Switched Reluctance Motor Drives with Fully Pitched Windings

Andrew Charlton Clothier

Department of Electrical and Electronic Engineering
University of Newcastle upon Tyne

A thesis submitted for the degree of Doctor of Philosophy

To my wife, Mandy

and son, Samuel

Abstract

Switched reluctance motors with fully pitched windings are a relatively recent advancement in motor technology having only been in existence since the early 1990's. They have been shown previously to offer greater torque per unit copper loss, and hence higher torque density, than conventional switched reluctance machines with short pitched windings. Early work by Mecrow and Barrass has demonstrated operation of prototype machines, developed and assessed various methods of control strategy, and made some comparisons of machine efficiency and inverter rating. The results presented here build on this early work by, in essence, examining the aspects of machine design, control strategy and inverter topology that affect drive performance and cost.

Detailed comparisons of inverter rating and machine efficiency are made under equal conditions with the various methods of excitation that are possible. This is achieved with results from a test rig, including temperature rise tests, and the use of accurate dynamic simulation. The latter is developed to accurately model the motor with its strong mutual coupling between phases, various inverter topologies and the details of the controller such as digital PWM. As a result comparisons between simulated and measured results are shown to be very good.

The fundamentals of machine design are examined with a view to optimising the machine for fully pitched windings. Previous work has indicated that good results are achieved when a conventional machine is simply rewound, however it is shown that further improvements can be made.

Proposals are made to improve the drive in terms of both machine performance and power electronic rating. A search method is proposed that optimises current waveshape for either maximum torque per unit copper loss, or smooth torque for lowest loss. The method works over the entire speed range, as the rate of change of flux linkage is taken into account. Three alternative power electronic converters are developed, one of which is also particularly suitable for the short pitched winding machine. Aspects of silicon rating, current controllability, and current sensor requirements are discussed.

Acknowledgements

It all seems such a long time ago now, but there was a great community spirit down in the UG lab, who's members over my three years included Pete, Eugene, Howard, Chris F, Chris M, Jim H, Jim K, Berhard, Volker, Ken, Gavin, Jawad, Ibrahim and Alun. I think we all learnt a lot from each others work and experience.

I would like to thank Alan, Paul, everyone in the electronics and mechanical workshop, and most of all Barrie, of course, for all the support, ideas and direction that have enabled me to get this far. I would also like to thank my wife Mandy, and now baby Sam, for all the spare time it has taken to write up this thesis.

Table of Contents

List of Symbols and Abbreviations

Symbols

1,2,3	Subscripts referring to short pitched winding phases
A,B,C	Subscripts referring to fully pitched winding phases
g	Air gap
i,I	Current
I_{dem}	Demanded current
L	Inductance
L_{stk}	Stack Length
M	Mutual Inductance
N	Number of turns per phase
r_b	Resistance in IGBT equivalent circuit
r_{rotor}	Radius of rotor
r_{stator}	Radius of stator
R	Resistance
t	Time
t	Tooth width
t/λ	Tooth width to tooth pitch ratio
T	Torque
V	Voltage
V_S	Star point voltage
V_{dc}	DC link voltage
W'	Co-energy
W_{slot}	Slot Width
θ	Rotor position
ψ	Flux linkage in phase

Abbreviations

BDCM	Brushless Direct Current Machine
CBD	Core Back Depth
DC	Direct Current
DSP	Digital Signal Processor
EMF	Electro Motive Force
Eoff	Turn off energy loss
Eon	Turn on energy loss
FE	Finite Element
FEA	Finite Element Analysis
FP	Fully Pitched
FPGA	Field Programmable Gate Array
IGBT	Insulated Gate Bipolar Transistor
MMF	Magneto Motive Force
MOSFET	Metal Oxide Field Effect Transistor
OD	Outside Diameter
PID	Proportional, Integral and Derivative (current controller)
PWM	Pulse Width Modulation
SOA	Safe Operating Area
SP	Short Pitched
SR	Switched Reluctance
SRM	Switched Reluctance Motor
VA	Volt-Amp

List of Figures

List of Tables

References

[1.1] Mechanics Magazine, Vol. XXXII, pp.693-696, 1840.

[1.2] Anderson AF, "Robert Davidson – father of the electric locomotive", IEE History of Electrical Engineering Conference, pp. 8/1-8/18, 1975.

[1.3] Mackie D, "The prospects of electromagnetism as a prime mover", The Practical Mechanic and Engineering Magazine, Nov. 1842.

[1.4] Bedford BD, US Patent No.3678352 and 3679953, 1972.

[1.5] Bausch H, Rieke B, "Speed and torque control of thyristor-fed reluctance motors", ICEM Proceedings, Part 1, pp.128.1-128.10, 1976.

[1.6] Lawrenson PJ, Stephenson JM, Blenkinsop PT, Corda J, Fulton NN, "Variable-speed switched reluctance motors", IEE Proceedings, Part B, Vol.127, No.4, pp.253-265, 1980.

[1.7] Byrne JV, Lacy JG, "Characteristics of saturable stepper and reluctance motors", IEE Conference Publication 136, Small Electrical Machines, pp.93-69, 1976.

[1.8] Stephenson JM, Corda J, "Computation of torque and current in double salient reluctance motors from nonlinear magnetisation data", IEE Proc. B, Electr. Power Appl., 1979, 126, pp.393-396.

[1.9] Miller TJE, "Converter volt-ampere requirements of the switched reluctance motor drive", IEEE Industrial Applications Society Annual Meeting, Chicago, Il, October 1984.

[1.10] Ray W, Lawrenson P, Davis R, Stephenson JM, Fulton NN, Blake R, "High performance switched reluctance brushless drives", IEEE Transactions on Industry Applications, Vol. IA-22, No.4 July/August 1986.

[1.11] Pollock C, "Power converter circuits for switched reluctance motors with minimum number of switches", PhD thesis, University of Heriot Watt, 1989.

[1.12] Pollock C, Williams BW, "Power converter circuits for switched reluctance motors with the minimum number of switches", IEE Proc. B, 1990, Vol. 137, No. 6, pp.373-384.

[1.13] Pollock C, Williams BW, "The design and performance of a multiphase switched reluctance drive", EPE Conference Proceedings, Aachen, pp.29, 1989.

[1.14] Xu L, Lipo TA, "Analysis of a variable speed single-salient reluctance motor utilizing only two transistor switches", IEEE, 1988.

[1.15] Harris MR, Finch JW, Mallick JA, Miller TJE, "A review of the integral horsepower switched reluctance drive", IEEE Transactions on Industry Applications, vol.22, No.4, pp.716, 1986.

[1.16] Cameron DE, Lang JH, Umans SD, "The origin and reduction of acoustic noise in the switched reluctance motor drive", IEEE IAS Conference Record, Vol. 1, pp.106-113, 1993.

[1.17] Wu CY, Pollock C, "Time domain analysis of vibration and acoustic noise in the switched reluctance motor", IEE Conference Publication No.377, pp.558, 1993.

[1.18] Mecrow BC, "New winding arrangements for doubly salient reluctance machines", IEEE IAS Conference Proceedings, Vol.1, pp.249, 1992.

[1.19] Mecrow BC, "SRM and stepping motor design" UK Patent application 9 126 206.3, Dec 1991.

[1.20] Mecrow BC, "Fully pitched-winding switched-reluctance and stepping motor arrangements", IEE Proceedings-B, Vol. 140, No.1, Jan 1993.

[1.21] Barrass PG, “High performance switched reluctance motor drives”, PhD thesis Oct 1995.

[1.22] Barrass PG, Mecrow BC, Clothier AC, “The unipolar operation of fully-pitched winding switched reluctance drives”, ICEM Conference Proceedings, Vol.1, pp.71, 1994.

[1.23] Barrass PG, Mecrow BC, Clothier AC, “Bipolar operation of fully-pitched winding switched reluctance drives”, IEE EMD Conference Proceedings, pp.252, 1995.

[2.1] Moreira JC, Lipo TA, "Simulation of a four phase switched reluctance motor including the effects of mutual coupling", Beijing International Conference on Electrical Machine (BICEM 89) Aug 10-14, 1987, China.

[2.2] Mecrow BC, "Fully pitched-winding switched-reluctance and stepping motor arrangements", IEE Proceedings-B, Vol. 140, No.1, Jan 1993.

[2.3] Mecrow BC, "New winding configurations for doubly salient reluctance machines", IEEE Industrial Applications Society Transactions, 1996.

[2.4] Barrass PG, Mecrow BC, Clothier AC, “The unipolar operation of fully pitched switched reluctance motor drives”, ICEM, Paris, Sept.1994.

[2.5] Barrass PG, “High performance switched reluctance motor drives”, PhD thesis Oct 1995.

[2.6] Barrass PG, Mecrow BC, Clothier AC, “Bipolar operation of fully-pitched winding switched reluctance drives”, IEE EMD Conference Proceedings, pp.252, 1995.

[3.1] Chai HD, “A mathematical model for single-stack step motors”, IEEE Trans.,1975, PAS-94, pp.1508-1517.

[3.2] Singh G, Kuo BC, "Modelling and simulation of variable-reluctance step motors with application to a high performance printer system", IEE Trans., 1975,IA-11, pp.373-383.

[3.3] Pickup IED, Tipping D, "Method for predicting the dynamic response of a variable reluctance stepping motor", Proc. IEE, 1973, 120, (7), pp.757-765.

[3.4] Pickup IED, Tipping D, "Prediction of pull-in rate and settling-time characteristics of a variable-reluctance stepping motor and effect of stator-damping coils on these characteristics", ibid., 1976, 123, (3), pp.213-219.

[3.5] Blenkinsop PT, "A novel, self-commutating, singly-excited motor", PhD thesis, University of Leeds, Oct. 1976.

[3.6] Byrne JV, Dwyer JB, "Saturable variable reluctance machine simulation using exponential function", Proc. of the international conference on stepping motors and systems, University of Leeds, July 1976, pp.11-16.

[3.7] Acarnley PP, "Analysis and improvement of the steady-state performance of variable-reluctance stepping motors", PhD thesis, University of Leeds, Oct. 1977.

[3.8] Stephenson JM, Corda J, "Computation of torque and current in double salient reluctance motors from nonlinear magnetisation data", IEE Proc. B, Electr. Power Appl., 1979, 126, pp.393-396.

[3.9] Torrey DA, Lang JH, "Modelling a nonlinear variable-reluctance motor drive", IEE Proc., Vol. 137, Pt B, No. 5, Sept 1990.

[3.10] Miller TJE, "Nonlinear theory of the switched reluctance motor for rapid computer-aided design", IEE Proc., Vol. 137, Pt. B, No. 6, Nov 1990.

[3.11] Miller TJE, "PC CAD for switched reluctance drives", IEE EMD, 16-18 Nov 1987, Conf. Publication No.282.

[3.12] Jack AG, Finch JW, Wright PW, "Adaptive mesh generation applied to switched-reluctance motor design", IEEE Transactions on Industry Applications, Vol.28, No.2, March/April 1992.

[3.13] Moreira JC, Lipo TA, "Simulation of a four phase switched reluctance motor including the effects of mutual coupling"

[3.14] Mecrow BC, "New winding configurations for doubly salient reluctance machines", IEEE Industrial Applications Society Transactions, 1996.

[3.15] Barrass PG, "High performance switched reluctance motor drives", PhD thesis, Oct 1995.

[4.1] Horst G, US Patent No.5122687, Horst G, 1992.

[4.2] El-Khazendar MA, Stephenson JM, "Analysis and optimisation of a 2-phase self starting switched reluctance motor', International Conference on Electrical Machines, pp.1031-1034, Munich, Germany, 1986.

[4.3] Pollock C, Wallace M, "The flux switching motor, a DC motor without magnets or brushes", IEEE Industrial Applications Society Annual Meeting 1999, pp1980-1987.

[4.4] Michaelides A, Pollock C, '"A new magnetic flux pattern to improve the efficiency of the switched reluctance motor", Conf. Proc. IEEE Industrial Applications Society Annual Meeting, pp.226-234, Houston, USA, Oct. 1992.

[4.5] Faiz J, Finch JW, "Aspects of design optimisation for switched reluctance motors", IEEE Trans. Energy Conversion, Vol. 8, No.4, pp.704-713, Dec 1993.

[4.6] Miller TJE, "Switched reluctance motors and their control", Clarendon Press, Oxford, 1993.

[4.7] Jack AG, Finch JW, Wright PW, "Adaptive mesh generation applied to switched-reluctance motor design", IEEE Transactions on Industry Applications, Vol.28, No.2, March/April 1992.

[5.1] Barrass PG, "High performance switched reluctance motor drives", PhD thesis Oct 1995.

[5.2] Cameron DE, Lang JH, Umans SD, "Origin of acoustic noise in variable-reluctance motors", IEEE IAS Conference Record, pp.108-115, 1989.

[5.3] Wu CY, Pollock C, "Time domain analysis of vibration and acoustic noise in the switched reluctance motor", IEE Conference Publication No.377, pp.558, 1993.

[6.1] Miller TJE, "Converter volt-ampere requirements of the switched reluctance motor drive", IEEE Industrial Applications Society Annual Meeting, Chicago, Il, October 1984.

[6.2] Davis RM, "Inverter drive for switched reluctance motor: circuits and component ratings", Proc. Inst. Elec., Pt. B, vol.128, pp.126-136, March 1981.

[6.3] Ray W, Lawrenson P, Davis R, Stephenson JM, Fulton NN, Blake R, "High performance switched reluctance brushless drives", IEEE Transactions on Industry Applications, Vol. IA-22, No.4 July/August 1986.

[6.4] Clemente S, Dubashi A, Pelly B, Dokopoulos G, "IGBT characteristics", International Rectifier Application Note AN-983A

[6.5] Barrass PG, "High performance switched reluctance motor drives", PhD thesis Oct 1995.

[7.1] Ilic'-Spong M, Miller TJE, MacMinn SE, Thorp JS, "Instantaneous torque control of electric motor drives", IEEE PESC Conference Record, pp.42-48, 1985.

[7.2] Taylor DG, "An experimental study on composite control of switched reluctance motors", IEEE Control Systems magazine, Vol.11, No.2 pp.31-36, 1991.

[7.3] Reay DS, Green TC, Williams BW, "Minimisation of torque ripple in a switched reluctance motor using a neural network" IEE Conference Publication, No.372, 3rd International Conference on Artificial Neural Networks, pp.224-226, 1993.

[7.4] Reay DS, Green TC, Williams BW, "Application of associative memory neural networks to the control of a switched reluctance motor" IEEE IECON Conference Proceeding, pp.200-206, 1993.

[7.5] Barrass PG, "High performance switched reluctance motor drives", PhD thesis Oct 1995.

[7.6] Barrass PG, Mecrow BC, "Flux and torque control of switched reluctance machines", IEE Proceeding, Part B, Nov.1998

[8.1] Lawrenson PJ, Stephenson JM, Blenkinsop PT, Corda J, Fulton NN, "Variable speed switched reluctance motors", IEE Proc., Vol. 127, Pt. B, July 1980, pp.253-265.

[8.2] Stephenson JM, El Khazendar MA, "Saturation in doubly salient reluctance motors", IEE Proc. B, 1989, Vol. 136, No. 1, pp.50-58.

[8.3] Bryne JV, McMullin MF, O'Dwyer JB, "A high performance variable reluctance drive: a new brushless servo", Motor-Con Proceedings, October 1985, pp.147-160.

[8.4] Pollock C, Williams BW, "Power converter circuits for switched reluctance motors with the minimum number of switches", IEE Proc. B, 1990, Vol. 137, No. 6, pp.373-384.

[8.5] Le-Huy H, Viarouge P, Francoeur B, "A novel unipolar converter for a switched reluctance motor", IEEE Trans. Power Electronics, 1990, pp.469-475.

[8.6] Davis RM, European Patent Application No. EP 0 692 862 A2

[8.7] Miller TJE, "Converter volt-ampere requirements of the switched reluctance motor drive", IEEE Industrial Applications Society Annual Meeting, Chicago, Il, Oct. 1984.

[8.8] Ray W, Lawrenson P, Davis R, Stephenson JM, Fulton NN, Blake R, "High performance switched reluctance brushless drives", IEEE Transactions on Industry Applications, Vol. IA-22, No.4 July/August 1986.

[8.9] Harris MR, Finch JW, Mallick JA, Miller TJE, "A review of the integral horsepower switched reluctance drive", IEEE Transactions on Industry Applications, Vol.22, No.4, pp.716, 1986.

[8.10] Clothier AC, Mecrow BC, "Inverter topologies and current sensing methods for short pitched and fully pitched winding SR motors", IEEE APEC Conference Proceedings, 1999.

Publications by the Author

"The Unipolar Operation of Fully-Pitched Winding Switched Reluctance Drives", Barrass PG, Mecrow BC, Clothier AC, ICEM Conference Proceedings, Vol.1, pp.71, 1994.

"Bipolar Operation of Fully-Pitched Winding Switched Reluctance Drives", Barrass PG, Mecrow BC, Clothier AC, IEE EMD Conference Proceedings, pp.252, 1995.

"High performance switched reluctance drives using novel windings", Mecrow BC, Clothier AC, invited presentation at IEE Colloquium on machines and drives for electric vehicles, June 1996.

"Operation of switched reluctance machines from three phase bridge inverters", Clothier AC, Mecrow BC, EMD, Cambridge, Sept. 1997.

"Drive configurations for fully pitched winding switched reluctance machines", Mecrow BC, Clothier AC, Barrass PG, Weiner C, Industrial Applications Society, Oct. 1998.

"Inverter topologies and current sensing methods for short pitched and fully pitched winding SR motors", Clothier AC, Mecrow BC, IEEE APEC Conference Proceedings, 1999.

Chapter 1 - INTRODUCTION

1.1 Historical Background to the Switched Reluctance Motor

The switched reluctance motor can, paradoxically, be described as being both a very new and a very old machine at the same time. Faraday famously made the first demonstration of the conversion of electrical energy into mechanical energy in 1822. His apparatus consisted of a metal rod suspended over a pool of mercury, the centre of which contained a powerful magnet. Only a short time later, in 1838, WH Taylor obtained a patent for his "electromagnetic engine", details of which are given in [1.1]. This consisted of a wooden wheel containing seven pieces of soft iron and four stationary electromagnets. A mechanical commutator was used to magnetise one of the electromagnets, causing the wheel to rotate and hence a torque to be produced. The wheel rotated until the pole piece came into alignment with the electromagnet, at which point no further torque was produced and the electromagnet was turned off. Because the number of electromagnets and pole pieces differed, it was then possible to continue to produce torque by switching on one of the other electromagnets. This demonstrated the basic principles of the switched reluctance motor, that is, production of torque by the alignment principle and the need to maintain motion by the switching on and off of electromagnets at the correct time and position.

An early application of a switched reluctance motor was demonstrated in 1842 by R Davidson, when he powered a locomotive on the Edinburgh to Glasgow railway [1.2, 1.3]. Performance was, however, restricted to 4mph, thus demonstrating some of the problems associated with these earliest of motors such as electromagnetic design and the control of power to the electromagnets. The latter meant that DC and induction machines became dominant over the next century due to their simplicity of control.

Besides the invention of the stepper motor by Walker in the 1920's, no significant development work continued until the 1970's, after the invention of semiconductor devices. Semiconductor devices made a significant advance in two main areas within the

SR motor. Firstly, power electronic devices such as the thyristor could be used to efficiently control the flow of power to the electromagnetic coils (or phases). Secondly, control electronics could be used to synchronise the currents in the phases with the position of the rotor. In 1972 Bedford [1.4] described some of the earliest examples of such control methods, and the following decade saw the development and understanding of the SR motor as it is today. Notable papers during this time include Bausch *et al* [1.5], Lawrenson *et al* [1.6], Byrne *et al* [1.7], Stephenson *et al* [1.8], Miller *et al* [1.9], and Ray *et al* [1.10]. These papers described the control, design, characterisation, simulation and power electronic rating of the modern SR motor.

Since then much work has concentrated, for example, on the reduction of cost and any impact on drive performance. The SR motor itself is fundamentally robust and low cost due to its simple stator windings and geometry. This machine, however, cannot be connected direct to an AC supply as an induction motor or universal machine can. The power electronics and control needed to drive the SR motor are a large proportion of the overall cost, and much work has concentrated on new converter topologies with a lower number of switches per phase. In addition the number of phases itself has a large impact on cost and performance. Examples of such work are by Pollock *et al* [1.11], [1.12], [1.13], Lipo *et al* [1.14], Harris *et al* [1.15]. Other areas of work included the reduction of acoustic noise and torque ripple, for example Cameron *et al* [1.16], Wu *et al* [1.17].

In the early 1990's Mecrow made a significant advance in the fundamental design of SR machines. A new winding arrangement is described in [1.18] and the patent application of 1991 [1.19], its aim being to increase winding efficiency and hence increase torque output in a given motor frame size. The windings were "fully pitched", meaning that a winding enclosed as many stator teeth as there were phases. In contrast, a conventional SR motor winding only encloses one stator tooth. The motor was characterised by strong mutual coupling between phases, and torque was produced when two or more phases were excited at a time, when this mutual coupling changed with position. Chapter 2 will describe this phenomenon in detail.

Initial work was carried out by Mecrow on a prototype machine to measure flux linkage and static torque characteristics [1.20]. The first real time operation of a fully pitched

winding motor was developed by Barrass [1.21]. Subsequent papers have described control with unipolar phase currents (Barrass, Mecrow, Clothier [1.22]) and bipolar currents (Barrass, Mecrow, Clothier [1.23]). Further work by Barrass [1.20] included the use of flux linkage control and genetic algorithms to improve performance, and acoustic measurements.

1.2 SR Motor Characteristics and Applications

Figure 1.1 shows a cross section of a typical modern day three phase SR motor. In the machine shown, one phase consists of two stator coils connected in series. The motor is operated by sequentially exciting each phase in turn, with torque being produced by the alignment principle i.e. the rotor will tend to turn into such at position to minimise the reluctance of the excited magnetic path. Chapter 2 will describe this operation in more detail. However, it can be seen that to operate in an efficient manner the machine requires a controller to determine which phase should be excited, and power electronics to control the flow of power to the relevant phase. Typically, then, the controller would require feedback from a position detection device such as an optical encoder or hall effect sensor to determine the rotor position. Current is usually controlled to a fixed value during phase excitation, primarily as a means of controlling torque and protecting the power electronic devices.

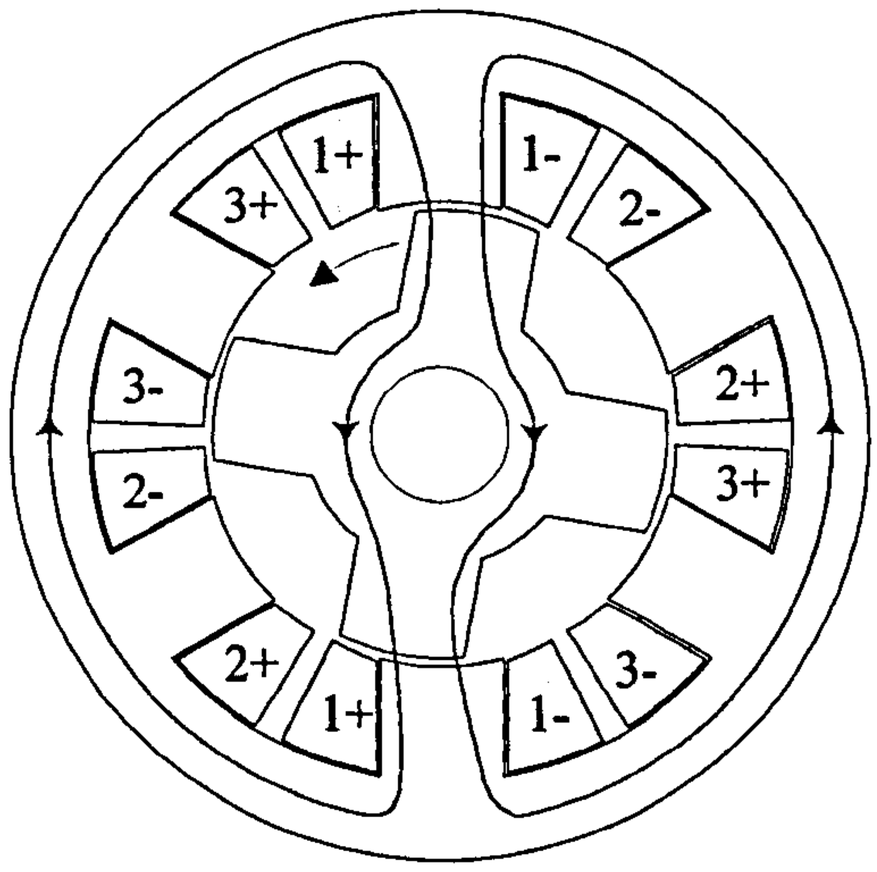

Figure 1.1 Cross section of a typical three phase SR motor with short pitched windings , showing a representation of the flux produced with phase 1 conducting.

Compared to a DC or induction motor the design of both the magnetic circuit and the windings are very simple, and therefore robust. The rotor in particular differs from any other type of machine in that it does not contain a winding or require brushes. It is therefore highly suitable for applications requiring high speed operation. Starting torque in the three phase machine is high, and the machine exhibits excellent controllability and efficiency over its entire speed range, in contrast for example with the induction motor.

Figure 1.2 shows the most common power electronic topology, the asymmetric half bridge, to control the phase currents (see Lawrenson et al [1.6]). Energy is typically supplied from a rectified AC supply and is fed into the DC link capacitor shown in Figure 1.2. Each phase has two controlled power electronic devices and two diodes. Thyristors were initially used for the controlled power electronic devices, but have been replaced in recent years by superior devices such as IGBTs (Insulated Gate Bipolar Transistor) and MOSFETs (Metal Oxide Field Effect Transistor). This topology offers maximum flexibility. When both controlled devices are turned on, the DC link voltage is applied across the phase, rapidly increasing the current. When the devices are turned off, current continues to flow in the winding due to the phase inductance, and is therefore forced to flow through the diodes. This applies the negative of the DC link voltage to the phase, rapidly decreasing the current. This is important for high speed operation when the phases must be turned on and off rapidly to maintain performance. If current continues to flow in a phase after the rotor and stator poles have aligned a negative torque will be produced.

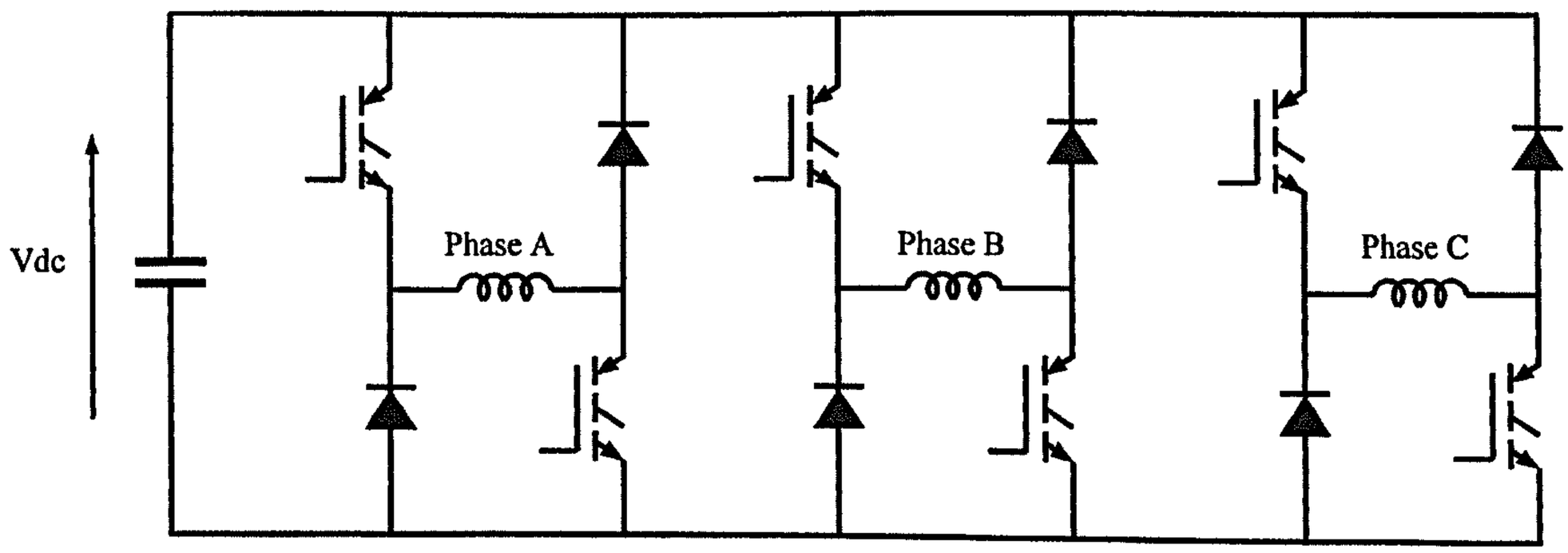

Figure 1.2 Three phase asymmetric half bridge inverter.

Much work has focussed on reducing the power electronic cost, which is a large proportion of the overall cost of the SR drive. This can be achieved by reducing the number of phases and reducing the controlled switches per phase with alternative topologies (see Pollock [1.17]). While this does reduce cost, there is always a reduction of some kind in machine performance. A two phase machine, for example, only requires four switches, but suffers from very low starting torque. However, in a fan load application this may not be important.

The SR motor, then, can be designed with a wide variety of power electronic topologies, number of phases, and lamination designs. These produce marked differences in overall cost and performance. This is of benefit, in that particular combinations of motor, power electronics, and control design can be targeted and optimised for particular applications. SR motors are suitable, and becoming increasingly competitive, in applications as diverse as domestic appliances, standard industrial drives and servos. Note that this wide variety of configurations and applications makes the assessment of advancements in fundamental design, such as the fully pitched winding, difficult to generalise.

1.3 Objectives of the Work

The objectives of the work carried out by the author are as follows:

- Development of an accurate dynamic simulation of both the short pitched and fully pitched winding SR machines.
- Design of a machine optimised towards the fully pitched winding, if possible.
- Use of simulation and test rig results to evaluate performance in terms of:
  - Power electronic rating
  - Torque rating
  - Development of design improvements to increase torque output further and reduce power electronic rating.

1.4 Overview of the Thesis

Chapter 2 describes the definition of a short pitched and a fully pitched winding SR machine. Operation of the machines is described in terms of the desired phase current shape, and how torque is subsequently produced. The concept of "transformation matrices" to aid understanding and simulation of the fully pitched winding machine is introduced.

Chapter 3 describes the method of simulation, and how the model was developed to accurately cope with variation of mutual coupling with position and magnetic saturation. The full effects of PWM control are included so that, for example, power electronic rating comparisons can be accurately made.

Chapter 4 uses the simulation and finite element analysis to optimise the design of a 12-8 SR machine. Assessments are also made of designs with 1, 2, 3, 4 and 5 phases in terms of desired phase current shapes and copper losses.

Chapter 5 shows operation of the prototype motor on the purpose-built test rig, and compares waveforms such as current and torque to validate the accuracy of the simulation model. Comparisons are made with a variety of excitation methods e.g. unipolar and bipolar currents. Bipolar operation with star connected winding is also possible and, as will be shown, is particularly difficult to simulate.

Chapter 6 uses the test rig combined with simulation results, to assess machine performance, torque rating, and power electronic rating with the various methods of excitation under the same conditions.

Chapter 7 describes a search method that was developed to find the optimal current waveshape to achieve either the highest torque per unit copper loss, or smooth torque output for the lowest copper loss. As will be seen, power electronic rating is also reduced for a given machine power output.

Chapters 8 and 9 describe three novel power converters developed for operation of three phase machines with either short pitched or fully pitched windings. Significant advantages will be demonstrated particularly in the fully pitched machine in terms of power electronic rating and control costs.

1.5 The Contribution to Knowledge

The following is a summary of achievements that the author believes are previously unpublished:

- A full dynamic simulation of the fully pitched winding machine.
- A machine lamination design optimised for fully pitched windings.
- Power electronic ratings comparisons of unipolar and bipolar operation of the fully pitched and short pitched winding machines for the same machine output.
- Determination of torque rating for a given winding temperature rise with unipolar and bipolar operation of the fully pitched winding machine.
- A new search method to find optimal fully pitched winding bipolar currents for either highest torque per unit copper loss, or smooth torque with lowest copper loss, at any speed.
- Three novel power converters and development of current sensing arrangements and control strategies for the fully pitched winding machine.
- Development of a dead time compensation technique to improve current waveshape in the above inverters.
- Current sensing and control strategy for the short pitched winding machine operated from a modified three phase bridge circuit
- A dead time compensation technique for the above inverter to improve current waveshape.

Chapter 2 - SWITCHED RELUCTANCE MACHINES WITH FULLY PITCHED WINDINGS

2.1 Introduction

Traditional switched reluctance machines come in many varieties. The number of phases, the number of poles, the shape of the stator/rotor teeth, the control strategy, and the type of inverter can all be varied over a wide range. Each one in turn can be considered advantageous depending on the demands of the specific application. They all, however, have one feature in common, which is that the windings are short pitched i.e. wound around a single pole.

This chapter examines the definition and characteristics of the short pitched winding. The concept of the fully pitched winding will then be introduced and its possible modes of operation, method of torque production, and potential benefits will be explained.

2.2 The Short Pitched Winding Machine

The cross sectional view of a typical SRM with short pitched windings is shown in Figure 2.1. In this instance the machine has 3 phase windings, 6 stator teeth, 4 rotor teeth and is hence referred to as having a 6-4 geometry. Each stator tooth has a coil wrapped around it. In a three phase machine the coil on every third stator tooth is connected together in series to form one phase winding. Therefore in the case of the 6-4 geometry shown, the two coils directly opposite each other are connected together. If a current is forced into one of the phases a MMF is produced down each of the associated stator teeth and a flux is produced. Fig 2.1 shows a representation of the flux pattern that would be produced with phase 1 excited (Figure 2.7 later in this chapter shows flux plots produced from finite element analysis).

The salient nature of the rotor and the stator results in the self inductance of a phase varying with position. In other words, the reluctance of the magnetic circuit that each

phase 'sees' varies with position. With one of these phases excited there will be a tendency to minimise this reluctance by bringing the rotor and stator teeth into alignment, hence torque is produced.

It can be seen from Figure 2.1 that the flux produced by phase 1 does not link with either of the other phases, hence there is no mutual inductance or coupling between phases. In practice there is usually some coupling but in most cases it is small enough to ignore (Moreira and Lipo [2.1] investigated the validity of this assumption). Torque is only produced by variation of self inductance with rotor position. If no saturation of the magnetic circuit occurs then torque can be calculated as follows:

$$T = \frac{1}{2} i^2 \frac{dL}{d\theta} \tag{2.1}$$

Figure 2.2 shows how the self inductance of a phase varies with position in an idealised unsaturated machine. It is shown simplified here, with rising inductance for one third of the electrical cycle, falling inductance for one third, and no variation for the other third. As indicated in Equation 2.1 the direction of the change in inductance with position determines whether positive or negative torque is produced (i.e. motoring or generating). Therefore, to produce a continuous positive torque on the rotor, the unipolar currents shown in Figure 2.2 should be forced into the machine.

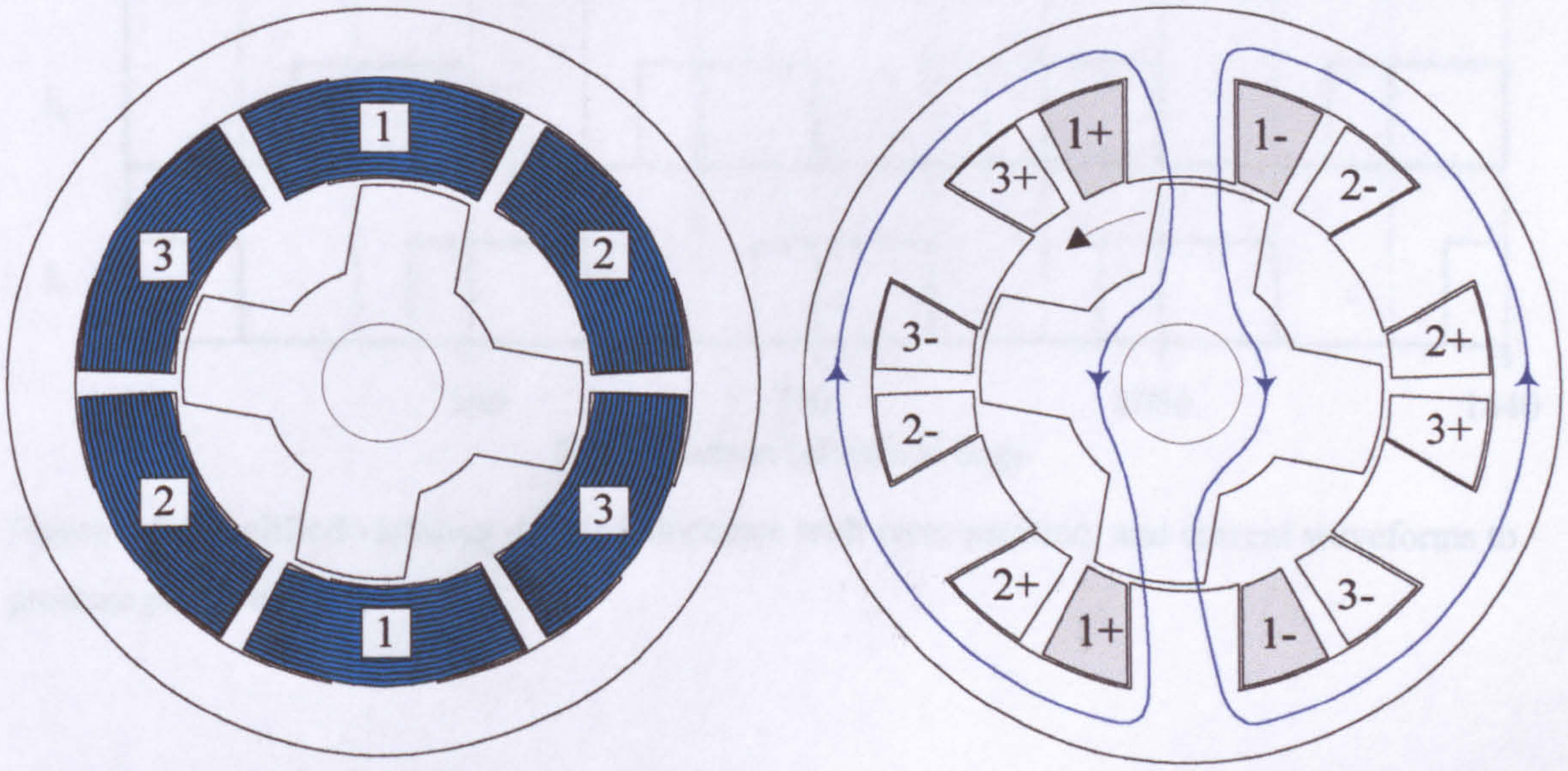

Figure 2.1 Cross Section of a 3 phase 6-4 SRM with short pitched windings. Representation of the flux pattern produced with phase 1 excited.

Note that in practice inductance varies more sinusoidally with position and therefore it is possible to produce a small amount of extra torque by extending the period of excitation up to one half of the electrical cycle, as indicated by the dotted lines in Figure 2.2.

Equation 2.1 also shows that the direction of the current has no effect on the direction of torque produced. Only the timing of the excitation makes a difference, hence the need for knowledge of rotor position. This analysis shows that both the electrical and magnetic circuits are under utilised, particularly the former as only one third of the available copper in the machine is being excited at a time.

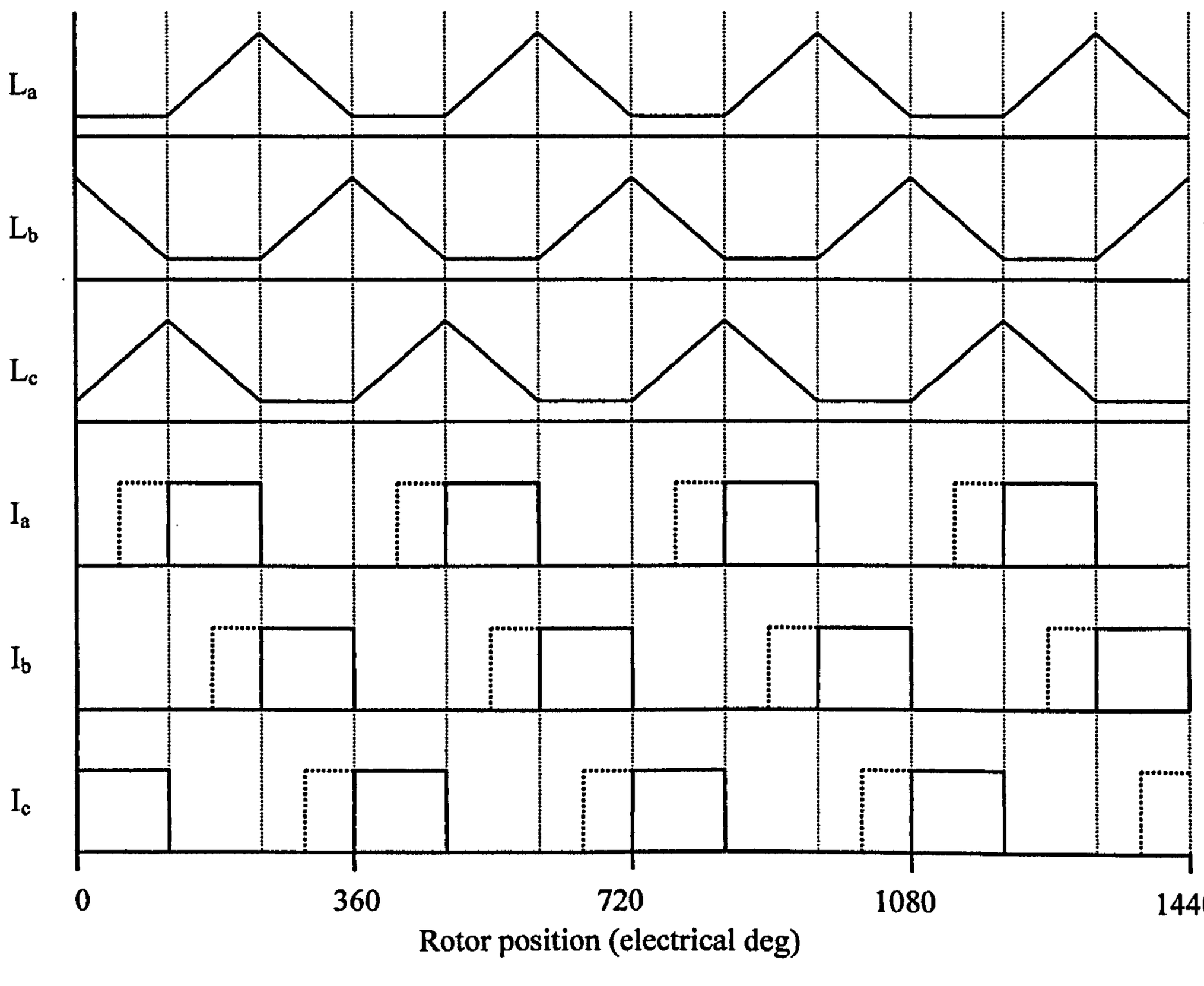

Figure 2.2 Simplified variation of self inductance with rotor position, and current waveforms to produce positive torque.

2.3 The Fully Pitched Winding Machine

The winding arrangement for the fully pitched winding SRM is shown in Figure 2.3. In contrast to the short pitched arrangement each winding encloses three stator teeth in a three phase machine, and is hence fully pitched. Mecrow [2.2] first described this arrangement and demonstrated its potential for reducing copper loss for a given torque output. Further publications by Mecrow [2.3], Barrass *et al* [2.4], Barrass [2.5], Barrass *et al* [2.6] went on to demonstrate its operation and performance in more detail. Unlike the short pitched winding machine, operation is possible with both unipolar and bipolar currents as will be demonstrated over the next two sections.

2.3.1 Unipolar Operation

Figure 2.3 shows Phases B and C excited with a unipolar current and it can be seen that this produces the same flux pattern as the short pitched winding machine (see Fig. 2.2). The difference is that twice the amount of copper is utilised to achieve this same level of flux in the stator teeth (and hence the same torque). If the same number of turns per slot is assumed, then the current in each phase can be halved to achieve the same torque output. This is an example of how the fully pitched winding machine can achieve lower copper losses for a given torque output.

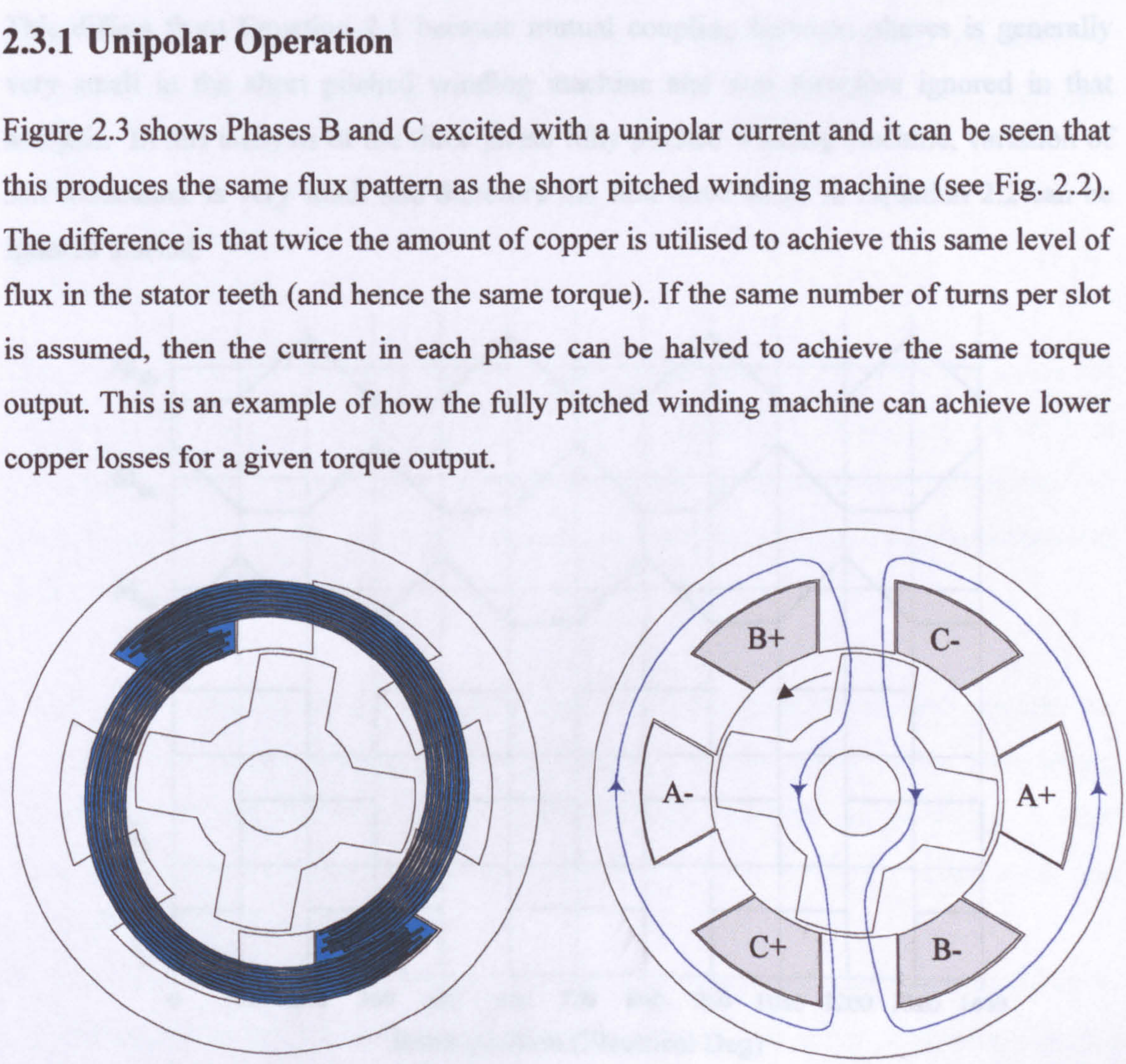

Figure 2.3 Cross Section of a 3 phase 6-4 SRM with fully pitched windings (only one phase shown for clarity and wound in a double layer arrangement). Flux pattern shown for phases B and C excited.

Inspection of Figure 2.3 reveals that the self inductance of each phase essentially does not vary with position - there is a constant area of overlap between the three stator teeth that the winding encloses and the rotor teeth. There is now, however, a large amount of mutual coupling between phases. This is indicated in Figure 2.3 by the fact that the flux now links all three phases. The amount of mutual coupling between phases varies strongly with position, and a simplified version is shown in Figure 2.4. A more general expression for the torque generated in a SRM is given in Equation 2.2.

$$T = \frac{1}{2} i_a^2 \frac{dL_a}{d\theta} + \frac{1}{2} i_b^2 \frac{dL_b}{d\theta} + \frac{1}{2} i_c^2 \frac{dL_c}{d\theta} + i_a i_b \frac{dM_{ab}}{d\theta} + i_b i_c \frac{dM_{bc}}{d\theta} + i_c i_a \frac{dM_{ca}}{d\theta} \qquad (2.2)$$

This differs from Equation 2.1 because mutual coupling between phases is generally very small in the short pitched winding machine and was therefore ignored in that analysis. In this analysis of the three phase fully pitched winding machine, variation of self inductance is very small and therefore the first three terms in Equation 2.2 can be ignored instead.

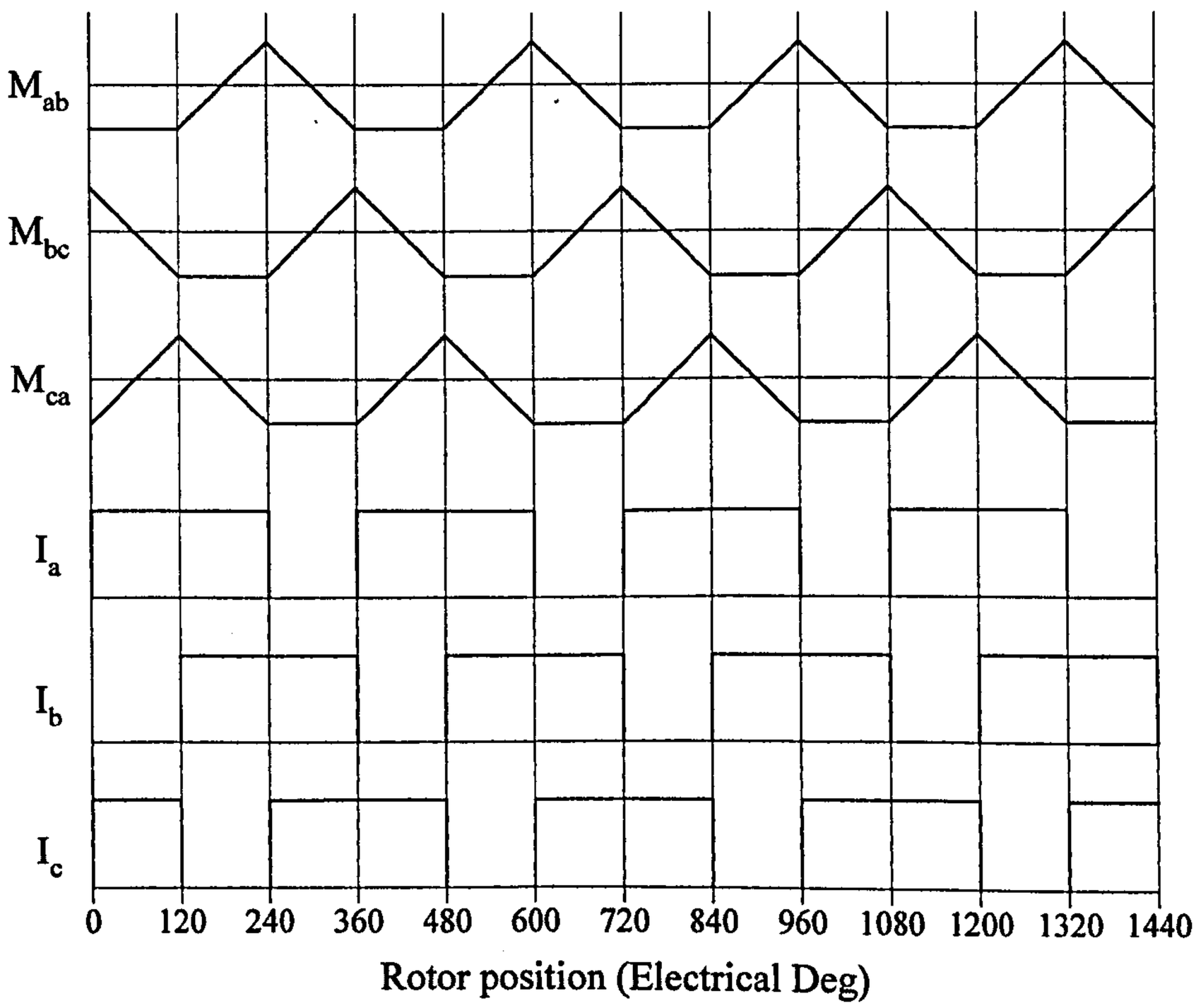

Figure 2.4 Simplified variation of mutual inductance with rotor position, and current waveforms to produce positive torque.

The equation shows that with a rising mutual coupling between two phases a positive torque can be produced if those two phases conduct with a positive current. This leads to the waveforms shown in Figure 2.4. These waveforms relate to the flux pattern shown in Figure 2.3. Two fully pitched phases excited with positive currents produce the same pattern as the short pitched winding machine with only one phase excited i.e. an MMF is produced down one pair of stator teeth only. The difference is that torque is derived from the variation in the mutual coupling between the two excited phases, rather than variation of self inductance.

A simplistic analysis of the copper losses can now be performed. If the same number of turns are assumed per slot as in the short pitched winding machine, then the current in each fully pitched winding is half to achieve the same total number of ampere-turns driving flux down that stator tooth. Two phases, however, conduct at any one time, therefore:

$$\frac{Loss_{FP}}{Loss_{SP}} = \frac{2*(0.5)^2 R_{FP}}{1*(1)^2 R_{SP}} \tag{2.3}$$

If R_{FP} is assumed to be equal to R_{SP}, then copper losses in the fully pitched machine are reduced to half that of the short pitched winding machine. It then follows that, in a machine where the magnetic circuit does not saturate, the torque output for a given loss increases by a factor of 2. In a real machine, however, two effects reduce this apparent gain in specific output.

- The endwinding length is inevitably longer in the fully pitched winding machine i.e. $R_{FP} > R_{SP}$ (compare Figures 2.1 and 2.3). The relative effect of the endwinding depends on both the aspect ratio of the machine and also the geometry. A 12-8 geometry has a smaller endwinding length than a 6-4 machine for instance (as will be demonstrated in Chapter 4).
- The magnetic circuit saturates in any SR machine operated at rated torque output. In this region torque is no longer proportional to the square of the current, it becomes more proportional to the current.

2.3.2 Bipolar operation

Further inspection of Equation 2.2 reveals that it is possible to produce positive torque in the region where the mutual inductance between phases is falling, as long as one of the phase currents is negative and the other positive. Figure 2.5 shows that the current waveforms necessary to achieve this are the same as that used in many brushless DC motors i.e. alternating 120° periods of constant positive and negative current. Note that in this instance the electrical period has, in fact, been defined over a period of 720°, and therefore 240° conduction occurs. This is simply to avoid confusion when relating conduction periods with bipolar waveforms to those with unipolar waveforms - with this definition the same electrical period (360°) corresponds to a rotation of one rotor tooth pitch in both cases.

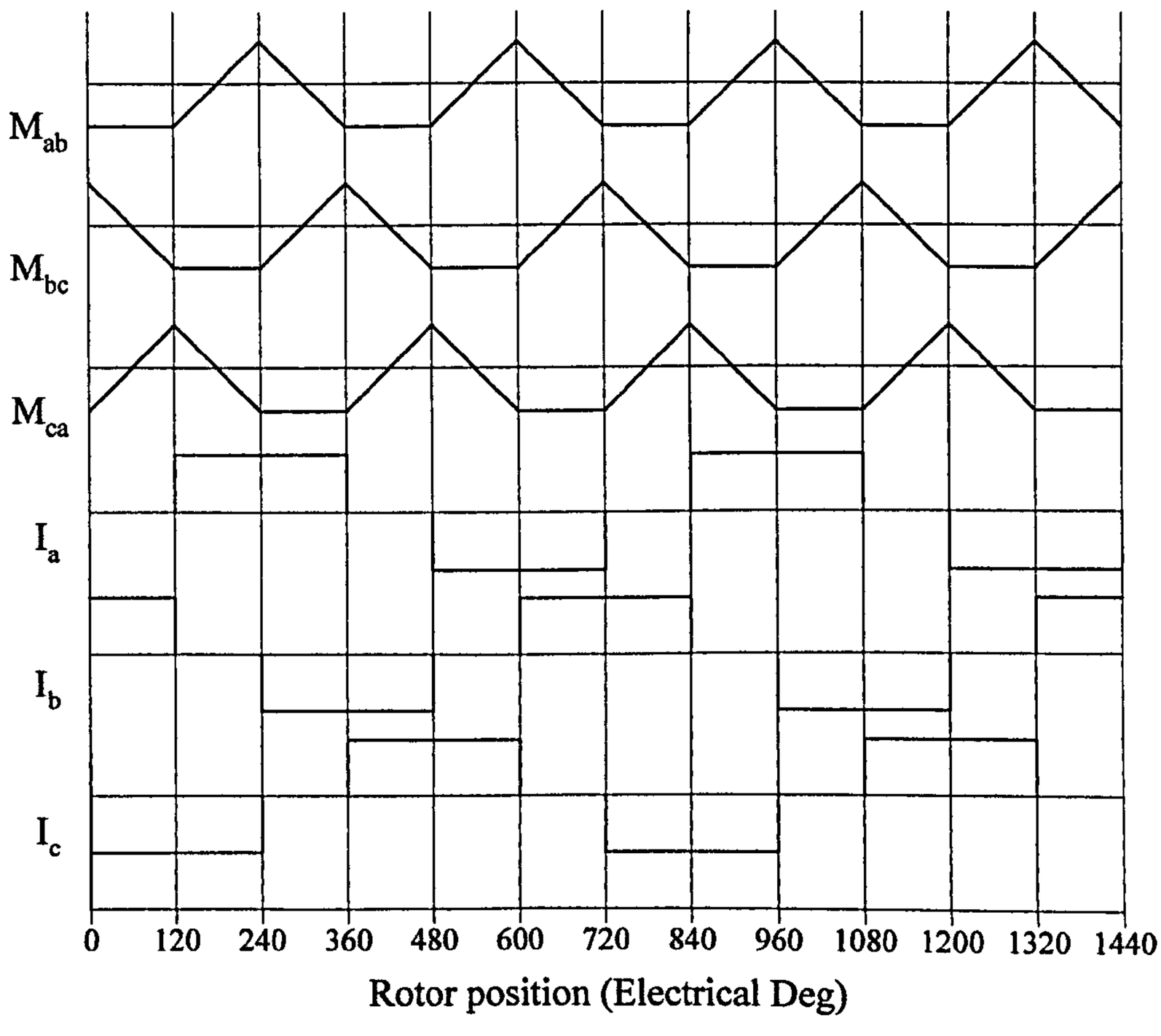

Figure 2.5 Idealised variation of mutual inductance with rotor position, and 240° bipolar current waveforms to produce positive torque.

Another case to consider is where both the rising and falling mutual inductances are utilised. Figure 2.6 shows this case, where all phases conduct at the same time, carrying a squarewave of current. The resulting flux pattern can be seen in Figure 2.7 and is shown in comparison to the other two basic excitation methods. In all three cases the rotor is at, or near, its aligned position.

It can be seen that bipolar squarewave excitation utilises all the copper in the machine at the same time and in that respect is making the best utilisation of the electric circuit. Not all of the flux, however, can be directed down the desired stator teeth and negative torque is therefore produced on some stator teeth (see Fig. 2.7). A variation on this excitation method is to use sinusoidal shaped currents instead of square. It is unclear at this stage as to which bipolar waveform is best in terms of torque per unit copper loss as well as other important criteria, such as power electronic rating. Simulation work and results from a test rig are used to make an assessment later in this thesis, including comparisons with other modes of operation.

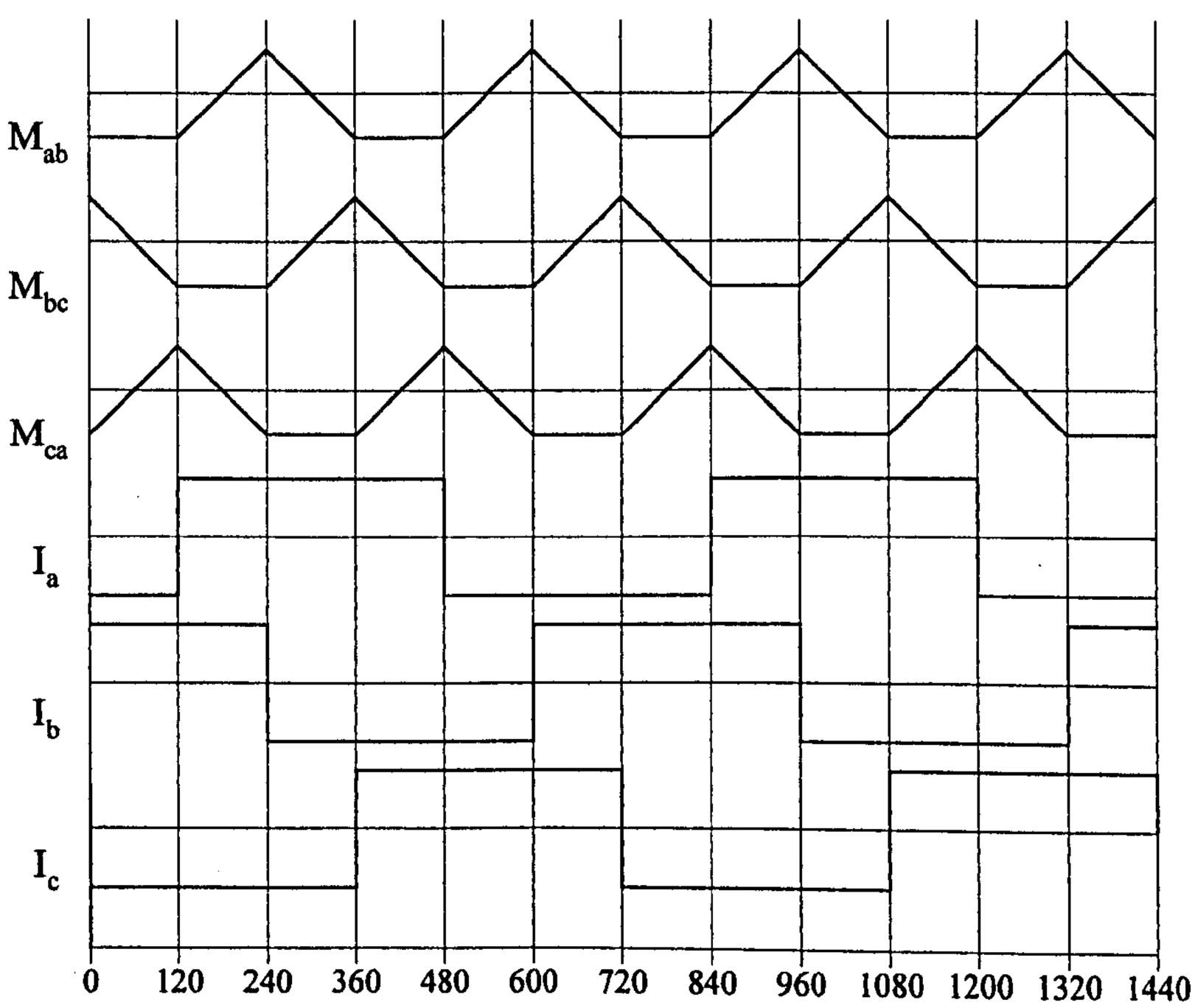

Figure 2.6 Idealised variation of mutual inductance with rotor position, and 360° bipolar current waveforms to produce positive torque.

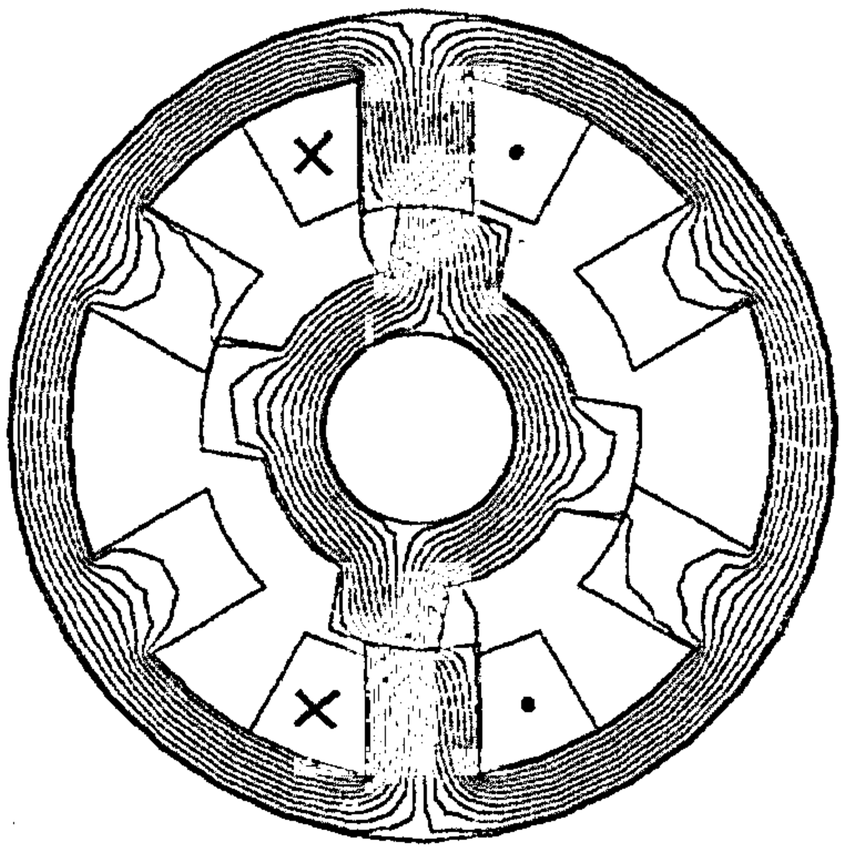

(a) One phase excitation of the short pitched winding machine

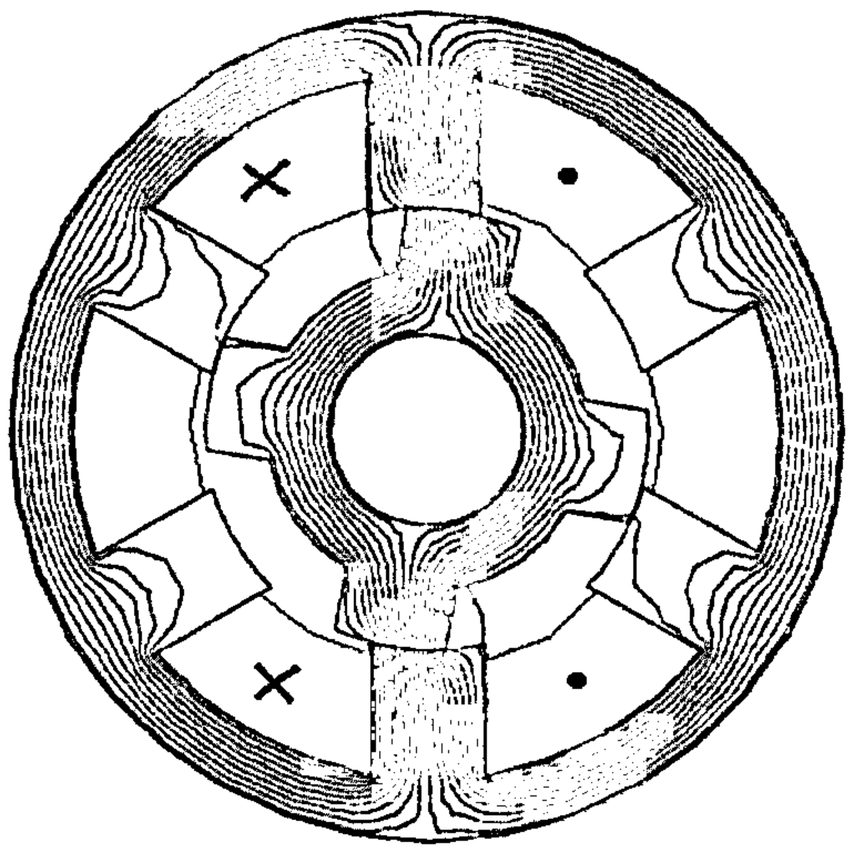

(b) Two phase unipolar excitation of the fully pitched winding machine

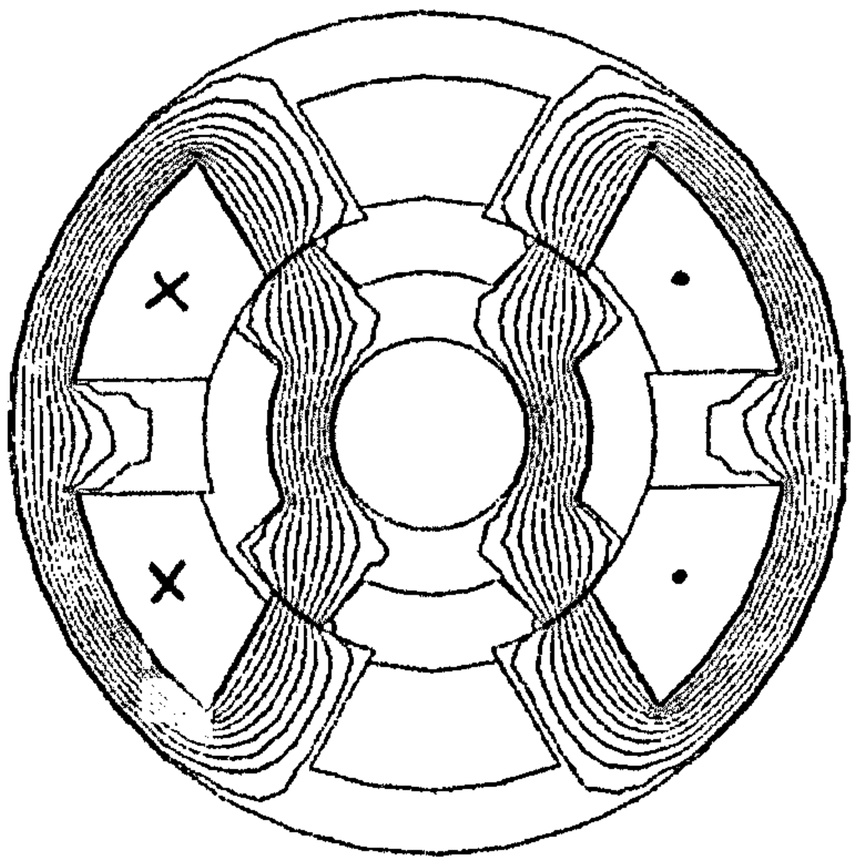

(c) Two phase bipolar excitation of the fully pitched winding machine

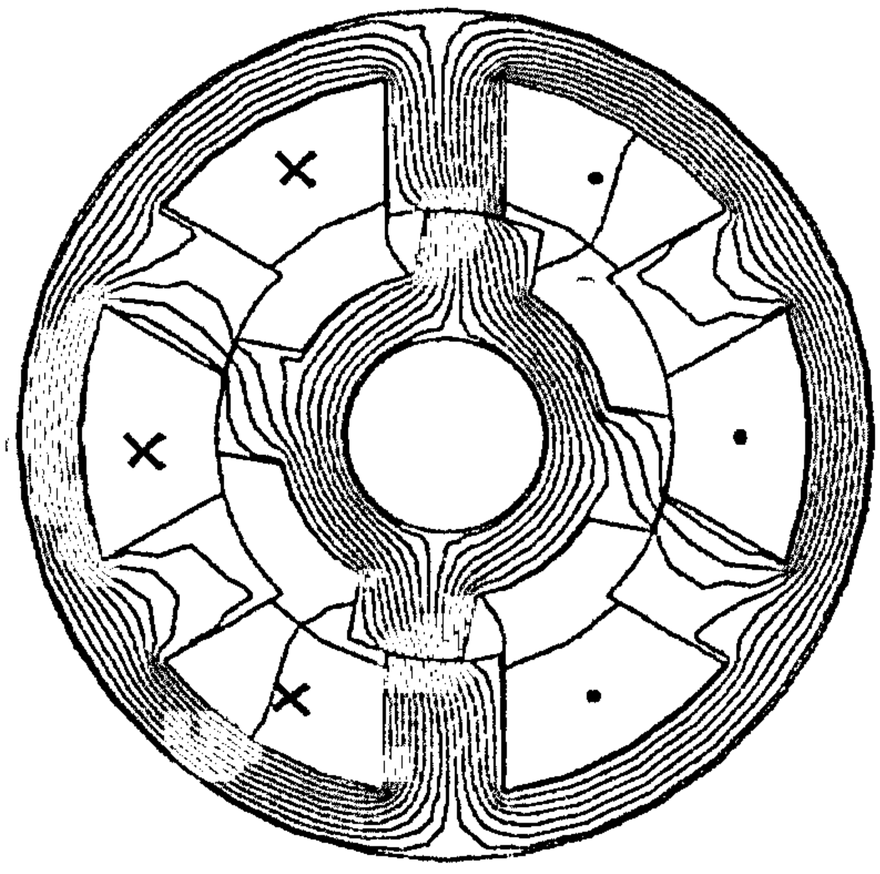

(d) Three phase bipolar excitation of the fully pitched winding machine

Figure 2.7 Flux plots generated from FE for the short pitched and fully pitched winding machines

2.3.3 Transformation Matrices

The concept of transformation matrices used with fully pitched winding machines was first introduced by Mecrow [2.3]. It will be shown that the use of the matrices considerably simplifies the analysis and the simulation of this type of machine.

So far the comparison between the operation of a fully pitched and a short pitched winding machine has been made assuming no saturation in the machine. In practice large amounts of saturation occur in the magnetic circuit, and it is therefore fundamentally important to take this into consideration when designing or simulating a machine. In the short pitched winding machine, saturation means that flux linkage in a phase is a non-linear function of rotor position and the current in that phase. Either finite element analysis or measurements on an actual machine can be made to measure this flux linkage at various different currents and rotor positions. The machine can then be 'characterised' with a set of curves of phase flux linkage versus phase current at various different rotor positions. Once this information is known it can be used to predict, for example, the current in a phase or the torque produced from it. Fortunately there is no, or very little, mutual inductance or coupling between phases. This means that the analysis need only consider each phase independently, as operation of each has no effect on the others. This is a relatively simple problem to solve.

In the case of the fully pitched winding machine, however, flux linkage in a phase is a non-linear function of rotor position and the currents in *all phases*. This is a highly complex problem in comparison, and is due to the large amount of mutual coupling between phases. It makes the machine both very difficult to simulate and difficult to understand.

To get over this problem Mecrow [2.3] introduced a set of transformation matrices which could be used to convert parameters such as current, flux linkage and voltage into corresponding values in a set of fictitious short pitched windings. More appropriate terminology for 'fictitious short pitched' parameters is perhaps 'single tooth' parameters. This, then, had the effect of decoupling the phases and hence greatly simplifying the problem.

Consider the following example of unipolar excitation. Figure 2.8 shows the fully pitched winding machine with phases B and C excited. The resulting flux pattern due to these currents is also shown. The same figure also shows the same machine, except with short pitched windings. To produce the same flux pattern phase 1 needs to be excited.

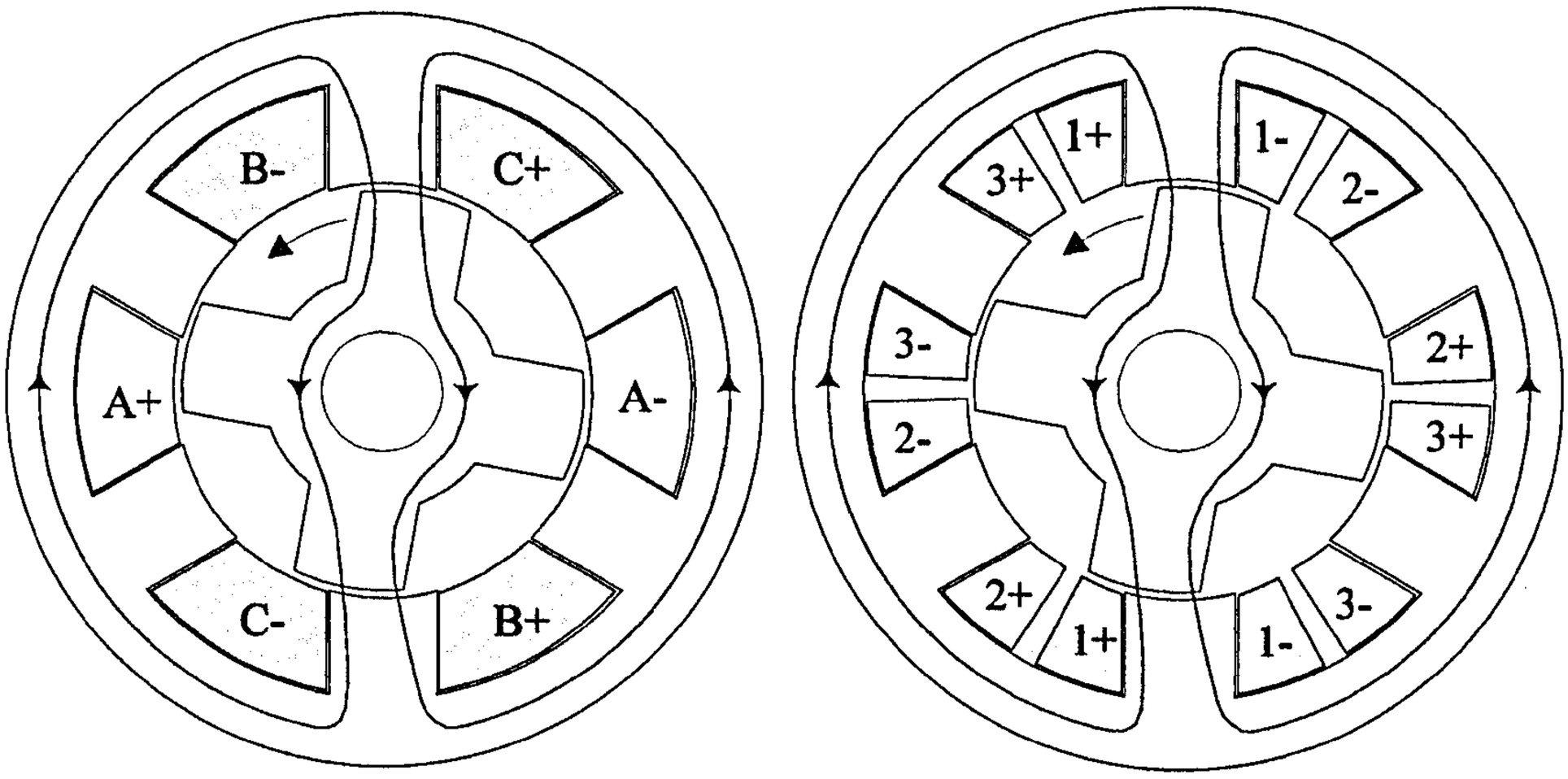

Figure 2.8 Unipolar excitation showing phase currents to produce the same flux in the fully pitched and short pitched winding machines.

The MMFs in each slot can now be examined. If the same number of turns per slot is assumed, then by inspection the following equivalence is derived:

$$I_A = -\frac{I_2}{2} - \frac{I_3}{2} \tag{2.4}$$

$$I_B = -\frac{I_1}{2} - \frac{I_3}{2} \tag{2.5}$$

$$I_C = -\frac{I_1}{2} - \frac{I_2}{2} \tag{2.6}$$

This is summarised with the following matrix:

$$\begin{bmatrix} I_A \\ I_B \\ I_C \end{bmatrix} = \begin{bmatrix} 0 & -½ & -½ \\ -½ & 0 & -½ \\ -½ & -½ & 0 \end{bmatrix} \begin{bmatrix} I_1 \\ I_2 \\ I_3 \end{bmatrix} \tag{2.7}$$

Therefore for the example shown in Figure 2.8 where I_2 and I_3 are zero:

$$I_A = 0$$

$$I_B = -\frac{I_1}{2}$$

$$I_C = -\frac{I_1}{2}$$

In other words, with unipolar excitation the current in the short pitched phase needs to be twice that of the fully pitched phases.

By inverting the above matrix Equation 2.7 can be rewritten in terms of the single tooth currents:

$$\begin{bmatrix} I_1 \\ I_2 \\ I_3 \end{bmatrix} = \begin{bmatrix} 1 & -1 & -1 \\ -1 & 1 & -1 \\ -1 & -1 & 1 \end{bmatrix} \begin{bmatrix} I_A \\ I_B \\ I_C \end{bmatrix} \tag{2.8}$$

This introduces the concept that with any combination of currents in the fully pitched machine it is possible to calculate an equivalent set of currents in a short pitched winding machine using a transformation matrix. A similar analysis of the machine is done to derive the following transformation matrices for flux linkage and voltage. Notice the transformation matrix is the inverse of the one used for currents.

$$\begin{bmatrix} \Psi_A \\ \Psi_B \\ \Psi_C \end{bmatrix} = \begin{bmatrix} 1 & -1 & -1 \\ -1 & 1 & -1 \\ -1 & -1 & 1 \end{bmatrix} \begin{bmatrix} \Psi_1 \\ \Psi_2 \\ \Psi_3 \end{bmatrix} \tag{2.9}$$

$$\begin{bmatrix} V_A \\ V_B \\ V_C \end{bmatrix} = \begin{bmatrix} 1 & -1 & -1 \\ -1 & 1 & -1 \\ -1 & -1 & 1 \end{bmatrix} \begin{bmatrix} V_1 \\ V_2 \\ V_3 \end{bmatrix} \tag{2.10}$$

The above equivalences make the following assumptions:

- The position of a winding within a slot does not affect tooth MMFs or leakage fluxes.
- The excitation of more than one pole pair does not saturate the core back any further than it would have done with only one pair excited. The transformations rely on the ability to treat pole pairs separately, but the core back region is an area where flux paths are common.

The use of the transformation matrices means that at any instance in time the fully pitched winding machine parameters can be converted into the equivalent single tooth parameters. Once this has been achieved the machine can be analysed as if it were a short pitched winding machine, which considerably simplifies the problem as in this situation the phases are not mutually coupled together and can therefore be treated independently. Some examples of how this can be used in a practical situation are as follows:

- *Flux linkage 'characterisation' of a fully pitched winding machine*

  Measuring the flux linkage characteristics of one phase in a three phase fully pitched winding machine is very difficult as the flux depends on four variables – current in all three phases and rotor position. This is too complex to measure or analyse. It is much easier to analyse the machine as if it were a single tooth winding machine and use the transformation matrices to convert the currents and fluxes into equivalent single tooth values. The flux linkage characteristics of these equivalent single tooth windings needs to be determined. This is achieved by connecting two of the fully pitched windings in series and passing a current through both of them. As can be seen in Figure 2.8 these two fully pitched phases now act in the same way as the equivalent single tooth phase would. The machine is therefore characterised as if it were a single tooth winding machine, where flux linkage only varies with the current in that phase itself and rotor position. This is described in more detail in Appendix A. The same principle was used during finite element modelling.

- *Calculation of torque in a fully pitched winding machine*

  Once the flux linkage characteristics are known, the torque characteristics can be calculated using the principle of co-energy i.e. curves of torque against current for different rotor positions. The method for doing this is described in Chapter 3. These torque characteristics are, however, for one fictitious short pitched phase. To utilise this data in the real machine the transformation matrices are used to convert the fully pitched winding currents into the equivalent single tooth values. Torque can then be calculated for each of these fictitious phases and then summed together to determine the total machine torque.

- *Simulation*

  Chapter 3 will describe how the simulation uses the flux linkage/current/rotor position data to predict current at the end of each time step. Flux linkage is determined by integrating the voltage applied to a phase by the inverter; position at each time step is known as a fixed speed is assumed. Knowledge of two of the parameters means that the third, the current, can be calculated. Again, however, this flux linkage data is based on short pitched windings. Simulation of a fully pitched machine involves using the transforms to convert parameters into their single tooth equivalents during the calculations that take place every time step. Briefly, phase flux linkage, which is known, is converted into the equivalent single tooth flux linkage using Equation 2.9. Position is also known, so the flux linkage data can then be used to calculate the equivalent single tooth current. Finally, Equation 2.7 is used to convert the current back into the real fully pitched winding current. These steps are then repeated for the next time step.

Note from Equation 2.7 that the polarity of the currents change when converting between fully pitched winding and short pitched winding values. Torque production is independent of current direction in the short pitched winding machine, therefore for clarity in the forthcoming chapters the equivalent single tooth values will generally be shown with positive values.

2.4 Summary

The fully pitched winding SR machine has been introduced. Cross sectional diagrams of a typical machine have been used to define what is meant by a 'fully pitched' winding, and what is meant by a 'short pitched' winding.

It has been demonstrated that the nature of the fully pitched winding leads to strong mutual coupling between phases. Due to the salient nature of the SR machine the magnitude of this mutual coupling varies with rotor position. In addition, in the case of the three phase machine, the self inductance of a phase varies very little with position. In the short pitched winding machine the exact opposite is true - variation of self inductance with position is dominant and any mutual coupling between phases is usually small enough to ignore.

The generalised expression for the torque generated in any SR machine has been used to demonstrate that both variation of self inductance and variation of mutual inductance with position can be used to produce torque (Equation 2.2). The conclusion from this equation is that, in the case of the short pitched winding machine, positive torque can only be produced when a phase conducts during its period of rising self inductance, which is the case for approximately one third of the electrical cycle. This leads to the commonly adopted 120^{o} conduction period.

In the fully pitched winding machine the equation shows that numerous excitation patterns are possible. If only unipolar phase currents are used then phases should only conduct when the mutual inductance between one phase and another is rising. If bipolar currents are used then both the periods of rising and falling mutual inductance can be utilised. A summary of the main excitations patterns that are possible is as follows:

- Unipolar, square shaped, 240^{o} conduction
- Bipolar, trapezoidal, 240^{o} conduction
- Bipolar, squarewave, 360^{o} conduction
- Bipolar, sinusoidal, 360^{o} conduction

The idea of the fully pitched winding is to increase the utilisation of the electric circuit by operating at least two of the three phases at a time (in the case of a three phase machine). The flux pattern produced by unipolar operation with two phases conducting has been shown to be identical to the short pitched winding machine with one phase conducting. The result is a 50% reduction in copper loss for the same torque. This, however, has ignored the fact that endwinding length with fully pitched windings must be longer and therefore this apparent large gain in efficiency will not be so great. The machine aspect ratio and pole number will determine the relative length of the endwinding and therefore the magnitude of any gain in efficiency. Chapter 4 "Machine Design" will examine these effects in detail.

The concept of 'transformation matrices' has been introduced. The flux linkage in a fully pitched winding is a non-linear function of rotor position and the currents in all three phases, which makes the machine both very difficult to simulate and difficult to understand. The transformation matrices enable values of phase flux linkage, current and voltage to be converted into the equivalent parameters in a short pitched winding machine. This makes analysis and simulation very much easier, as in the short pitched winding machine each phase is magnetically decoupled from the others and so each phase can be considered separately. The transformations are used extensively in the dynamic simulation software that is described in Chapter 3 to greatly simplify the problem.

Chapter 3 - SIMULATION

3.1 Introduction

The ability to simulate the fully pitched winding SRM, when fed from a power electronic converter, is highly desirable for two reasons. Firstly, it enables direct comparison on a like-for-like basis with the equivalent short pitched winding machine. Secondly, it can be used in conjunction with FE modelling to assess the impact that different machine geometries, inverter topologies and excitation patterns have on overall drive performance, including inverter rating, without having to construct every combination. It will therefore be used in creating the new machine design described in Chapter 4, and also help in explaining results from measured performance in Chapters 5 and 6.

An existing package called 'BDCM' had already been developed in the University using C code for simulation of Brushless DC Motors. This forms the basis of the SRM simulation, as the same core model that 'BDCM' used is also very appropriate for SR motors.

This chapter discusses the theory behind the simulation, and how it was developed for both the short pitched and fully pitched winding machines. The model needs to cope with the highly saturating nature of the magnetic circuit in both types of machine, but in the fully pitched winding machine must also correctly model the strong mutual coupling between phases.

Some comparisons with measured values and waveforms are shown, however the majority of simulation results will be presented in Chapters 5 and 6, where more extensive comparisons will be made with measured results using the new prototype machine that will be described in Chapter 4.

3.2 Background

An example of some of the earliest work on modelling of switched reluctance motors is that of Chai [3.1]. This work took no account of magnetic saturation, and therefore had severe inherent limitations in its accuracy. Further work by Singh and Kuo [3.2], Pickup and Tipping [3.3, 3.4], Blenkinsop [3.5], Byrne and Dwyer [3.6] and Acarnley [3.7] all introduced magnetic saturation into the model. In each case either inductance or flux linkage was approximated with methods such as cosines, polynomials or Fourier series.

Stephenson and Corda reviewed these methods in 1979 [3.8], in which they argued that inaccuracies in these models were due to the need to calculate the differential coefficients $\frac{d\psi}{di}(\theta,i)$ and $\frac{d\psi}{d\theta}(\theta,i)$ from curve fits of the tabulated data. Their method used the following circuit equation in its simplest form to avoid the need for these differential coefficients:

$$\psi = \int (V - iR).dt \tag{3.1}$$

The machine was first characterised in terms of flux linkage against current over a range of rotor positions i.e. $\psi(\theta,i)$ (typical data is shown later in this chapter in Figure 3.1). This data was then inverted to give a table of $i(\theta,\psi)$. Equation 3.1 was then used to calculate the values of ψ and i during a time step. A 4th order Runge Kutta integration method was used to improve accuracy. Excellent agreement between calculated and measured results was shown.

Later work concentrated in two main directions. Curve fitting techniques were developed to simplify computation by avoiding the need for interpolation of the magnetic data. Torrey and Lang [3.9], for example, used equations based on a Fourier cosine series and good curve fits were achieved. Problems, however, were encountered with unwanted higher order harmonics on the curve fit, which fed through to ripple on the torque waveforms. Other work, for example by Miller *et al* [3.10, 3.11], was aimed at substantially reducing computation time, at the expense of some accuracy, by producing empirical approximations to the flux linkage/current/angle data (other

approaches require relatively slow finite element analysis or measurements from an actual motor). Miller's method involved calculation of the aligned and unaligned flux linkage curves, with data for other positions being interpolated using an empirical formula. Note, however, that the introduction of more automated FEA techniques (Jack *et al* [3.12]) and ever increasing computer power have significantly increased the speed of the FEA approach.

The emphasis on the simulation developed here for the fully pitched winding SR motor is accuracy rather than speed of computation. Accurate comparisons are needed between different machines in terms of torque, torque ripple, and copper loss as well as power electronic losses and rating. It is based substantially on the method described by Stephenson and Corda. Flux linkage data is either generated from FEA or measurements from an existing motor. This data is used in its tabulated form with quadratic interpolation used to calculate values between points. This approach can be seen as a form of curve fitting, however the key difference is that the curve is forced to go through all of the known points. This is a computationally intensive technique, but enables very accurate interpretation of the data. As with the Stephenson and Corda approach a 4^{th} order Runge Kutta method is used to improve the accuracy of the flux linkage integration during a time step. The increase in computational speed since the original paper means that accuracy can be further improved using smaller time steps together with more accurate interpolation of the flux linkage data.

As will be described, this forms the basis for the core model of the simulation for the short pitched winding machine. The fully pitched winding machine, on the other hand, requires further modelling to take into account the strong mutual coupling between phases. Moreira and Lipo [3.13] modelled mutual coupling between phases in a four phase machine with short pitched windings. This used a cubic spline model of the flux linkage/current/angle data to model phase self inductance, together with extra terms using fixed values for mutual inductance. The amount of coupling in these short pitched winding type machines is small in comparison, and this can justify the use of fixed values of mutual inductance.

In the fully pitched winding machine, however, the majority of torque is produced from variation of mutual inductance with position (see Chapter 2). This means that the mutual coupling must be modelled very accurately, including the full effects of saturation within these terms. This, then, implies a highly complex model, as flux linkage in a phase is a non-linear function of rotor position and the currents in *all three phases*. In the short pitched winding machine flux linkage is only dependent on the rotor position and the current within the phase itself.

As discussed in Chapter 2, transformation matrices developed by Mecrow [3.14] enable this problem to be significantly simplified. This utilises the fact that at any instant in time a unique set of currents can be calculated in a set of fictitious short pitched phases that produce exactly the same flux with the magnetic circuit as the actual fully pitched phases. This has the effect of decoupling the magnetic sources and fluxes, so that each flux can then be solved independently from the others.

Barrass [3.15] described a simulation model for the fully pitched winding machine, which utilised these transformation matrices as described here. Considerable simplification of the problem was, however, achieved by assuming perfect current control or voltage control and also ignoring resistive voltage drop in the flux integration equation. This eliminated the need to perform the time stepping calculations, including the PWM current control effects, because either the current (in the case of perfect current control) or the flux linkage (in the case of voltage control) could be predetermined over the entire electrical cycle.

In contrast, the simulation described here calculates the changes in current and flux linkage on a step by step basis, including resistive voltage drop, and taking winding voltage information from a current control loop. This gives the simulation the ability to show realistic, rather than ideal waveforms, over the whole speed range. Results shown later in this chapter and in Chapters 5 and 6, for example, will show significant effects on current waveform due to mutual coupling between phases.

In addition to accurate modelling of the machine itself, it is important to be able to assess control strategies and power electronic ratings and topologies. This means that the simulation must also include the following components:

- PWM current control (including emulation of both analogue and digital control systems).
- Optimisation of on and off angles (advance and conduction angles), for example for automatic torque-speed curve generation.
- Different number of phases.
- A range of power converter topologies, including asymmetric half bridge, H bridge, star and delta connections.
- Inverter device loss (switching and conduction loss).
- DC link components e.g. DC link capacitor and inductor.

All of the above should help to ensure simulation results that closely resemble real conditions and make relative assessments of cost sensitive components such as power electronic devices and controller requirements. Note that iron loss calculations are not included in the model.

3.3 Simulation Method

The simulation method is split into several distinct parts -

- **Current Controller** - decides the voltage applied to each winding based on knowledge of current demand, actual current, type of inverter, rotor position, on/off angles and type of current controller. See Section 3.3.3 for more detail.
- **Current Solver** - determines for phase currents based on knowledge of phase voltages, position, machine characteristics, current and flux linkage values from the previous time step calculation. See Section 3.3.1. for more detail.
- **Torque Solver** - the calculation of instantaneous electrical torque from knowledge of phase currents and position. See Section 3.3.2. for more detail.
- **Performance Evaluation** - Once the phase currents and instantaneous torque have been determined, values such as average torque, torque ripple, copper loss, inverter loss, and efficiency can be calculated.

A Runge Kutta time stepping method is used and so the first two parts (the Current Controller and the Current Solver) are executed during each step. The PWM frequency is used to automatically determine the length of the time step to be used, as this gives a good guide to the time constant of each winding. It was found that fifty time steps per PWM period give a good compromise between the accuracy and the speed of the result. Therefore, in the case of the motors being modelled here, one step constitutes 2μs. The time stepping calculations continue for several machine electrical cycles until convergence occurs. Convergence here is defined as the difference between the currents during one electrical cycle and the currents from the previous electrical cycle being small enough.

Once convergence has taken place the Torque Solver determines torque developed by each phase at each machine electrical degree. The Performance Evaluation can then be performed.

3.3.1 Current Solver

This is where the simulation differs, depending on whether a fully pitched or short pitched winding machine is being used. As will be explained, the routine to solve for currents in the fully pitched winding machine requires some additional sections.

The Short Pitched Winding Machine

The ability to simulate a conventional short pitched winding SRM depends heavily on how well it can model the strong variation of flux linkage in a phase winding. The two factors that influence this are rotor position, and saturation within the magnetic circuit. Mutual coupling effects between phases are usually ignored, as they are generally considered small.

For this reason, a particular machine is characterised with flux linkage as a function of phase current and rotor position. A dynamic, or instantaneous, inductance can therefore be calculated at any instance in time and each phase can be considered separately.

Typical flux linkage/current/position data is shown in Figure 3.1. This data can be generated in three ways:

- FE analysis, as used in the machine design of Chapter 4, together with knowledge of the machine geometry.
- Measurements on an actual machine (as described in Appendix A).
- Empirically as described by Miller [3.10, 3.11].

A Runge Kutta time stepping routine is used to solve for current and this is based on the following equation:

$$\psi = \int (V - iR).dt \tag{3.2}$$

Equation 3.2 is therefore used to calculate the flux linkage in a phase by integrating the voltage applied by the inverter over time. Note that, as this equation shows, the flux linkage attained is reduced by a voltage drop due to the resistance of the phase.

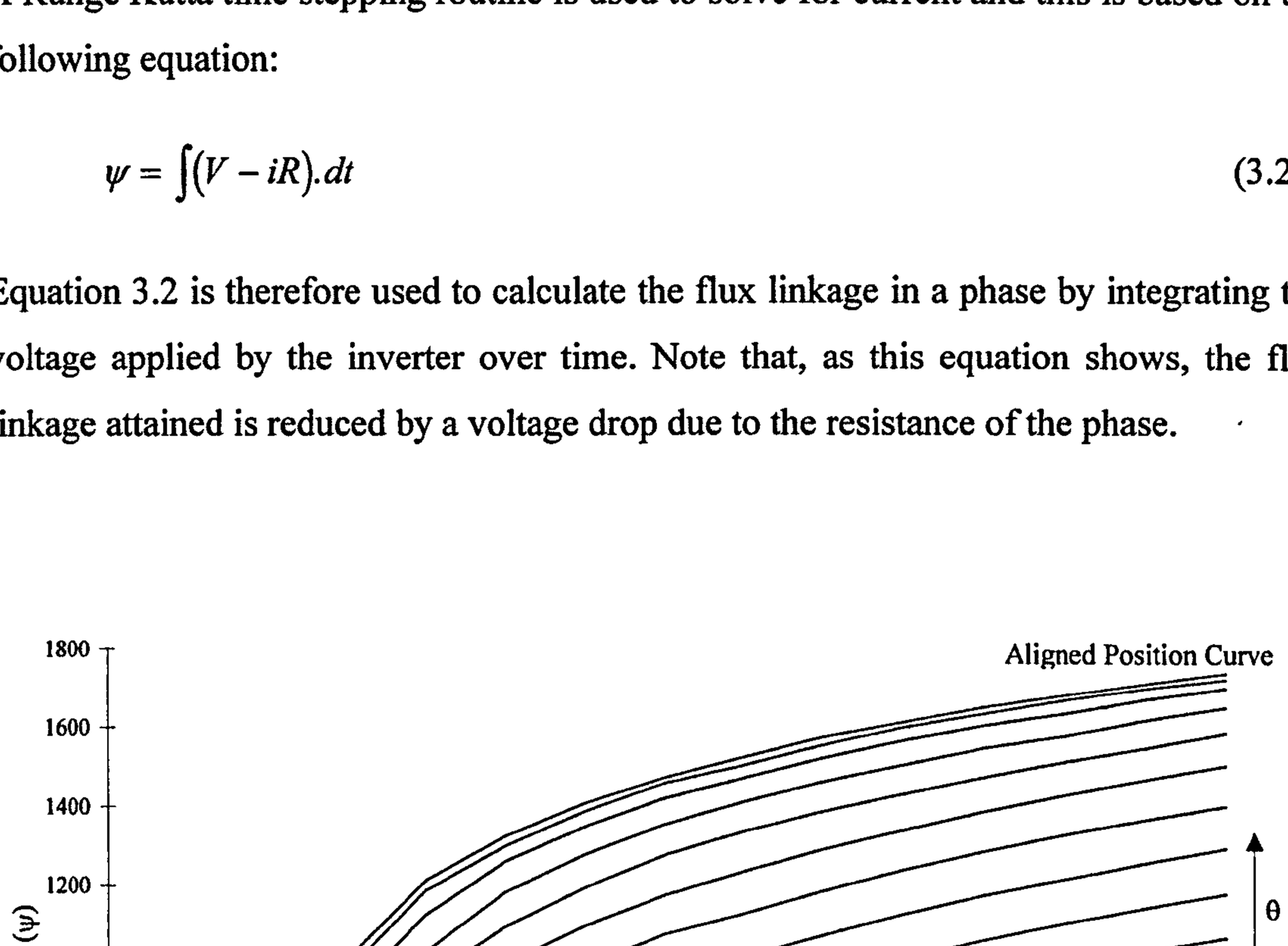

Figure 3.1 Typical flux linkage/current/position data

One time step is described as follows as is repeated for each of the phases:

1. At the start of a time step the rotor position is known, as well as the phase currents from the previous time step. Position is calculated from the motor speed and the value of the fixed time step. The current from the last time step $i_{(n-1)}$ and the latest value of position, θ_n, are used to find a new value for the instantaneous inductance, L_n. As shown in Figure 3.1 this is achieved by using the flux linkage data to find a new value for ψ and using the following equation:

$$L_n = \frac{\psi}{i_{(n-1)}}$$

Quadratic interpolation is used in both the current and position axis, to calculate values of flux linkage between points. This new value of instantaneous inductance can then be used throughout the rest of the time step as a means of calculating a new value for current with each new value of flux linkage.

2. A change in flux linkage can then be calculated using Equation 3.2, knowing the voltage that the inverter has applied to that phase and the current from the last time step (to calculate the resistive volt drop). The first estimate for one time step of the change in flux linkage is:

$$\Delta\psi(1st)_{(n)} = (V_{(n)} - i_{(n-1)}R).t_s$$

3. The first estimate of the total flux linkage in the phase can then be determined using the total flux linkage from the previous time step.

$$\psi(1st)_{(n)} = \psi_{(n-1)} + \Delta\psi(1st)_{(n)}$$

4. The first estimate of the new phase current $i_{(n)1}$ is then:

$$i(1st)_{(n)} = \frac{\psi(1st)_{(n)}}{L_{(n)}}$$

The Runge Kutta method means that the above process of calculating a new value of current is carried out four times with the result fed back into the initial parameters to obtain a more accurate result i.e. $i(1st)_{(n)}$ is fed back into Step 2 in place of $i_{(n-1)}$. Step 3 and 4 are then repeated to produce $i(2nd)_{(n)}$ and so on.

5. The Runge Kutta equation to estimate the final value of flux linkage for the time step is calculated as follows:

$$\psi_{(n)} = \psi_{(n-1)} + \frac{\left[\Delta\psi(1st)_{(n)} + 2(\Delta\psi(2nd)_{(n)} + \Delta\psi(3rd)_{(n)}) + \Delta\psi(4th)_{(n)}\right]}{6}$$

6. Final values for current are given by:

$$i_{(n)} = \frac{\psi_{(n)}}{L_{(n)}}$$

This completes a time step for one phase. Steps 1 to 6 are then repeated for the other phases. Treating each phase separately is allowable, as the assumption is made that there is no electromagnetic coupling between phases.

The next time step starts again at the Current Controller (described in more detail later) where new phase voltages are determined. These new voltages are used in the next time step in the Current Solver stage to determine the change in flux linkage. Time steps continue through the Current Controller and Current Solver stages until several machine electrical cycles have been calculated and steady state conditions are reached.

Note that the above method makes the approximation of keeping L_n constant throughout each Runge Kutta time step. This saves substantially on computation time with minimal error as long as the electrical angle of rotation per time step is kept small. All simulation results shown use a 2μs time step.

Note also that the use of the term inductance is only a way of expressing the ratio of flux linkage to current at a particular instance within a time step. It should not be confused

with simulation methods that solely use inductance values rather than flux linkage/current/position data to solve for current.

The Fully Pitched Winding Machine

The short pitched winding machine model ignores the effects of mutual coupling between phases, as it is small. A fully pitched winding machine, however, derives the majority of its torque from variation of mutual coupling between phases. As described in Chapter 2 and earlier in this chapter, the mutual coupling effects can be modelled accurately by using transformation matrices. These are able to convert phase current and flux linkage into equivalent short pitched winding values, magnetically decoupling the phases, and allowing each phase to be solved independently, as with the method described for the short pitched winding machine. The transformation matrix for current is:

$$\begin{bmatrix} i_1 \\ i_2 \\ i_3 \end{bmatrix} = \begin{bmatrix} +1 & -1 & -1 \\ -1 & +1 & -1 \\ -1 & -1 & +1 \end{bmatrix} \begin{bmatrix} i_A \\ i_B \\ i_C \end{bmatrix} \tag{3.3}$$

where i_{123} are equivalent short pitched (or "single tooth") winding currents and i_{ABC} are fully pitched winding currents. The equivalent equation for flux linkage is:

$$\begin{bmatrix} \psi_A \\ \psi_B \\ \psi_C \end{bmatrix} = \begin{bmatrix} +1 & -1 & -1 \\ -1 & +1 & -1 \\ -1 & -1 & +1 \end{bmatrix} \begin{bmatrix} \psi_1 \\ \psi_2 \\ \psi_3 \end{bmatrix} \tag{3.4}$$

Let $$[C] = \begin{bmatrix} +1 & -1 & -1 \\ -1 & +1 & -1 \\ -1 & -1 & +1 \end{bmatrix} \tag{3.5}$$

The inverse of [C] is: $$[C]^{-1} = \begin{bmatrix} 0 & -\frac{1}{2} & -\frac{1}{2} \\ -\frac{1}{2} & 0 & -\frac{1}{2} \\ -\frac{1}{2} & -\frac{1}{2} & 0 \end{bmatrix} \tag{3.6}$$

The inverse of Equations 3.3 and 3.4 are then:

$$\left[i_{ABC}\right]=\left[C\right]^{-1}\left[i_{123}\right] \tag{3.7}$$

$$\left[\psi_{123}\right]=\left[C\right]^{-1}\left[\psi_{ABC}\right] \tag{3.8}$$

Equations 3.7 and 3.8 are the ones used in the Current Solver routine for the fully pitched winding machine. This routine is identical to that of the short pitched winding machine with the following extra stages (here "real" is defined as the actual fully pitched winding parameters and "equivalent per tooth" is the set of fictitious short pitched winding parameters):

- Real flux linkage is converted to equivalent single tooth flux linkage using Equation 3.8.
- Equivalent single tooth current is calculated as before from the flux linkage/current/ angle data (via the equivalent single tooth instantaneous inductance).
- Equivalent single tooth current is converted back to real phase current using Equation 3.7.

The complete routine is as follows with each section repeated for each phase as appropriate:

1. Calculate the instantaneous inductance of the equivalent single tooth windings using the equivalent single tooth currents from the previous time step and the present position (θ_n):

$$L_{1(n)}=\frac{\psi_{1(n)}}{i_{1(n-1)}}$$

where $\psi_{1(n)}$ has been determined from the equivalent single tooth flux linkage/current/position data using $i_{1(n-1)}$ and θ_n.

2. Calculate the first estimate of the change in real flux linkage in each phase over the time step due to the phase voltages that are being applied:

$$\Delta\psi_A(1st)_{(n)} = (V_{A(n)} - i_{A(n-1)}R).t_s$$

3. Total real flux linkage is calculated:

$$\psi_A(1st)_{(n)} = \psi_{A(n-1)} + \Delta\psi_A(1st)_{(n)}$$

4. Calculate equivalent single tooth flux linkage:

$$[\psi](1st)_{123(n)} = [C]^{-1}[\psi](1st)_{ABC(n)}$$

5. The first estimate of the new equivalent single tooth phase current $i_1(1st)_{(n)}$ is then:

$$i_1(1st)_{(n)} = \frac{\psi_1(1st)_{(n)}}{L_{1(n)}}$$

6. The first estimate of the new real phase currents are then:

$$[i](1st)_{ABC(n)} = [C]^{-1}[i](1st)_{123(n)}$$

7. Repeat from step 2 replacing $i_{A(n-1)}$ with $i_A(1st)_{(n)}$ to obtain the four parts of the Runge Kutta equation i.e. $\psi_A(1st)_{(n)}, \psi_A(2nd)_{(n)}$, $\psi_A(3rd)_{(n)}$ and $\psi_A(4th)_{(n)}$.

8. The final estimate of real flux linkage uses the Runge Kutta equation:

$$\psi_{A(n)} = \psi_{A(n-1)} + \frac{\left[\Delta\psi_A(1st)_{(n)} + 2(\Delta\psi_A(2nd)_{(n)} + \Delta\psi_A(3rd)_{(n)}) + \Delta\psi_A(4th)_{(n)}\right]}{6}$$

9. Use the equations in steps 4, 5 and 6 to obtain the final values of the real currents $i_{ABC(n)}$.

This completes one time step of the Current Solver. As before, new winding voltages are determined from the Current Controller stage, and the whole cycle is then repeated over several electrical cycles until convergence occurs.

A potential problem, however, arises when a phase is switched off. Calculation of the equivalent single tooth flux linkage in Step 4 requires that all three real phase flux linkages be known. This is because in the fully pitched machine all three phases contribute to the flux in any given tooth. They all therefore contribute to the flux linkage in an equivalent single tooth winding. The flux linkage in the 'off' phase can only be calculated if the volts being applied to it are known. During the turn off process, with an asymmetric half bridge inverter, the two transistors controlling one particular phase would simply be turned off. With positive current still flowing the diodes would apply a negative voltage and bring the current down to zero. The calculation during this stage is therefore still straightforward. Once at zero, however, the voltage that is applied to the winding by the diodes is not known, and hence flux linkage cannot be calculated. It is therefore necessary in the simulation to control the current to zero simply by setting the current demand to zero during the off period. In this way the Current Controller knows the voltage being applied and therefore the problem is overcome. This, however, does assume that the Current Controller is good enough to maintain the current at zero.

The above methods described for the short pitched and fully pitched winding machines are used with all inverter/machine configurations, except when the machine windings are connected in a star. This requires some additional code and is described in more detail in Section 3.3.3.3 "Star Connected Inverter".

3.3.2 Torque Solver

At any given rotor position and with any given phase currents the machine has a certain amount of co-energy stored within itself. The machine flux linkage characteristics (shown in Figure 3.1) can be used to calculate this energy:

$$W' = \int_0^i \psi(\theta, i)\, di \tag{3.9}$$

Any change in this co-energy will result in a corresponding electrical torque being applied. Therefore torque can also be derived:

$$T_e = \frac{dW'(\theta,i)}{d\theta}\Big|_{i=const} \tag{3.10}$$

Combining Equations 3.9 and 3.10 gives:

$$T_e = \frac{d}{d\theta}\int_0^i \psi(\theta,i)\Big|_{i=const} \cdot di \tag{3.11}$$

Therefore once the machine flux linkage/current/position characteristics have been entered (whether by calculation or measurement) a corresponding torque/ current/position characteristic can be determined. Typical characteristics are shown in Figure 3.2.

Once the time stepping calculations have converged, the final phase currents are known over a complete electrical cycle. Therefore instantaneous torque can easily be determined at each rotor position (in this case torque is calculated at every electrical degree). Quadratic interpolation is used to calculate values of torque between data points. The torque characteristic derived from the flux linkage is for one phase of the machine. The torque in the other phases is calculated simply by offsetting the values by the appropriate number of pole pitches. The torques are then summed together to give a total machine torque at each position. Once the torque waveforms are known for each phase, average torque and torque ripple can be calculated.

In the case of the fully pitched winding machine, the equivalent single tooth currents must be used for this calculation. This is because the flux linkage data is based on the use of these equivalent single tooth currents. Therefore in the calculation of torque at each position the 'real' currents are first converted into the equivalent single tooth currents.

The torque/current/position data is then interrogated to calculate the torque due to each equivalent single tooth phase, or, in other words, the torque due to each pole of the machine. The torques from each of the equivalent short pitched phases are then summed together to give the total torque at each position for the fully pitched winding machine.

Note: The torque due to each fully pitched phase cannot be calculated and is irrelevant. This is because torque in these 'real' phases is derived from the interaction, or mutual coupling, between two or more phases. Torque can only be calculated once parameters have been converted into the equivalent single tooth values so that each phase can be considered separately.

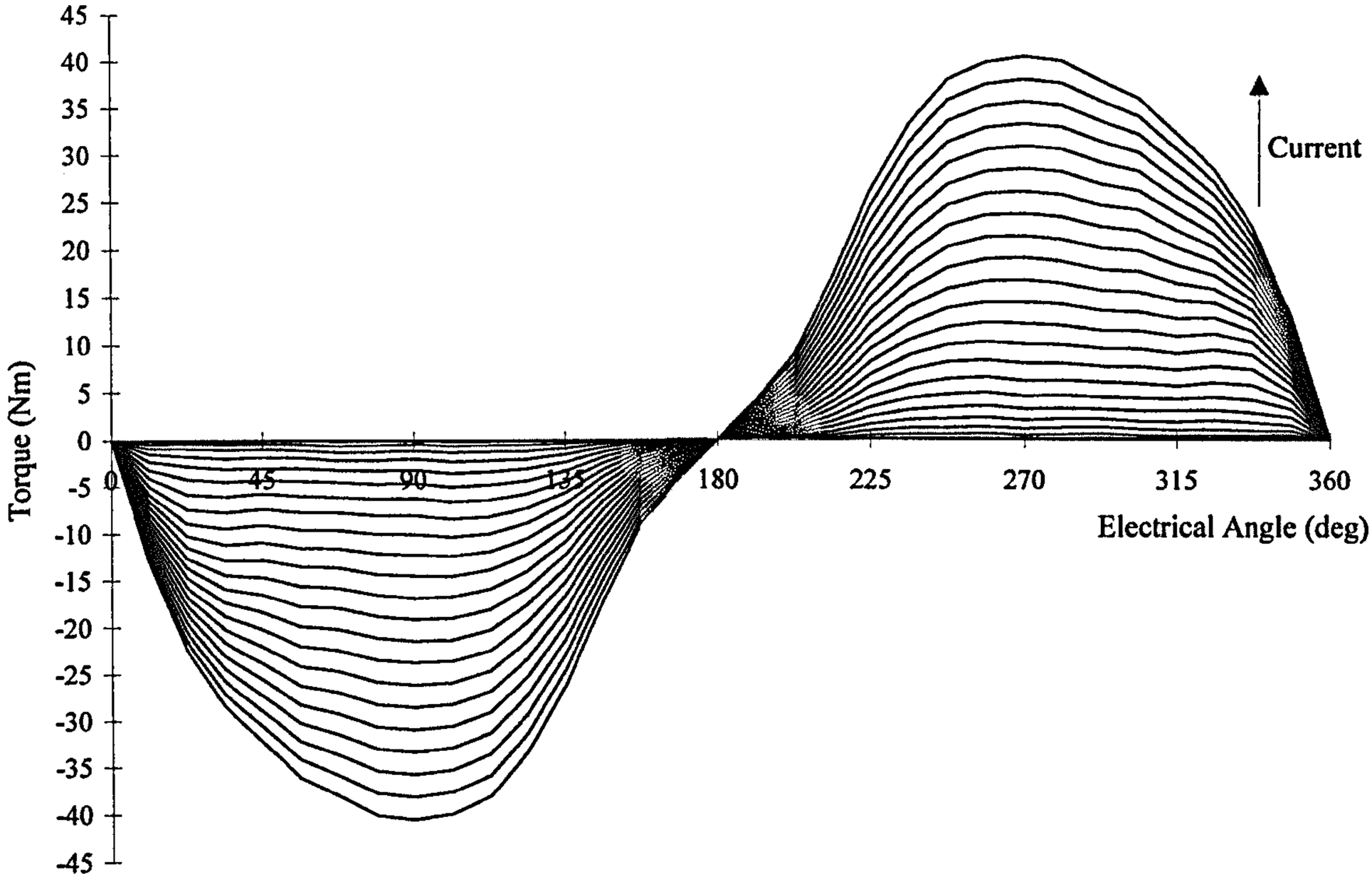

Figure 3.2 Torque against rotor position shown over one electrical cycle for various values of phase current.

3.3.3 Current Controller and Inverter Configurations

The Current Controller part of the simulation takes knowledge of the desired current, rotor position, desired on/off angles and outputs the voltages that should be applied to the windings for use in the Current Solver. Different controllers are used with different types of inverter. This is to take into account any restrictions on the available phase voltage and phase currents e.g. the star connected inverter where the sum of the phase currents must be zero.

3.3.3.1 Analogue and Digital Current Controllers

PWM current control is used with values such as PWM frequency and the PID gains as control variables. Both digital and analogue controllers can be simulated.

The digital controller is based as closely as possible on the DSP controller developed for the test rig. This is described in detail in the "Controller" section of Appendix C. The simulation is able to control the timing of two critical events within each PWM period i.e. the timing of current sampling and timing of the voltage reference output from the PID controller. The timings are important to the stability of a digital control system as they introduce lag. Section 6.6 of Chapter 6 will use the simulation to assess differences in control requirements in terms of bandwidth and PID gains between the short pitched and fully pitched winding machines.

With the analogue current controller the voltage reference is adjusted on a continual basis. In a real circuit only the slew rates and small propagation delays in the hardware would detract from this ideal, as well as any drift problems that would be encountered. In the simulation, the analogue controller is assumed to be ideal, but of course the output is only updated at the end of each time step period. This time step can be set independently, but throughout all simulations its value was set to be $1/50^{th}$ of the PWM period i.e. 2μs. The simulation of the analogue controller, therefore, should be very close to ideal.

3.3.3.2 Asymmetric Half Bridge and Full 'H' Bridge Inverter

As explained in Chapter 2 there are several inverter configurations that can be used in conjunction with a fully pitched winding SRM. The 'H' bridge, shown in Figure 3.3, can supply both unipolar and bipolar currents. Here the PID controller supplies $+V_{ref}$ to control leg 1 and $-V_{ref}$ to control leg 2 of the bridge (where V_{ref} is the voltage reference value defining the required voltage duty cycle to be applied to the winding).

Figure 3.4 shows an example of the PWM control showing the triangular wave, voltage references, gate signals and subsequent phase voltage. Complimentary switching results in the conduction and switching losses being shared equally between each transistor. A

further benefit is that the switching frequency of the voltage actually applied to the winding is twice that of the switching frequency of each transistor.

The same PWM controller and inverter can be used when both unipolar and bipolar currents are required. This is because with unipolar currents only half of the devices in the 'H' bridge would conduct, as shown in Figure 3.5. These are the same devices as in an asymmetric half bridge and so the controller can be used in either case.

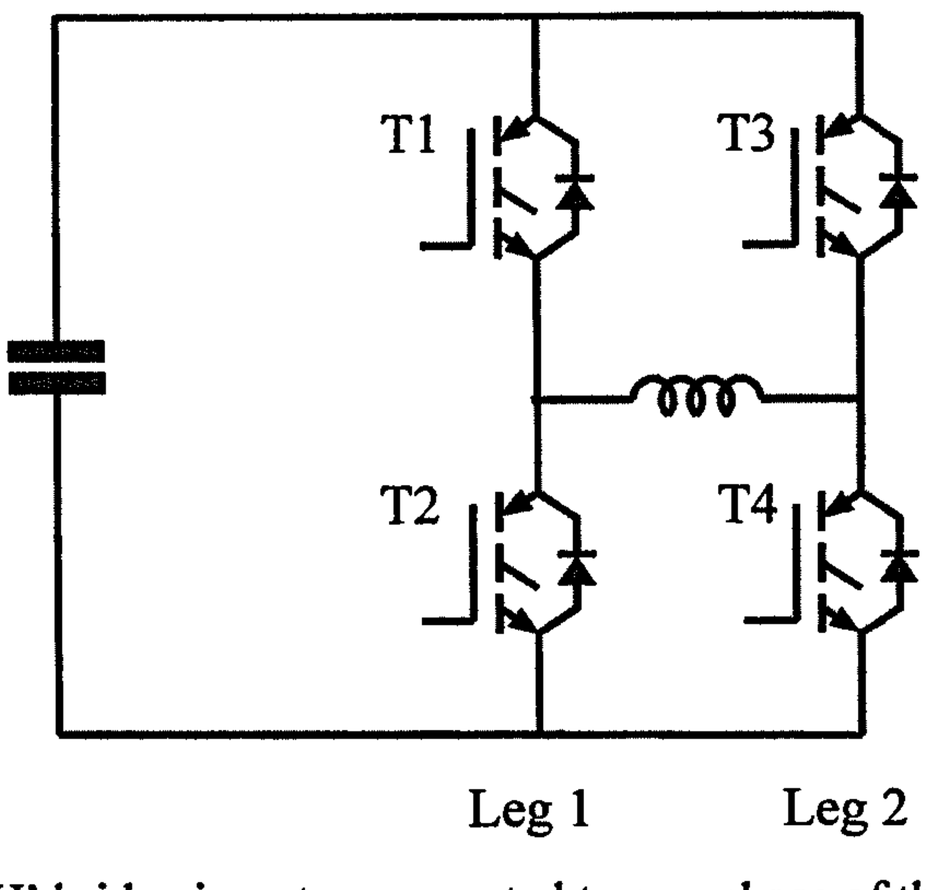

Figure 3.3 An 'H' bridge inverter connected to one phase of the machine.

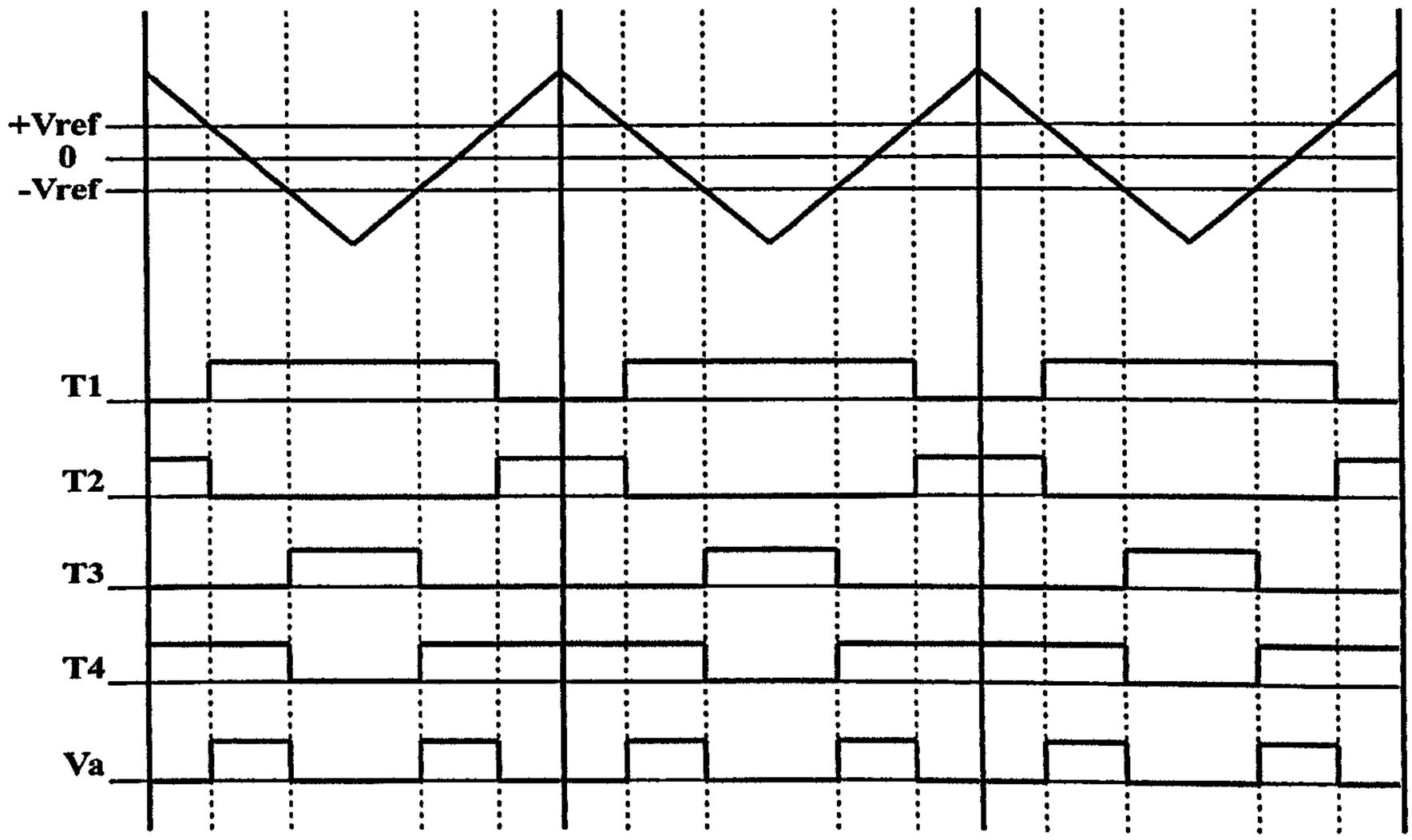

Figure 3.4 PWM control of the 'H' bridge inverter. +Vref and -Vref are the voltage control signals supplied from the PID controller, T1, T2, T3, T4 are the transistor gate signals, V_A is the voltage subsequently imposed on winding.

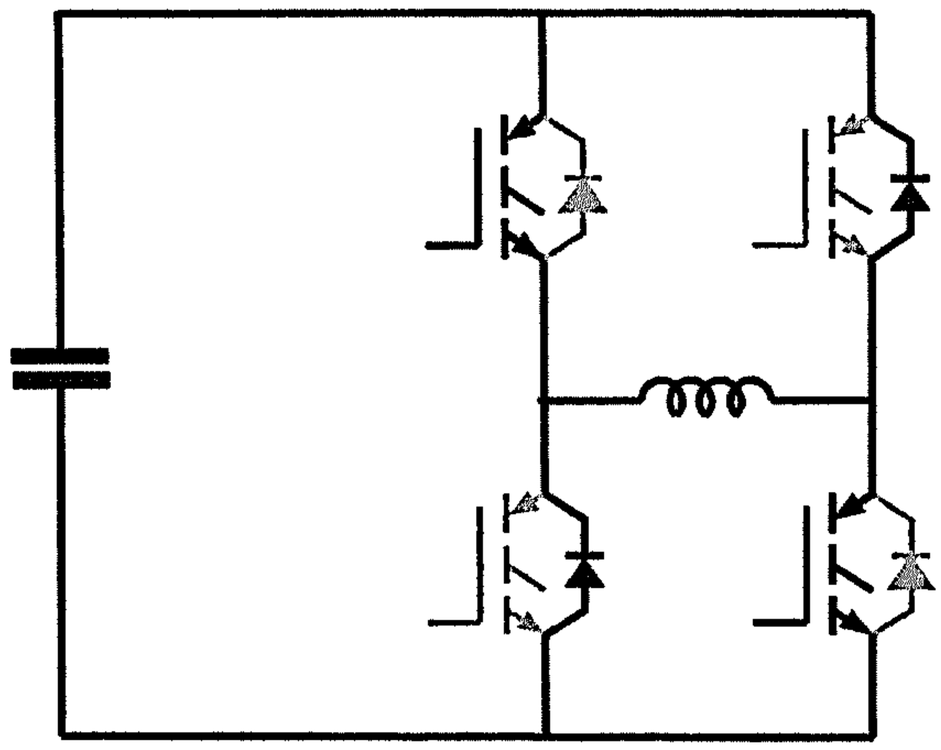

Figure 3.5 Devices conducting with unipolar currents in the 'H' bridge configuration shown in black, those not conducting shown in grey.

3.3.3.3 Star Connected Inverter

The star connected inverter is a special case. The star point forces the sum of the phase currents to be zero, and because the star point is not directly controlled by the Current Controller, its voltage is not known (Figure 3.6 shows the star connected motor drive). The Current Solver requires the voltage across each winding to be known to calculate its change in flux linkage, and therefore the star voltage needs to be determined for the simulation to work.

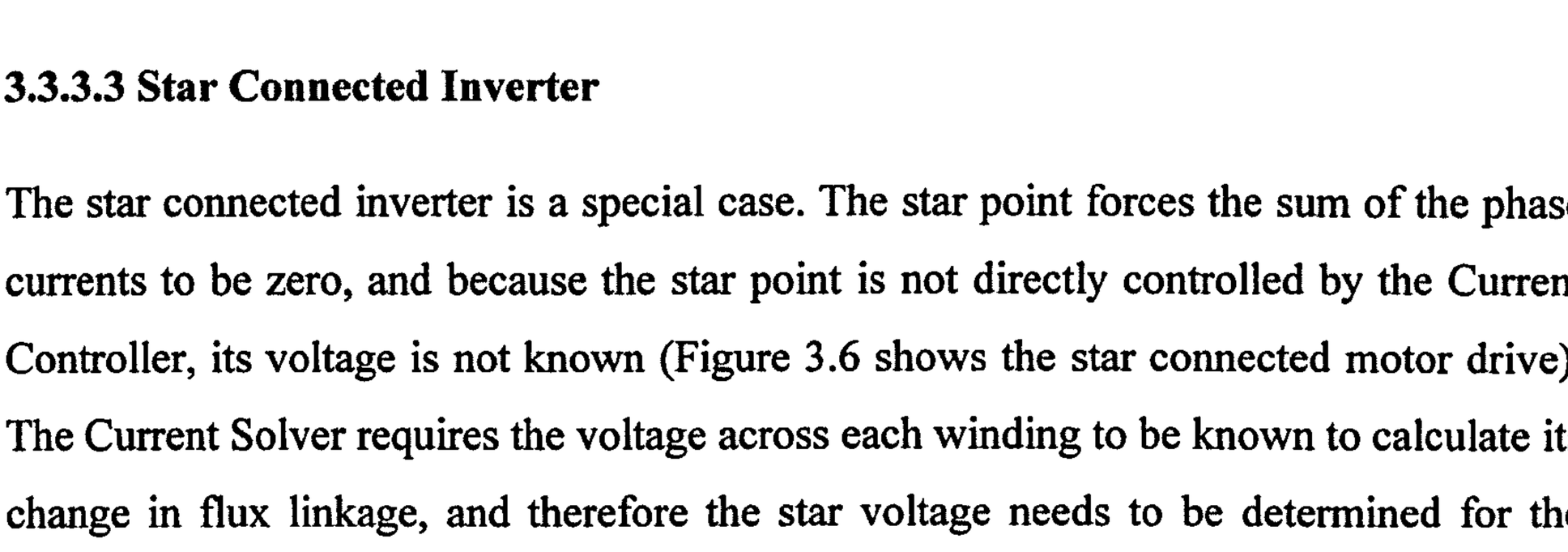

Figure 3.6 The star connected inverter.

The method used to solve for the star point voltage is an iterative one. Most of the steps are the same as before, with the addition of the extra steps to calculate the star voltage.

The time step is entered assuming the star voltage has not changed from the last time step. It is used to calculate the voltage imposed across each winding. The new currents can then be calculated as before. The sum of these new currents should be zero, but almost inevitably this will not be the case, and an error current is produced. The star voltage is then adjusted in the appropriate direction by an estimated amount and the whole time step restarted until the sum of the currents is zero (or within a nominal error). Note that the accuracy of the estimated correction voltage does not affect the accuracy of the final solution – it only affects the speed at which convergence is achieved. Figure 3.7 shows a top level flow diagram of a time step in the Current Solver routine. A detailed list of the equations used at each stage follows this, with the extra steps required over the previous routine being shown in Italics.

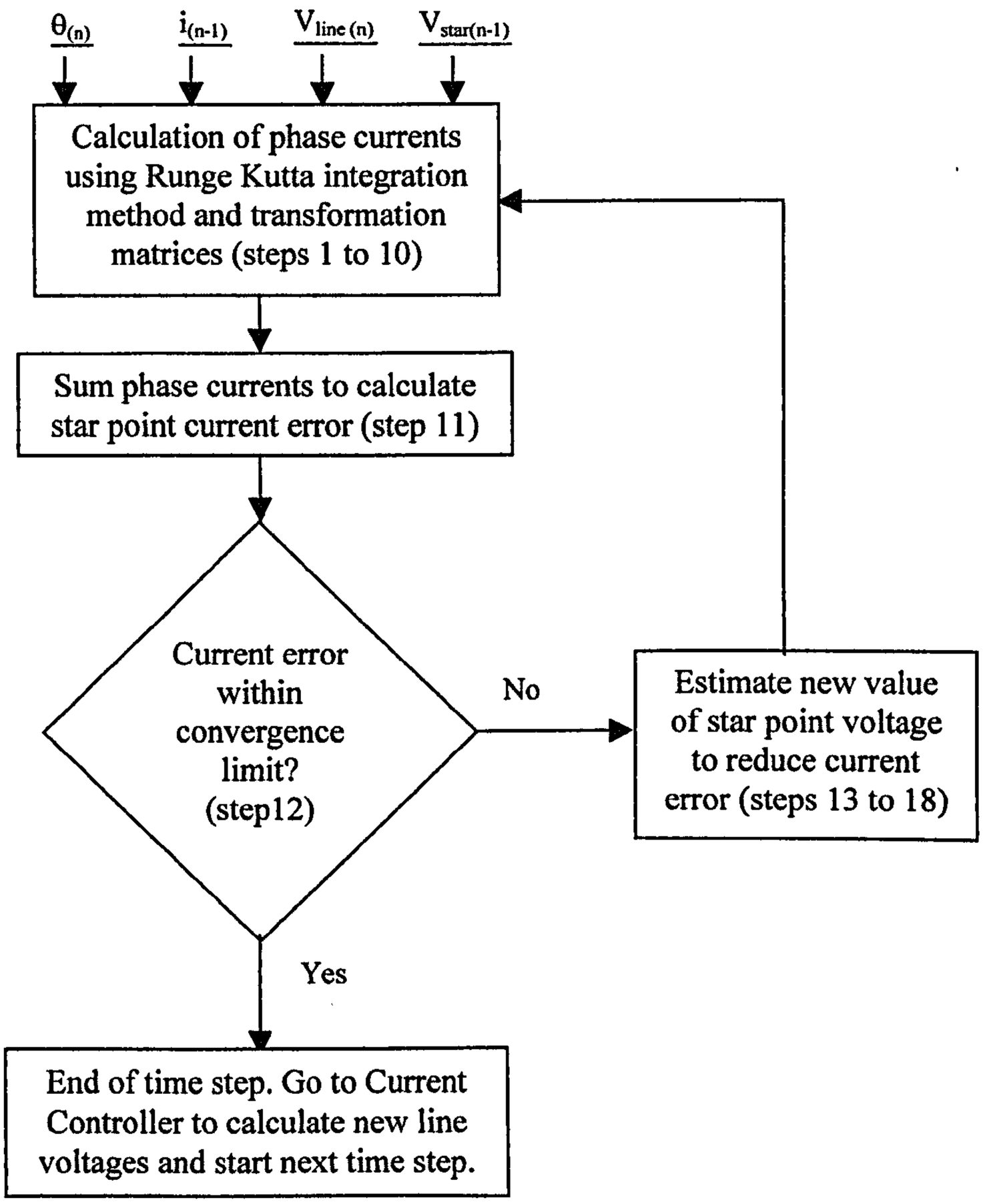

Figure 3.7 Flow chart for Current Solver stage with motor connected in a star connection.

1. Calculate the instantaneous inductance of the equivalent single tooth windings using the equivalent single tooth currents from the previous time step and the present position (θ_n):

$$L_{1(n)} = \frac{\psi_{1(n)}}{i_{1(n-1)}}$$

where $\psi_{1(n)}$ has been determined from the equivalent single tooth flux linkage/ current/position data using $i_{1(n-1)}$ and θ_n.

2. *Calculate the voltage imposed across each winding for the time step knowing the line voltage supplied from the inverter and the last calculation of the star point voltage:*

$$V_{A(n)} = V_{line\_A(n)} - V_{star(n-1)}$$

3. Calculate first estimate of the change in real flux linkage in each phase over the time step due to the phase voltages that are being applied:

$$\Delta\psi_A(1st)_{(n)} = (V_{A(n)} - i_{A(n-1)}R).t_s$$

4. Total real flux linkage is calculated:

$$\psi_A(1st)_{(n)} = \psi_{A(n-1)} + \Delta\psi_A(1st)_{(n)}$$

5. Calculate equivalent single tooth flux linkage:

$$[\psi]_{123}(1st)_{(n)} = [C]^{-1}[\psi]_{ABC}(1st)_{(n)}$$

6. The first estimate of the new single tooth phase current $i_1(1st)_{(n)}$ is then:

$$i_1(1st)_{(n)} = \frac{\psi_1(1st)_{(n)}}{L_{1(n)}}$$

7. The first estimate of the new real phase current $i_A(1st)_{(n)}$ is then:

$$[i]_{ABC}(1st)_{(n)} = [C]^{-1}[i]_{123}(1st)_{(n)}$$

8. Repeat from step 3 replacing $i_{A(n-1)}$ with $i_A(1st)_{(n)}$ and so on, to obtain the four parts of the Runge Kutta equation i.e. $\psi_A(1st)_{(n)}$, $\psi_A(2nd)_{(n)}$, $\psi_A(3rd)_{(n)}$ and $\psi_A(4th)_{(n)}$.

9. The resulting estimate of real flux linkage uses the Runge Kutta equation:

$$\psi_{A(n)} = \psi_{A(n-1)} + \frac{\left[\Delta\psi_A(1st)_{(n)} + 2(\Delta\psi_A(2nd)_{(n)} + \Delta\psi_A(3rd)_{(n)}) + \Delta\psi_A(4th)_{(n)}\right]}{6}$$

10. Use the equations in steps 5, 6 and 7 to obtain the final values of the real currents $i_{ABC(n)}$.

11. Sum the three phases currents together to produce the error current:

$$i_{error(n)} = i_{A(n)} + i_{B(n)} + i_{C(n)}$$

12. Check whether error is within the convergence band:

$$-\text{convergence limit} < i_{error(n)} < \text{convergence limit}$$

where convergence limit is set to be 0.01% of the peak current demand. If the error is above the specified convergence limit then the star point needs to be adjusted so as to reduce the error. Stages 13 to 17 are used to calculate the magnitude and direction of the adjustment to the star point voltage. This process involves reversing the usual direction of the transformation matrices. The aim is to estimate the change in phase voltage necessary (and hence star point voltage) to achieve a given change in phase current that will consequently enable all three phase currents to sum to zero.

13. Adjust the currents to reduce the error (the factor of 10 used here is a nominal value that was found to give fast convergence results):

$$i_{A(n)} = i_{A(n)} - \frac{i_{error(n)}}{10}$$

14. Calculate the new equivalent single tooth currents:

$$[i]_{123(n)} = [C][i]_{ABC(n)}$$

15. Calculate new single tooth flux linkages:

$$\psi_{1(n)} = L_{1(n)} i_{1(n)}$$

16. Calculate new real flux linkages:

$$[\psi]_{ABC(n)} = [C][\psi]_{123(n)}$$

17. Estimate a new adjusted star voltage for each phase by combining the equations in steps 2 and 3 and rearranging:

$$V_{star\_A(n)} = (V_{line\_A(n)} - i_{A(n)} R) - \frac{(\psi_{A(n)} - \psi_{A(n-1)})}{t_s}$$

18. The final estimate of the next star point voltage to try is then the average of the voltages calculated for each of the phases.

$$V_{star(n)} = \frac{(V_{star\_A(n)} + V_{star\_B(n)} + V_{star\_C(n)})}{3}$$

19. Repeat from step 2 through to 18 until the error current in Step 12 is within the convergence limit.

Typically several iterations are required to solve for the star point voltage each time step, resulting in an entire simulation taking approximately two or three times as long.

Current control for the star connected inverter

PWM control is used here as with the asymmetric half bridge inverter. However, the control for each of the phases now only controls one of the inverter legs. The PID control supplies a reference voltage (V_{ref}) which is then compared to the triangular wave (V_{tri}). The top transistor is switched on if V_{ref} is greater than V_{tri}. If not, the bottom transistor is switched on.

3.3.3.4 Delta Connected Inverter

The delta connected inverter (Figure 3.8) presents no problem to the simulation as unlike the star connected inverter the controller directly controls the voltage across each winding. Therefore that voltage is always known and so the currents and flux linkages can be solved as with the asymmetric half bridge circuit. The only difficulty comes with the methodology used in the Current Controller itself. The voltage applied to one phase directly affects the voltage available to be supplied to the other two phases, so direct control of the current in individual phases is not possible.

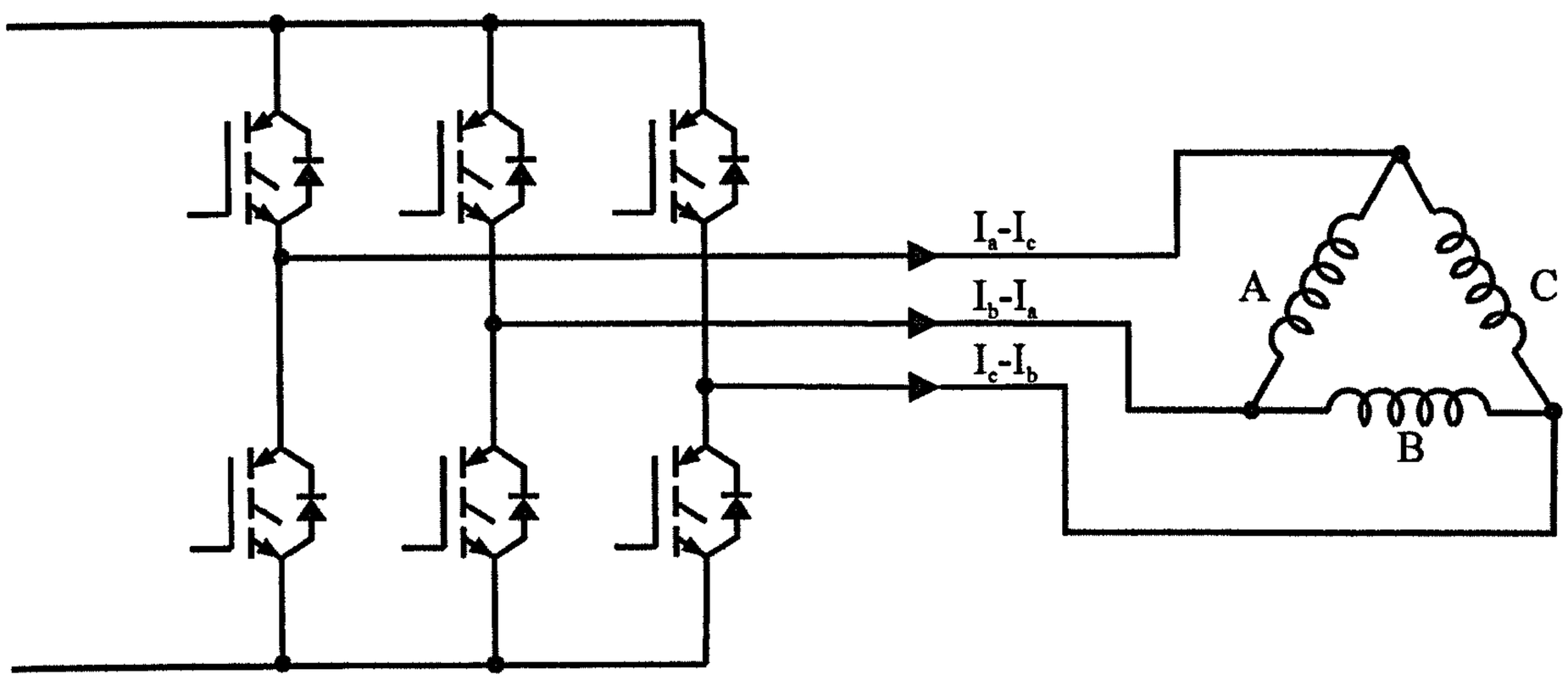

Figure 3.8 The delta connected inverter.

3.4 Performance Evaluation

Once the Current Solver and the Torque Solver have completed their calculations, the Performance Evaluation can take place. The Torque Solver calculates instantaneous torque for each phase of the machine at intervals of one electrical degree. Total electric machine torque, average torque and torque ripple are easily determined from this. Torque ripple is defined here in the following way:

$$T_{ripple} = \left[\frac{T_{\max} - T_{\min}}{T_{av}} \right] \% \tag{3.12}$$

where T_{av} is average torque, $T_{\min}$ and $T_{\max}$ are the minimum and maximum instantaneous total torques in the machine. Machine winding loss (copper loss) is calculated using the following equation:

$$\sum_{\theta=0}^{\theta=360} \frac{3(I_a^2 R)}{360} \tag{3.13}$$

3.4.1 Torque-Speed Characteristic Generation

Generation of the torque-speed curve is achieved by performing the above calculations above over a range of speeds, with a fixed current demand and DC link voltage. However, as with any SR motor, the desired 'on' and 'off' angles need to be changed with speed to ensure maximum torque is achieved at each point. For the torque-speed curve to be generated automatically a reliable method of optimising these on/off angles was found. The method used for doing this is explained as follows:

3.4.1.1 Optimisation of 'On' and 'Off' Angles

The aim of the optimisation is to maximise average torque at each speed, with the constraint of a fixed current demand and a fixed DC link voltage. The method to achieve this is an iterative one, as opposed to any form of calculated method. This is very appropriate in this case as the fully pitched winding machine has not been simulated in this detail before, and so a 'dumb' search method is the simplest way of reliably arriving at the correct values.

The simulation initially asks for the range of speeds the torque-speed curve is to be generated over. An estimation of the on and off angles at the first speed is then entered (a bad estimation of the correct values simply leads to a longer search time). A maximum and minimum search step is also entered.

The simulation then starts by calculating the average torque at the estimated on and off angles, and at the on and off angles +/- the maximum search step. An example is shown in Figure 3.9 with the initial estimate of on angle being 200°, off angle 320° and the search step 10 °. Note that on and off angles are defined with reference to the aligned position as can be seen in Figure 3.2.

Initially the torque at positions T1 to T9 is calculated. In this example suppose T3 is found to have the highest torque of the nine values. The search then moves off in the

direction of T3. Another nine values of torque then need to be calculated centred around the latest maximum value. Only T10 to T14 have to be calculated as T2, T3, T5 and T6 have already been determined. This carries on until the maximum torque is found in the centre of the nine latest values. In this example T11 is found to have the highest torque out of T2, T3, T13, T10, T11, T12, T15, T16 and T17.

The search step can then be reduced to obtain a more accurate result. Therefore eight more values are calculated around T11, now with a step size of 5°. The search continues until the highest torque found is again in the centre of the nine values calculated. The search step is then reduced again until the desired accuracy is achieved.

The size of the initial search step and the rate at which the search step reduces are a compromise between total processing time and the need not to miss the optimum turn 'on' and turn 'off' angles. It was found that the variation of torque with these angles was a smooth one and therefore the search was not very susceptible to local maximums. This, combined with the fact that the initial estimate was usually quite accurate meant that the initial search step could be relatively large. A step of 10 ° was generally used, with this step halving in size when the point of highest torque was found in the centre of the nine values. A minimum search step of 2° was used.

Turn Off Angle

Turn On Angle	270	280	290	300	310	320	330	340	350	360
150										
160										
170						T15	T16	T17		
180						T10	T11	T12		
190					T1	T2	T3	T13		
200					T4	T5	T6	T14		
210					T7	T8	T9			
220										
230										
240										

Figure 3.9 Search method used to optimise 'on' and 'off' angles

This optimisation is performed at each speed to be calculated in the generation of the torque-speed curve. The final on and off angles from the previous speed are used as the starting point for the search on the next speed.

This method produced very reliable results within a reasonable time frame. At no point was it found that with all the different drives and their different excitation patterns that the search had not optimised the on and off angles correctly. This was checked by giving the search routine a variety of different initial on and off angles and ensuring that the same result is achieved in each case. Processing time of course depends on the number of speed points to be calculated, but total time needed would be in the order of one hour on a Sun workstation.

3.4.2 Inverter Loss Calculation

The aim of the inverter loss calculation was to be able to perform comparative studies between different drives and assess their impact on power electronic rating in terms of device loss, as well as device peak current.

The characteristics of several different diodes and switching devices are available to be selected from the menu system. Additionally new device characteristics can be entered manually. Devices are characterised in a reasonably simple way as it is the comparative performance of the drive rather than the comparative performance of individual devices that are being assessed.

Conduction loss of a diode, IGBT or MOSFET is based on a y=mx+c model. Therefore in the case of an IGBT three parameters are entered as shown in Figure 3.10. Vce(on) at zero current and Vce(on) at a current I_1. This is a first order approximation to the real curve, a typical example of which is also shown in Figure 3.10.

A choice of the method to calculate switching loss of an IGBT or MOSFET is offered. One way is to enter the energy per switch at turn on (Eon) and the energy per switch at turn off (Eoff). The device current and volts that this energy is based on is also entered. Eon and Eoff are then scaled proportionally in the simulation to suit the actual currents

and voltages being used. This method is particularly suitable for IGBTs as the energy per switch is directly quoted in the data sheet and includes 'tail' losses as well additional losses due to the recovery of the freewheel diode.

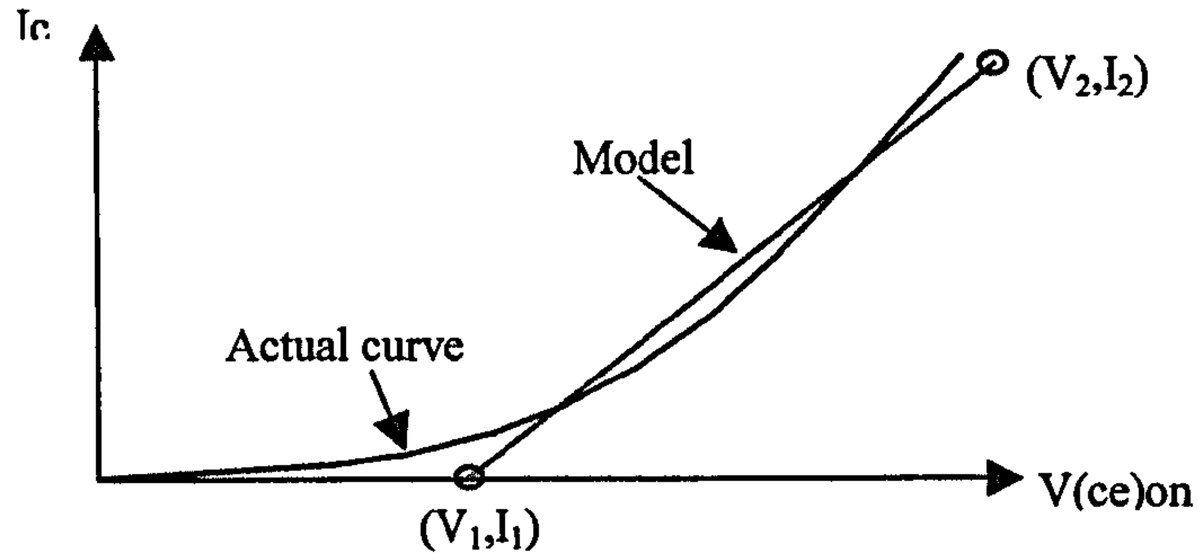

Figure 3.10 IGBT conduction loss characterisation

The second method is to enter rise and fall times for the device with the energy per switch then being calculated using:

$$E = \frac{1}{2}VIt$$

The latter method is more suitable to MOSFETs, where only rise and fall times are quoted in the data sheet. This model, however, is much more simplistic as no account is taken of variation in rise/fall time with current or losses due to diode reverse recovery. Inverter loss calculations shown throughout this thesis are based on the more accurate energy per switch method, and use 600V rated IGBTs and ultrafast diodes.

If inverter loss calculations are to be performed then to reduce computation time the calculation is only performed once the simulation has fully converged. One more electrical cycle is completed, this time also calculating inverter loss as well. At the end of each time step the inverter loss routine checks to see how much current a device has conducted and whether the device has changed switching state or not. The energy loss in the device is then determined using the appropriate characteristics. The energy losses are summed together over the electrical cycle so that average conduction loss and switching loss per device can be displayed. Note that, for simplicity, power electronic voltage drops are not included in the determination of phase flux linkage.

3.5 Example Waveforms

In addition to the calculated parameters such as torque, copper loss, and inverter loss, the following waveforms can be plotted over an electrical cycle:

- Phase current
- Phase flux linkage
- Phase voltage
- Flux linkage/current locus
- Phase torque (equivalent single tooth phase for the fully pitched machine)
- Total torque
- Inverter current (DC link capacitor to motor)
- DC link current (Rectifier to DC link capacitor)
- DC link voltage
- PWM triangle and voltage reference signals

The fully pitched winding machine has the following in addition:

- Equivalent single tooth phase current
- Equivalent single tooth phase flux linkage
- Equivalent single tooth flux linkage/current locus

Machines with a star connected inverter also have:

- Star point voltage
- Line voltage

All of the above are plotted at intervals of one electrical degree over one electrical cycle. The following waveforms have a high resolution facility to monitor outputs after each time step:

- Phase current
- PWM triangle and voltage reference signals

Figures 3.11 to 3.15 show examples of simulated waveforms of both the fully pitched and short pitched winding machines. The waveforms are summarised as follows:

- Figure 3.11, 120° excitation of the short pitched winding machine at low speed. Phase current (I_{123}), flux linkage (Ψ_1) and single phase and total torque (T) are shown.
- Figure 3.12, 240° unipolar excitation of the fully pitched winding machine. Phase current (I_{ABC}), flux linkage (Ψ_A), equivalent single tooth current (I_1), equivalent single tooth flux linkage (Ψ_1) are shown together with torque. Figure 3.13 shows a plot of the ψ_A/i_A locus. Figure 3.14 shows a plot of the equivalent single tooth ψ_1/i_1 locus.
- Figure 3.15, sinusoidal excitation of star connected fully pitched winding machine. Phase current (I_A), flux linkage (Ψ_A), line voltage (V_{L1}), phase voltage (V_A), star point voltage (V_S) and equivalent single tooth current (I_1) are shown together with torque.

Explanations of the shapes of these waveforms will be given in Chapters 5 and 6.

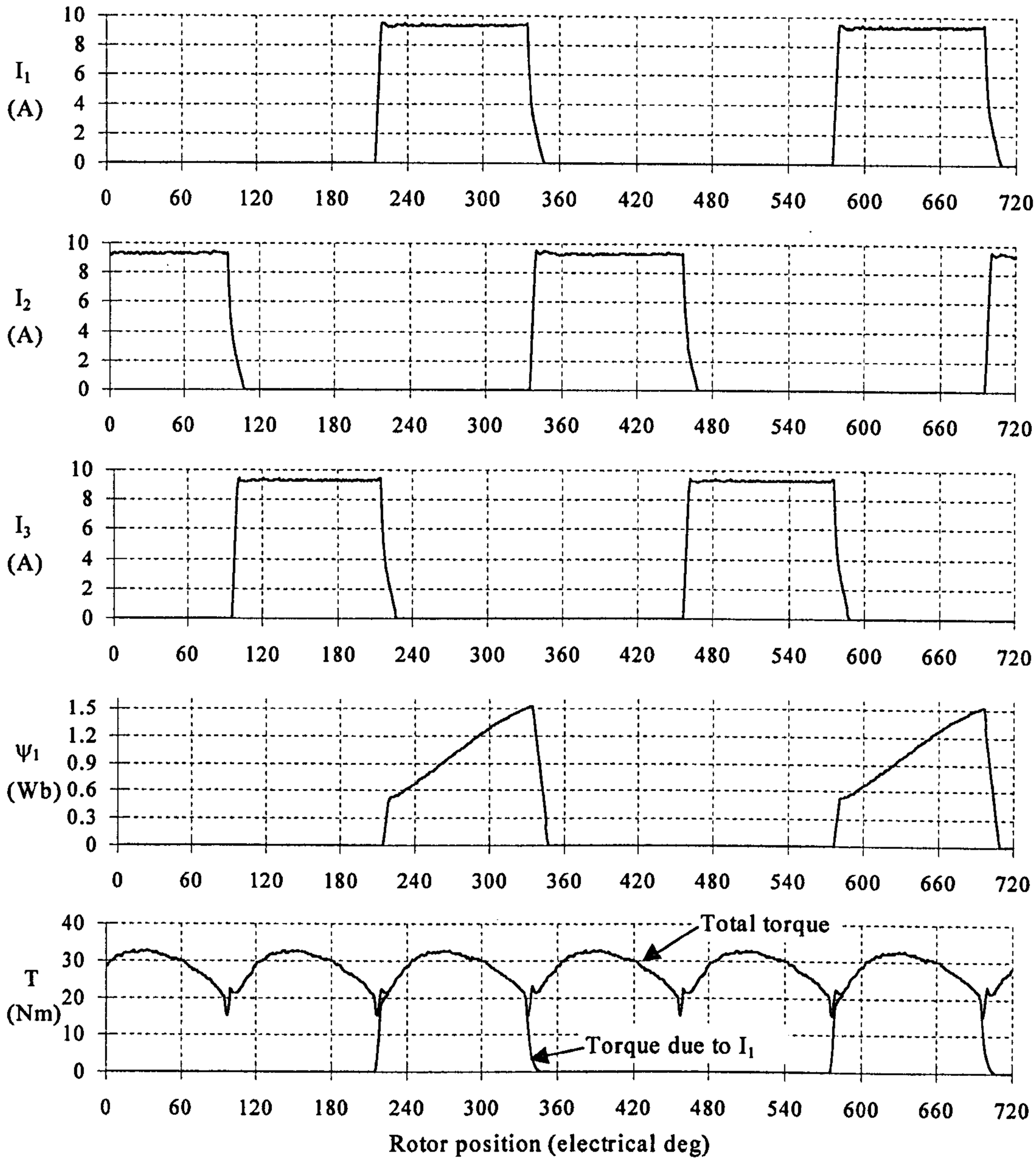

Figure 3.11 Simulated waveforms at low speed for the short pitched winding machine

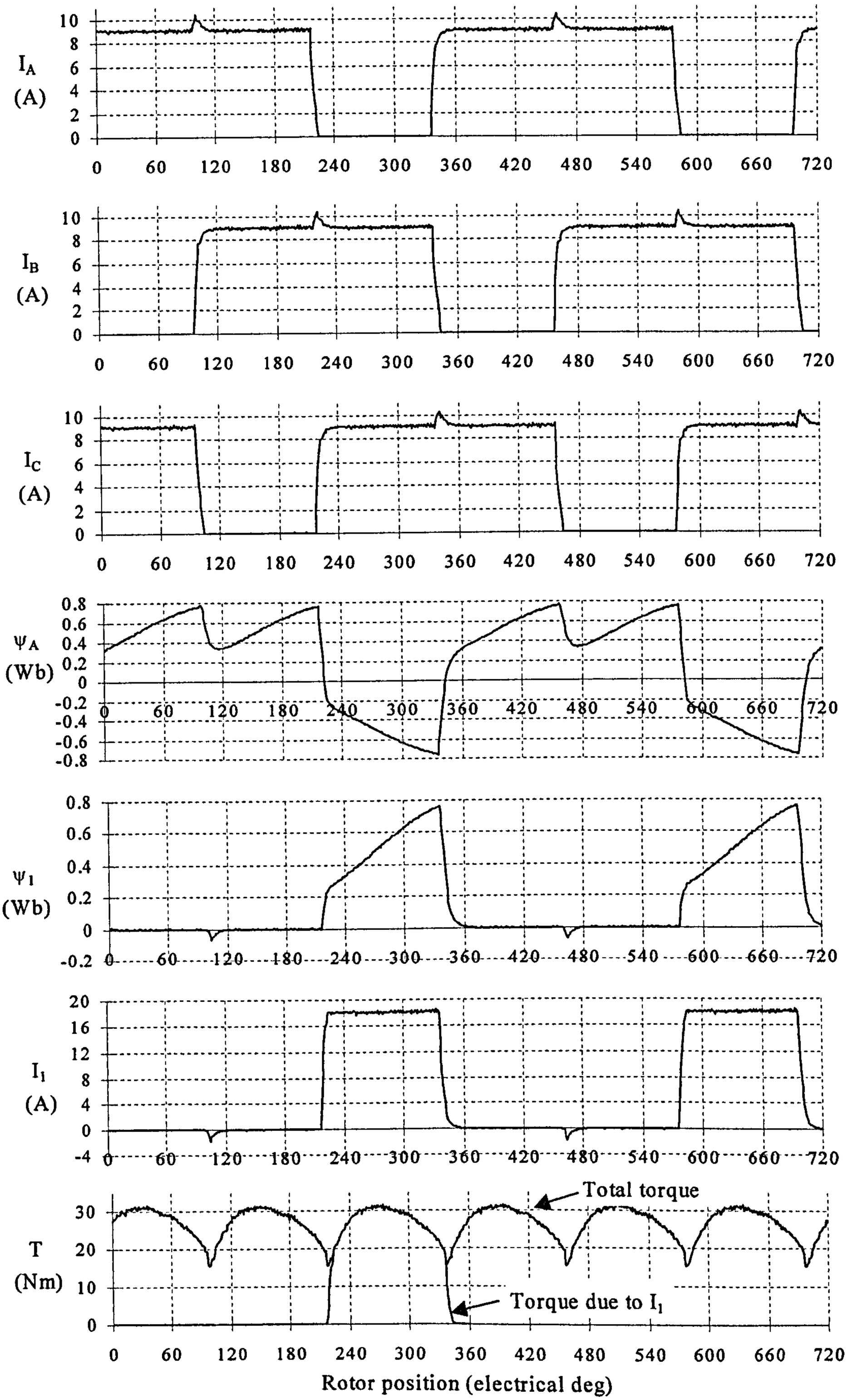

Figure 3.12 Simulation of unipolar operation of the fully pitched winding machine at low speed

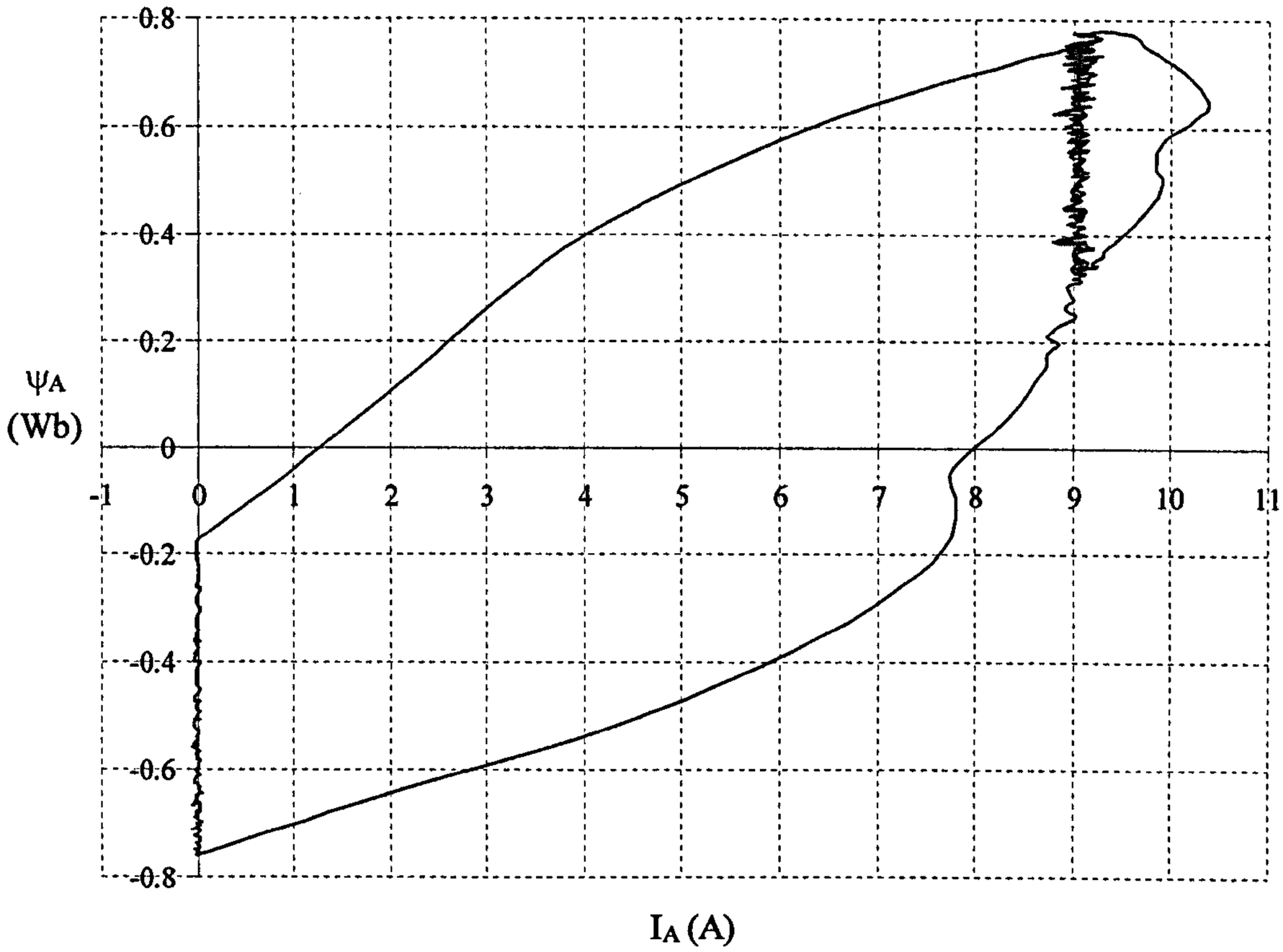

Figure 3.13 Simulated ψ/i locus of the fully pitched winding machine with unipolar operation

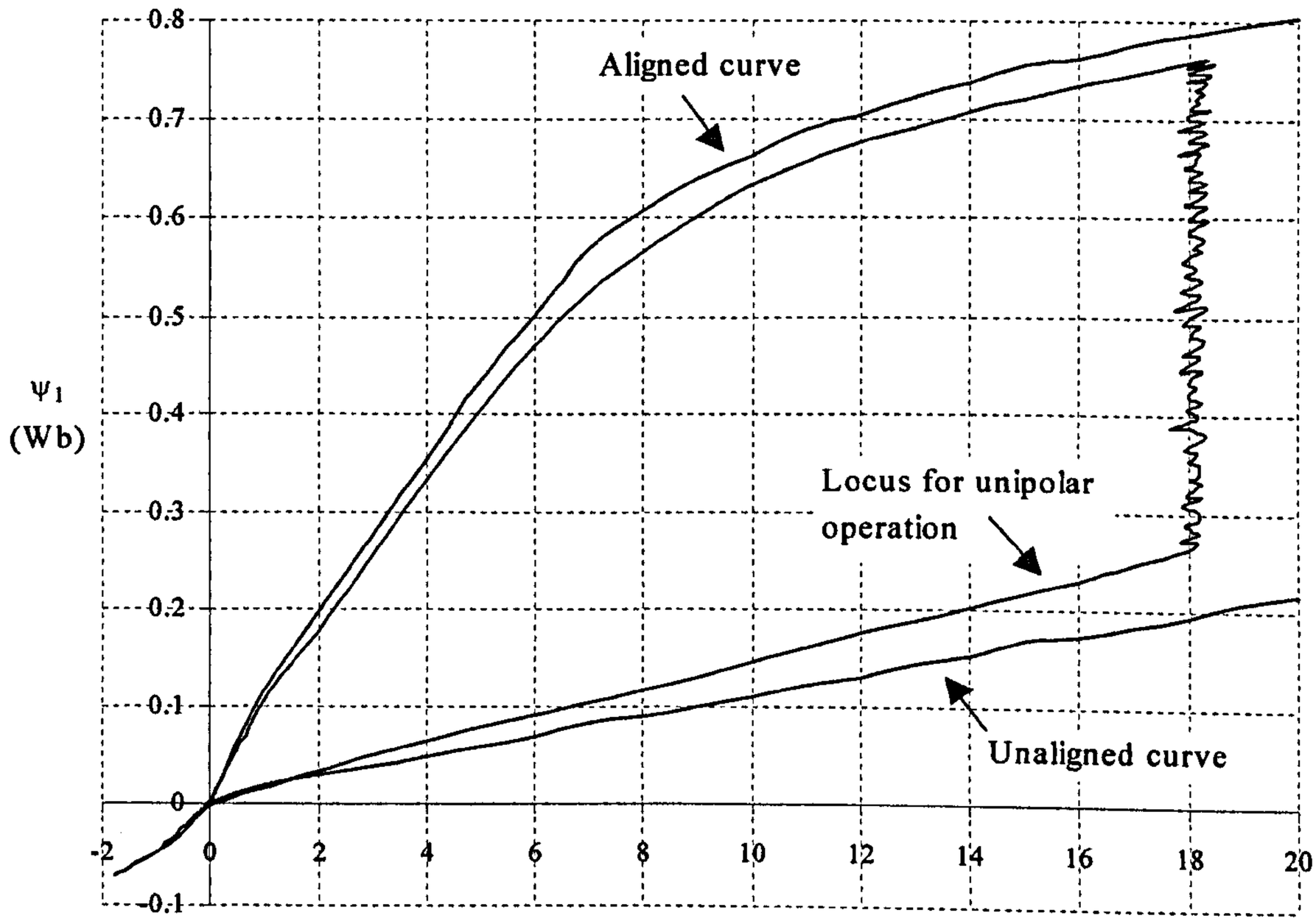

Figure 3.14 Simulated ψ/i locus of the equivalent single tooth parameters with unipolar operation

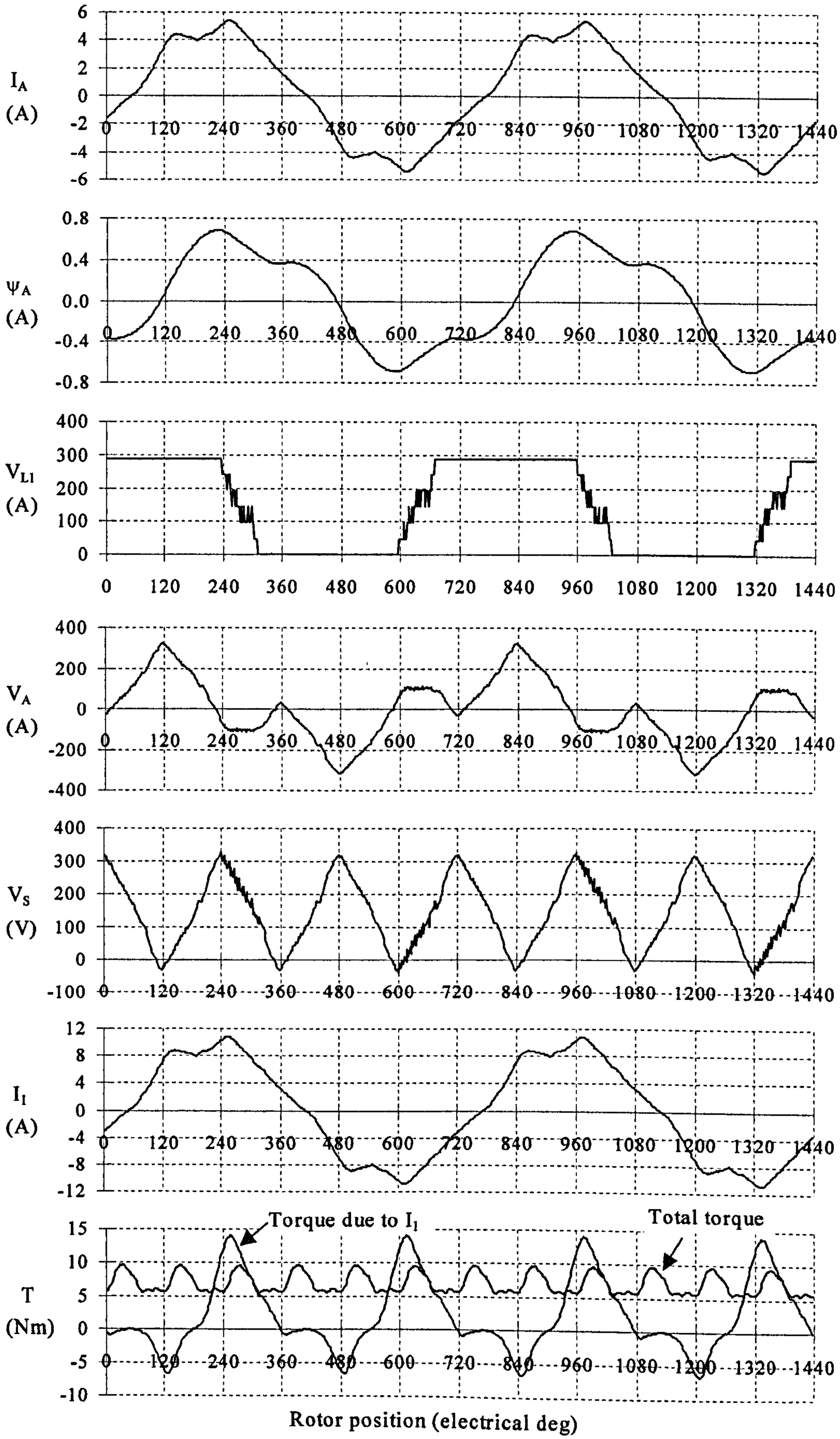

Figure 3.15 Simulation of star connected operation at base speed.

3.6 Summary

Previous simulation methods have been reviewed, and these have been compared to the simulation developed here with the aim of justifying the techniques used.

The primary objective was to have the ability to perform accurate simulations of both the fully pitched and short pitched winding machines, taking into account both magnetic saturation and mutual coupling effects. The latter is so strong in the fully pitched winding machine that saturation within the mutual coupling needed to be part of the model. This is something that is usually neglected in short pitched winding simulations as mutual inductance is normally very low in comparison to self inductance.

The Current Solver core model, which was developed from an existing brushless DC simulation, is based substantially around that first described by Stephenson and Corda [3.8]. The machine is characterised in terms of flux linkage against current and rotor position. Flux linkage is determined using a time stepping integration technique, further improved with a 4^{th} order Runge Kutta equation. Current is determined by quadratic interpolation of the flux linkage/current/position data. Whilst relatively computationally intensive in comparison to other techniques, this ensures accurate results.

This core model is extended to be able to cope with fully pitched windings with the use of transformations matrices developed by Mecrow [3.14]. Current and flux linkage are converted into their equivalent single tooth values, enabling decoupling of the phases to take place. Current is then determined from flux linkage in exactly the same way as with the short pitched winding machine i.e. using the flux linkage/current/position data.

Built around the Current Solver core model are the Current Controller, Torque Solver and Performance Evaluation. The Current Controller is able to model the full effects of both analogue and digital PWM control schemes, ensuring realistic PID gains are used, and enabling comparisons of the required controller bandwidth between machines. The Current Controller can be used with a variety of power electronic topologies, including star connection. The latter requires an additional stage in the model to determine the star connection voltage.

The Performance Evaluation calculates averaged parameters such as torque, copper loss, and inverter loss. Plots of all the relevant waveforms are available. Also included is a search routine that is able to automatically determine the best on and off angles over a speed range to maximise torque output for a given current demand.

Example waveforms have been shown for both types of machine, and these will be explained in more detail in Chapters 5 and 6. Chapter 5 will show direct comparisons with test rig results.

Chapter 4 - MACHINE DESIGN

4.1 Introduction

Chapter 2 has described the various basic ways it its possible to excite the three phase fully pitched winding machine. Unlike the short pitched winding machine, both unipolar and bipolar excitation patterns are possible. This brings about the following reasons as to why the fundamental geometry of the laminations should be re-examined with a view to optimising performance further:

1) An excitation method that produces flux in a different way to that of the short pitched machine results in different amounts of saturation in various parts of the magnetic circuit. Therefore the thickness of the core back or the poles, for example, may need some adjustment.
2) Unipolar excitation of the fully pitched winding machine results in very similar flux patterns to the short pitched winding machine, and so the machine geometry is likely to be fairly similar. Some optimisation, however, may be possible to overcome some of the disadvantages of a fully pitched winding e.g. the total amount of copper required.
3) Machine design is a balance between the magnetic and electric design. The fully pitched winding machine has improved winding efficiency. It should therefore be appropriate to shift the balance of the design towards improving the magnetic design, at the expense of the electric design. In other words, achieve point 2) by reducing the amount of copper, hopefully without compromising torque for a given stack size.

The fully pitched winding machine need not necessarily have three phases - many other geometry configurations with different numbers of phases are possible. Therefore the first section in this chapter will review some of the more promising configurations with a different number of phases, examining the potential reduction in copper loss as well as the power electronic requirement.

After the number of phases has been selected for the prototype machine design, the effect that pole number and machine aspect ratio have on efficiency will be shown. This is then followed by the detailed design of the other critical parameters such as split ratio (ratio of rotor to stator diameter), tooth width etc.

The chosen parameter to be optimised is torque per unit copper loss with the aim of maximising the torque output from the given frame size. Other very important performance criteria, however, are also taken into account, including the torque-speed curve achievable and the power electronic rating. Practical issues such as level of acoustic noise need to be taken into account. This can be reduced, for instance, by increasing the core back thickness to stiffen the mechanical construction. This has the effect of compromising the electromagnetic design to some extent and therefore should be incorporated into this design so that comparisons can be made with other machines on a like-for-like basis.

Designs were evaluated with the aid of 2D finite element software (which had already been developed within the Department) to generate the flux linkage characteristics. This data was then input to the simulation (which was described in Chapter 3) to perform the dynamic analysis of the drive including the power electronics and control. Once the design had been finalised it was constructed for experimental analysis. The results of this experimental work are presented in Chapters 5 and 6.

4.2 Basic Machine Geometries

4.2.1 Number of Phases

Switched reluctance machines in general can be designed with a wide variety of geometries and number of phases. The following section examines the effect the number of phases has on the basic operation and performance of a fully pitched winding SR machine.

4.2.1.1 Single Phase Machines

The lowest number of phases a switched reluctance motor can have is one. In its simplest form this would consist of 2 stator teeth and two rotor teeth. It is characterised

by large periods of zero torque output, which makes starting difficult and results in very high torque ripple. Horst [4.1] described the use of a parking magnet to overcome this starting problem.

A single phase winding machine is already fully pitched, and therefore no other fundamentally different winding configurations are possible. It is interesting to note that although the winding is fully pitched, torque is still produced purely by variation in self inductance with position. Its operation is therefore fundamentally different from fully pitched winding machines with two or more phases where a large component of the torque is produced by variation of mutual inductance with position.

4.2.1.2 Two Phase Machines

Lower torque ripple is produced with a two phase machine, as the period of zero torque output is reduced to positions where the rotor is completely aligned to the stator. Starting, however, can still be difficult and many schemes have been suggested to overcome this problem. For example, a stepped air gap has the effect of producing a variation in inductance with one phase, even when the rotor is fully aligned with the other phase, and is hence able to produce torque (see El-Khazendar *et al* [4.2]). Even with this scheme, however, starting torque is still low and is in a fixed direction (at least initially).

A two phase fully pitched winding machine is possible, and is shown in Figure 4.1. In this machine it is necessary to have bipolar currents in at least one of the phases to produce a rotating magnetic field on the stator. For example, to produce an MMF down stator teeth '1' in Figure 4.1, both phases A and B should be conducting with a positive current. The only way to produce an MMF down stator teeth '2', however, is to excite one of the phases with a negative current. Figure 4.1 shows this excitation pattern with phase B being bipolar and phase A permanently on with a unipolar current. The current 'I_1' is the equivalent current in a winding that is short pitched around stator teeth '1' with the same total number of turns as the fully pitched windings (i.e. the equivalent single tooth current). Note that the magnitude of this current needs to be twice that of the fully pitched winding currents to produce the same MMF. This is because only one phase is contributing to the MMF, as opposed to two in the fully pitched winding machine, and

therefore twice the current is needed for the same number of ampere-turns. The transformation matrix to convert between currents in a 2 phase fully pitched winding machine and a 2 phase short pitched winding machine is as follows:

$$\begin{bmatrix} I_1 \\ I_2 \end{bmatrix} = \begin{bmatrix} 1 & 1 \\ 1 & -1 \end{bmatrix} \begin{bmatrix} I_A \\ I_B \end{bmatrix} \tag{4.1}$$

This two phase fully pitched winding machine should therefore show a significant improvement as all the copper in the machine is being utilised at the same time to produce torque - with the short pitched winding machine only one phase can contribute to torque production at any one time. If endwinding effects are ignored for simplicity, the reduction in copper loss for the same tooth MMF can be estimated as follows:

$$\frac{Loss_{FP}}{Loss_{SP}} = \frac{2 * I_{FP}^{\ 2} * R_{FP}}{I_{SP}^2 * R_{SP}} \tag{4.2}$$

where $I_{SP} = 2I_{FP}$ and assuming $R_{SP} = R_{FP}$, then:

$$\frac{Loss_{FP}}{Loss_{SP}} = 0.5$$

This will be an underestimate as the fully pitched end windings will clearly be longer than the short pitched ones. The stack aspect ratio will determine the relative effect endwinding length has on phase resistance, but in most cases there would be a substantial saving in copper loss for the same torque output.

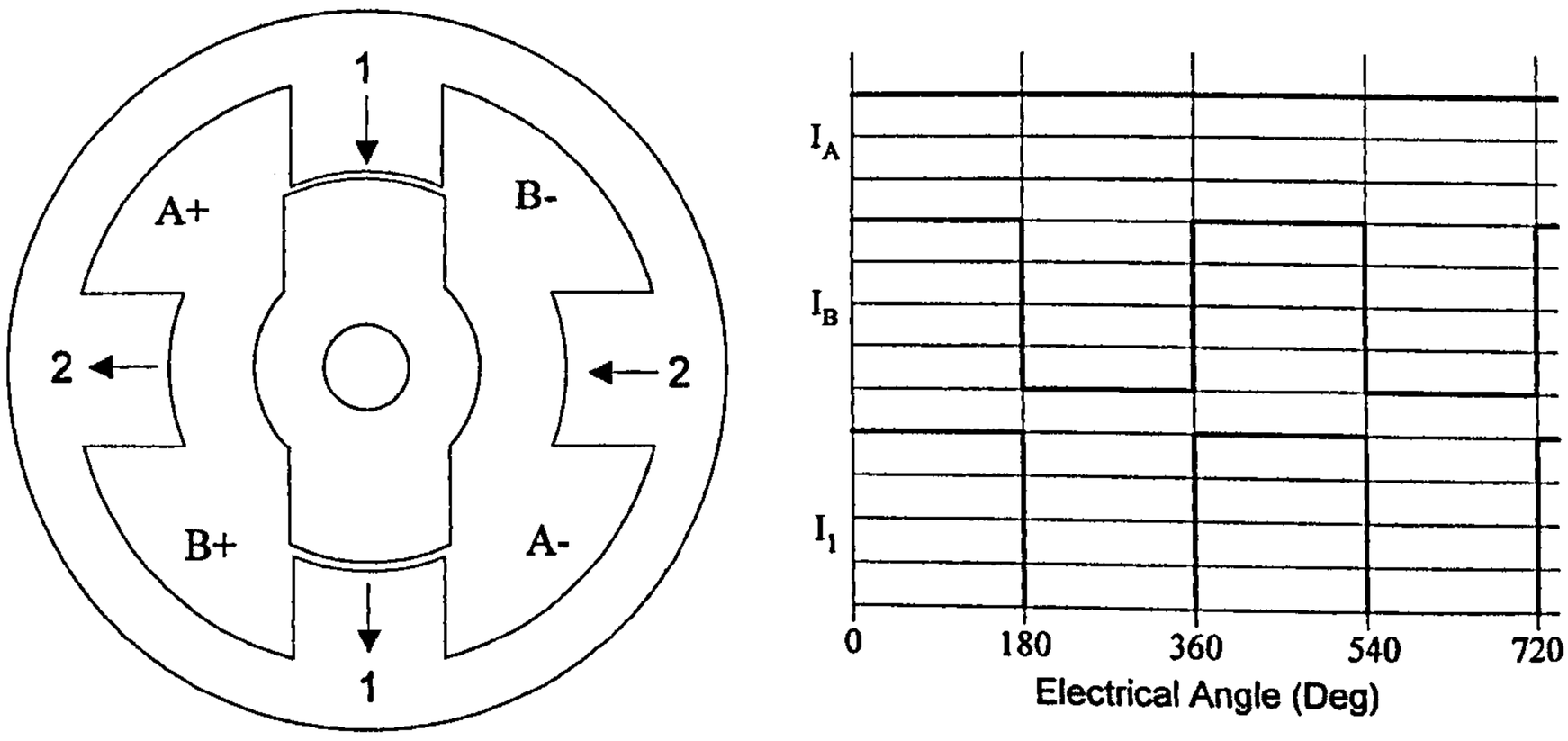

Figure 4.1 Two phase, 4/2, fully pitched winding machine with proposed excitation pattern.

One drawback is that bipolar currents are needed in one of the phases and so the power electronics needed to control the current may become more complex. On the other hand the continuous DC current in Phase A simplifies matters. It may be possible to use a topology where the windings are in effect in series with each other and the power electronic switches alternate the current through phase B e.g. the topology in Figure 4.2.

In this circuit T1, T2, T3 and T4 would be used to control the direction of current in phase B. The diode across Phase A would be required to allow the energy from phase B to flow back into the DC link capacitor during commutation. Additionally it is thought that the mutual coupling between phases will induce positive going current spikes during commutation in Phase A, and therefore the diode would allow this current to freewheel. This circuit should be very efficient in that only two active devices conduct at any one time, keeping inverter losses to the minimum. Also during commutation the full DC link voltage would be applied across Phase B, resulting in good high speed performance. The combination of these facts will reduce inverter VA rating and hence cost should be minimised.

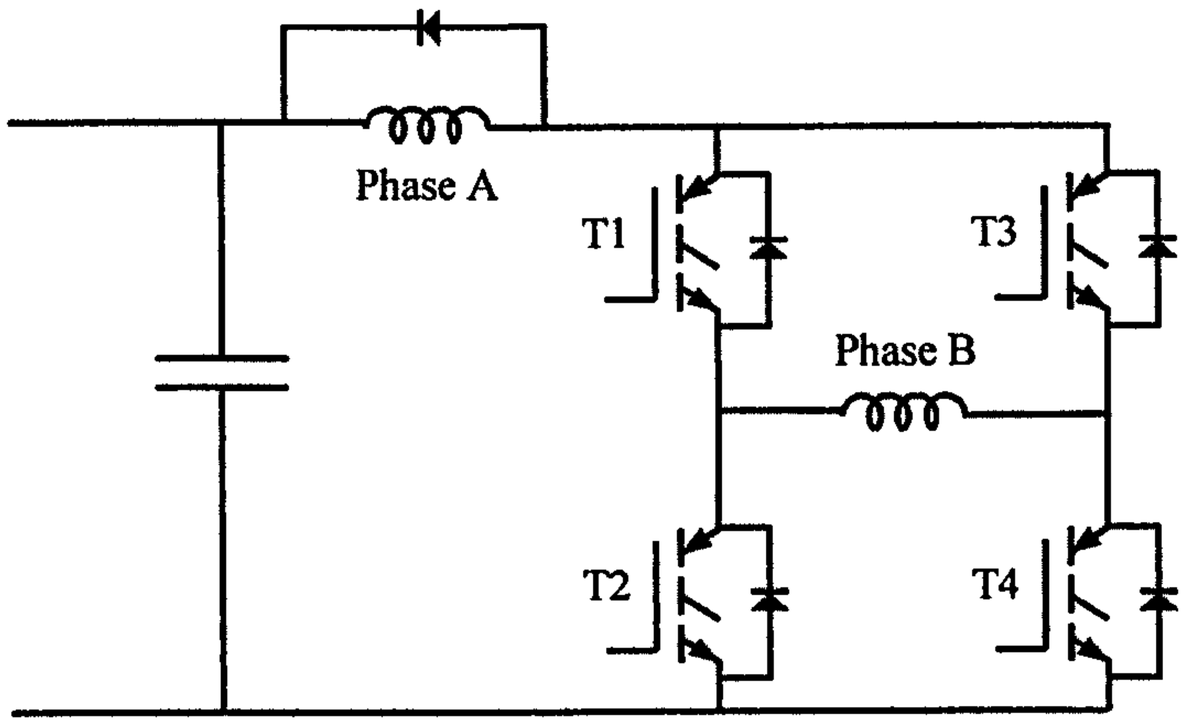

Figure 4.2 Proposed topology for two phase fully pitched machine.

Other topologies have been developed for the two phase fully pitched winding SR motor by Pollock [4.3]. This involves bifilar winding the bipolar excited phase, so that only low side power electronic switches are required. This should lower cost, particularly as high side gate drive circuits are no longer required. Also, with the addition of an extra "commutation" capacitor, thyristors can be used. One disadvantage, however, is that there is up to a 50% reduction in copper utilisation of the bipolar phase.

4.2.1.3 Three Phase Machines

This is one of the most popular choices as it is the minimum number of phases to produce full starting torque in either direction. No zero torque producing zones are present and torque ripple is much reduced compared to the two phase machine.

The fully pitched winding equivalent machine is shown in Figure 4.3. As discussed in Chapter 2 both unipolar and bipolar currents are possible. The excitation pattern shown here is for unipolar currents with a 240° conduction angle i.e. two phases conducting at any one time. Figure 4.3 shows the equivalent single tooth current 'I_1' that is needed to flow in a short pitched winding around stator teeth '1', with the same number of turns per phase as the fully pitched windings. Note that the magnitude of this current needs to be twice that of the fully pitched winding currents to produce the same MMF.

The reduction in copper loss with unipolar currents can be estimated using the same equation as for the two phase machine (Equation 4.2). Therefore if endwinding length is ignored for simplicity, copper loss would be reduced by 50% for the same torque output.

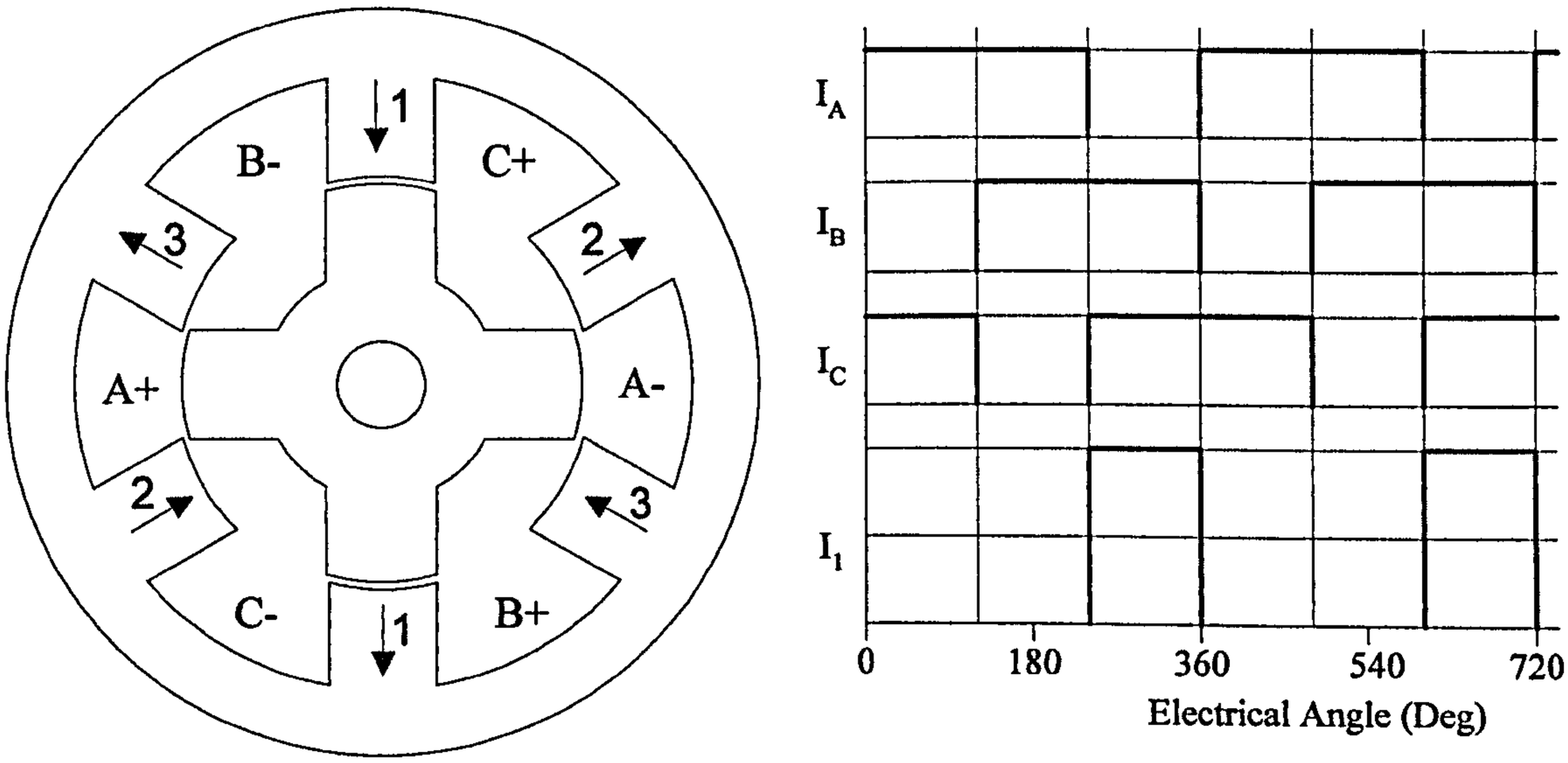

Figure 4.3 Three phase, 6/4, fully pitched winding machine shown with unipolar excitation.

4.2.1.4 Four Phase Machines

The four phase machine with short pitched windings offers the advantage of even lower torque ripple than the three phase machine. This is because two phases can be excited at one time to produce a MMF down two pairs of stator teeth. It is more difficult for the

fully pitched winding machine to produce the same effect, due to the number of phases in the machine being even. Figure 4.4(b) shows an attempt at unipolar excitation, however, as can be seen, it becomes necessary to reverse the direction of current in one of the phases at the end of one electrical cycle to maintain the sequence in which the stator teeth are excited. Furthermore with this excitation pattern only one stator tooth is magnetised at a time and therefore torque ripple will be relatively poor.

The currents shown in Figure 4.4(c) enable two stator teeth to be excited at a time, however, there is a major disadvantage in that two of the phases have bipolar currents, which may lead to an expensive power converter.

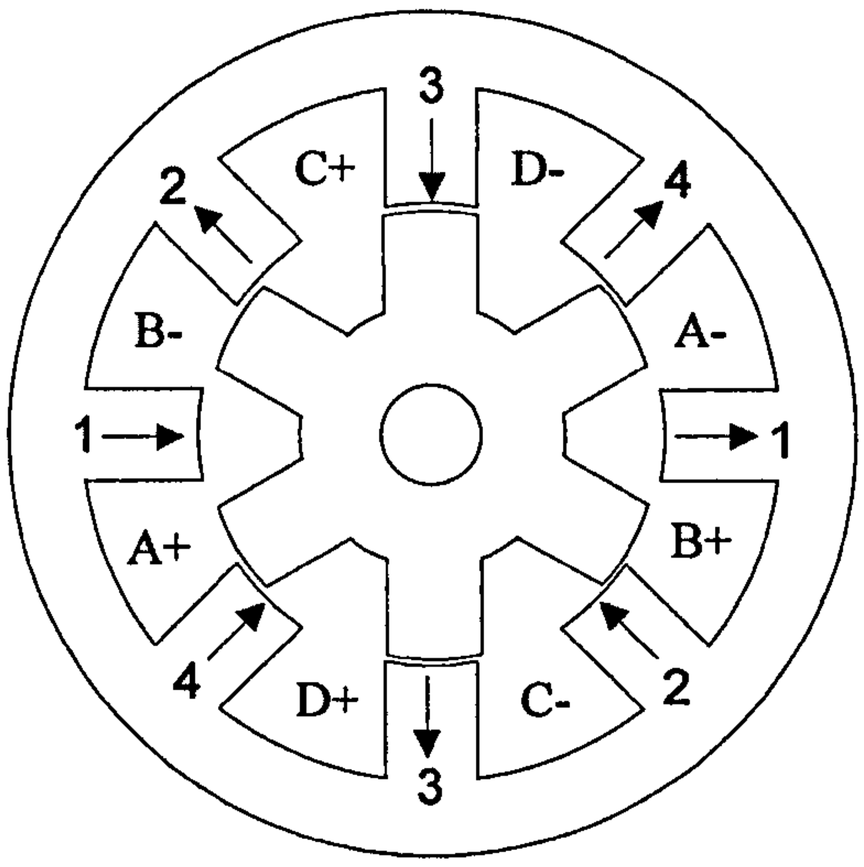

Fig.4.4(a) Winding configuration

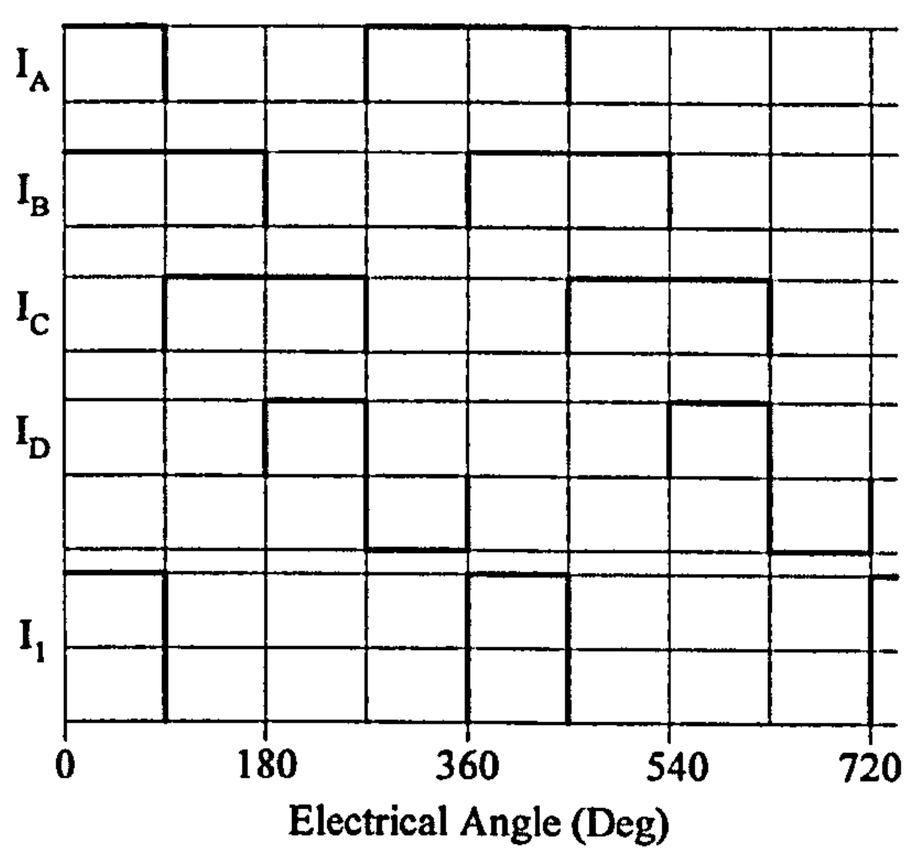

Fig.4.4(b) Single tooth excitation

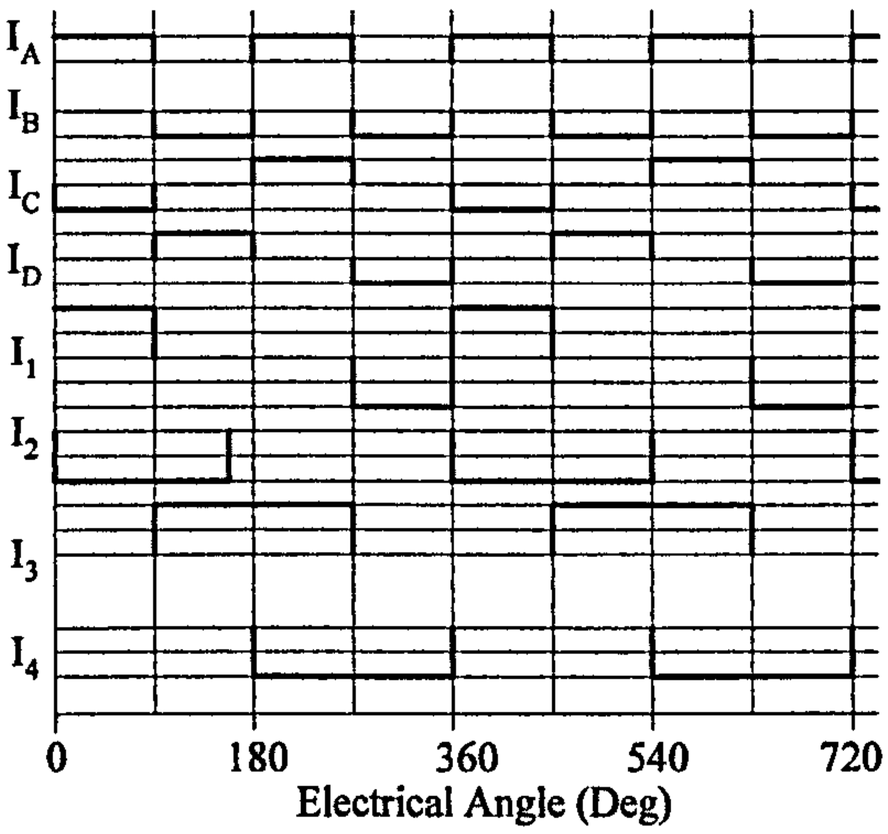

Fig.4.4(c) Double tooth excitation

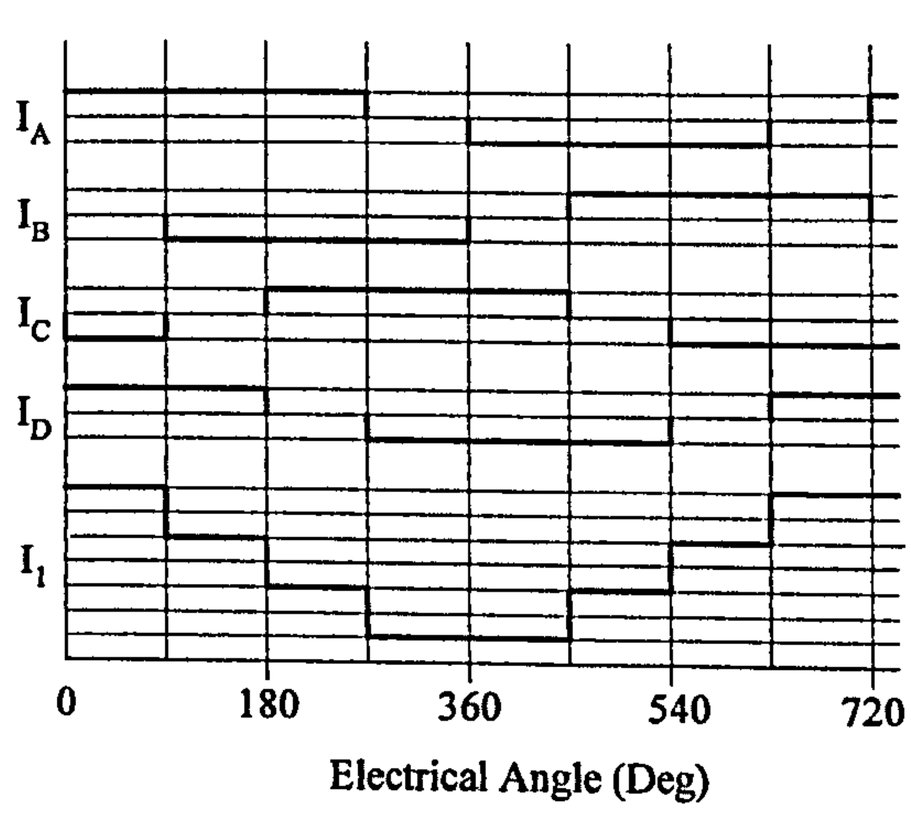

Fig.4.4(d) Multiple tooth excitation

Figure 4.4. Four phase, 8/6, fully pitched winding machine, with proposed excitation patterns. I_{ABC} = fully pitched winding currents, I_{123} = equivalent single tooth currents.

Using bipolar currents in all four phases is perhaps the best solution in that three out of the four phases are contributing to torque production at the same time (Figure 4.4(d)). This can be seen in the equivalent single tooth current, I_1, which has a current three times that of the fully pitched winding currents for half of the electrical cycle, thereby maximising torque output during the positive torque producing region. Some negative torque will also be produced from the much lower current during the rest of the cycle. An estimate of the winding losses with this excitation pattern in the fully pitched winding machine can be made compared to the short pitched winding machine with two phases excited producing approximately the same torque output.

$$\frac{Loss_{FP}}{Loss_{SP}} = \frac{3 * I_{FP}^{2} * R_{FP}}{2 * I_{SP}^{2} * R_{SP}} \tag{4.3}$$

where $I_{SP} = 3I_{FP}$ and assuming $R_{SP} = R_{FP}$ (i.e. ignore endwinding length), then:

$$\frac{Loss_{FP}}{Loss_{SP}} = 0.166$$

This figure underestimates the copper loss in the fully pitched winding machine as endwinding length is not been taken into account, as well as the periods of small negative torque production. It clearly indicates, however, that a significant advantage can be gained in terms of efficiency. There is, of course, an impact on the power electronics - twice the number of switches are needed, although each of these switches is rated for significantly less current. It may be possible to use a topology where some of the switches are shared between phases e.g. three half bridges connected to two of the phases.

4.2.1.5 Five Phase Machines

The five phase short pitched winding machine offers the advantage of inherently low torque ripple, as with the 4 phase machine, when two adjacent phases are excited at the same time. A further advantage can be gained with the use of use of 'short flux loops' as described by Michaelides, Pollock [4.4] that can only be realised in machines with an odd number of phases. If two adjacent teeth are excited with opposite magnetic polarity

then the magnetic flux has only to travel between the two teeth rather than around the whole machine via the core back. This decreases the MMF required for a given torque output, thereby increasing efficiency.

There are many excitation patterns possible with a fully pitched winding version of the five phase machine. Three of these are shown in Figure 4.5. The first two show unipolar excitation, which is possible in this machine as it has an odd number of phases. Figure 4.5(b) shows unipolar excitation of two fully pitched windings to excite three stator teeth at the same time. This produces the equivalent single tooth winding current (I1) shown in the same figure, and reveals that excitation of a stator tooth occurs for 3/5 of the electrical cycle with twice the magnitude of the fully pitched winding currents. Unfortunately, however, the direction of this equivalent single tooth current must reverse half way through its conduction period, which may well cause problems at high speed. As the equivalent single tooth excitation period is 3/5 of the electrical cycle some negative torque production is inevitable. There will, however, still be a significant reduction in copper loss for a given torque output. This can be estimated, as follows, if this situation is compared with a short pitched winding machine excited for 2/5 of its electrical cycle.

$$\frac{Loss_{FP}}{Loss_{SP}} = \frac{2 * I_{FP}{}^{2} * R_{FP}}{2 * I_{SP}^{2} * R_{SP}} \tag{4.4}$$

where $I_{SP} = 2I_{FP}$ and assuming $R_{SP} = R_{FP}$ (i.e. ignore endwinding length), then:

$$\frac{Loss_{FP}}{Loss_{SP}} = 0.25$$

The second unipolar excitation pattern shown in Figure 4.5(c) is interesting in that it produces the short flux loops that are possible in the short pitched winding machine. For example with phases A, B and C conducting, flux will circulate around stator teeth 4 and 5. Twice the current, however, is needed in the phase between the two excited teeth to do this, and therefore there is only a small benefit in terms of copper loss over the short pitched winding machine. The major problem with a five phase machine, though, is the

number of power electronic switches that are required to drive even unipolar currents into each phase.

The pattern shown in Figure 4.5(d) is one of the possible bipolar versions. The major advantage is that the equivalent single tooth winding current is four times that of the actual fully pitched winding current. This occurs for 2/5 of the electrical cycle, which is a good proportion of the positive torque region. There is some magnetisation during the negative torque producing region, but its magnitude will be small.

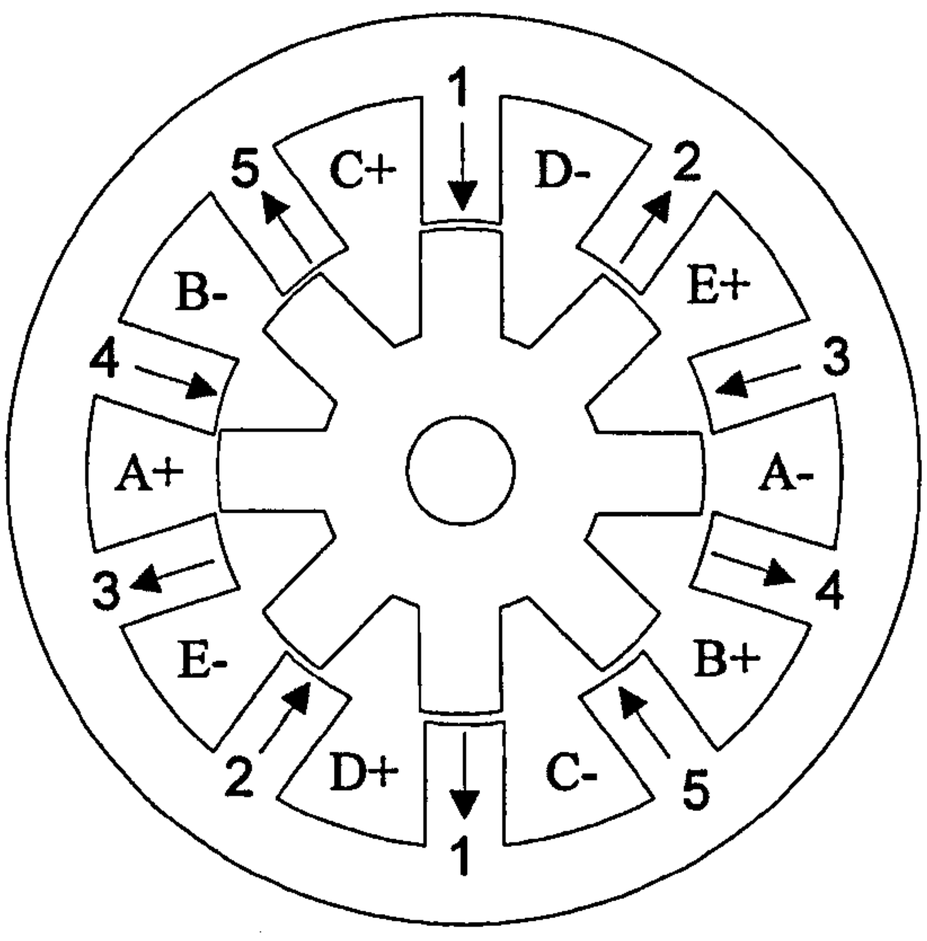

Fig.4.5(a) Winding configuration

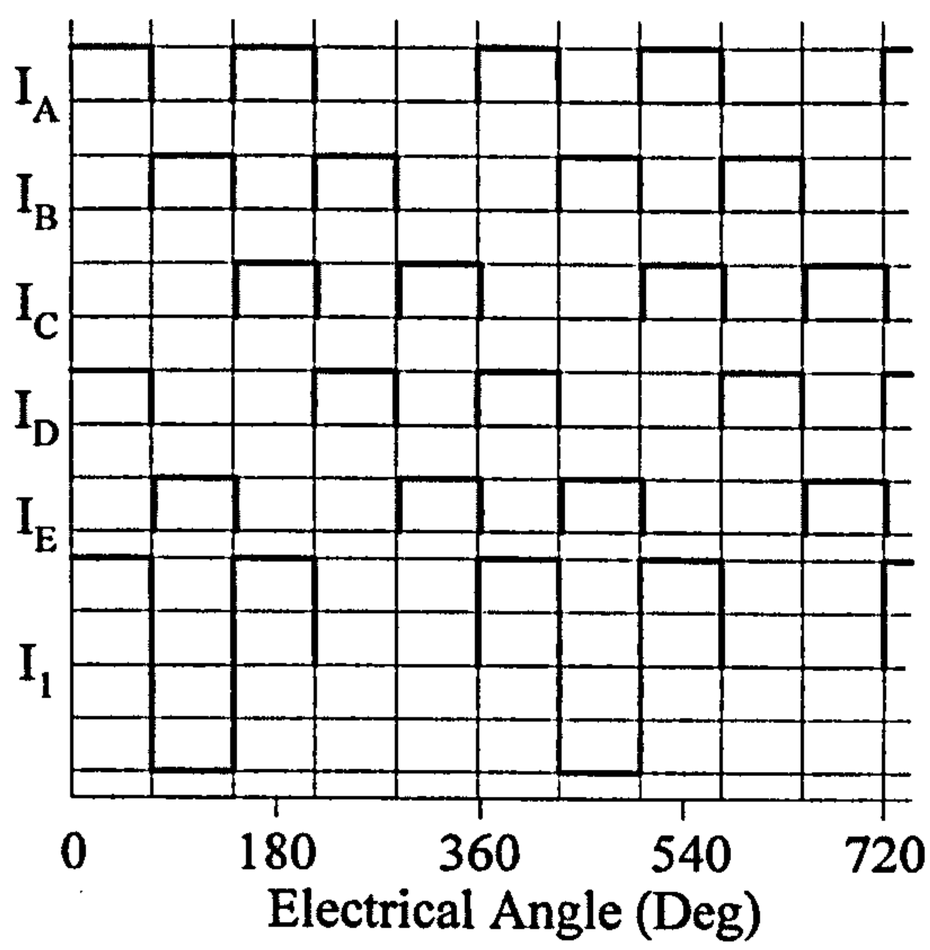

Fig 4.5(b) Triple tooth excitation

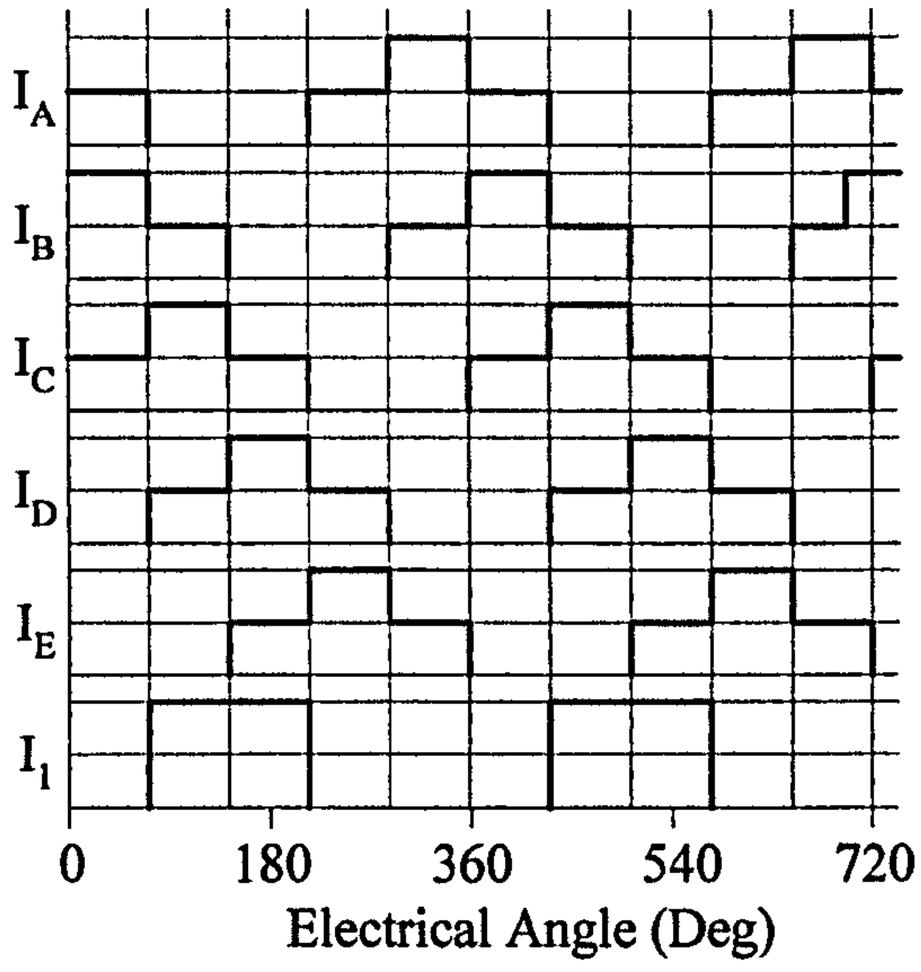

Fig.4.5(c) Double tooth excitation

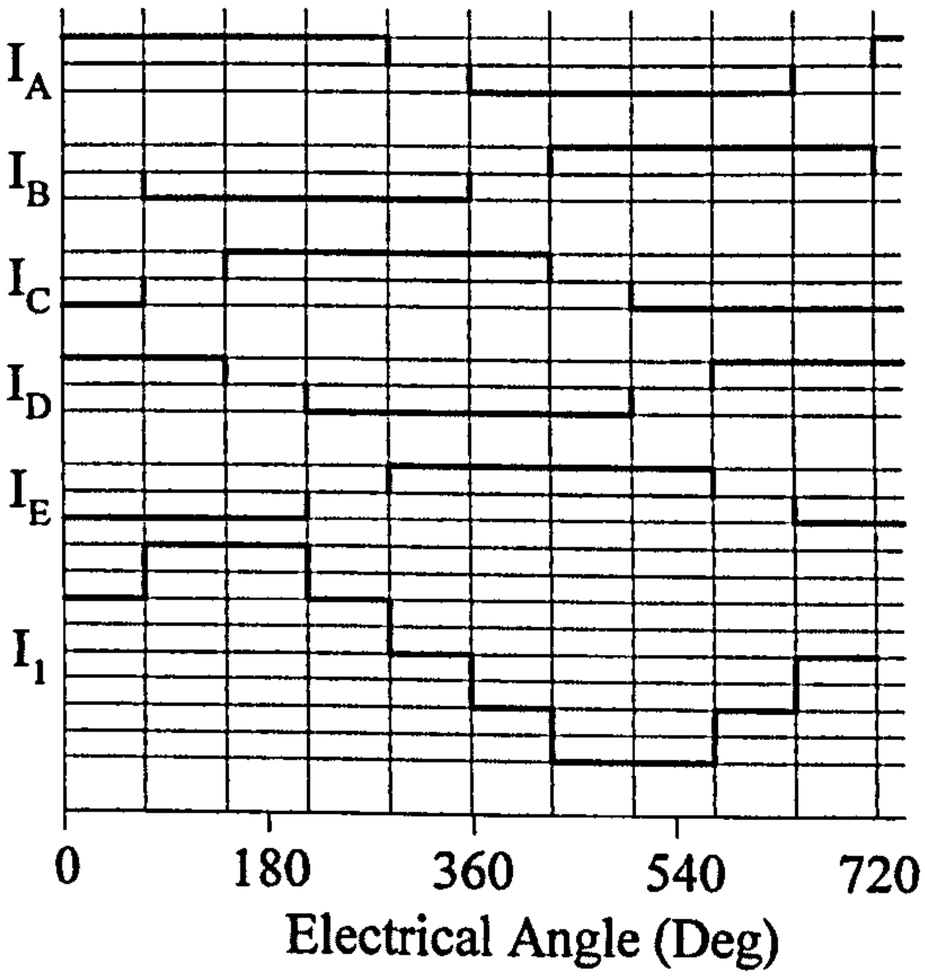

Fig.4.5(d) Multiple tooth excitation

Figure 4.5 Five phase, 10/8, fully pitched wound machine, with proposed excitation patterns. I_{ABC} = fully pitched winding currents, I_{123} = equivalent single tooth currents.

The following equation compares the losses with this excitation pattern compared to a five phase short pitch winding machine with 2 phases excited at a time:

$$\frac{Loss_{FP}}{Loss_{SP}} = \frac{4 * I_{FP}^{2} * R_{FP}}{2 * I_{SP}^{2} * R_{SP}} \tag{4.5}$$

where $I_{SP} = 4I_{FP}$ and assuming $R_{SP} = R_{FP}$, then:

$$\frac{Loss_{FP}}{Loss_{SP}} = 0.125$$

This is a similar ratio to the four phase machine, and as before, assumes no extra end winding length, and that the effect of the small negative torque production periods are insignificant. The problem, again, is the number of power electronic switches required to supply bidirectional currents to five phases. Twenty switches would be required if an 'H' bridge was used to control each phase, although the current rating of each would be substantially lower compared to a machine with a lower number of phases. As the phase currents sum to zero, however, an alternative would be to connect the phases in a star connection. This would reduce the number of switches required to 10 (5 half bridges).

4.2.1.6 Phase Number Selection

A three phase machine was selected for the prototype machine. This is because three phase is the most common machine configuration, offering full starting torque in either direction. Four phase machines cannot operate with unipolar excitation and five phase machines require too many power devices. It should be possible to optimise the machine further for operation with fully pitched windings. The machine can then be constructed and compared directly to other standard SR machines in terms of torque output for a given temperature rise.

The two phase machine deserves further research as torque per unit copper loss is good at the same time as having potentially a very low power electronic requirement. Also the four phase machine with bipolar operation should offer the highest torque per unit copper loss, but is likely to require an expensive inverter.

4.2.2 Winding Resistance Versus Pole Number and Aspect Ratio

The winding resistance for a three phase machine can be estimated using Equation 4.6, where N is the total number of turns in a phase, L_{stk} is the stack length, W_{slot} is the average slot width, 'a'and 'b'are defined in Figure 4.6.

$$R_{phase} = \frac{N\left[2L_{stk} + 4b + 2a\right]}{\sigma A} \tag{4.6}$$

Parameters 'a' and 'b' can be estimated using the following equations depending on the machine type (these equations were formulated from estimates made on typical machine geometries):

Short pitched winding machine

$$a = 2r\pi \cdot \left(\frac{40}{360}\right) \quad \text{for a 6-4 machine} \tag{4.7}$$

$$a = 2r\pi \cdot \left(\frac{20}{360}\right) \quad \text{for a 12-8 machine} \tag{4.8}$$

$$b = \frac{W_{slot}}{2} \tag{4.9}$$

Fully pitched winding machine

$$a = \frac{2r\pi}{2} \quad \text{for a 6-4 machine} \tag{4.10}$$

$$a = \frac{2r\pi}{4} \quad \text{for a 12-8 machine} \tag{4.11}$$

$$b = W_{slot} \tag{4.12}$$

A comparison of winding resistance can now be made between the fully pitched and short pitched winding machines with a 6-4 and 12-8 geometry with different stack lengths. The values shown in Table 4.1 have been calculated for a stack with an outside diameter of 150mm, and lengths of 75mm, 150mm and 300mm. The machine design described later in this Chapter has a 12-8 geometry with an outside diameter of 150mm and a length of 150mm , and so these theoretical numbers relate directly to that design.

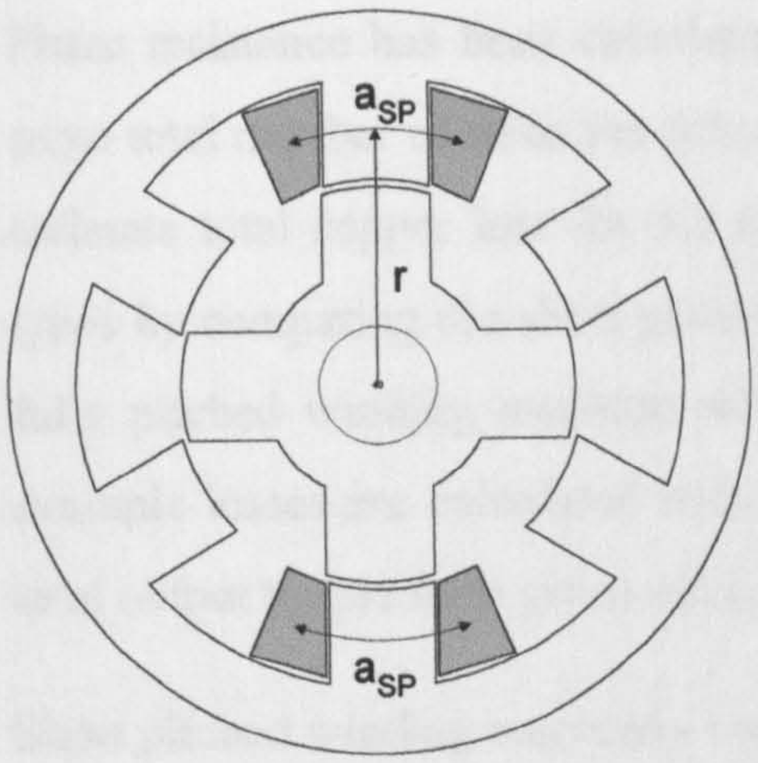

Fig 4.6(a) 6-4, short pitched winding

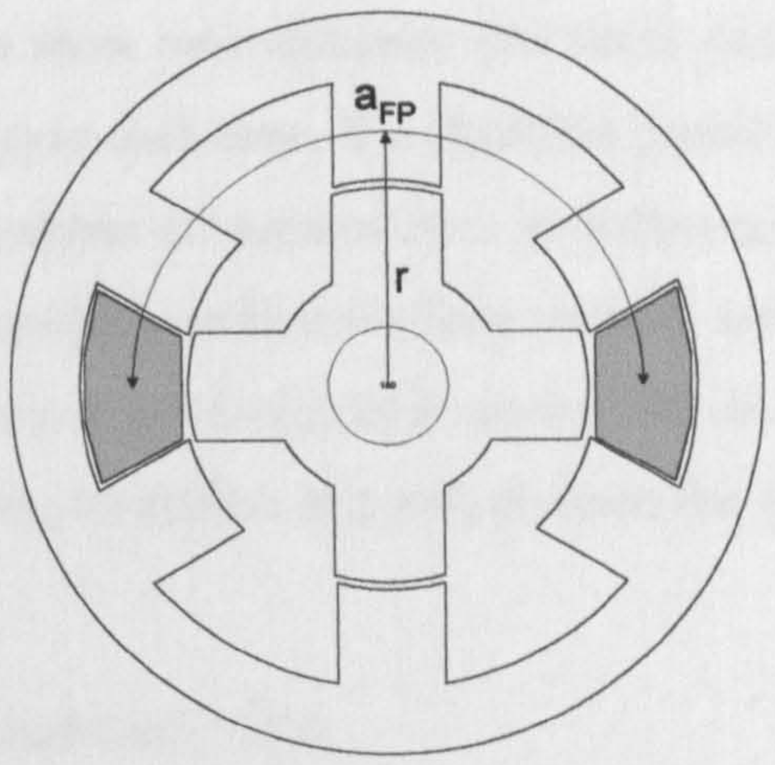

Fig 4.6(b) 6-4, fully pitched winding

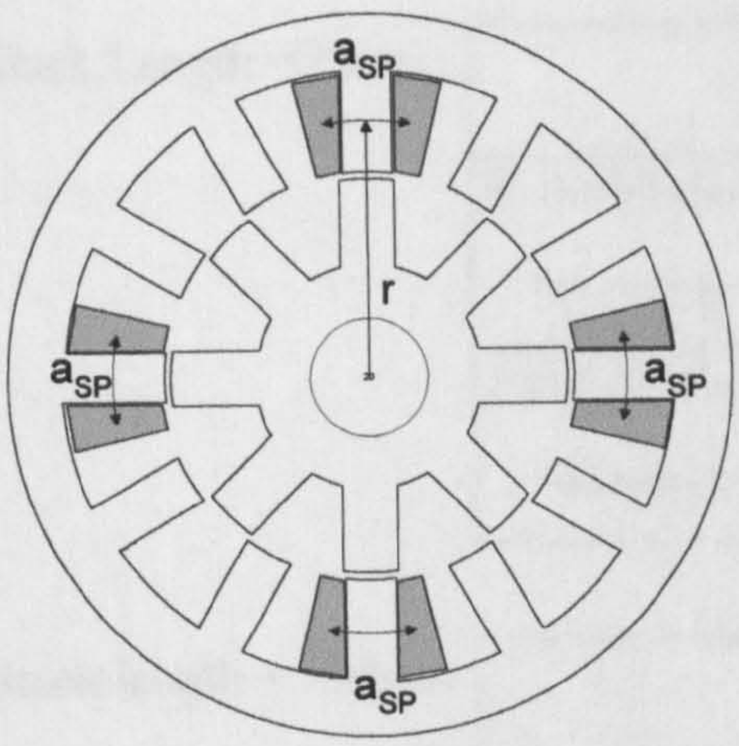

Fig 4.6(c) 12-8, short pitched winding

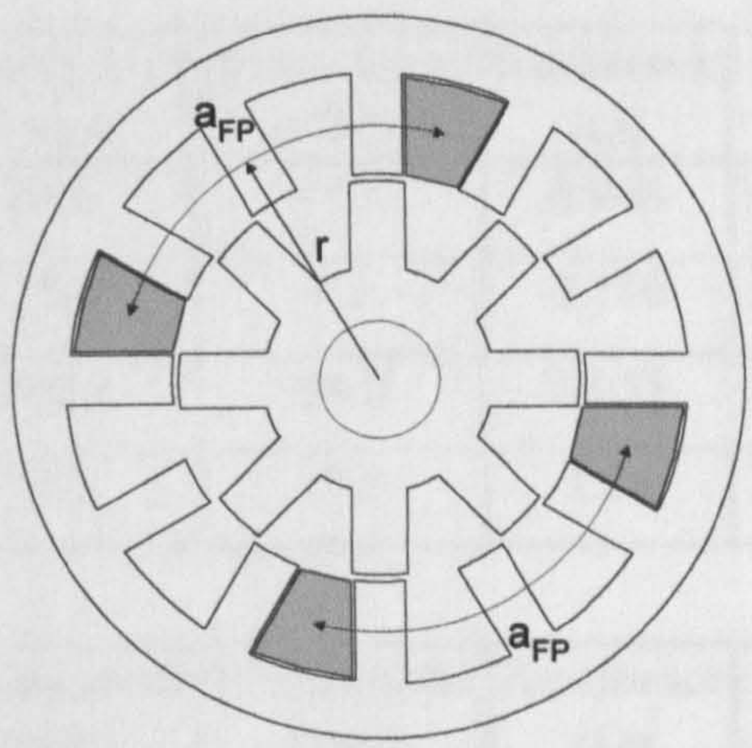

Fig 4.6(d) 12-8, fully pitched winding

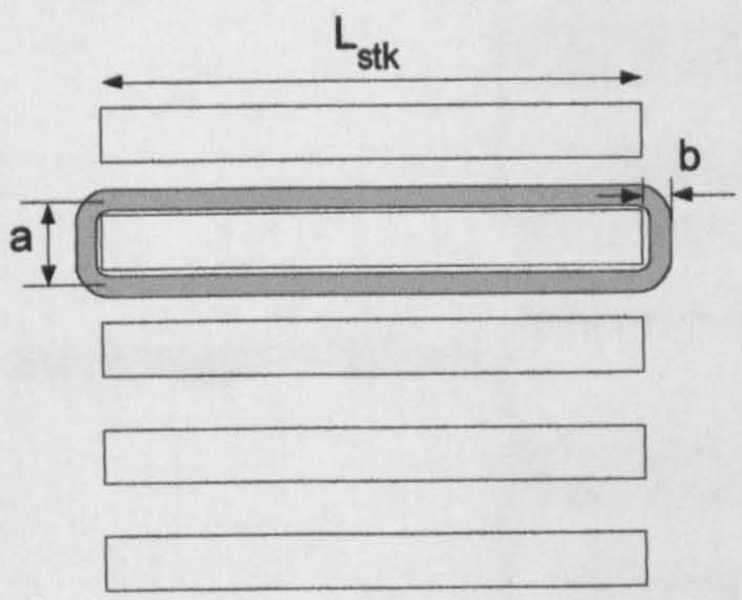

Fig 4.6(e) axial view of a short pitched Winding

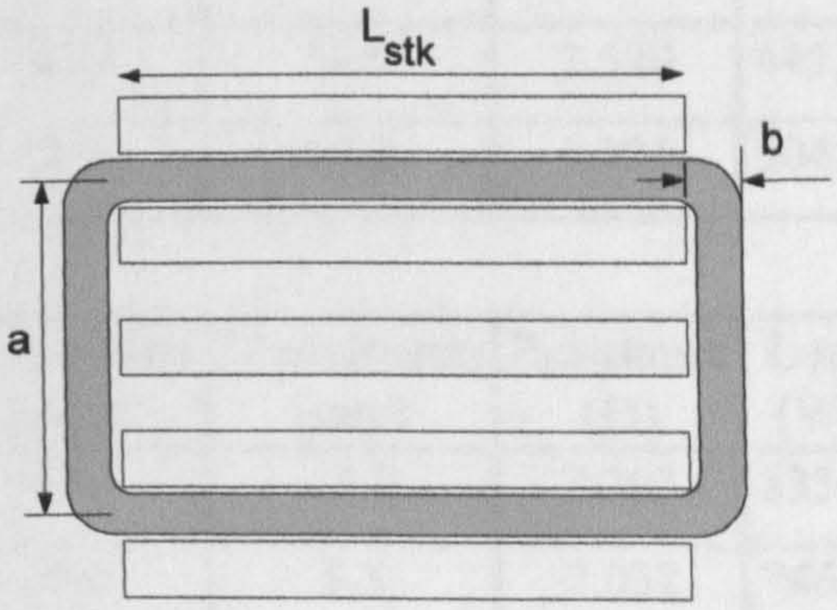

Fig 4.6(f) axial view of a fully pitched winding

Figure 4.6 Definition of parameters for winding resistance calculation.

Phase resistance has been calculated using the same wire diameter (0.85mm) and the same total number of turns per phase (102 turns) in each case. It is therefore possible to estimate total copper loss for the same total number of ampere-turns in both machine types by comparing the short pitched winding machine with one phase excited, and the fully pitched winding machine with two phases excited (unipolar excitation). In this example losses are calculated with the following excitation and will produce the same total output torque for a given stack length:

Short pitched winding machine - one phase excited with 18.8A

Fully pitched winding machine - two phases excited with 9.4A each.

Stack Length =75mm

		'a' parameter (mm)	'b' parameter (mm)	Resistance (Ω)	Loss (W)
Short Pitched Winding	6-4	47.1	17.0	0.968	342.1
	12-8	23.6	8.5	0.716	253.2
Fully Pitched Winding	6-4	188.5	34.0	2.055	363.1
	12-8	94.2	17.0	1.26	222.7

Stack length = 150mm

		'a' parameter (mm)	'b' parameter (mm)	Resistance (Ω)	Loss (W)
Short Pitched Winding	6-4	47.1	17.0	1.433	506.4
	12-8	23.6	8.5	1.181	417.5
Fully Pitched Winding	6-4	188.5	34.0	2.520	445.3
	12-8	94.2	17.0	1.725	304.8

Stack length = 300mm

		'a' parameter (mm)	'b' parameter (mm)	Resistance (Ω)	Loss (W)
Short Pitched Winding	6-4	47.1	17.0	2.203	835.1
	12-8	23.6	8.5	2.032	746.1
Fully Pitched Winding	6-4	188.5	34.0	3.142	609.6
	12-8	94.2	17.0	2.501	469.2

Table 4.1 Comparison of phase resistance with different geometries and stack lengths. Total copper loss calculated with I=18.8A for short pitched and I=9.4A for fully pitched winding machines and idealised current control. Stator outside diameter = 150mm in all cases.

Figure 4.7 shows the variation of copper loss with stack length. These figures are based on unipolar excitation with the same number of ampere-turns per tooth in each case. It is clear from these figures that the difference in losses between a short pitched and fully pitched winding machine is more marked with a 12-8 geometry, which is a consequence of the relative length of the endwinding. It can also be seen that with a 12-8 machine it becomes beneficial to use a fully pitched winding with stack lengths greater than 50mm i.e. a stack length greater than ⅓ the outside diameter. With a 6-4 machine it only becomes beneficial when the stack length is greater than ⅔ the outside diameter.

A stack length equal to the stack diameter can be considered a common aspect ratio. If a 12-8 geometry is considered, then Table 4.1 shows that the unipolar excited fully pitched winding machine has 73% of the losses of the short pitched winding machine for the same output torque. This compares with the estimate in Section 4.2.1.3 of 50%, which did not take into account the extra endwinding length of the fully pitched winding machine.

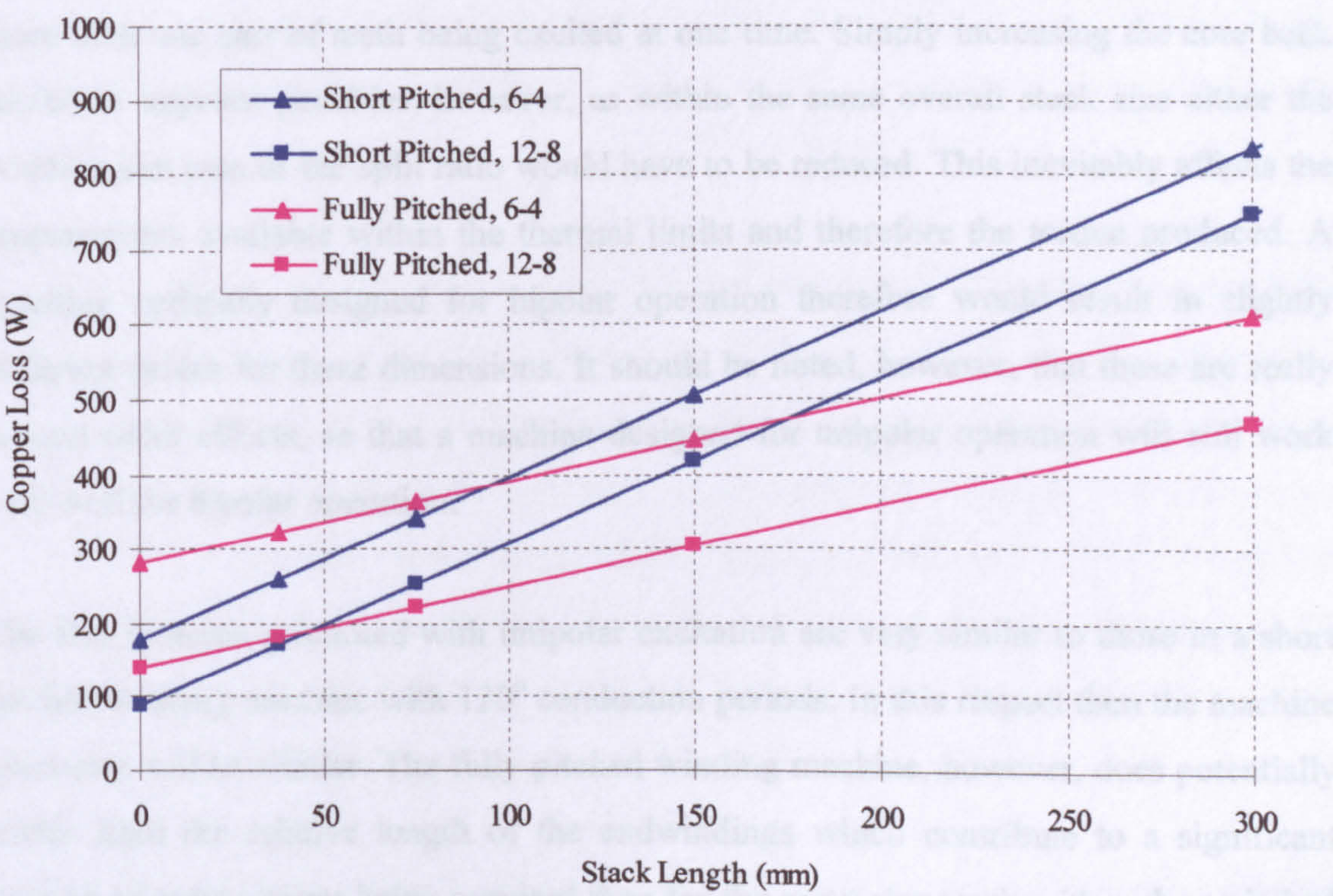

Figure 4.7 Total machine loss for the same total number of ampere-turns in the short pitched and unipolar excited fully pitched winding machine (stack OD = 150mm).

4.3 Design of a 3 Phase 12-8 SRM with Fully Pitched Windings

4.3.1 Design Aims

It was decided to design the machine primarily for unipolar operation. This is due to the fact that it seems to be the best compromise between the improvement in machine efficiency and the power electronic rating/cost. Chapter 6 - 'Performance Comparisons' will describe in more detail the tradeoffs between excitation patterns and inverter VA rating. It is necessary to either simulate or run practical tests with each inverter topology and each excitation pattern to determine both high and low speed torque output. High speed torque output may in fact differ between each arrangement, and this ultimately must be taken into account before the real inverter rating can be found.

Bipolar operation was decided to be of secondary importance. The basic difference is that higher flux density is encountered in the core back with bipolar operation due to more than one pair of teeth being excited at one time. Simply increasing the core back thickness imposes penalties, however, as within the same overall stack size either the winding slot area or the split ratio would have to be reduced. This inevitably affects the ampere-turns available within the thermal limits and therefore the torque produced. A machine optimally designed for bipolar operation therefore would result in slightly different values for these dimensions. It should be noted, however, that these are really second order effects, so that a machine designed for unipolar operation will still work very well for bipolar operation.

The flux patterns generated with unipolar excitation are very similar to those in a short pitched winding machine with 120° conduction periods. In this respect then the machine geometry will be similar. The fully pitched winding machine, however, does potentially suffer from the relative length of the endwindings which contribute to a significant amount of extra copper being required than for the same size stack with a short pitched winding. The amount of extra copper can be estimated from Table 4.1 by taking the ratio of the phase resistance values (with the same pole number and stack length). Therefore, for example, a machine with a stack length of 150mm and a stator OD of 150mm

requires 46% more copper. It would be advantageous from a cost point of view to reduce the amount of copper, as long as machine performance is not affected. Two points need to be borne in mind when comparing the amount of copper required in the short pitched and fully pitched winding machines:

1. **Reduction of fully pitched winding copper volume to force copper losses to be equal to that in the short pitched winding machine** - The amount of copper needed is greater in the fully pitched machine for the same size stack and assuming the same slot area. An analysis, however, can be done where the same slot area is assumed in both machines, but the amount of copper in the fully pitched winding machine is reduced by an amount to equalise the copper losses in both machines for the same torque output. This analysis is detailed in Appendix B. It is shown that when the losses are equalised, the ratio of fully pitched winding copper volume to short pitched winding copper volume is $\alpha^2/2$. Here, α is defined as the ratio of fully pitched winding to short pitched winding phase resistance from Table 4.1. Therefore, for example, α=1.46 for the 12-8 machine with a stack length of 150mm (and stator OD of 150mm). In this instance, then, the ratio of copper volumes in the two machines would be 1.066 for the same loss and torque output i.e. approximately the same.

   Note, however, that to equalise the losses the total cross sectional area of the fully pitched winding is reduced by the factor β (=1.37, see Appendix B). This means that the slot area could be reduced by the same factor, which would allow, for example, the stator tooth width or the split ratio to be increased. These have the effect of increasing torque for a given MMF. In this situation described, the MMF is equal in both machines, so the conclusion is that even with the same copper weight and the same copper loss, the fully pitched winding machine would still produce more torque for the same stack size.

2. **Increase of short pitched winding copper volume to that of the fully pitched winding machine** - Could the short pitched winding machine benefit by using the same amount of copper as the fully pitched winding machine (in the same size stack)? It is possible to increase efficiency by increasing the slot area and so use extra

copper to decrease current density. This is, however, at the expense of the magnetic area available, which in turn has an effect on the maximum amount of torque that can be produced within the thermal limits of the machine. These trade-offs between the electrical and magnetic aspects of the machine will be discussed in greater detail later in this chapter. The fully pitched winding machine, on the other hand, uses this 'extra' copper in a fundamentally different way, increasing efficiency significantly *at the same time* as increasing torque output from a given frame size. This is something that the short pitched winding machine cannot do with any extra amount of copper.

The major aim of this design was to optimise the fully pitched winding machine further by minimising the volume of copper without having significant detrimental impact on efficiency (at rated torque output), torque per unit copper loss, or inverter VA rating. In other words, remove some cost from the overall system. Other secondary design considerations were reduction in acoustic noise or torque ripple. The design aims are summarised below in order of importance:

1. Maximise efficiency at rated torque output for unipolar operation, thereby maximising torque output within the given frame size
2. Maximise torque per unit copper loss for unipolar operation
3. Minimise the amount of copper
4. Minimise inverter VA rating
5. Reduce acoustic noise
6. Reduce torque ripple

It was decided to use a standard induction motor frame so that direct comparisons can be made. A D100L frame was selected for this purpose.

4.3.2 Critical Dimension and Material Selection

In order to optimise the geometry of any SR machine the following dimensions should be considered.

- Tooth width to tooth pitch ratio (t/λ)
- Split Ratio (ratio of stator outside diameter to rotor outside diameter)
- Ratio of core back depth (CBD) to half of tooth width (t/2)
- Air gap (g)

Figure 4.8 defines these parameters on a typical 12-8 machine geometry. This design is, in fact, an Allen West 7.5kW SRM (with short pitched windings), and will be used in this chapter as a reference design of a typical SR machine.

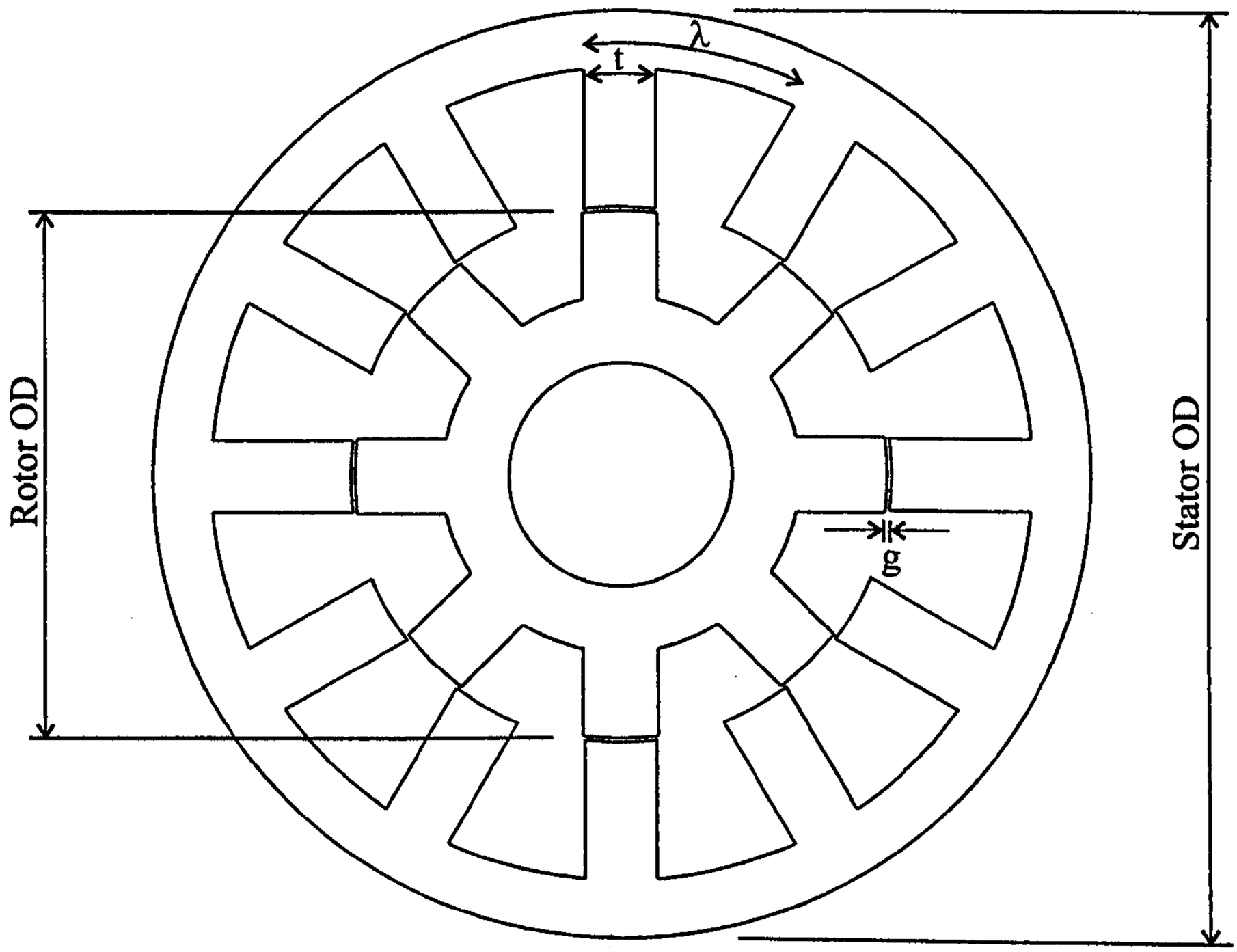

Stator OD=209.54mm, Rotor OD=120.08mm, t=16mm, CBD=13mm, g=0.37mm, L_{stk}= 193.5mm, λ=48, t=16, t/λ =0.33, CBD/(t/2) = 1.625, split ratio = 0.58.

Figure 4.8 Definition of machine dimensions on the Allen West 7.5kW SRM

Several papers have been written concerning methods of computationally determining the optimum values of each of these parameters. One such paper by Faiz and Finch [4.5] suggested optimum values for a 6-4 machine based on a relatively accurate machine model in which the complete aligned and unaligned magnetisation characteristics were calculated, thus forming the basis for determining the average torque produced. At the same time slot dimensions and hence winding resistance could be estimated, based on the basic dimensions. As both the magnetic and electrical loading were considered at the same time, the trade-offs between the available ampere-turns and the reluctance of the core could be established e.g. if the stator tooth or core back depth was widened with the aim of increasing the magnetisation of the aligned curve, then the available slot area for the winding must be reduced (assuming the same split ratio). For the same number of turns the wire diameter must be reduced to fit in the slot, resistance increased, and so the current must be reduced for the same temperature rise.

The paper suggested three basic criteria as a means of optimising the machine - maximisation of torque (taking into account the slot area available for the winding), maximum torque per unit copper loss and efficiency. The latter took high speed performance into account and included iron loss. One of the most critical dimensions is the ratio between tooth width and tooth pitch, t/λ. The paper found that t/λ should be in the range 0.33 - 0.40 to maximise torque production capability in the machine, but to maximise torque per unit copper loss it should be in the range 0.27-0.30. For maximum efficiency it should be in the range of 0.25 to 0.35. The recommended value was between 0.35 and 0.40 as the best compromise to maximise both torque production and efficiency.

Varying the split ratio (the ratio of rotor outside diameter and stator outside diameter) had an effect similar to t/λ in that increasing it produced more torque for the same ampere-turns. Slot area, however, was reduced at the same time, meaning that the number of ampere-turns available was reduced. To maximise torque per unit copper loss the split ratio should be between 0.42 and 0.5. To purely maximise electromagnetic torque capability, however, it should be as large as practically possible. The paper suggested a split ratio of 0.57 to 0.63 as the optimal range for maximum torque production and maximum torque per unit copper loss.

The core back depth was optimised in a similar way. The recommended ratio of CBD to t/2 was in the range 1.1 to 1.3. Again this was the best compromise between torque production and torque per unit copper loss, but took no account of acoustic noise.

The last important dimension was the air gap, g. The smaller the air gap the more torque could be produced, so in practice it is mechanical considerations that form the determining factor.

The emphasis in this design is to eliminate as much copper as possible, therefore t/λ, CBD to t/2 ratio and split ratio need to be set towards the upper end of the suggested ranges. To achieve a t/λ of around 0.4, say, would mean widening the stator teeth compared to the Allen West design shown in Figure 4.8. Widening the tip of the stator tooth, however, has an impact on the unaligned inductance as the rotor teeth would be closer to the stator teeth in this situation. It also affects the shape of the torque versus angle curves. To avoid this, the tooth is tapered so that it is 30% wider at the base of the tooth compared to the tip. The shape of the torque versus angle curve, therefore, remains the same, but the tooth reluctance is minimised. Miller [4.6] referred to the use of taper teeth to minimise tooth reluctance and concentrate the MMF drop across the air gap. There are several other advantages of using a tapered tooth, and these are summarised as follows:

- The mechanical strength of the lamination is increased, mainly in the lateral direction. This is improved further if the corner between the base of the tooth and the core back has a radius. This may improve acoustic noise, as one noise source in a SR machine is the deformation of the lamination as torque is produced in a stator pole.
- The shape of the slot becomes more square shaped, making winding insertion easier.
- The slot area is reduced (as desired) without affecting the shape of the torque/angle curve.

The same tapering can be applied to the rotor tooth as a means of lowering the reluctance of the circuit in the aligned position as the effective tooth width increases. The effects of tapering the stator and rotor teeth can be seen with the aligned and unaligned flux linkage curves shown in Figure 4.9. These curves are the result of finite

element analysis using the 2D magnetostatic software that had already been developed in the Electric Machines and Drives Group at Newcastle University. 2D analysis means no account is taken of end effects. The basic geometry shown in Figure 4.8 is used with a short pitched winding of 61 turns and a stack length of 193mm. When tapering of the teeth is used, the tip is maintained at the same width and the base is widened by 33%. So the stator tooth tip width is 16mm and base width 21.3mm.

Figure 4.9 shows that the tapering of the teeth does indeed increase magnetisation for the same number of ampere-turns, and this effect only occurs in the region of saturation of the iron. The unaligned curve is unaffected and therefore torque output will be increased (assuming the same number of ampere-turns).

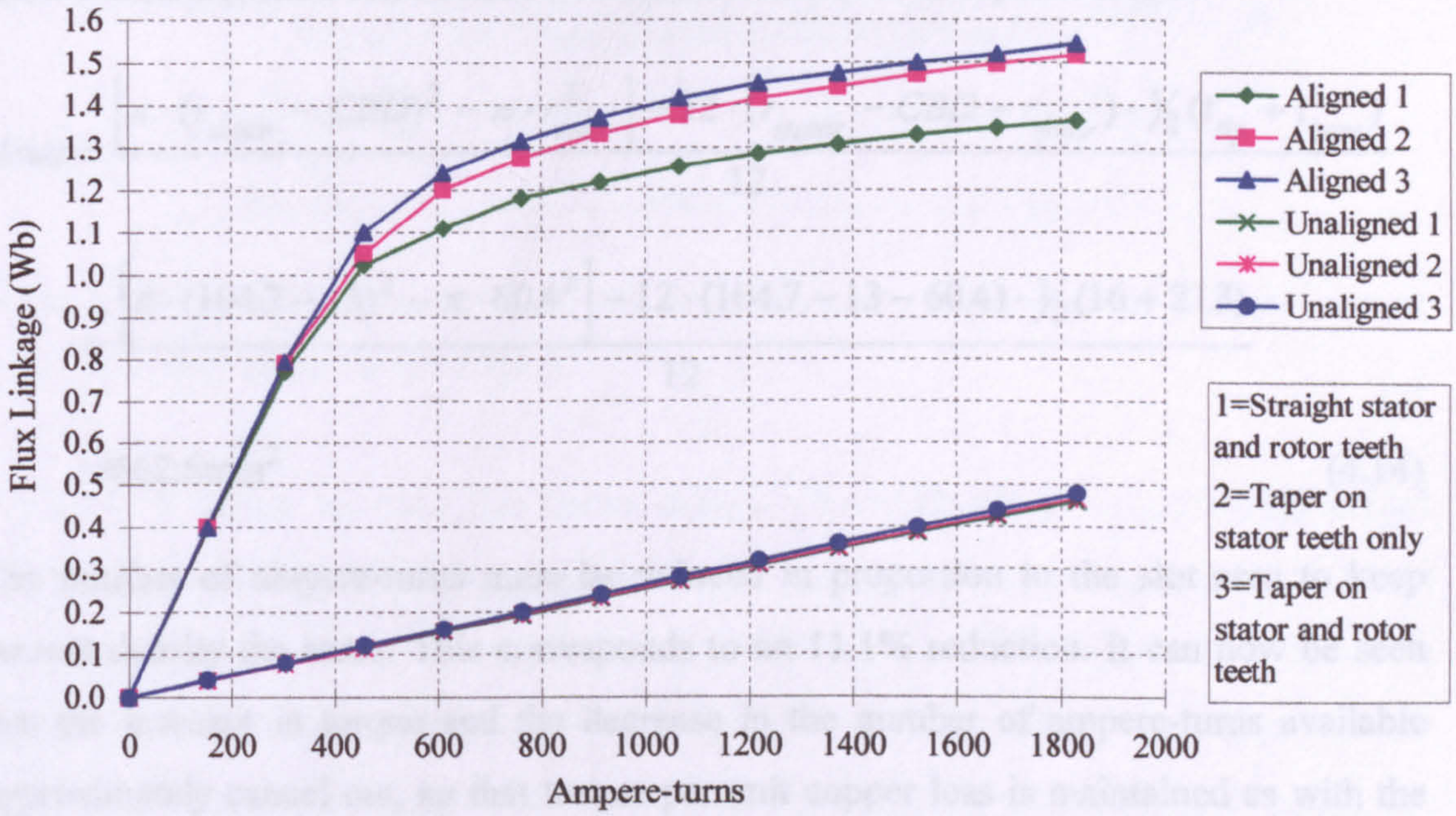

Figure 4.9 Aligned and Unaligned flux linkage curves for the 7.5kW AllenWest machine with different shaped stator and rotor teeth (all other conditions the same)

The area enclosed by the aligned and unaligned flux linkage curves is directly proportional to the amount of torque obtainable (Chapter 3 discussed how torque can be derived from the flux linkage/current/position data using co-energy). It is therefore straightforward to calculate the extra amount of torque obtainable with the tapered teeth by calculating the area enclosed between the two curves up to the number of ampere-turns the machine is operated at. For this machine approximately 1250 ampere-turns should correspond to rated output. Therefore by tapering the teeth an extra 11.9% torque

is available for the same number of ampere-turns. The effect of the tapering on the available slot area now needs to be analysed. The following equation can be used to estimate the slot area with straight teeth:

$$Area = \frac{\left[\pi \cdot (r_{stator} - CBD)^2 - \pi \cdot r_{rotor}^2\right] - 12 \cdot (r_{stator} - CBD - r_{rotor}) \cdot t}{12}$$

$$= \frac{\left[\pi \cdot (104.7 - 13)^2 - \pi \cdot 60.4^2\right] - 12 \cdot (104.7 - 13 - 60.4) \cdot 16}{12}$$

$$= 745.5\text{mm}^2 \qquad (4.13)$$

and a similar equation can be used to estimate slot area with tapered teeth:

$$Area = \frac{\left[\pi \cdot (r_{stator} - CBD)^2 - \pi \cdot r_{rotor}^2\right] - 12 \cdot (r_{stator} - CBD - r_{rotor}) \cdot \tfrac{1}{2}(t_{tip} + t_{base})}{12}$$

$$= \frac{\left[\pi \cdot (104.7 - 13)^2 - \pi \cdot 60.4^2\right] - 12 \cdot (104.7 - 13 - 60.4) \cdot \tfrac{1}{2}(16 + 21.3)}{12}$$

$$= 662.6\text{mm}^2 \qquad (4.14)$$

The number of ampere-turns must be reduced in proportion to the slot area to keep current density the same. This corresponds to an 11.1% reduction. It can now be seen that the increase in torque and the decrease in the number of ampere-turns available approximately cancel out, so that torque per unit copper loss is maintained as with the original design using straight teeth. The advantage is that the amount of copper needed is significantly reduced without apparently affecting performance.

Design for a D100L frame size

The fundamental principles of how to minimise the amount of copper required have been established and they can now be applied to the D100L frame size.

The dimensions of the D100L frame are shown in Figure 4.10. The inside diameter of the frame is 152mm and the length of the main body is 180mm. A sensible stack length,

therefore, is around 150mm. This leaves more than enough room to accommodate the endwindings.

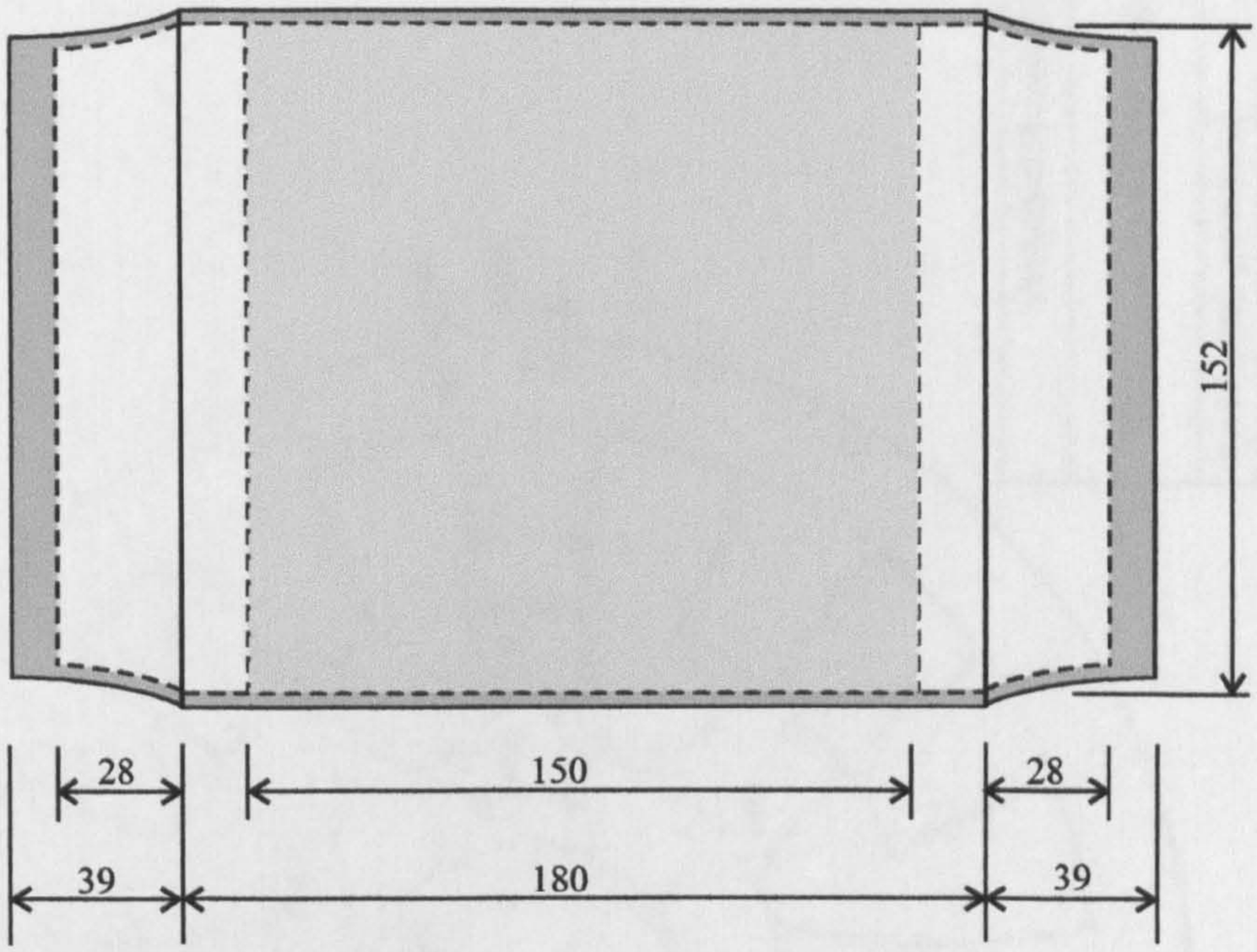

Figure 4.10 Basic dimensions of the D100L frame shown with a 150mm length stack (shown without cooling fins and terminal box).

Figure 4.11 shows the final lamination design. The tooth design is essentially scaled from the tapered tooth design discussed on the 7.5kW Allenwest machine. The stator tooth tip is 12.05mm wide and the base width 16mm. The average tooth width is therefore 14mm, which corresponds to a t/λ of 0.407. A 3mm radius is added at the base of the teeth to give extra mechanical strength. The tooth tip also contains a 'tang', the main purpose of which is location of a wedge to hold the winding in place. It does, however, have a slight effect on the flux linkage curves, as shown in Figure 4.12. The unaligned curve is raised slightly as in this position the tang shortens the gap between the stator and rotor teeth slightly, at a time when they should be as far apart as possible. In the aligned position, mainly under lower MMFs, the curve is again slightly higher. This is thought to be due to the larger stator to rotor surface area in this position, reducing the MMF drop across the air gap. The two effects essentially cancel each other out.

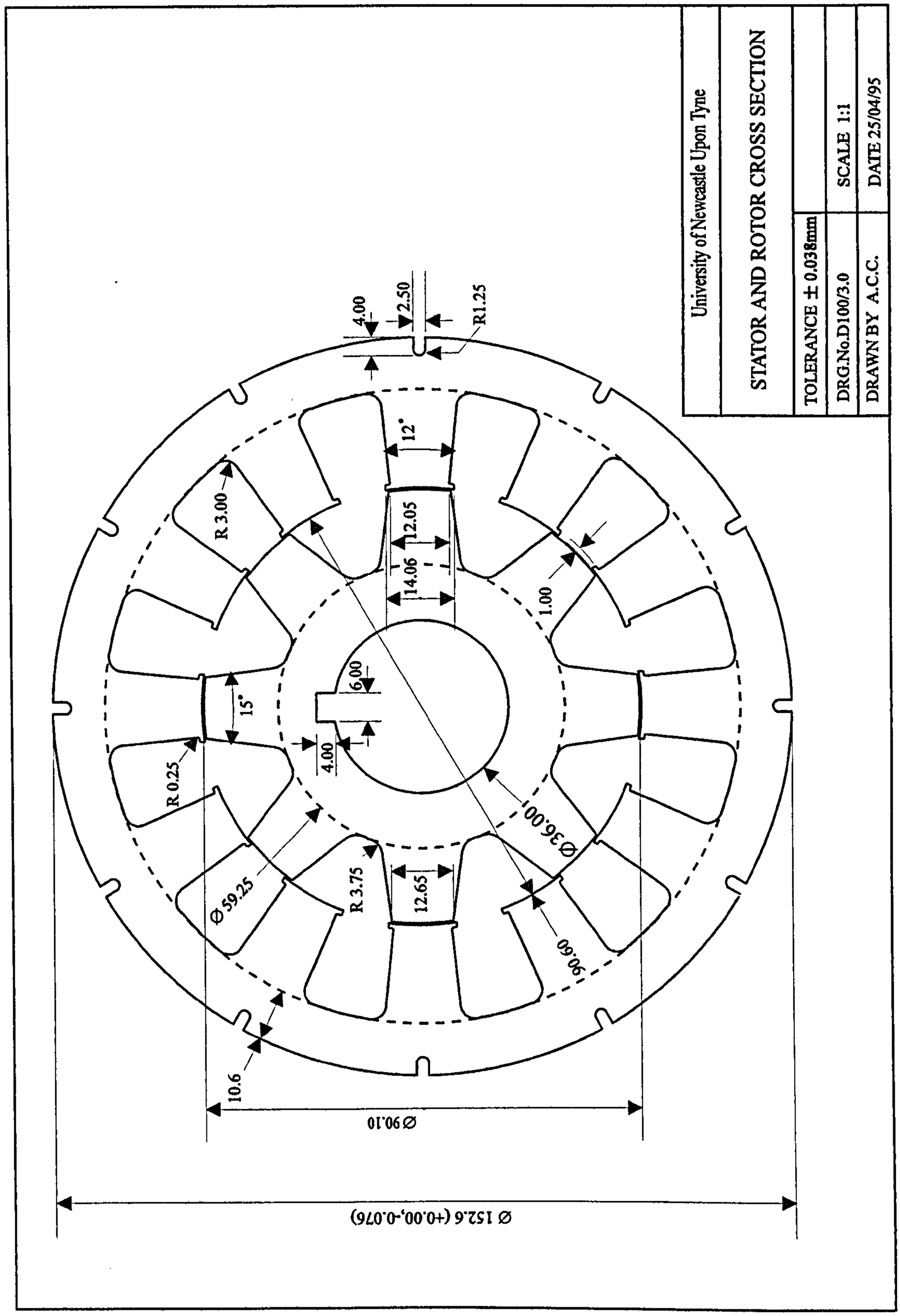

Figure 4.11 Stator and rotor design for the D100L frame. Dimensions shown in mm.

The rotor teeth are designed in a similar way to the stator teeth, with the tip maintained at its normal width and the base widened by 33% to lower the reluctance, as indicated in

Figure 4.9. The split ratio is set to 0.594, and the core back depth 10.6mm. This gives a CBD/(t/2) ratio of 1.51, if the average tooth width is assumed. This is more than the 1.1 to 1.3 recommended by Faiz and Finch [4.5], however it is advantageous to set it higher than this theoretical value for two reasons:

- A thicker core back will lead to a mechanically stiffer design and should result in less acoustic noise.
- It will allow better operation with bipolar operation, where the flux densities in this region are higher than with unipolar excitation.

Twelve slots are placed in the core back (see Fig.4.11) to accommodate bolts that run axially down the whole length of the stack to hold the laminations together. According to the FE analysis these slots should have very little effect on the electromagnetic design. On the rotor lamination a keyway is used to locate it onto the rotor shaft. The rotor laminations are then held in place axially by two rotor endcaps.

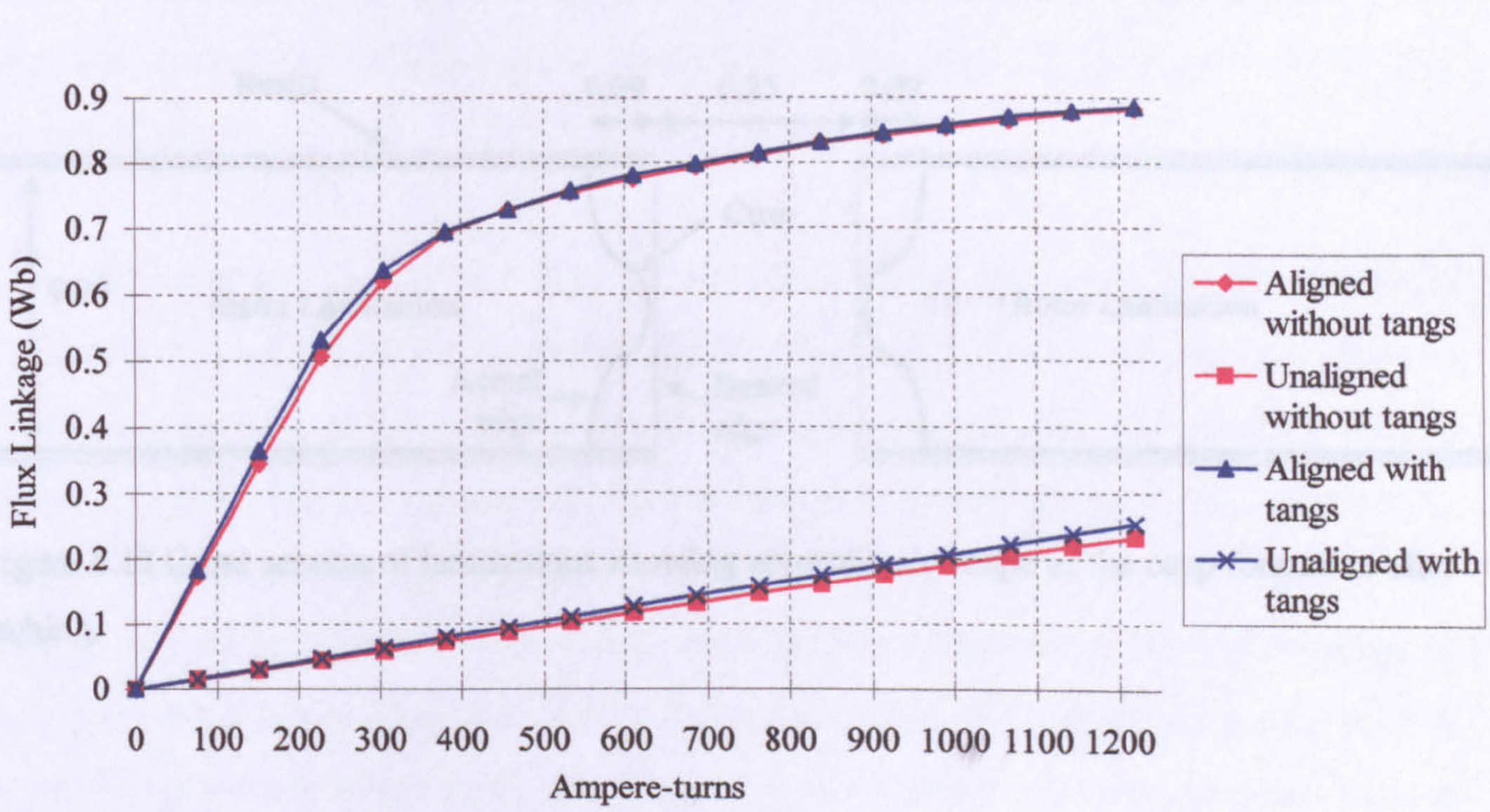

Figure 4.12 Aligned and Unaligned flux linkage curves for the 3kW D100L machine showing the effect of the tangs. (The rotor is not tapered with these results).

The air gap is set to 0.25mm. As discussed earlier in the chapter this number should be as small as possible, but is ultimately set by mechanical considerations, such as the

tolerances associated with eccentricity of the rotor/bearing assembly. This size of air gap is thought to be acceptable for a machine of this frame size.

Transil 335 material is used for the lamination material. This is 0.35mm thick and has low iron loss compared to other materials such as Newcore or Losil and is therefore more appropriate for this 12-8 machine with its higher electrical frequency. It is, however, a high cost material, which may make it prohibitive for some applications. Newcore has the advantage of higher permeability (which should lower copper loss), and Losil is a compromise between the two. The laminations can be manufactured to the required shape by several techniques such as laser cutting, stamping or etching. The latter proved to be the most cost effective for the small number being made. The basic tolerances of this process are very good at +/-0.04mm, however it should be remembered that the etching process does not lead to an even finish on the edge of the lamination. A cusp formation is left as the outside material is dissolved before the centre (see Figure 4.13). The height of this cusp is approximately one quarter of the lamination thickness.

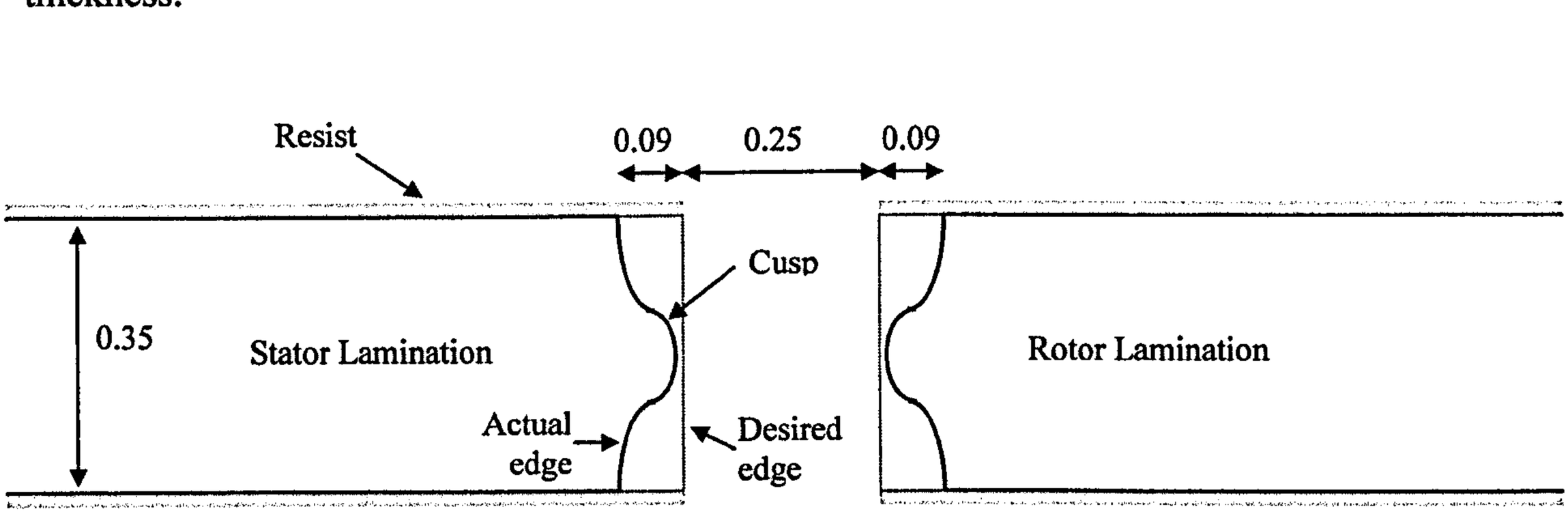

Figure 4.13 Cross section of laminations showing approximate shape of the cusp formation after etching.

4.3.3 FEA modelling and ψ/i Characteristics of the Final Machine

For the purposes of simulation, flux linkage values are required over a range of rotor positions and MMFs. Some examples of the FEA modelling required to calculate this are shown in Figure 4.14. FEA software developed within the Electrical Machines and Drives Group at Newcastle University was used. Jack e*t al* [4.7] described the software, which considerably speeds up the process by automating the mesh preparation and boundary source. Figure 4.14 shows the lines of flux at various rotor positions. Symmetry is used to reduce the amount of modelling required, so that in the aligned and unaligned positions only one eighth of the machine needs to be modelled. At all other positions one quarter of the machine needs to be modelled.

The rotor was moved in steps of 30° (electrical) from the aligned to the unaligned position, and the current in steps of 76.25 ampere-turns from 0 to 1220 ampere-turns. The complete set of flux linkage data generated from FEA is shown in Figure 4.15.

Once the flux linkage data had been generated it was input into the simulation software (that was described in Chapter 3) to check the performance of the machine with fully pitched windings.

It should be noted that all the flux linkage data that is presented in this chapter is calculated for a short pitched winding machine i.e. a machine in which each phase is electromagnetically independent from each other with no mutual coupling effects between phases. This is necessary, as the simulation needs this data to solve for the fully pitched winding currents. It works by first converting real (fully pitched winding) flux linkage into the equivalent single tooth MMF and flux linkages, so that decoupling of the phases takes place. The 'short pitched' flux linkage/current/angle data is then used to solve for equivalent single tooth currents, and these currents are then converted back to the real phase currents. This method of decoupling the phases before solving for the currents makes simulation of the fully pitched winding machine, with its mutually coupled windings, very much easier.

The simulation was used to determine the exact number of turns needed to produce the rated power output of 3kW at 1500rpm (i.e. a torque of 19.1Nm). The simulation allows for easy adjustment of the number of turns by use of a 'winding turns factor' to adjust the scaling on the flux linkage/current data. Once an adjustment has been made the simulation produces the torque-speed envelope of the machine for a fixed current demand and DC link voltage. The advance and conduction angles are automatically optimised for maximum torque production at each speed setting. This determined that 184 series turns are needed in each slot for a fully pitched machine.

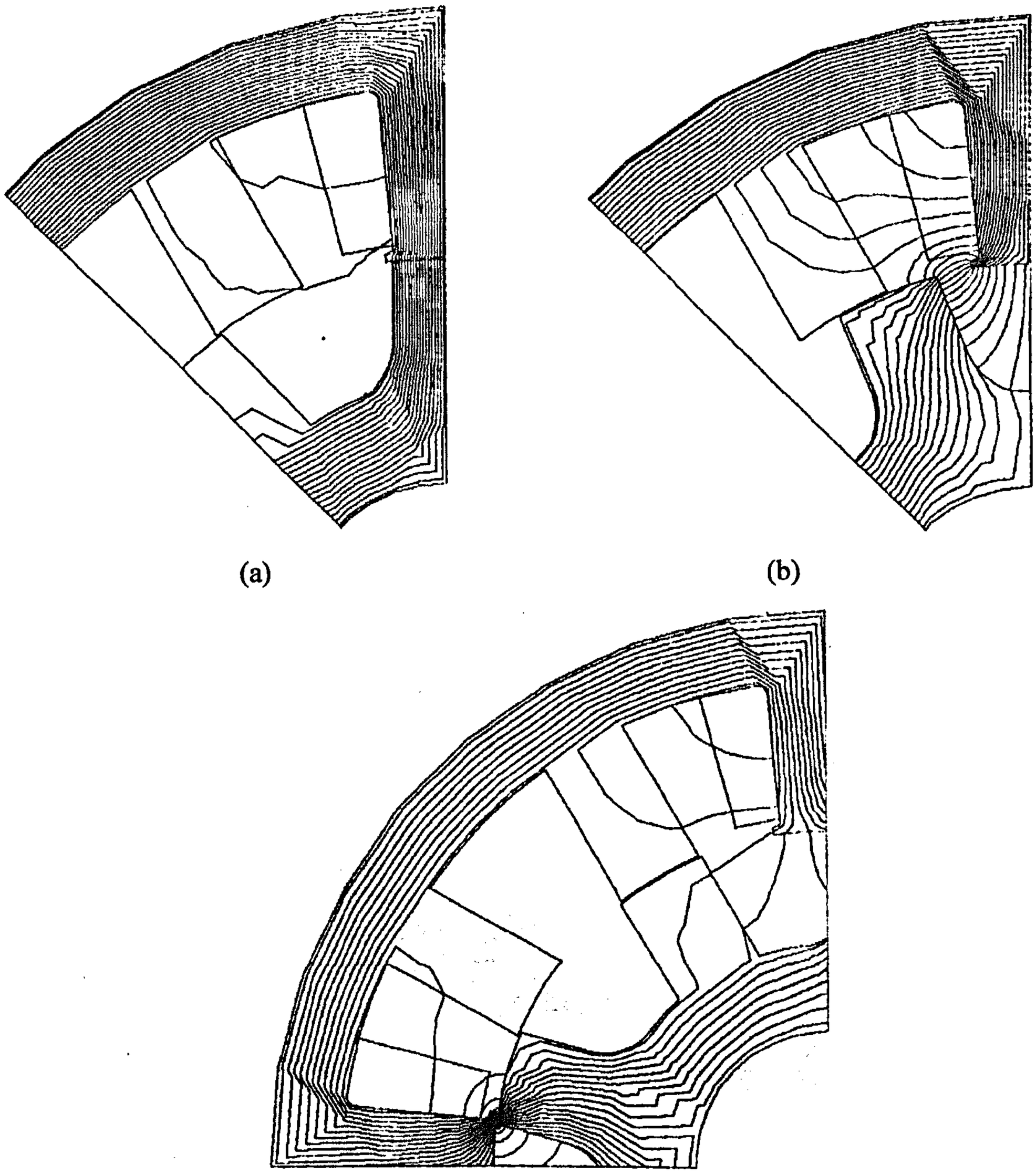

Figure 4.14 FE calculation of flux lines in the new machine design at different rotor positions - (a) aligned, (b) unaligned and (c) 120° electrical (15° mechanical) from aligned position.

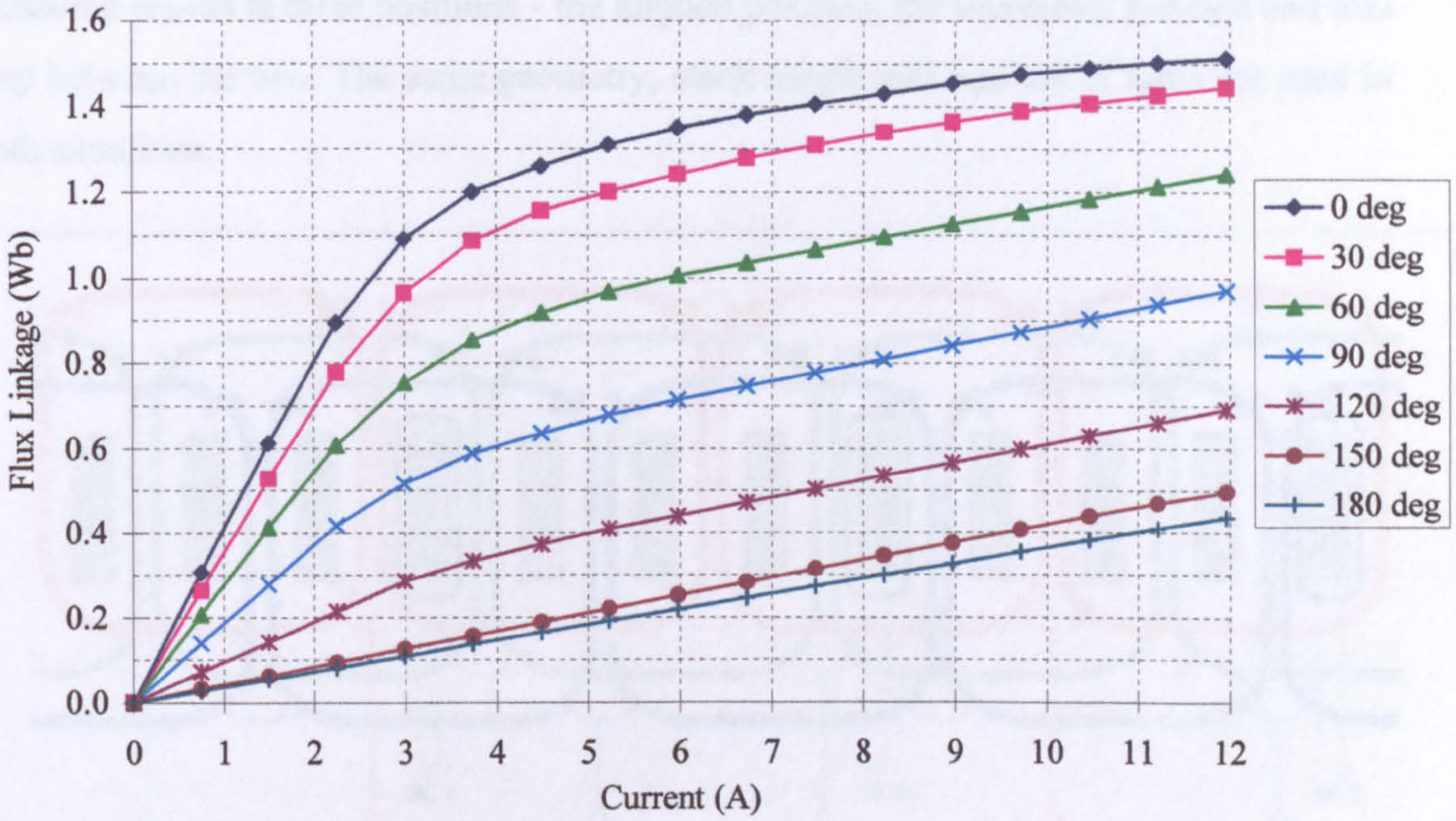

Figure 4.15 Complete flux linkage/current/angle curves for the prototype machine generated from FE. Number of series turns per slot = 102, stack length =150mm. Angular positions are in electrical degrees, with 0 degrees being the aligned position.

It was decided to wind the fully pitched winding as a double layer winding as shown in Figure 4.16 as this makes the endwinding easier to arrange as it comes out of the slot. In the 12-8 machine this means 4 separate coils. Two parallel paths were then chosen. Thus if 92 series connected turns are needed in each slot, then each of the four coils requires 92 turns.

The available slot area was calculated to be 289mm^2. This is defined as the area of the slot from the core back up to the tang. If a fill factor of 0.4 is assumed then a wire of diameter 0.89mm is required. The nearest wire size to this is 0.85mm, therefore when the calculations are reversed this corresponds to 102 turns per coil being possible. The fact that 102 turns are used instead of the desired 92 means that the base speed of the machine will be reduced from 1500rpm by that ratio. With this size wire and number of turns the fill factor remains at 0.4.

The flux linkage data generated from FEA in Figure 4.15 was calculated using 102 turns per coil. After the machine had been constructed flux linkage measurements were made using the method described in Appendix A. Figure 4.17 compares the theoretical and the

measured results at three positions - the aligned position, the unaligned position and mid way between the two. The same geometry, stack length and number of turns are used in both situations.

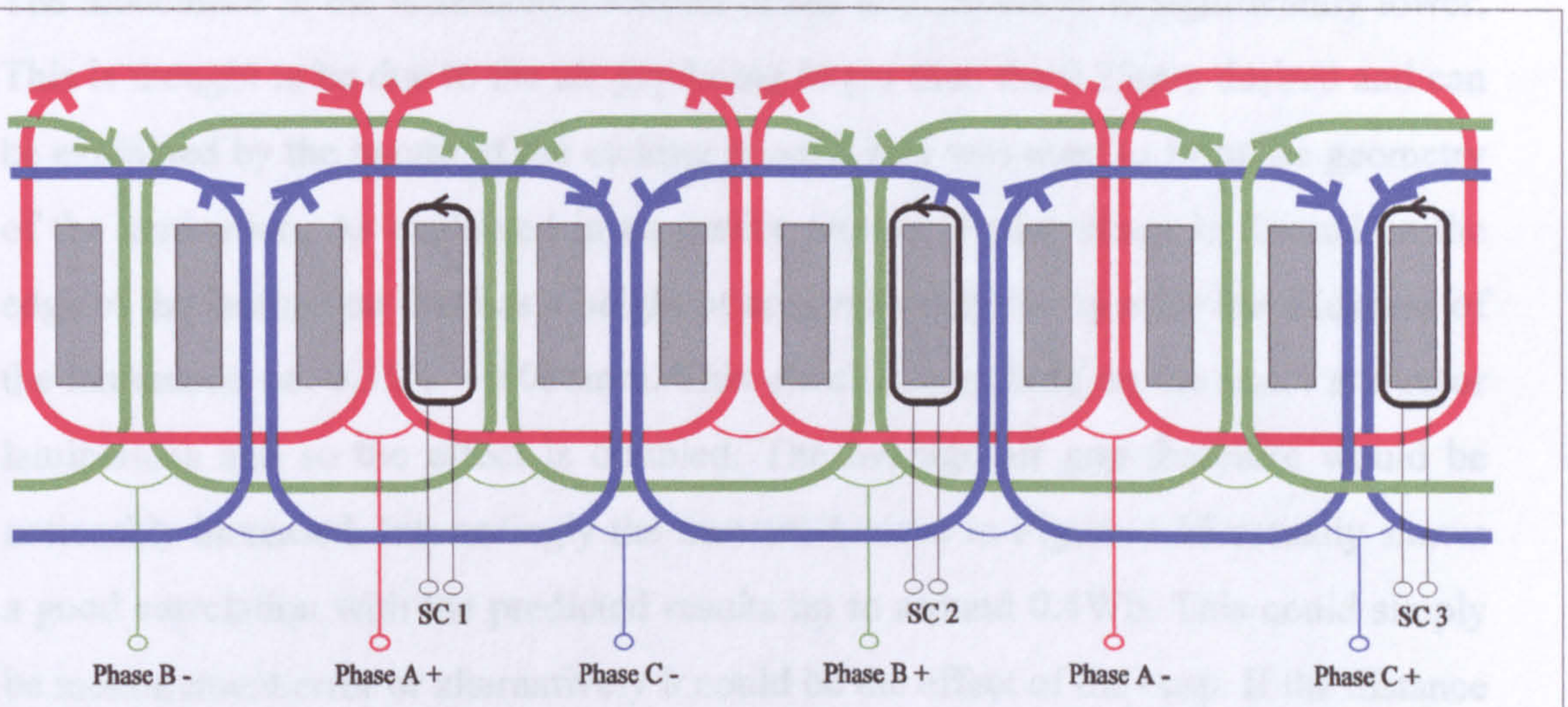

Figure 4.16 Winding arrangement of the fully pitched machine shown on the 'rolled out' stator.

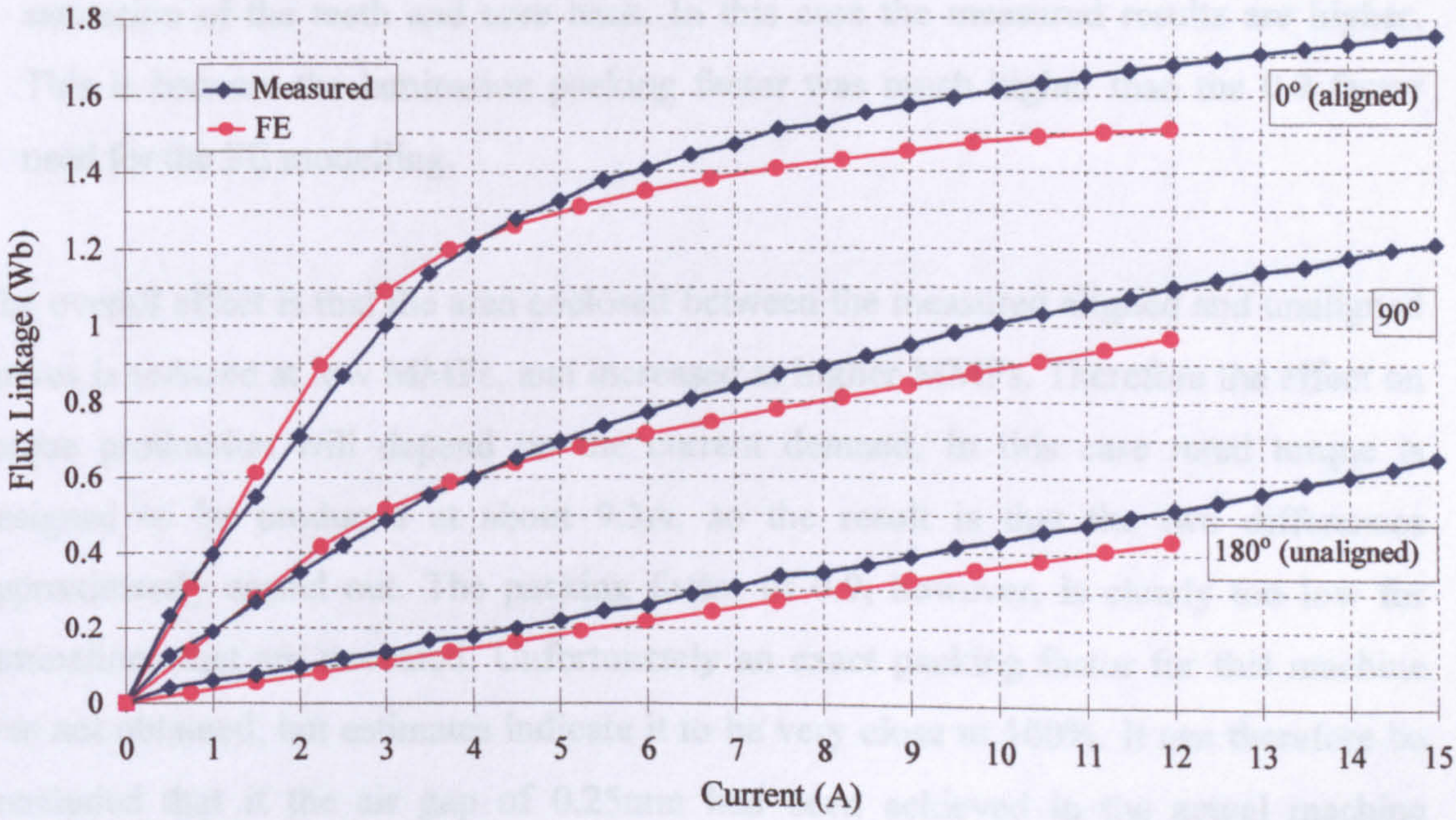

Figure 4.17 A comparison of measured and FE generated flux linkage/current characteristics for the prototype machine. Number of series turns per slot = 102, stack length =150mm.

The differences between the two sets of results are thought to be due to the following:

- The unaligned inductance is higher in reality due to the end winding leakage effects and the fact that the 2D FE modelling cannot take this into account.
- The inductance in the unsaturated section of the aligned curve is significantly lower. This is thought to be due to the air gap being larger than the 0.25mm desired and can be explained by the nature of the etching process that was used to form the geometry of the lamination. As explained in an earlier section, a cusp shape is formed on the edge of the lamination that has a height of approximately one quarter the thickness of the lamination i.e. 0.35/4 = 0.088mm. This effect is seen both on the stator and rotor laminations and so the effect is doubled. The average air gap therefore would be noticeably increased. Interestingly the measured curve in Figure 4.16 actually shows a good correlation with the predicted results up to around 0.4Wb. This could simply be measurement error or alternatively it could be the effect of the cusp. If the distance between the tip of the cusp on the stator and that on the rotor produces the correct air gap of 0.25mm, then this would produce the correct aligned curve up until the point the cusp section becomes heavily saturated. The effective air gap would then increase, resulting in the difference between the measured and theoretical curves.
- There is a difference between the measured and theoretical results in the region of saturation of the teeth and core back. In this case the measured results are higher. This is because the lamination packing factor was much higher than the 0.9 factor used for the FE modelling.

The overall effect is that the area enclosed between the measured aligned and unaligned curves is reduced at low MMFs, and increased at higher MMFs. Therefore the effect on torque production will depend on the current demand. In this case rated torque is designed to be produced at about 9.3A, so the result is that the two differences approximately cancel out. The packing factor of 0.9, however, is clearly too low for laminations that are uncoated. Unfortunately an exact packing factor for this machine was not obtained, but estimates indicate it to be very close to 100%. It can therefore be concluded that if the air gap of 0.25mm had been achieved in the actual machine together with this high packing factor, then more torque could have be produced. Note that there was no turning or grinding of the rotor outside diameter or the stator bore,

which would have helped to improve the air gap. Figure 4.18 shows a photograph of the constructed machine with the rotor removed for clarity.

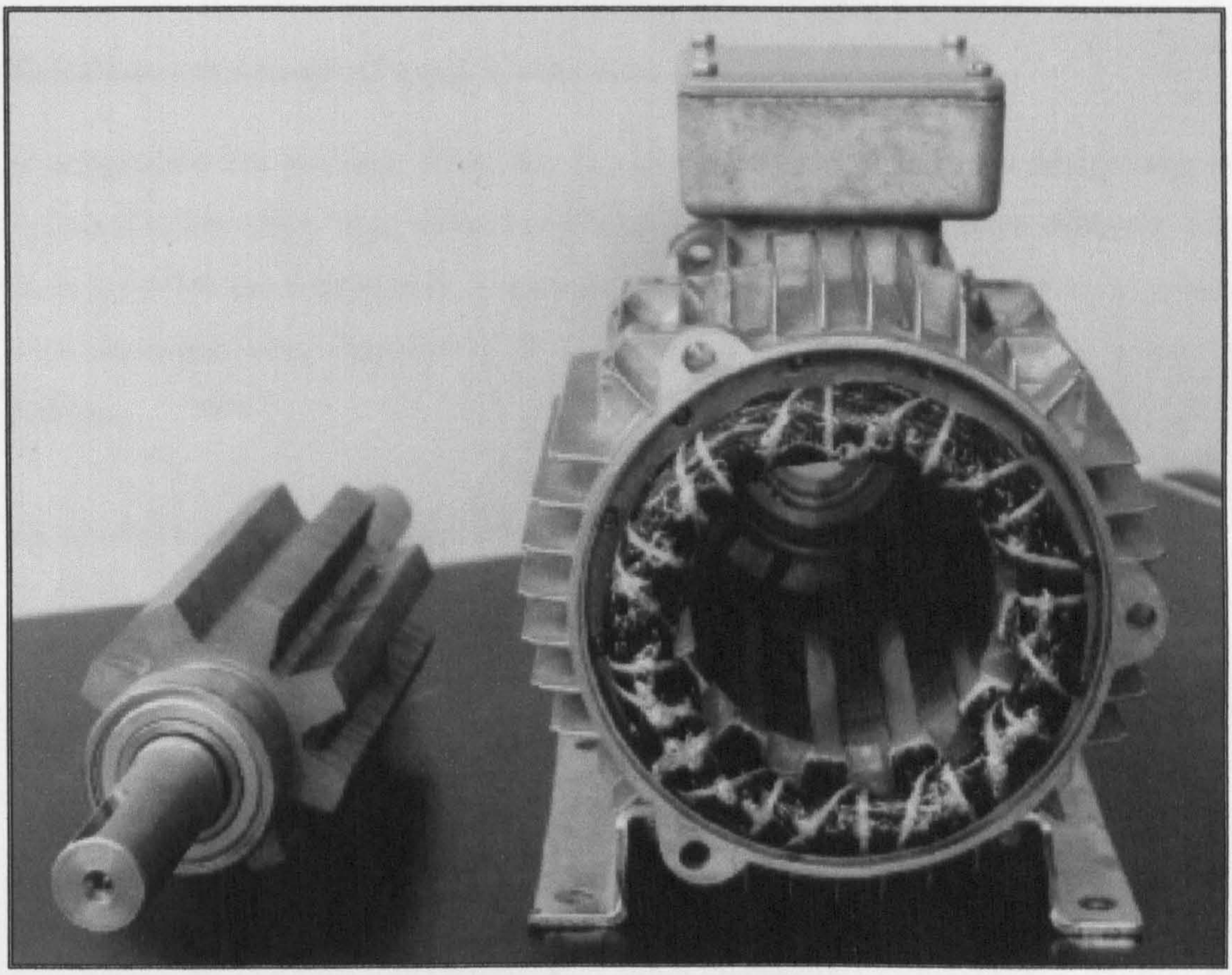

Figure 4.18 Prototype machine in D100L frame.

Winding Resistance

The resistance of one of the four fully pitched coils can be estimated using Equation 4.6 as follows:

$$R_{coil\_fp} = \frac{102[(2*0.15)+(4*0.017)+(2*0.0942)]}{5.8*10^{7}*0.567*10^{-6}} \tag{4.15}$$

$$=1.726\Omega \quad (\text{at } 20^{\circ}C)$$

Four coils are used in this machine per phase. As two pairs of series connected coils are then connected in parallel, the resistance of one phase is the same as the individual coil resistance. Therefore $R_{ph} = 1.726\Omega$.

After the machine was constructed the actual phase resistance was measured to be 1.825Ω. Unfortunately this was more than the predicted value due to the way the

machine was wound. As can be seen on Figure 4.18, the windings protrude out of the slots much further than they needed to before turning the 90° to form the endwinding.

Calculation of amount of copper reduction

A comparison can be made of the amount of copper used in this new design with that required in the Allen West reference design. The two machines have different frame sizes therefore the comparison is made in terms of the ratio of the slot area to stator cross sectional area. Equation 4.13 can be used to estimate slot area, giving the following values:

D132 (Allen West machine) slot area = $753.4mm^2$
D100 (Prototype machine) slot area = $289mm^2$

The ratio of slot area to stator cross sectional area is therefore:

D132 (Allen West machine) = 0.02185
D100 (Prototype machine) = 0.01580

Comparing these figures shows that the prototype machine has reduced the amount of copper required with fully pitched windings by 27.7%. 2.5% of this is due to the inclusion of tangs, 13% is due to the increase in the split ratio and the slight increase in the average stator tooth width, and 12% is due to the tapering of the stator teeth and the radius at the base of the stator teeth.

A comparison can now be made between the amount of copper in the prototype machine with fully pitched windings and the amount of copper in a machine with short pitched windings with the same frame size and an *unmodified geometry*. This is useful because, as stated in Section 4.3.1, the fully pitched winding machine requires significantly more copper due to its endwinding length if the same slot area is used. Phase resistance can be used for this comparison if the same number of turns and the same wire diameter is used. Phase resistance with fully pitched windings in the prototype machine has already been calculated using Equation 4.15 to be 1.726Ω. Phase resistance with short pitched

windings and an unmodified geometry can be calculated using a modification to Equation 4.6 as follows:

$$R_{coil\_sp} = \frac{102 * (0.02185/0.0158) * [(2 * 0.15) + (4 * 0.01) + (2 * 0.0210)]}{5.8 * 10^{7} * 0.567 * 10^{-6}}$$

$$= 1.636\Omega \quad (\text{at } 20^{\circ}C)$$

The additional factor of (0.02185/0.0158) is included to account for the slot area in the unmodified geometry being larger by this factor.

It can now be seen that phase resistance, and therefore copper weight, is now only 5.5% higher with this fully pitched winding machine. As stated in Section 4.3.1, without these design modifications the fully pitched winding machine required 46% more copper than the short pitched winding machine (with this aspect ratio and a 12-8 geometry).

4.3.4 Torque Characteristics

Torque was calculated from the measured flux linkage data using the same method that was described for the simulation in Chapter 3 i.e. using the principle of co-energy. This data is shown in Figure 4.19, and was used extensively by both the simulation and the test rig for determining instantaneous torque from current. Note that current is the equivalent single tooth current; in the fully pitched machine the phase currents must first be converted into the equivalent single tooth current using the transformation matrices before this data can be used.

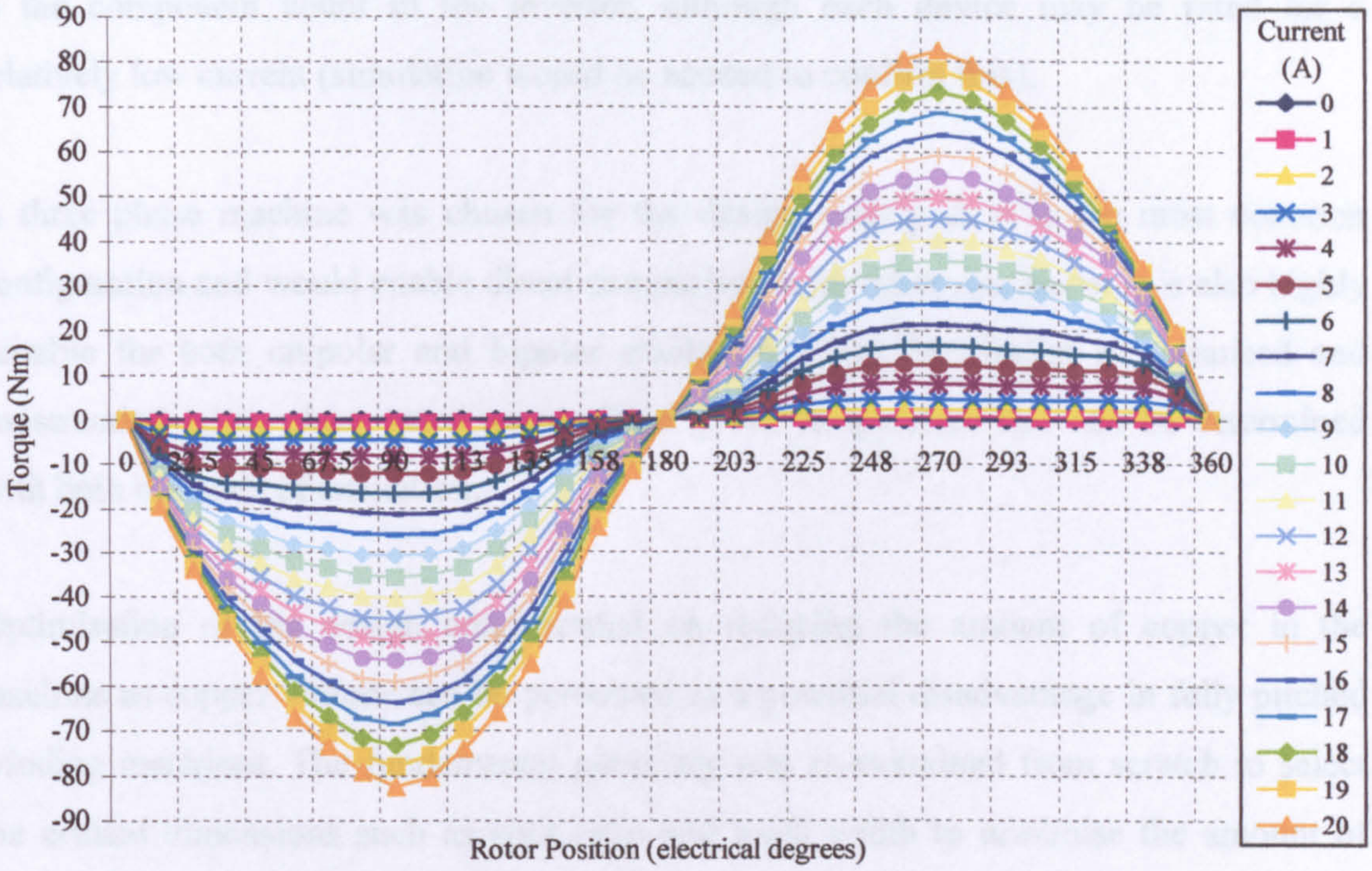

Figure 4.19 Torque against current and rotor position for the prototype machine calculated from the measured flux linkage data.

4.4 Summary

Fully pitched winding machines with 1,2,3,4 and 5 phases have been examined and some of the possible excitation patterns evaluated in terms of torque per unit copper loss and power electronic requirement.

A two phase machine should have approximately the same reduction in copper loss as a three phase machine when compared to a short pitched winding machine. The additional advantage of the two phase machine is that potentially the power electronics could be less expensive due to the lower component count.

It has been shown that the four phase machine cannot be excited with unipolar currents: this is the case with any fully pitched wound machine with an even number of phases. However bipolar operation has been shown to be exceedingly efficient, due to three of the phases contributing to torque at the same time. This results in each stator tooth being excited for half of the electrical cycle, thereby maximising torque output. The drawback

is the component count in the inverter, although each device may be rated for a relatively low current (simulation would be needed to confirm this).

A three phase machine was chosen for the design mainly as it is the most common configuration and would enable direct comparison with other machines. It is also highly suitable for both unipolar and bipolar excitation. Once the design is optimised and construction taken place, rated torque for a given temperature rise can be determined with both methods of excitation.

Optimisation of the design concentrated on reducing the amount of copper in the machine as copper volume can be perceived as a potential disadvantage in fully pitched winding machines. The fundamental geometry was re-examined from scratch to select the critical dimensions such as split ratio and tooth width to minimise the amount of copper. Tapered teeth were included to reduce the amount of copper, without adversely affecting the variation of flux linkage with position. A 12-8 machine was also shown to be highly beneficial for the fully pitched winding (more so than the short pitched winding). It has been shown that with the above improvements slot area has been reduced by 27.7% compared to the Allen West design when scaled to the same frame size. This results in copper weight and volume now being only 5.5% greater than the Allen West design with short pitched windings. Previous comparisons showed that with the same machine design the fully pitched winding would require 46% more copper.

FEA has been used to calculate flux linkage/current/rotor position data. This has been used with the simulation to predict dynamic performance, which has concluded that the reduction in copper required is achieved while maintaining torque per unit copper loss.

After construction the measured phase resistance was found to be higher than expected, and this is thought to be mainly attributable to the unnecessary length of the endwinding. Comparisons have also been made with measured flux linkage data and some differences have become apparent. Reasons for these differences have been postulated.

Chapter 5 - MACHINE OPERATION AND COMPARISON TO SIMULATION

5.1 Introduction

The fully pitched machine can be excited with several methods of excitation, some of which require a different inverter to the standard asymmetric half bridge commonly used with SR machines. The following excitation methods have been investigated:

- Unipolar.
- Bipolar squarewave.
- Sinusoidal (with H bridge inverter).
- Sinusoidal (with star connected inverter).

A test rig was specifically designed and constructed for this purpose. Briefly, this consisted of the following:

- The prototype three phase fully pitched winding machine described in Chapter 4 coupled to a DC load machine.
- A DSP/FPGA based control system designed to allow flexible control strategies and to capture and calculate data to assess motor drive performance. This was linked to a host PC and DSP emulator that allow software development and data capture.
- An IGBT based power electronic inverter, configurable in a variety of topologies.

Appendix C describes the rig, its control methods and measurement techniques in more detail. This chapter shows the prototype machine running on this test rig with each method of excitation – Chapter 6 goes on to make the performance comparisons. Current waveforms are measured and the DSP processes this data to calculate various other useful waveforms such as the equivalent single tooth current and torque. This additional information makes the understanding of the way torque is produced in the machine easier. Following this, simulation results are shown under the same operating conditions for direct comparison. General reference should be made to the PhD thesis by Barrass [5.1], which describes the first development of a current controlled fully pitched winding machine with both unipolar and bipolar excitation patterns.

5.2 Unipolar Operation

Low speed

Figure 5.1 shows the measured phase currents of the fully pitched wound machine with unipolar excitation during low speed operation. At this speed they are very close to the ideal 240° conduction described in Chapter 2. The equivalent single tooth current, I_1, is also shown and is calculated using the transformation matrices (these are described in Chapter 2). This calculation is done in real time by the DSP controller with knowledge of the measured phase currents. The equivalent single tooth current is very useful in understanding machine operation. This is the current that would be needed to flow in a phase of a short pitched winding machine to produce the same amount of flux in each tooth. In this respect therefore, Figure 5.1 shows that 240° unipolar conduction in a fully pitched winding machine is the equivalent of 120° conduction in a short pitched winding machine.

The torque due to the current in the equivalent single tooth phase is also calculated. As described in Appendix C, this is done using the curves of torque against current and rotor position for the prototype machine. The torque due to the I_1 is shown in Figure 5.1, in addition to the total torque due to all three phases.

Note that the equivalent single tooth parameters are calculated on the basis that these equivalent phases have the same number of turns as the actual fully pitched windings. Therefore with two phases excited and the same number of turns per phase, the amplitude of I_1 is twice that of I_A.

Half way through the conduction period the current has a large tendency to increase due to the commutation of the other two phases and the large amount of mutual coupling in this type of machine. The inverter is actually capable of applying enough volts to prevent this from occurring, but in this instance the controller bandwidth is not high enough to completely cope with the situation and the current rises beyond the demanded value slightly. It is now useful to compare these results to the simulation shown in Figure 5.2, which was performed using measured ψ–i data.

It can been seen that the phase currents are almost identical, including the magnitude of the commutation spike in the middle of the conduction period. The whole waveform shape is modelled very well by the simulation. This is due to two main reasons:

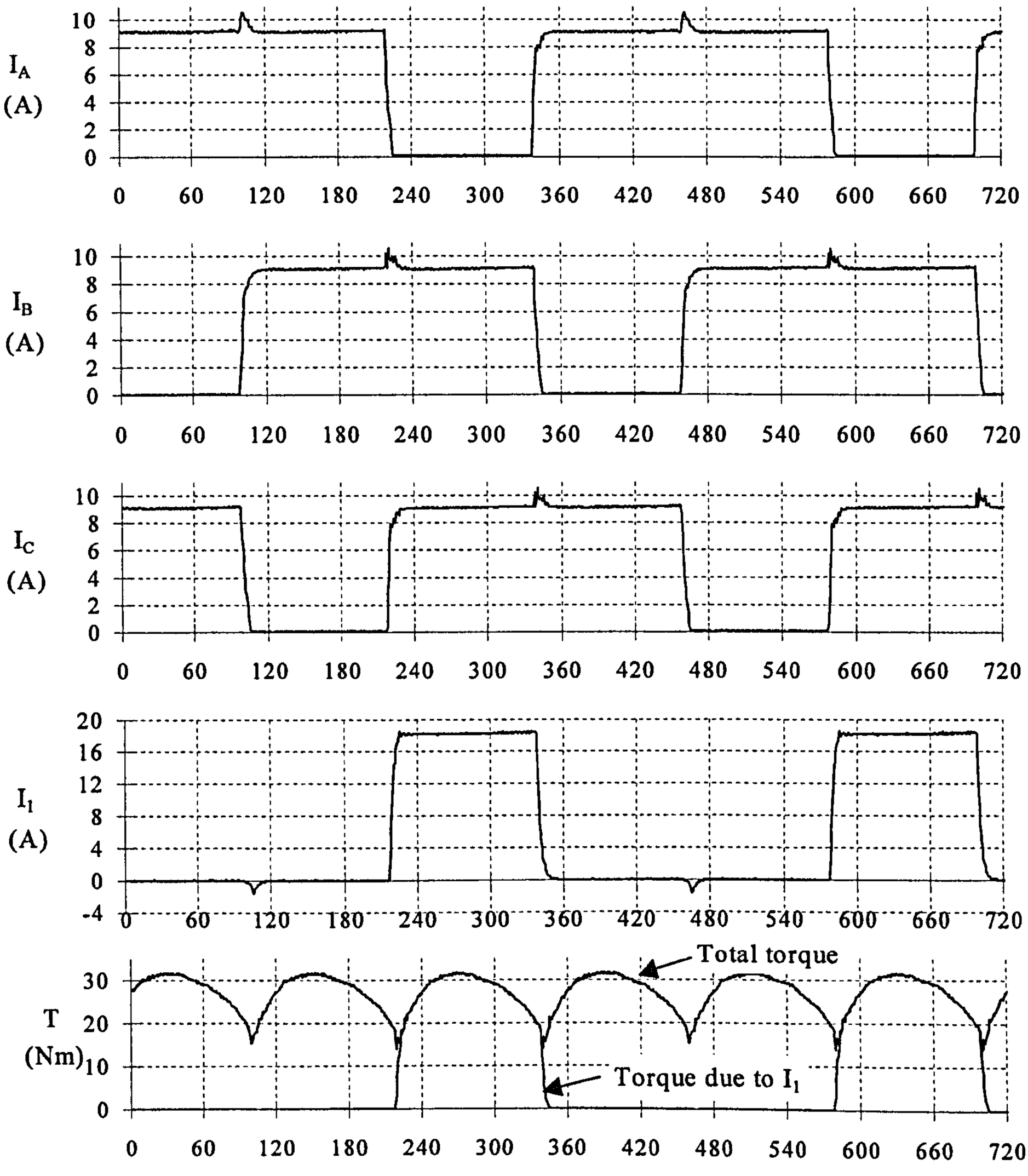

Figure 5.1 Measured waveforms of unipolar operation. Real currents are measured, equivalent single tooth current and torque are calculated. I_{dem}=9.2A, V_{dc}=580V, Speed=200rpm.

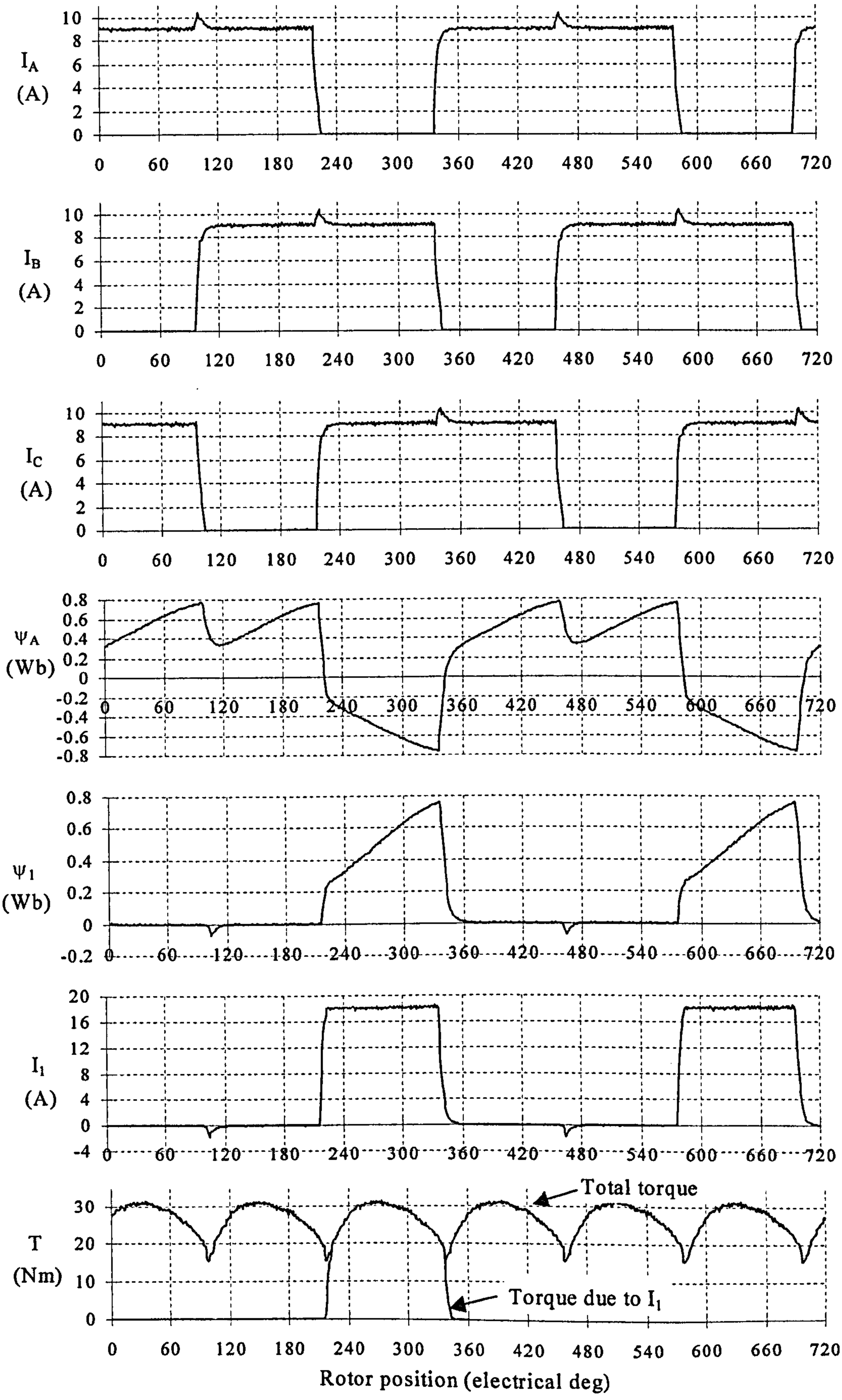

Figure 5.2 Simulation of unipolar operation. I_{dem}=9.2A, V_{dc}=580V, speed=200rpm.

- The core model of the simulation is accurate because of the combined use of Runge Kutta time stepping method, the flux linkage/current/rotor position data, and the transformation matrices. This method is able to cope with the strong mutual coupling and magnetic saturation in this type of machine.
- The current controller is completely modelled. This predicts effects that are likely to be seen in practical situations where controller bandwidth is not infinite and therefore current control is not perfect. In this case the controller on the test rig is digital with current sampling every 100μs and 10kHz switching frequency. The same current controller PID gains are used, and current sampling occurred as the same point within a PWM period. (Appendix C describes the digital controller in more detail).

The simulated results also show the flux linkage waveform. The flux linkage for phase A is shown in Figure 5.2. During the first half of the conduction period flux rises gradually as torque is produced in the machine. At the half way point the full effect of the other two phases commutating can now be seen. A large voltage needs to be applied to the phase to reduce the flux linkage and prevent the current rising beyond the current demand. Following this point flux again starts to rise more gradually, again as torque is produced. At the end of the conduction period negative volts are applied to bring the current and flux linkage down to zero. In this machine, however, the flux linkage in fact needs to fall below zero during the time that the phase is off. This is as a consequence of the mutual coupling between phases.

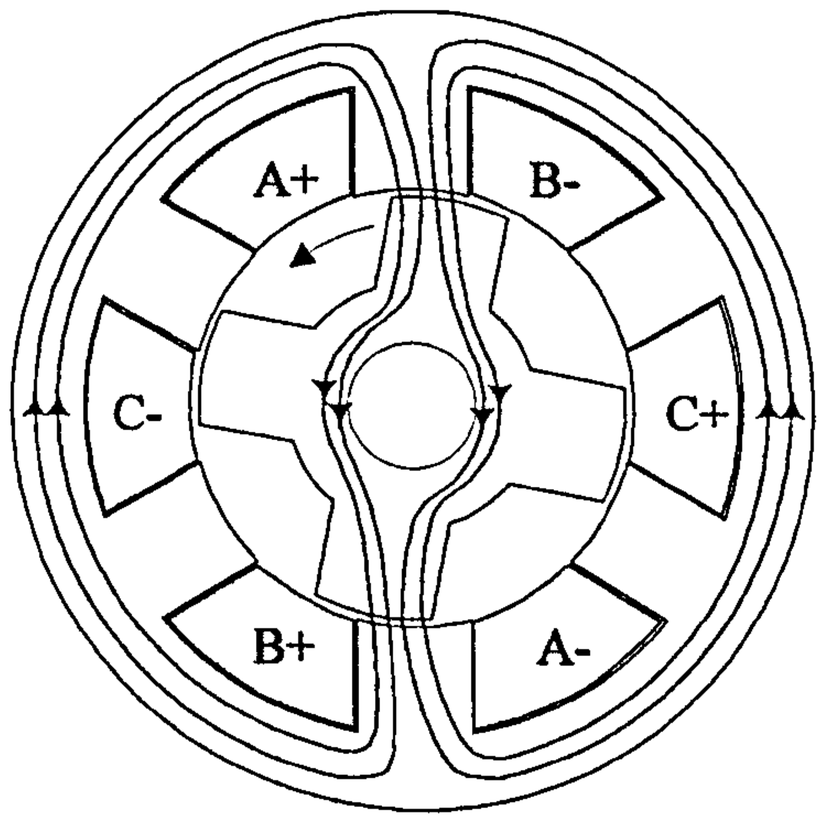

Figure 5.3 Cross section of the machine with phases A and B conducting.

Figure 5.3 shows a cross section of the machine with phases A and B conducting with a representation of the resulting flux pattern. It can be seen that this flux completely links phase C as well, and as a result a voltage must be applied to keep the current at zero. Consequently the shape of the flux linkage during its negative region is the mirror image of that during one half of the positive region.

Figure 5.4 shows the ψ/i locus with unipolar operation i.e. an x-y plot of flux linkage against current. The area enclosed by the locus can be used to calculate the torque being produced, as with ψ/i loci in short pitched winding SR machines. In the fully pitched winding machine, however, the flux linkage in a phase is a function of rotor position and the current in that phase, as well as the currents in the other two phases. It is therefore difficult to draw any further conclusions from it. Instead it is much more useful to look at the equivalent single tooth ψ/i locus derived using the transformation matrices. This is now the much more familiar shape of the ψ/i locus where the phase flux linkage only depends on rotor position and the current in that phase. The aligned and unaligned curves taken from the measured flux linkage data for the machine is also shown for comparison. This indicates how much of the machines' potential to produce torque is being utilised.

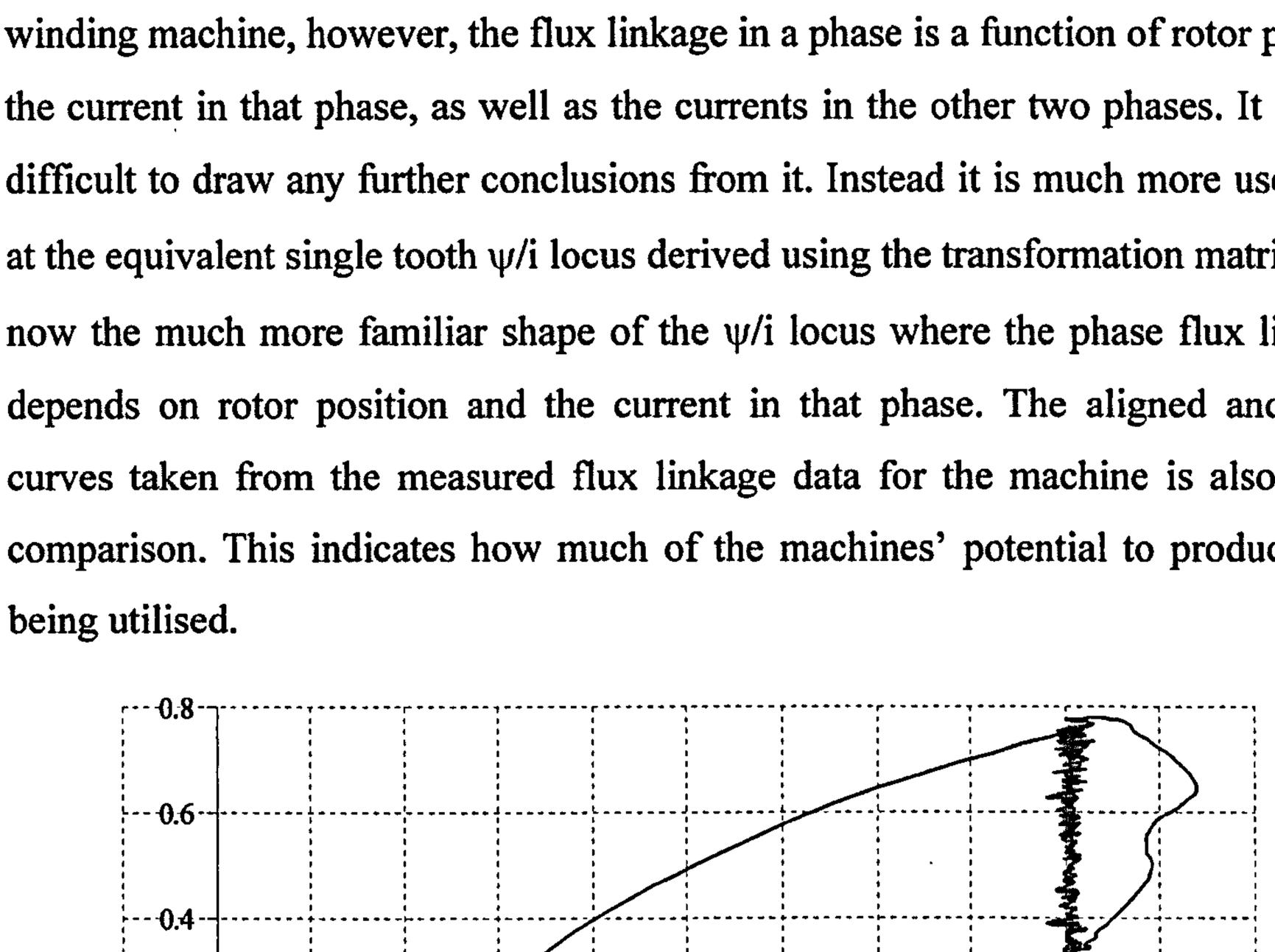

Figure 5.4 Simulated ψ/i locus of the fully pitched winding machine with unipolar operation.

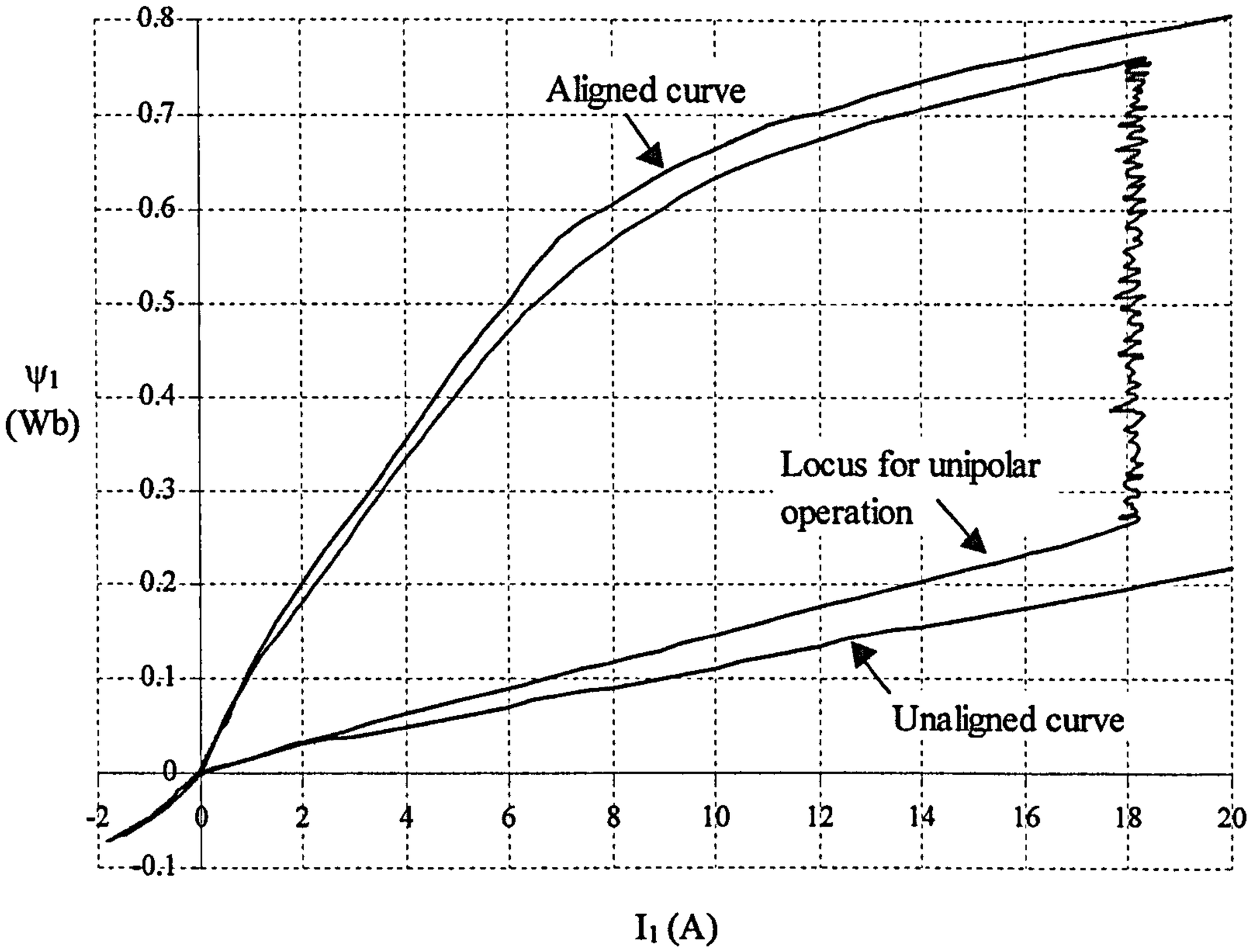

Fig. 5.5 Simulated ψ/i locus of the equivalent single tooth parameters with unipolar operation.

Comparisons of machine efficiencies with this mode of operation are made in Chapter 6, together with the other modes of operation and the same machine with short pitched windings.

High speed

Figure 5.6 shows real and simulated current waveforms with unipolar excitation at the equivalent of base speed (675rpm) and twice base speed (1350rpm). Base speed is 675rpm here because the drive is being operated at a reduced DC link of 290V to avoid over-speeding the DC generator load.

The current demand is still 9.2A, and at higher speeds it is beneficial to reduce the conduction period slightly below 240° (see Chapter 6 for a graph of conduction angle versus speed). At base speed and beyond the back EMF is such that the inverter 'runs out of volts' and the current waveform starts to move to the shape it becomes in full voltage control. This is the waveform in the bottom graph of Figure 5.6 that resembles a twin peak.

The waveforms for the simulation are very close to the measured results. The only significant difference is at twice base speed, where there is a mismatch in the on and off angles. This is thought to be due to the limitations of the bandwidth of the position sensing part of the control system on the test rig, which the simulation did not fully model i.e. position sampling takes place every 100uS, and at 1350rpm this corresponds to a rotation of 6.5° (electrical). Therefore the test rig on and off angles can be incorrect by an amount up to this value – the simulation on the other hand assumed the exact desired values.

Finally, for unipolar operation, a comparison of torque-speed curves between measured and simulated results is shown in Figure 5.7.

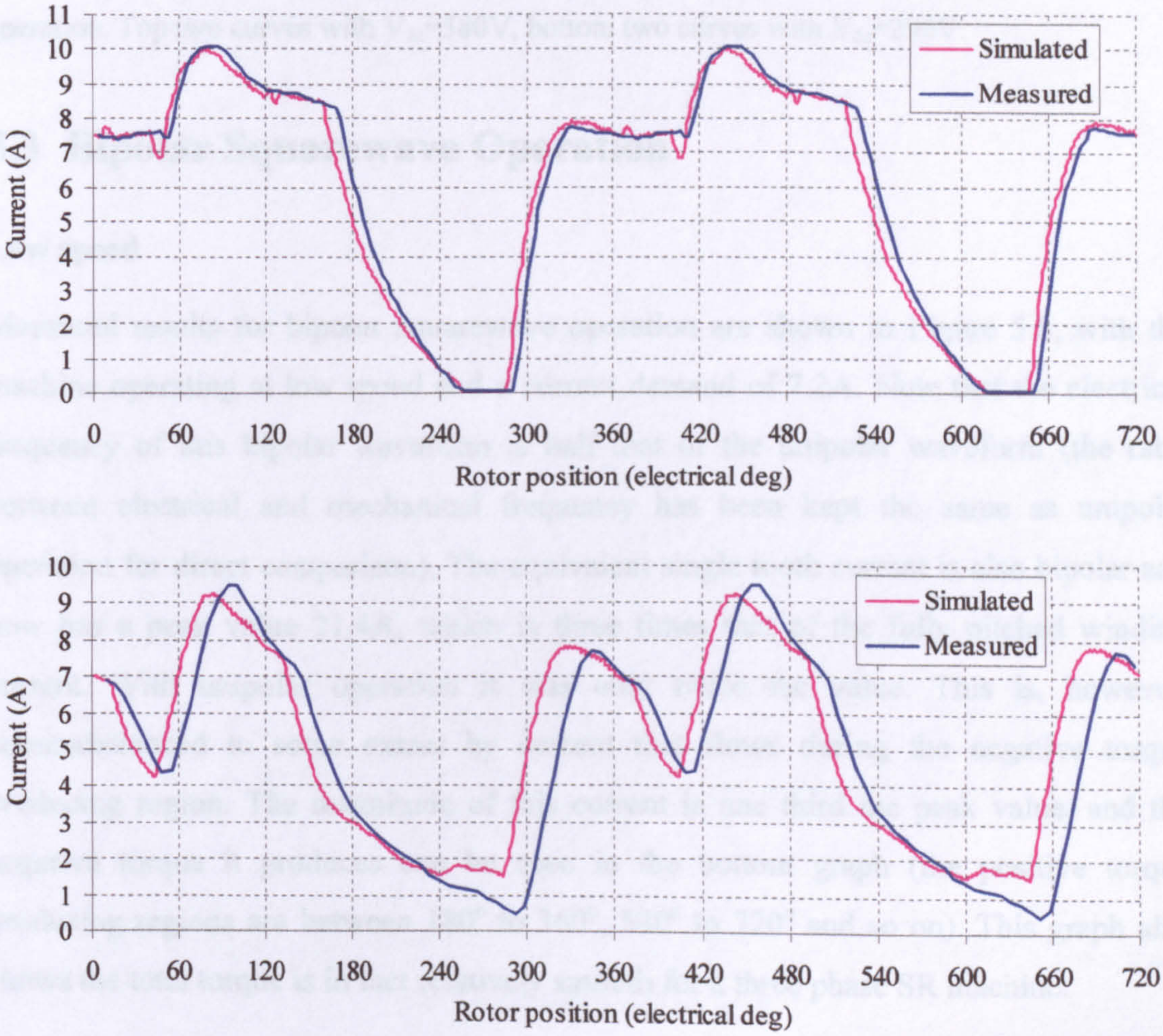

Figure 5.6 Comparison of real and simulated unipolar currents. I_{dem}=9.2A, V_{dc}=290V. Top graph at 675rpm, bottom graph at 1350rpm.

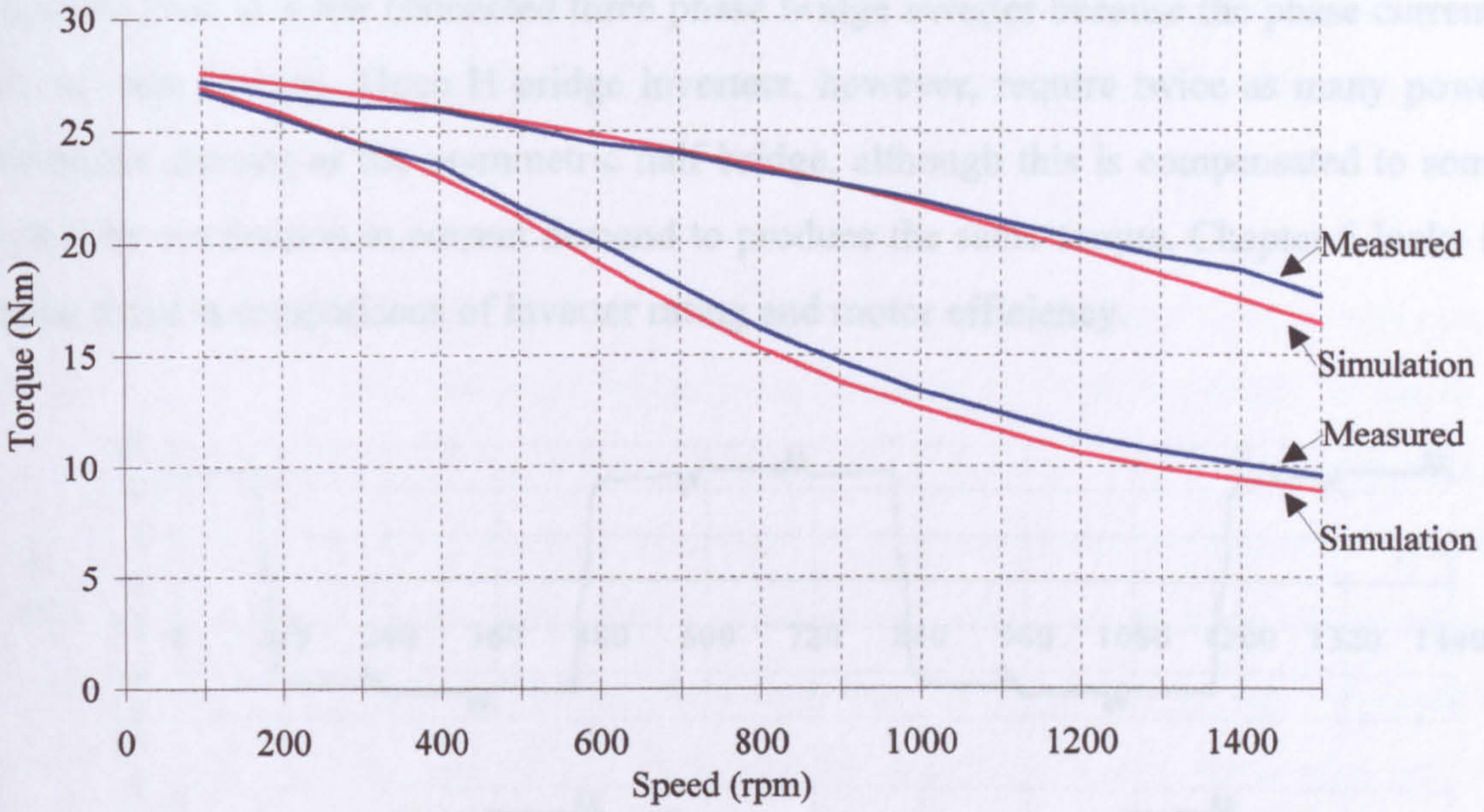

Figure 5.7 Comparison of real and simulated torque-speed characteristics for unipolar operation. Top two curves with V_{dc}=580V, bottom two curves with V_{dc}=290V.

5.3 Bipolar Squarewave Operation

Low speed

Measured results for bipolar squarewave operation are shown in Figure 5.8, with the machine operating at low speed and a current demand of 7.2A. Note that the electrical frequency of this bipolar waveform is half that of the unipolar waveform (the ratio between electrical and mechanical frequency has been kept the same as unipolar operation for direct comparison). The equivalent single tooth current is also bipolar and now has a peak value 21.4A, which is three times that of the fully pitched winding current. With unipolar operation it was only twice the value. This is, however, counterbalanced to some extent by current that flows during the negative torque producing region. The magnitude of this current is one third the peak value, and the negative torque it produces can be seen in the bottom graph (the positive torque producing regions are between 180° to 360°, 540° to 720° and so on). This graph also shows the total torque is in fact relatively smooth for a three phase SR machine.

To achieve these currents a more complex inverter is required i.e. an H bridge inverter which allows full independent control of each phase. These currents could not for

example flow in a star connected three phase bridge inverter because the phase currents do not sum to zero. Three H bridge inverters, however, require twice as many power electronic devices as the asymmetric half bridge, although this is compensated to some extent by a reduction in current demand to produce the same torque. Chapter 6 looks in more detail at comparisons of inverter rating and motor efficiency.

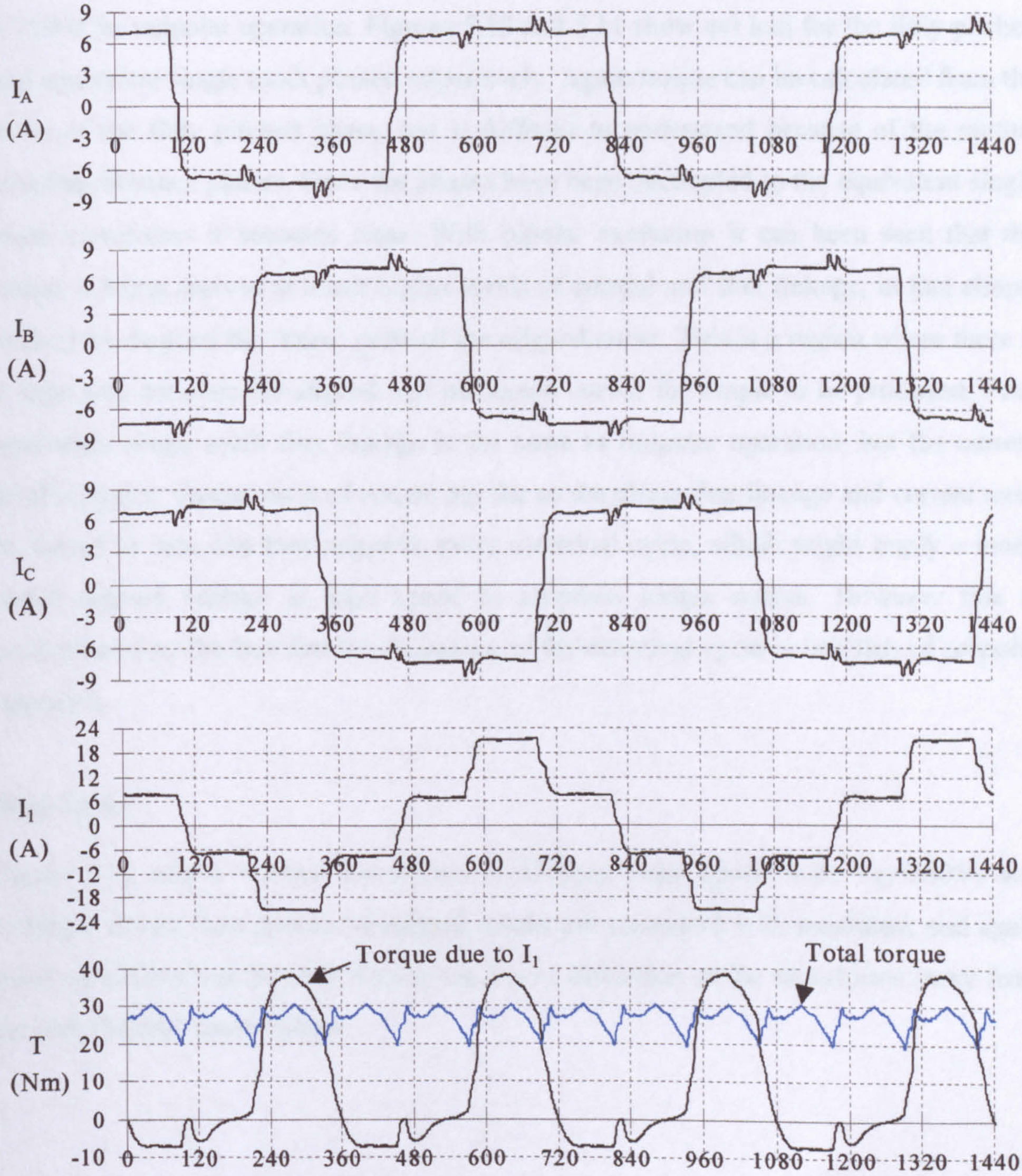

Figure 5.8 Measured waveforms of bipolar squarewave operation. Real currents are measured, equivalent single tooth and torque calculated. I_{dem}=7.1A, V_{dc}=290V, speed=100rpm.

Simulated waveforms are shown in Figure 5.9 and are almost identical to the measured ones. Again details such as the disturbances caused by commutation in the other phases is modelled very well.

Phase flux linkage in a fully pitched phase, as well as an equivalent single tooth phase, are shown. Notice that the peak value of the former is 1.15Wb which compares to 0.75Wb for unipolar operation. Figures 5.10 and 5.11 show ψ/i loci for the fully pitched and equivalent single tooth phases respectively. Again torque can be calculated from the locus of the fully pitched phase, but is difficult to understand because of the mutual coupling between phases. Once the phases have been decoupled to the equivalent single tooth waveforms it becomes clear. With bipolar excitation it can been seen that the torque is being derived at much higher levels of current and flux linkage, in fact almost exclusively beyond the 'knee' point of the aligned curve. This is a region where there is a large area between the aligned and unaligned curves for torque to be produced. Peak equivalent single tooth flux linkage is the same as unipolar operation, but the current level is higher. Operation is of course bipolar so the phase flux linkage and current must be forced to zero and then negative every electrical cycle, which might imply a much larger applied voltage at high speed to maintain torque output. However this is counteracted by the fact that the frequency of the electrical cycle is half that of unipolar operation.

High speed

Figure 5.12 shows current waveforms at 675rpm (base speed with V_{dc}=290V) and 1350rpm (twice base speed). Simulated results are compared with measured, and again good correlation can be seen despite the heavy distortion of the waveforms away from the ideal bipolar square shape.

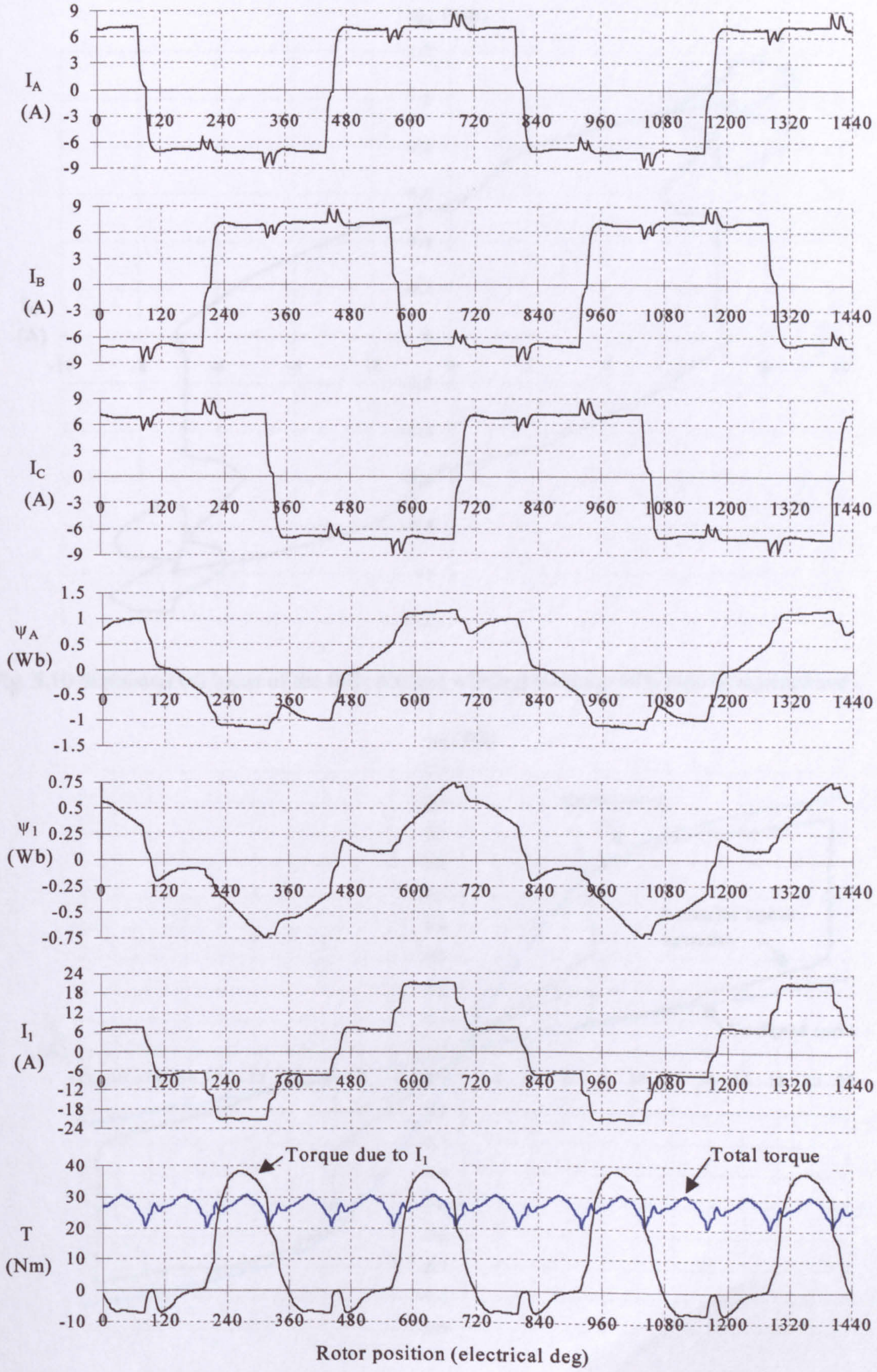

Figure 5.9 Simulation of bipolar squarewave operation. I_{dem}=7.1A, V_{dc}=290V, speed=100rpm.

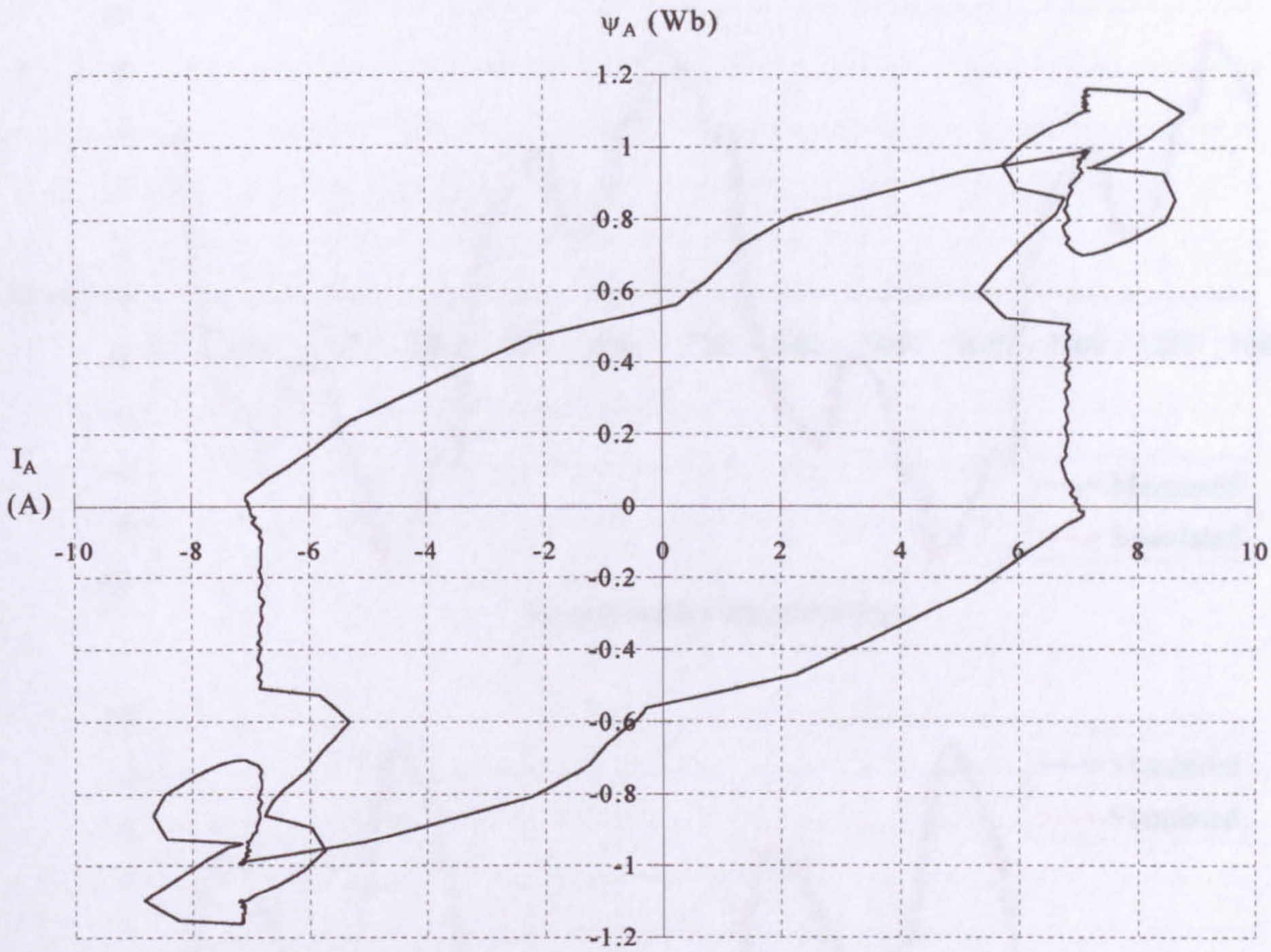

Fig. 5.10 Simulated ψ/i locus of the fully pitched winding machine with bipolar squarewave.

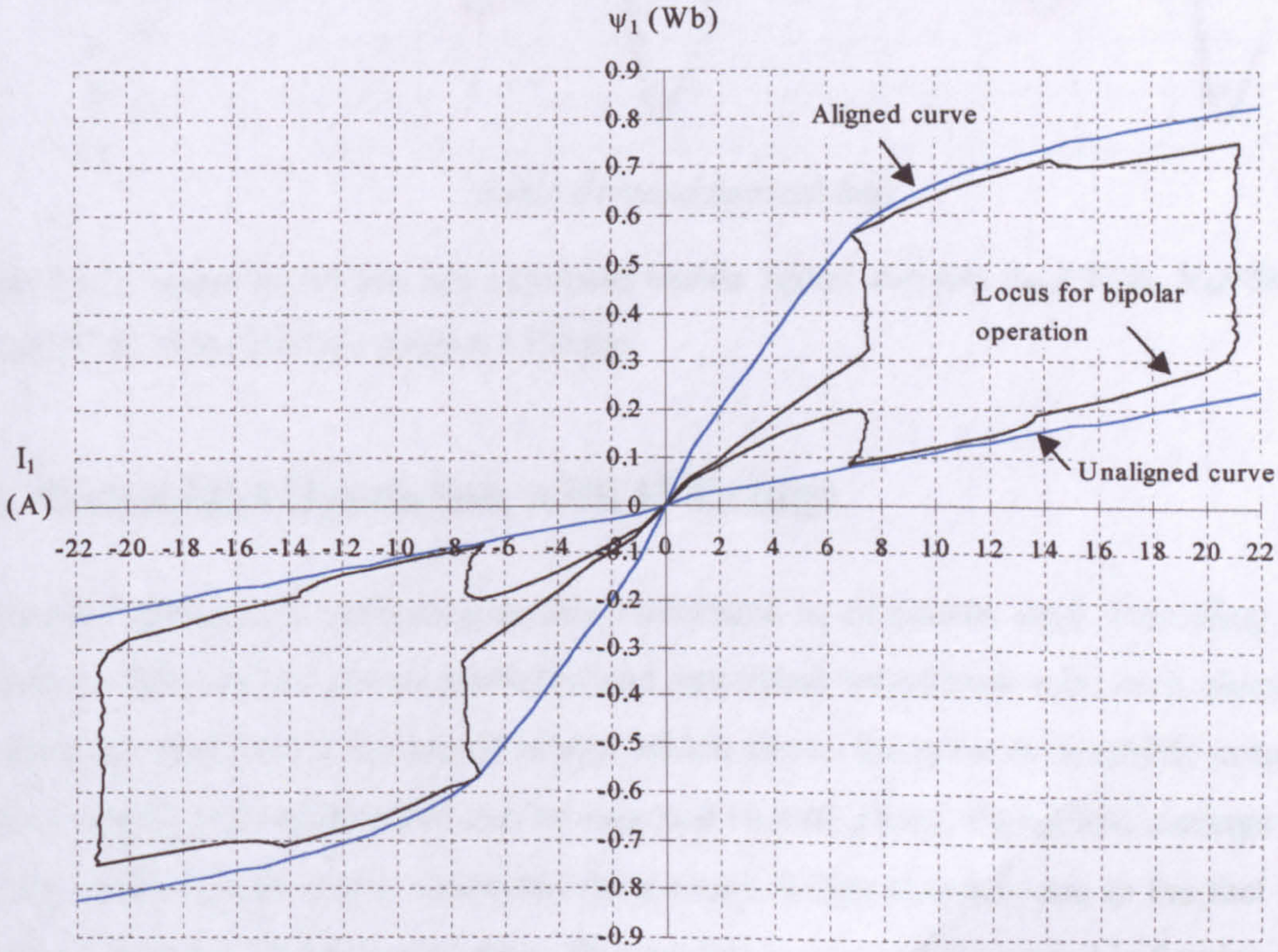

Fig. 5.11 Simulated ψ/i locus of the equivalent single tooth parameters with bipolar squarewave.

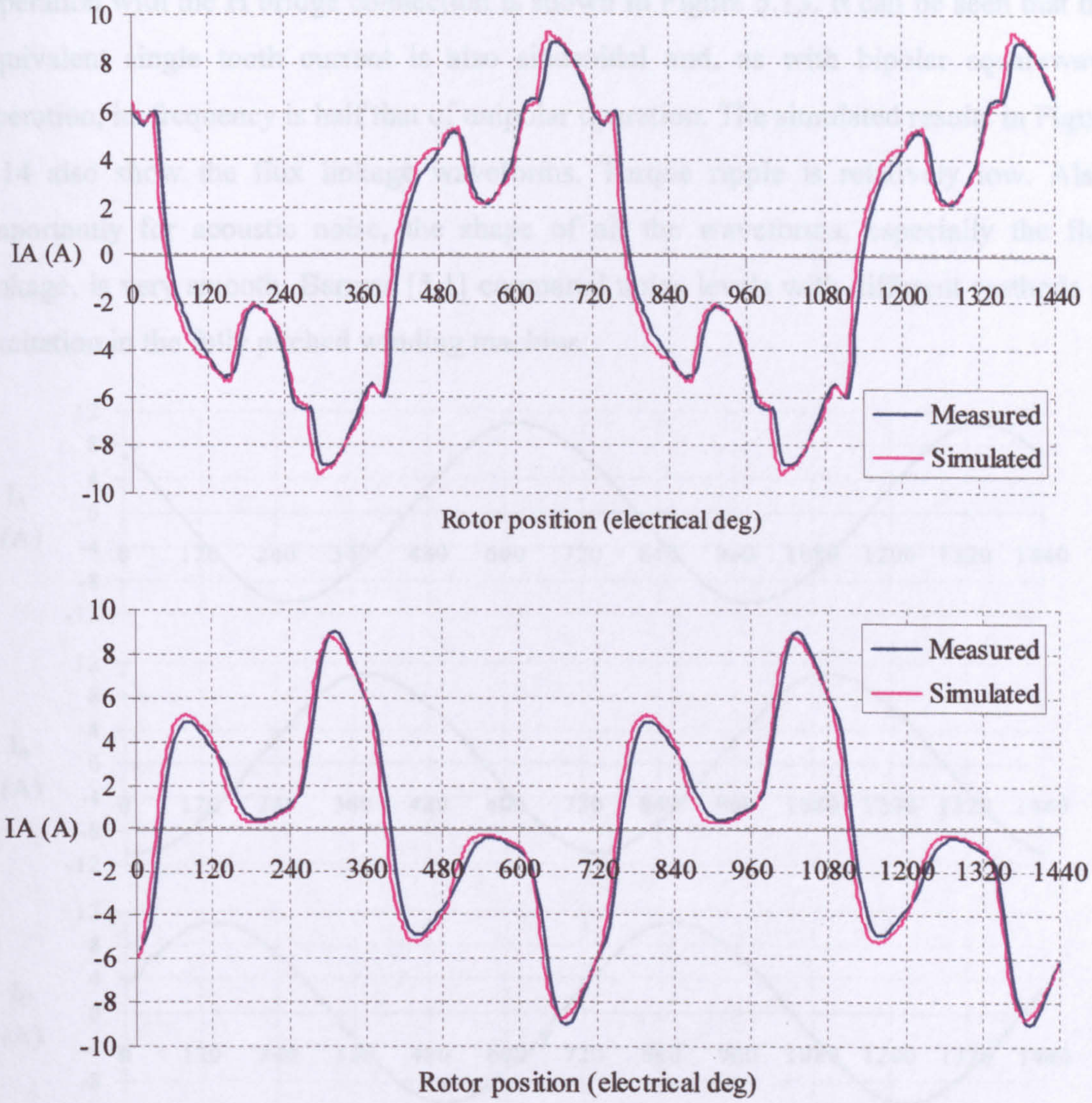

Figure 5.12 Comparison of real and simulated bipolar square currents. I_{dem}=7.1A, V_{dc}=290V. Top graph at 675rpm, bottom graph at 1350rpm.

5.4 Sinusoidal Operation with H Bridge

Sinusoidal operation is interesting as this waveshape is, of course, used with many AC machines. This section shows measured and simulated waveforms with each phase of the machine connected to its own H bridge, which allows the greatest flexibility in terms of the voltages and currents that can be supplied to each phase. Sinusoidal currents can also be produced with a star connected three phase bridge inverter, due to the fact that the phase currents always sum to zero. This mode of operation is covered in Section 5.5. Results in terms of machine efficiency and inverter rating with both inverters are presented in Chapter 6.

Operation with the H bridge connection is shown in Figure 5.13. It can be seen that the equivalent single tooth current is also sinusoidal and, as with bipolar squarewave operation, its frequency is half that of unipolar operation. The simulated results in Figure 5.14 also show the flux linkage waveforms. Torque ripple is relatively low. Also, importantly for acoustic noise, the shape of all the waveforms, especially the flux linkage, is very smooth. Barrass [5.1] compared noise levels with different methods of excitation in the fully pitched winding machine.

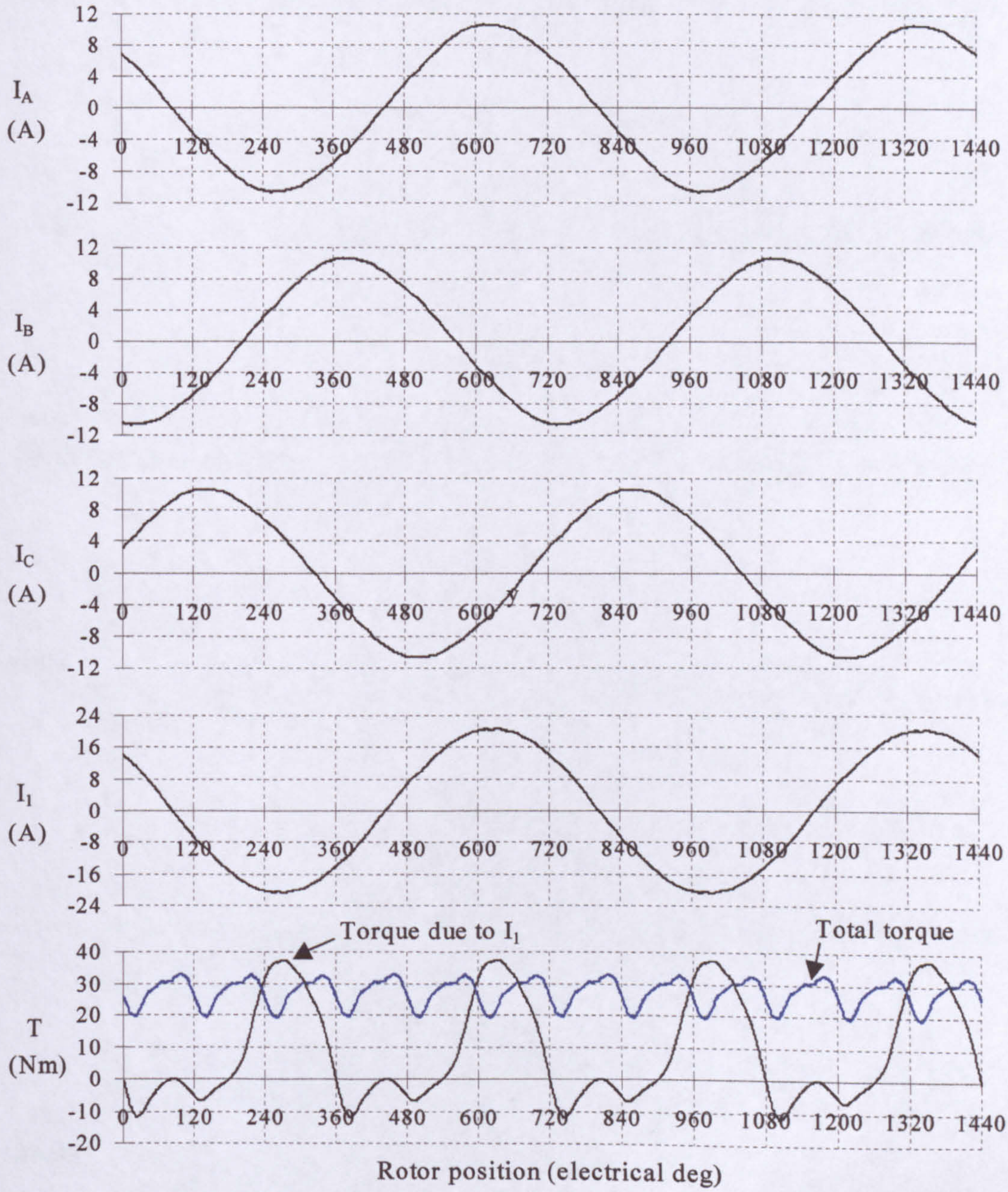

Figure 5.13 Measured waveforms of sinusoidal operation. Real currents are measured, equivalent single tooth current and torque are calculated. I_{dem}=10.5A(pk), V_{dc}=290V, speed=100rpm.

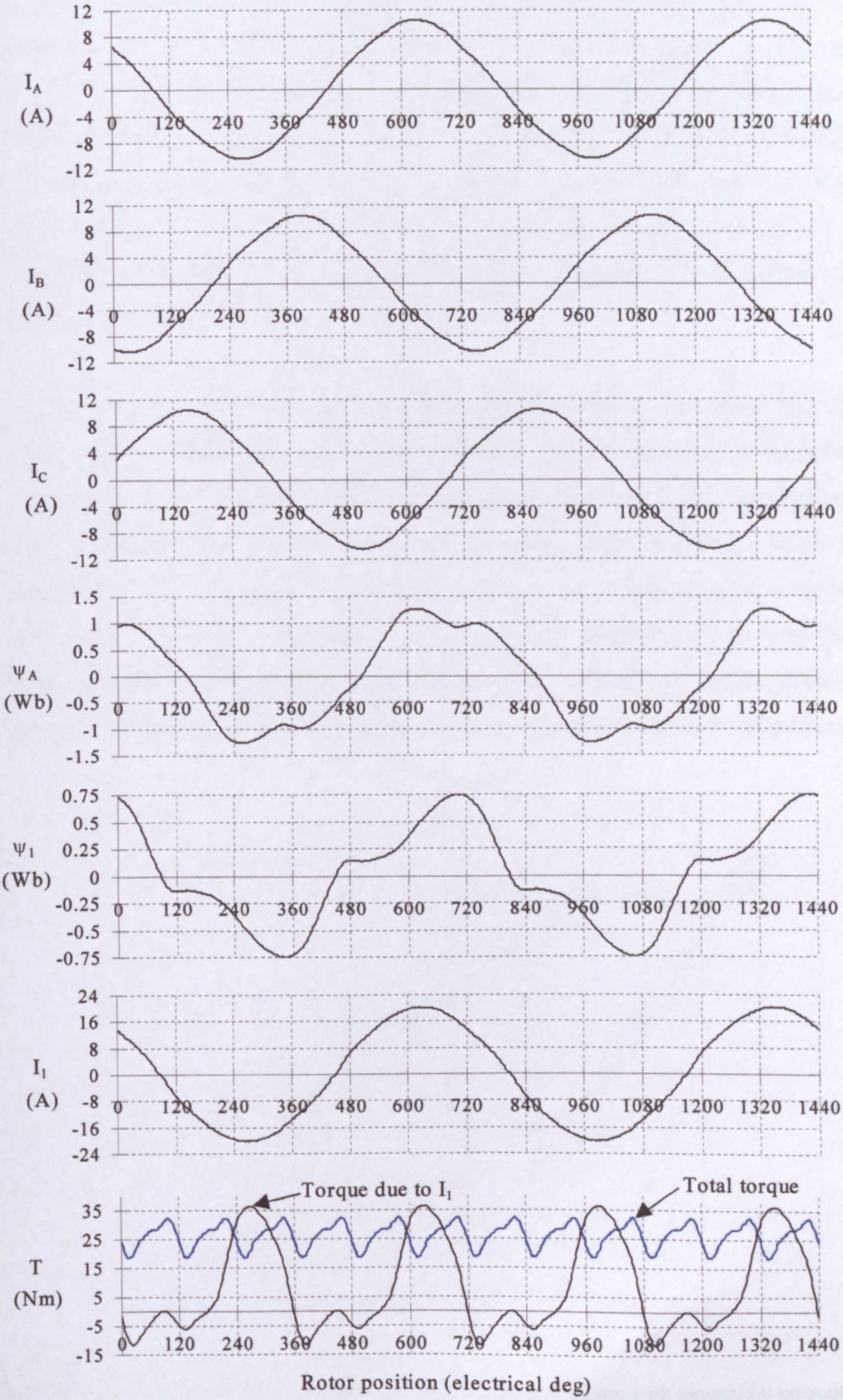

Figure 5.14 Simulation of sinusoidal operation. I_{dem}=10.5A(pk), V_{dc}=290V, speed=100rpm.

Barrass found that the rate of change of flux linkage and current, particularly at, or near, the aligned position, was the dominant factor in the noise level produced. This agreed with the conclusions of Cameron *et al* [5.2], and Wu *et al* [5.3], that noise is a result of oscillations caused by the effects of the stator "ovalising". Measurements by Barrass [5.1] found that sinusoidal operation was significantly quieter than unipolar operation with the same machine because of these smoother waveforms. While no acoustic measurements were made on this test rig, this mode of operation was noticeably quieter than those with step changes in current demand.

The ψ/i locus for sinusoidal operation is shown in Figures 5.15. Note that current demands for all modes of operation shown through this Chapter produce the same low speed torque. The ψ/i locus shows that both peak current and peak flux linkage are higher than those with bipolar squarewave operation, which tends to indicate that a larger inverter will be required to produce the same torque at high speed. The equivalent single tooth ψ/i locus is shown in Figure 5.16. This emphasises how smooth both changes of current and flux are in each machine pole. A significant amount of the locus is realised in terms of torque production, but it is not as good as unipolar operation.

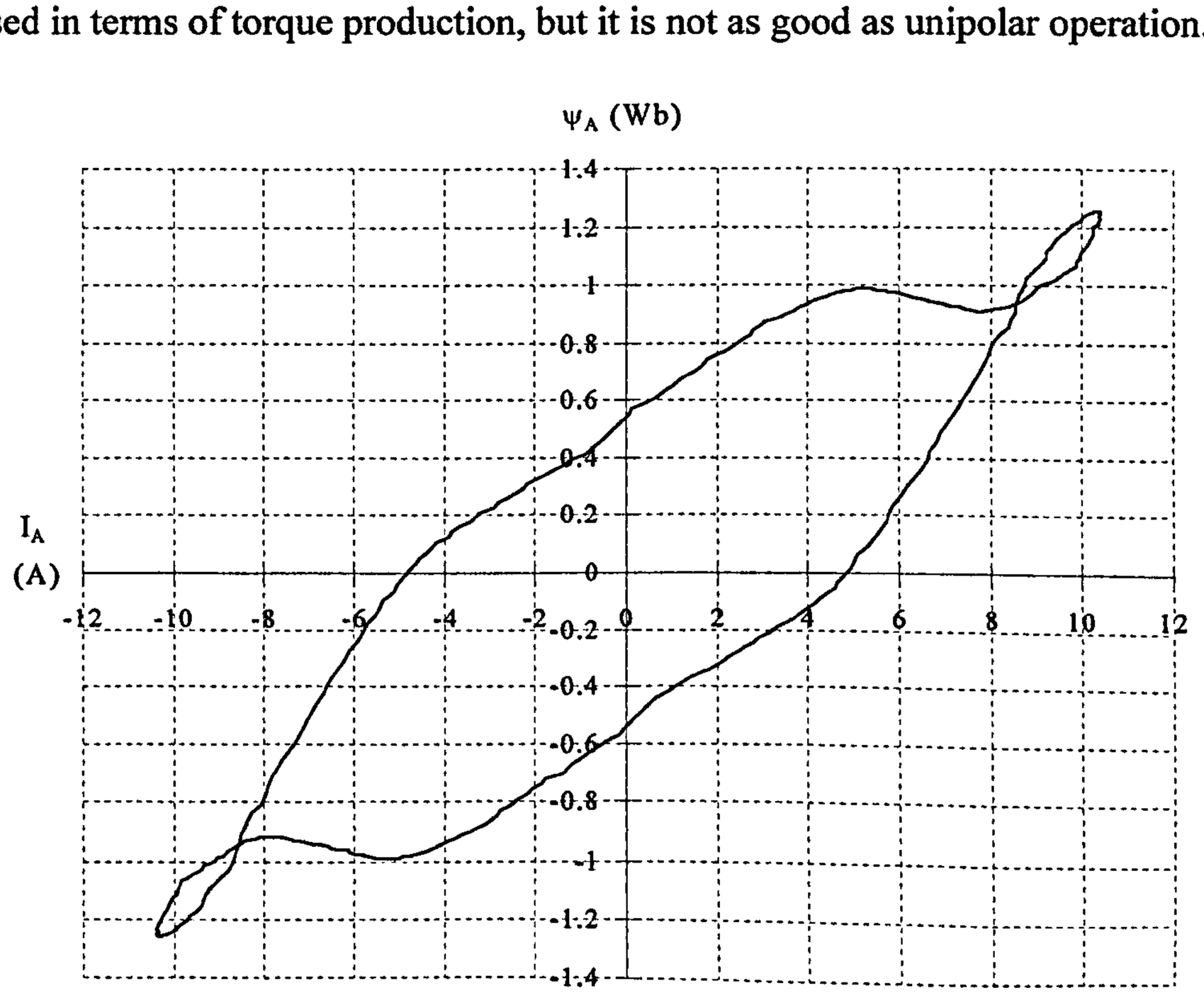

Fig. 5.15 Simulated ψ/i locus of the fully pitched winding machine with sinusoidal currents.

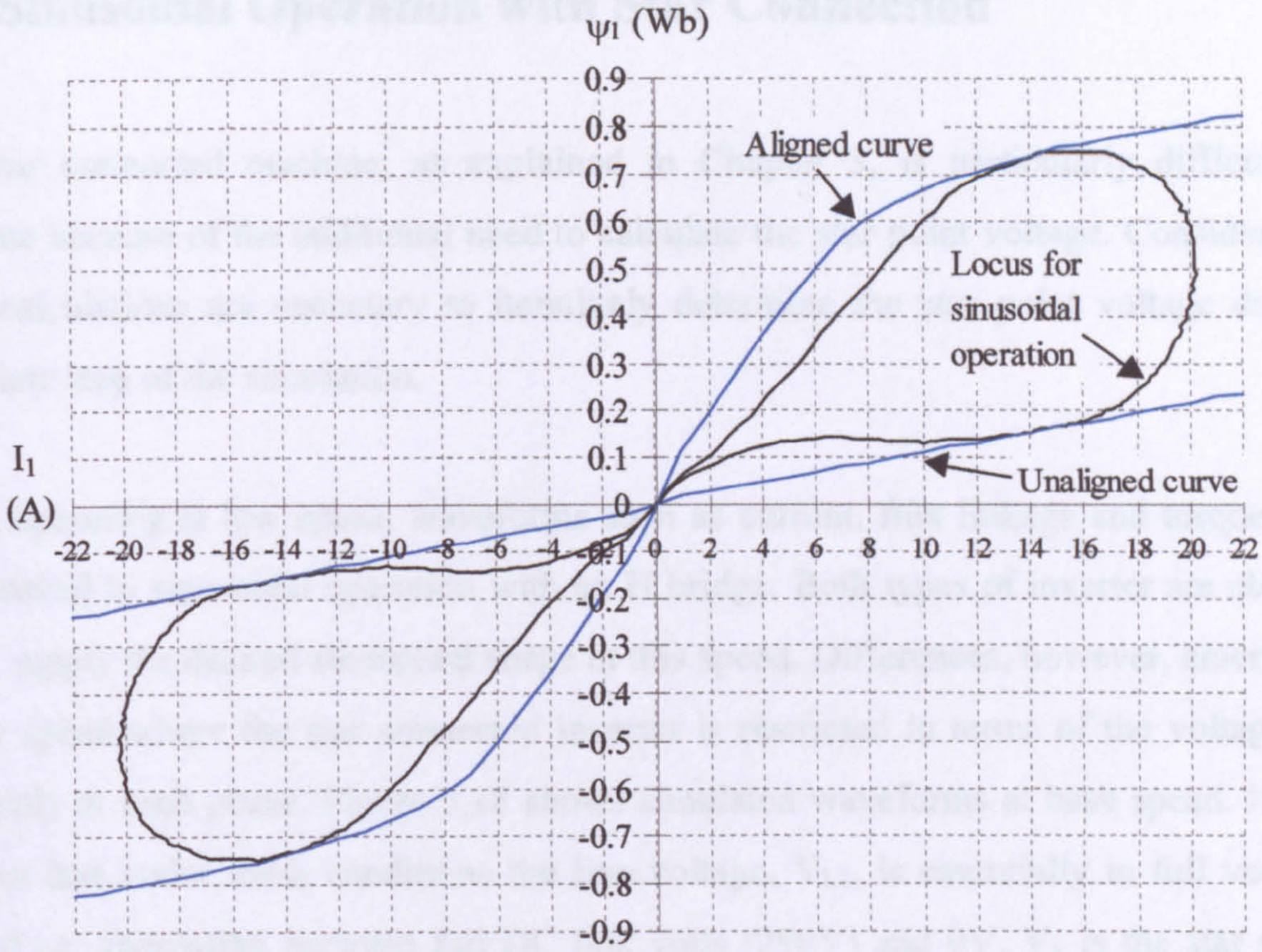

Fig. 5.16 Simulated ψ/i locus of the equivalent single tooth parameters with sinusoidal current.

High speed

Measured phase current at base speed is shown in Figure 5.17 (675rpm with V_{dc}=290V). This is compared directly with the simulated waveform and again very good correlation was found. Heavy distortion from the ideal sinusoidal shape is apparent at this speed.

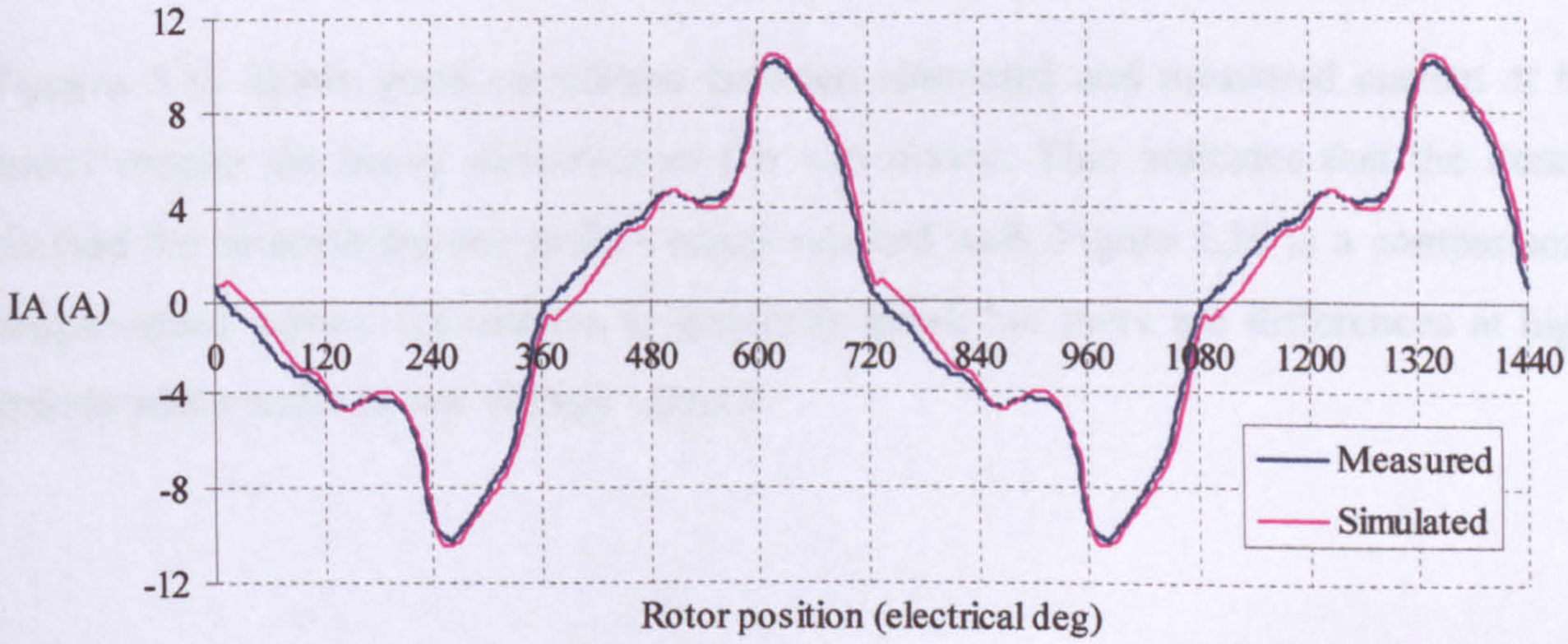

Figure 5.17 Comparison of real and simulated sinusoidal operation with H bridge. I_{dem}=10.5A(pk), V_{dc}=290V, speed=675rpm.

5.5 Sinusoidal Operation with Star Connection

The star connected machine, as explained in Chapter 3, is particularly difficult to simulate because of the additional need to calculate the star point voltage. Considerable extra calculations are necessary to iteratively determine the star point voltage during each time step of the simulation.

When operating at low speed, waveforms such as current, flux linkage and torque, are all identical to sinusoidal operation with an H bridge. Both types of inverter are able to easily supply the desired sinusoidal shape at this speed. Differences, however, emerge at higher speed where the star connected inverter is restricted in terms of the voltages it can apply to each phase. Figure 5.18 shows simulated waveforms at base speed. It can be seen that under these conditions the line voltage, V_{L1}, is essentially in full voltage control i.e. alternating between full DC link volts (290V) and 0V. V_S is the star point voltage which swings between the two rail voltages but in a triangular shape and at three times the frequency of the current waveform. The voltage across phase A, V_A, is the difference between V_{L1} and V_S. As a result the voltage available to be supplied to a phase is considerably less than with H bridge operation, which inevitably means lower torque at high speed. Figures 5.17 and 5.18 can be compared directly to see the difference in the resulting currents at base speed with the same current demand and the same DC link voltage.

Figures 5.19 shows good correlation between simulated and measured current at base speed despite the heavy distortion of the waveforms. This indicates that the iterative method for determining star point voltage worked well. Figure 5.20 is a comparison of torque-speed curves. Correlation is generally good, but there are differences at higher speeds while under heavy voltage control.

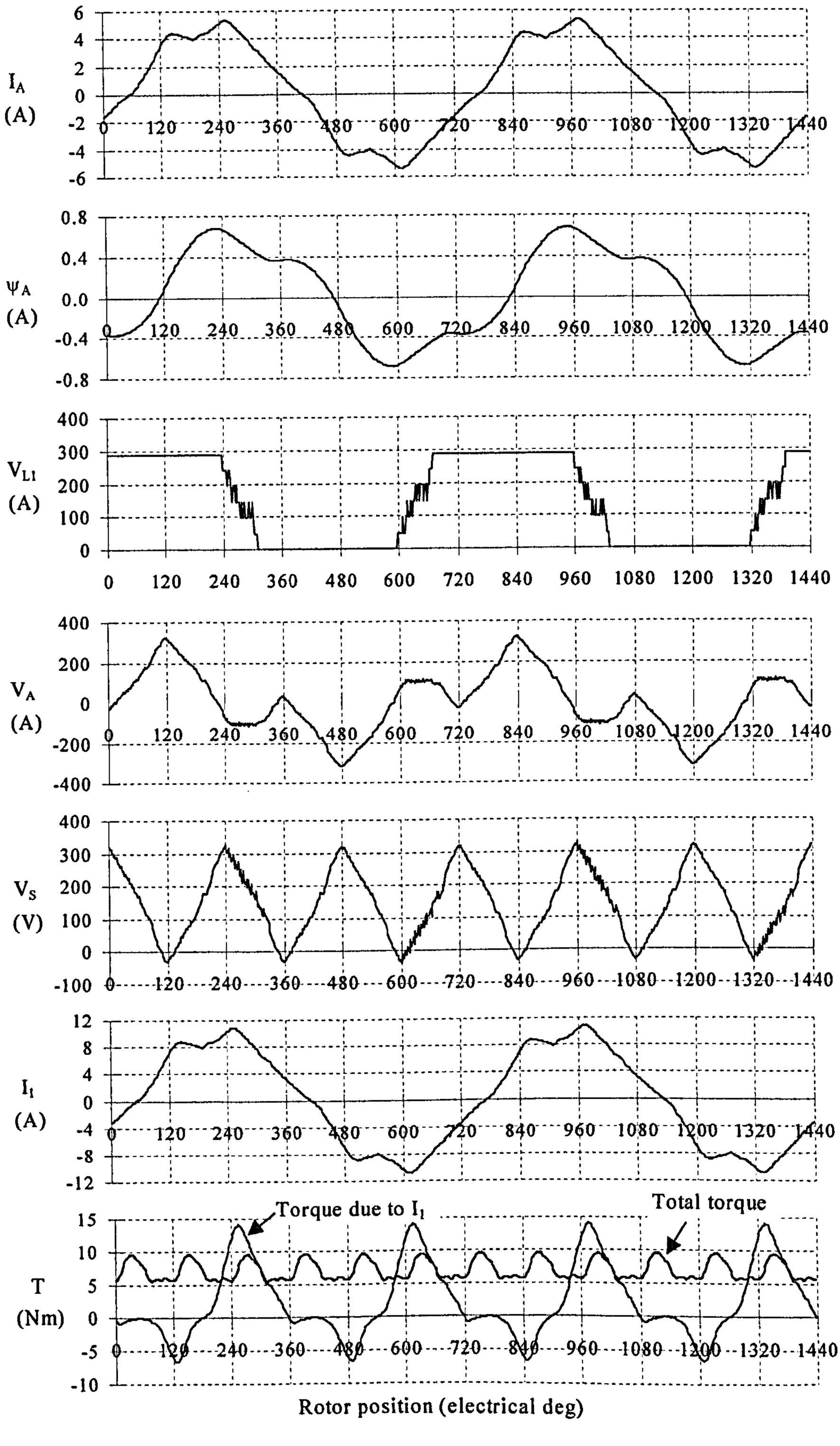

Figure 5.18 Simulation of star connected operation. I_{dem}=10.5A(pk), V_{dc}=290V, speed=675rpm.

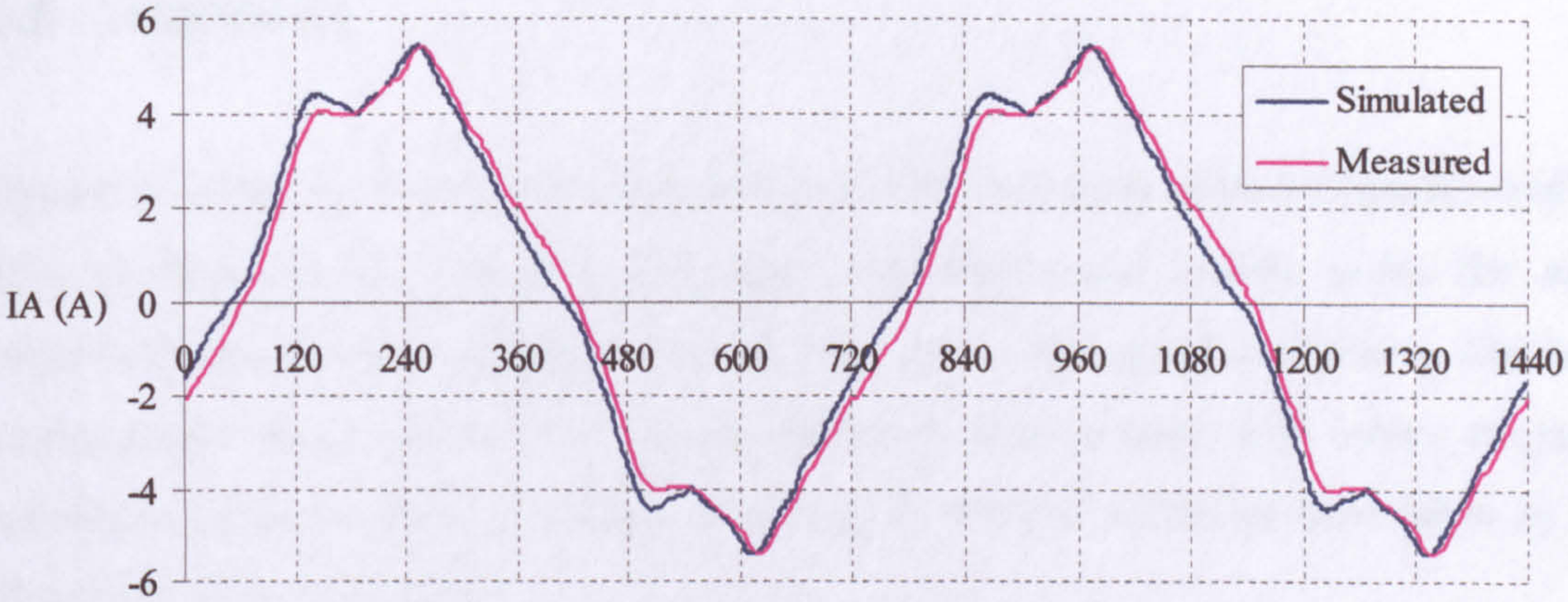

Figure 5.19 Comparison of real and simulated star connected operation. I_{dem}=10.5A(pk), V_{dc}=290V, speed=675rpm.

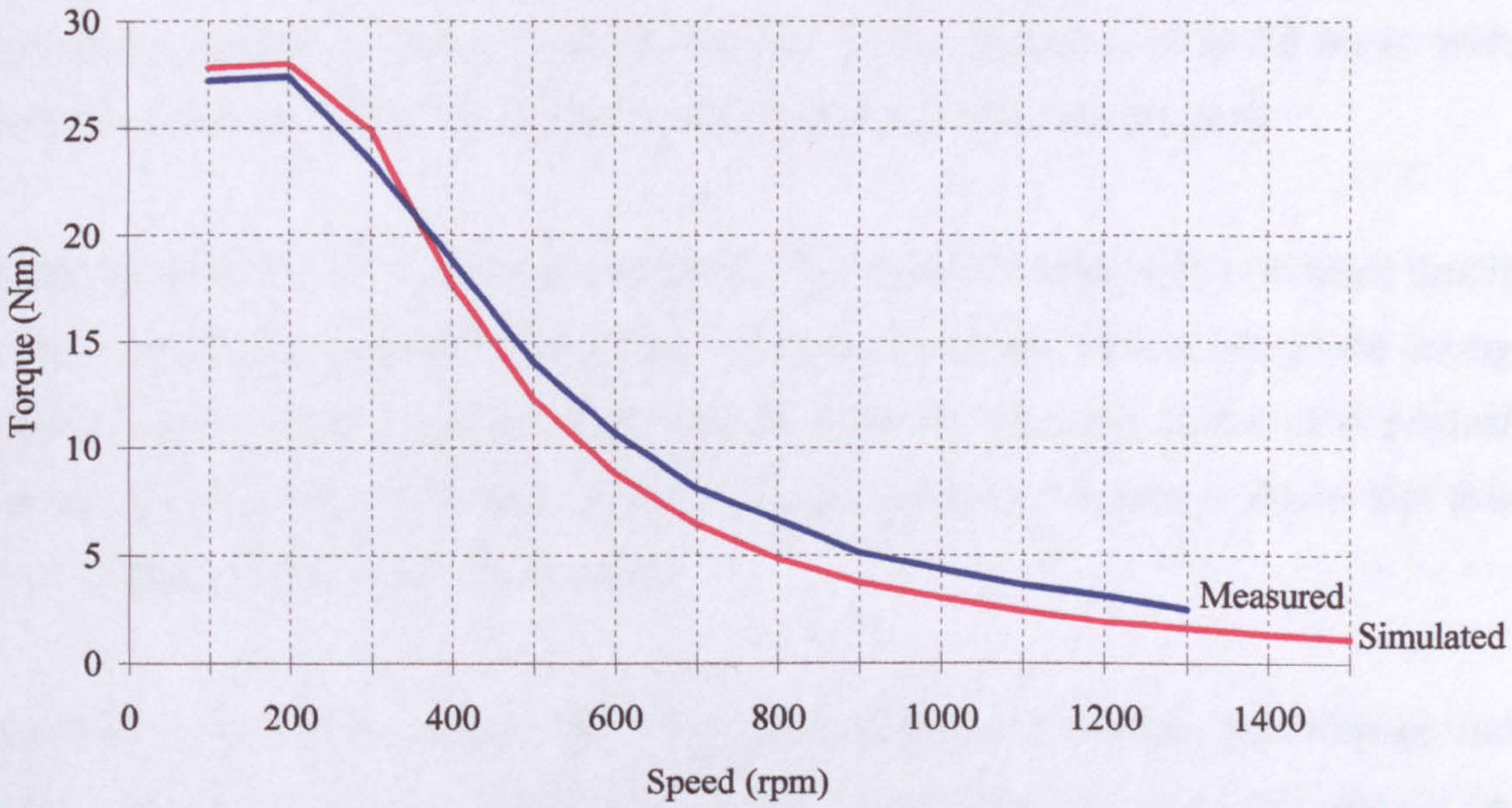

Figure 5.20 Comparison of real and simulated torque-speed characteristics for star connected operation with V_{dc}=290V, I_{dem}=10.5A

5.6 Summary

Operation of the test rig has been demonstrated with each basic mode of operation of the fully pitched winding machine. Simulated waveforms and results under the same conditions have been compared directly. Generally very good correlation has been demonstrated which shows that the simulation is able to cope with heavy magnetic saturation, large amounts of mutual coupling, as well as subtleties introduced by the digital PWM control system.

The benefits of using the transformation matrices has been demonstrated. These have been used to calculate the equivalent single tooth current, flux and torque and have helped to explain how the machine works. For example 240° unipolar operation has been shown to be very similar in some respects to 120° operation of an SR motor with short pitched windings i.e. the single tooth currents and fluxes are the same.

Examination of the flux linkage waveforms with unipolar operation has revealed that it in fact needs to go negative during the off period of a phase. This is due to the strong mutual coupling between phases and is unlike unipolar operation of the short pitched winding machine where the flux linkage is always positive. Chapter 6 shows that this has a significant effect on inverter rating.

Operation with bipolar currents has been demonstrated with current, flux linkage and torque waveforms. The equivalent single tooth waveforms aided in the analysis by showing what happens in each stator tooth so that comparisons can more easily made with the short pitched winding machine. Bipolar operation cannot use the asymmetric inverter commonly used with the SR motor. Instead operation has been demonstrated with both the H bridge inverter and a three phase bridge in star connection.

Chapter 6 - PERFORMANCE COMPARISONS

6.1 Introduction

The last chapter showed measured and simulated waveforms with each different mode of excitation of the machine. This chapter looks at how well they compare in terms two main criteria:

- The rating of inverter required to achieve a given machine output power.
- Torque per unit copper loss and machine efficiency.

Initially, measured torque-speed characteristics will be compared with a fixed current demand. Tests were performed on the test rig with the new machine design described in Chapter 4. In each case the same DC link voltage and the same number of turns per phase were used. The results from this show that there are differences in the torque-speed characteristics, so it therefore becomes necessary to adjust the number of turns in each phase and adjust the current demand to attempt to produce the same machine output over the whole speed range. Simulation results are used for this comparison as the number of turns per phase can be infinitely adjusted with ease (use of the simulation has been justified by the results shown in Chapter 5). Inverter ratings can then be truly compared, with each drive producing the same torque and power output. Comparisons will be made in terms of peak VA as well as average device losses. This is necessary, as the nature of a given application will determine which of the two is more important, as will be discussed.

Machine efficiency and torque per unit copper loss is demonstrated by copper loss comparisons over the speed range. In addition, temperature rise tests were performed for unipolar and bipolar squarewave operation with thermocouple results from various strategic points within the motor. These results are used to demonstrate maximum continuous torque for this new prototype design of fully pitched winding machine. Short term torque and losses are also assessed with the aid of simulation work.

6.2 Inverter Rating Comparison

6.2.1 Torque-Speed Characteristics with the Same Number of Phase Turns and the Same DC Link Voltage

Torque-speed characteristics were measured on the test rig for the various different excitation methods previously described i.e.

- Unipolar (240° conduction using an asymmetric half bridge inverter).
- Bipolar squarewave (360° conduction using an H bridge inverter).
- Sinusoidal (using an H bridge inverter).
- Sinusoidal star connected (using a three phase bridge inverter).

Measurements were taken under the following conditions:

- The prototype machine (described in Chapter 4) with 204 series turns per phase.
- Results were taken with a DC link voltage of 580V (rated voltage) and also at a reduced voltage of 290V to see effects at higher speed without over-speeding the DC load machine.
- On and off angles optimised for maximum average torque throughout the speed range.
- Current demand set at low speed in each case to give the same torque of 27.2Nm, which in the case of unipolar operation corresponds to the nominal rated torque of 19Nm at 1350rpm.

As these results are taken from test rig measurements no comparison is made here with the short pitched winding machine. However, simulated results later in this chapter will make that comparison.

Figures 6.1 and 6.2 show the torque-speed curves at V_{dc}=580V and V_{dc}=290V respectively. The current demands used to achieve these are detailed in Table 6.1. There are clearly differences between each mode of operation, and the reasons will be explained over the forthcoming sections. Note that the results shown are machine

electrical torque calculated by the DSP, as opposed to shaft torque. Appendix C details the method used and a crosscheck with measurements from a torque transducer on the shaft.

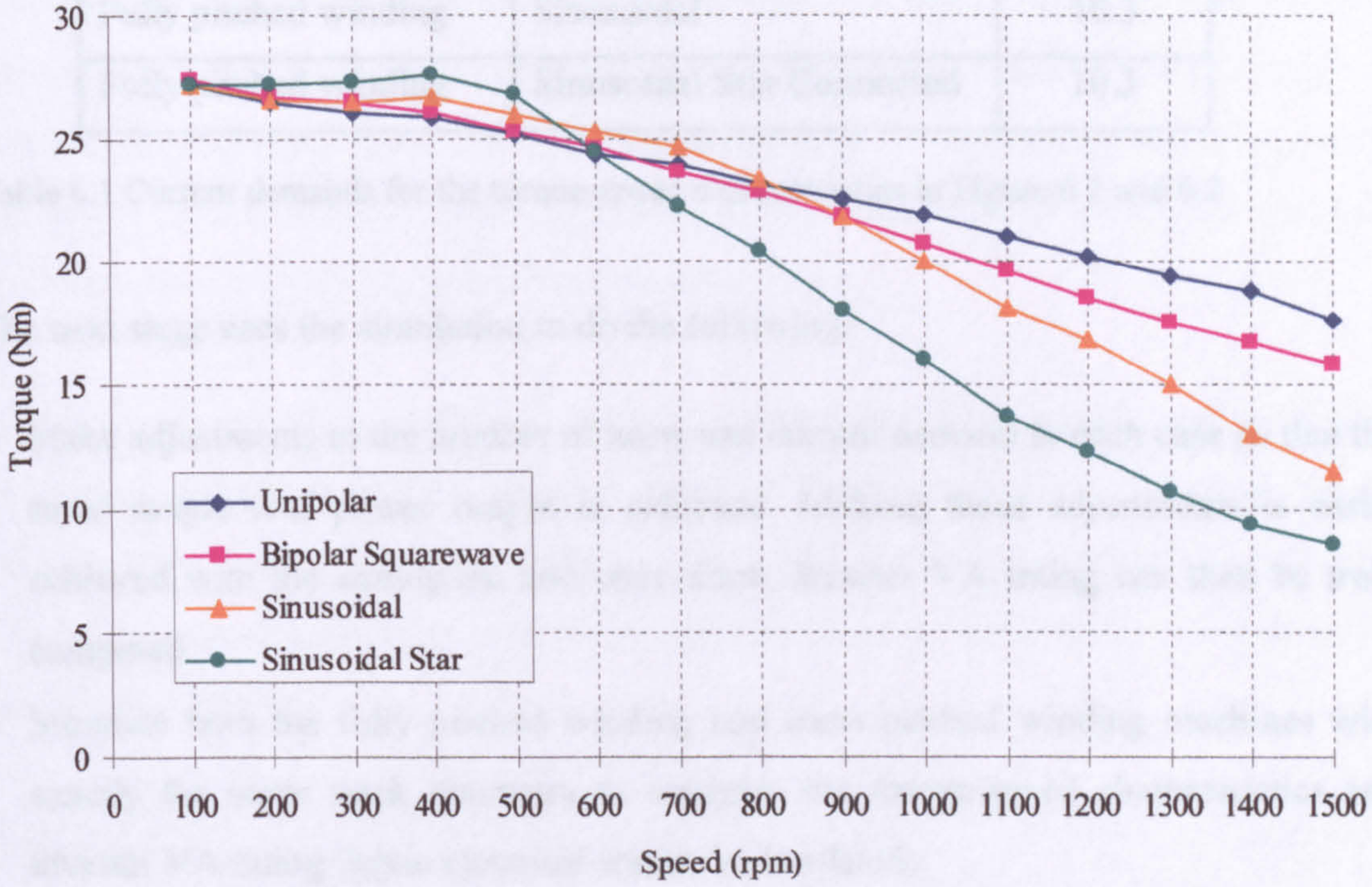

Figure 6.1 Torque-speed characteristics with V_{dc}=580V. Current demands as Table 6.1.

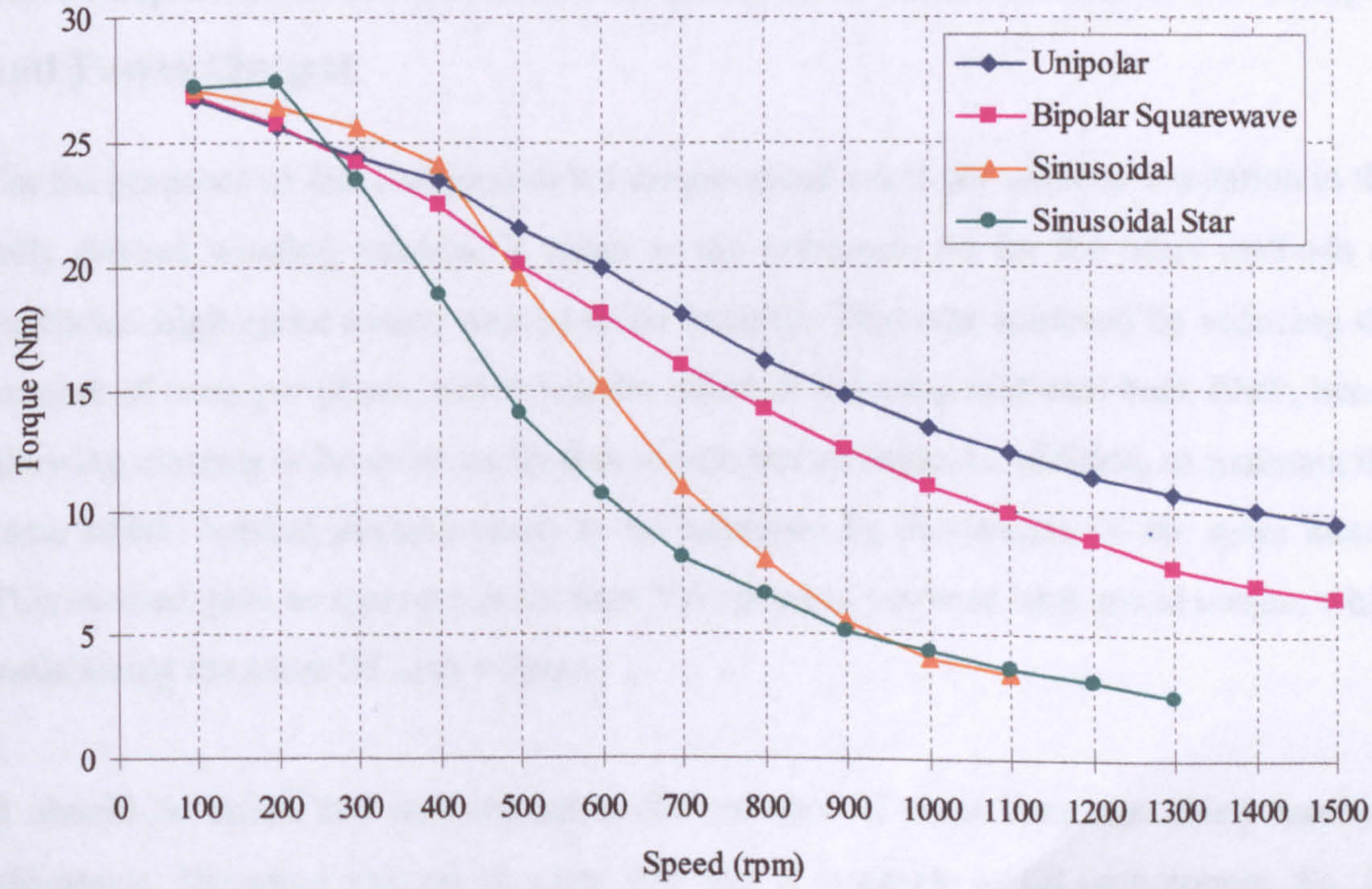

Figure 6.2 Torque-speed characteristics with V_{dc}=290V. Current demands as Table 6.1.

Machine type	Excitation method	Idem
Fully pitched winding	Unipolar	9.2
Fully pitched winding	Bipolar Squarewave	7.1
Fully pitched winding	Sinusoidal	10.3
Fully pitched winding	Sinusoidal Star Connected	10.3

Table 6.1 Current demands for the torque-speed characteristics in Figure 6.1 and 6.2

The next stage uses the simulation to do the following:

- Make adjustments to the number of turns and current demand in each case so that the same torque *and* power output is achieved. Making these adjustments is easily achieved with the simulation and once done, inverter VA rating can then be truly compared.
- Simulate both the fully pitched winding and short pitched winding machines with exactly the same stack geometry to compare the torque-speed characteristics and inverter VA rating (again electrical torque is simulated).

6.2.2 Adjustment to Machine Parameters to Achieve Matched Torque and Power Output

For the purposes of this comparison the torque-speed curve for unipolar excitation in the fully pitched winding machine is taken as the reference. So for the other methods of excitation high speed torque needed to be boosted. This was achieved by reducing the number of turns per phase, which has the effect of reducing motional back EMF, hence allowing currents to be more easily forced into the machine. In addition, to maintain the same MMF, current demand needs to be increased by the inverse of the same factor. This method gave an increase in inverter VA rating to increase high speed torque, while maintaining the same DC link voltage.

It should be noted that any change in the number of turns does not affect machine efficiency. The same amount of stator slot area is available to fill with copper. So, for example, if the number of turns is halved and the current demand doubled, copper losses

(I^2R losses) remain constant because the conductor cross sectional area per turn is doubled.

The different torque-speed curves reduce with speed at slightly different rates, so it is impossible to match the curves over the entire speed range. It makes sense, though, to matched them at two points - low speed and base speed. Base speed is the point at which the desired power output is first achieved. Advance and conduction angles are again optimised at each point for maximum average torque.

Table 6.2 shows the conditions used to match the torque-speed curves. Before adjustment each machine had the same number of turns per phase. The 'turns factor' refers to the relative adjustment to the number of turns needed to achieve the matching. The current demands are also adjusted by the inverse of the same factor to maintain the same MMF as before.

Machine type	Excitation method	Turns factor	Number of series turns	Idem after adjustment
Fully pitched winding	Unipolar	1	204	9.4
Fully pitched winding	Bipolar Squarewave	0.88	180	8.3
Fully pitched winding	Sinusoidal	0.82	167	12.8
Fully pitched winding	Sinusoidal Star Connected	0.6	122	17.5
Short pitched winding	Unipolar	2	408	9.4

Table 6.2 Adjustments to the number of turns and current demand.

The short pitched winding machine is now included in this comparison and control of this machine is complicated by the fact that the conduction angle can be set to any value between 120° and 180°. More torque is always achieved with 180° conduction with lower torque ripple, but there is a severe penalty in terms of copper loss, especially at low speed. Beyond base speed, however, 180° is desirable to maximise power output for a given inverter size. To present the best case for the short pitched winding machine conduction angle is varied with speed. At low speed 120° is used to maximise torque per unit copper loss. Conduction angle is then raised gradually with speed to values between 130° and 140 °. This still maintains good torque per unit copper loss but lowers torque

ripple significantly and raises torque output for a given current demand. Only in the region of base speed and above does the conduction angle become close to 180° to maximise torque output. Advance angle is optimised at each speed. The angles used for the short pitched winding machine, and those for each mode of operation of the fully pitched winding machine, are shown in Figure 6.3.

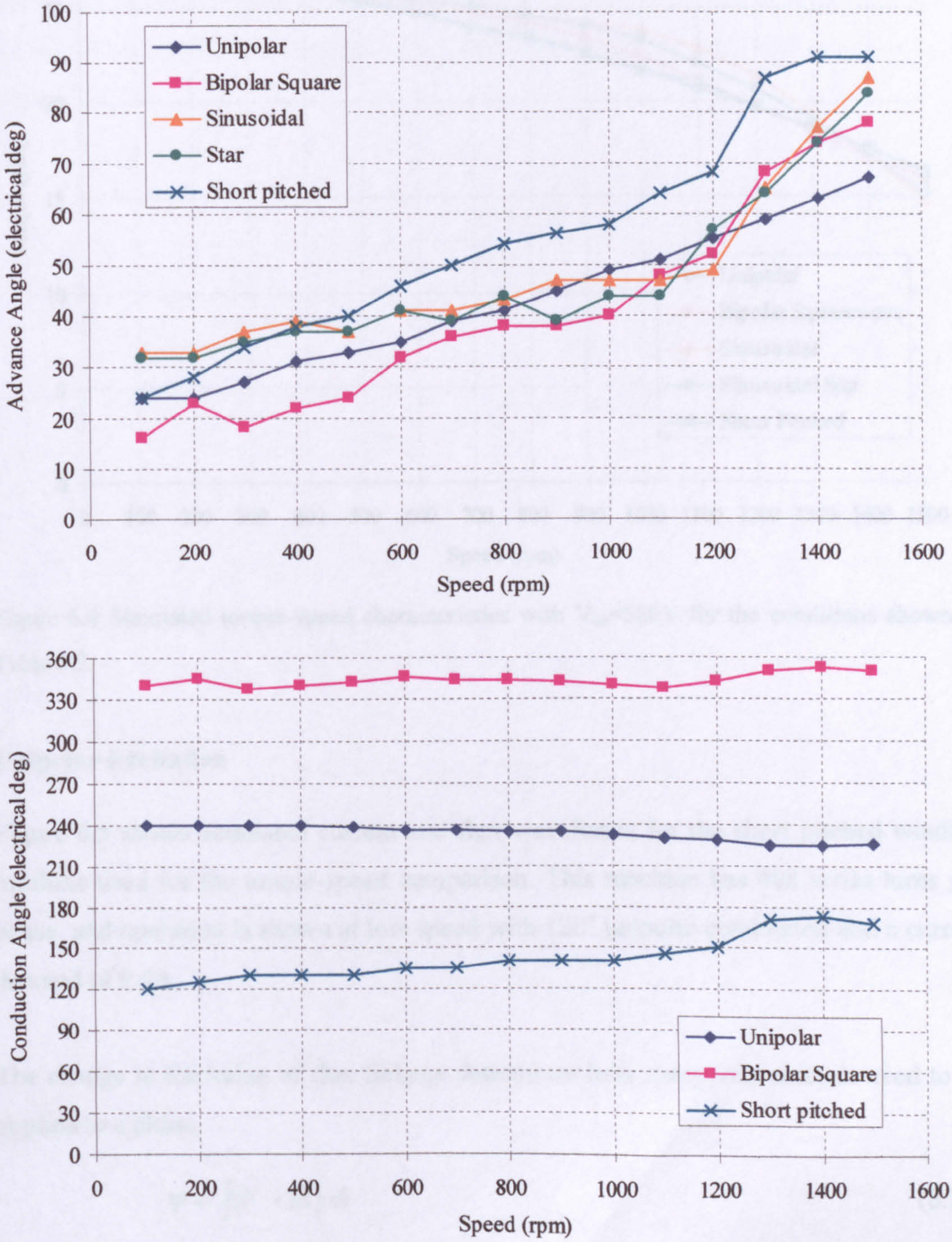

Figure 6.3 Advance and conduction angles used for the torque output shown in Figure 6.4

Figure 6.4 shows the resulting torque-speed curves and confirms that the torque has been matched at low speed as well as base speed. The following sections explain the need for the adjustments to number of turns per phase.

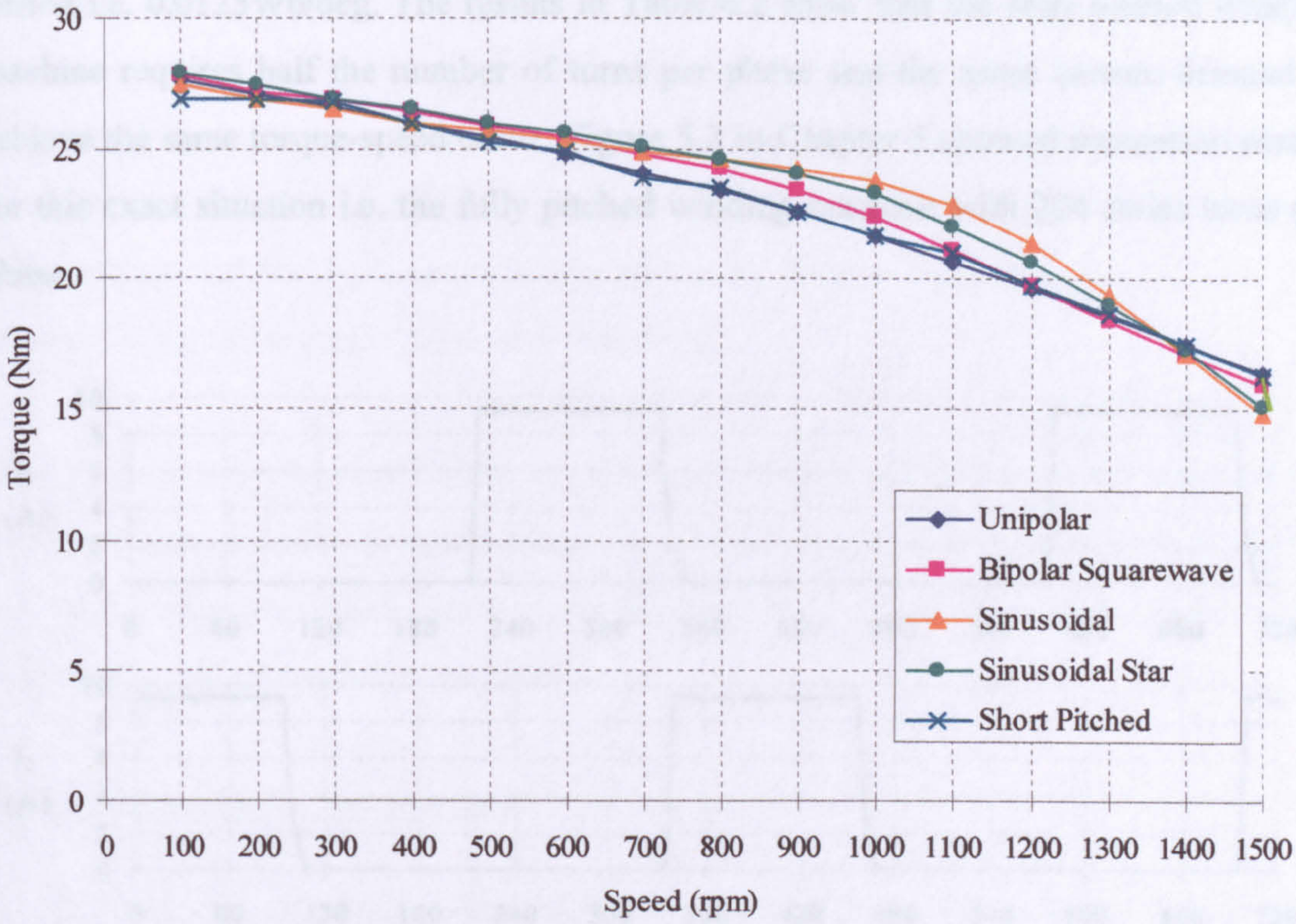

Figure 6.4 Simulated torque-speed characteristics with V_{dc}=580V for the conditions shown in Table 6.2.

Unipolar Excitation

Figure 6.5 shows simulated current and flux waveforms for the short pitched winding machine used for the torque-speed comparison. This machine has 408 series turns per phase, and operation is shown at low speed with 120° unipolar conduction and a current demand of 9.4A.

The change in the value of flux linkage determines how many volt-seconds need to be applied to a phase.

$$\psi = \int (V - iR).dt \tag{6.1}$$

where 'V'is the applied voltage to the phase, 'iR' is the volts drop across the phase due to its resistance.

This will consequently determine the speed at which the inverter is no longer capable of forcing the required current into the machine, which leads to torque output falling off with increasing speed. The change in flux linkage here is 1.5Wb and occurs over a 120° period i.e. 0.0125Wb/deg. The results in Table 6.2 show that the fully pitched winding machine requires half the number of turns per phase and the same current demand to achieve the same torque-speed curve. Figure 5.2 in Chapter 5 showed simulation results for this exact situation i.e. the fully pitched winding machine with 204 series turns per phase.

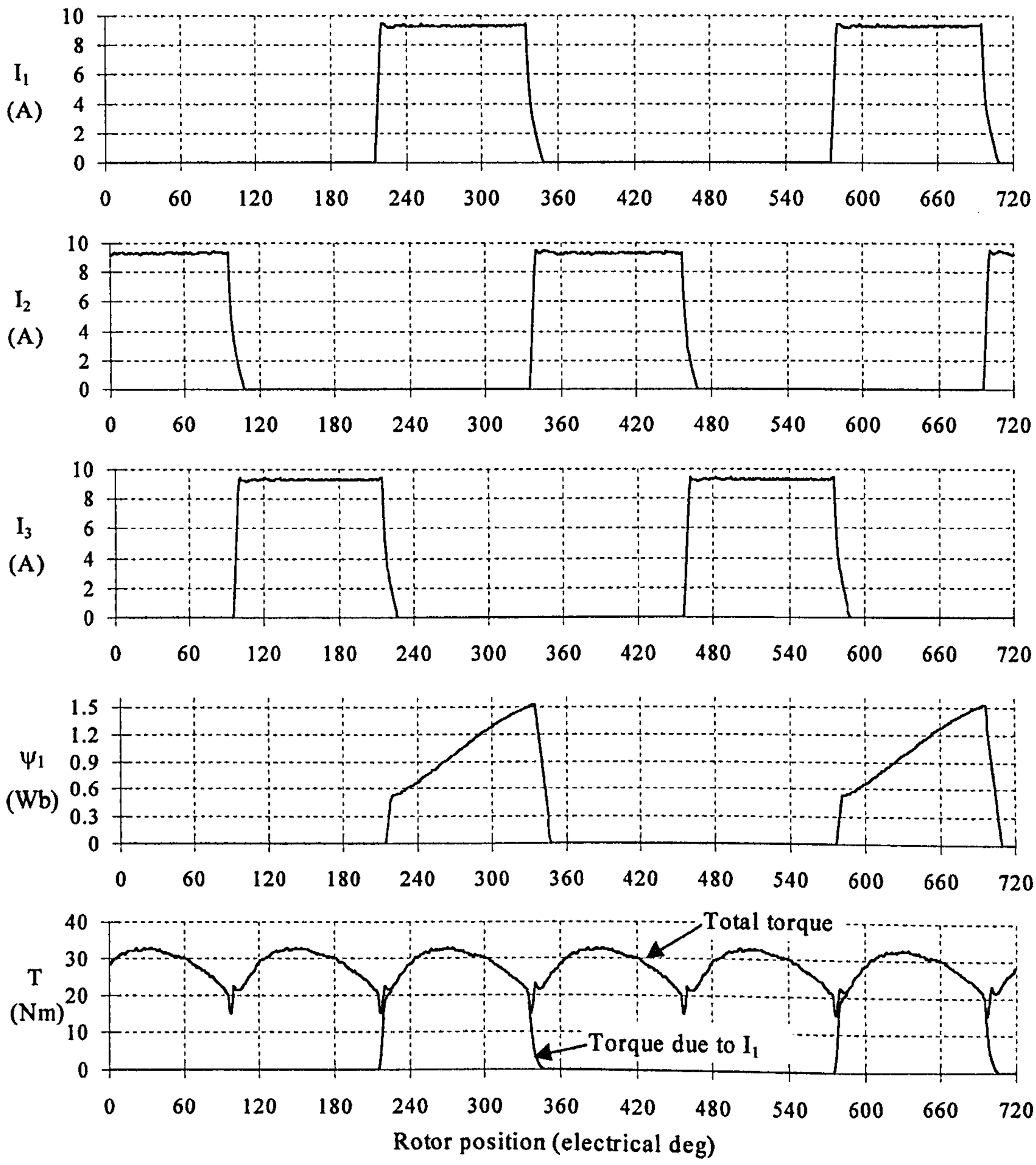

Fig. 6.5 Simulated low speed current and flux waveforms for the short pitched winding machine.

Figure 5.2 shows that during its conduction period of 240° the flux linkage rises to a level of 0.75Wb – half that of that of the short pitched winding machine. This is as expected as the fully pitched winding machine has half as many turns and the same current demand. During the off period of the phase, however, the flux linkage needs to go negative by the same value due to the mutual coupling between phases (the flux in the two phases that are conducting also links the phase that is off). At high speed, therefore, the rate of fall of flux linkage at turn off of a phase is the same in both the fully pitched and short pitched winding machines. This explains why torque now falls off with speed at the same rate in both machines.

Note that the same level of MMF in each tooth is also maintained in the fully pitched winding machine and so the same torque is produced. In comparison to the short pitched winding machine current demand is now the same, the number of turns per phase is half, but two phases are excited at the same time.

Bipolar Squarewave Excitation

Current and flux waveforms were shown in Figure 5.9 for the fully pitched winding machine with bipolar squarewave operation. These waveforms are before the adjustments to the number of turns i.e. 204 series turns per phase as with unipolar excitation. This mode of operation is a little more difficult to compare directly with unipolar operation as the waveforms are quite different. It is therefore difficult to assess the exact required rate of change of flux required at high speed. However, the highest general rate of change of flux is, for example in the period between 80 ° and 225°. Here the total change of flux linkage is 2.1Wb, which corresponds to a rate of change of 0.0145Wb/deg. This is slightly higher than unipolar operation and goes some way to explaining why the number of turns needs to be reduced by a factor of 0.88 to match the torque-speed characteristics.

Sinusoidal Excitation

This is very similar to bipolar square operation in that both are operated from the same H bridge inverter and both waveforms are bipolar. The difference is that the sinusoidal shape of the current demand is detrimental to high speed performance. Figures 6.6 and

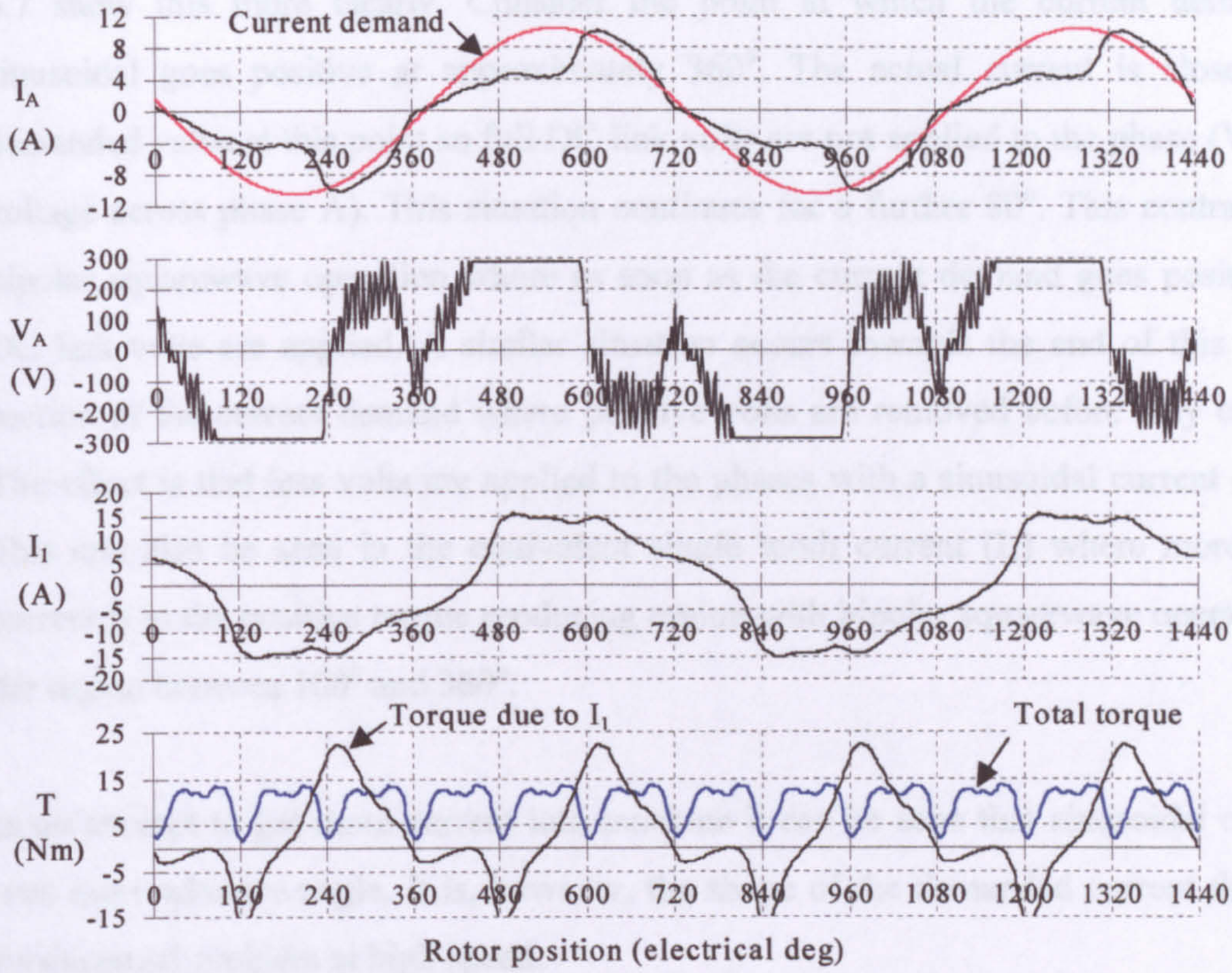

Fig.6.6 Simulated waveforms of sinusoidal operation with V_{dc}=290V, speed=675rpm.

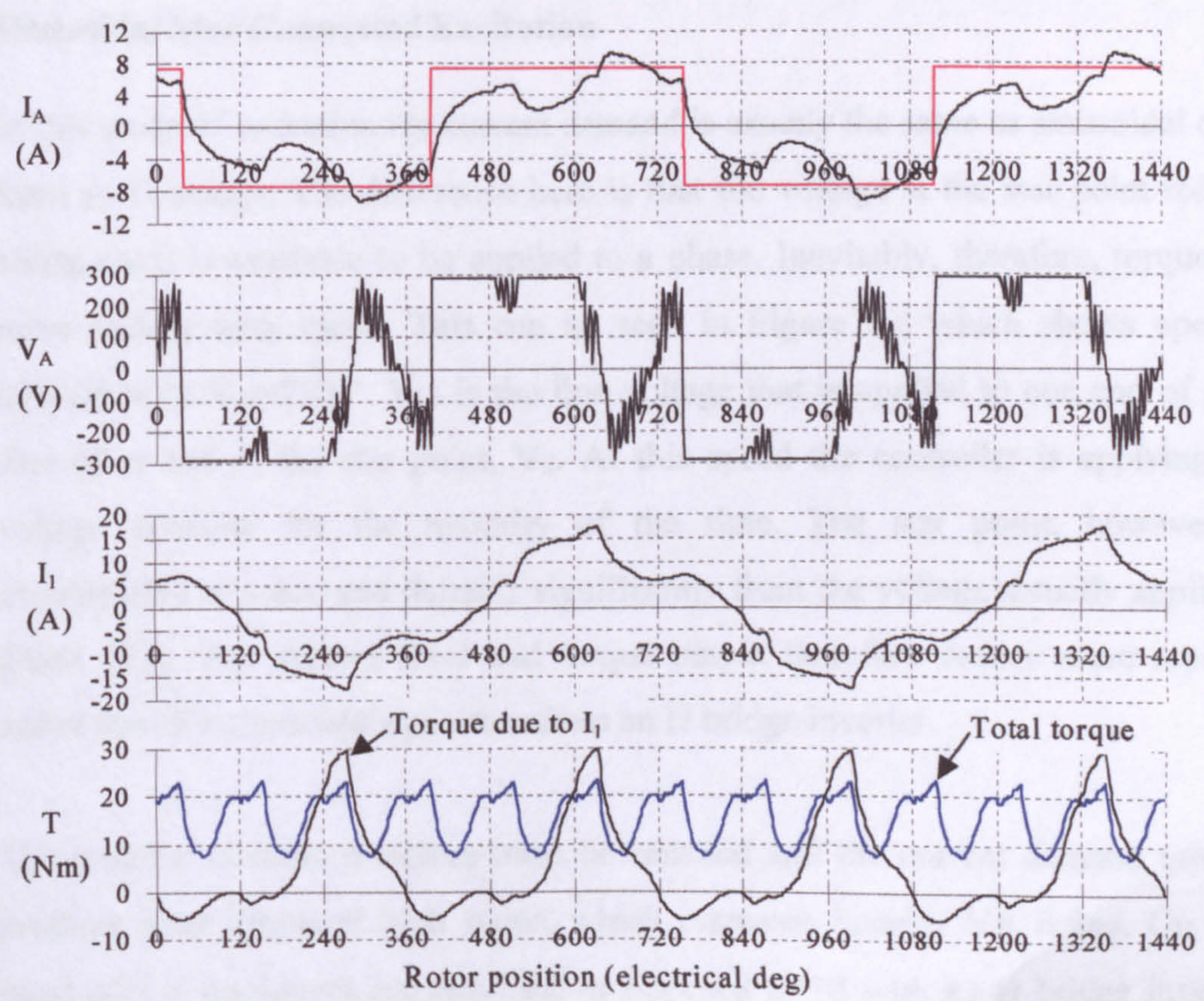

Fig. 6.7 Simulated waveforms for bipolar squarewave operation with V_{dc}=290V, speed=675rpm.

6.7 show this more clearly. Consider the point at which the current demand for sinusoidal goes positive at approximately 360°. The actual current is close to the demanded value at this point so full DC link volts are not applied to the phase (V_A is the voltage across phase A). This situation continues for a further 80°. This contrasts with bipolar squarewave operation where as soon as the current demand goes positive, full DC link volts are applied. A similar situation occurs towards the end of this positive section of the current demand where positive volts are removed before they could be. The effect is that less volts are applied to the phases with a sinusoidal current demand. This can also be seen in the equivalent single tooth current (I_1) where more of this current is in the positive torque producing region with bipolar squarewave operation e.g. the region between 180° and 360°.

In an attempt to get more current into machine it can be seen that sinusoidal operation uses more advance angle. It is, however, the shape of the demanded current that is the fundamental problem at high speed.

Sinusoidal Star Connected Excitation

In this mode of operation the current demand is exactly the same as sinusoidal operation from an H bridge. The difference here is that the voltage at the star point reduces the voltage that is available to be applied to a phase. Inevitably, therefore, torque reduces more rapidly with speed. This can be seen in Figure 6.8 which shows operation at 675rpm with V_{dc}=290V. V_{L1} is the line voltage that is applied to one end of phase A. The other end is the star point, V_S. At this speed the controller is applying the full voltage possible for the majority of the time. The star point, however, varies considerably in value and detracts significantly from the voltage actually applied to the phase (V_A). The current level and torque output therefore reduce more rapidly with speed than for sinusoidal operation from an H bridge inverter.

The number of turns therefore must be reduced and the current demand increased to produce more torque at high speed, which increases inverter VA rating. On the other hand only 6 transistors are required, as opposed to 12 with an H bridge inverter. The next section compares the overall effect in terms of inverter size and rating.

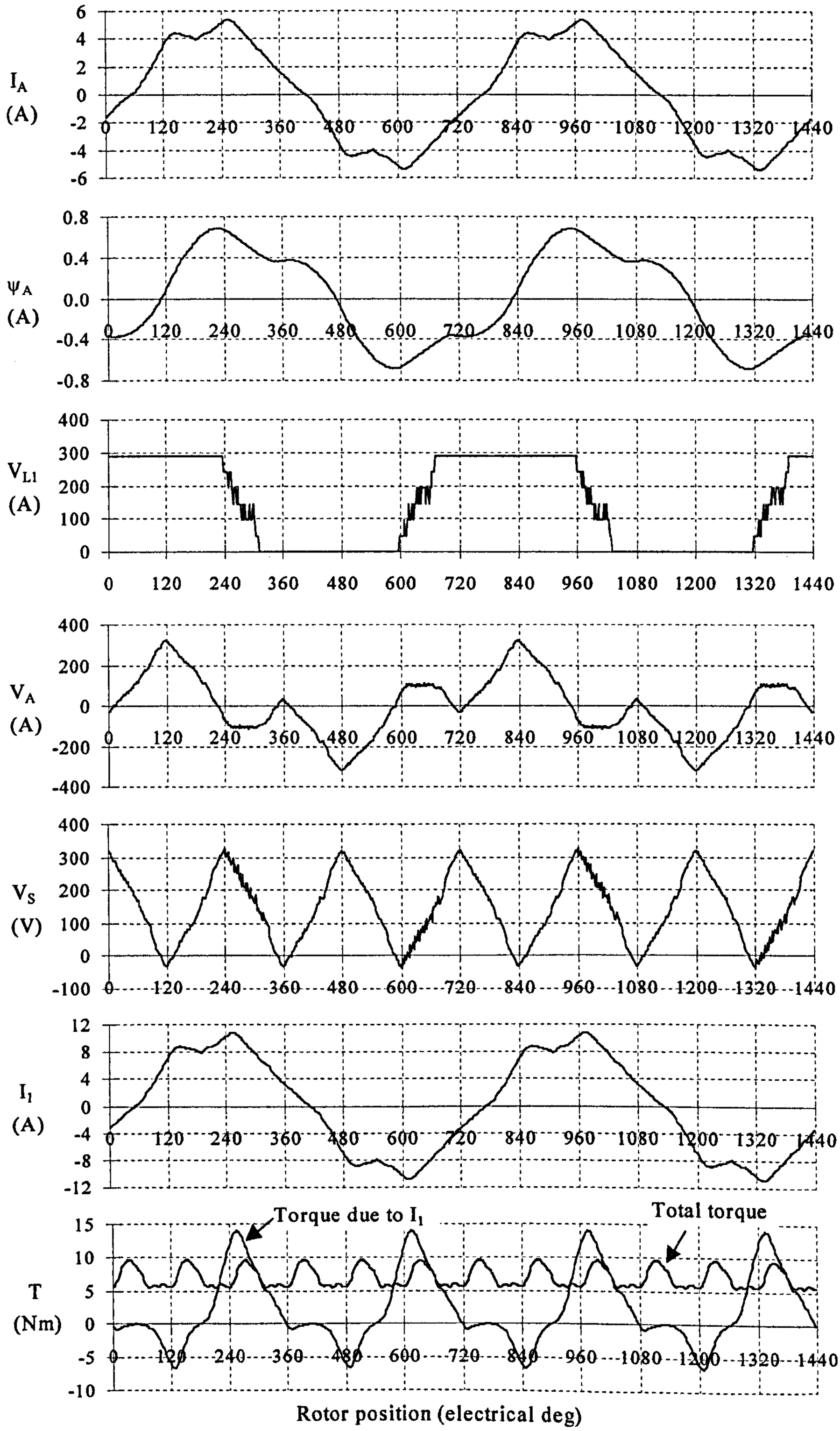

Figure 6.8 Simulation of star connected operation. I_{dem}=10.5A(pk), V_{dc}=290V, Speed=675rpm.

6.2.3 Inverter Rating

Several papers have been published on methods to evaluate the inverter VA rating of SR machines for example Miller [6.1], Davis *et al* [6.2] and Ray *et al* [6.3]. Two commonly used techniques are:

- Calculate the peak volts and current that each power electronic device must withstand, and multiply this by the number of switches in the circuit. Inverter rating is then expressed in terms of kVA per kW of motor power.
- Calculation of device rms current and peak voltage, again expressed in terms of kVA/kW.

It will be seen that these two different methods of comparison unfortunately yield different relative results, and which one is more important depends on the application conditions. The majority of power circuits today are constructed using either MOSFETS or IGBTs. It is true to say that in both cases these devices are much less sensitive to peak currents than they used to be. For example SOAs (Safe Operating Areas) are very wide and dynamic switching effects such as 'latch up' in IGBTs have been eliminated with improvements in design (see Clemente *et al* [6.4]). This is caused when excessive currents are attempted to be turned off in a device – a high density of hole currents flow in the resistor r_b in the IGBT equivalent circuit, and the result is the device turns back on and latches like a thyristor.

The main factor that determines the selection of a device is the calculation of its peak junction temperature, which is determined by the losses in the device and its thermal resistance to the heatsink. There are two basic calculations that need to be performed:

- Calculation of junction temperature at high speed. In this situation it is the *average* device losses that should be used for the calculation. This assumes that the thermal time constant of a device is long, so that junction temperature will not vary across an electrical cycle.
- Calculation of junction temperature at minimum speed. If the motor speed is low enough then the junction temperature will reach its steady state value at the point in the electrical cycle with the *peak* current. The junction temperature calculation should then be based on the losses in the device at this point. Note that if the minimum

motor speed is not low enough to reach this steady state value a more complex calculation must be done that takes in to account the thermal time constant of the device. This involves use of the 'Effective Transient Thermal Impedance' of the device published in its datasheet.

Clearly the application conditions need to be known before it can be determined whether it is the peak losses or the average losses that are more important. In other words whether inverter rating should be based on the peak VA calculation or the rms current/peak voltage calculation.

The following are additional points to consider in the assessment of the 'size' or cost of an inverter drive:

- **Number of switches.** Both of the above analyses take this into account by calculating the individual VA rating of each switch and multiplying by the total number. This is a very simplistic assumption. The cost of one device is not necessarily twice the cost of two devices of half the VA rating. In addition, a larger number of smaller devices tend to take up more space, cost more to assemble and require more drive and control circuits. The relative effect of these will be different in a small drive compared to a large one. For example the cost of a drive circuit in a low power drive is close to that of the switch itself, whereas in a larger drive there may well be an order of magnitude difference in the cost. For these reasons it is likely that more preference should be given to the inverter with a lower number of switches.

Besides purely the number of switches, circuit topology can be an important factor. If the freewheel diodes are in parallel to the switches they can easily be placed within the same package and hence reduce component count. This is the case with both sinusoidal operation (H bridge) as well as sinusoidal star connected operation (three phase bridge). Total cost of the power devices is not generally reduced, but there would be indirect saving due to the fact that the physical layout would be much smaller e.g. PCB material, insulating washers, heatsink mounting area and assembly cost. A further advantage of star connected operation is that standard three phase bridge modules could be used.

- **Total inverter loss.** This is important for selecting the heatsink size and hence its cost. Take, for example, a situation where two different drives have the peak instantaneous loss per device and indeed the same peak current and voltage. The same size device is then selected for both drives on the basis of the same heatsink temperature. However in one drive two phases may be conducting at a time, and in the other only one phase. The same size device can be selected but one has twice the *total* inverter loss. This drive will therefore need twice the heatsink rating, which will cost more and take up more space.

The following two sections detail the comparisons using the two basic techniques described above. It should also be noted that the results were obtained from the accurate dynamic simulation of machine and controller. Many papers such as the ones referenced above make the comparisons on the basis of simple linear or quasi-linear models of the motor which inevitably cannot be such an accurate reflection of true life conditions.

6.2.3.1 Peak VA Comparisons

The following table summarises the inverter rating for different machines and excitation methods on the basis of peak current and volts. This assessment is made after the matching of the torque-speed characteristics previously described and which involves a change in the number of turns per phase and the current demand. The last column in the table 'Rel. size' is the ratio of the inverter rating for each case compared to the short pitched winding machine.

On this basis the fully pitched winding machine with unipolar excitation requires the same size inverter as the short pitched winding machine. All the bipolar methods, however, need a very large inverter in comparison. Sinusoidal operation with an H bridge needs a particularly large inverter due to the high peak current of the sinusoidal shape, combined with the fact that high speed performance is not good. The latter leads to the number of turns being reduced to improve performance, which makes peak current worse again. Sinusoidal star operation on the other hand fairs relatively well overall – the torque-speed performance is very poor, meaning that the number of turns and current demand has to be altered substantially, but this is more than compensated by

the fact that only six switches are required, compared to the 12 that bipolar squarewave and sinusoidal require.

Machine Type	Excitation Method	No. of Devices	Current Demand (pk, A)	Peak Volts (V)	Device kVA	Inverter Rating (kVA/kW)	Rel. Size
Fully pitched winding	Unipolar	6	9.4	580	0.545	12.85	1
Fully pitched winding	Bipolar Squarewave	12	8.3	580	0.481	22.70	1.77
Fully pitched winding	Sinusoidal	12	12.8	580	0.742	35.01	2.72
Fully pitched winding	Sinusoidal star	6	17.5	580	1.015	23.93	1.86
Short pitched winding	Unipolar	6	9.4	580	0.545	12.85	1

Table. 6.3 Inverter rating based on peak volts and current (for output power of 2545W at 1350rpm with V_{dc}=580V).

6.2.3.2 Device Loss Comparisons

Total inverter losses are shown in Figure 6.9. These relate directly to the matched torque-speed curves of Figure 6.4. Losses are based on a model of the IRGBC50KD2 device which combines a 1200V IGBT with an ultra fast recovery epitaxial diode (FRED). Losses include conduction losses in the IGBT and diode, in addition to switching losses in the IGBT, which is based on a switching frequency of 10kHz (the calculation method used by the simulation is described in Section 3.4.2 of Chapter 3).

Tables 6.4 and 6.5 give a more detailed breakdown of where the losses are occurring at low speed (100rpm) and base speed (1350rpm) respectively.

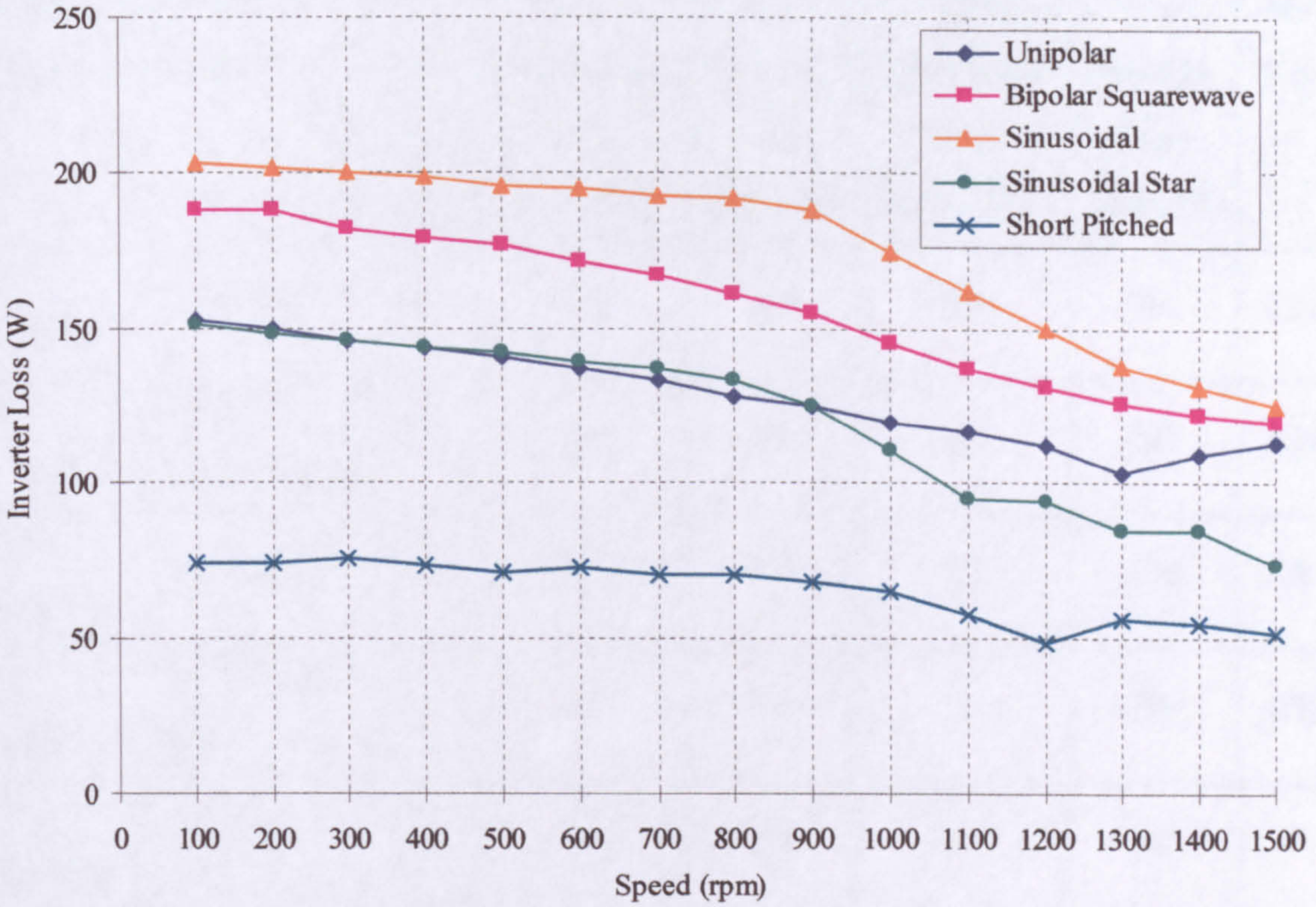

Figure 6.9 Simulated total inverter losses for different machines and excitation methods.

Machine Type	Excitation Method	No. of Dev-ices	Trans. Conduction Loss (Av., W)	Trans. Switch Loss (Av., W)	Diode Conduction Loss (Av., W)	Total Inverter Loss (Av., W)	Rel. Size
FP winding	Unipolar	6	6.4	13.2	5.9	153	2.07
FP winding	Bipolar squarewave	12	3.8	8.3	3.6	188	2.54
FP winding	Sinusoidal	12	4.2	8.8	4.1	205	2.77
FP winding	Sinusoidal star	6	6.8	12.2	6.4	152	2.05
SP winding	Unipolar	6	3.4	6.4	2.6	74	1

Table 6.4 Breakdown of device losses at 100rpm (simulated). SP=short pitched, FP=fully pitched.

Machine Type	Excitation Method	No. of Dev-ices	Trans. Conduction Loss (Av., W)	Trans. Switch Loss (Av., W)	Diode Conduction Loss (Av., W)	Total Inverter Loss (Av., W)	Rel. Size
FP winding	Unipolar	6	6.8	6.9	3.8	105	1.91
FP winding	Bipolar squarewave	12	3.3	4.9	2.1	123	2.24
FP winding	Sinusoidal	12	3.9	4.7	2.7	136	2.47
FP winding	Sinusoidal star	6	6.1	4.9	3	84	1.53
SP winding	Unipolar	6	5.1	2.5	1.7	55	1

Table 6.5 Breakdown of device losses at 1350rpm (simulated). SP = short pitched winding, FP = fully pitched winding.

Some of these results clearly contrast with the comparisons made on the basis of peak VA rating, due to variations in the period that each device conducts during an electrical cycle. Unipolar excitation of the fully pitched winding machine has approximately twice the device and total inverter loss compared to the short pitched winding machine throughout the speed range. This contrasts with the peak VA comparison which indicates both inverter sizes are the same. This is due to the fact that once the torque-speed curves have been matched both machines have the same current demand. The conduction period in the fully pitched winding machine, though, is twice that of the short pitched winding machine at 240°, thereby doubling the *average* device losses.

It is a similar situation with bipolar squarewave operation, which shows an increase of approximately 50% in the relative inverter size between the two methods of comparison. This is explained by the fact that in a bipolar waveform the device conduction period is 180°, which is 50% larger than the 120° conduction period in the short pitched winding machine.

The inverter size with both sinusoidal excitation methods hardly increases at all between the two methods of determining inverter size. This is explained by the fact that one half of a sinusoid (180° conduction period) is very similar in area to a squarewave of 120° conduction period with the same height, as shown in Figure 6.10. There is, therefore, only a relatively small increase with this inverter rating method, compared to the short pitched winding machine.

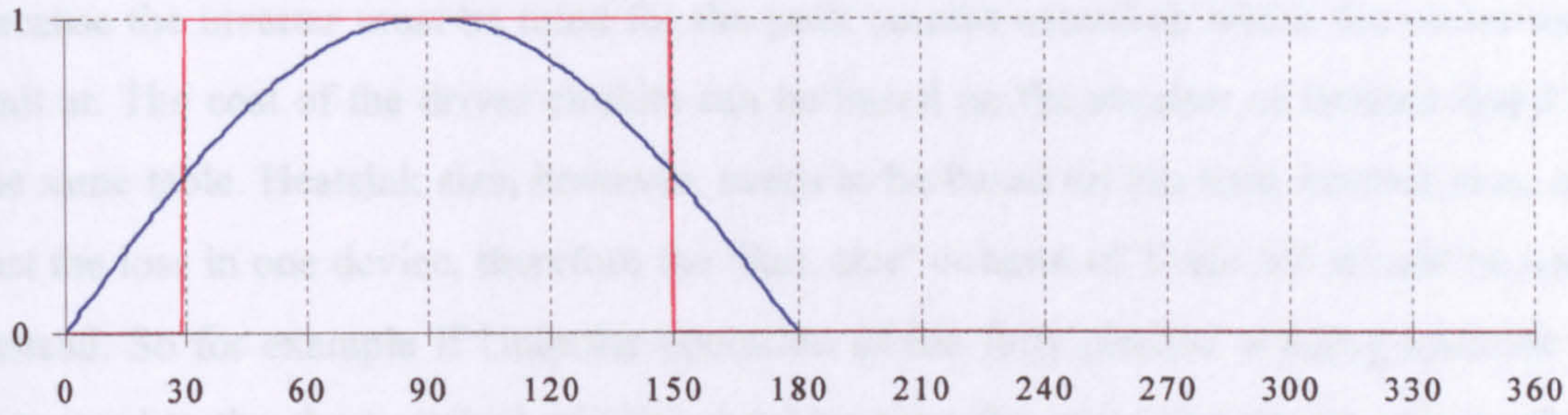

Figure 6.10 Comparison of area of a 120° squarewave and half of a sinusoid

Notice that sinusoidal star connected is the best of the bipolar waveforms – as explained in the previous method of comparison, current demand needs to be high due to the poor high speed performance, but only 6 switches are required. An added advantage is that these switches are connected in the three phase bridge topology used with all other types of AC machine such as the induction motor. The advantage over the asymmetric half bridge is that the diodes are in parallel to the switches, resulting in only 6 discrete packages being required compared to 12.

Note that the relative inverter sizes compared to the short pitched winding machine, all reduce between Table 6.4 and Table 6.5. This is thought to be due to the increasing conduction period with speed in the short pitched winding machine i.e. greater than 120° conduction. The simulation search routine was set to find the optimum on and off angles for maximum average torque at each speed. At low speed, however, the conduction period is not allowed to exceed 120°, which maximises torque per unit copper loss in this machine and hence gives it its best torque per unit copper loss figure to compare to the fully pitched winding machine. At higher speed the conduction angle is allowed to increase up to a maximum value of 180°. This maximises torque output at higher speed for a given current demand and hence minimises the inverter peak VA rating. Inverter losses, on the other hand, do increase as a result.

6.2.3.3 Inverter Rating Summary

The above figures can now be used to 'cost' the inverter for each case depending on the application conditions.

Motor Stall Condition - If the worst case junction temperature occurs in a motor stall situation then device size can be based on the 'Rel. Size' column of Table 6.3. This is because the inverter must be rated for the peak current condition which the motor may stall at. The cost of the driver circuits can be based on the number of devices listed in the same table. Heatsink size, however, needs to be based on the total inverter loss, not just the loss in one device, therefore the 'Rel. size' column of Table 6.4 should be used instead. So for example if Unipolar operation of the fully pitched winding machine is compared to the short pitched winding machine then the same size devices are needed, but the heatsink needs to be twice the size.

High Speed Condition - This is the speed at which the silicon junction temperature is virtually stable across the electrical cycle, in other words the speed at which the thermal time constant of the device is much larger than one electrical cycle in the machine. It is only the average losses that need to be considered, so Table 6.5 can be used to assess the cost and size of the devices, drive circuits and heatsink.

Low Speed condition - This is the situation where the rotor is turning but the silicon temperature varies considerably across the electrical cycle. Peak current as well as average device losses are important. The relative inverter size and cost will be somewhere in between the figures given in Table 6.3 and 6.4. Heatsink size will still be based on the average losses i.e. Table 6.4.

Section 6.3 of this chapter now compares machine performance. Section 6.4 will summarise inverter rating and machine performance tradeoffs.

6.3 Machine Performance Comparison

6.3.1 Copper Loss Comparisons

Test Rig Results

Copper loss is measured on the test rig by the DSP controller. This continuously samples the phase currents and calculates copper loss using the measured DC phase resistance value of 1.825Ω (measured at 22°C). As with all measurements made by the DSP, values are measured over 10 electrical cycles to ensure a stable reading.

Measured copper losses for the prototype fully pitched winding machine are shown in Figure 6.11, and these correspond directly with the torque results shown in Figure 6.1. Note that these were produced with a fixed current demand across the speed range and are therefore not necessarily representative of rated machine torque against speed.

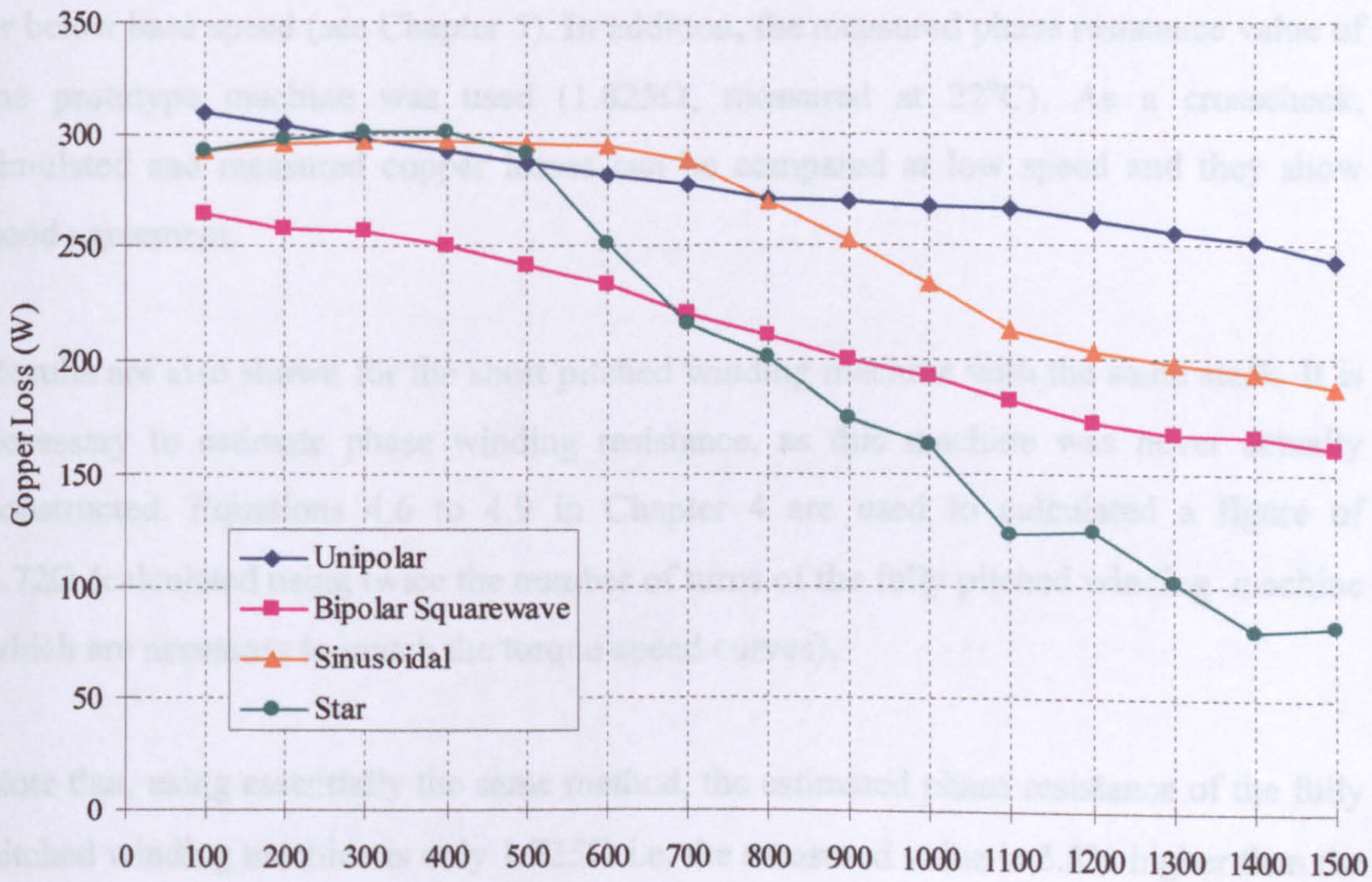

Figure 6.11 Copper losses for the torque shown in Figure 6.1 as measured by the DSP.

Comparisons of torque per unit copper loss between the different excitation methods can now be made at low speed where the torque output is the same. Direct comparisons cannot, however, be made at higher speed as torque output is not the same. This is because in an SR motor torque per unit copper loss is not constant with torque, due to the varying amount of saturation in the magnetic circuit.

Simulation Results

The advantage of using simulation is that the torque-speed curves can be matched by adjusting the number of phase turns and the current demand. Figure 6.4 showed torque matched as closely as possible up to base speed. The associated copper losses for these results are shown in Figure 6.12. Figure 6.13 shows these results in terms of torque per unit copper loss against speed.

The use of the simulation is justified because excellent correlation has been demonstrated between the simulated and measured waveforms, particularly at speeds at or below base speed (see Chapter 5). In addition, the measured phase resistance value of the prototype machine was used (1.825Ω, measured at 22°C). As a crosscheck, simulated and measured copper losses can be compared at low speed and they show good agreement.

Results are also shown for the short pitched winding machine with the same stack. It is necessary to estimate phase winding resistance, as this machine was never actually constructed. Equations 4.6 to 4.9 in Chapter 4 are used to calculated a figure of 4.72Ω (calculated using twice the number of turns of the fully pitched winding machine which are necessary to match the torque-speed curves).

Note that, using essentially the same method, the estimated phase resistance of the fully pitched winding machine is only 1.725Ω i.e. the measured value is 5.8% higher than the calculated. This is because the machine was unfortunately wound with longer than necessary endwindings. The results shown for the fully pitched winding machine are therefore pessimistic. Tabulated results of the above are shown in Tables 6.6 and 6.7 at 100rpm and 1350rpm respectively .

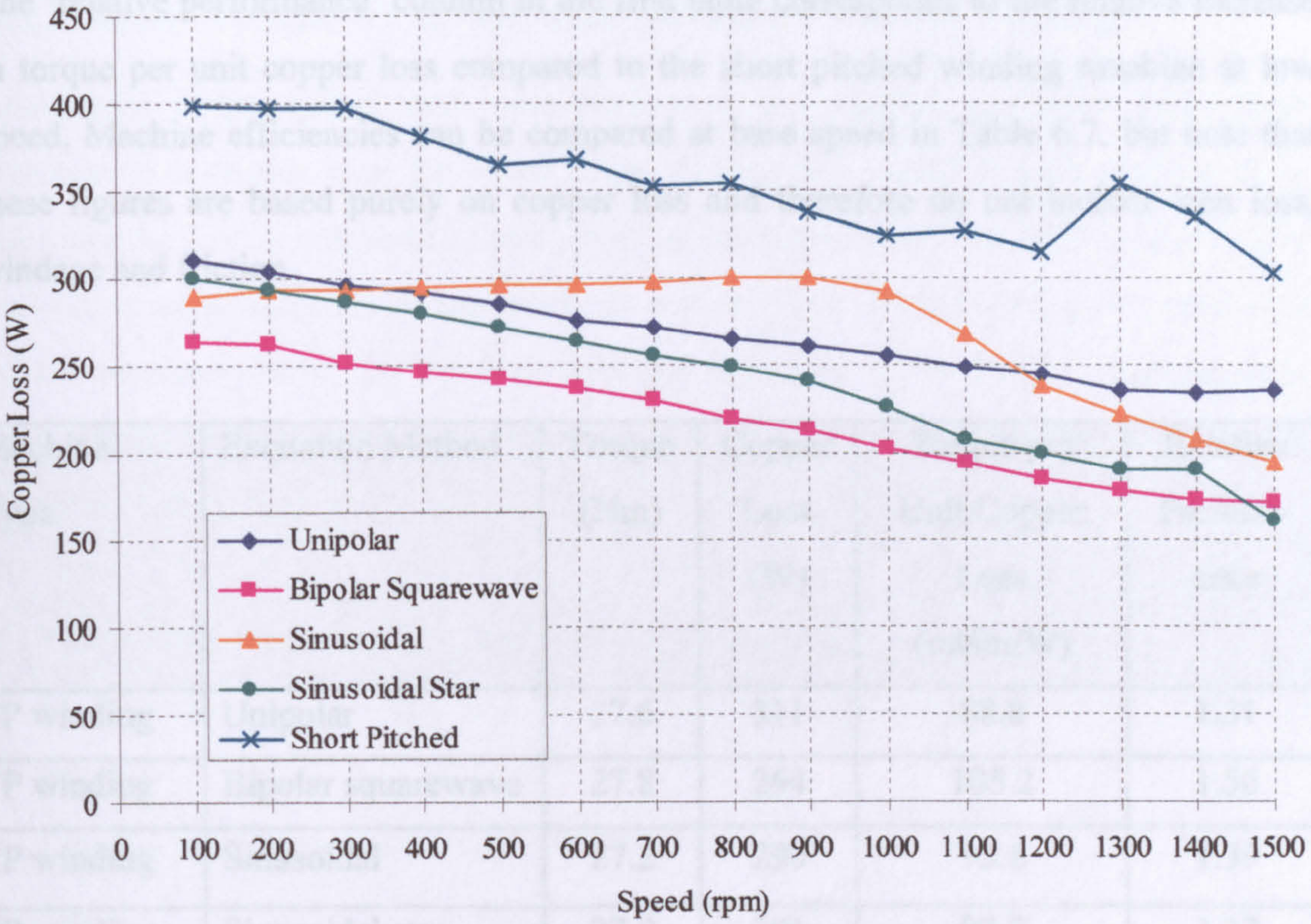

Figure 6.12 Simulated copper losses for the torque shown in Figure 6.4.

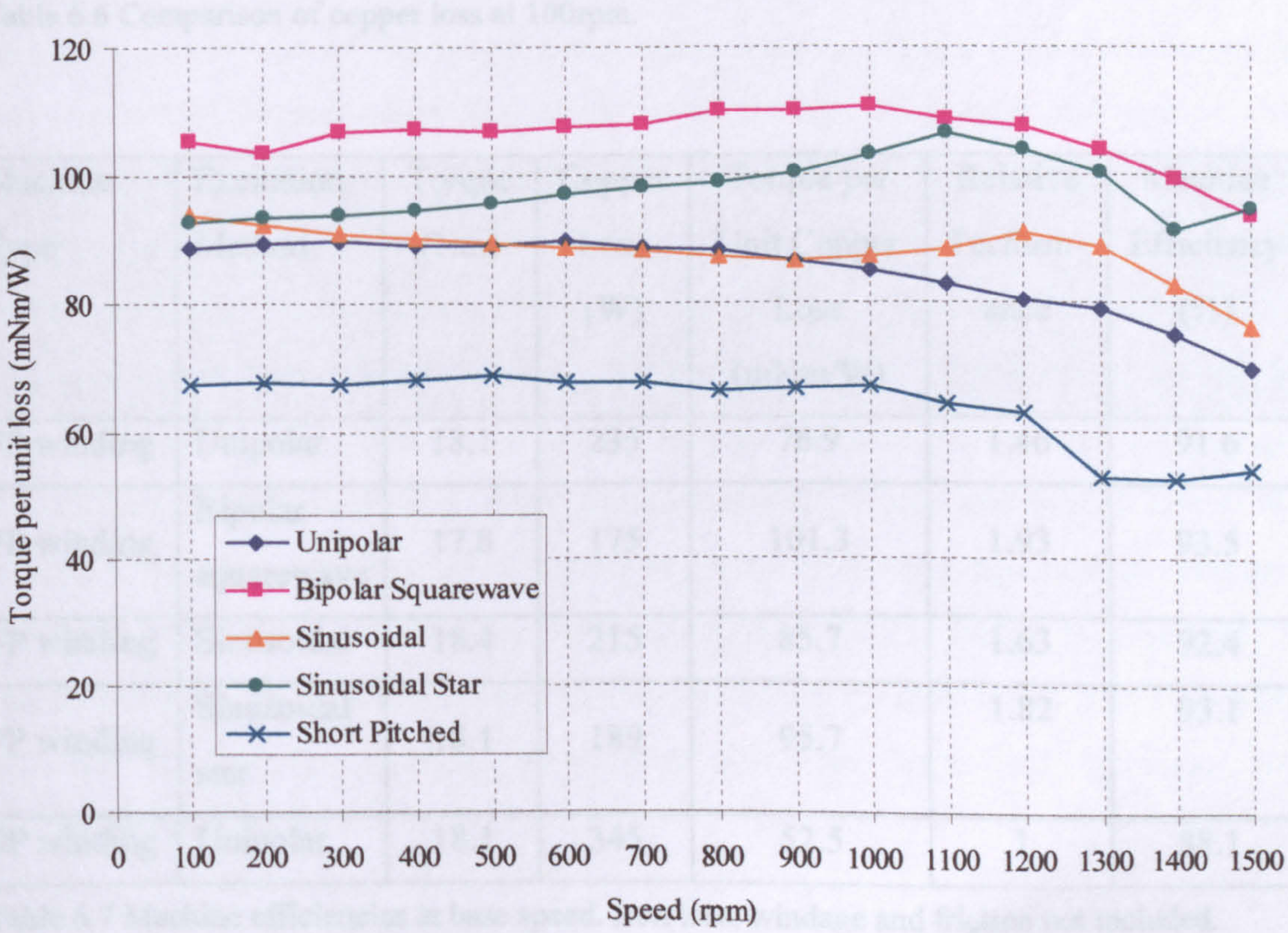

Figure 6.13 Simulated torque per unit copper loss for the torque shown in Figure 6.4.

The 'relative performance' column in the first table corresponds to the relative increase in torque per unit copper loss compared to the short pitched winding machine at low speed. Machine efficiencies can be compared at base speed in Table 6.7, but note that these figures are based purely on copper loss and therefore do not include iron loss, windage and friction.

Machine Type	Excitation Method	Torque (Nm)	Copper Loss (W)	Torque per Unit Copper Loss (mNm/W)	Relative Perform-ance
FP winding	Unipolar	27.6	311	88.8	1.31
FP winding	Bipolar squarewave	27.8	264	105.2	1.56
FP winding	Sinusoidal	27.2	290	93.8	1.39
FP winding	Sinusoidal star	27.9	301	92.7	1.37
SP winding	Unipolar	26.9	398	67.6	1

Table 6.6 Comparison of copper loss at 100rpm.

Machine Type	Excitation Method	Torque (Nm)	Copper Loss (W)	Torque per Unit Copper Loss (mNm/W)	Relative Perform-ance	Machine Efficiency (%)
FP winding	Unipolar	18.1	235	76.9	1.46	91.6
FP winding	Bipolar squarewave	17.8	175	101.3	1.93	93.5
FP winding	Sinusoidal	18.4	215	85.7	1.63	92.4
FP winding	Sinusoidal star	18.1	189	95.7	1.82	93.1
SP winding	Unipolar	18.1	345	52.5	1	88.1

Table 6.7 Machine efficiencies at base speed. Iron loss, windage and friction not included.

6.3.2 Rated Torque Vs Speed with Naturally Vented Cooling

Continuous torque rating tests were performed for unipolar excitation and bipolar squarewave excitation over the speed range. Torque was varied at each speed point by adjusting the current demand and re-optimising the advance and conduction angles, until the correct temperature rise in the windings was obtained. Motor cooling was only aided by the standard plastic fan supplied with the induction motor frame. Thermocouples were placed in the machine at various positions to monitor spot temperatures. The positions were as follows:

- Endwinding (in the centre of the winding, as it emerges from the slot).
- Slot (between the winding and the slot sleeving, approximately 50mm axially into the slot).
- Core back (at the base of a stator tooth).
- Case.

Motor temperature rise tests are normally based on an average winding temperature rise, as opposed to the rise of the hottest point on the winding. This is because temperature rise is normally determined by the change in the winding resistance, and hence it can only measure an average rise. On this test rig it was more convenient to use the thermocouples to measure the temperature rise as they could be used to easily continuously monitor the temperatures across the machine. A test therefore needed to be performed to ascertain the best way to calculate the average temperature rise from the spot readings. A DC current was passed through all three phases and the average temperature rise was monitored with measurements of voltage and current across the phases. It was found that the average temperature of the thermocouples at the first two positions correlated exactly with the value calculated from the change in resistance i.e. measurements in the endwinding and the outside of the winding in the slot. Following this test the average winding temperature rise was determined by these two thermocouple readings.

Temperature rise readings were taken with the machine having been run for several hours to make sure the machine had reached its steady state thermally. The thermal time

constant of the machine was measured in the stalled condition to be 40 minutes, with the temperatures reaching their final values after 5 hours. Figure 6.14 shows the continuous torque achievable in this machine for unipolar and bipolar operation with a 100°C average winding temperature rise (a figure commonly adopted for SRM ratings).
Simulated curves for the equivalent short pitched winding machine are also shown for comparison. Two curves are shown – one has its conduction angle rising from 120° at low speed towards 180° at high speed, as with the previous comparisons. The other has 120° conduction throughout the speed range for maximum efficiency.

Torque is calculated at each speed for the same copper loss as unipolar operation of the fully pitched winding machine. The assumption, therefore, is that the short pitched machine has the same iron loss as unipolar operation. This assumption should be a good one, as the equivalent single tooth flux waveforms are very similar – compare Figure 5.2 (Chapter 5) and Figure 6.5.

The results in Figure 6.14 show that bipolar squarewave operation is able to produce 25.7Nm, compared to 23.3Nm for unipolar operation at base speed (1350rpm). The simulated values for the short pitched winding machine are 19.2Nm and 16.7Nm, depending on the conduction angle used. Unipolar operation therefore produces 21% more torque than the most efficient operation of the short pitched machine at base speed, and bipolar squarewave produces 33.9% more.

These results are useful for comparing bipolar and unipolar operation as the effect of iron loss is included. Figure 6.15 shows the copper loss for the torques in Figure 6.14. At low speeds where iron loss is relatively low, both unipolar and bipolar squarewave are able to dissipate the same copper loss. At higher speeds, however, bipolar squarewave cannot dissipate as much copper loss, and this would suggest that its iron loss is relatively greater.

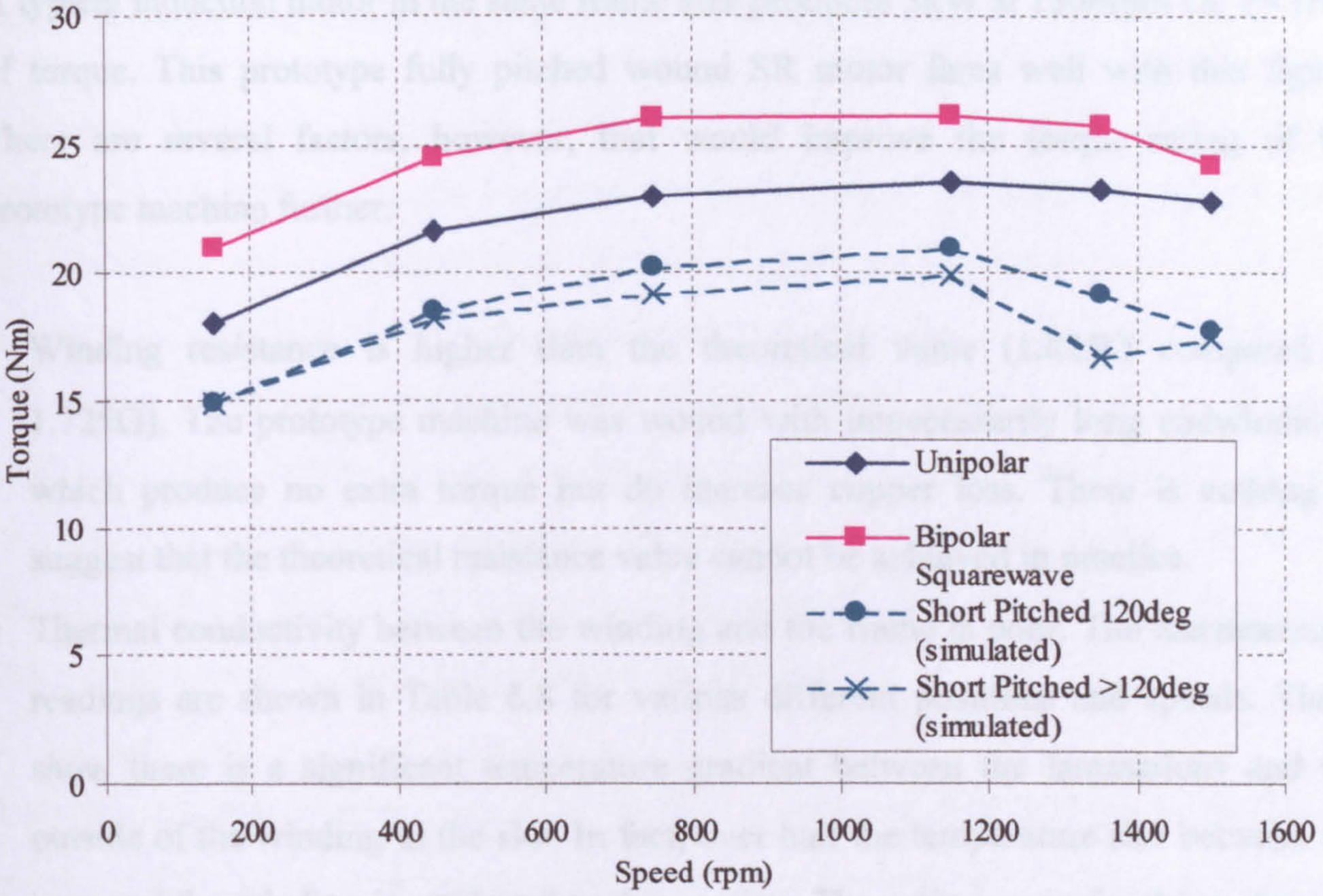

Figure 6.14 Continuous torque for 100°C average temperature rise. Curves for short pitched are simulated.

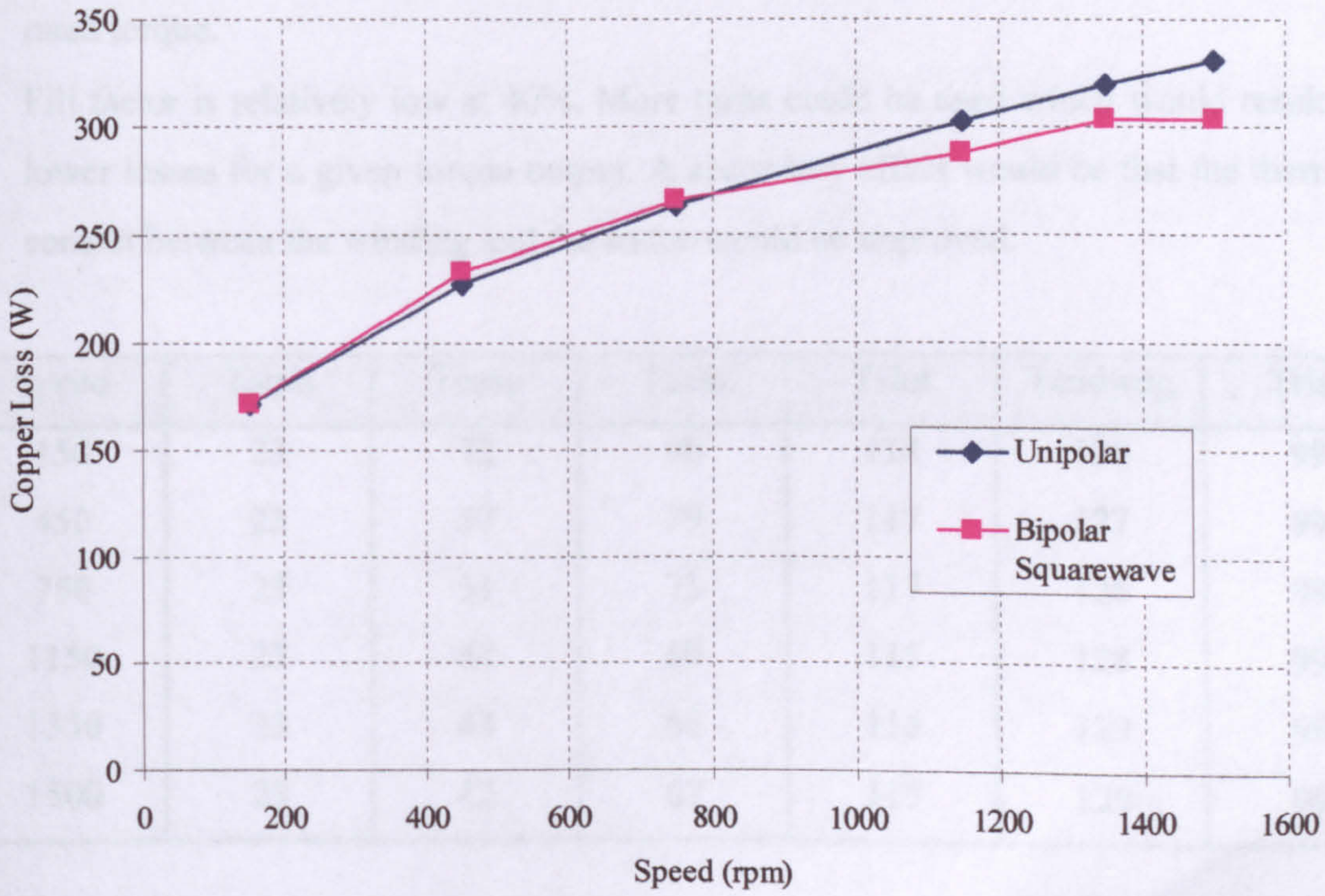

Figure 6.15 Copper loss for the torque shown in Figure 6.14.

A typical induction motor in the same frame size produces 3kW at 1500rpm i.e. 19.1Nm of torque. This prototype fully pitched wound SR motor fares well with this figure. There are several factors, however, that would improve the torque rating of the prototype machine further:

- Winding resistance is higher than the theoretical value (1.825Ω compared to 1.725Ω). The prototype machine was wound with unnecessarily long endwindings, which produce no extra torque but do increase copper loss. There is nothing to suggest that the theoretical resistance value cannot be achieved in practice.
- Thermal conductivity between the winding and the frame is poor. The thermocouple readings are shown in Table 6.8 for various different positions and speeds. These show there is a significant temperature gradient between the laminations and the outside of the winding in the slot. In fact, over half the temperature rise between the case and the winding is attributed to this section. The main reason for this is thought to be poor contact between the winding and the slot, and gaps of around 1mm were observed between the winding and the slot in the areas visible at the end of the stack. The effect of lower thermal conductivity is lower heat dissipation and hence lower rated torque.
- Fill factor is relatively low at 40%. More turns could be used which would result in lower losses for a given torque output. A secondary effect would be that the thermal contact between the winding and the stator would be improved.

Speed	Tamb	Tcase	Tiron	Tslot	Tendwdg	Trise
150	23	72	90	118	126	99
450	23	57	79	117	127	99
750	23	51	75	117	128	99
1150	23	44	69	115	128	99
1350	23	43	68	116	129	99
1500	23	42	67	115	129	99

Table 6.8 Thermocouple temperatures with unipolar operation and a 99° C average rise.

6.3.3 Torque Per Unit Copper Loss Vs Torque

In an ideal SR motor, torque is proportional to the square of the phase current. Copper loss is also proportional to the square of the phase current - it therefore follows that a given machine has a constant torque per unit copper loss. However, in a real machine the magnetic circuit becomes increasingly saturated with rising MMF levels. Torque per unit copper loss, then, becomes a function of torque itself. Figure 6.16 shows simulated results of torque against loss at low speed (100rpm) i.e. under good current control. Figure 6.17 shows the same figures but in terms of torque per unit copper loss against torque. Finally in Figure 6.18 torque per unit copper loss is shown normalised to the short pitched winding machine for ease of comparison.

It can be seen that in each case torque per unit copper loss falls with increasing torque output, and this is due to the increasing saturation in the magnetic circuit. It is, however, notable that the fully pitched winding machines with bipolar currents have a greater dependency on torque output than those machines with unipolar currents. The difference is that with bipolar currents some negative torque is always produced at certain positions in each stator pole (see sections 5.3 and 5.4 in Chapter 5). This is counteracted by a large amount of positive torque at other positions, but as the machine saturates it is the positive component of the torque that is affected first. The positive torque component is therefore reduced in comparison to the negative torque component, thereby reducing torque per unit copper loss.

It is interesting to see how torque per unit copper loss varies with torque for a number of reasons:

- Many motor driven systems run at very light loads for significant amounts of time. One of the major advantages of a variable speed drives is significant amounts of energy are saved under these conditions. It can be seen from Figure 6.18 that the fully pitched winding machine with bipolar type currents (bipolar squarewave and sinusoidal) fare especially well under these conditions.
- At low speed the amount of loss that a motor can dissipate is very limited if it is only cooled by the rotor mounted fan. The continuous low speed and stall torque of the machine will be determined by this loss together with the efficiency of the machine at

this speed. The previous section showed that with this cooling arrangement the prototype machine can dissipate approximately 160W of copper loss at 100rpm (see Figure 6.15). Figure 6.16 can be used to estimate rated torque for each machine under these conditions. It is notable that bipolar squarewave is particularly good under these conditions with a rated torque value of 20.8Nm compared to 14.5Nm for the short pitched winding machine (a gain of 43%). Values for unipolar and sinusoidal operation are 17.5Nm and 18.5Nm respectively (gains of 20.7% and 27.6%).

- Water cooled motors are able to dissipate much larger amounts of loss, hence these curves can be used to illustrate the relative differences at much higher levels of torque output. Figure 6.18 shows that throughout the range of torque outputs, unipolar excitation with the fully pitched machine maintains a constant advantage of a 28% increase in torque per unit copper loss for a given torque. Bipolar squarewave and sinusoidal operation generally have even higher torque per unit copper loss, but the difference does reduce with increasing torque output. Above 600W and 40Nm, sinusoidal operation in fact has lower torque per unit copper loss than unipolar operation.

Note that these values are pessimistic as they are based on the measured phase resistance of the fully pitched machine, which has been stated to be higher than it could have been.

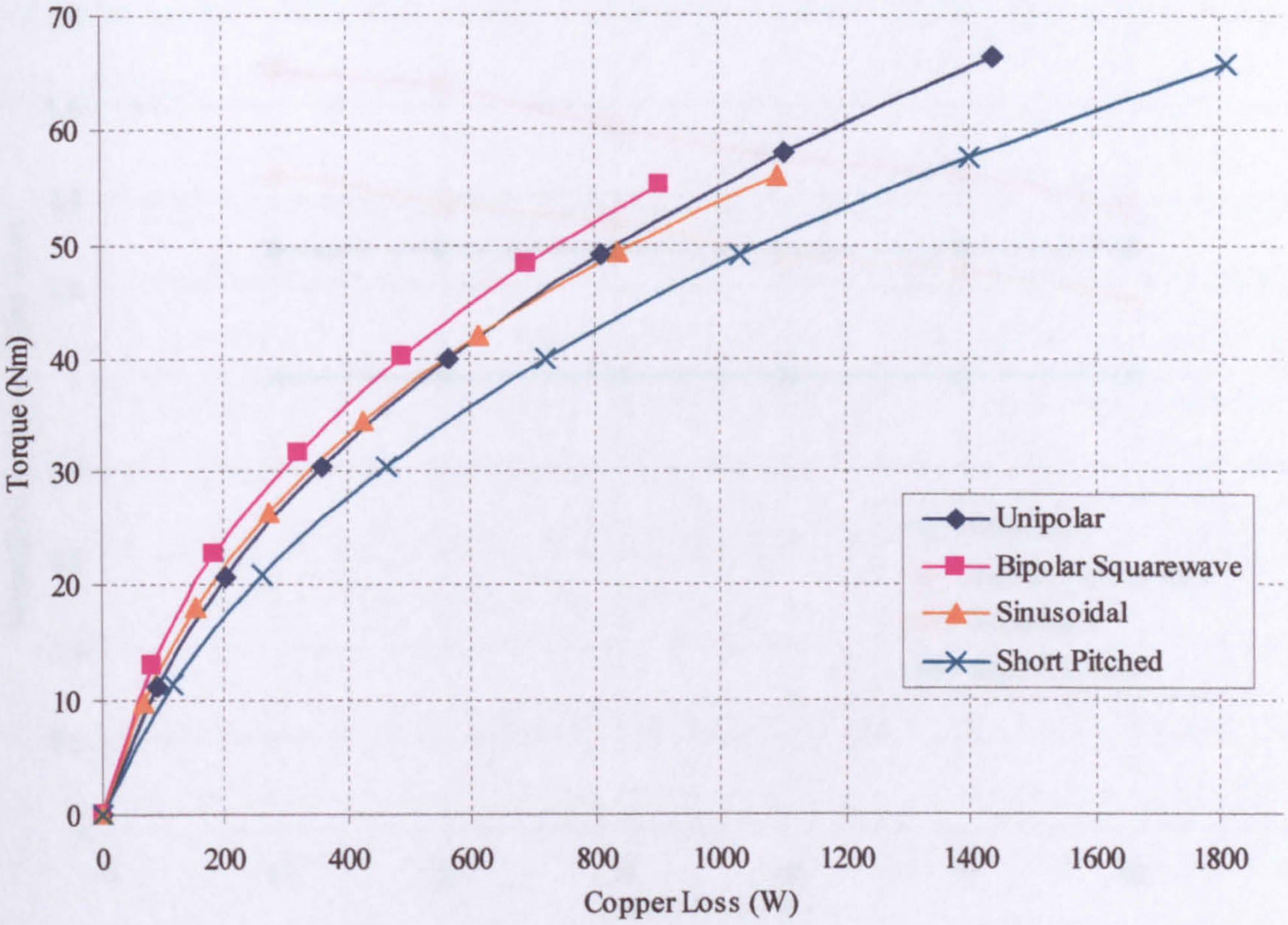

Figure 6.16 Simulated results of torque against copper loss (100 rpm , V_{dc} = 580V).

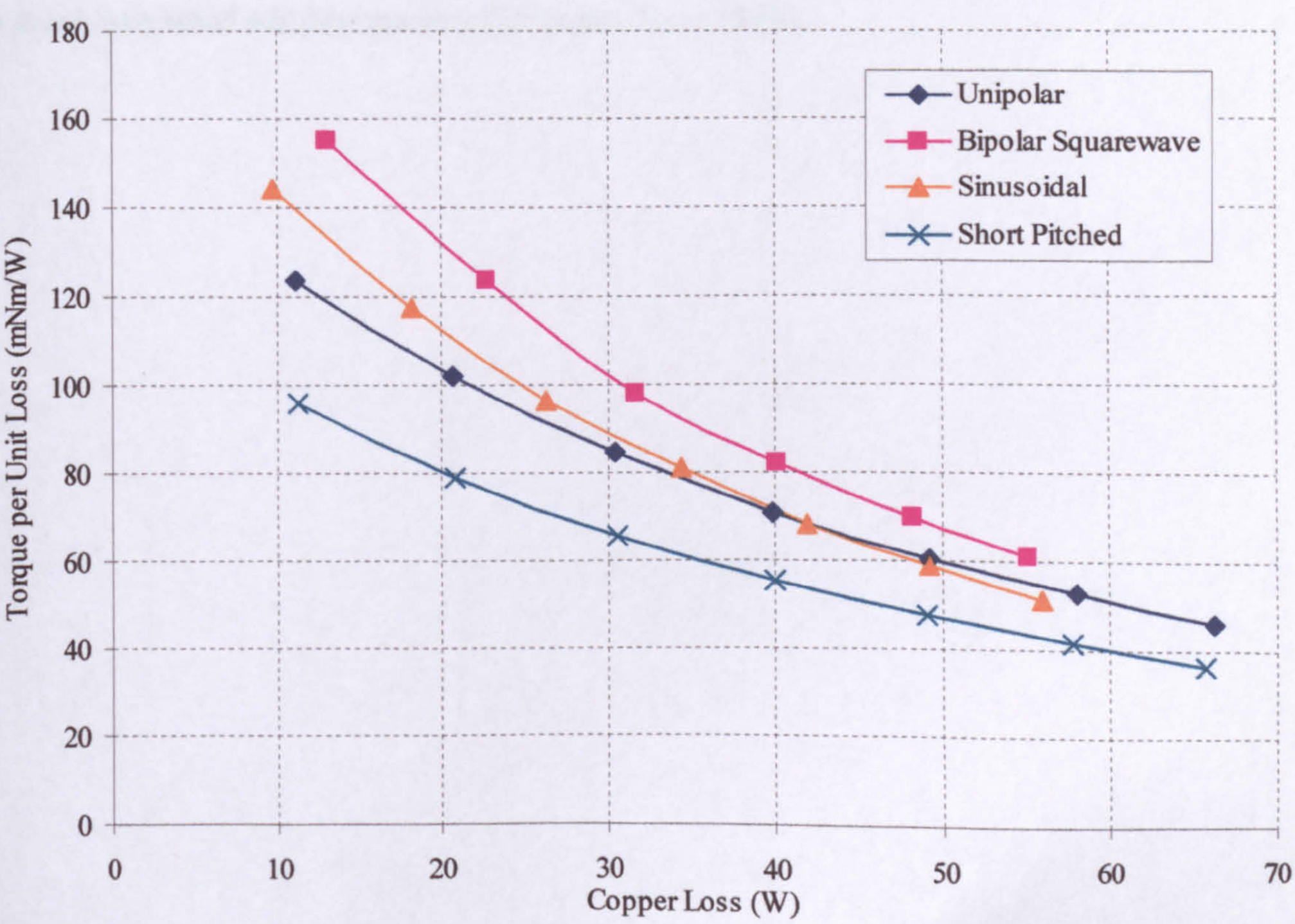

Figure 6.17 Simulated results of torque per unit copper loss against torque (100 rpm , V_{dc} = 580V).

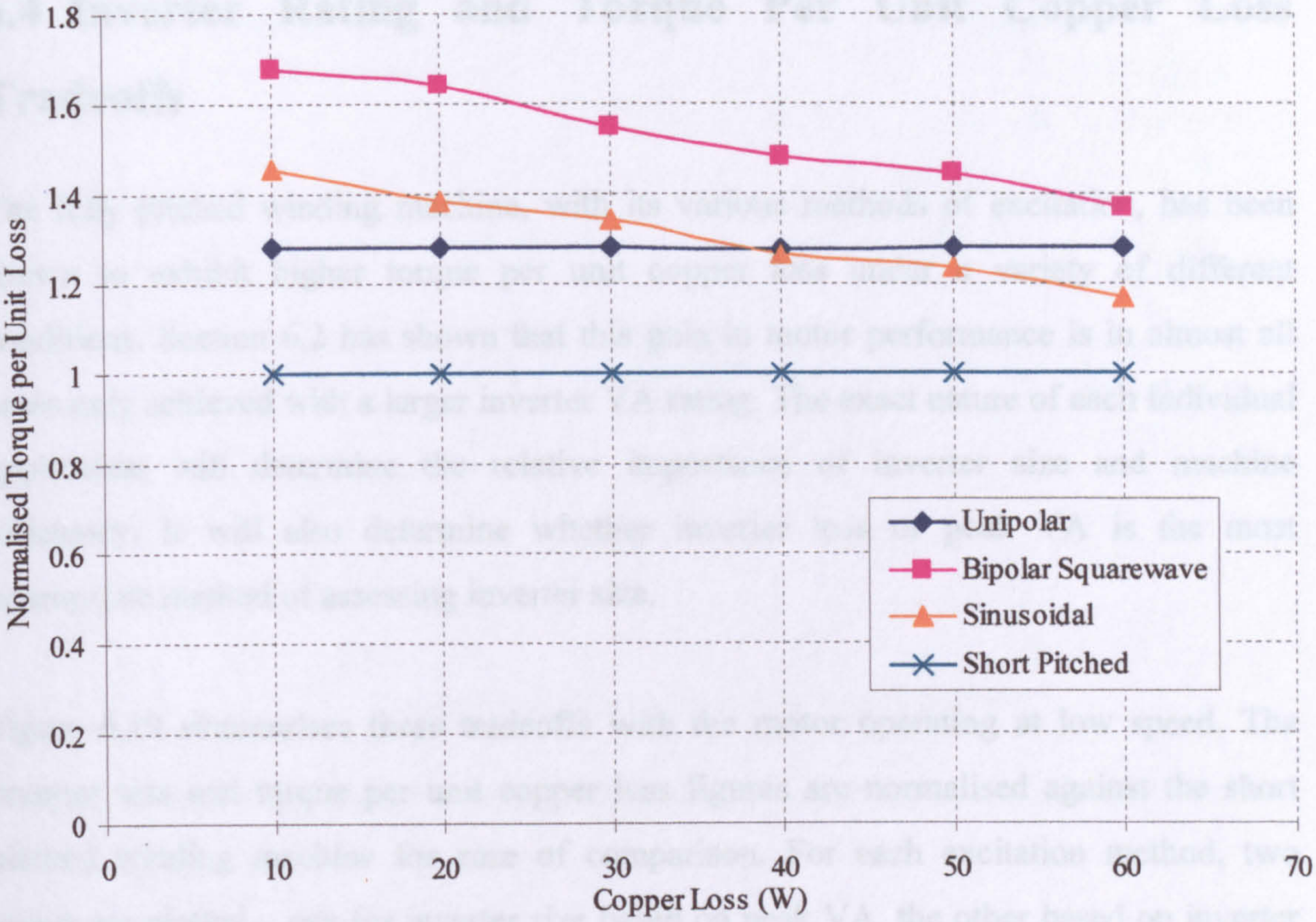

Figure 6.18 Simulated results of normalised torque per unit copper loss against torque, relative to the short pitched winding machine (100 rpm , V_{dc} = 580V).

6.4 Inverter Rating and Torque Per Unit Copper Loss Tradeoffs

The fully pitched winding machine, with its various methods of excitation, has been shown to exhibit higher torque per unit copper loss under a variety of different conditions. Section 6.2 has shown that this gain in motor performance is in almost all cases only achieved with a larger inverter VA rating. The exact nature of each individual application will determine the relative importance of inverter size and machine efficiency. It will also determine whether inverter loss or peak VA is the most appropriate method of assessing inverter size.

Figure 6.19 summarises these tradeoffs with the motor operating at low speed. The inverter size and torque per unit copper loss figures are normalised against the short pitched winding machine for ease of comparison. For each excitation method, two points are plotted – one for inverter size based on peak VA, the other based on inverter losses. Figure 6.20 shows values based on operation at base speed (the only difference between the two graphs is that torque per unit copper loss changes with speed). Note that these graphs are based on values taken from Figure 6.13 and Tables 6.3 to 6.6 i.e torque output is approximately 27Nm at low speed and 18Nm at base speed.

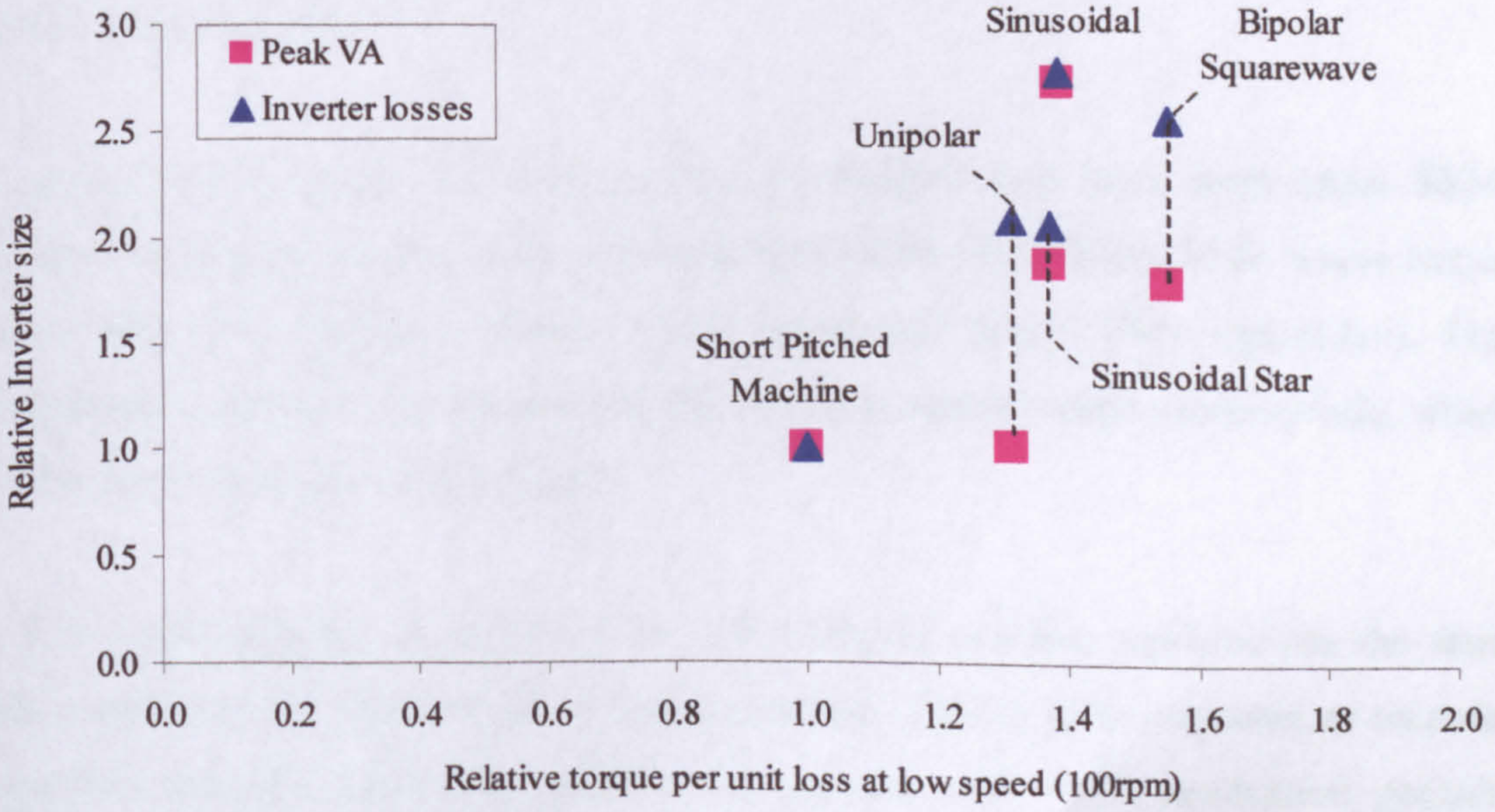

Figure 6.19 Relative inverter size versus relative torque per unit copper loss at low speed.

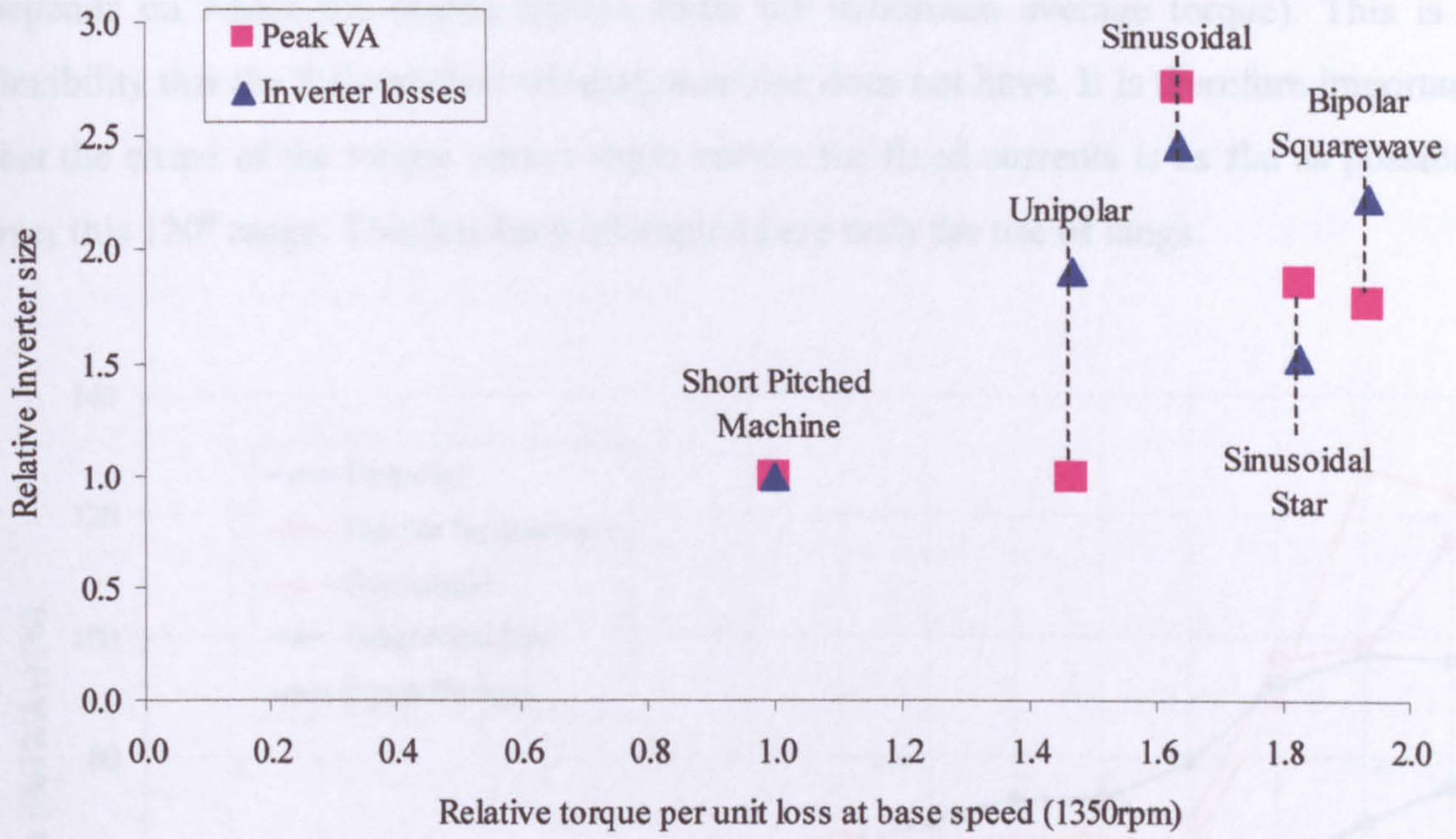

Figure 6.20 Relative inverter size versus relative torque per unit copper loss at base speed.

6.5 Torque Ripple

Figure 6.21 shows the torque ripple associated with the matched torque-speed curves shown in Figure 6.4. These can all be explained from the simulated waveforms shown in Chapter 5. These show the equivalent single tooth current which is used to calculate the torque produced by each pole of the machine, and which consequently contributes to total torque produced.

In general torque ripple with this machine is relatively low for a three phase SRM. Chapter 9 will show results with a standard Allen West D132 frame SRM where torque ripple with 120° unipolar currents at low speed was nearly 100% (pk-pk/av). This improvement is due to the broader and flatter torque against angle characteristic, which is a feature of this particular machine.

At low speed unipolar operation of the fully pitched winding machine has the same torque ripple as the short pitched winding machine. This is to be expected as unipolar operation produces equivalent single tooth currents with 120° conduction periods. Torque ripple for the short pitched winding reduces as speed rises in this case because the conduction angle is allowed to rise beyond 120° (see Figure 6.3 - the exact value

depends on where the search routine finds the maximum average torque). This is a flexibility that the fully pitched winding machine does not have. It is therefore important that the shape of the torque versus angle curves for fixed currents is as flat as possible over this 120° range. This has been attempted here with the use of tangs.

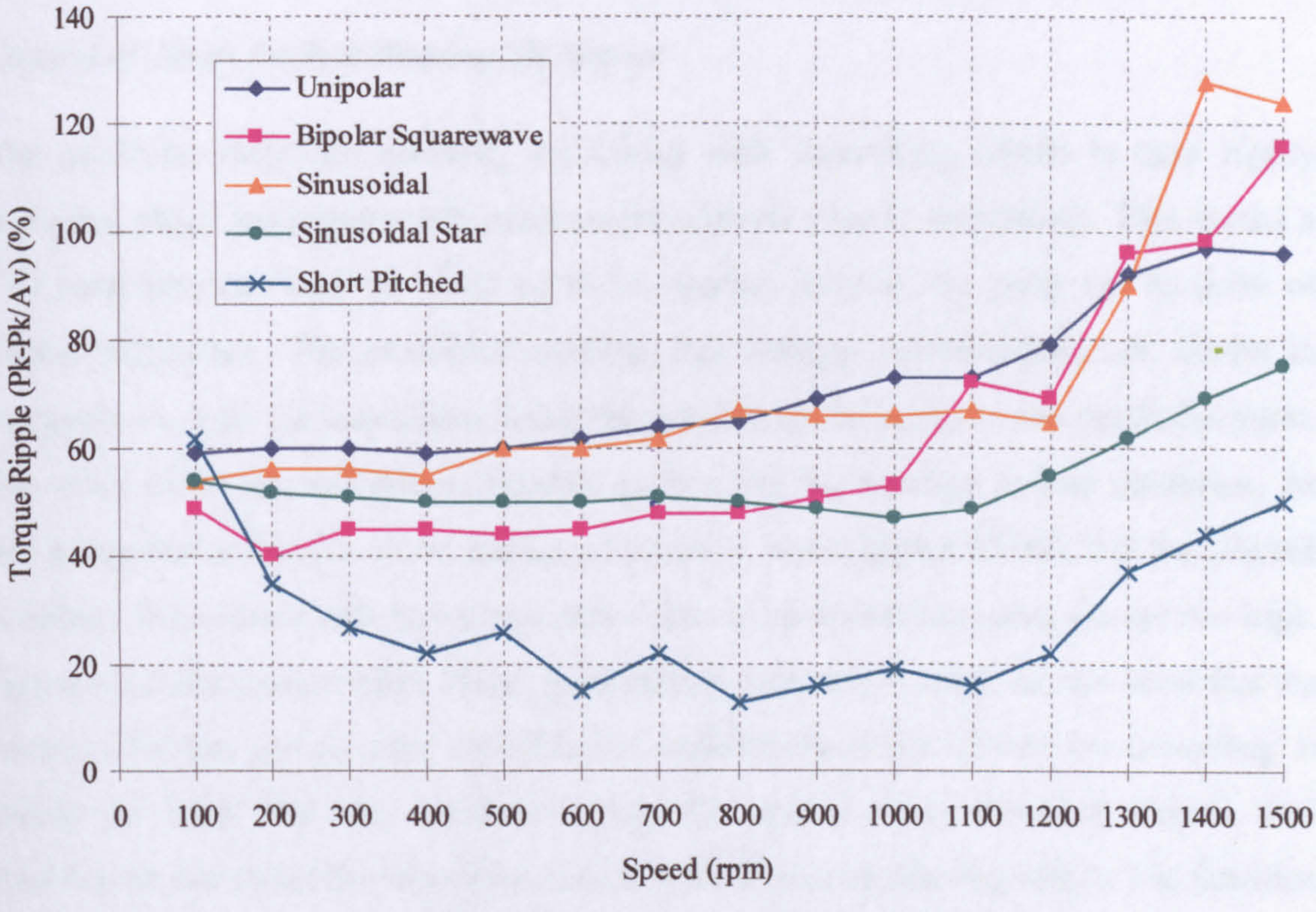

Figure 6.21 Torque ripple for the torque results shown in Figure 6.4.

6.6 Controller Requirements

The bandwidth requirement of a controller is an important consideration in the design of any electric drive. In a digitally controlled system this determines current sampling rate and current control loop processing speed.

Control of Short Pitched Winding SR Motors

The particular difficulty normally associated with controlling SRMs is their highly changing phase inductance with position and current (due to saturation). This means a PID controller can only be tuned up to its optimal level at one point i.e. its point of lowest inductance. The measured machine flux linkage characteristics are shown in Appendix A, with the inductance being the gradient of the curve at any particular point. The point of lowest inductance depends on how far the machine is into saturation. At low saturation levels this is the unaligned position, but at higher MMFs it is the aligned position. These areas will become unstable first if the controller gains are set too high. Figure 6.22 demonstrates this. Here, proportional gain only is used, set at a level that the control loop has just become unstable and oscillations in the current are occurring. It should be noted that the simulation plots the current every electrical degree, and therefore at this speed the waveform shown suffers from an aliasing effect. The machine here is highly saturated and the current becomes unstable near the aligned position.

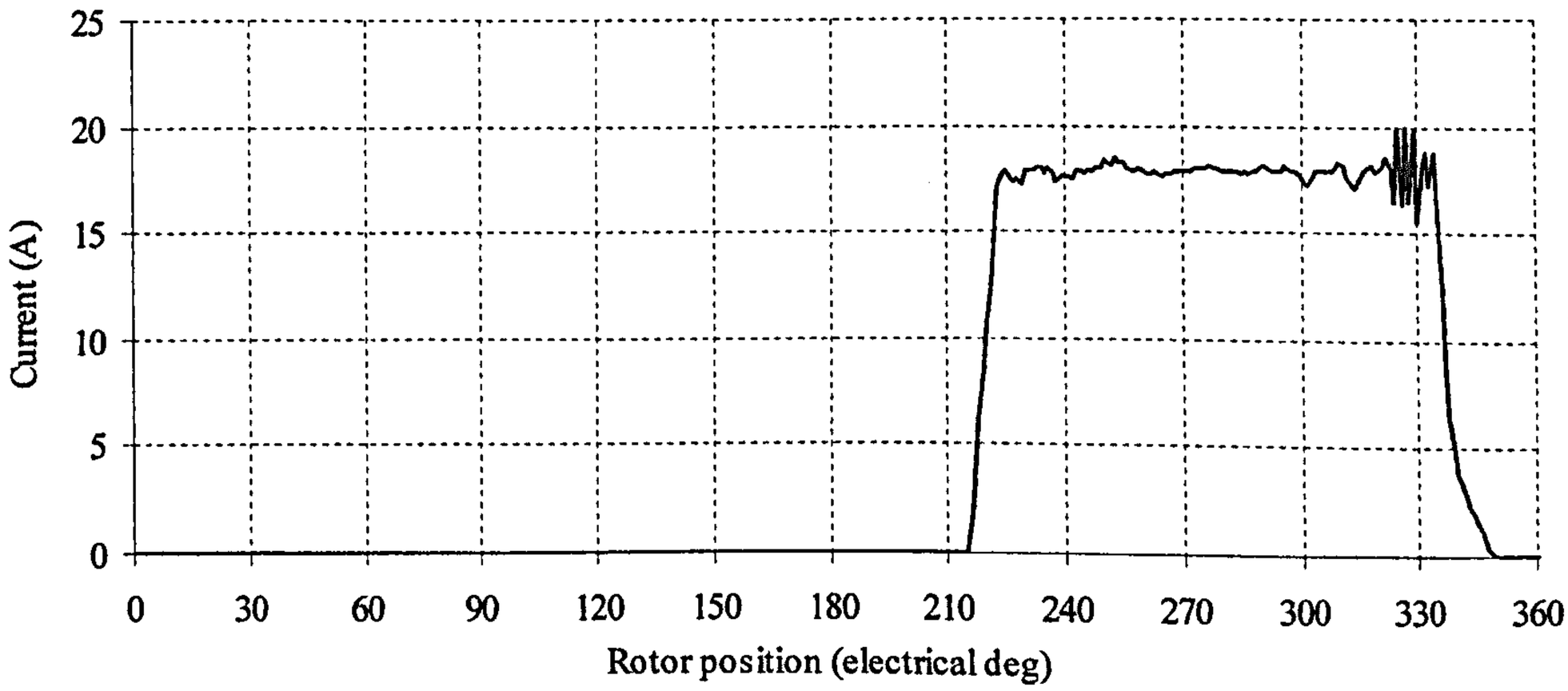

Figure 6.22 Simulation of phase current in short pitched machine at twice rated current.

Control of Fully Pitched SRMs

In the three phase fully pitched winding machine phase inductance is nearly constant with position. Controller stability is now determined by the very strong mutual coupling between phases. The action of each independent phase controller now affects not only the current in its own phase, but also affects the current in the other two phases as well.

Simulation was used to assess the relative stability of the same digital controller used on both types of machine. Its specification is as follows, and is designed to be as similar as possible to the one used in the test rig itself - 10kHz PWM frequency, 10kHz current control loop, current sampling 20μs before voltage reference implementation in the PWM controller. Details of this scheme are discussed in more detail in Appendix C. Proportional gain only is used, and the value of this gain before the onset of instability was determined. It was found that the gain for the short pitched winding machine could be set 2.5 times higher than the fully pitched winding machine. Clearly the interaction between each phase current controller due to the mutual coupling has a significant effect.

Two factors are predominant in determining the relative stability of a digital current controller - sampling rate and control lag. Sampling rate refers to the frequency at which currents are sampled and the PWM voltage reference is recalculated. Controller lag refers to the time between current samples and the updating of the voltage reference signal in the PWM controller. Simulation work showed the relative importance of each.

Increasing the sampling rate by a factor of five resulted in proportional gain being able to rise by a factor of 2.5. Reducing controller lag by moving the current sampling point from 100μs before PWM update to 20μs before, resulted in the gain being able to rise by a factor 4.

In theory both methods would involve a faster microprocessor to implement the code in a shorter available amount of time. In practice, however, moving the current sampling point closer to the PWM update point did not require more processing power. The order in which the code is executed was simply changed, leaving the code that actually required knowledge of the current until last. This method was used in the test rig and the increase in the maximum allowable proportional gain was confirmed.

This method of reducing lag maximises the bandwidth of the controller on the test rig to give good current control. It is, however, equally applicable to both the short pitched and fully pitched winding machines. The short pitched winding machine is still able to achieve better current control with the control system as it is naturally more stable. It therefore follows that to achieve the same level of current controllability the fully pitched winding machine requires faster current sampling and a faster current control loop i.e. extra cost.

One possible approach to improve the situation is to control the equivalent single tooth currents instead. These equivalent currents are decoupled and therefore do not suffer from the problem described above. A fully pitched drive control using these currents was reported by Barrass [6.5] and was mostly successful in achieving the decoupling. This involves converting the desired fully pitched currents into equivalent single tooth current demands. The same was done with the actual sampled phase currents and so equivalent single tooth voltage references are produced from the controller. These are then converted back into fully pitched winding voltage references and passed to the PWM output. Problems, however, were encountered when the PWM voltage reference saturated. When this happened, two or more of the equivalent single tooth voltage references were affected, resulting in controller decoupling not being achieved. A further effect is that the level of voltage reference saturation in the equivalent single tooth sense becomes variable, making integral anti-windup control difficult to achieve.

Current control stability will be addressed again in Chapter 8 where a completely different inverter is used. This enables control of all three phases from only one sample current, and will therefore show that instability problems are significantly reduced.

6.7 Summary

Measured results from the test rig have shown the differences in torque-speed curves for unipolar, bipolar squarewave, sinusoidal and sinusoidal star connected operation. Current demand was selected in each case to give the same low speed torque, and that current demand was then maintained throughout the speed range.

Simulated waveforms were useful in explaining the differences between each excitation method. Bipolar squarewave and unipolar operation have quite similar torque-speed curves, despite having completely different current waveshapes, which produce torque in the machine in fundamentally different ways. At any one time unipolar operation produces torque in the period of rising mutual inductance between two phases. Bipolar squarewave uses both rising and falling mutual inductance between all three phases. In terms of the rate of change of flux linkage at high speed to maintain the desired current waveform, however, bipolar squarewave requires slightly more and hence the number of turns need to be reduced to 0.88 that of unipolar (with a corresponding rise in the current demand). Sinusoidal operation should be similar to bipolar squarewave, however torque falls away much more rapidly with speed. Comparisons of the phase currents and current demands show that bipolar squarewave is able to produce more torque purely due to the fast change in the demand from positive to negative, and visa versa. This forces as much current into the machine as possible at the critical time during phase commutation. Sinusoidal operation on the other hand has a very slowly changing demand which means that the current controller does not apply full volts during commutation i.e. it current chops and hence cannot produce so much torque at high speed.

Compared to the short pitched winding machine, unipolar excitation is very similar in terms of its equivalent per tooth waveforms i.e. flux linkage, current and torque. However phase flux linkage of the fully pitched winding machine is quite different. This has been shown to go negative while a phase is off. This is necessary to maintain the current in that phase at zero, while the other phases, that are mutually coupled to it, are conducting. The overall effect is that, for the same MMF, unipolar operation of the fully pitched winding machine only requires half the current demand, but the flux linkage

excursion is double. This explains why unipolar operation with half the number of phase turns and the same current demand produced the same torque-speed curve in both machines.

To enable meaningful comparisons of inverter rating and machine performance the torque-speed curves were matched at two points – low speed and base speed. This was achieved by adjustment of the number of phase turns and current demand. The number of turns and the current demands to do this have been shown.

Two methods of calculating inverter size were used – peak VA rating and inverter losses. Both methods were used as the relevance of each changes with each application, particularly the need for low speed operation. Inverter losses are in all cases higher in the fully pitched winding machine and this is mainly due to the longer conduction periods compared to the short pitched winding machine. Additionally, in the case of bipolar type currents (bipolar squarewave, sinusoidal and sinusoidal star), either current demand or the number of power electronic switches is higher. Inverter size rating in terms of peak VA and inverter losses produce broadly similar results with the notable exception of unipolar operation. Here the same current demand is required as the short pitched winding machine, and therefore the same peak VA inverter is required. Under motor stall conditions, the same device losses are produced. Once the machine rotates, however, twice the average device losses are produced as the phase conduction period is twice as long.

Both measured results from the test rig and simulation work have been used to show the performance of the fully pitched winding machine with each excitation method. Results were taken in a variety of ways:

- Torque per unit copper loss up to base speed with a fixed current demand. With T=27Nm at low speed the fully pitched winding machine had between 1.31 and 1.56 times the torque per unit copper loss of the short pitched winding machine, depending on excitation method. At base speed and with T=18Nm the figures are between 1.46 and 1.93 times the torque per unit copper loss.
- Torque per unit copper loss against torque output (at low speed only). Torque per unit copper loss varied with torque due to saturation. There was a larger effect with

bipolar currents in the fully pitched winding machine. With T=10Nm for example bipolar squarewave has 1.68 times the torque per unit copper loss as the short pitched winding machine. This figure drops to 1.37 with T=60Nm. Unipolar operation showed a constant 1.28 times the torque per unit copper loss over the whole torque range. Sinusoidal operation actually becomes less efficient than unipolar at a torque of 40Nm.

- Rated machine torque over the speed range (i.e. for a fixed loss at each speed). Rated torque for unipolar and bipolar squarewave was measured at various speeds. Simulated results for the short pitched winding machine were also shown, and these were based on the same copper losses as unipolar operation of the fully pitched winding machine. At base speed bipolar squarewave is able to output 25.7Nm of torque. This compares to 19.18Nm with the most efficient operation of the short pitched winding machine i.e. with 120° conduction angle. Unipolar is able to output 23.3Nm. These figures correspond to a 33.9% and a 21% increase in torque respectively. At low speed bipolar squarewave is able to output 40% more torque. This further increase is because at low speed cooling is low, hence torque outputs are lower. Bipolar operation has been shown to be even more efficient at lower torque outputs.

Further increases in torque are thought possible with the fully pitched machine due to a number of factors – phase resistance was higher than the theoretical value, fill factor was low at 40% and the thermal conductivity between the winding and the frame appeared to be poor.

Torque ripple results have shown that at low speed the fully pitched winding machine has very similar values to the short pitched winding machine with 120° conduction. At higher speeds, though, the short pitched machine has lower torque ripple, mainly due to the fact that the conduction angle can increase beyond 120° i.e. overlapping phases. The prototype machine, however, had in all cases relatively good torque ripple, and this is thought to be due to the use of tangs at the tip of the stator teeth.

Current controller stability has been assessed, and it has been found that the fully pitched winding machine is relatively less stable. This due to the mutually coupled

phases, which results in disturbances being introduced on one phase by the switching action of the other two phases.

Chapter 7 - CURRENT PROFILING TECHNIQUES TO IMPROVE MACHINE PERFORMANCE

7.1 Introduction

Current control discussed in previous chapters is relatively simple in terms of current demand shape. Phase current is either controlled to a fixed desired value or is turned off, depending on rotor position. This keeps control simple and generally gives good performance in terms of torque output, machine loss, and power electronic rating. It can also reduce hardware requirements, as rotor position sensing can be of very low resolution, due to the fact that only the commutation points need to be determined.

It is well known, however, that profiling the currents to some other waveshape can improve machine performance, normally at the expense of controller and hardware complexity. Many methods have been proposed to do this, for example Ilic'-Spong *et al* [7.1], and Taylor [7.2]. Work by Reay *et al* [7.3] and Reay *et al* [7.4] proposed use of neural networks to determine phase current shape. Initial training of the system is achieved by feeding back measured torque so that current shape is adjusted to achieve a smooth torque output. The majority of methods, however, only consider low speed operation as ideal current control is assumed.

Work by Barrass [7.5, 7.6] has shown techniques that are also applicable to the fully pitched winding machine and goes further to take high speed operation into account. This was achieved by using flux linkage rather than current as the controlled parameter, which ensured that the inverter was always capable of forcing the required current into the machine. The flux linkage profile was defined by four regions of linearly rising flux ramps. It was found that there were many possible combinations of flux shape possible, and so a genetic algorithm was developed to optimise the ramps. Only unipolar operation of the machine was considered, and results showed good performance at both low and high speeds.

This chapter presents a novel search method to optimise performance in the fully pitched winding machine. It is empirical in nature, which is of benefit in this type of machine with its many potential excitation methods. It will be shown that the same search routine can be set to achieve one of two parameters to be optimised – profiles to achieve smooth torque with lowest rms current, and profiles to maximise torque per unit copper loss regardless of torque ripple.

As with the work by Barrass, optimisations can also be achieved at high speed by working with flux linkage rather than current. The technique is relatively fast, so that complete sets of profiled current or flux linkage waveforms can be built up for a range of torque outputs over the entire torque-speed envelope of the machine.

Both unipolar and bipolar basic modes of operation could be considered, however the work concentrated on optimising bipolar for two reasons. Chapter 6 showed that bipolar operation is the most efficient with square shaped currents, therefore the results from this optimisation should show the best that can possibly be achieved in the fully pitched winding machine. Additionally, torque production at high speed has been shown to fall off more rapidly with bipolar operation compared to unipolar operation of both the fully pitched and short pitched winding machines. As this optimisation technique can be used at high speed, an improvement in this situation may be possible.

The profiled currents for bipolar operation will assume use of an H bridge inverter on each of the three phases of the machine. Work was also carried out to establish whether an improvement of bipolar operation with a delta connected machine is possible. Bipolar operation with delta connected windings will be shown to be very poor, especially at low speed, so there is significant room for improvement. It will be shown that the search method can be adapted for use with the delta circuit, and the results will be presented.

7.2 Optimisation Methods

7.2.1 Maximum Mean Torque per Unit Copper Loss

The method chosen to solve for optimal currents depends on whether low speed or high speed operation is being considered.

Low Speed Operation

At low speed it can be assumed that the inverter can force any desired current into the machine. The requirement, therefore, is that the current waveform achieves the desired average torque over the electrical cycle at the same time as minimising winding loss.

As only an average torque needs to be achieved, it is not possible to solve this problem by taking each rotor position in turn and finding the currents that will achieve a certain torque. The torque at each position can either be smaller or greater than the desired torque, as long as the average of the torque over the electrical cycle meets the desired value. There are therefore many combinations of currents that might achieve that desired torque.

The total number of combinations, N, and therefore the computation time, depends on the number of rotor positions at which the calculation is performed, as well as the variation in current allowed at each position i.e. the current step used. The number of combinations possible is calculated as follows:

$$N = \left[\frac{I_{\max} - I_{\min}}{I_{step}} + 1 \right]^{N_\theta} \tag{7.1}$$

where N_θ is the number of rotor position points to be taken into consideration, $I_{\max}, I_{\min}$ are the maximum and minimum currents to be checked and I_{step} is the current step. Therefore if the current step is 0.25A over the range -10A to 10A, and the number of rotor positions to check is 12 (corresponding to an angle step of 30 electrical degrees), then N would be equal to 6.9E22 ! Computation time, therefore, would be

excessive if every combination of current was checked. A search routine was therefore developed to reduce the number of combinations to be checked.

The code starts by generating an approximate current waveform that achieves more than the desired torque. At each position only three possible currents are allowed, that is +I, -I, and zero. 'I' is normally set to the maximum possible current thought necessary to achieve the desire torque. Using Equation 7.1, this keeps the number of combinations down to 3^{12} = 531,441, assuming an angle step of 30 electrical degrees, which is acceptable in terms of computation time. The calculation for each combination involves the following steps:

- Take the particular combination of currents for phase A over 360 electrical degrees (consisting of 12 points). Use symmetry to calculate the current for the next 360 degrees (note that the complete electrical cycle for a bipolar waveform is 720°).
- Shift phase A by 240° at a time to calculate the current waveform in the other two phases.
- The equivalent single tooth currents at each rotor position are then determined using the transformation matrices. These are then used as inputs to a torque lookup table to calculate the instantaneous torque at each position.
- The average torque and winding loss is then obtained. If the average torque is above the desired torque, and the torque per unit copper loss is better than any previous combination of currents, then the new combination is stored.
- The above four steps are then repeated for each possible combination of currents. At the end of this sweep the best waveform is output.

This waveform can then be taken and improved. At each rotor position the current is again varied by I, the current step, from the original best waveform, but this time the current step is halved. Every combination is tried, so again 3^{12} computations are performed. This is shown in Figure 7.1 where the upper and lower waveforms define the limits of the new sweep.

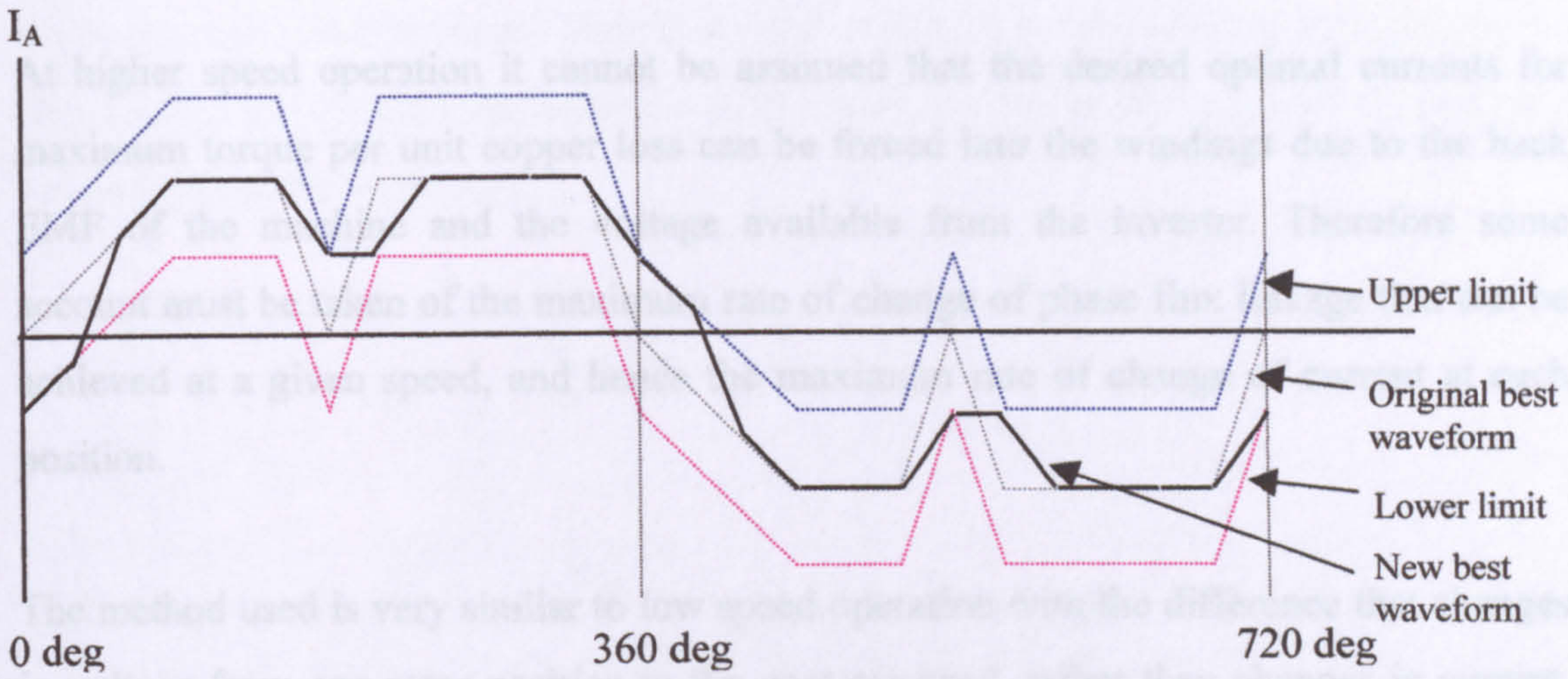

Figure 7.1 Upper and lower limits for search based on the previous best result, shown dashed. New best waveform shown with solid black line.

It can be seen from Figure 7.1 that the new "best" waveform has refined the original "best" waveform as the smaller current step allows finer control. It may still be possible to improve on this new waveform even with the same current step. Therefore another search is started centred around this new "best" waveform. This continues until no improvement in the waveform can be made with this current step value. This is defined in the following way: at the end of a sweep of 3^{12} combinations of currents the latest "best" waveform is checked against the upper and lower limits. If it is at the centre at every point then no improvement can be made in the waveform with that current step.

The current step can then be reduced and the whole procedure repeated, each time fine tuning the current waveform further. This method of "homing in" on the best waveform takes considerably less computation time than calculating every possible combination of current to the require accuracy in terms of the current step used. Also note that because the current is not constrained to start with zero current at 0°, then angle advance or retard is automatically achieved. Typical computation time is approximately 20 minutes to obtain an optimised current waveform for a given torque demand with an accuracy of 0.25A and a maximum current demand of 10A using a Pentium 133MHz PC.

High Speed Operation

At higher speed operation it cannot be assumed that the desired optimal currents for maximum torque per unit copper loss can be forced into the windings due to the back EMF of the machine and the voltage available from the inverter. Therefore some account must be taken of the maximum rate of change of phase flux linkage that can be achieved at a given speed, and hence the maximum rate of change of current at each position.

The method used is very similar to low speed operation with the difference that changes in voltage from one rotor position to the next are used, rather than changes in current. Again a 30^{o} angle step is used, so 12 rotor positions are considered. At each position a voltage is applied that is maintained until the next position. Therefore a *change* in flux linkage between each point can be determined, based on the speed of the machine and the change in angle between the points. Phase resistance is ignored in this part of the calculation for simplicity.

Now the *absolute* values of flux linkages need to be determined. This is explained with the aid of Figure 7.2. Initially the flux linkage at 0^{o} is assumed to be zero. A flux linkage waveform ('Waveform A' in Figure 7.2) can then determined from knowing the changes in flux linkage between points thereafter. However, the symmetry with a bipolar waveform means that the flux linkage at one position is the negative of the flux linkage 360^{o} later (remembering that the complete electrical cycle for a bipolar waveform in this machine has been defined as 720^{o}). So, for example, the flux linkage at 0^{o} is the negative of the flux linkage at 360^{o}. This can be achieved by shifting the whole waveform in the y axis until this condition is achieved, thus forming the first section of 'Waveform B' in Figure 7.2. Once the first 360^{o} are known, the next 360^{o} is simply the negative of the first 360^{o}. This now completes the full electrical cycle. Note that the angle advance does not have to be considered separately with this method, as flux linkage at the first position need not be zero.

Once the flux linkage waveform has been determined, phase current can be calculated using a lookup table of the machine's flux linkage/current/rotor position data. As with

low speed operation the equivalent single tooth currents are then calculated followed by the torque and winding losses. Note that computation time was reduced by indexing the flux linkage and torque look-up tables at 30° steps, so that interpolation of the data was not required in the angle axis.

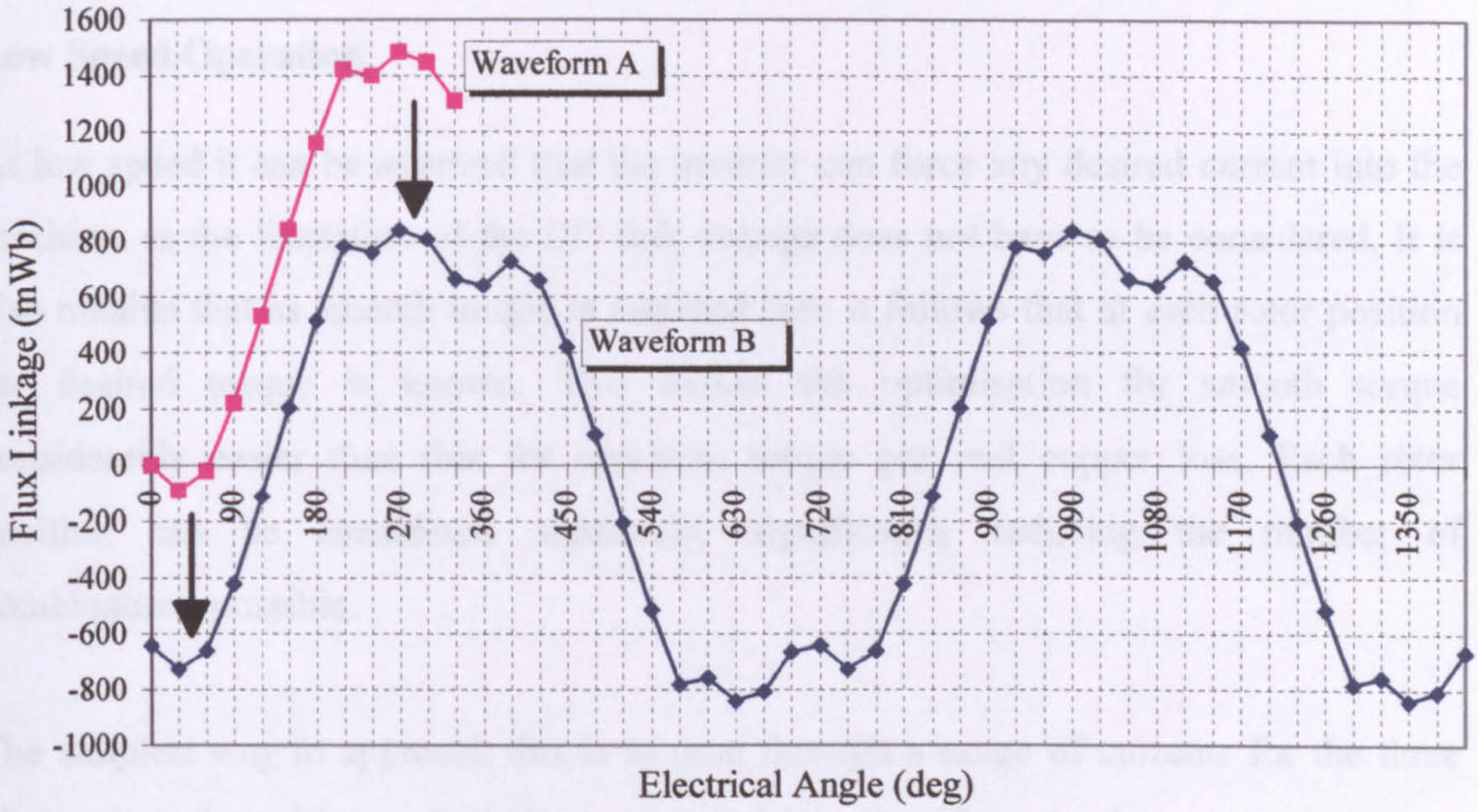

Figure 7.2 Method of completing the flux linkage waveform over the full electrical cycle.

The same method of 'homing in' on the optimum waveform is used. The code starts by only allowing $+V_{dc}$, 0 or $-V_{dc}$ at each rotor position i.e. +600, 0 or -600V for the machine being considered here. This is the same as using variations of +I, 0 or -I with low speed operation. The combination of voltages that produces the best torque per unit copper loss are noted.

This waveform is then refined by starting a new search, this time only allowing the voltage applied at each position to vary by one half the voltage of the previous case. Once more there are 3^{12} combinations to be calculated. As with the method for low speed operation it may be possible to improve on this combination further with the same voltage step. New searches therefore continue until the best voltage at each position is found to be at the centre of the sweep being considered.

The voltage step is then reduced and the whole process repeated. The optimisation stops when further reductions in the voltage step make no difference to the result.

7.2.2 Smooth Torque for Lowest Copper Loss

Again, two slightly different approaches are used, depending on whether low or high speed operation is being considered.

Low Speed Operation

At low speed it can be assumed that the inverter can force any desired current into the machine, as the limitation of the DC link voltage does not have to be considered. It is also notable that as smooth torque is required then it follows that at each rotor position the desired torque is known. This makes the optimisation for smooth torque considerably easier than that for optimum torque per unit copper loss. Each rotor position can be considered separately, significantly reducing the number of combinations possible.

The simplest way to approach this is to scan through a range of currents for the three phases at each position, calculating torque and loss as before. As the sweep progresses the combination of phase currents that achieves at least the desired torque with the greatest torque to loss ratio is noted. This method makes it unnecessary for a particular combination of currents to produce exactly the right torque, which is highly unlikely. The fact that torque per unit copper loss is also a criteria means that rms phase currents are reduced to the minimum possible to achieve the desired torque. The torque achieved at each position, therefore, only just meet the desired value with a small amount to spare due to the current step being used. The number of possible combinations of currents, N, is now given by:

$$N = N_\theta \left[\frac{I_{\max} - I_{\min}}{I_{step}} + 1 \right]^{N_p} \tag{7.2}$$

where N_θ is the number of rotor position points to be taken into consideration, $I_{\max}, I_{\min}$ are the maximum and minimum currents to be checked, I_{step} is the current step, and N_p is the number of phases.

So, for example, if I_{max}=10A, I_{min}=-10A, I_{step}= 0.25A, N_p = 3 and the angle step is 5 electrical degrees (N_θ = 24), then $N = 12.75*10^6$. Note that N_θ=24 as only 120° need be calculated, with the rest derived from symmetry. This was found to be an acceptable computation time and therefore no effort was put into a more intelligent way of speeding up the optimisation.

High Speed Operation

This is very similar to the optimisation for maximum torque per unit copper loss at high speed. Again changes in voltage between each rotor position are tried for one phase over 360° to take into account the limitations of the DC link voltage available. The voltage step reduces over progressive iterations, gradually homing in on the optimum waveform. The only difference is that each point must achieve the demanded torque so that a smooth torque output is achieved. Therefore for a particular combination of voltages applied, the flux, current and torque is calculated at each position. The best combination is noted where the torque achieved at each position is at least the demanded torque and the total losses are less than any previous best combination. If smooth torque cannot be achieved with any combination of voltages, then the one that produces the desired average torque with the least torque ripple is noted instead.

This method of considering the whole electrical cycle at the same time ensures that smooth torque will be achieved up to the highest speed possible. This is because if only single points are considered in isolation no account is taken of the change in flux linkage to get to the next or subsequent points. Note that the ability to achieve the desired smooth torque is the primary objective and winding loss is only a secondary consideration when there is more than one possible combination to achieve smooth torque.

7.2.3 The Delta Connected Drive

When the windings of any three phase machine are connected in a delta configuration to a three phase bridge inverter, there are certain restrictions on the voltages and currents that can be applied to the machine i.e.

$$V_A + V_B + V_C = 0 \tag{7.3}$$

and

$$I_{l1} + I_{l2} + I_{l3} = 0 \tag{7.4}$$

where V is the phase voltage I_l is the line current.

The same basic optimisation method is used as before with the addition of these restrictions. The code takes different combinations of *line* voltages and calculates the resulting phase voltages e.g. $V_A = V_{l1} - V_{l2}$. The phase currents are then solved in the normal way, and the line currents can then be calculated e.g. $I_{l1} = I_A - I_C$.

An extra optional restriction of limiting the line currents to a chosen value was found to be useful. Thus the effect of reducing peak line currents on the machine performance could be examined, with the aim of lowering inverter VA rating.

7.3 Comparison of Machine Performance with Current Profiling

7.3.1 Current Profiles for Maximum Mean Torque Per Unit Copper Loss

Low speed

The optimised currents for maximum mean torque per unit copper loss at low speed are shown in Figure 7.3, generated using the method described in Section 7.2.1. for the D100 prototype machine. For comparison, the simulated current waveform for bipolar squarewave is shown for 27Nm of torque (data taken from Chapter 5). Both machines have 204 series turns per phase. The difference in the shapes has the following effects:

- RMS phase current is reduced for the same torque output. For example, for 20Nm output, loss is reduced from 152W to 132W (a 13% reduction).
- Peak phase current demand is increased. For example for 20Nm output, peak current demand is increased from 5.5A to 6.75A (a 22.7% increase). Note this ignores the additional spikes of current due to phase commutation that is seen with bipolar squarewave due to commutation effects.

The increase in machine performance can be explained with the aid of the equivalent single tooth currents shown in Figure 7.4, and the torque produced by each equivalent single tooth phase (or each machine pole) shown in Figure 7.5. The normal equivalent single tooth current for bipolar squarewave operation is also shown for reference. The equivalent single tooth current is now shaped so as to reduce the current around the aligned and unaligned positions, or more specifically in the region just less than 180° and just greater than 360°. This is the region that, with normal square shape control, produces reasonable amounts of negative torque (see Figure 7.5). The reduction in this negative torque means that less positive torque needs to be produced in the region between 180° and 360°. Hence the current in this region is generally less than it was before. It is also shaped to essentially follow the torque profile of the machine - something which is seen with short pitched winding machines.

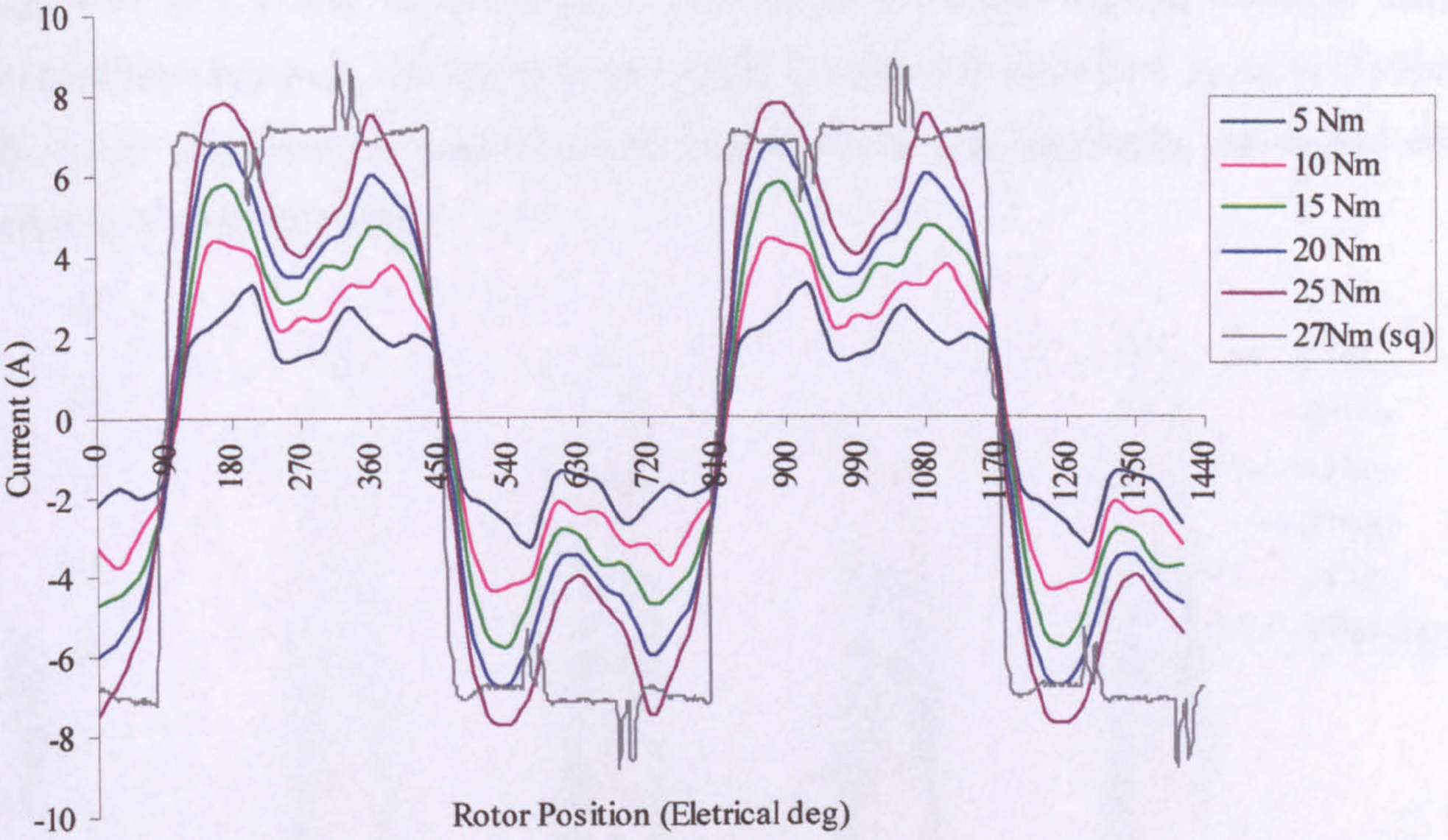

Figure 7.3 Current profiles for maximum mean torque per unit copper loss at low speed for a range of torque demands (data calculated at 30° intervals and smoothed). Bipolar squarewave shown, producing 27Nm.

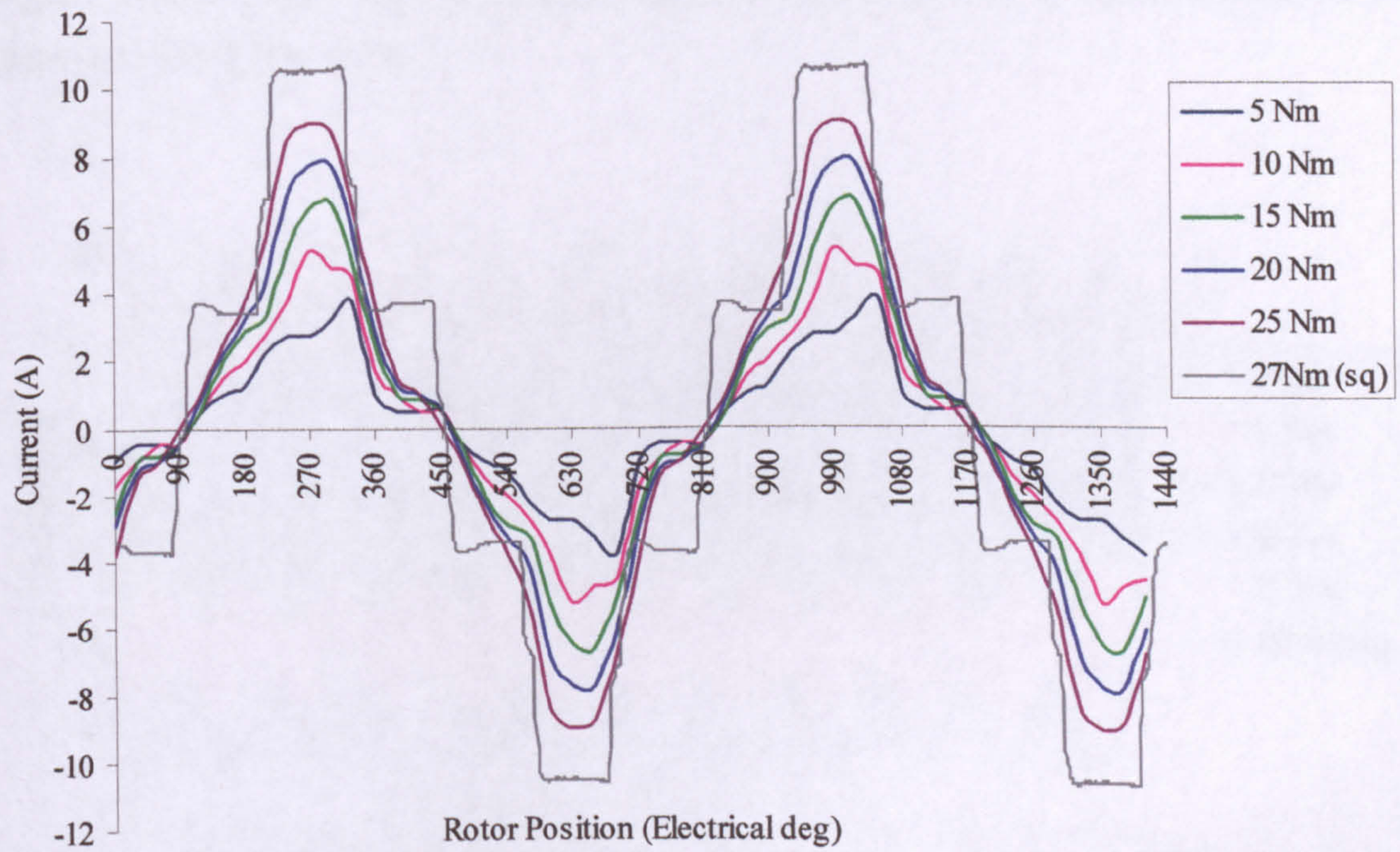

Figure 7.4 Equivalent single tooth currents for the phase currents shown in Figure 7.3.

Figure 7.6 shows total torque output. Unlike the short pitched winding machine, when profiled for maximum efficiency, torque ripple is relatively low (30% pk-pk at 20Nm). This is an indication that smooth torque output will be achieved easily and should still maintain a good efficiency.

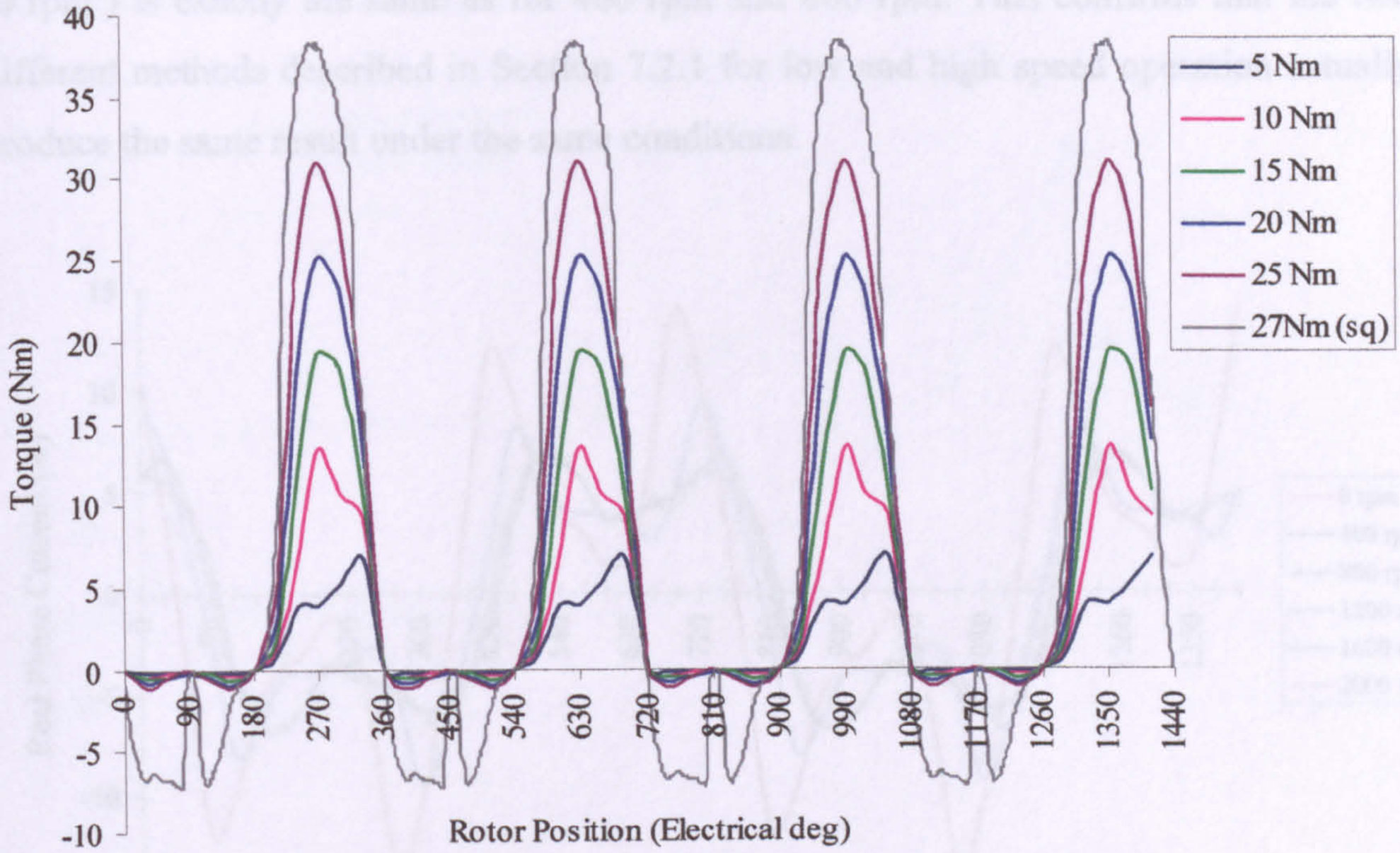

Figure 7.5 Equivalent single tooth phase torque (or torque due to one machine pole) for the phase currents in Figure 7.4.

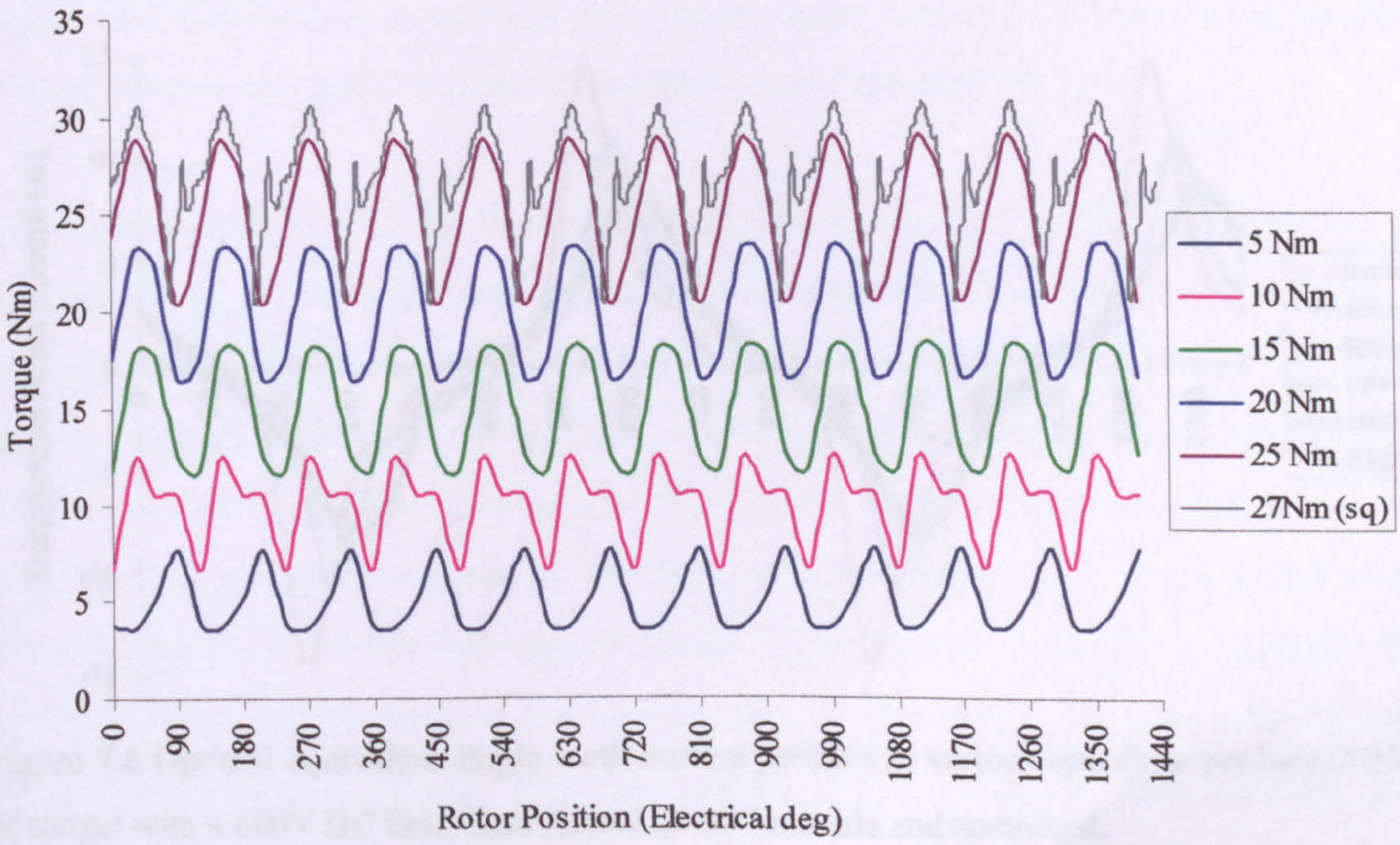

Figure 7.6 Total machine torque for the currents in Figures 7.3 and 7.4.

High Speed

Current profiles for operation at high speed are shown in Figure 7.7 and 7.8. These are generated using the method described in Section 7.2.1. The profile for low speed operation is also included for comparison. It can be seen that this profile (referred to as '0 rpm') is exactly the same as for 400 rpm and 800 rpm. This confirms that the two different methods described in Section 7.2.1 for low and high speed operation actually produce the same result under the same conditions.

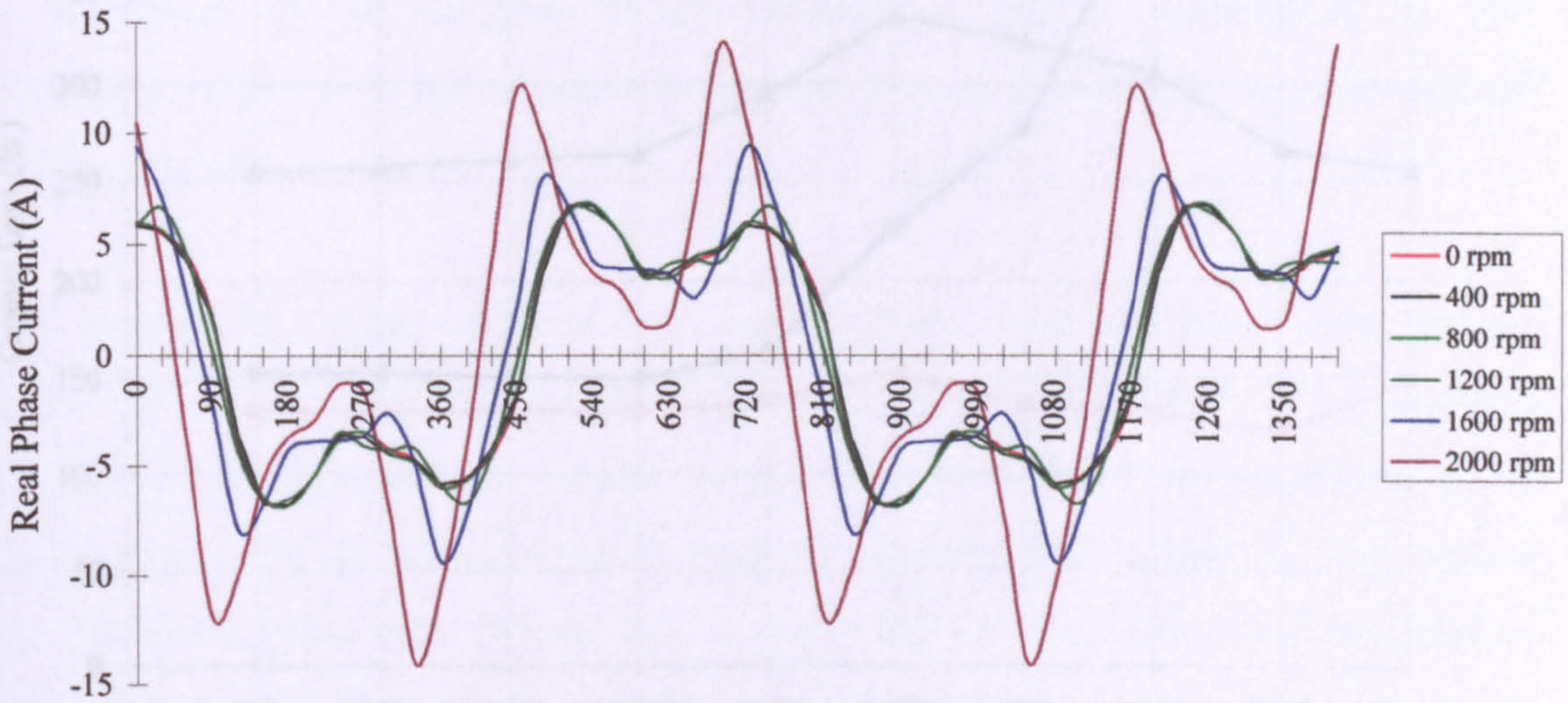

Figure 7.7 Optimal current profiles at various speeds to produce 20Nm of torque with a 600V DC link. Data plotted at 30° intervals and smoothed.

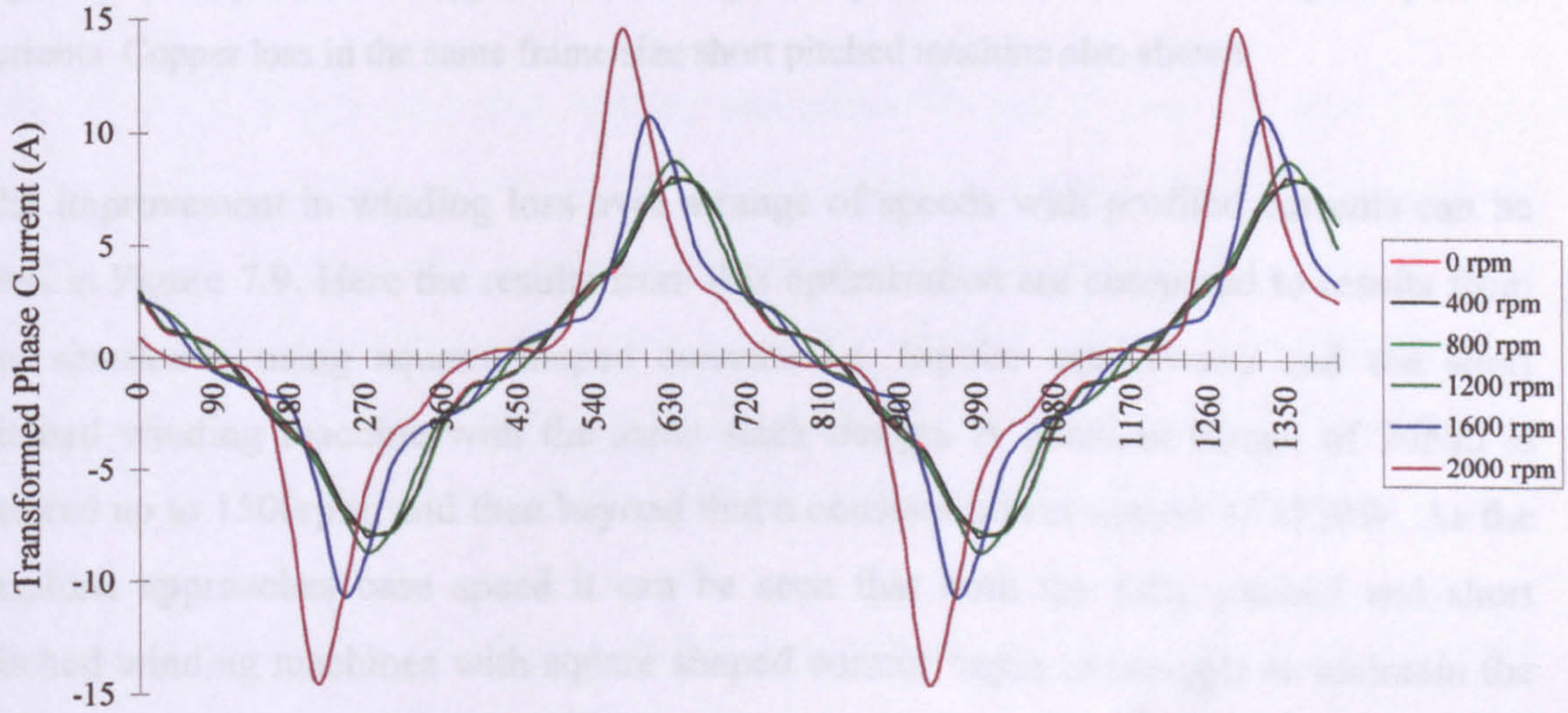

Figure 7.8 Optimal equivalent single tooth current profiles at various speeds to produce 20Nm of torque with a 600V DC link. Data plotted at 30° intervals and smoothed.

As the machine approaches base speed (1350rpm) it can be seen that it is no longer possible to force the ideal currents into the windings. The most optimal currents possible, within the constraints of the DC link voltage, are shown to become peakier and require more advance angle. The highest speed possible to produce 20Nm in this machine with 600V was found to be 2000rpm.

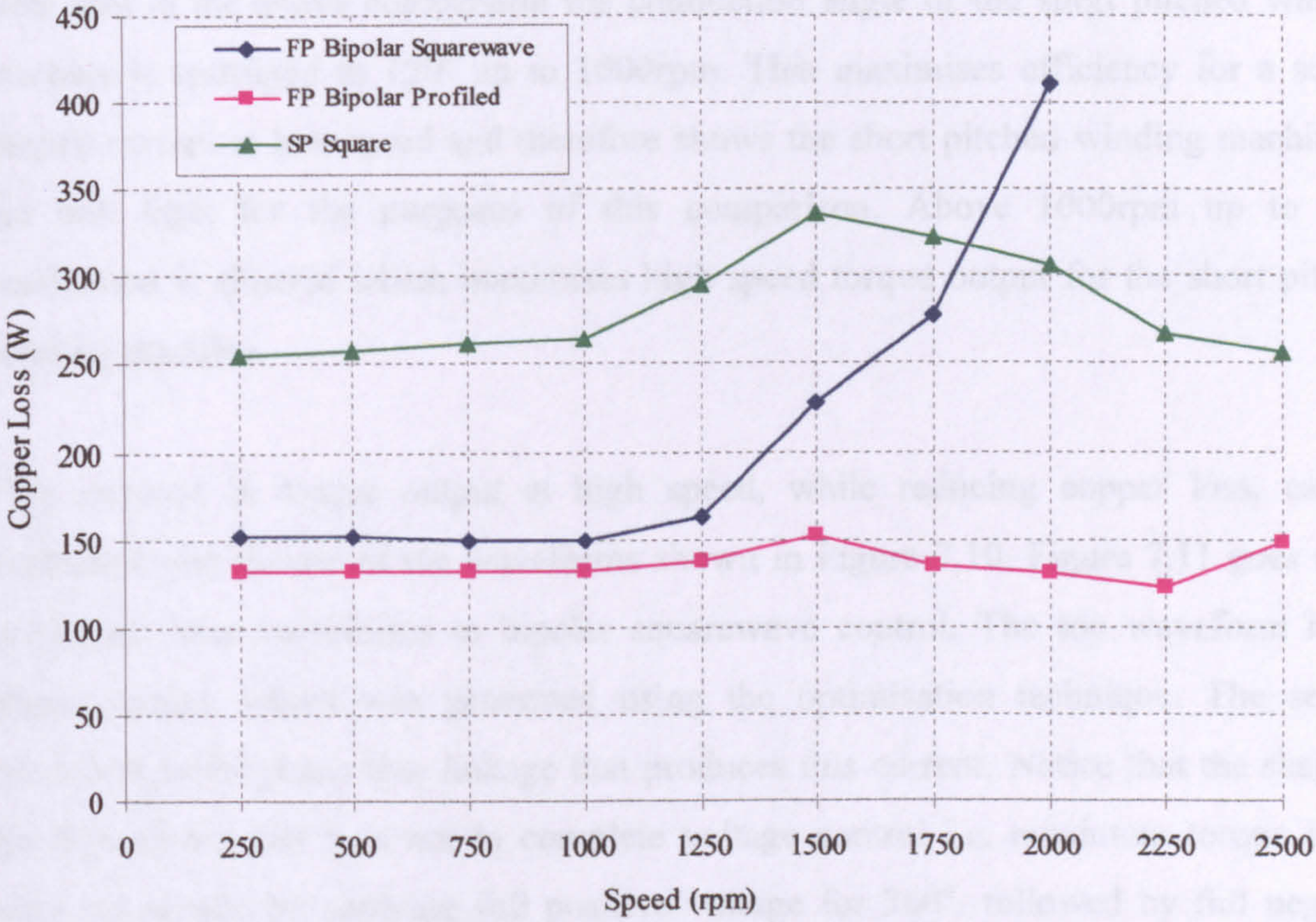

Figure 7.9 Comparison of copper loss with bipolar square currents (360°) and bipolar profiled currents. Copper loss in the same frame size short pitched machine also shown.

The improvement in winding loss over a range of speeds with profiled currents can be seen in Figure 7.9. Here the results from this optimisation are compared to results from the simulation using square shaped currents i.e. bipolar squarewave and the short pitched winding machine with the same stack design. A constant torque of 20Nm is desired up to 1500rpm, and then beyond that a constant power output of 3150W. As the machine approaches base speed it can be seen that both the fully pitched and short pitched winding machines with square shaped control begin to struggle to maintain the constant torque output. Copper loss consequently rises rapidly. In the constant power region torque output is lower, therefore copper loss is lower, however at 2000 rpm bipolar squarewave is unable to produce the required torque output. Results with

profiled currents show a substantial improvement, especially at high speed where constant power can be maintained at the same time as exhibiting very low copper loss.

At 1500rpm machine efficiency (ignoring iron loss) improves from 93.2% to 95.4% by profiling the currents. This compares with 89.2% for the short pitched winding machine. Note that in the above comparison the conduction angle of the short pitched winding machine is restricted to 120° up to 1000rpm. This maximises efficiency for a square shaped current at low speed and therefore shows the short pitched winding machine in the best light for the purposes of this comparison. Above 1000rpm up to 180° conduction is allowed which maximises high speed torque output for the short pitched winding machine.

This increase in torque output at high speed, while reducing copper loss, can be explained with the aid of the waveforms shown in Figure 7.10. Figure 7.11 goes on to compared these waveforms to bipolar squarewave control. The top waveform is the phase current, which was generated using the optimisation technique. The second waveform is the phase flux linkage that produces this current. Notice that the shape of the flux shows that it is not in complete voltage control i.e. maximum torque is not achieved simply by applying full positive voltage for 360°, followed by full negative voltage for the subsequent 360°.

The equivalent single tooth flux linkage and current is also shown in Figure 7.10. At 180° it can be seen that full equivalent single tooth volts are applied for a period of 60° resulting in a large increase in equivalent single tooth current. For the next 120° zero volts are applied, therefore the current falls off as positive torque is produced in the machine. Negative volts are then applied for a period of 60°, reducing the current back to zero. This whole cycle then repeats itself, but in the negative direction.

The final plot in Figure 7.10 shows the resulting equivalent single tooth torque, together with total machine torque (for reference the period between 180° and 360° is the region positive torque can be produced, and the period between 0° and 180° is the region negative torque can be produced).

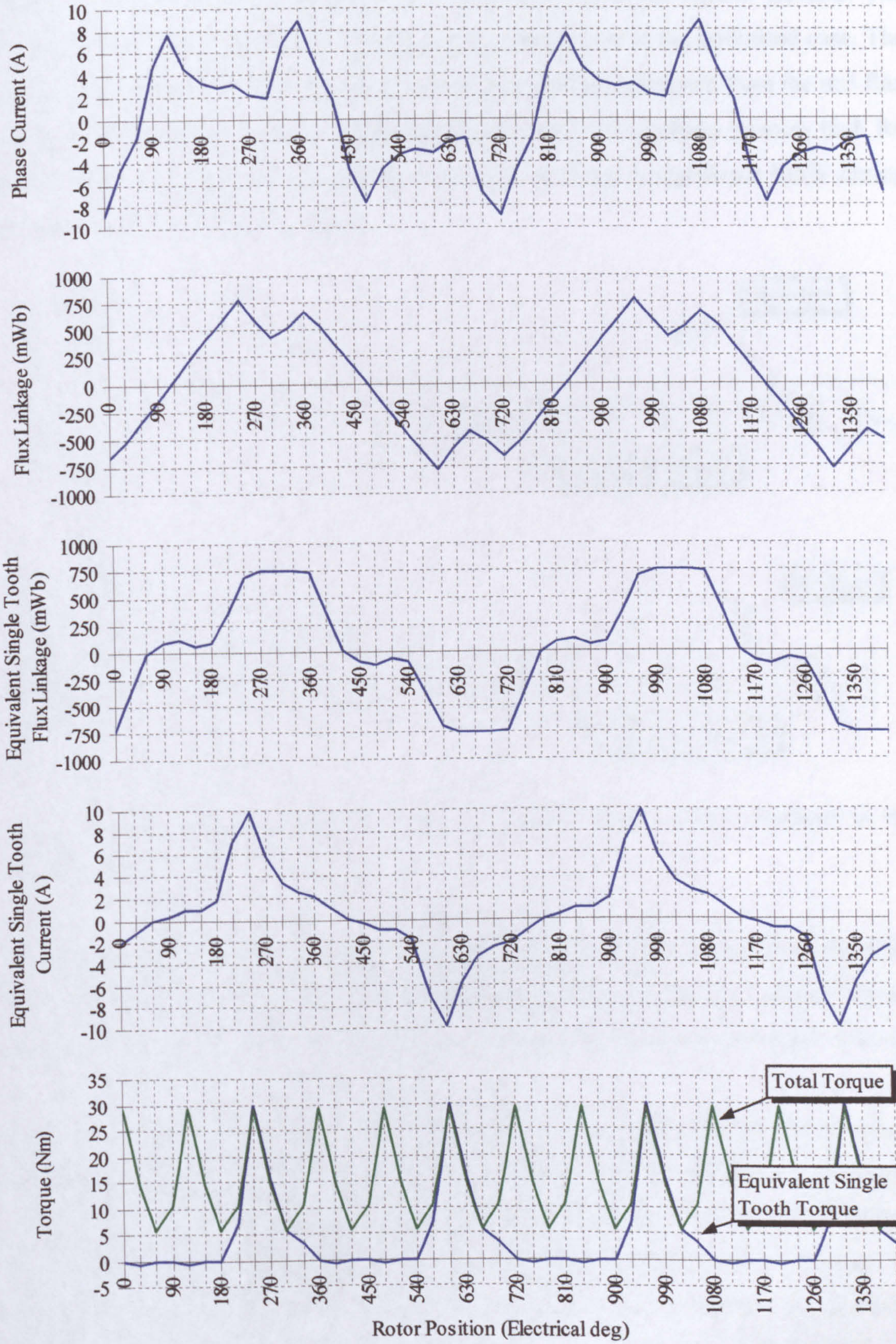

Figure 7.10 Waveforms at 2000rpm producing 15Nm torque using the optimisation technique.

Figure 7.11 shows why the optimisation is an improvement for bipolar currents. The first graph shows the full voltage control case in comparison to the optimised case. The second graph shows the equivalent single tooth flux linkage calculated from the real flux linkages. It can be seen that the equivalent single tooth flux linkage remains high for much longer in comparison to the optimised case, resulting in significant MMF during the negative torque producing region.

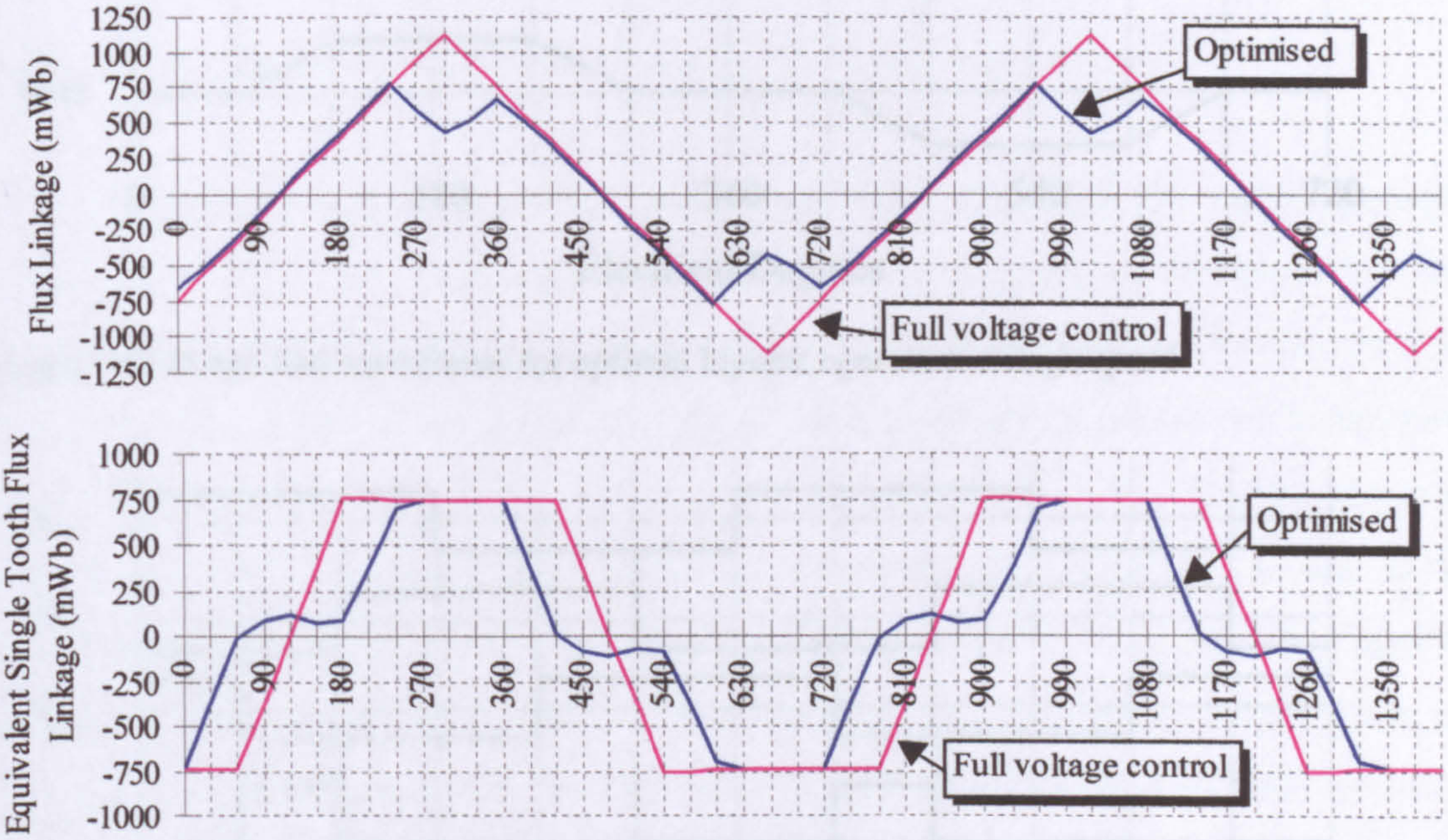

Figure 7.11 Flux linkage waveforms under full bipolar voltage control compared to the optimised waveforms.

The net effect is that less torque is produced for a greater copper loss as shown in Figure 7.9. This explains why profiling the currents is an improvement on ordinary bipolar control at high speed. The following section compares this situation to unipolar control.

Figure 7.12 shows, in simplified form, the phase and equivalent single tooth voltage waveforms that would produce the fluxes and currents shown in Figures 7.10. Figure 7.13 shows the same for unipolar control. It can be seen that the flux linkage waveforms are the same shape and magnitude, the only difference being that one is bipolar. As torque is independent of current (or flux) direction, this means the same torque will be produced. In other words bipolar operation can now match the same torque-speed envelope as unipolar operation.

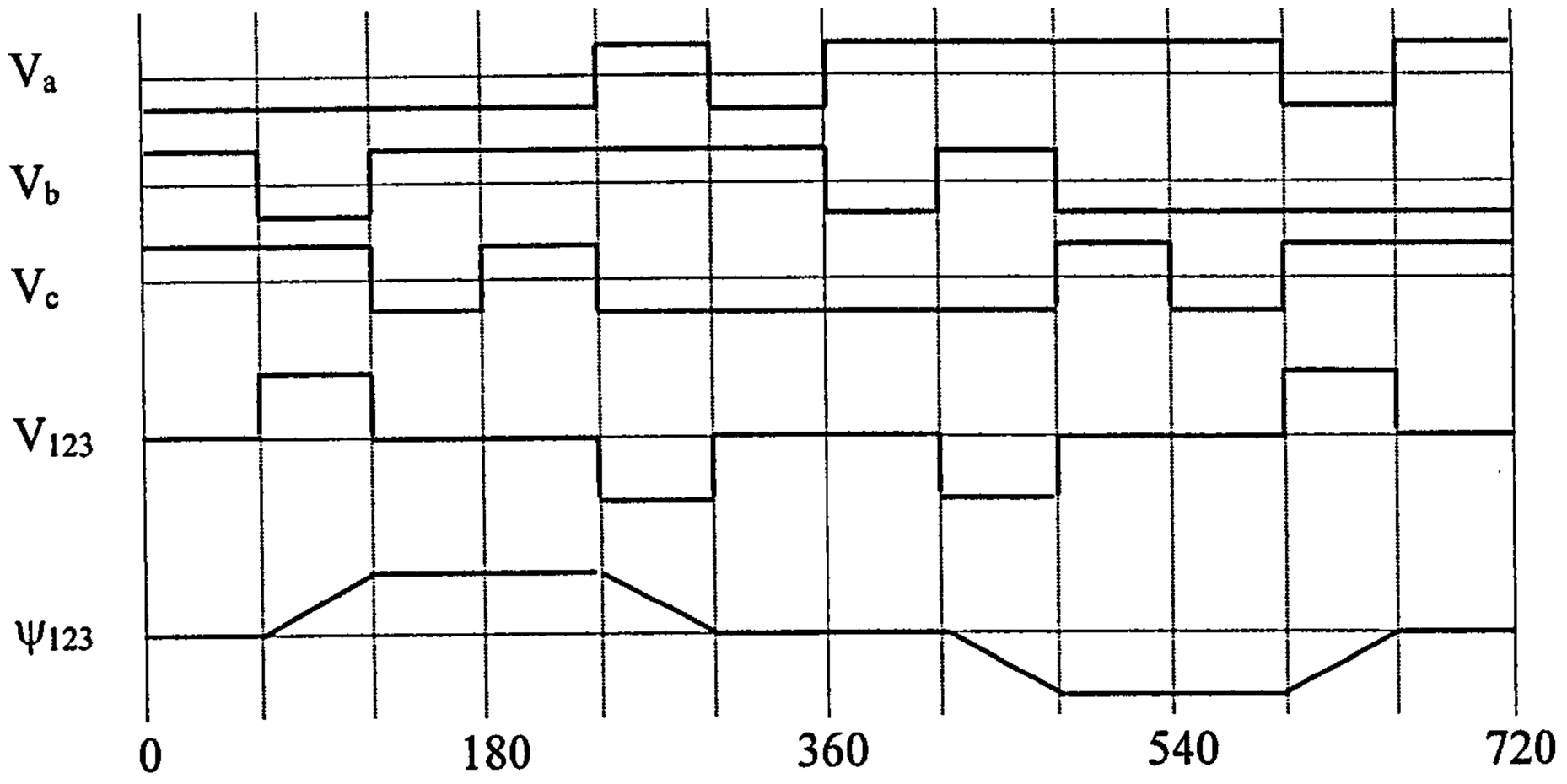

Figure 7.12 Simplified waveforms for optimal bipolar operation at high speed.

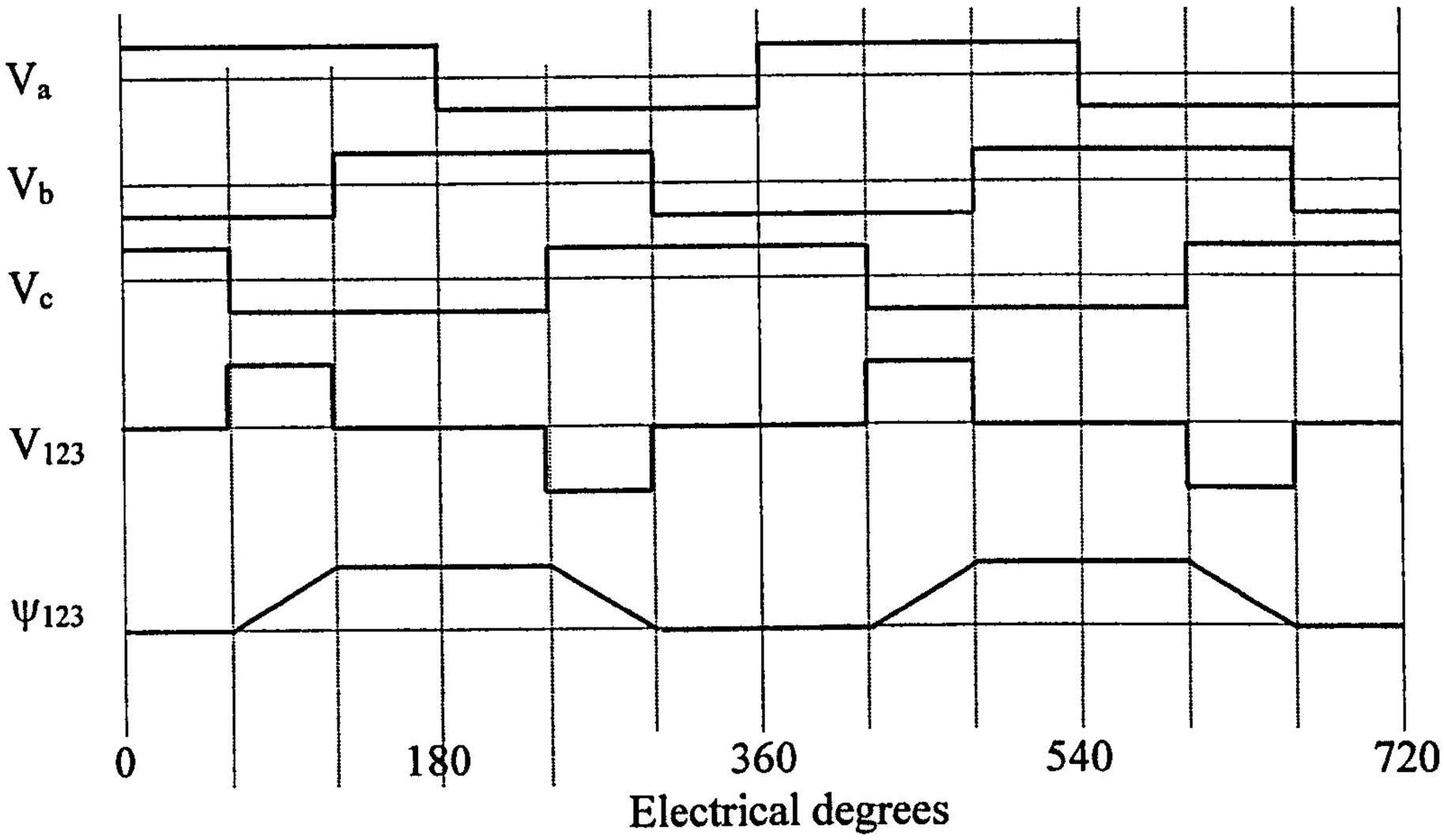

Figure 7.13 Simplified waveforms for voltage control with unipolar operation.

For reference, Figure 7.14 shows the short pitched winding machine in maximum voltage control i.e. full positive volts for 180° followed by full negative volts for 180°. A comparison with the fully pitched winding case shown in Figures 7.12 or 7.13 reveals that although the fully pitched winding machine has a much shorter period of equivalent per tooth voltage, it is at twice the magnitude. The overall effect was shown in Chapter 6 where the torque-speed envelopes of both machines were shown to be essentially the same.

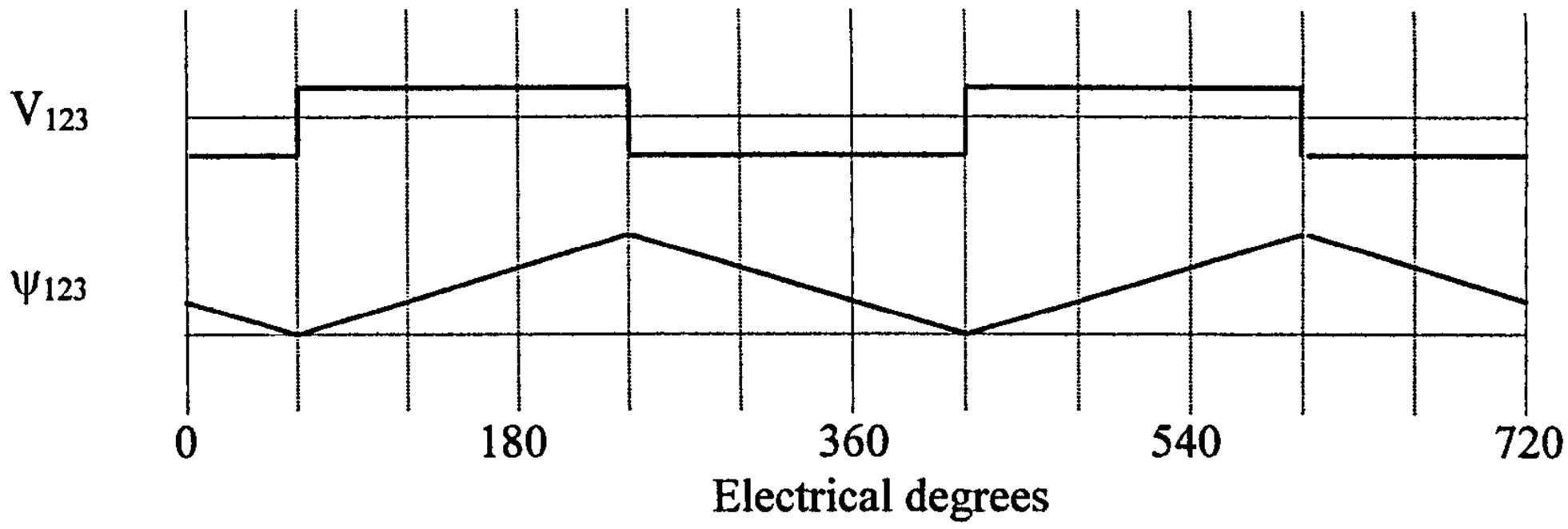

Figure 7.14 Voltage control (180°) with the short pitched winding machine

These results agree very well with the work described by Barrass [7.5], where the same voltage waveform shown in Figure 7.12 was proposed for high speed operation. The work described here has confirmed that the voltage waveform described by Barrass is in fact basically the best possible for high speed bipolar operation. However, it has now taken this further by developing this method to calculate the best current demand references over the entire torque-speed envelope of the machine i.e. the same optimisation and control method is used to minimise losses at low speed and also to maximise torque output and torque per unit copper loss at high speed. Furthermore, as optimum current references can be calculated for any given speed, a smooth transition between low and high speed operation can take place.

Implementation of the above scheme requires a matrix of current (or flux linkage) reference waveforms to be stored in the controller to cover the speed and torque range required. In practical terms this means a digital processor with a sufficient amount of memory and processing power. However this does not appear to be a problem as:

- The amount of memory required can be kept low by keeping the number of current references stored to a minimum. Simple interpolation techniques can be used to quickly calculate a waveshape between two stored references. This should work well as the current references do not change very rapidly with speed or torque, and are in fact the same up base speed.
- Processor costs have dropped dramatically in recent years, resulting for example in powerful DSP controllers with enough memory, even in the lowest cost applications.

7.3.2 Current Profiles for Smooth Torque with Lowest Copper Loss

Low speed

The optimised currents for smooth torque at low speed are shown in Figure 7.15 and have been generated using the method described in Section 7.2.2. i.e. these are the currents that give smooth torque for the lowest copper loss. When these current profiles are compared to those for maximum torque per unit copper loss, shown in Figure 7.3, it can be seen they are rather similar. Table 7.1 is a summary of the effect on peak and rms currents for the three cases of smooth torque, maximum torque per unit copper loss and normal square bipolar currents during low speed operation. It is interesting to note that when compared to the case of maximum torque per unit copper loss, smooth torque can be achieved with a slightly lower peak current and only a slightly higher winding loss.

Figure 7.16 shows the equivalent single tooth currents derived from Figure 7.15. Figure 7.17 shows the resulting equivalent single tooth phase torque, together with the total machine torque.

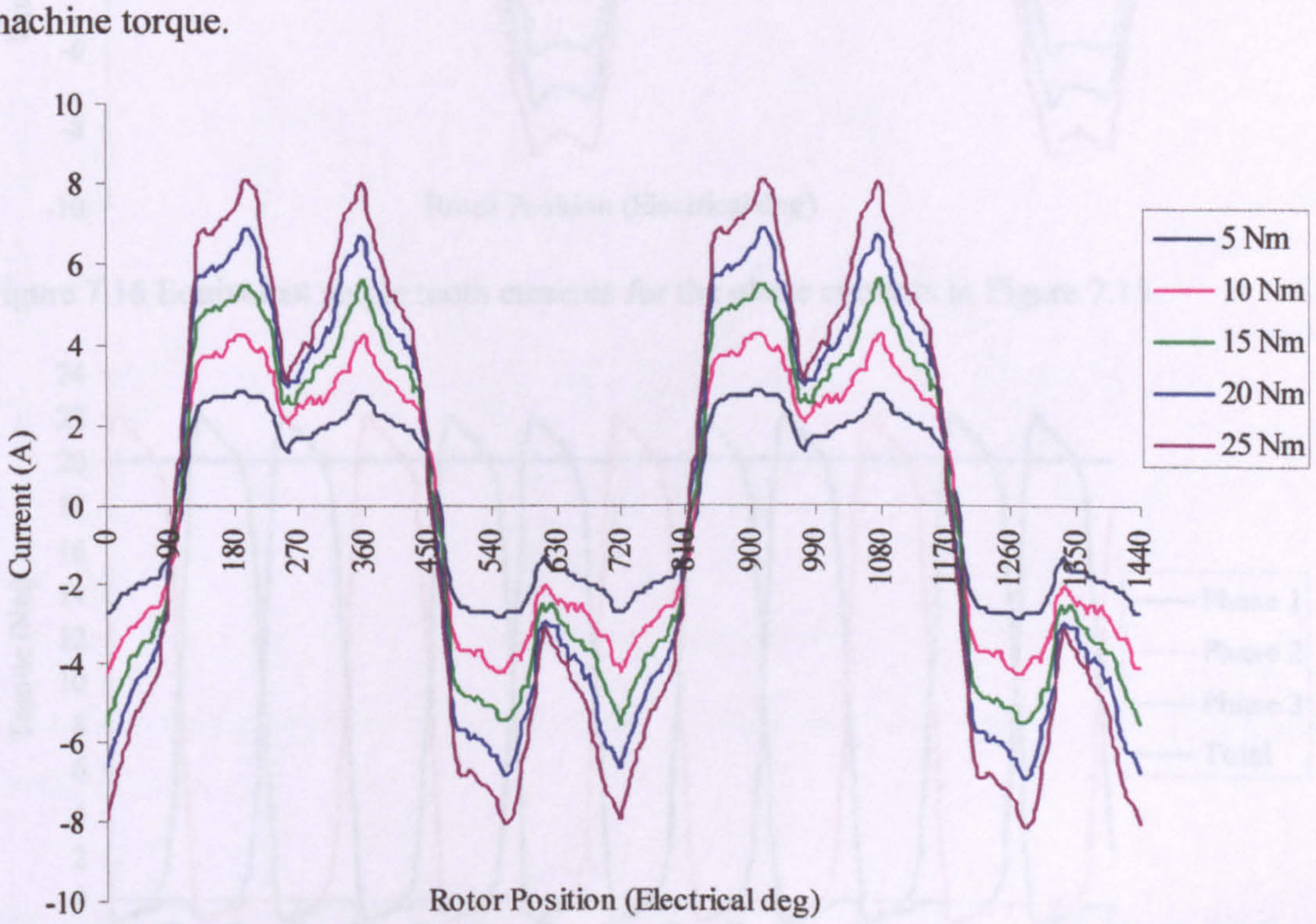

Figure 7.15 Current profiles for smooth torque at low speed for a range of torque demands (waveforms have been calculated at 5° (electrical) intervals and then smoothed).

	Winding Loss (W)	Peak Current (A)
Bipolar square	152	5.5
Profiled for Max. Torque per Unit Copper Loss	132	6.75
Profiled for Smooth Torque	137	6.63

Table 7.1 Comparison of RMS and peak currents demand for the three methods of current control, each producing 20Nm of torque at slow speed.

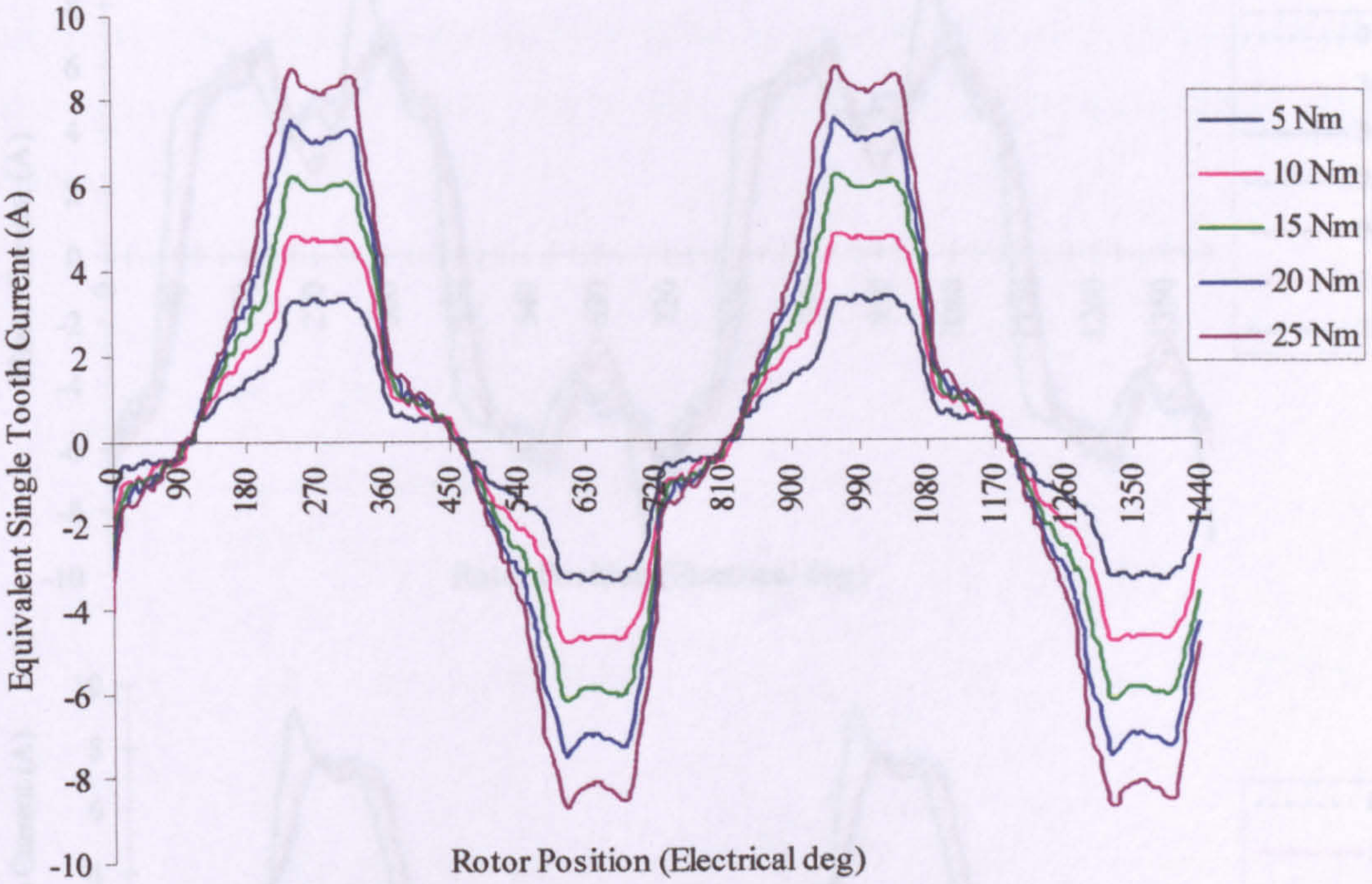

Figure 7.16 Equivalent single tooth currents for the phase currents in Figure 7.15.

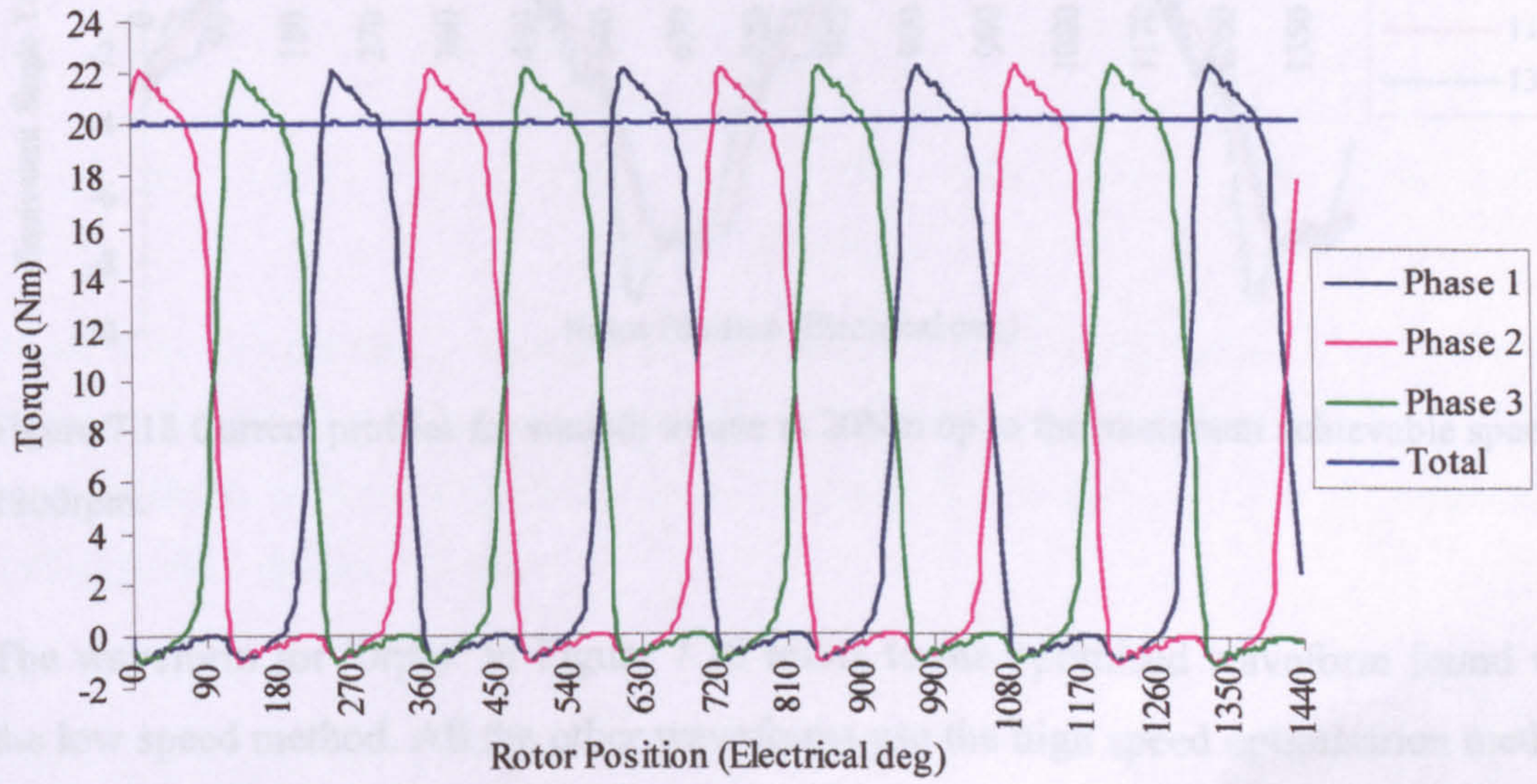

Figure 7.17 Equivalent single tooth phase torque, together with total machine torque for 20Nm smooth torque operation. Data plotted at 5° intervals.

High speed

Figure 7.17 shows the results of the optimisation method described in Section 7.2.2 for smooth torque during high speed operation. The maximum speed while obtaining 20Nm of smooth torque was found to be 1300rpm with a 600V DC link i.e. approximately the base speed and power of the drive.

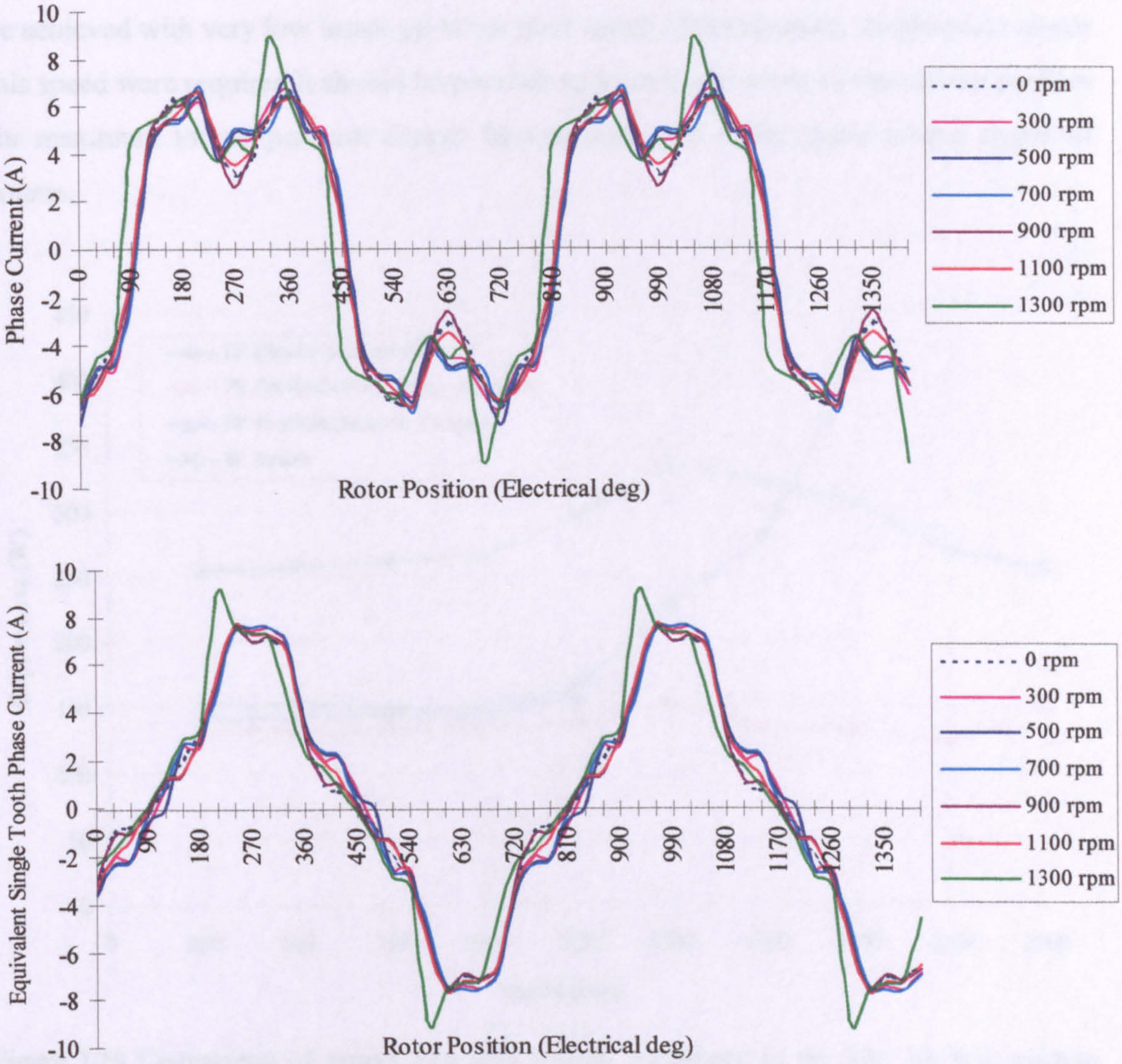

Figure 7.18 Current profiles for smooth torque at 20Nm up to the maximum achievable speed of 1300rpm.

The waveform for '0rpm' in Figure 7.18 refers to the optimised waveform found with the low speed method. All the other waveforms use the high speed optimisation method. In general there is no particular shift in the waveforms as speed increases. The waveforms only differ because a range of currents achieve a very similar result in terms

of torque and loss. The exception is the waveform at 1300rpm, where some extra advance angle is required and the currents become peakier before smooth torque is no longer achievable.

Figure 7.19 compares copper losses using smooth torque control against the other methods of control that have already been discussed. This shows that smooth torque can be achieved with very low losses up to the base speed of the machine. If operation above this speed were required it should be possible to seamlessly revert to the current profiles for maximum torque per unit copper loss instead, and suffer some torque ripple of course.

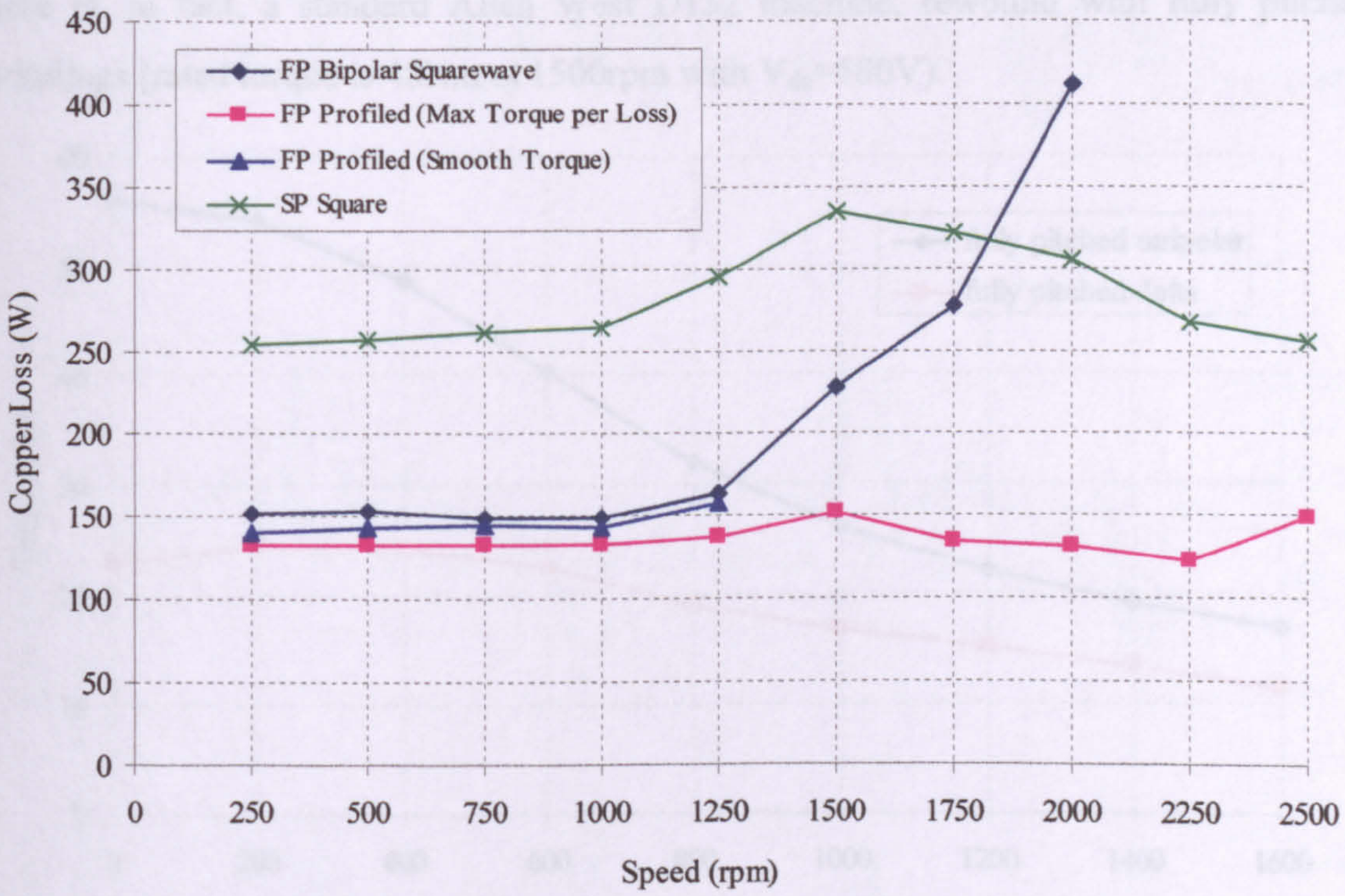

Figure 7.19 Comparison of copper loss with current waveshape in the fully pitched winding machine. Copper loss in the same machine but with short pitched windings also shown. A constant torque of 20Nm is produced up to 1500rpm, then a constant power of 3150W above 1500rpm. Base speed is 1350rpm.

7.3.3 Current Profiles for the Delta Connected Drive

The main difficulty when using the delta circuit is that an applied line voltage affects two phase voltages. This makes independent current control of individual phases impossible, leading to poor phase current control. As the simulated results in Figure 7.20 show, this leads to very poor torque production for a given current demand, especially at low speeds. The comparison here is made on the basis of the same peak current demand and the same DC link voltage. Control of the delta connected machine is with square shaped bipolar line current demands. Advance and conduction angles were optimised at each speed for maximum torque production, and in the delta connected case the best conduction angles were found to be approximately 240°. The machine simulated here is, in fact, a standard Allen West D132 machine, rewound with fully pitched windings (rated torque is 48Nm at 1500rpm with V_{dc}=580V).

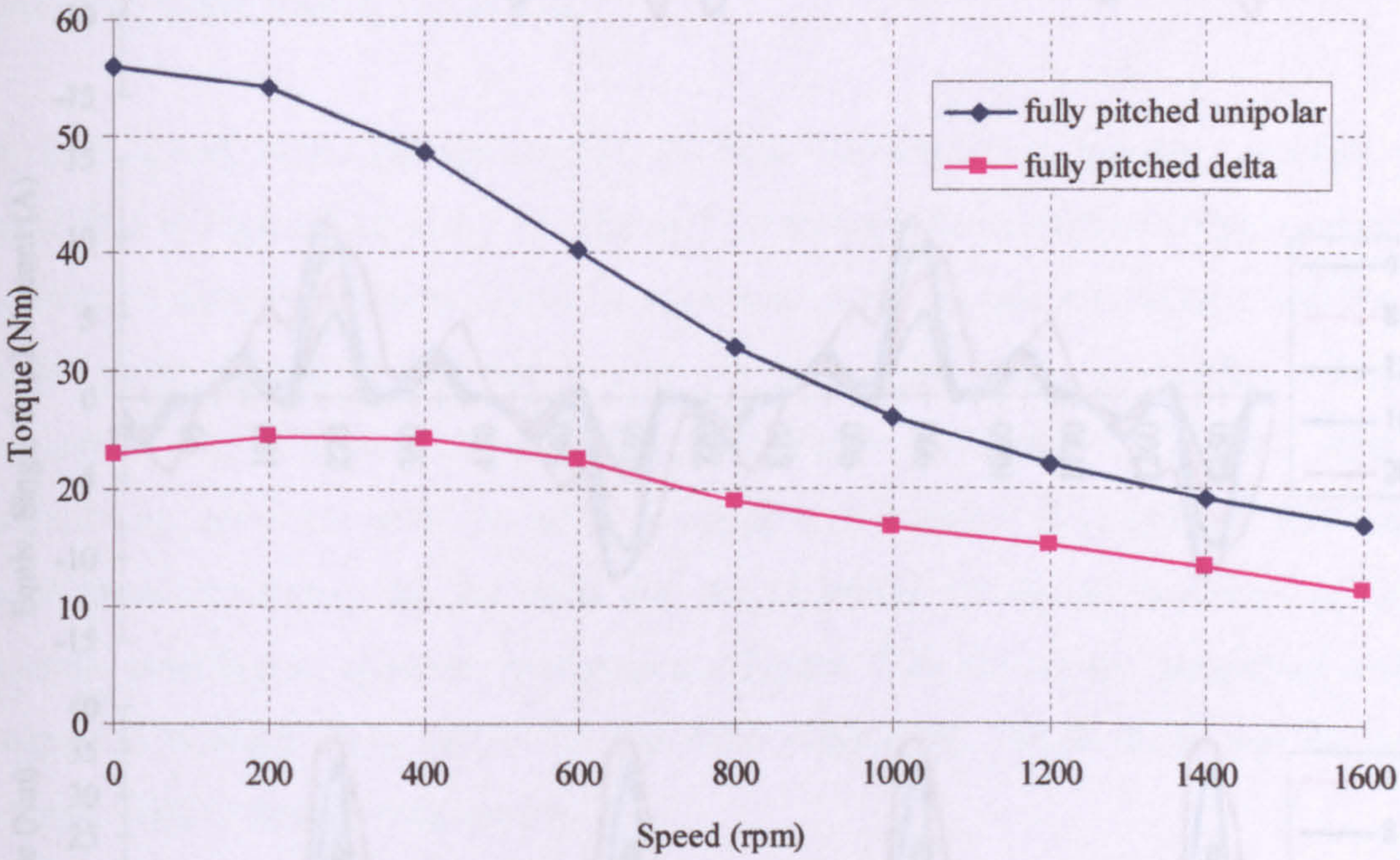

Figure 7.20 Comparsion of simulated torque-speed curves for unipolar excitation/assymetric half bridge versus bipolar excitation/delta connection. Allen West D132 machine, I_{dem}=10A, V_{dc}=240V.

The delta connection optimisation technique described in Section 7.2.3. is an attempt to take into account these facts and find some different shaped line currents that result in better machine performance. These new line currents are shown in Figure 7.21, and were calculated for the D100 prototype machine, as before with 204 turns per phase.

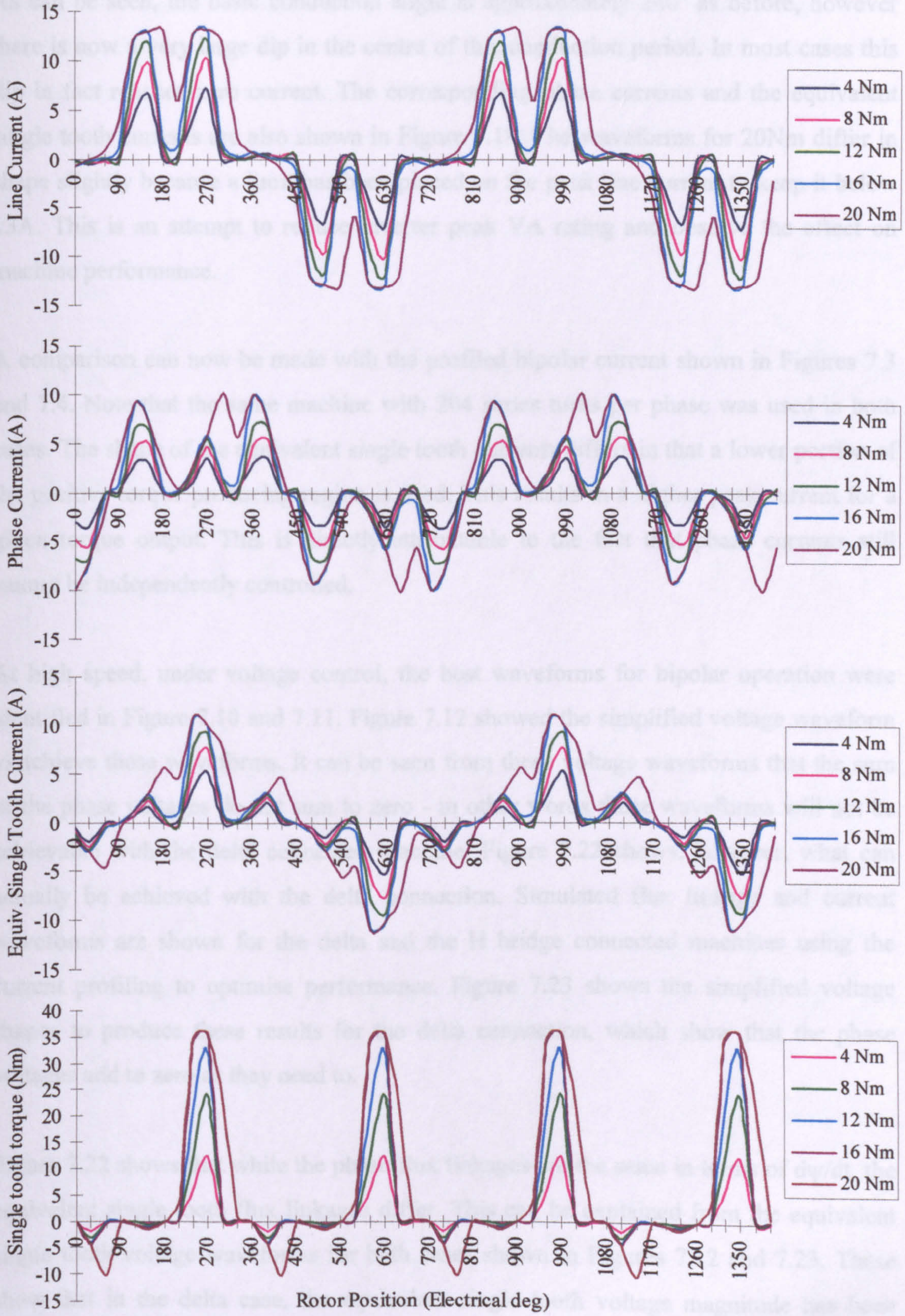

Figure 7.21 Profiled currents for the delta connected machine at 500 rpm for a range of torque outputs. Waveforms for 20Nm differ, as the line current is limited to 13A maximum. Torque due to the equivalent single tooth current also shown.

As can be seen, the basic conduction angle is approximately 240° as before, however there is now a very large dip in the centre of this conduction period. In most cases this dip in fact reaches zero current. The corresponding phase currents and the equivalent single tooth currents are also shown in Figure 7.19. The waveforms for 20Nm differ in shape slightly because a limit has been placed on the peak line current to keep it below 13A. This is an attempt to reduce inverter peak VA rating and observe the effect on machine performance.

A comparison can now be made with the profiled bipolar current shown in Figures 7.3 and 7.4. Note that the same machine with 204 series turns per phase was used in both cases. The shape of the equivalent single tooth currents differs in that a lower portion of the positive torque producing region is used. This results in a higher peak current for a given torque output. This is directly attributable to the fact that phase currents still cannot be independently controlled.

At high speed, under voltage control, the best waveforms for bipolar operation were identified in Figure 7.10 and 7.11. Figure 7.12 showed the simplified voltage waveform to achieve these waveforms. It can be seen from these voltage waveforms that the sum of the phase voltages do not sum to zero - in other words those waveforms will not be achievable with the delta connected machine. Figure 7.22 shows, however, what can actually be achieved with the delta connection. Simulated flux linkage and current waveforms are shown for the delta and the H bridge connected machines using the current profiling to optimise performance. Figure 7.23 shows the simplified voltage shapes to produce these results for the delta connection, which show that the phase voltages add to zero as they need to.

Figure 7.22 shows that while the phase flux linkages are the same in terms of $d\psi/dt$, the equivalent single tooth flux linkages differ. This can be explained from the equivalent single tooth voltage waveforms for both cases shown in Figures 7.12 and 7.23. These show that in the delta case, the equivalent single tooth voltage magnitude has been halved, but its period is twice as long. This results in the rate of rise of equivalent single tooth flux linkage being half that with the H bridge connection, but the period of that rise is doubled, resulting in the same magnitude of flux linkage still being reached. The

effect on the equivalent single tooth currents and torque can be seen in Figure 7.22 where slightly more current is evident in the negative torque producing region. Overall, however, the waveforms are remarkably similar, considering the voltage restrictions inherent in the delta circuit and the poor phase current controllability.

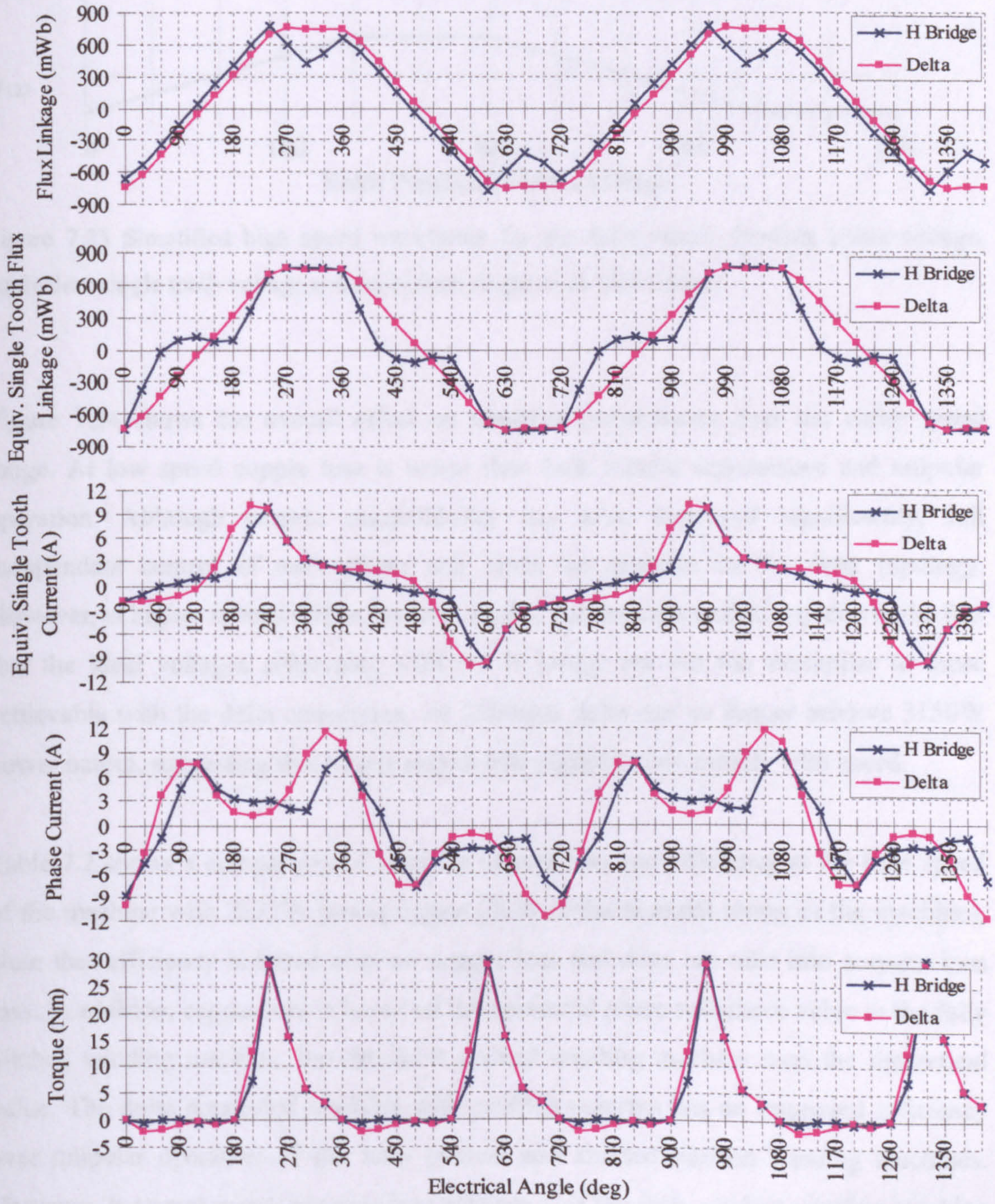

Figure 7.22 Simulated flux linkage and current waveforms at 2000rpm, producing 15Nm of torque. Waveforms for control with the H bridge circuit and the delta connected circuit are shown, both being having being derived from the optimisation technique.

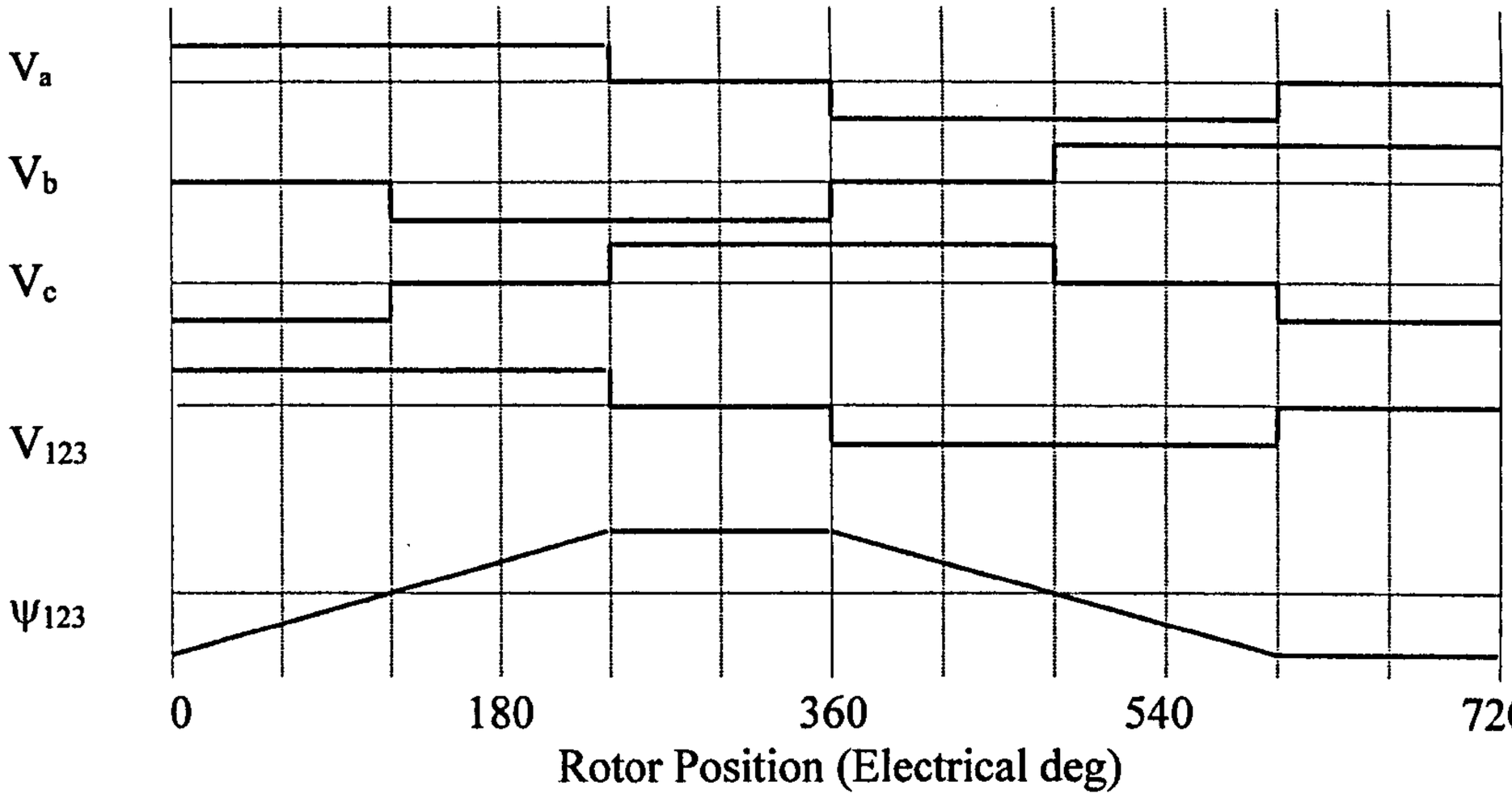

Figure 7.23 Simplified high speed waveforms for the delta circuit showing phase voltage, equivalent single tooth voltage and equivalent single tooth flux linkage.

Figure 7.24 shows the overall effect on machine performance over the entire speed range. At low speed copper loss is worse than both bipolar squarewave and unipolar operation. Although current controllability has been improved significantly, full independent control of each phase will never be possible in the delta topology. However, at higher speeds torque per unit copper loss improves relatively due to the fact that the ideal voltages achievable with the H bridge are not too dissimilar to those achievable with the delta connection. At 2500rpm delta can no longer achieve 3150W power output, suggesting that torque output falls slightly more rapidly with speed.

Table 7.2 shows a comparison of machine copper loss and efficiency at the base speed of the machine with 2827W power output (3kW is the nominal rating of the machine). Note that efficiency is based only on copper loss and does not take into account iron loss. In addition, copper loss is based on the measured phase resistance value in the fully pitched winding machine, but the short pitched winding machine uses the theoretical value. The delta connected machine with profiled currents has an improved efficiency over unipolar operation of the fully pitched and shorted pitched winding machines. However, it cannot match the excellent efficiency of the fully pitched winding machine using an H bridge inverter with profiled currents.

In terms of inverter rating two comparisons need to be made. The first is at very low speed or stall where peak current in a device will determine its rating due to its relatively short thermal time constant. Table 7.3 shows a comparison of peak device currents for the various drives.

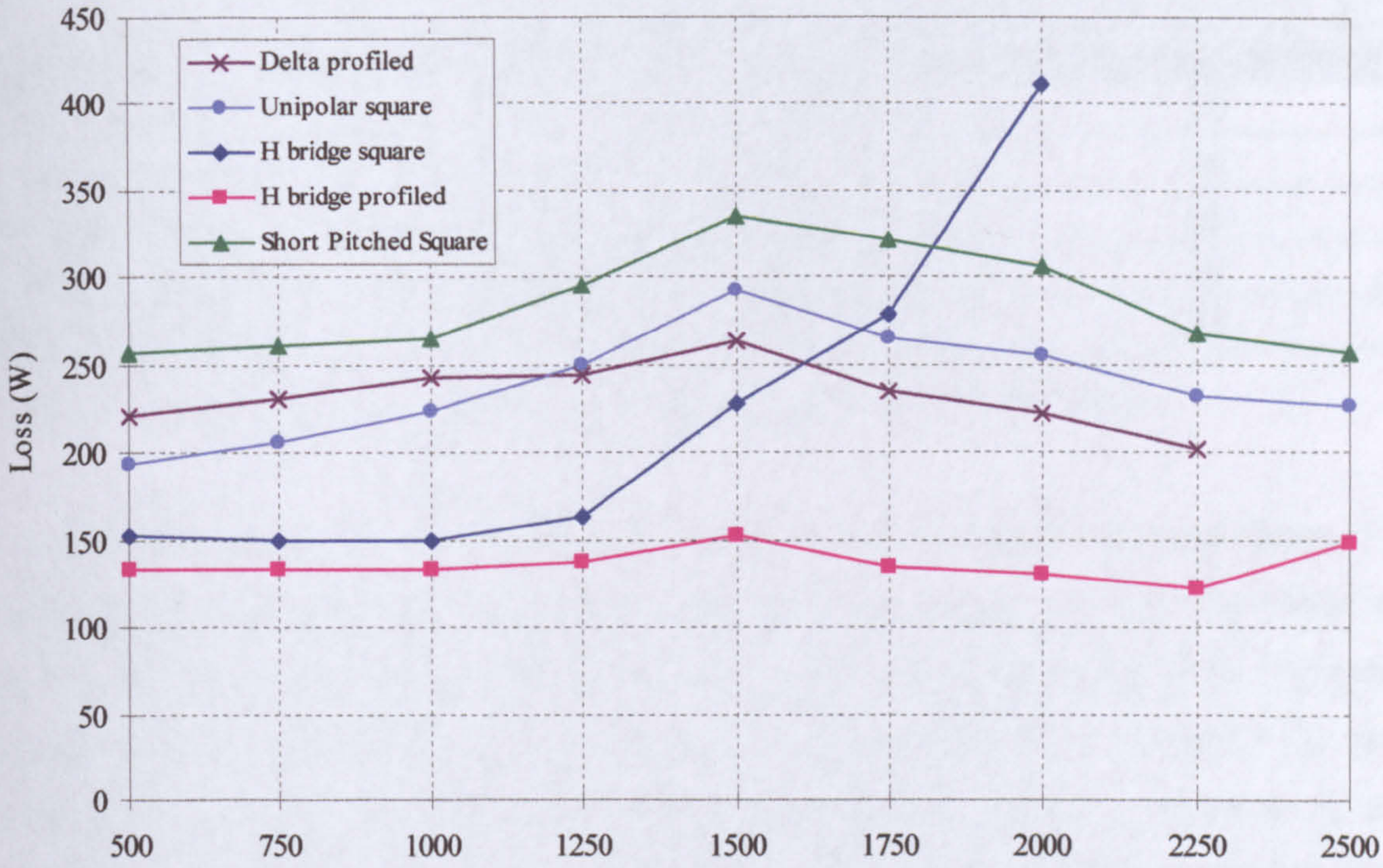

Figure 7.24 Comparison of copper loss with current waveshape. Copper loss in the same machine but with short pitched windings also shown. Losses correspond to a constant torque of 20Nm up to 1500rpm, and a constant power of 3150W above 1500rpm. Base speed is 1350rpm.

	I_{pk} (A)	Copper Loss (W)	Machine Efficiency (%)
Delta Profiled	13	252	91.8
Unipolar square	9.4	267	91.4
H bridge square	6.1	189	93.7
H bridge profiled	7.7	143	95.2
Short pitched square	8.5	311	90.1

Table 7.2 Comparison of machine performance at base speed (1350rpm) for 2827W power output. I_{pk} is inverter device peak rating. Efficiency does not include iron loss.

The relative size of each inverter will therefore be the product of the peak current at low speed and the number of active devices (the same DC link assumed for each). This gives the inverter rating shown in the table. It can be seen that the peak line current of the delta connection severely affects low speed operation rating.

	Peak Current (A)					
Speed (rpm)	<500	1000	1500	2000	N	Inverter rating (@500rpm)
Delta Profiled	13	13	13	12.65	6	78
Unipolar square	7.7	9.9	9.9	9.5	6	46
H bridge square	5.5	6.5	6.5	10.2	12	66
H bridge profiled	6.8	9.3	9.3	8.8	12	82
Short pitched square	7.5	8.9	8.9	8.8	6	45

Table 7.3 Comparison of peak inverter device current and peak inverter rating.

A comparison, however, also needs to be made in terms of device average losses. At higher electrical frequencies where device losses tend to average out over the electrical cycle, it is the average rather than the peak loss that is the determining factor. Inverter losses cannot be estimated as they were using the simulation in Chapter 6 as the optimisation routine used here is simplistic in comparison. Table 7.4, however, is an attempt to estimate relative losses based on the current demand and the estimated duty cycle of each device. The total inverter rating is therefore the product of these two values and the number of active devices in the inverter.

	I (A)	Duty Cycle	N	Inverter rating
Delta Profiled	13	0.33	6	25.8
Unipolar square	9.9	0.66	6	39.6
H bridge square	6.5	0.5	12	39.0
H bridge profiled	9.3	0.5	12	57.0
Short pitched square	8.9	0.39	6	20.8

Table 7.4 Comparison of device rating at base speed. Estimates based on product of peak current demand, device duty cycle and total number of devices.

The delta connection now looks more favourable, as although peak device current is high, its duty cycle is low. This is due to the fact that at any one time only two devices are needed to supply current to two phases in the delta circuit. With unipolar operation

using the asymmetric half bridge four devices need to conduct at any one time (two per phase for two thirds of the time). Bipolar squarewave using H bridges requires six to conduct (2 out of 4 per phase continuously).

As with many SR motor configurations the relative merits of the delta topology both in terms of machine efficiency and inverter rating is highly dependent on the application. A pump or fan application would perhaps be most suitable, where the start up torque is low and power electronic rating is determined at high rather than low speed.

Further points to consider with the delta topology are as follows:

- A major advantage of the delta connection is that the number of power electronic packages is reduced to six, as the switch and diode can now be contained within the same component. In contrast, the asymmetric half bridge topology, for example, requires 12 packages as the six switches and six diodes must be contained in their own package due to the connectivity of the circuit. The delta connection uses the same three phase bridge topology used with the vast majority of AC machines such as the induction motor. Complete inverters are therefore available as standard within one module.
- Further advantages are that only three power connections are required between the inverter and the motor. This is useful where large distances are encountered between the two. Another less obvious situation, for example, is in a refrigerator compressor where expensive seals are required in the motor housing for each motor connection. This is one major reason why brushless DC machines rather than SR machines are currently being developed for variable speed purposes.
- Line current sensing with only two sensors is possible, as the third line current can be calculated.
- A 3kW induction motor requires a peak line current of 8.5A. In comparison the delta topology with profiled currents requires 13A, therefore power electronic rating appears to be high. Note, however, that all SR machines have the advantage under voltage control at high speed that very little device switching takes place, resulting in lower losses for the same conducted current.

7.4 Implementation of Current Profiling Using a Flux Control Method

The current profiles generated by the optimisation techniques described in this chapter were implemented on the test rig. Thus, it was possible to discover whether these waveforms truly gave the predicted increase in performance.

Current reference look-up tables were stored in the memory of the DSP for a range of torque demands and positions as follows: 5Nm to 25Nm at intervals of 5Nm, 0 to 360° at intervals of 11.25°. For simplicity in the trial, only references for a speed of 1000 rpm were used. The current controller implemented the following steps each PWM cycle. The timing of these steps are shown in Figure 7.25.

- Sample position
- Calculate desired phase currents with knowledge of torque set point (input via hardware) and the measured position. Linear interpolation used to calculate the value between the stored points.
- Sample currents
- Use a PID controller to generate the voltage references (or voltage demands) to send to the PWM controller based on the current error.

The results of this method are shown in Figure 7.26. The actual current lags substantially behind the desired current reference. The effect is a drop in performance due to the fact that torque output is much lower than expected.

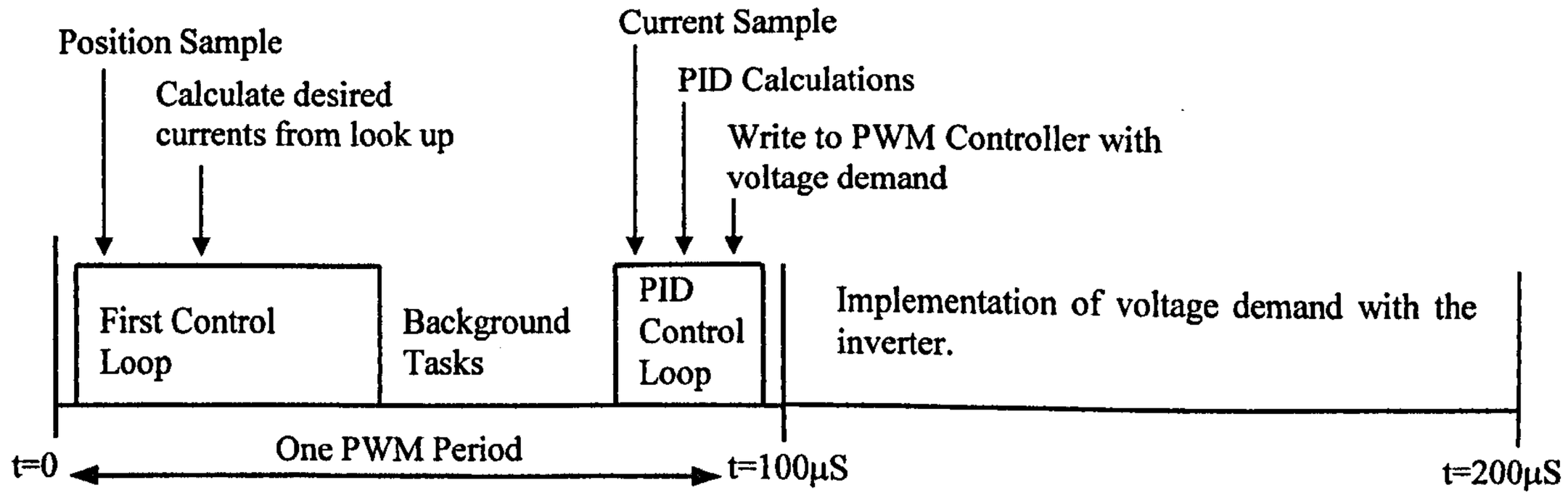

Figure 7.25 Implementation of profiled currents using a PID Current control

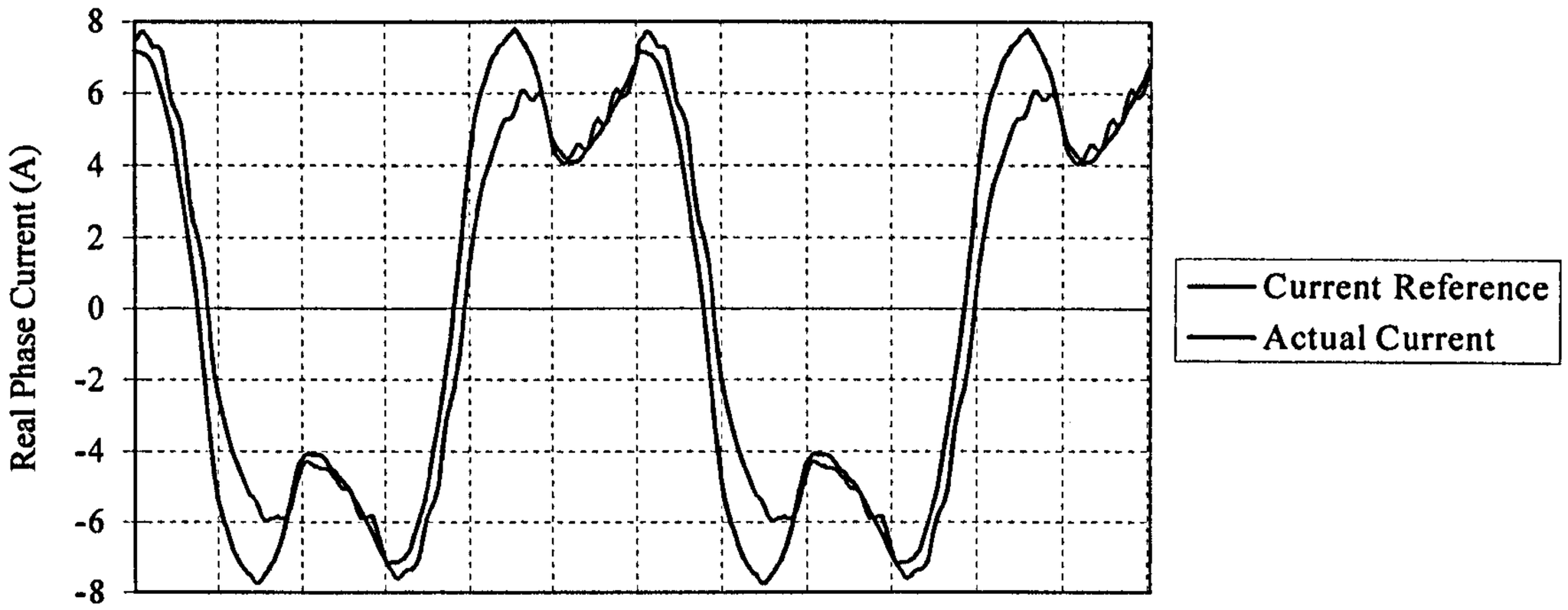

Figure 7.26 Comparison of a profiled current reference to the current actually achieved in the machine with the PID current controller described.

The lag and incorrect magnitude of the actual current is due to two problems. Firstly, a PID current controller relies on current error to generate the voltage demand. A certain steady state error that is dependent on the proportional gain will always exist. In a situation where the current demand is constant, integral gain can be used to help eliminate this error. However, in this situation the current reference is constantly changing and therefore there will always be an error. Secondly, the speed of the machine means that the current demand will always be incorrect by the time the PID loop has implemented its voltage demand on the machine. This can be seen in the timing diagram of Figure 7.25, where the inverter is implementing the voltage on the machine one PWM cycle after all the calculations have been done. In this case the position sampling makes the situation worse as this is performed at the start of a PWM period, meaning it is nearly two periods 'out of date' by the time the voltage demand has been fully implemented. At 1000rpm the rotor will turn over 7 electrical degrees during a PWM period of 100μs in a 12-8 machine, thus leading to significant error.

The second problem of controller lag can be substantially reduced by predicting where the position of the rotor will be by the time the controller has implemented its voltage demand on the system. The speed of the machine is essentially fixed over a PWM period and therefore a good prediction can be made of the position at the end of the subsequent PWM period.

This improves the situation somewhat, but still leaves an error in the current magnitude. A fundamental problem is that the effective inductance of a phase winding changes with position, and therefore a PID current controller will only be tuned optimally at one point. In other words, when a certain voltage is applied to a phase the controller does not have knowledge of the change in current that will result, and that change in current will be different at different rotor positions. To optimally tune the system the controller must know the change in current to expect, otherwise either instability or poor control will occur. Both these effects are evident in the waveforms of Figure 7.24. Poor control can be seen at the first peak in the waveform where a large difference between demanded and actual current has occurred. In the dip in the waveform that follows, oscillations are evident indicating that the system is on the point of instability at this position.

A controller can be given knowledge of the expected change in current due to an applied voltage with use of the machine's flux linkage/current/position characteristics. If the present position and currents are known, then these characteristics can be used to calculate the exact change in flux required to achieve a certain current at a subsequent position. This is shown in Figure 7.27. Here $\psi(\theta_n, i_n)$ is known as current and position have been sampled. A certain time later the rotor will be at a new position and require a new current demand. $\psi(\theta_{n+1}, i_{n+1})$ can now be calculated. The change in flux linkage needed to achieve the desired change in current is therefore:

$$\Delta\psi = \psi(\theta_n, i_n) - \psi(\theta_{n+1}, i_{n+1}) \tag{7.5}$$

It is also known that:

$$\psi = \int (V - iR).dt \tag{7.6}$$

Rearranging Equation 7.6 gives

$$V = \frac{\Delta\psi}{t} + iR \tag{7.7}$$

Therefore the exact voltage required to achieve the desired change in flux can be calculated, thus achieving optimal control at every point. Barrass and Mecrow [7.6] used a very similar scheme to implement desired waveforms for torque control purposes. An addition to the scheme is that position is also predicted, as there is a lag between calculating the required voltage and its implementation in the inverter.

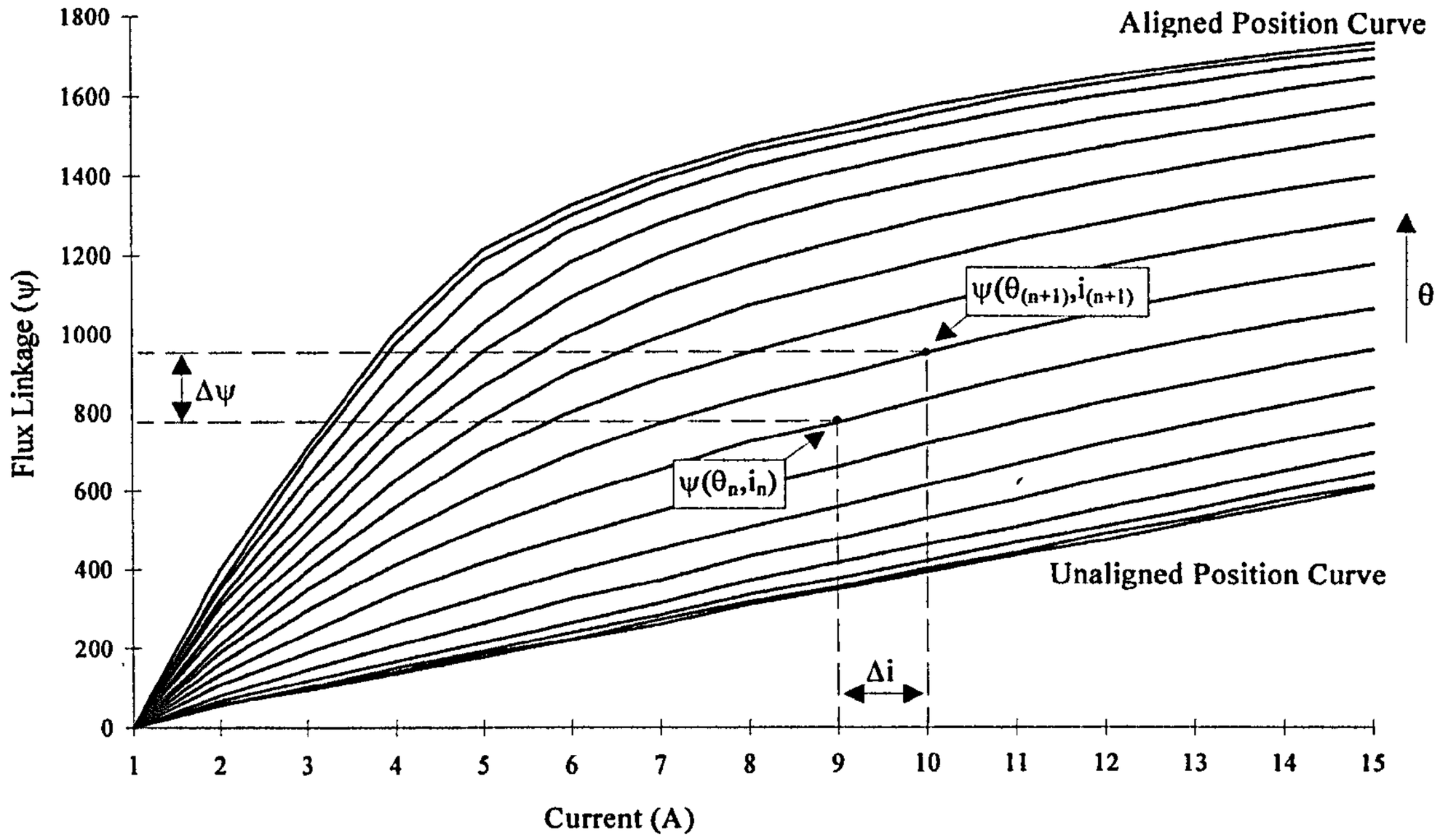

Figure 7.27 Use of the flux linkage characteristics with a flux controller.

It is more convenient in practice to store the desired profiled waveforms that have been presented in this chapter as flux linkage rather than current. This simply saves computation time, as the desired current does not have to be converted to desired flux every time.

When implemented on a fully pitched winding motor, values need to be converted into their equivalent single tooth parameters before the flux linkage data can be used. The following summarises the complete set of steps necessary during one PWM cycle:

- Sample position.
- Calculate the predicted position in the next PWM period.
- Find desired flux linkage values from interpolation of the stored reference waveforms using knowledge of the predicted position and the desired torque.
- Sample actual phase currents.
- Convert actual phase currents to the actual equivalent single tooth currents using the transformation matrices.
- Use the flux linkage/current/position data to obtain actual equivalent single tooth flux linkage.

- Convert actual equivalent single tooth flux linkage to actual flux linkage using the transformation matrices.
- Calculate the change in flux linkage necessary to achieve the new desired value of flux linkage (Equation 7.5).
- Calculate the voltage required, and hence PWM duty cycle, to achieve the desired change in flux linkage (Equation 7.7).
- Send value to PWM controller.

The timing diagram for this is shown in Figure 7.28. The above method therefore solves the two problems identified as causing the poor performance i.e. the controller looks ahead to see what the desired current value (or flux linkage value) will be by the time the required voltage demand has been implemented in the inverter. The exact voltage to achieve that desired current is calculated from knowing the machine characteristics. It should be noted that even if there is a slight error in the volt-seconds applied during one PWM period (e.g. due to a variation in the DC link voltage), this is compensated for in the next period. This is because the actual current is always sampled every PWM period and so cumulative errors cannot build up.

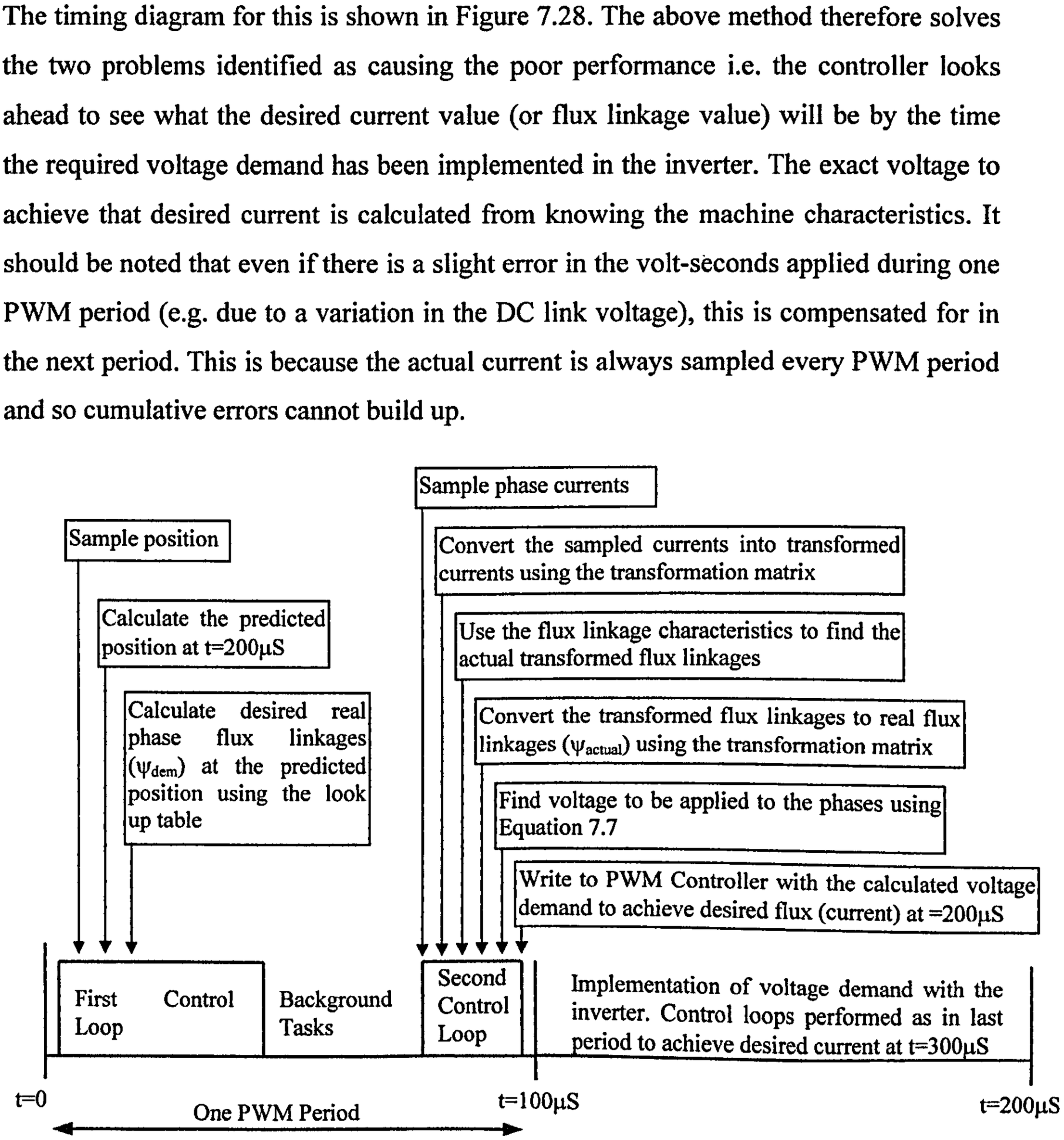

Figure 7.28 Implementation of profiled waveforms using a flux controller.

When tried on the test rig excellent results were achieved. As discussed at the start of this section, profiles for operation at 1000rpm were stored in memory and the torque demand set via hardware. Linear interpolation was used to calculate points between torque profile curves and between stored positions. With the torque demand set, the excitation of the DC load machine was adjusted so that the SR motor was driving it at the desired speed of 1000rpm. The torque and copper losses produced were estimated using the techniques described in Chapter 5. Torque did indeed now match the demanded value confirming that the flux controller was achieving the desired current profiles. Furthermore it showed that those demanded values were achievable in the machine at this speed. Losses also matched the predicted values confirming that the overall improvement in machine performance with profiled currents is correct.

7.5 Summary

A method of finding the optimum currents in the fully pitched winding machine with bipolar currents has been described. It is empirical in nature, and needing no initial starting values, is able to quickly scan through many combinations of possible waveform shape, gradually becoming more and more accurate. The method is able to optimise the currents either for maximum mean torque per unit copper loss or for smooth torque with the lowest copper loss. The technique works for both high and low speed operation due to the fact that the maximum change in current at any position can be taken into account. The method does not work on a point by point basis, but takes the whole electrical cycle into consideration at once thereby producing the best results possible.

The results show a significant improvement. When optimised for maximum mean torque per unit copper loss, copper loss is reduced by 13% at low speed compared to bipolar squarewave operation. This is achieved at the same time as having a relatively low torque ripple of 30% pk-pk. On the other hand, when the currents are optimised in a different way smooth torque can be achieved up to base speed, while still maintaining a saving in copper loss over bipolar squarewave. These optimisation methods bring copper loss down towards half the value in the same size short pitched winding machine for the same torque.

At higher speeds there is an even larger effect. While trying to maintain a constant power output bipolar squarewave operation shows rapidly increasing copper losses. The optimisation method has shown that this is due the fact that full voltage control should not be used with bipolar currents. More torque can be produced with lower copper losses by profiling the currents, even at the highest speeds.

Comparisons with unipolar voltage control show that the profiled shape is in fact the bipolar equivalent, and therefore shows that the torque-speed envelope of unipolar machine can now be achieved with bipolar currents. The drawback, however, is that twice the number of power electronic devices are needed to achieve this (although peak device current and devices losses are lower). Therefore this drive is likely only to be

appropriate where machine performance, rather than power electronic cost, is paramount.

The optimisation method has been shown to work for the delta connected drive by taken into account the restrictions on the available phase voltages (the sum of the phase voltages must be zero). A delta allows the use of low cost standard inverter modules and current feedback with two line sensors. Profiling of the currents to the waveforms shown drastically improves low speed machine performance in terms of torque for a given current demand, as well as losses, thereby making the drive a realistic option. Machine performance is now broadly similar to unipolar operation. Power electronic rating, and therefore cost, is highly dependent on speed. Peak line current is high, meaning that low speed inverter rating is poor in comparison. At high speed, however, device losses are more important, and they are low due to the low device duty cycle (only two devices need to conduct in the inverter at any one time). Estimates show that this results in a lower inverter rating than either unipolar or bipolar squarewave operation.

Lower cost drives may be able to simplify the optimised waveforms to achieve good performance while minimising controller costs. This could be especially true in the delta connected version which could be suitable for a low cost fan/pump application. It has been shown, however, that to achieve the exact current waveforms is very difficult with normal PWM current control. A flux controller was developed to improve performance by calculating the exact voltage to be applied in the subsequent PWM period by using the flux linkage characteristics of the machine.

Chapter 8 - NEW INVERTER TOPOLOGIES FOR UNIPOLAR OPERATION

8.1 Introduction

The asymmetric half bridge circuit (AHB) is by far the most common topology used with switched reluctance motors [8.1]. With this configuration there is a separate half bridge for each phase, so that the voltages and currents supplied to each phase are completely independent of all other phases. Thus this offers the maximum degree of flexibility of all unipolar converter options. There have been many other developments, examples of which are given in [8.2-8.5], driven predominantly with the aim of reducing the number of devices, but almost without exception these have inherent limitations in terms of motor controllability. Consequently the half bridge circuit generally remains the preferred choice for unipolar excitation.

Unipolar operation of the fully pitched winding SRM with a standard AHB converter has been discussed in Chapters 5 and 6. It has been shown that with the same peak current and voltage rating this type of inverter can deliver the same torque-speed envelope as a short pitched winding SRM, but with much improved machine efficiency. Inverter losses on the other hand were shown to be up to twice that of the short pitched winding machine due to the fact that each phase needs to conduct for 240° rather than 120°. Although peak VA is the same, in many applications the increased device losses will lead to higher rated components and a larger heatsink rating.

With this in mind, possible new inverters were considered that would reduce this inverter loss, but at the same time maintain good enough control of the phase currents so machine performance is not significantly affected. Three new inverters were developed that satisfied these requirements and these are explained in this chapter. They all have the same basic principle behind them, which is to control two phases at the same time with only two switches. This is in contrast to the asymmetric half bridge arrangement, which requires four switches to control the two conducting phases.

8.2 Ideal Current and Voltage Waveforms

Figure 8.1 shows the ideal currents at low rotor speed for the fully pitched winding machine. Two phases conduct at any one time with the same unipolar current and so this brings about the opportunity to 'connect ' the conducting phases in series, with the aim of reducing the number of power electronic switches conducting.

When two windings are, however, simply connected in series the voltage applied across the pair will be shared in proportion to the impedance of each. This could result in reduced torque output at high speed as the full DC link voltage would not be available across each winding at the commutation positions.

It was, however, noticed that the machine did not require full DC voltage across each phase all of the time when operating at high speed (base speed and above). The machine in fact does not go into full voltage control as normally experienced with the short pitched winding machine. In other words, there are significant periods when current chopping takes place and either little or no volts are applied to the winding. Figure 8.2 shows the voltage waveform required at high speed in an idealised manner. Measured phase currents with this idealised voltage waveform are shown in Figure 8.3, and these can be seen to be similar to the high speed waveforms shown in Figure 5.6 of Chapter 5.

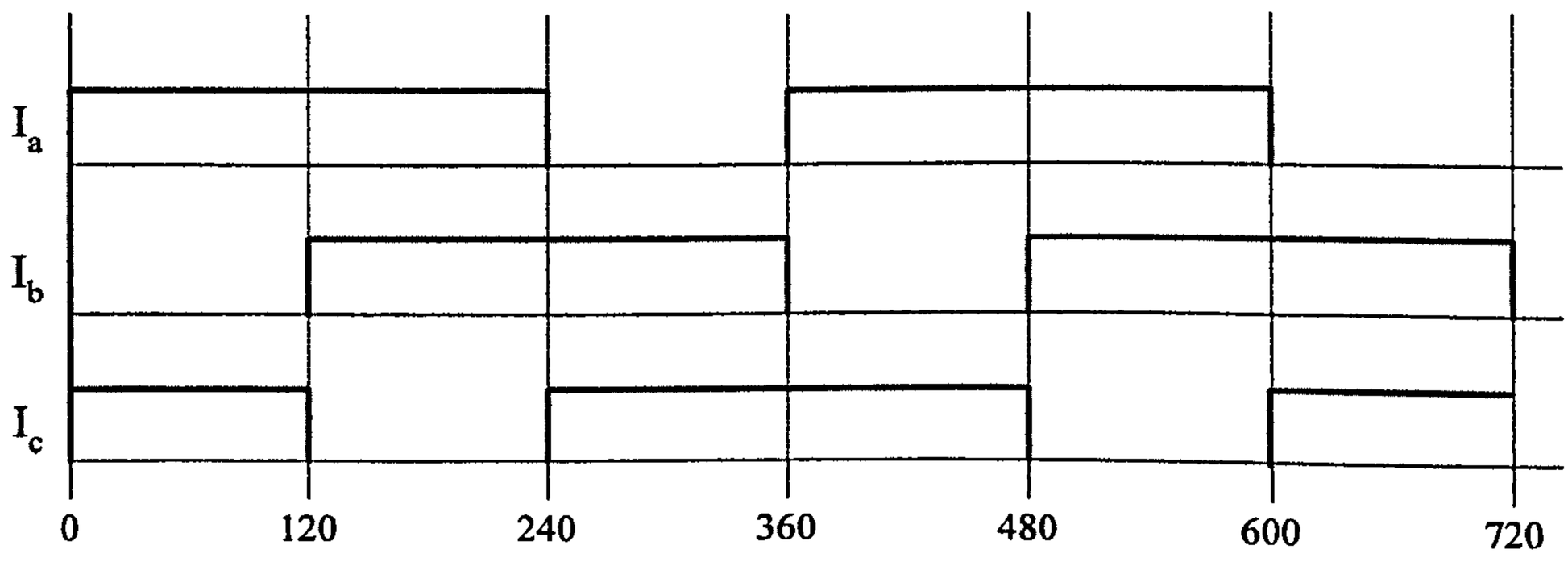

Figure 8.1 Ideal current waveforms under current control.

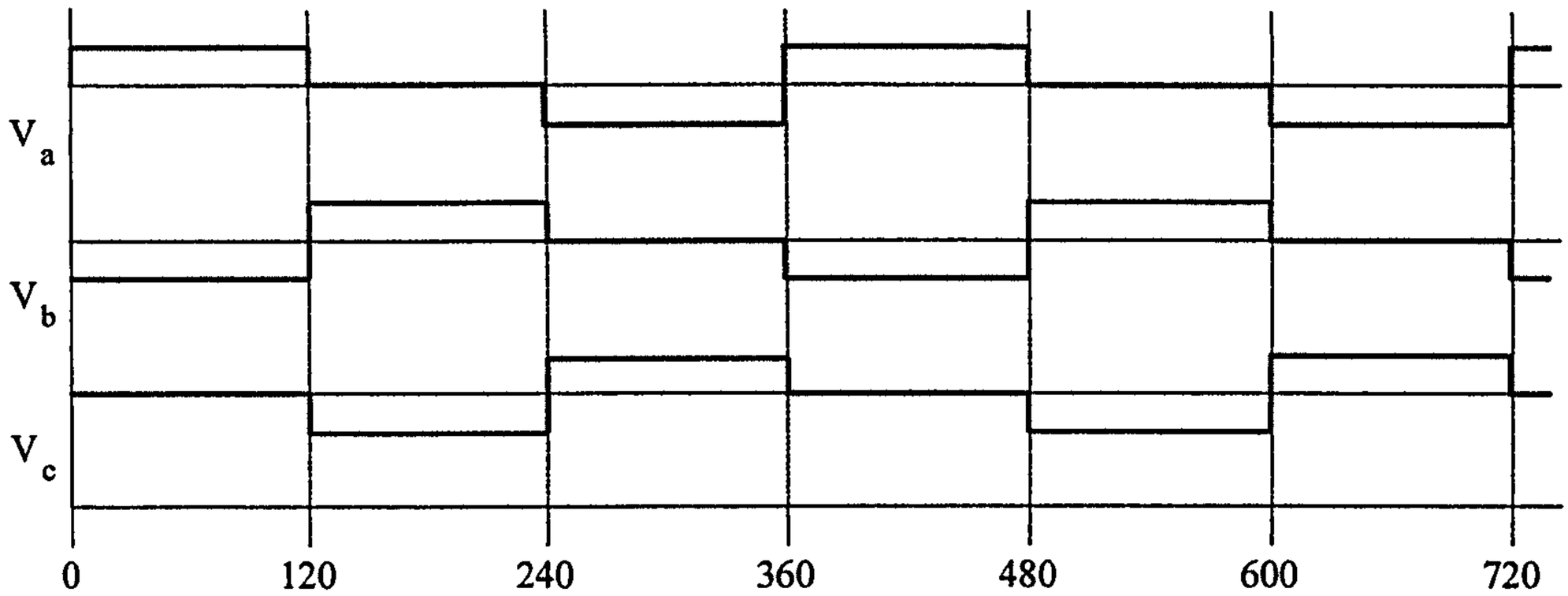

Figure 8.2 Ideal phase voltage waveform at base speed (shown here with no phase advance for direct comparison with Figure 8.1.

Figure 8.2 and 8.3 show that during high speed operation voltage only has to be applied to the phase turning on and the phase turning off. No voltage need be applied to the phase that remains conducting. In other words, out of the two phases that need to be connected in series during each 120 degree period, one needs the full DC link voltage applying to it, while the other requires nothing. The conclusion therefore is that an inverter is needed that can effectively connect the two conducting phases together in series and selectively apply the full DC link voltage to one of those phases. If this is achieved then high speed machine performance will not be affected and inverter loss should be reduced, as only two devices are needed to drive the two windings.

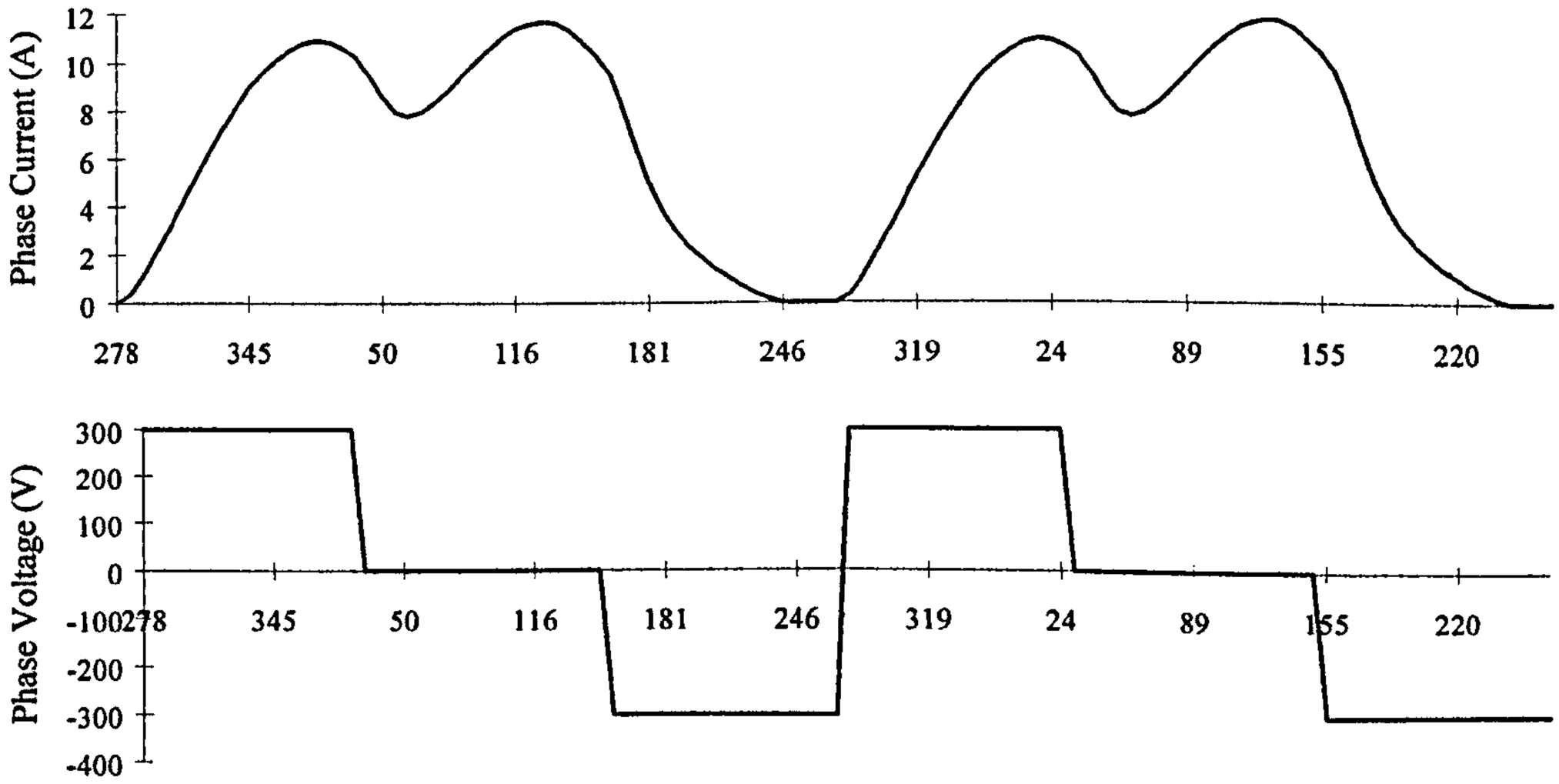

Figure 8.3 Measured phase current shown with the idealised voltage waveform.

8.3 Delta Connection with Interphase Diodes (DID)

8.3.1 Inverter Description

The arrangement for this inverter is shown in Figure 8.4. Visually there are two differences between this inverter and the asymmetric half bridge. Firstly, the diodes D1-D6 are now connected only across their associated switches T1-T6. This is advantageous as switches are commonly available complete with an associated diode, keeping connections and component count to a minimum. Secondly, three extra diodes are connected between phases. This gives the inverter its ability to control two phases at once, while keeping the current unidirectional.

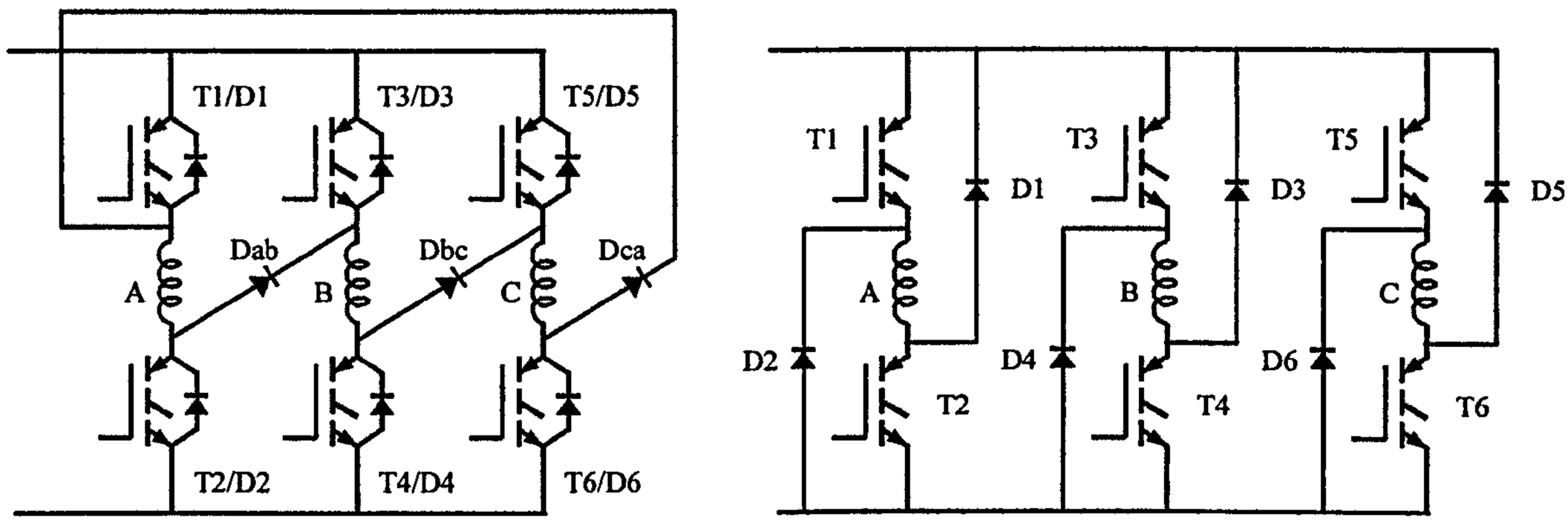

(a) (b)

Figure 8.4 (a) Delta Connection with Interphase Diodes Inverter, (b) Asymmetric Half Bridge.

Operation is described with the example of phases A and B being desired 'on', and phase C desired 'off' (see Figure 8.1 for desired current waveforms). Switches T1 and T4 are used to apply volts to the conducting phases. With both these switches on (and all the others off) phases A and B are essentially connected in series across the DC link through diode D_{AB}. In this situation it might be expected that the DC link voltage would be shared in some way across each winding. In fact, the way it is shared depends entirely on the difference in currents flowing in each of the windings. If I_A is less than I_B, then the difference between I_A and I_B must flow up through diode D2. The effect is to connect phase A across the DC link and freewheel phase B. If I_B is less than I_A, then the difference (I_A - I_B) flows up through D3, applying full DC link voltage across phase B and freewheeling phase A. There is, therefore, a large tendency for the currents in the

two phases to equalise naturally under these conditions, without any control effort being required.

Phase C, the 'off' phase, also needs consideration. If any current flows in this phase then, with T5 and T6 both off, full negative DC link voltage will be applied bringing the current down as rapidly as possible. When the current reaches zero, diode D_{BC} stops the current from going negative, therefore maintaining the unidirectional nature of the currents.

It can now be seen that the basic requirements of the inverter, as described in section 8.2, are satisfied. At the commutation point the appropriate two switches are turned on across the two phases that are desired to conduct. One of those phases will have zero current, while the other has already been conducting with some value of positive current. The phase with zero current will then receive the full DC link voltage until such time as the two currents are equal, at which point the DC link voltage will be shared between the two. The third phase, that is desired off, receives the full negative DC link voltage until its current reaches zero.

Another way of viewing this inverter is that the phases are connected in a configuration similar to a delta connection with diodes in series with each of the phases.

The fundamental operation of this new inverter has now been explained and it has been demonstrated that high speed performance should be unaffected as the correct voltages can be applied to the windings at the right time. Control is achieved with only two switches, instead of the four required with asymmetric half bridges, which should substantially reduce device losses. The following sections will now describe the inverter in more detail, in particular -

- Switching states and a current control method for low speed operation.
- Voltage control with high speed operation.
- Drive performance - inverter losses, torque-speed characteristics etc.

8.3.2 Switching States and Current Control

Operation of a SR motor with the asymmetric half bridges is straightforward in that each phase has its own inverter. This means that the switch state of each is purely dependant on the current in its own phase. The "Delta with Inter-phase Diodes" (DID) inverter, on the other hand, is more complex to analyse because the phases are connected together in the same inverter. The voltage across a particular winding is now a function of the three phase currents, as well as the inverter switch state. It becomes apparent that certain combinations of phase voltages cannot be applied with this inverter and this can be summarised by the following equation:

$$V_A + V_B + V_C \geq 0 \tag{8.1}$$

One of the main repercussions of this is that it is not possible to apply negative DC link volts to more than one phase at a time. This can be demonstrated by way of the following example. Suppose phase C is conducting and negative volts are required to be applied to it. This requires that devices T4/D4 conduct, connecting the anode of D_{BC} to the negative of the DC link. Correspondingly, devices T1/D1 need to conduct to connect the cathode of D_{CA} to the positive of the DC link. It therefore follows that the "top" side of phase A is also connected to the positive of the DC link, and the "bottom" end of phase B is connected to the negative of the DC link. In this situation, positive volts will be applied to either phase A or phase B depending which one has the least current. In other words, it is impossible to apply negative volts to a phase without applying positive volts to at least one of the other phases. This means that negative volts cannot be applied to more than one phase at a time.

It is, however, possible to apply positive volts to more than one phase at a time. For example if all six transistors were switched on positive volts would be applied to all the phases at once. An important conclusion from Equation 8.1 is that, even with these restrictions in voltage states, it is still possible to achieve the ideal phase voltage waveforms that were shown in Figure 8.2. An inspection of these waveforms shows that at any one time the phase voltages actually sum to zero i.e.

$$V_A + V_B + V_C = 0 \tag{8.2}$$

Current control strategy

Table 8.1 summarises the inverter switch states that were found to be useful for current control purposes. Notice that with some switch states the voltage applied is also dependant on the phase currents flowing, while with others it is independent of current e.g. if either all three top devices or all three bottom devices are switched on, this guarantees freewheeling of all three phases regardless of current.

Phases desired on	Switches On	Condition	Phase A Voltage	Phase B Voltage	Phase C Voltage
A & B	T1, T4	$I_A > I_B$	0	$+V_{dc}$	$-V_{dc}$
	T1, T4	$I_A < I_B$	$+V_{dc}$	0	$-V_{dc}$
	T1, T3, T5	-	0	0	0
	T2, T4, T6	-	0	0	0
B & C	T3, T6	$I_B > I_C$	$-V_{dc}$	0	$+V_{dc}$
	T3, T6	$I_B < I_C$	$-V_{dc}$	$+V_{dc}$	0
	T1, T3, T5	-	0	0	0
	T2, T4, T6	-	0	0	0
C & A	T5, T2	$I_C > I_A$	$+V_{dc}$	$-V_{dc}$	0
	T5, T2	$I_C < I_A$	0	$-V_{dc}$	$+V_{dc}$
	T1, T3, T5	-	0	0	0
	T2, T4, T6	-	0	0	0

Table 8.1 Summary of the switching states used for current control and the resulting winding voltages.

A current controller ideally needs three states – one state to apply positive DC link volts, one to supply negative DC volts and a third to apply zero volts (freewheel). It can be seen from Table 8.1 that these three states can be applied to each of the phases, but with the restriction defined in Equation 8.1.The current controller developed using these switch states is explained with the following example:

Phases A and B are desired on and phase C is desired off. This corresponds to the period between point 1 and point 4 in Figure 8.5 which shows measured current waveforms

with this method of control. Phase B is in the first half of its conduction period and phase A is in its second half. The current that is in the first half of its conduction period, in this case phase B, is sampled and the result of this sample is used to determine the switch state of the whole bridge. There are three possible switch states to choose from, as detailed in Table 8.1, and they are determined as follows:

- If the current is below its current demand, T1 and T4 are turned on. One of two consequences will then follow. If $I_A > I_B$ then phase B will receive positive volts and phase A will receive zero volts. If $I_A < I_B$ then phase A will receive positive volts and phase B will receive zero. Thus the currents in the two conducting phases will tend to equalise, even though only one of them is being 'controlled'. In either case, with T1 and T4 switched on, negative DC link volts will be applied to phase C.
- If the current is above its current demand then either turn T2, T4, and T6 on, or T1, T3, T5. This will apply zero volts to all three phases.

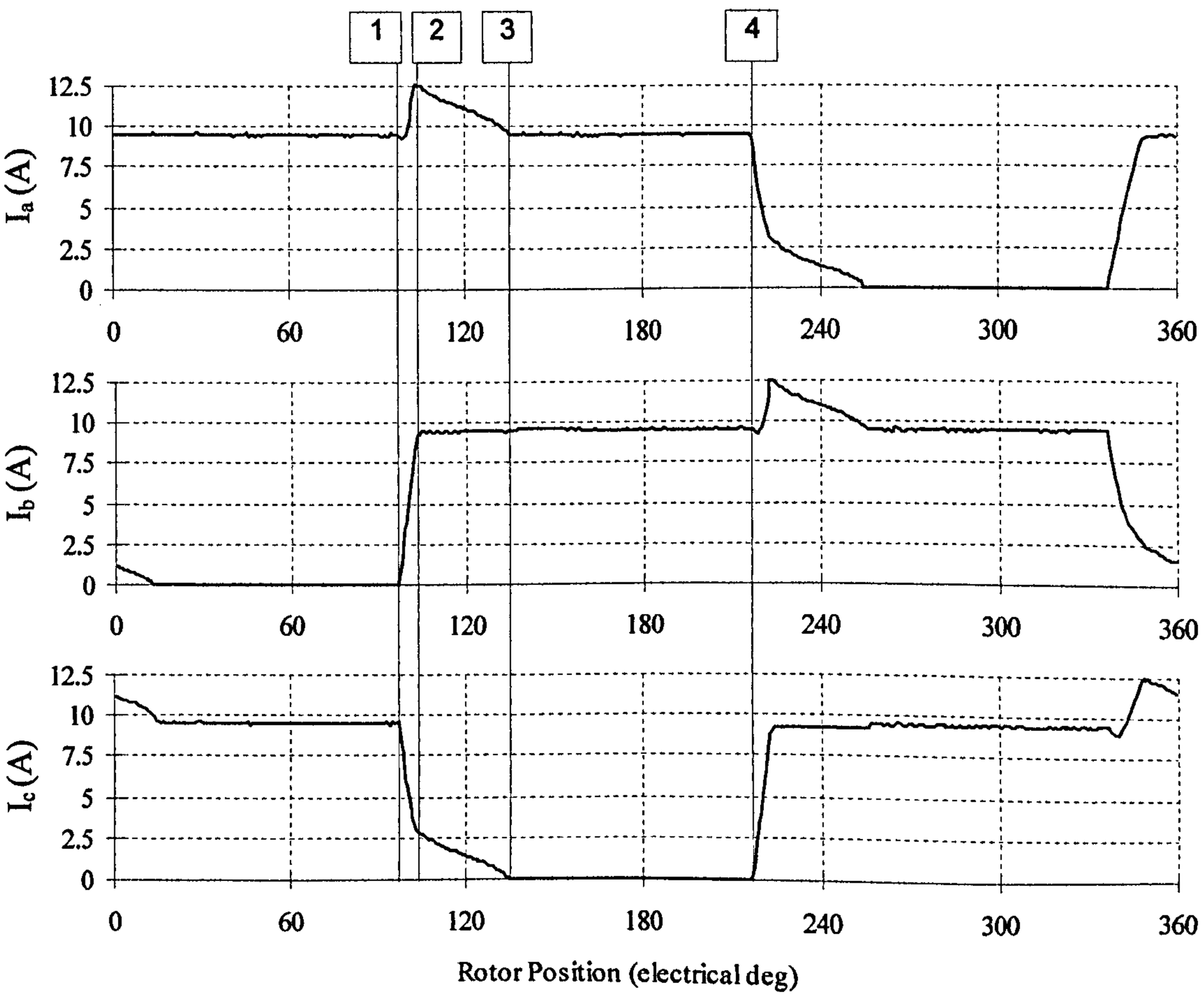

Figure 8.5 Measured low speed current waveforms with DID inverter.

In effect this forms the basis for a hysteresis current controller. The same switching strategy can be implemented in PWM and this is detailed in Appendix D. The appendix explains a slightly more sophisticated method of PWM control that produces a voltage output from the inverter with twice the frequency that the transistors are switching at. The waveforms shown in Figure 8.5 are achieved using this PWM control. It can be seen that the desired ideal current waveforms of Figure 8.1 are not quite achieved with this current control strategy and the reasons for this are explained as follows:

At point 1 the current in phase B is sampled. It is below its current demand and therefore T1 and T4 are turned on. As $I_B < I_A$ at this point, phase B receives positive volts, phase A receives zero volts, and phase C receives negative volts. The effect, that is not immediately obvious, is that the current in phase A rises rapidly, even though no volts are being applied to it by the inverter. This is due to the mutual coupling between phases and the large di/dt that are occurring in the other two phases at this time. If reference is made to the idealised variation of mutual inductance with position shown in Figure 2.4 (Chapter 2), this effect can be predicted. This effect is not nearly so prominent with the AHB inverter as at this point it is able to apply a larger amount of negative voltage to phase A to keep the current nearly constant (see Figure 5.1 and 5.2 in Chapter 5). Unfortunately with this inverter nothing can be done about it - as Equation 8.1 shows the voltages that are applied to the windings must sum to zero or be greater than zero. The full negative DC link voltage cannot be applied to more than one phase, and in this case priority must be given to the phase turning off (phase C in this example). Therefore, with zero volts across phase A, the flux linkage only gradually reduces due to the resistance of the phase and the voltage drop in the power electronics. Eventually the current reduces to the same value as phase B (point 3 in Figure 8.5), and from this point on, the positive voltage applied to the machine is shared between these two phases, and they are both controlled to the desired values as if they were one.

A further effect occurs due to the limitation of the voltages that can be applied to the windings at any one time. The current in phase B reaches its current demand at point 2 in Figure 8.5. However, the current in phase C has not reached zero and, as Equation 8.1 indicates, negative volts cannot be applied to a winding without positive volts being applied to one of the other phases. Therefore from this point on negative volts can only

be applied to phase C at the same (reduced) rate that positive volts are applied to phase B. A tail in the current of the phase turning off inevitably occurs.

In summary then two deviations from the desired current waveforms occur directly as a result of the limitations of the voltages that can be applied by this inverter. The following sections will now examine overall drive performance in terms of torque per unit copper loss, torque-speed envelope (performance under voltage control) and inverter rating (device losses, peak current and volts).

8.3.3 Drive Performance

8.3.3.1 Measurement Techniques

Comparisons between the drives in terms of inverter losses and machine performance are made on the basis of real time measurements and calculations made by the DSP. Details of the arrangement are described in Appendix C. Currents and position are sampled every PWM period (i.e. every 100μs) and this is used with a lookup table to estimate the instantaneous torque produced. Calculations such as average torque, copper loss, torque ripple and device losses are displayed directly on the PC via a serial link and are averaged over several electrical cycles. Waveforms are also captured and downloaded to the PC. All waveforms shown are therefore subject to 100μs sampling.

8.3.3.2 Low Speed Operation

Figure 8.6 details the differences between the two inverters in terms of current, flux linkage, equivalent single tooth current, equivalent single tooth flux linkage and torque at low speed. Both have the same current demand of 9.1A at the same speed of 100rpm, although slightly different values are actually achieved due to differences in the current controller gains achievable. The flux linkage waveforms show clearly the differences in voltages that can be applied to the windings. The shape of the equivalent single tooth current is of interest as this is used to calculate the torque produced by each stator pole and hence total machine torque. This shows that a small tail in the current at turn off now occurs with the DID inverter. The effect on *machine* performance therefore is not significant as the tail actually produces a net positive torque, and the additional copper

losses are small. Table 8.2 shows a comparison of torque and copper losses for the two drives at low speed.

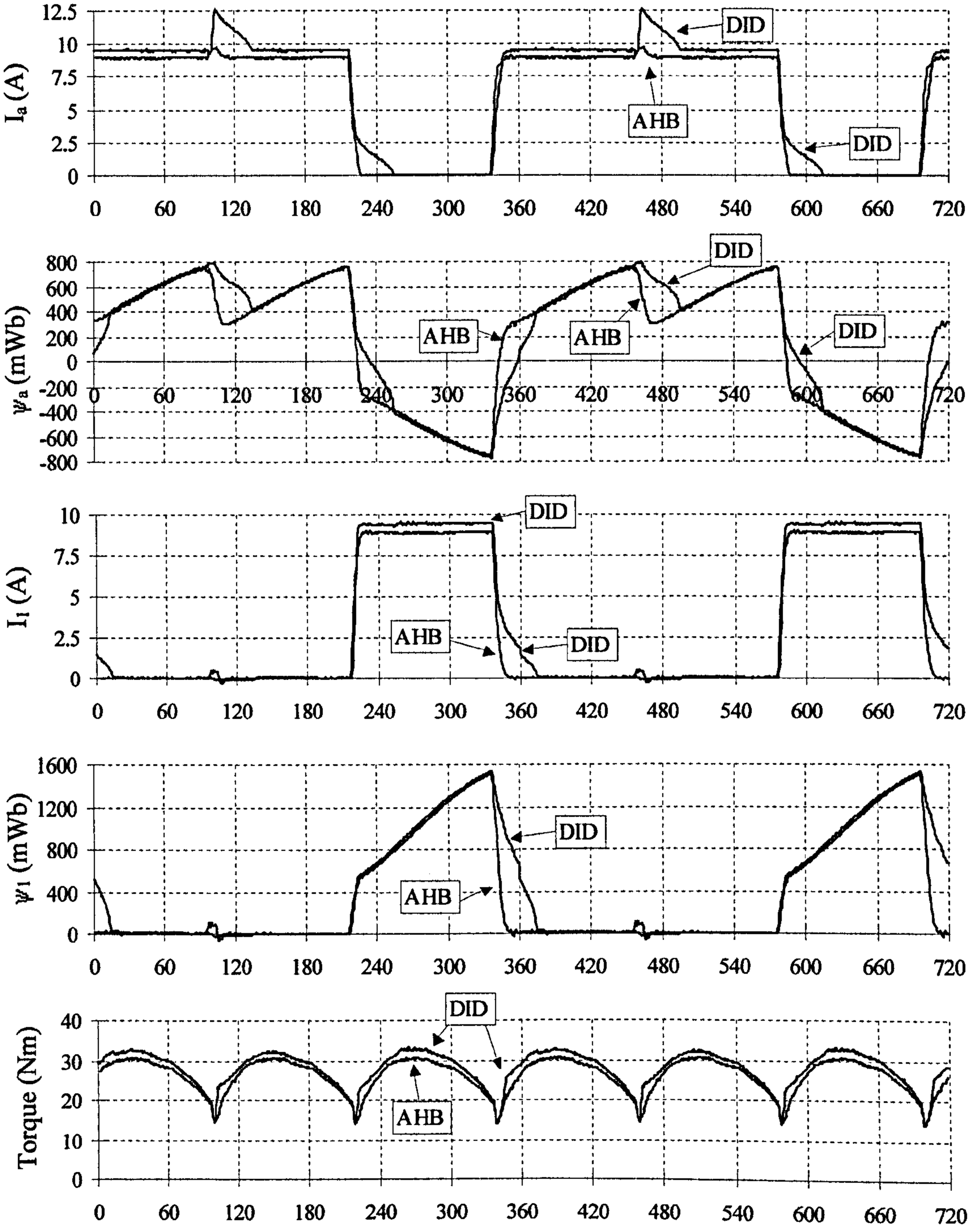

Figure 8.6 A comparison of phase current, flux linkage, equivalent single tooth current, equivalent single tooth flux linkage and torque between the AHB and DID inverters at 100rpm with V_{dc}=290V. Phase currents are measured, and all other waveforms are calculated (equivalent single tooth current and flux linkage shown inverted for clarity).

Inverter Type	Torque (Nm)	Copper Loss (W)	Torque per Unit Copper Loss (mNm/W)
AHB	26.3	296	88.9
DID	27.8	319	87.25

Table 8.2 Comparison of torque and loss with the AHB and DID inverters. Prototype machine (D100 frame), 100rpm, V_{dc}=290V, I_{dem}=9.1A.

8.3.3.3 High Speed Operation

Figure 8.7 shows a comparison between the AHB and DID inverters at 675rpm with a DC link voltage of 290V and a current demand of 9.1A. This is the equivalent of 1350rpm with 580V and therefore corresponds to the base speed of the machine (the DC link voltage was halved so that performance at twice base speed could be measured without over-speeding the DC load machine). Figure 8.8 shows the corresponding waveforms at twice base speed. In all cases advance angle is optimised for maximum torque production and in the case of the AHB inverter conduction angle is also optimised.

These results show that the waveforms produced are broadly similar and therefore the torque-speed curve can be expected to be very similar. It can, however, be seen that the AHB drive is able to make the phases conduct for slightly longer, almost going in to continuous conduction at twice base speed. This is especially apparent in the equivalent single tooth currents, and therefore explains the torque-speed curve shown in Figure 8.9.

Machine copper loss versus speed is shown in Figure 8.10, and torque per unit copper loss versus speed is shown in Figure 8.11. Both of these curves are for the torque-speed curve of Figure 8.9. It can be seen that torque per unit copper loss is basically the same at low speed. At high speed torque per unit copper loss is slightly lower with the AHB inverter. This is because this drive is achieving the extra torque by going almost into continuous conduction and this results in a significant rise in copper loss for the extra torque achieved.

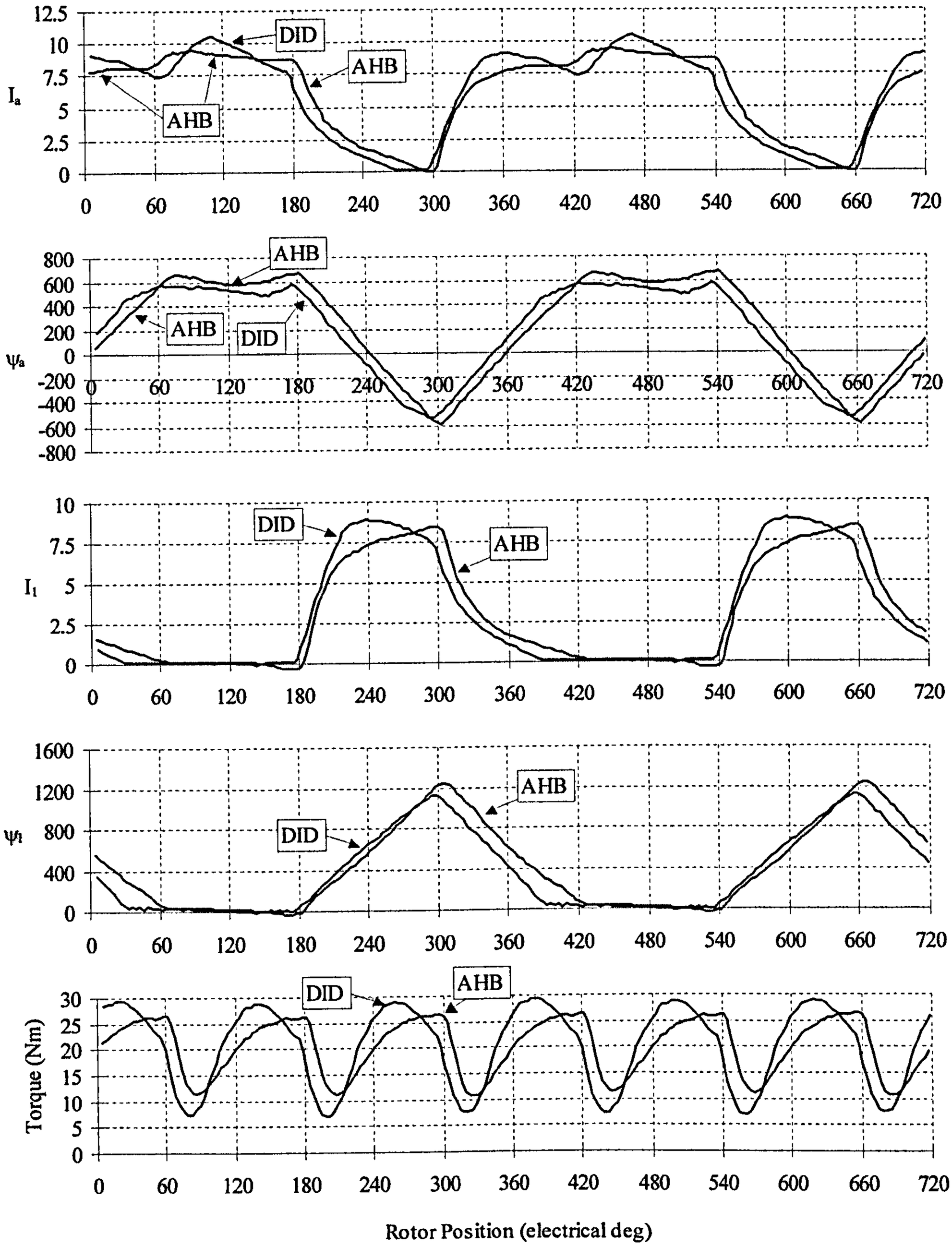

Figure 8.7 A comparison of phase current, flux linkage, equivalent single tooth current, equivalent single tooth flux linkage and torque between the AHB and DID inverters at 675rpm with V_{dc}=290V. The phase currents are measured and all other waveforms are calculated from them (equivalent single tooth current and flux linkage shown inverted for clarity).

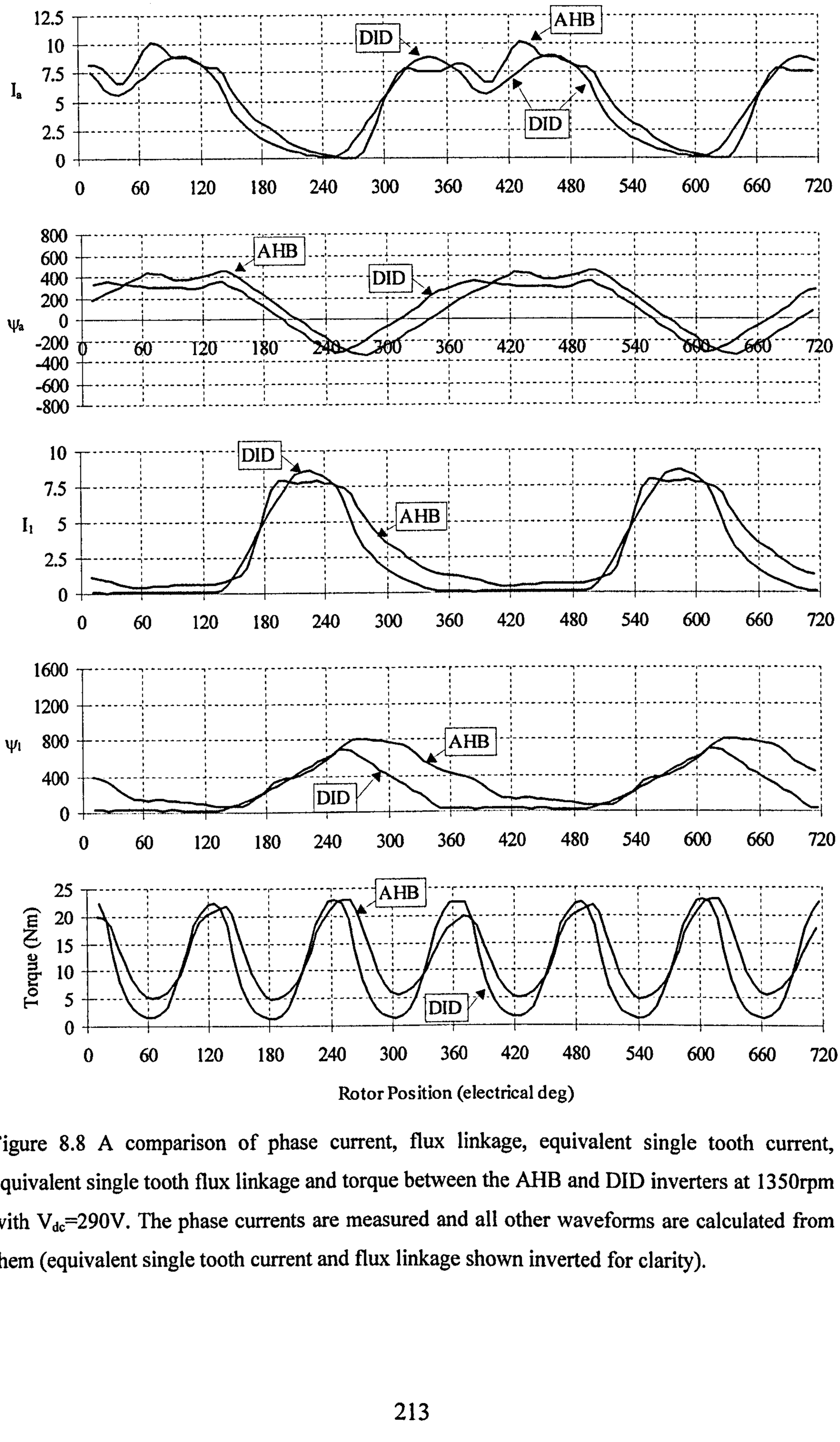

Figure 8.8 A comparison of phase current, flux linkage, equivalent single tooth current, equivalent single tooth flux linkage and torque between the AHB and DID inverters at 1350rpm with V_{dc}=290V. The phase currents are measured and all other waveforms are calculated from them (equivalent single tooth current and flux linkage shown inverted for clarity).

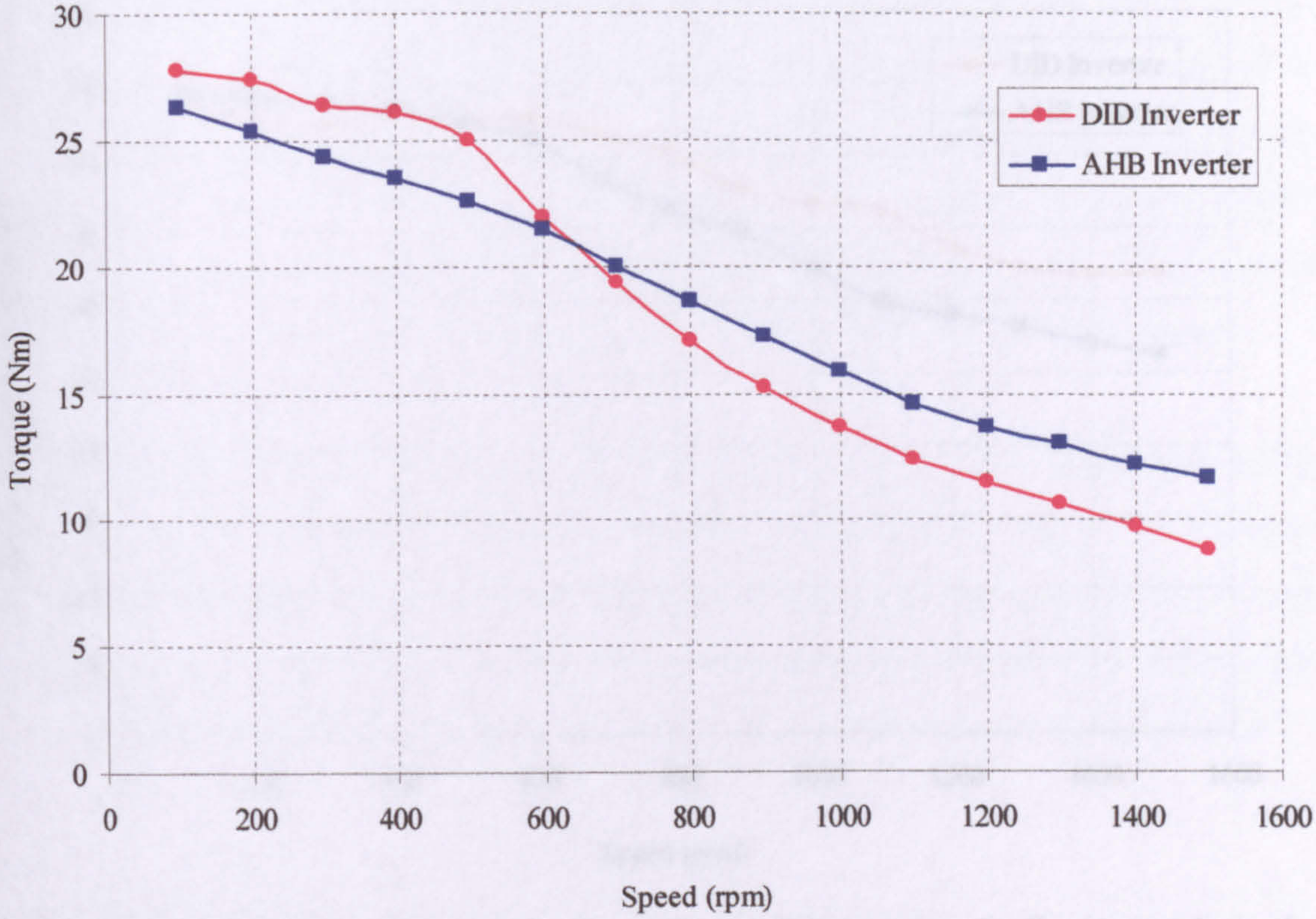

Figure 8.9 Torque-speed characteristics with I_{dem} =9.1A, V_{dc}=290V.

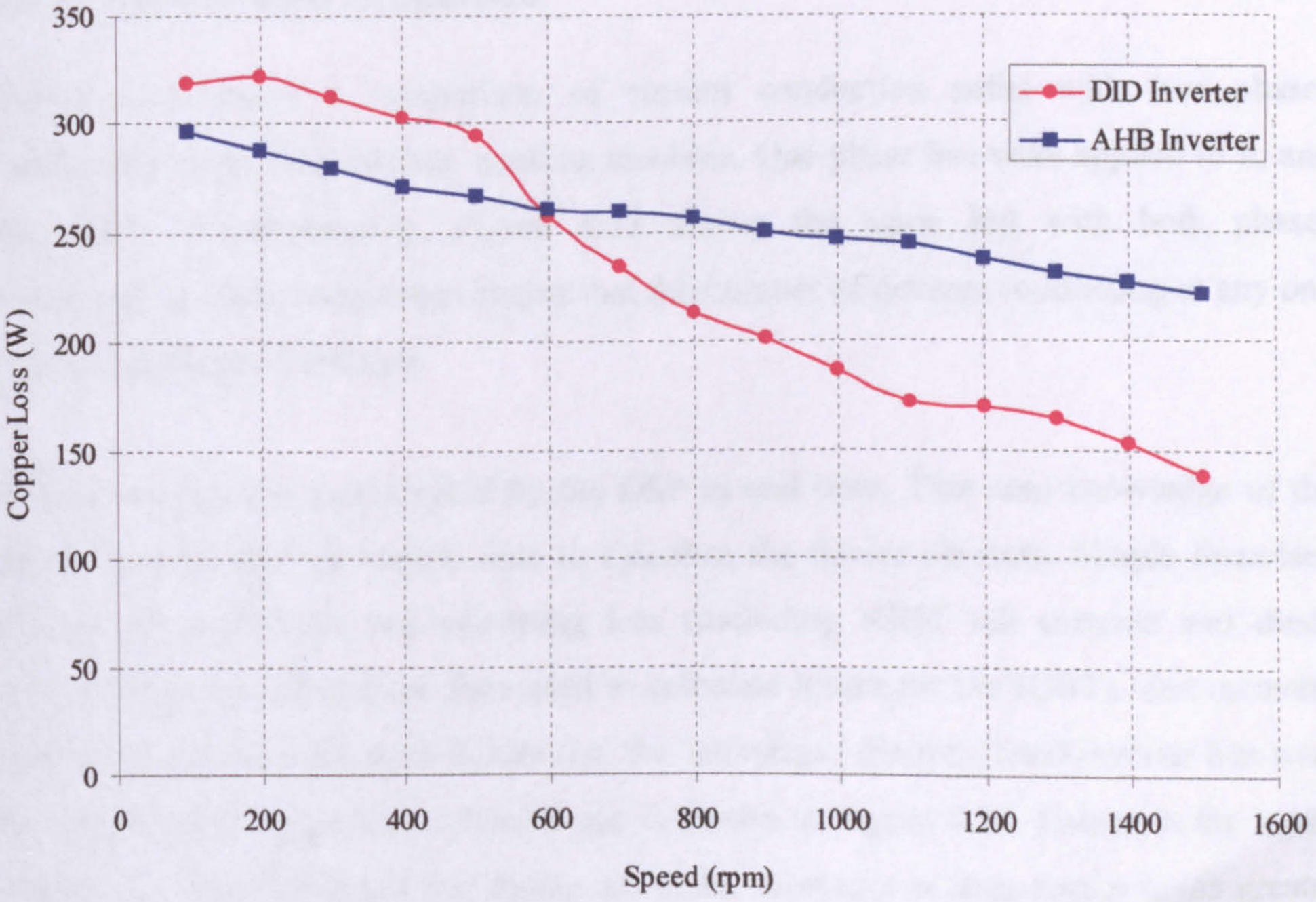

Figure 8.10 Copper loss with the AHB and DID inverters for the torques shown in Figure 8.9.

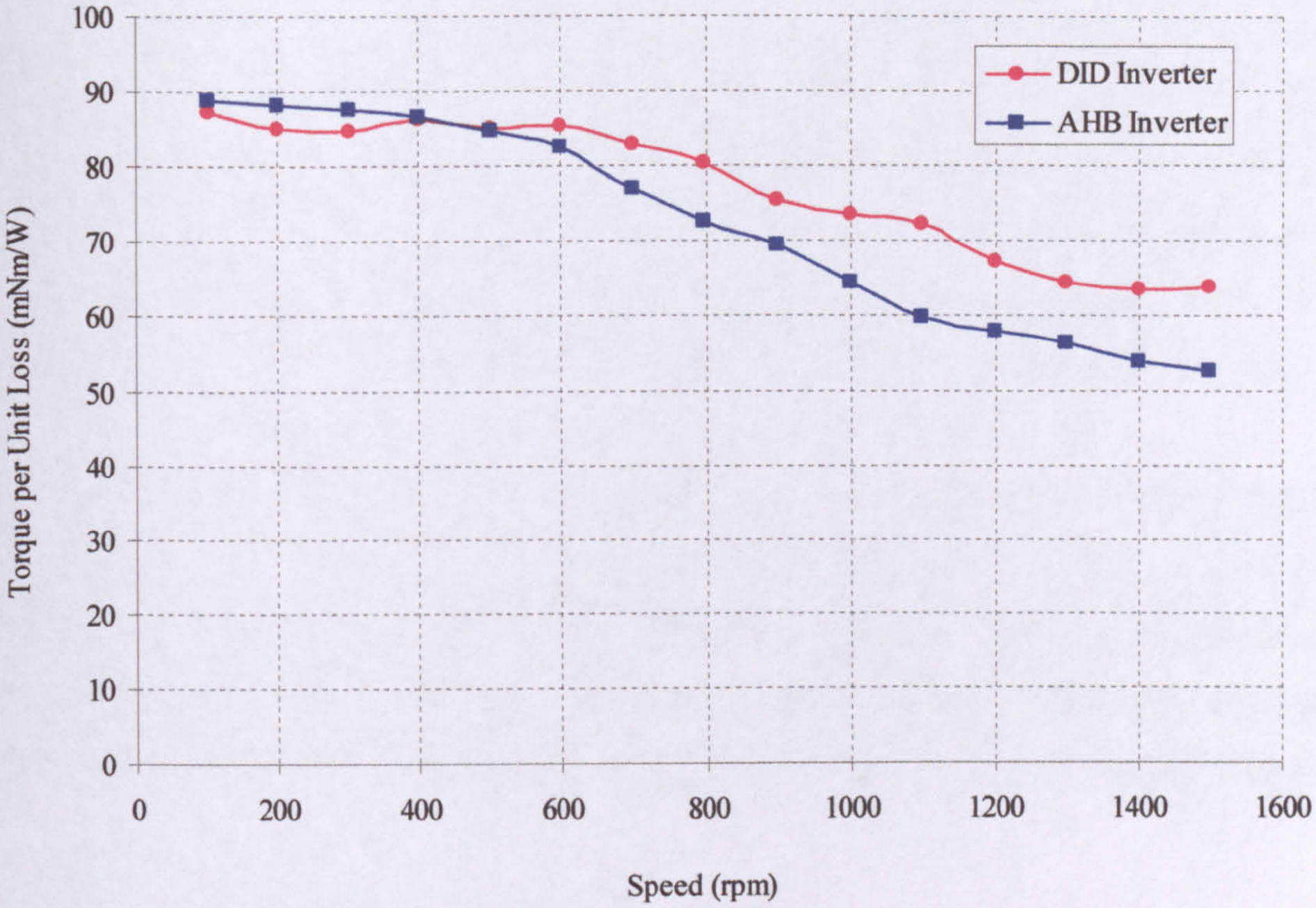

Fig. 8.11 Torque per unit copper loss for the AHB and DID inverters for the torque shown in Fig. 8.9.

8.3.3.4 Inverter Loss Comparison

Figure 8.12 shows a comparison of current conduction paths with two phases conducting in the fully pitched winding machine. One phase has volts applied to it, and the other is freewheeling. Figure 8.13 shows the same but with both phases freewheeling. This comparison shows that the number of devices conducting at any one time is significantly reduced.

Actual inverter loss is estimated by the DSP in real time. This uses knowledge of the phase currents and the switch state to calculate the device currents. Simple linearised models of conduction and switching loss (including IGBT tail currents and diode reverse recovery effects) are then used to calculate losses for the IGBTs, fast recovery diodes and standard recovery diodes (i.e. the 'interphase' diodes). Total inverter loss over the whole speed range was collected and is shown in Figure 8.14. Losses in the 'main' inverter i.e. the IGBTs and fast diodes are more important as their cost is much greater than the interphase diodes. Therefore two curves are shown with and without the interphase diode loss.

As predicted by the analysis of conduction paths, inverter loss is halved at low speed in the main part of the inverter due to the fact that only half the number of switches need to conduct (at low speed by far the largest majority of time is spent in the freewheeling state shown in Figure 8.13). Device duty cycle and therefore device losses are now approximately the same as in a short pitched winding machine being driven by an AHB inverter. This is achieved while having no adverse effect on machine performance.

At high speed there is an even larger beneficial effect. Inverter losses in the main bridge are reduced to approximately one quarter that of the AHB inverter. This is explained by Figure 8.15, which compares transistor currents with phase currents at twice base speed i.e. under full voltage control. Consider the period between 0° and 120°. During this period with an AHB inverter the transistor current would be equal to the phase current.

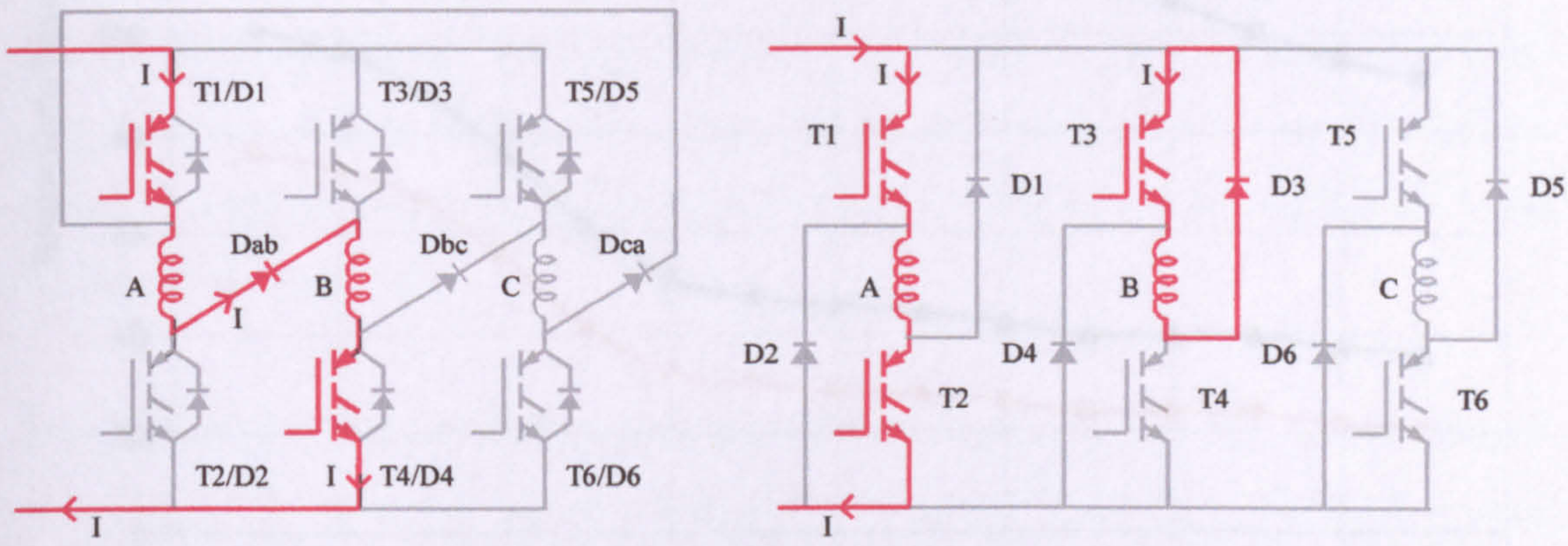

Figure 8.12 A comparison of conduction paths in the two inverters with voltage applied to the phases, assuming $I=I_A=I_B$. Conduction path shown in red, non conducting shown grey.

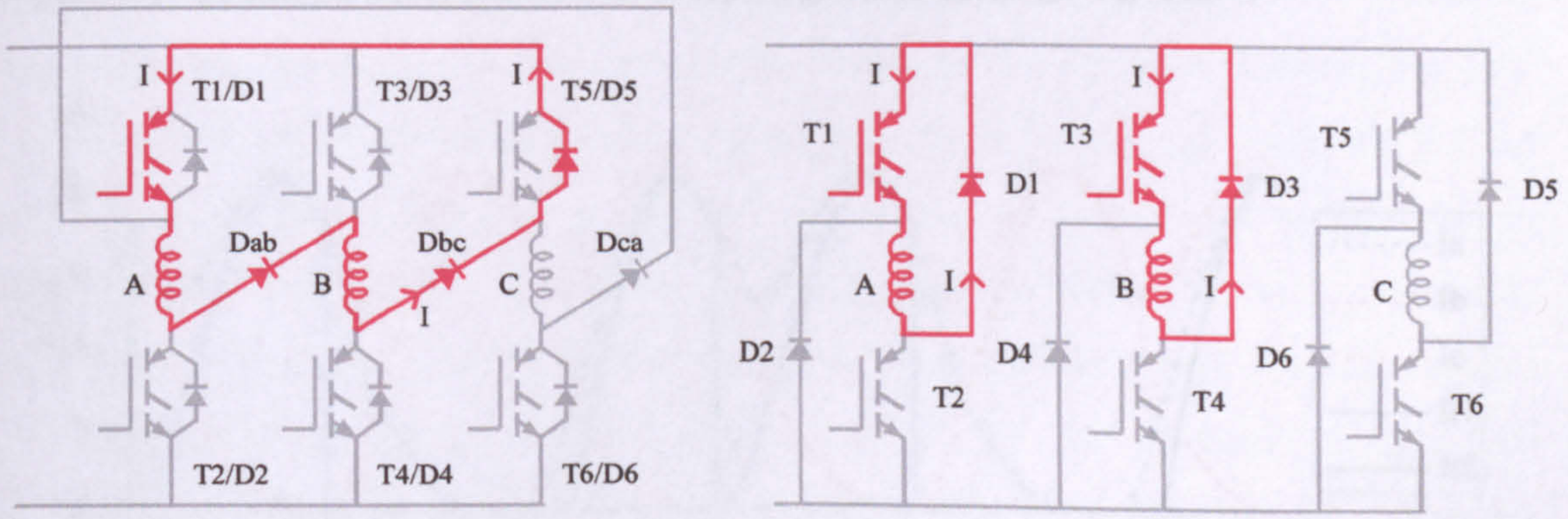

Figure 8.13 A comparison of conduction paths in the two inverters during one of the freewheeling states, assuming $I=I_A=I_B$. Conduction path shown in red, non conducting shown grey.

With the DID inverter, however, the transistor current is the difference between two phase currents. So during this period the current in transistor 1 (It1) is equal to the difference between I_A and I_C, which results in the current being substantially less than the phase current. In other words, when a phase turns off it is able to feed directly into the next phase via the interphase diodes. This substantially reduces the amount of energy that has to be extracted from a phase at turn off via the fast recovery diodes, and then conducted back into the next phase turning on via the transistors.

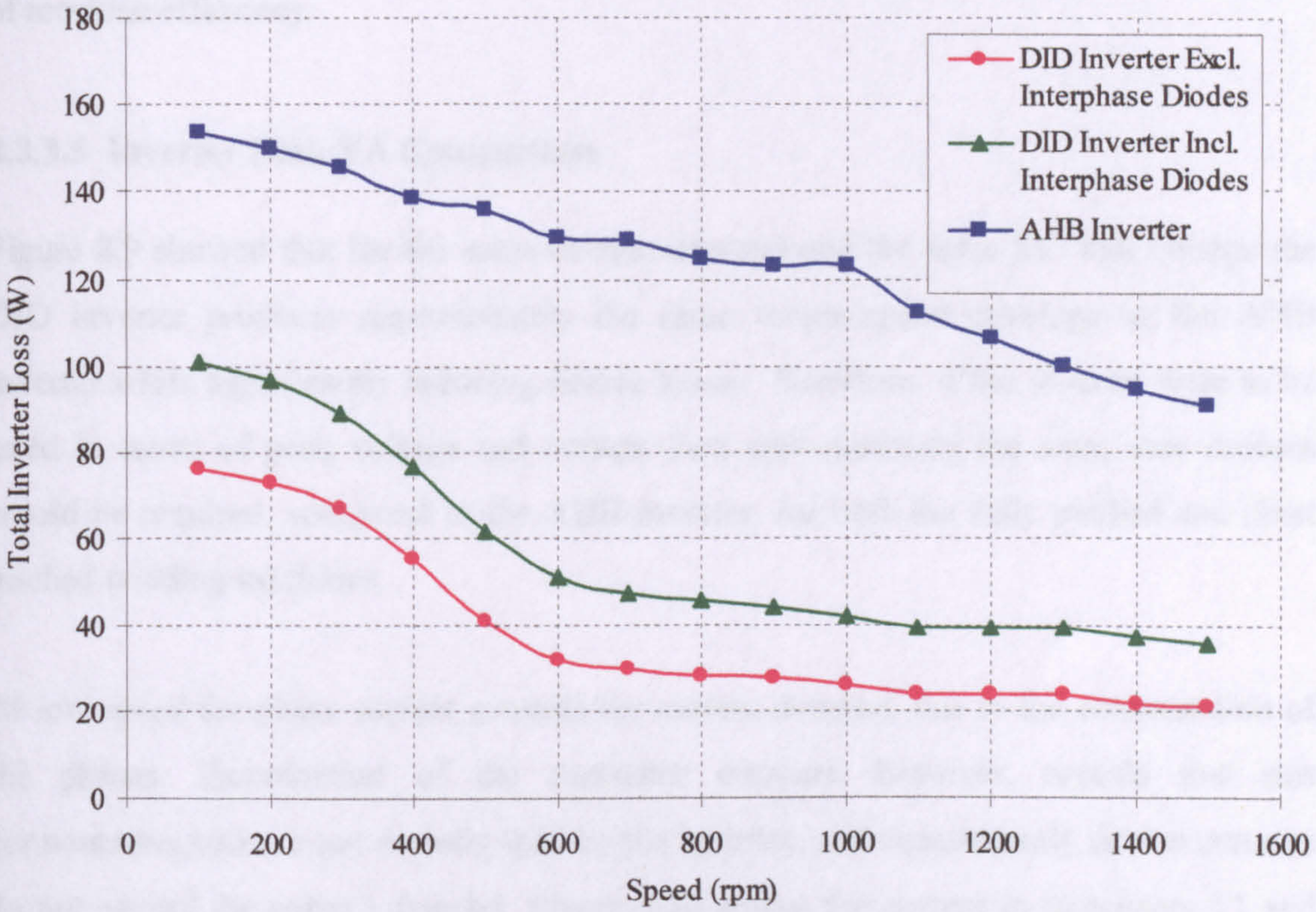

Figure 8.14 Estimated total inverter loss. Switching losses based on V_{dc}=600V.

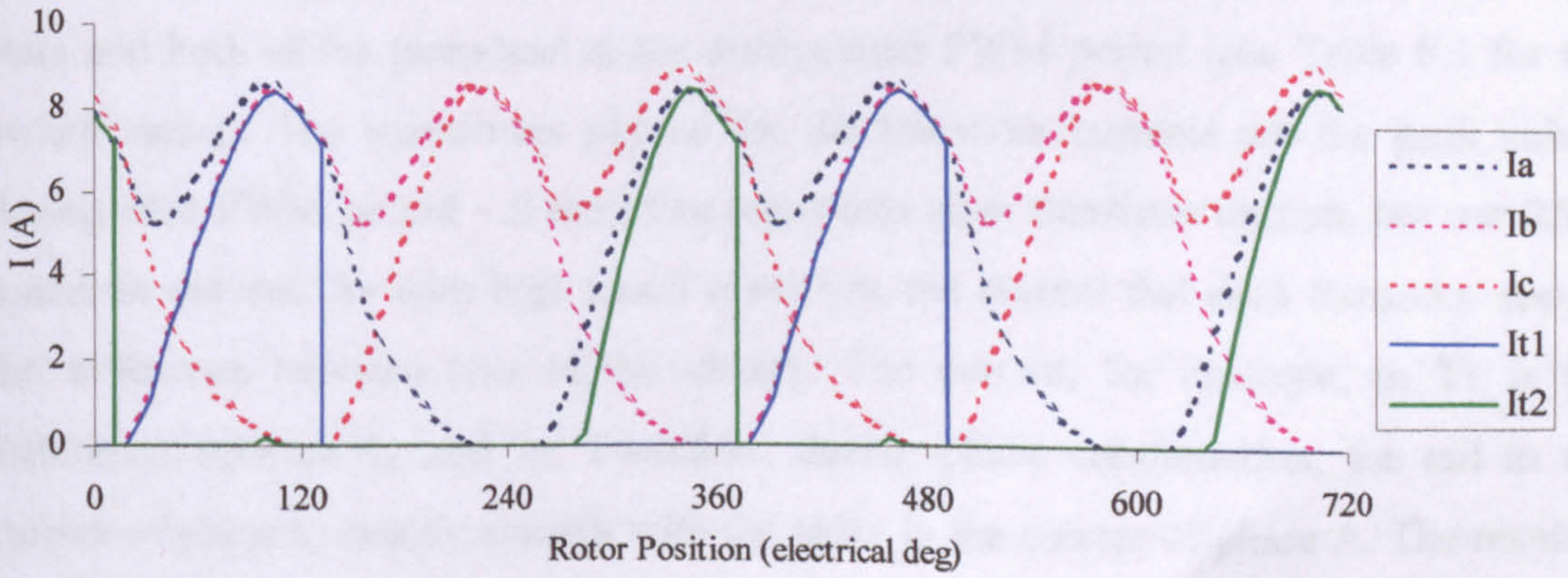

Figure 8.15 Transistors currents at twice base speed for the DID inverter.

A comparison can now be made with the short pitched winding machine, driven by the AHB inverter. Figure 6.9 in Chapter 6 showed that, for the same torque-speed curve, inverter loss with unipolar operation of the *fully pitched winding machine* driven by an AHB inverter was approximately double over the whole speed range. It can now be seen, therefore, that a fully pitched winding machine with the DID inverter has approximately the same inverter losses at low speed as the short pitched winding machine, and at high speed the losses are approximately one half. This is achieved at the same time as maintaining the advantage the fully pitched winding machine has in terms of machine efficiency.

8.3.3.5 Inverter Peak VA Comparison

Figure 8.9 showed that for the same current demand and the same DC link voltage the DID inverter produces approximately the same torque-speed envelope as the AHB inverter while significantly reducing device losses. Therefore, if the inverter were to be rated in terms of peak voltage and current then approximately the same size devices would be required, compared to the AHB inverter, for both the fully pitched and short pitched winding machines.

At low speed the phase current exceeds the current demand, due to the commutation of the phases. Examination of the transistor currents, however, reveals that this commutation spike is not actually seen by the inverter, and consequently device currents do not exceed the current demand. Figure 8.16 shows the current in transistors T1 and T2 compared to the phase currents at low speed. Note that the machine is in current control at this speed, and so the switch state of the inverter changes between the "on" state and both of the freewheel states during each PWM period (see Table 8.1 for the switch states). The waveforms plotted for the transistor currents are the peak values during each PWM period – it therefore represents peak transistor current, but not RMS transistor current. As with high speed operation, the current that each transistor sees is the difference between two of the phases. The current, for example, in T1 is the difference between I_A and I_C. Therefore, during phase commutation, the tail in the current of phase C exactly cancels with the spike in the current of phase A. The result is that the transistors do not see a current in excess of the demanded current.

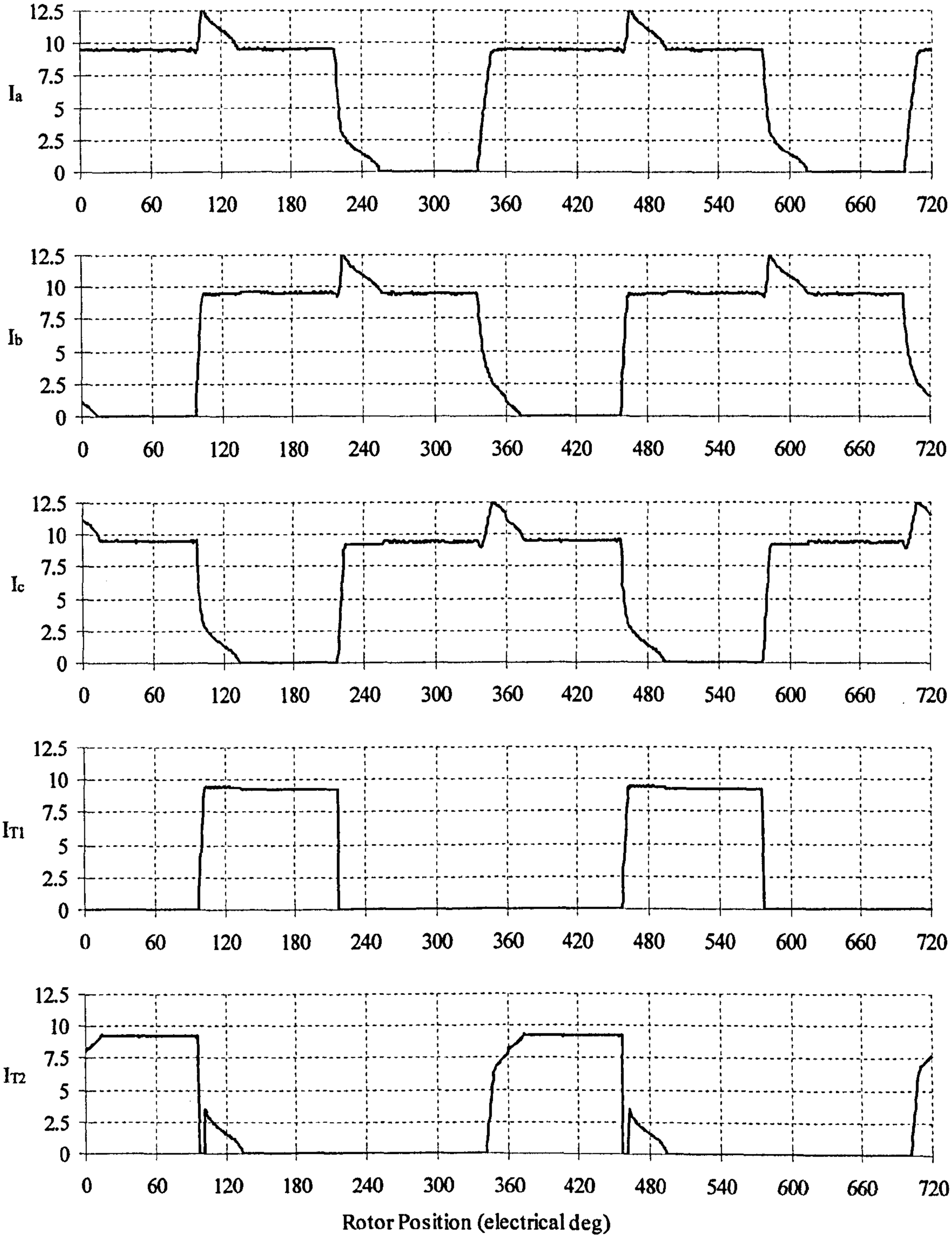

Figure 8.16 Phase currents and transistors currents at low speed for the DID inverter. Transistor currents are shown are the peak current during a PWM period.

8.4 Delta Connection with Phase Diodes (DPD)

8.4.1 Inverter Description

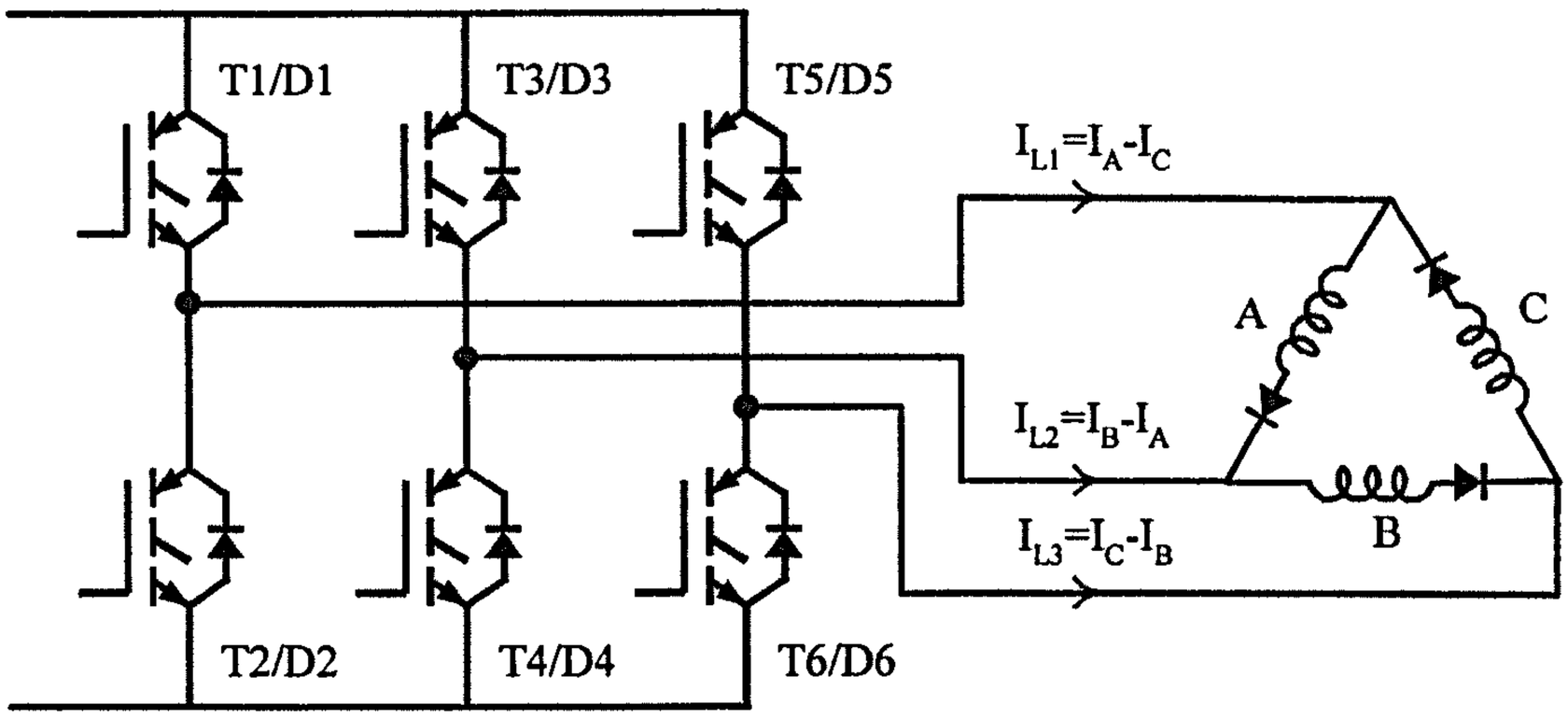

Figure 8.17 Delta connection with phase diodes.

This is a conventional three phase bridge in a delta connection, with the addition of a diode in series with each phase. The function of the diodes is to ensure only unidirectional phase currents flow; without them an AC phase current would be inevitable because the phase voltages must sum to zero in a delta circuit. If this circuit is rearranged, as shown in Figure 8.18, it reveals itself to be very similar to the DID inverter. The only difference is the position of the extra three diodes. Initially unknown to this research, this topology seems to have also been developed independently by two other separate sets of researchers for the short pitched winding SR motor: Davis via a patent application in 1995 [8.6], and researchers in the USA, who disseminated the same converter circuit in a Small Machines Manufacturers Association (SMMA) seminar in 1995[1].

The advantage of this circuit is that it can run from a completely standard three phase bridge. This allows the use of standard motor drive power electronic modules that commonly contain the complete three phase bridge, rectifier, brake circuit, current and temperature sensors. If the phase diodes are placed in the terminal box of the motor then only three wires are needed between the inverter and the motor rather than six - this can

[1] Private communication from Mr. DF Warne. This work is not in the public domain, so its extent is unknown.

be an important consideration in some applications where the motor can be tens of metres away from the inverter. This does assume that current control can be achieved with sensors placed at the inverter end, otherwise the object would be defeated. Current sensing methods to achieve this will be discussed later in the chapter.

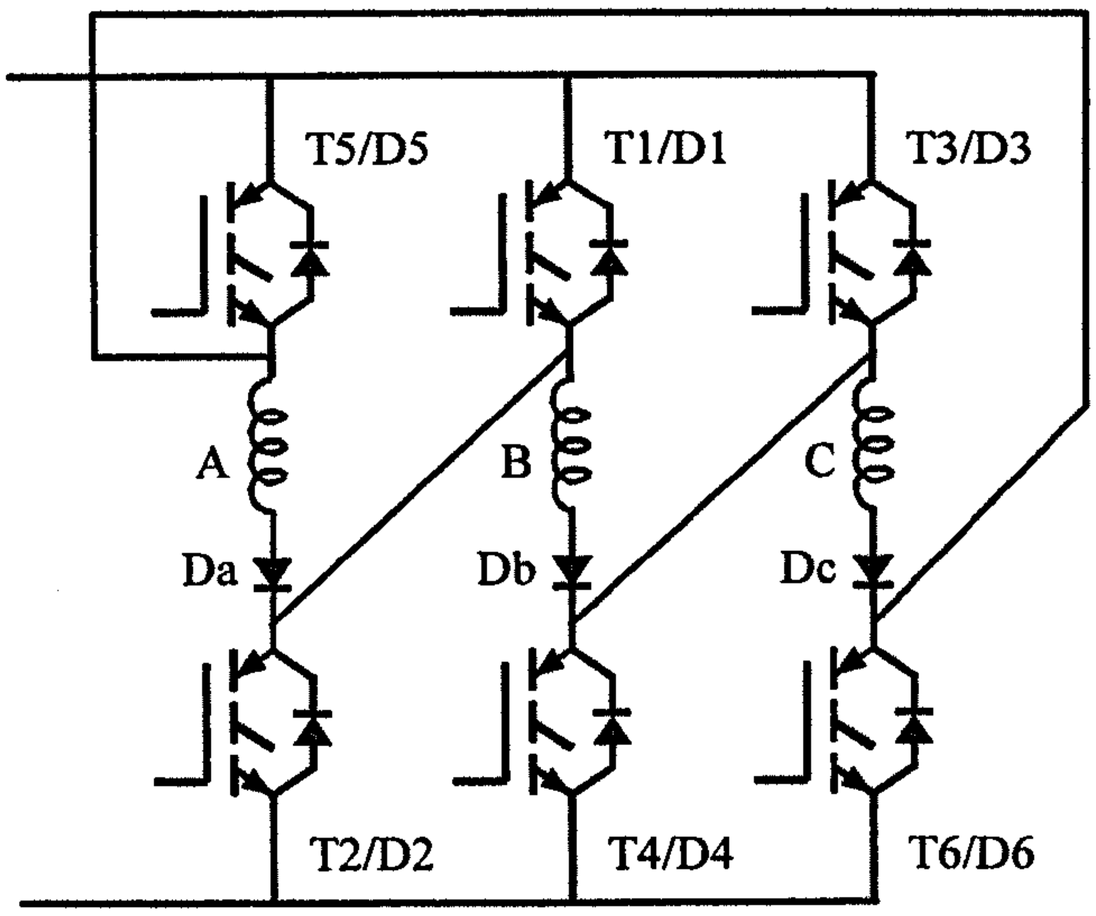

Figure 8.18. The delta (DPD) inverter redrawn for comparison to Figure 8.17.

Another consideration is that dead time control is needed to prevent shoot through. This is, however, a common requirement in inverters and is relatively simple to implement without additional cost. It does not affect the choice of short circuit rated or non short circuit rated silicon. Short circuit rated devices' primary function is to protect the silicon in the event of a motor winding failure or earth fault and allows time for the control circuit to detect this situation, and shut down the drive. If there is no advantage of this feature in a given application then non short circuit rated devices are used, even in three phase bridge circuits, as they are generally more efficient and therefore have higher current ratings.

As with the DID inverter, a simple assessment of potential performance can be carried out by examining any restrictions that this inverter has in terms of the voltages that are available to apply to the windings. With any delta circuit the sum of the voltages applied to the windings must be equal to zero. This differs slightly from the DID inverter where the sum of the phase voltages has to be zero or greater than zero. The control method, however, that was used with the DID inverter did not utilise a switch state with positive DC voltage applied to all three phases at the same time. It therefore follows that both

inverters can use a very similar control strategy and achieve very similar results in terms of machine and inverter performance.

8.4.2 Drive Performance

This inverter configuration was implemented in the same test rig as the DID inverter and performance in terms of machine efficiency, torque-speed envelope for a fixed current demand, and inverter loss were assessed. All results were, in all practicality, identical to the DID inverter as predicted by the theory.

It should be noted, however, that it may be possible to exploit the DID's ability to have the phase voltage sum greater than zero. With a suitable control strategy, a net DC voltage could be applied to each winding which would result in the current in a phase never returning completely to zero. This may well have the effect of increasing torque at high speed for a given inverter VA rating at the expense of machine efficiency.

8.5 Asymmetric Half Bridge with Interphase Diodes

8.5.1 Inverter Description

This topology is simply three asymmetric half bridges with diodes connected between phases to allow two phases to conduct using only two switches (see Figure 8.19). It is very similar to the DID inverter except for the position of the freewheel diodes which are no longer directly in antiparallel with the transistors.

In terms of the voltages that can be applied to the windings, the situation is similar to the DID inverter i.e. the sum of the phase voltages must be zero or greater than zero. Performance can therefore be expected to be the same as the DID and DPD inverters, although this topology was never actually tried in practice on the test rig.

The potential advantage of this topology is that total inverter loss should be reduced. This is because in the freewheel state the current only has to conduct through one switch, one freewheel diode and one interphase diode. With the other two topologies two interphase diodes need to conduct. This however is only of marginal benefit as the

interphase diodes are relatively low cost compared to the switching devices and fast recovery diodes. The disadvantages with this circuit are that six wires are needed between the inverter and the motor and the advantage of having the switching devices and diodes in full antiparallel is lost.

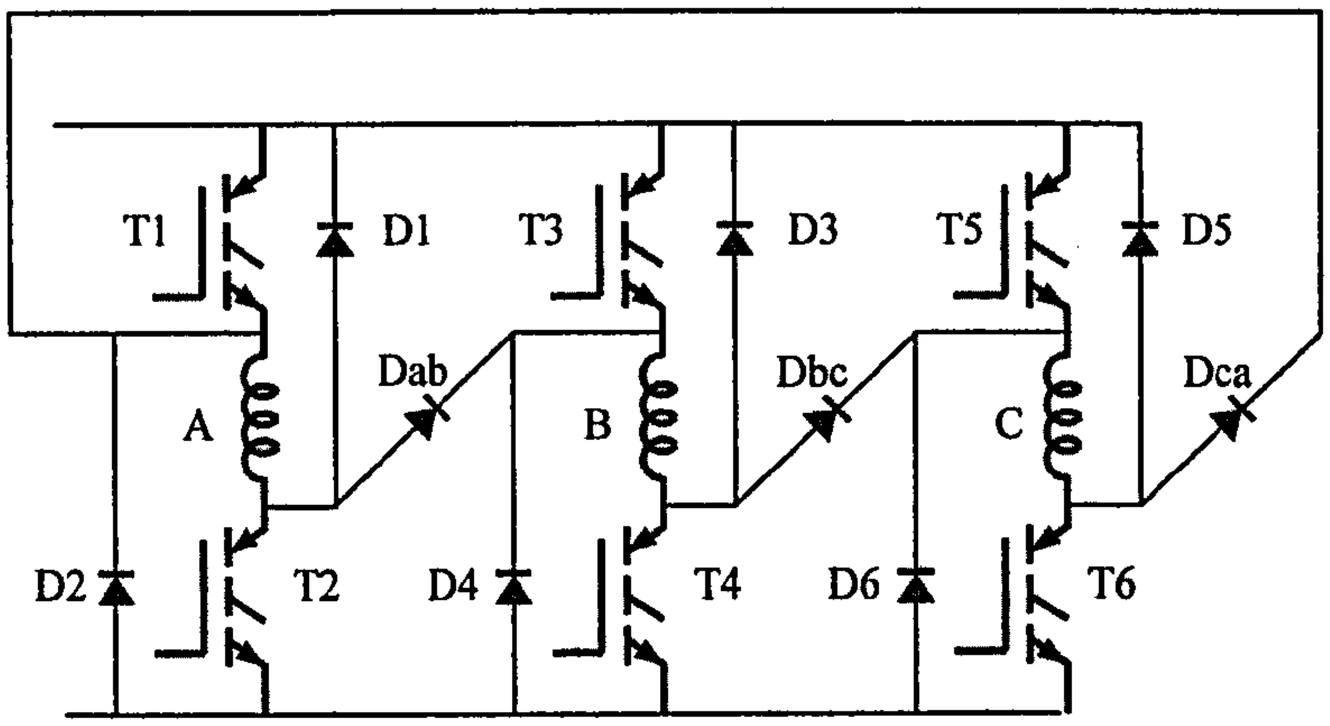

Figure 8.19 Asymmetric half bridge with interphase diodes topology.

8.6 Current Sensors

The waveforms shown in the previous sections of this chapter were achieved using a PID current controller operating from sensors measuring phase current. It would be advantageous with the DPD topology to mount the phase diodes in the motor, as this would mean that only three power connections would be required to link the inverter to the motor. The problem with this is that the phase current sensors would also need to be located in the motor. A much more convenient and cost effect solution would be to control the machine using sensors located in the inverter. Three schemes were developed – sensing of line currents, inverter leg currents, and DC link current. Over the next few sections the impact of the schemes on current controllability and hence performance will be discussed.

8.6.1 Control with Line Current Sensors

The waveforms shown in Figure 8.20 are for the DPD inverter, controlled with two line current sensors. This is achieved as follows. To work as before, the controller needs to sample one phase current during each third of the electrical cycle and control it to the demanded value. The problem is that the line currents are by definition the *difference*

between two phase currents, so the required phase current cannot be determined directly. Fortunately, it will be seen that during each third of the electrical cycle one of the line currents equals the phase current that is desired to be controlled.

Figure 8.20 shows line current I_{L1}, which is the difference between I_A and I_C. It can be seen that for the period that this is positive, i.e. one third of the electrical cycle, it equals the current in phase B. Consequently, during this time, I_{L1} can be used to control the phase currents A and B to their demanded values. This is made possible because during the majority of this period the phase current Ic is zero, and therefore the line current I_{L1} becomes simply equal to I_A. There is a period where Ic is not zero because it is still in the process of turning off. However, as with the DID inverter, the transistor currents are the difference between two of the phase currents – the commutation spike in phase A and the tail in phase C cancel out, and the transistor current (i.e. the line current) remains equal to phase B.

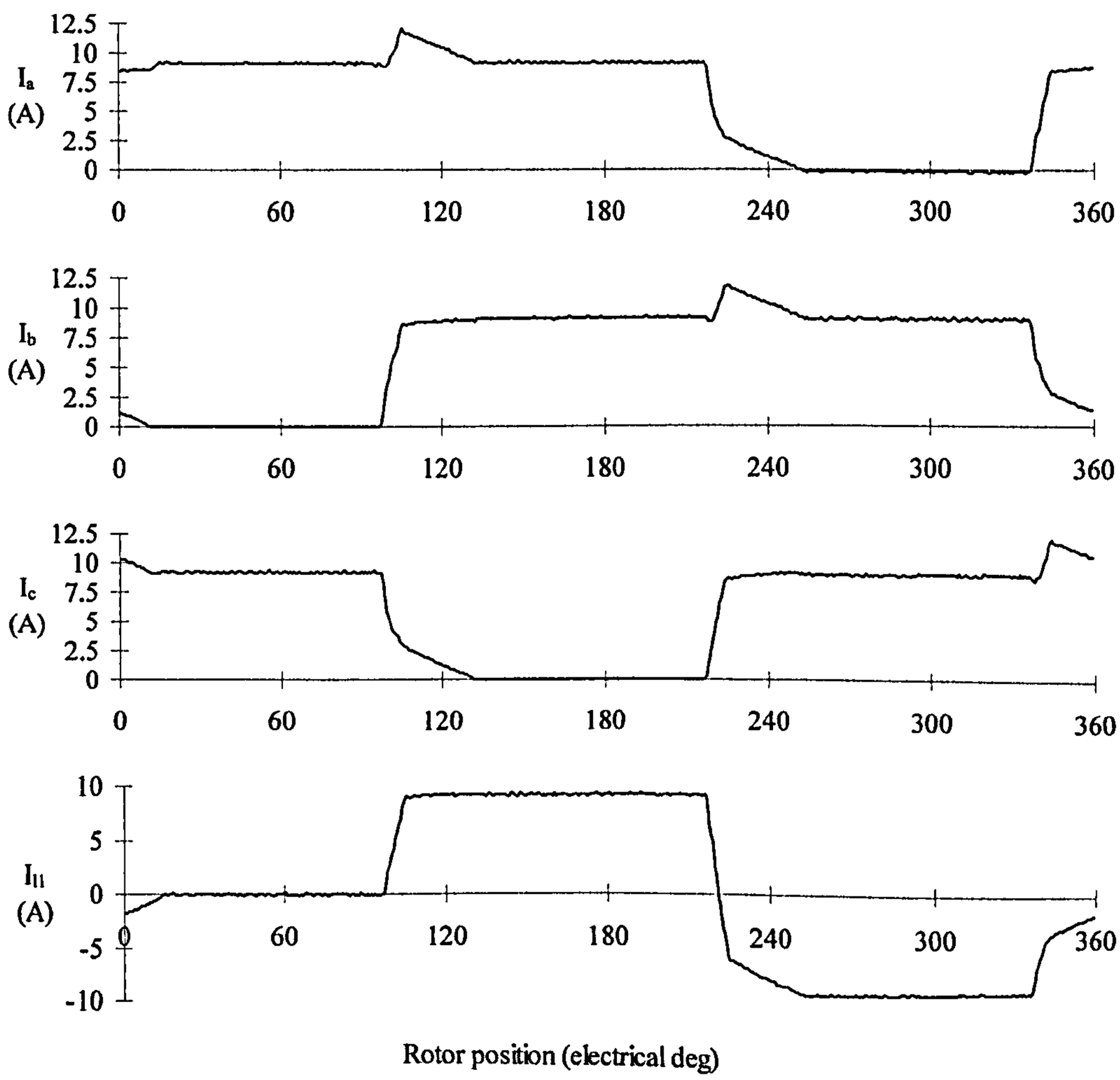

Figure 8.20 Measured current waveforms with current control using line current sensors.

During the remaining two thirds of the electrical cycle the other two line currents are used as appropriate. A benefit of this system is that only two line currents sensors are required - the third current can always be calculated, as the line currents must always sum to zero. This method of control has been implemented on the test rig and the resulting current waveforms are near identical to direct phase current sampling over the whole speed range.

8.6.2 Control with Shunt Resistors in Each Inverter Leg

It is common practice in smaller inverter drives, especially SR motor drives, to measure current using shunt resistors. This is possible when currents are low enough to obtain a good voltage output without dissipating large amounts of power. They can be lower cost due to the fact that voltage isolation is no longer necessary between the sensors and the controller (assuming the controller can be referenced to the negative DC bus). With the DID and DPD inverters, control with a current shunt in the bottom of each leg of the bridge is possible, but with some restrictions on when currents can be sampled. This is because current flow sometimes only occurs in one of the lower sections of a leg, meaning that the line current needed for control purposes cannot be measured directly or calculated. Interestingly, the restrictions on when the correct current can be sampled depend on the direction of rotation of the motor. In one direction it is possible to measure the desired line current in one of the freewheeling states and in the "on" state. In the other direction it is only possible to measure the current in one of the freewheel states. In this situation it is therefore impossible to apply full voltage to a winding continuously at the commutation points and sample currents at the same time.

If the shunt resistors are placed in the upper half of the bridge legs, i.e. referenced to the positive DC bus, then the problem is overcome as the current desired to be measured always flows in one of those devices regardless of motor direction. The only exception to this is one of the two freewheel states.

8.6.3 Control with a DC link Shunt Resistor

Current control using only one DC link current sensor is highly desirable, as this minimises cost and power dissipation. In addition, voltage isolation between the sensor

and the controller is not necessary. It is also common practice for semiconductor manufacturers to incorporate DC link sensors in power modules for overcurrent protection, and therefore the sensor is often already available.

As an example, Figure 8.21 shows the currents that flow in the DC link with phases A and B excited in the fully pitched winding machine. First consider the situation when the transistors are in a state when a positive DC link voltage is being applied to the excited phases i.e. with T1 and T6 switched on. In this situation, assuming $I_A > I_B$, the current in the DC link becomes equal to I_B-I_C. Inspection of Figure 8.5 reveals that this current will not be constant during the period when phases A and B are excited due to the tail in I_C as it turns off. Therefore, if the line current I_B-I_C is controlled to a fixed current demand during this period, the resulting phases currents will differ from those achieved using line current sensors.

The resulting measured waveforms are shown in Figure 8.22. The tail in the current at turn off of phase C is, in effect, added to the current in phase B. Notice that the current I_B-I_C (=-I_{L1}) is now flat topped during the period with phase A and B conducting, as that is the parameter now being controlled. The line currents, and consequently the transistors, also see a higher peak current due to the overshoot in the phase currents at turn on. A further consequence of this is that the commutation spike in the middle of the phase conduction period becomes larger due to the mutual coupling between phases.

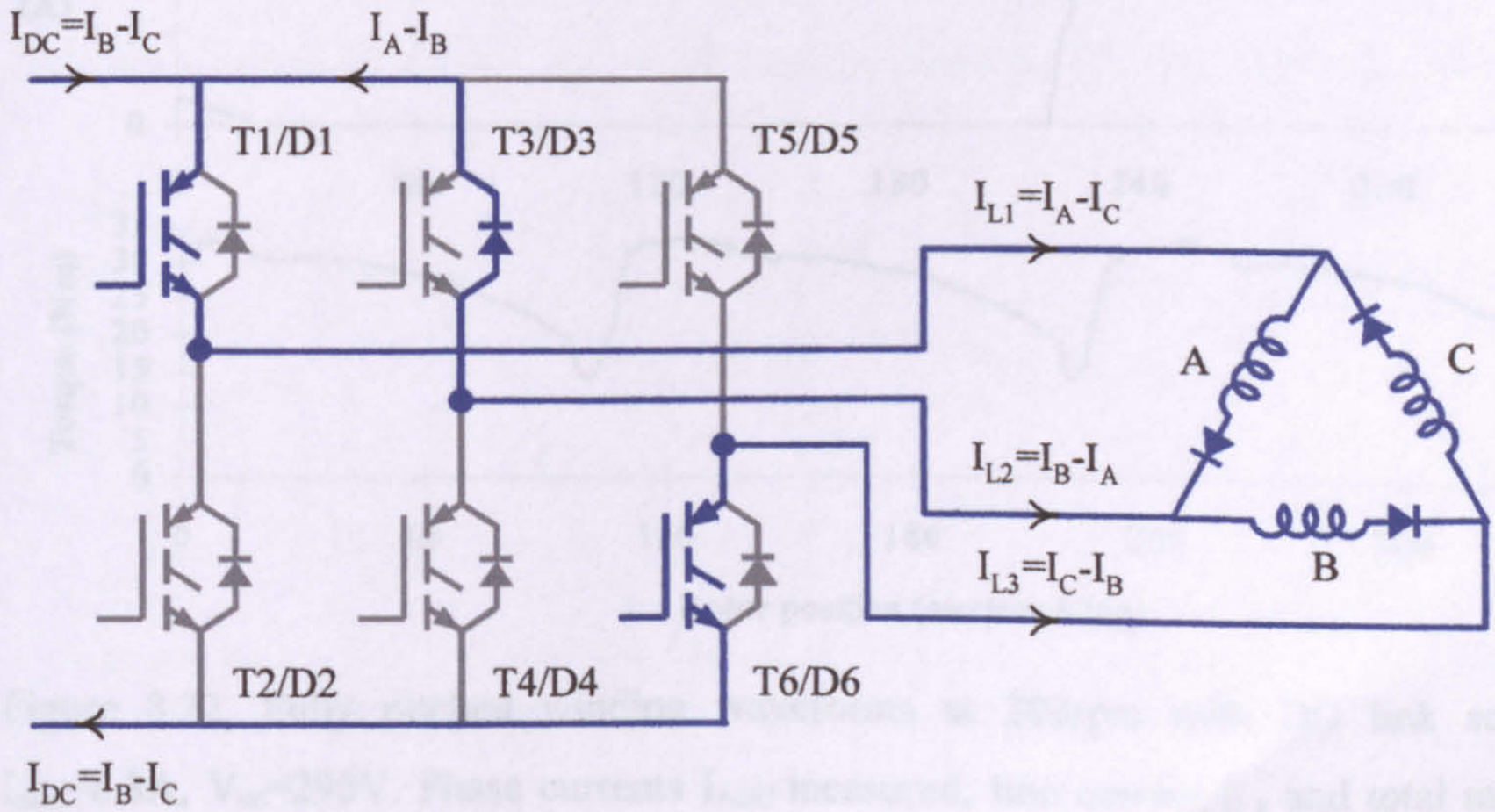

Figure 8.21. Current flow with phases A and B desired on, T1 and T6 on, $I_A > I_B > I_C$. Conducting parts of the circuit are shown in blue.

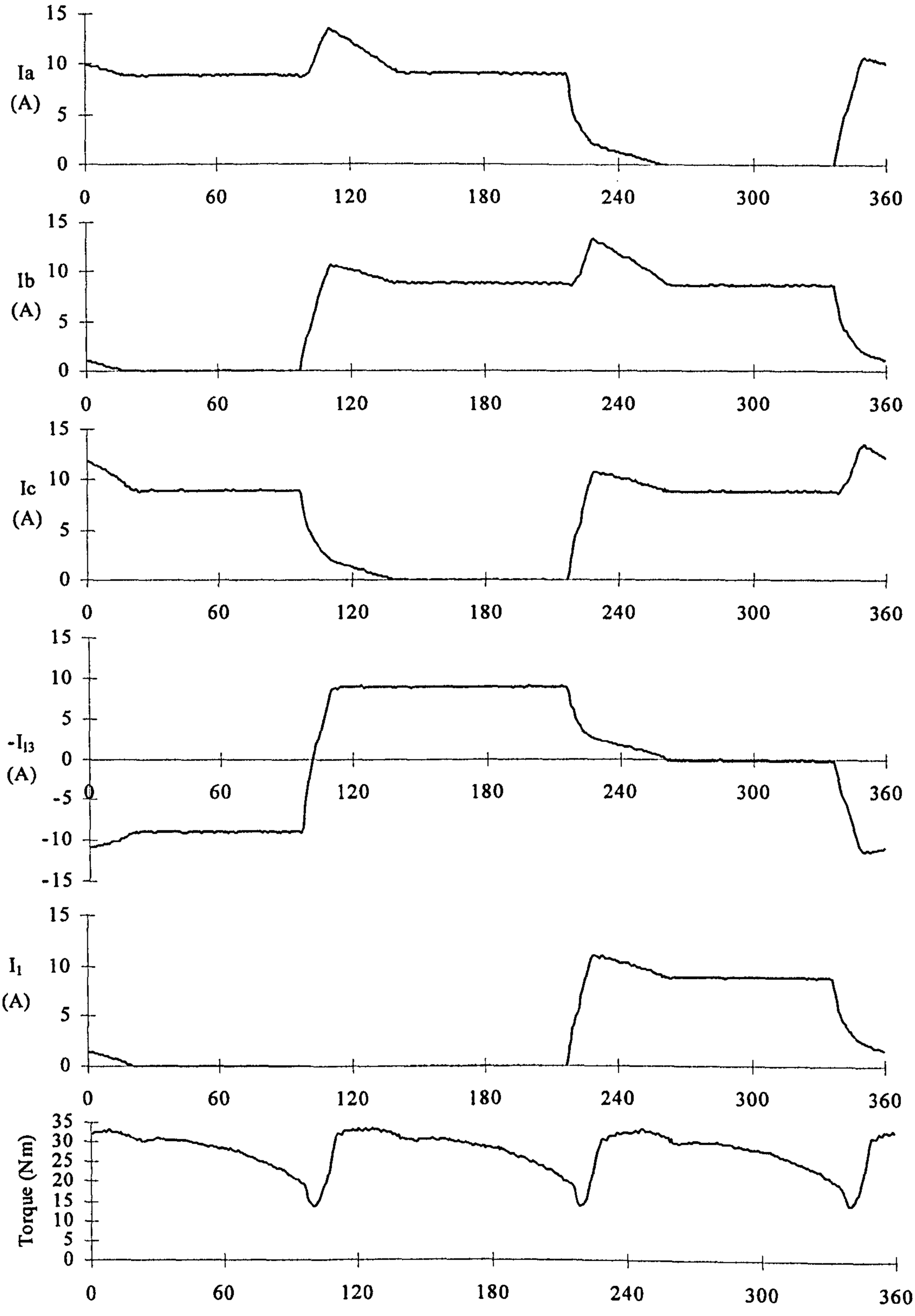

Figure 8.22. Fully pitched winding waveforms at 200rpm with DC link sensor control. I_{dem}=8.8A, V_{dc}=290V. Phase currents I_{ABC} measured, line current I_{L1} and total machine torque calculated.

The overall effect on the power electronic rating and the motor efficiency are in fact quite small and it is quite realistic to control this inverter drive with this single current sensor. The actual current demand for the same torque is reduced from 9.1A to 8.9A, however peak device current is 11.3A as the commutation spike no longer cancels with the turn off tail current. Machine torque per unit copper loss is now 84.4mNm/W at low speed and Table 8.3 summarises a comparison with the other inverters/sensing arrangements already discussed. As the machine approaches base speed and beyond the phase current waveforms become more and more like the waveforms with phase sensor control. Figure 8.23 shows there is no difference at base speed between DC link sensor control and line sensor control. The efficiency at rated power and the torque-speed envelope is therefore the same. DC link sensor control is equally applicable to the DID inverter.

Inverter Type	Torque (Nm)	Loss (W)	Torque Per Unit Copper Loss (mNm/W)
AHB	26.3	296	88.9
DPD/DID (with phase sensors)	27.8	319	87.25
DPD/DID (with DC link sensor)	27.3	324	84.4

Table 8.3 Comparison of torque and loss with the AHB, DID and DPD inverters. Prototype machine, 100rpm, V_{dc}=290V, I_{dem}=9.1A (except DID with DC link sensor I_{dem}=8.9A).

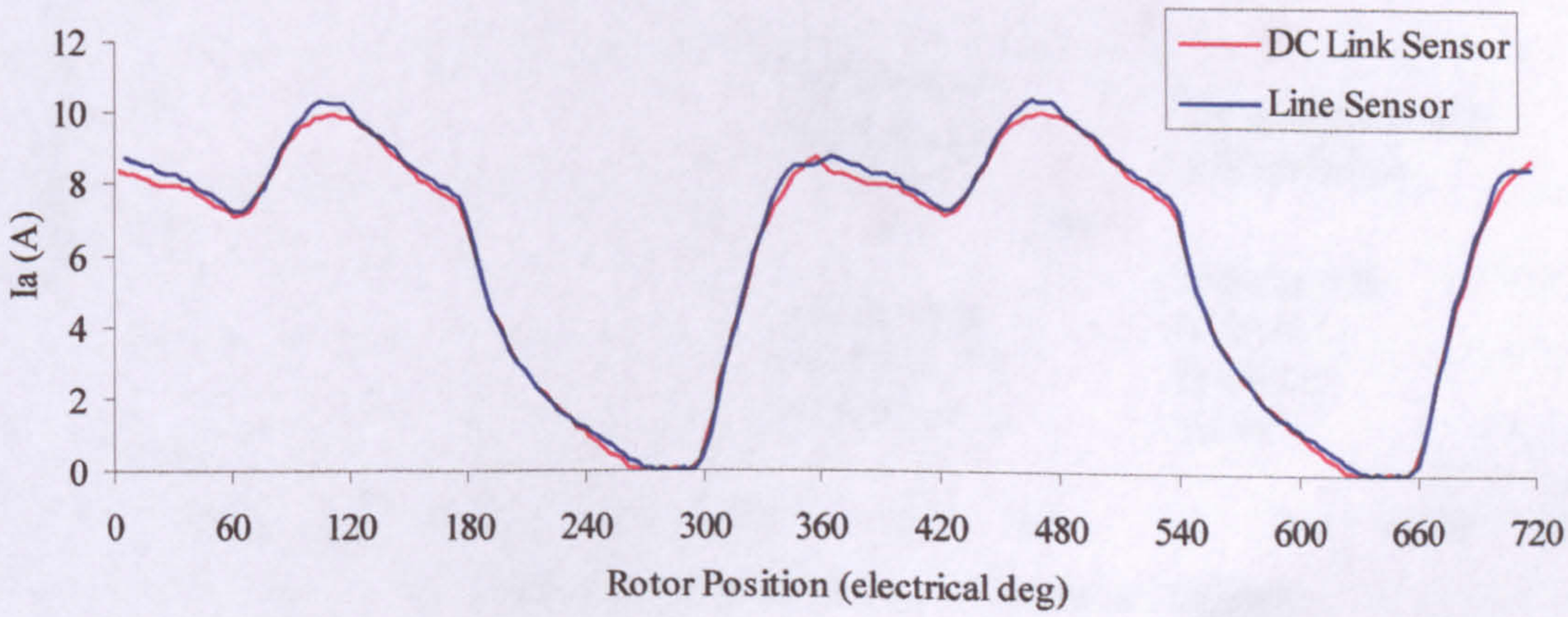

Figure 8.23. Comparison of phase currents at base speed with line sensor control and DC link sensor control.

It is worth noting that the currents are never out of control, but it is not possible to control them to their exact desired waveshape using a constant level of current demand on the parameter that can be sampled. It may well be possible to predict the value of the tail current and therefore compensate the current demand by the appropriate amount to achieve the desired phase currents.

There are restrictions on when the desired current can be sampled. This is more simple than before, as it does not depend on the direction of rotation of the motor – the current can only be sampled in the "on" state i.e. when there is a current flowing from the DC link capacitor to the inverter.

8.7 Inverter Rating and Torque Per Unit Copper Loss Tradeoffs

Figures 8.24 and 8.25 summarise the relative differences in machine and inverter performance and low speed and base speed, respectively. This is the same graph as discussed in Chapter 6, with the addition of results for the DID and DPD inverter with phase, line, and DC link sensor control.

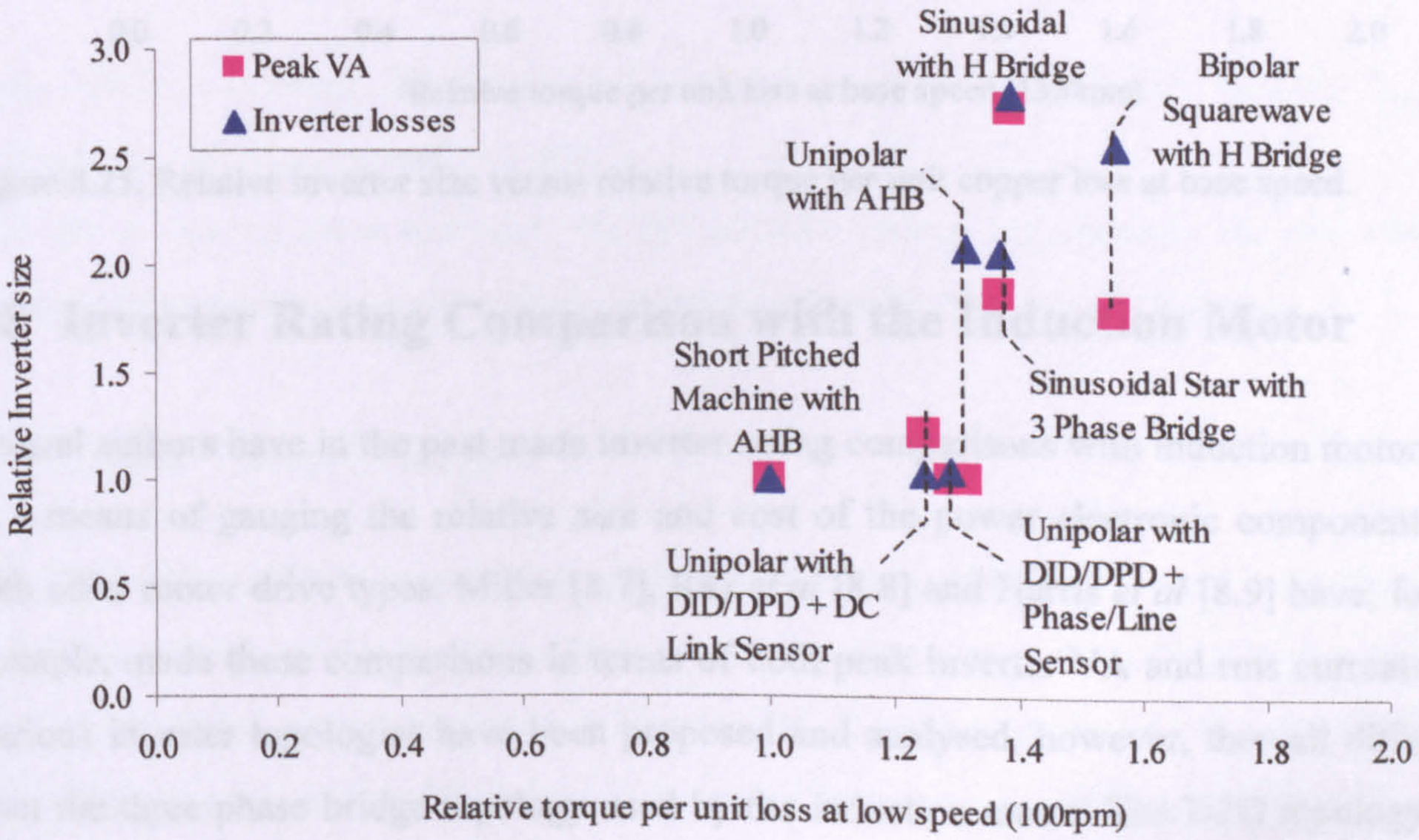

Figure 8.24. Relative inverter size versus relative torque per unit copper loss at low speed.

The figures shown in Figures 8.24 and 8.25 are based on the following assumptions:

- Torque per unit copper loss and for the DID and DPD inverters are based on data from Figures 8.9 and 8.11. There are differences in the torque-speed curves and no account of this has been taken in these comparisons.
- Similarly, inverter peak VA and loss figures are based on the same torque-speed curve.
- Inverter rating does not include the additional 3 diodes. These diodes do not need to be fast recovery types as the others do, and therefore they are relatively low cost.

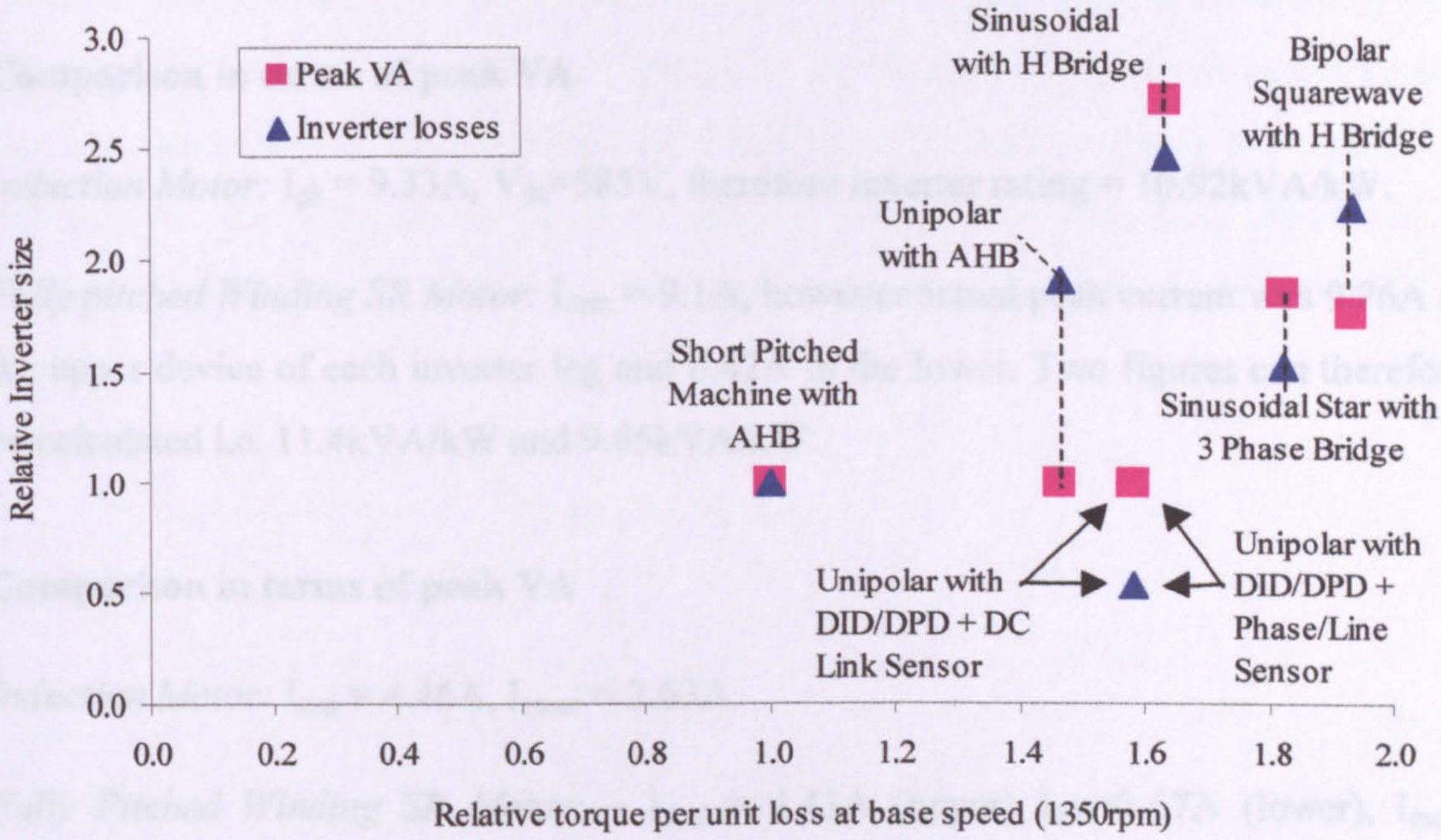

Figure 8.25. Relative inverter size versus relative torque per unit copper loss at base speed.

8.8 Inverter Rating Comparison with the Induction Motor

Several authors have in the past made inverter rating comparisons with induction motors as a means of gauging the relative size and cost of the power electronic components with other motor drive types. Miller [8.7], Ray *et al* [8.8] and Harris *et al* [8.9] have, for example, made these comparisons in terms of both peak inverter VA and rms currents. Various inverter topologies have been proposed and analysed, however, they all differ from the three phase bridge topology used by the induction motor. The DPD topology, on the other hand, now enables the closest comparison possible of a unipolar excited SR

motor versus the bipolar excited induction motor. Details of such a comparison have been given in [8.10], and the results from this are summarised below.

The evaluation was based on a simulation of the induction motor and experimental results from the fully pitched winding SR motor (the same motor and test rig and described in this thesis). The induction motor was operating in PWM with a modulation depth of 1.15 at base speed. Fundamental output current = 6.6A, power factor = 0.85, machine efficiency = 0.85, DC link ripple voltage = ±10%, machine output power = 3kW (accounting for efficiency).

Comparison in terms of peak VA

Induction Motor: I_{pk} = 9.33A, V_{dc}=585V, therefore inverter rating = 10.92kVA/kW.

Fully pitched Winding SR Motor: I_{dem} = 9.1A, however actual peak current was 9.76A in the upper device of each inverter leg and 8.42A in the lower. Two figures can therefore be calculated i.e. 11.4kVA/kW and 9.85kVA/kW.

Comparison in terms of peak VA

Induction Motor: I_{rms} = 4.46A, I_{mean} = 2.63A

Fully Pitched Winding SR Motor: – I_{rms} = 4.43A (upper) I_{rms}=3.67A (lower), I_{mean} (upper) = 2.38A, I_{mean} (lower) = 1.81A.

The above figures show that very similar inverter ratings are required for two very different three phase machines driven by near identical inverter topologies.

8.9 Dead Time Effects

When using the DPD inverter with the three phase bridge, dead time control is needed to prevent an upper and lower device being on at the same time. The effect of this dead time on the phase current is shown in Figure 8.26. Here the current is being controlled with phase current sensors. The effect of the dead time is to bring the commutation spike down faster than it would have done, and to worsen the tail current at turn off. This is because, for the period of the dead time, negative volts are being applied to the

commutation spike rather than the tail current. There is a subsequent effect on the equivalent single tooth phase currents as well as the line currents. It would be desirable to remove this effect, as there will be inevitably be a degree of worsening of torque per unit copper loss. In addition, if the inverter was now to be controlled with line current sensors, rather than phase current sensors, then the result would be an overshoot in the phase current waveform. This would be of the same magnitude as the dip in the line current waveform shown in Figure 8.26.

A scheme to remove this effect was developed. This uses compensating terms that are added to the PWM voltage reference. The scheme is simple to implement and only uses a few lines of code in the controller. Figure 8.27 shows current waveforms under exactly the same conditions as Figure 8.26 except with the compensation scheme in operation. It can be seen that with the correct level of compensation the dead time effect can be completely removed. Details of the dead time compensation method are described in Appendix D.

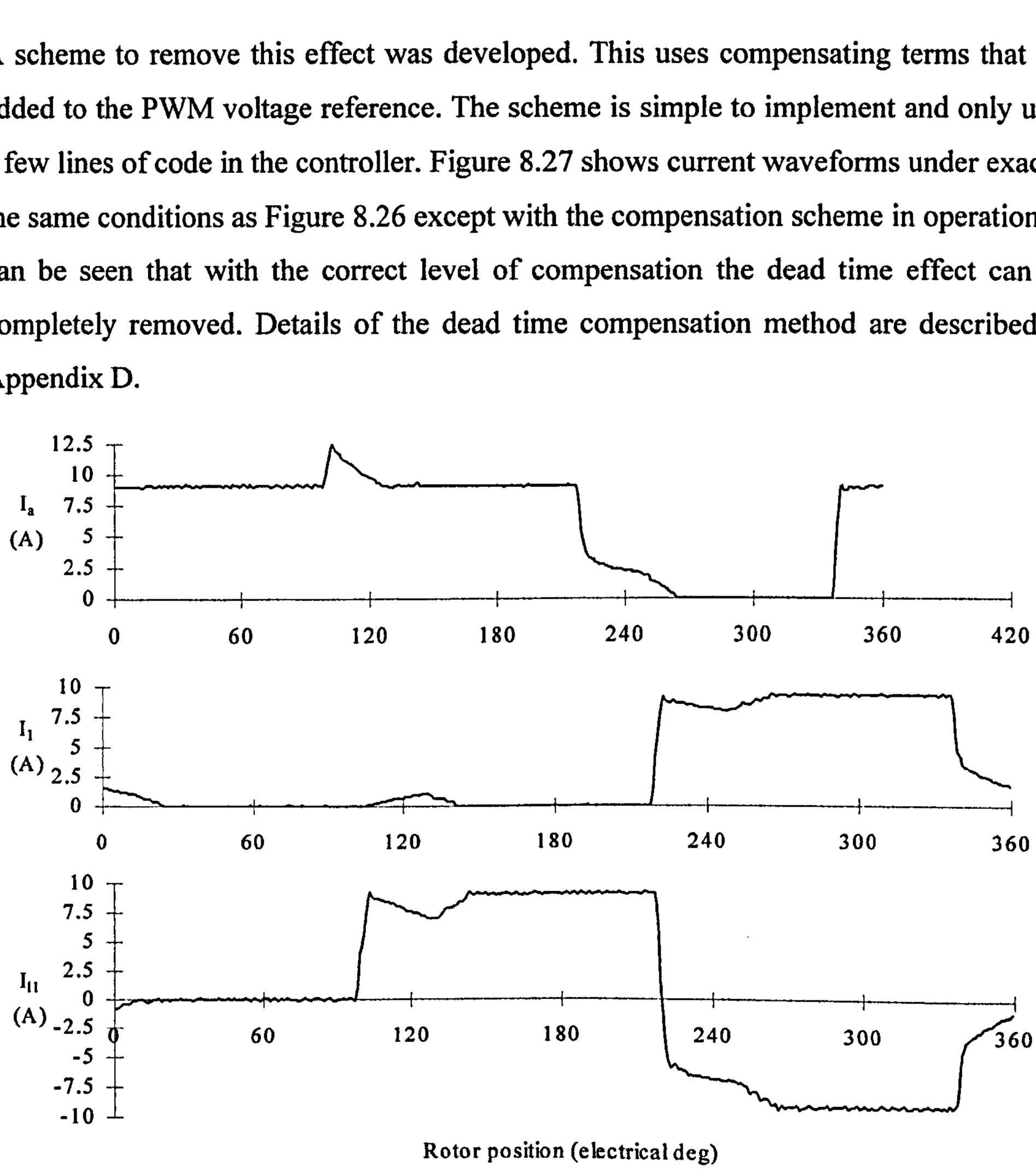

Figure 8.26 The effect of 4μs of dead time on current waveforms with the DPD inverter. I_{dem}=9.1A, V_{dc}=600V.

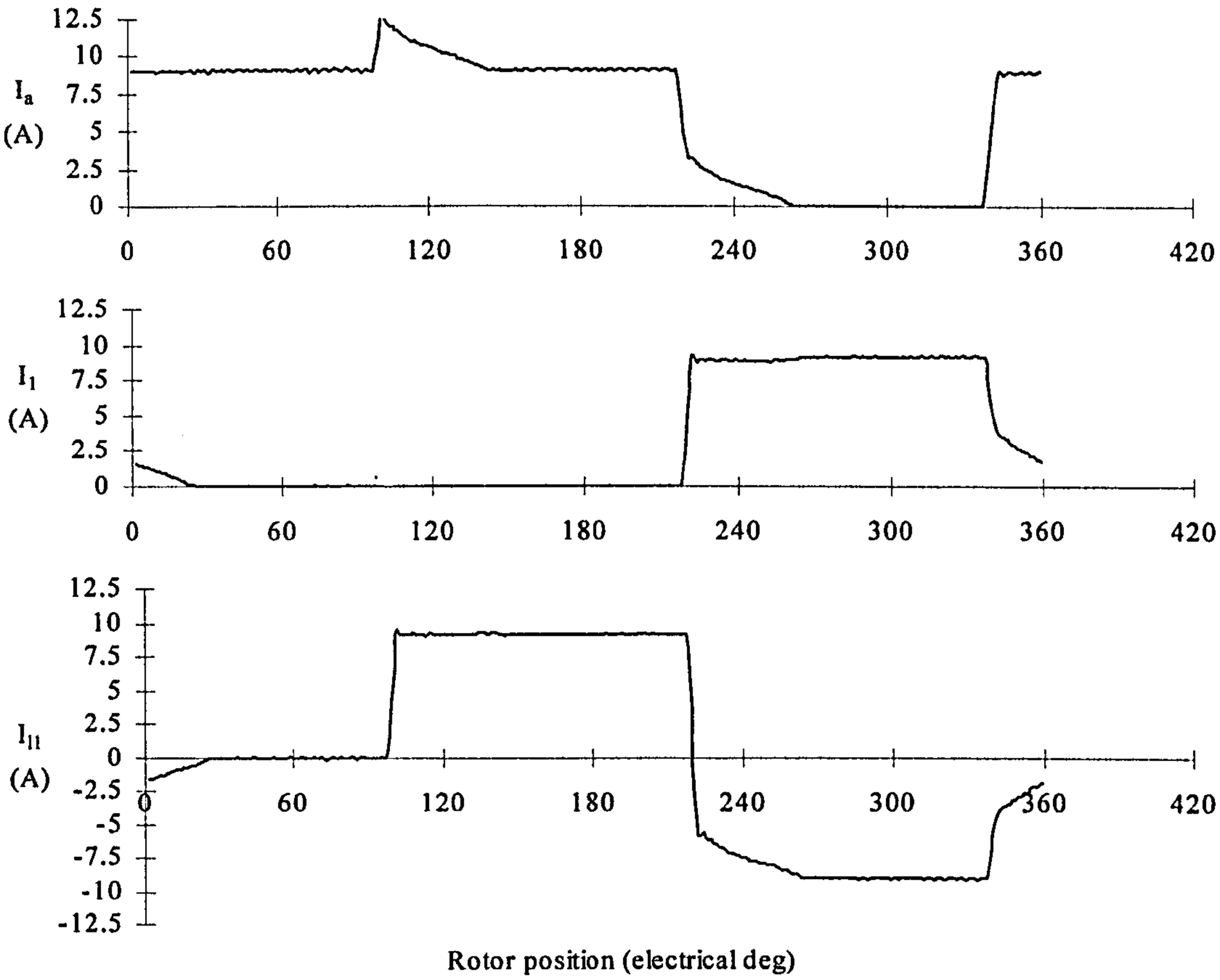

Figure 8.27 The measured effect of dead time compensation on current waveforms with the DPD inverter. Dead time 4μs, I_{dem}=9.1A, V_{dc}=600V.

8.10 Control Loop Stability

Results from the test rig showed that with both the DPD and DID inverters control bandwidth could be significantly increased. It was found that the proportional gain on the PID controller could be increased by a factor of three. As discussed in Chapter 6, the asymmetric half bridge (AHB) inverter has its own independent control loop on each phase. The fully pitched winding machine has very strong mutual coupling between phases, so the result is that a change in output of one of these control loops will potentially cause a disturbance in the control loop on another phase. It was found that the fully pitched winding machine needed to have its proportional gain reduced by a factor of 2.5 compared to the short pitched winding machine to maintain control loop stability. To achieve good current control with a digital control system, then, would require an increase in control loop frequency and hence possibly cost.

The difference with the DPD and DID inverters is that there is only one control loop for the whole bridge. There is therefore no adverse interaction between different control loops. In addition, with the current control method described, there is always a natural tendency for the two phases that are desired to conduct to naturally equalise their currents. If one phase has less current than the other, then it will naturally receive full positive DC link volts first until the two phases equalise their currents.

It was also found that the integral gain could be increased to a great extent, mostly because the control loop no longer sees the commutation spike in the middle of the conduction period. This is because control only takes place on the first half of the conduction period of a phase and therefore stops just before the commutation spike occurs.

8.11 Summary

Three novel power electronic topologies have been proposed and investigated with the aim of reducing inverter loss with unipolar operation of the fully pitched winding machine. It has been demonstrated that in theory all three inverters should have the ability to supply the necessary currents during low speed operation and apply the necessary voltages during high speed operation. This theory implies that the torque-speed envelope of the motor drive will be similar to the asymmetric half bridge with the same current demand and the same DC link voltage.

The test rig has been used to demonstrate two of the inverters, namely the DID and DPD inverters. A control method has been developed which 'connects' two of the desired phases in series to achieve the desired objective of controlling two phases at once with only two switches. This is in contrast to the four switches that need to conduct in the asymmetric half bridge topology.

The results have shown that the torque-speed curve and torque per unit copper loss are very similar to the AHB. At the same time inverter losses have been shown to be approximately one half at low speed and one quarter at high speed. The latter has been demonstrated to be the result of being able to feed current from the phase turning off

directly in to the next phase turning on. This reduces even further the rms currents that the transistors and freewheel diodes have to conduct. With these inverters the fully pitched winding machine is now able to achieve its gain in machine efficiency without an increase in inverter rating.

Current sensing schemes have been investigated, including control with three phase sensors, two line sensors, three inverter leg shunts, and one DC link shunt. The tradeoffs in terms of drive performance versus cost have been discussed. Line current sensing with the DPD inverter enables the motor to be situated remotely, with only three power connection between the two. The main part of the inverter is a standard three phase bridge which would facilitate the use of standard motor drive power electronic modules. In addition, only two line sensors are required as the third can be calculated. The main drawback is that the phase diodes need to be mounted in the motor (most likely in the terminal box).

DC link sensor control is a particularly interesting option for low cost as only one sensor is required, which does not necessarily need isolation if the controller is referenced to the negative side of the DC link. It can be used with either the DPD or DID inverters. Torque per unit copper loss and inverter rating have been shown to be only slightly affected with this sensing method.

It was found that control loop stability could be substantially increased due to the fact that the whole bridge is being controlled by only one current control loop. This solved the problem of the three separate control loops (one on each phase) in the AHB inverter continually introducing disturbances in to each other's system due to the strong mutual coupling between phases. Proportional gain could be increased by a factor of three, thereby significantly improving current waveshape.

Dead time was found to have a detrimental effect on current waveshape as during the period of the dead time incorrect voltages are applied to the windings. A method to overcome this has been demonstrated on the test rig. This involves adding appropriate compensating values to the PWM duty cycles and it has been shown that with the correct values the effect is completely overcome.

Chapter 9 - A NEW INVERTER TOPOLOGY FOR THE SHORT PITCHED WINDING MACHINE

9.1 Introduction

The delta type inverters described in Chapter 8 can also be used with short pitched winding SR machines. The delta with phase diodes inverter (DPD) in particular will be examined, as this offers the benefit of being able to use the standard three phase bridge topology. This enables the use of standard motor drive modules intended for induction motor drives. As current sensors are commonly already contained in these modules, current sensing methods will be examined to see how these can be utilised.

The ideal currents and voltages that are required by the short pitched winding machine will be examined to demonstrate the theoretical suitability of this type of inverter. Drive performance was evaluated on the test rig with the same controller and inverter as the fully pitched winding machine, except with a standard Allen West D132 12-8 SRM. Results for inverter and machine performance will be presented in terms of torque-speed characteristics, inverter loss, and peak VA ratings.

9.2 Theoretical Analysis

9.2.1 Description of the DPD Inverter

Figure 9.1 shows the DPD inverter. It consists of a conventional three phase bridge in a delta connection, with the addition of a diode in series with each phase. The function of the diodes is to ensure only unidirectional phase currents flow; without them AC phase currents would inevitably have to flow, because the phase voltages must sum to zero in a delta circuit. This topology is exactly the same as that used with the fully pitched winding machine.

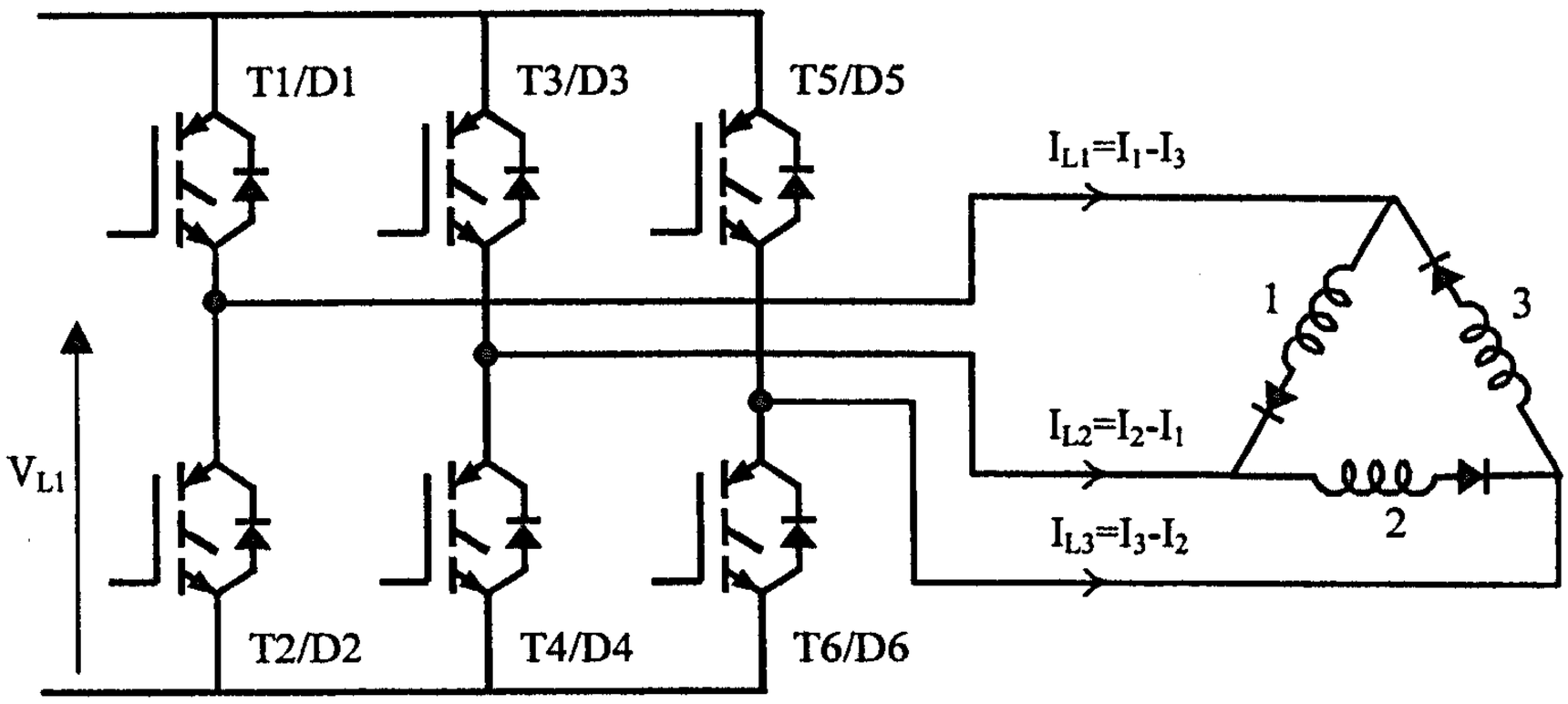

Figure 9.1 Delta connection with phase diodes.

9.2.2 Ideal Current and Voltage Waveforms

Figure 9.2 shows the ideal currents at low rotor speed for the short pitched winding machine. The line current that would be needed from the three phase bridge is also shown. This demonstrates that this type of inverter will be able to conduct the required phase currents at low speed without any problems such as high peak transistor currents.

Unlike the fully pitched winding machine, only one phase conducts at a time i.e. the phase conduction period is 120°. This means that with the asymmetric half bridge inverter (AHB) only two transistors are needed to control the machine at any one time (c.f. the four that are needed with the fully pitched winding machine). With the proposed delta type circuit two transistors will still be needed, so there will be no fundamental improvement in device duty cycle, as can be achieved with the fully pitched winding machine.

It should be noted that the short pitched winding machine can be controlled in a variety of ways in terms of the phase conduction angle. The method shown in Figure 9.2 is probably the most common and yields the highest torque to loss ratio. It is possible to increase the conduction period from 120° up to 180° which increases torque output slightly for a given current demand, and it also reduces torque ripple, but this is at the expense of greatly increased copper loss.

The ideal phase voltages required at high speed are shown in Figure 9.3. The voltage V_{L1} is also shown, and this is the voltage that would be required from one of the outputs of the three phase bridge. This shows that it will be possible at high speed to apply the correct voltages to the windings to produce the 120° conduction period. This analysis demonstrates, however, that it would not be possible to increase the phase conduction period beyond 120°, as the required V_{L1} could not be achieved without greatly increasing the DC link voltage. Another way to look at this is that with any delta circuit the sum of the phase voltages must be zero, so that the full volts cannot be applied to all the phases at once.

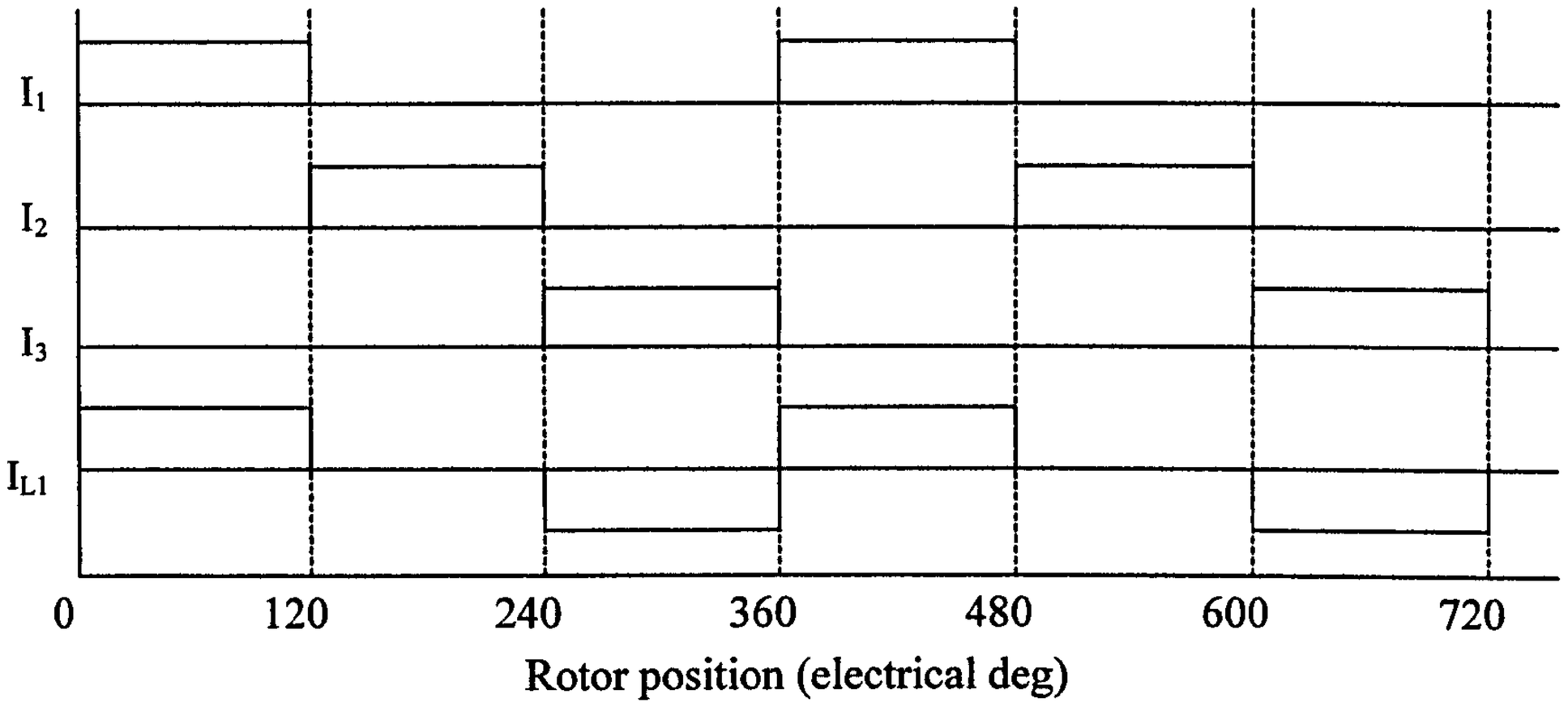

Figure 9.2 Ideal phase and line current waveforms under current control.

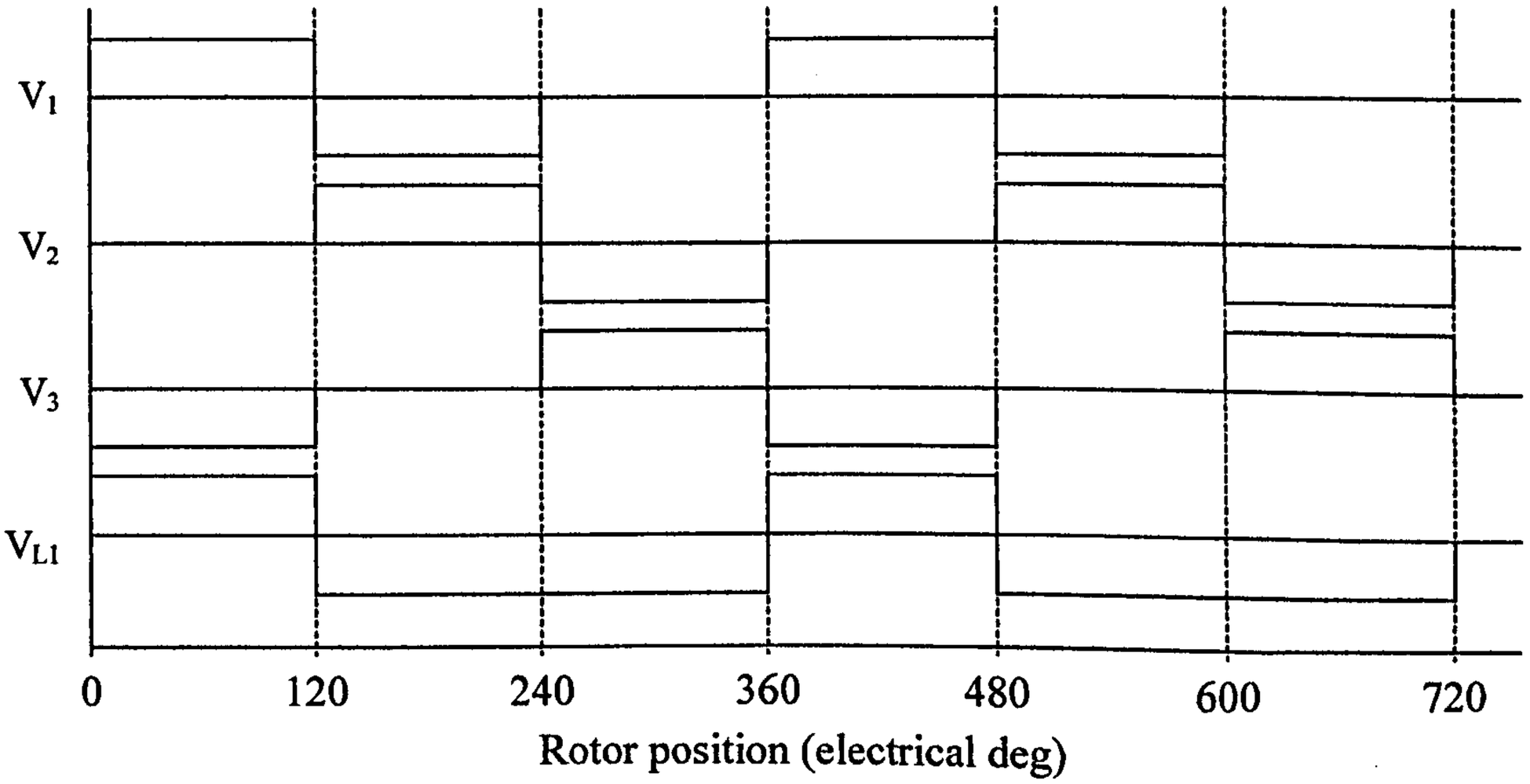

Figure 9.3 Ideal phase and line voltage waveforms at high speed (shown here with no phase advance for direct comparison with Figure 9.2).

9.3 Inverter Operation

Control is very similar to that of the fully pitched winding machine with this inverter. The only difference is that the switching states are changed slightly so that one phase is excited rather than two. Table 9.1 shows the switching states that are used to control this machine. For each phase that is desired to conduct there are three basic states:

1) The first applies positive volts to the phase that is desired to conduct. Negative volts are automatically applied to whichever of the other two phases has the greatest current i.e. the phase that is turning off would usually receive the negative volts, as the current in the phase that is already off should be zero. This therefore achieves the desired aim of turning one phase on, one phase off, and applying nothing to the third phase.

2) The other two states will both freewheel all the phases. Both of these states should ideally be used alternately to spread losses as evenly as possible between devices.

Phase desired on	Switches On	Condition	Phase 1 Voltage	Phase 2 Voltage	Phase 3 Voltage
1	T1, T4	$I_3 > I_2$	$+V_{dc}$	0	$-V_{dc}$
	T1, T4	$I_2 > I_3$	$+V_{dc}$	$-V_{dc}$	0
	T1, T3, T5	None	0	0	0
	T2, T4, T6	None	0	0	0
2	T3, T6	$I_1 > I_3$	$-V_{dc}$	$+V_{dc}$	0
	T3, T6	$I_3 > I_1$	0	$+V_{dc}$	$-V_{dc}$
	T1, T3, T5	None	0	0	0
	T2, T4, T6	None	0	0	0
3	T5, T2	$I_1 > I_2$	$-V_{dc}$	0	$+V_{dc}$
	T5, T2	$I_2 > I_1$	0	$-V_{dc}$	$+V_{dc}$
	T1, T3, T5	None	0	0	0
	T2, T4, T6	None	0	0	0

Table 9.1 Summary of the useful switching states for current control and the resulting winding voltages.

These switching states can be applied to the machine in PWM in a very similar way to the method described in Appendix D. The duty cycle for the PWM is generated from a PID controller. This works by sampling the current of the phase that is desired to conduct and comparing it to a fixed current demand. The voltage reference output (or duty cycle) from the PID control loop is simply based on the error between this fixed reference and the sampled current. So the overall effect is that the phase that is desired to conduct is controlled directly by the control loop and will receive positive volts accordingly. The voltages that are applied to the other two phases are the exact negative of this voltage, and whichever of these other two phases has the greatest current will receive this negative voltage.

9.4 Drive Performance

Performance was measured on the test rig using a standard Allenwest 7.5kW 12-8 SR motor in a D132 frame size. Rated torque output is 48Nm at 1500rpm. Static torque measurements had been previously measured for this machine and these were used by the DSP as a basis for estimating machine electrical torque output from knowledge of the phase currents and position.

9.4.1 Low Speed Performance

Figure 9.4 shows the phase current waveforms that result from the current control method described in the last section. It can be seen that the waveforms do deviate from the ideal ones shown in Figure 9.2, and this is explained as follows:

- At point A phase 1 is desired to turn on and phase 2 is desired to turn off. Therefore the control applies the state with transistors T1 and T4 switched on. Positive volts are applied to phase 1, and because the current in 2 is greater than that in 3, negative volts are naturally applied to phase 2.

- At point B the current in phase 1 reaches its current demand, and therefore current chopping is required. At this stage phase 2 has not yet turned off, but negative volts can only be applied to it at the same rate as positive volts are applied to phase 1. This is now at a reduced rated because phase 1 has reached its current demand. A tail in the current at turn off therefore occurs.

The effect of the phase diodes can also be seen – they block voltage from the time that a phase turning off reaches zero current, and the time the next phase turns on. If the diodes were removed then the phase current would become an AC rather than a DC waveform.

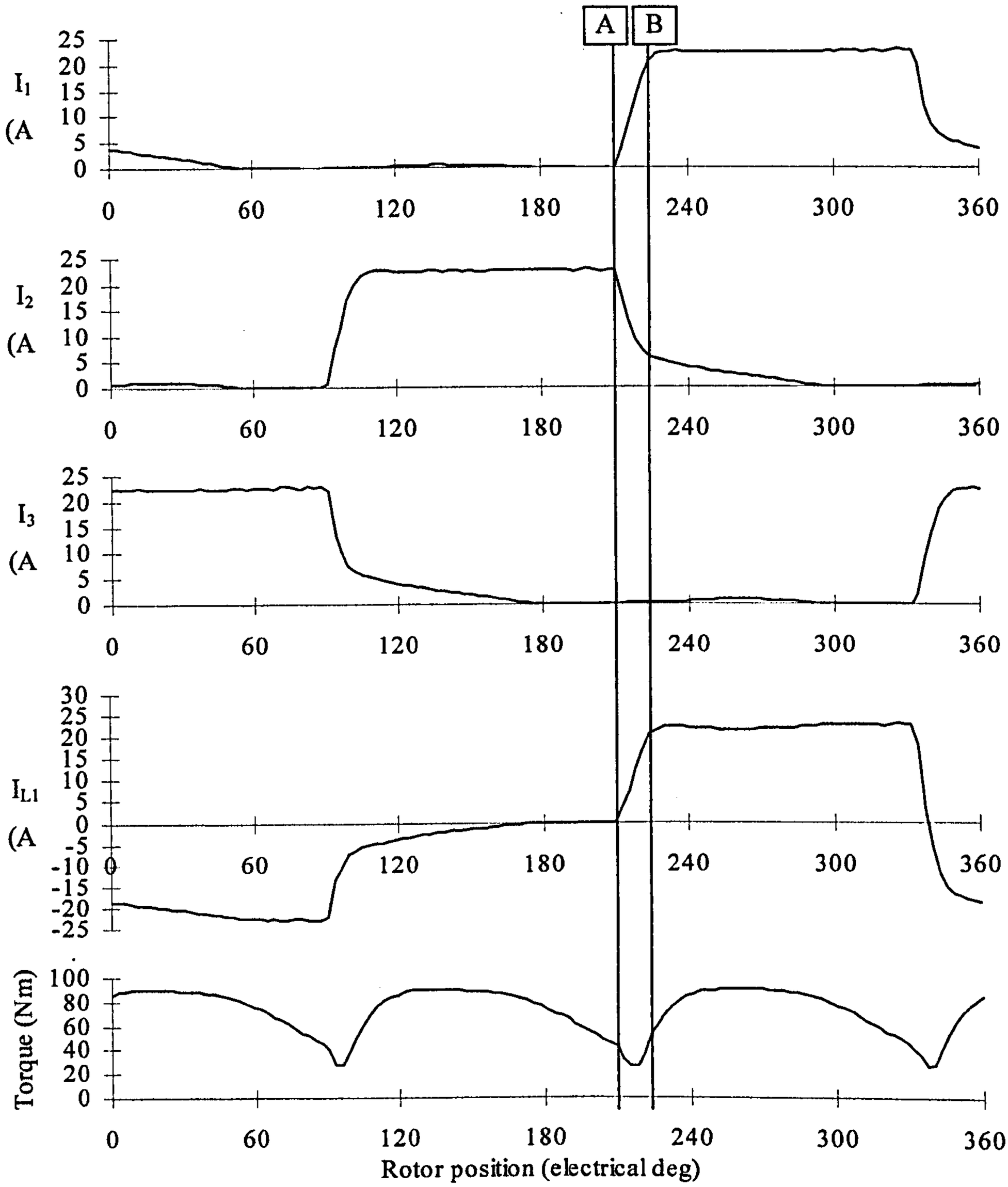

Figure 9.4 Measured phase current, line current and torque waveforms at 200rpm with the DPD inverter. V_{dc}=290V, I_{dem}= 22.4A. Current waveforms measured (sampling every100μs), torque waveform calculated from static torque curves.

Interestingly, the shape of this phase current with its characteristic tail is the same as the equivalent single tooth current of the fully pitched winding machine when run from the same inverter (see Figure 8.6 in Chapter 8). In other words the shape of the torque produced by each stator pole is the same.

In terms of machine performance at low speed there is almost no difference between the DPD and the AHB inverters using the same current demand and the same DC link voltage. This assumes that conduction angle with the AHB inverter is 120° (which achieves the best torque to loss ratio). Torque output with I_{dem}=22.4A was calculated from static torque curves to be 71.4Nm with the AHB inverter, and 72.5Nm with the DPD inverter. Torque per unit copper loss is the same to within less than 0.5%.

9.4.2 High Speed Performance

Performance at base speed is shown in Figure 9.5 and is compared directly with the AHB under the same conditions i.e. I_{dem}=22.4A, V_{dc}=290V, speed=750rpm. Advance angles are optimised in both cases for maximum torque production. The only difference is that conduction angle with the AHB inverter has now been optimised for maximum torque output for a given current demand, which at this speed corresponds to a conduction angle of 175°. This demonstrates what the delta inverter cannot achieve. Under these conditions average torque output for the AHB is 49.5Nm compared to 45Nm for the DPD inverter. Therefore at base speed an extra 10% torque can be achieved with the AHB, but at the same time copper loss increases by 45%. The DPD inverter is in effect forcing the machine to operate in a very efficient manner and will have a slightly reduced power capability for a given peak VA rating.

Figure 9.6 shows operation at twice base speed (1500rpm with V_{dc}=290V). Again advance angles have been optimised in both cases for maximum torque production, as has the conduction angle for the AHB inverter. It can be seen that the waveforms are the same, except that with the AHB inverter can conduct each phase for longer and consequently produce more torque (the phase actually switches off here at approximately 315° compared to 255 ° with the DPD inverter). Torque produced is

27.5Nm compared to the 23.8Nm produced by the DPD connected machine (15% more).

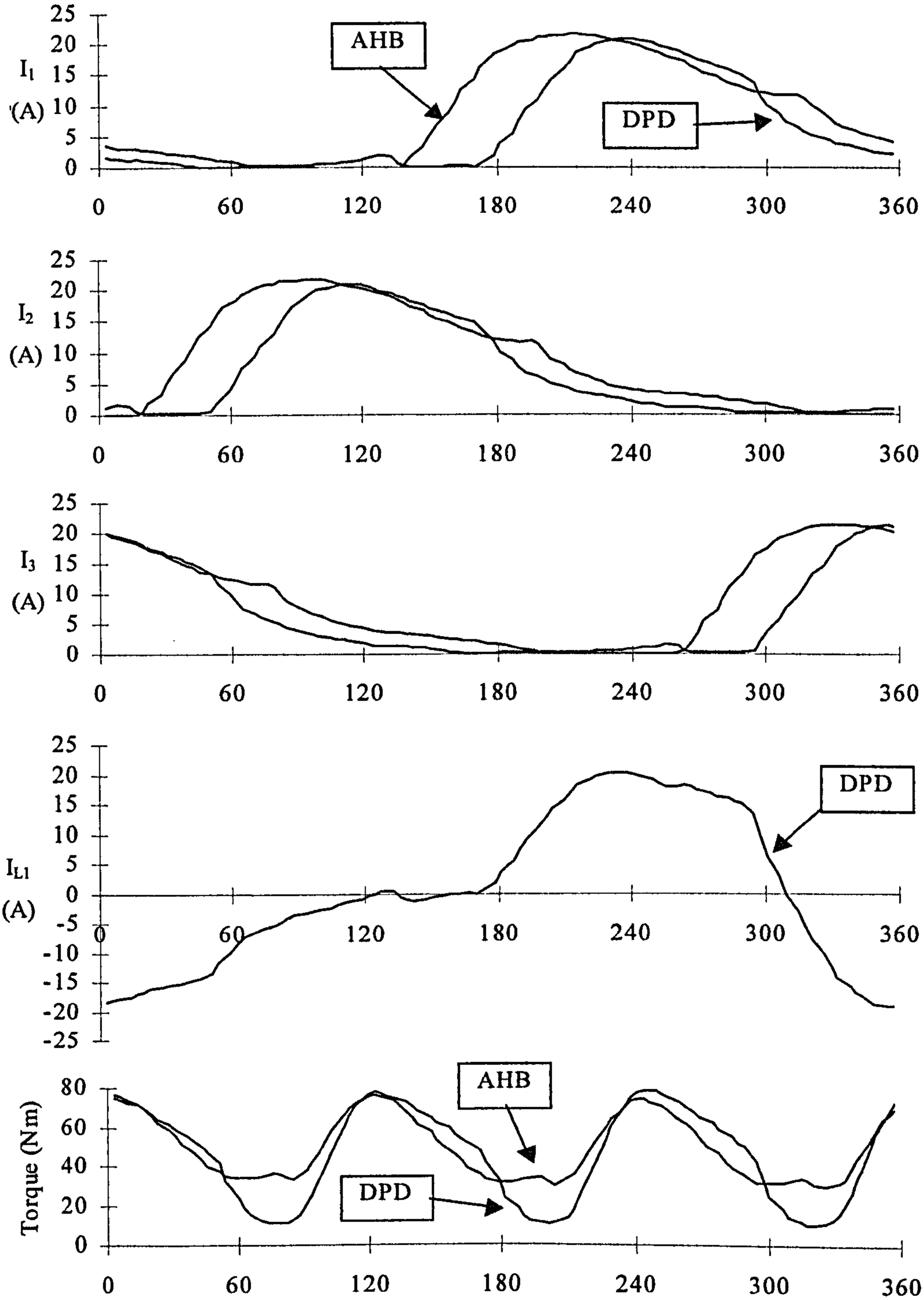

Figure 9.5 A comparison of measured performance at base speed with the AHB and DPD inverters. Phase currents are measured. Line current and torque are calculated (static torque curves). Advance angle optimised for maximum torque in both cases, conduction angle optimised for maximum torque for the AHB.

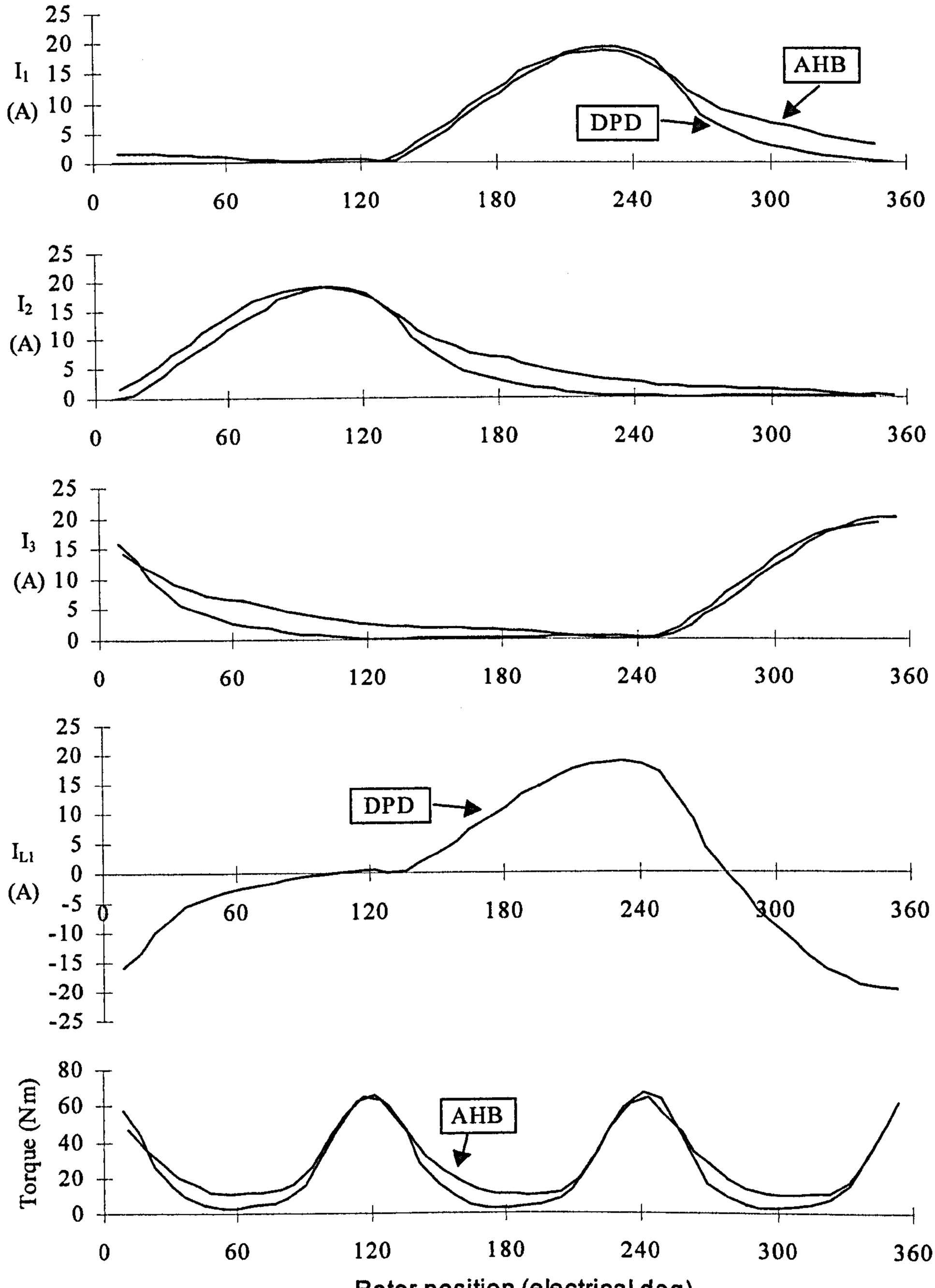

Figure 9.6 A comparison of measured performance at twice base speed, with the AHB and DPD inverters. Phase currents are measured. Line current and torque are calculated (static torque curves). Advance angle optimised for maximum torque in both cases, conduction angle optimised for maximum torque for the AHB.

9.4.3 Torque-Speed Curve

Torque-speed curves for both drives are shown in Figure 9.7 for a current demand of 22.4A and a DC link voltage of 290V. It is possible to control the short pitched winding machine with the AHB in a variety of ways, but the comparison was made in a way which was thought to be as fair as possible. This meant that at low speed conduction angle was limited to 120° – higher angles are possible but the gain in torque is not good compared to extra copper losses, and therefore is not likely to be operated in this manner. If more torque were required it would be better to increase current demand rather than increase conduction angle (from the point of view of both copper loss and inverter loss).

At higher speeds, however, it is advantageous to obtain maximum torque output from the available DC link voltage. At these speeds the machine is in full voltage control and therefore increasing the current demand will have no effect. The only way to increase torque output is to increase conduction angle up towards 180°. The difference in the two curves at high speed therefore essentially demonstrates the difference between 120° and 180° control. Machine copper loss, torque per unit copper loss and torque ripple are shown in Figure 9.8. The advance and conduction angles used are shown in Figure 9.9.

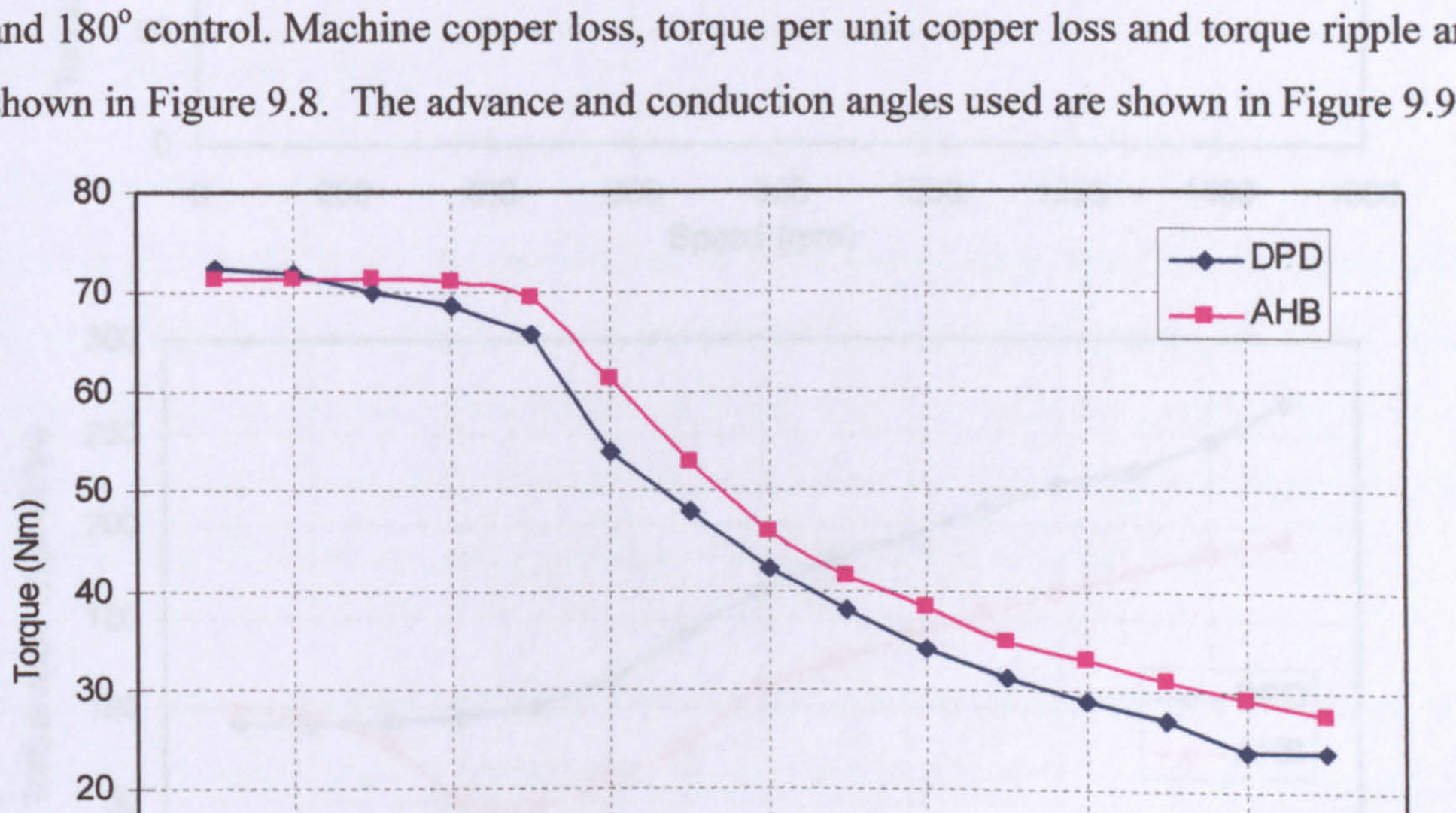

Figure 9.7 Torque-speed curve for the AHB and DPD inverter. I_{dem} = 22.4A, V_{dc} = 290V.

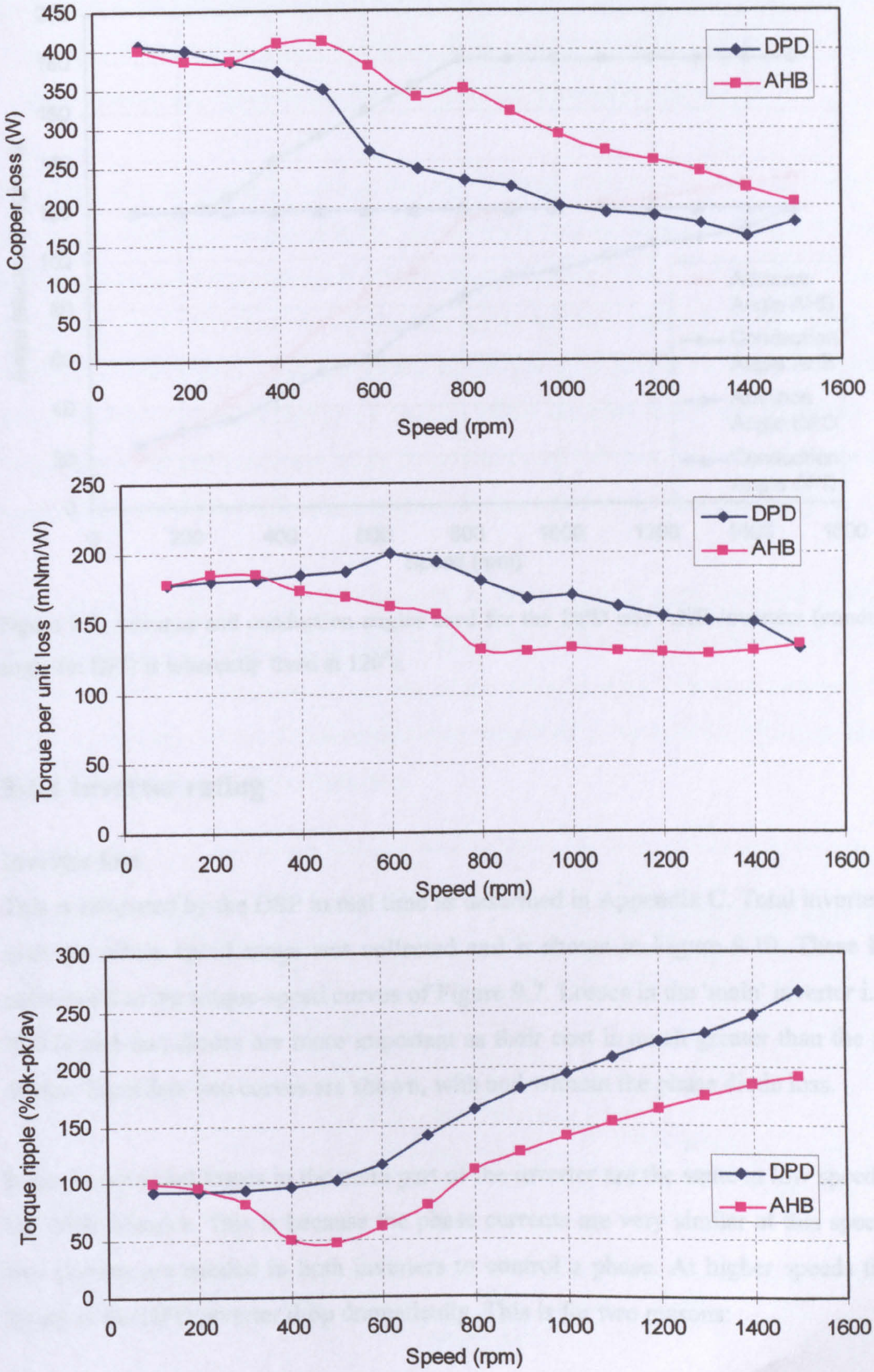

Figure 9.8 Comparison of copper loss, torque per unit copper loss, and torque ripple in the DPD and AHB inverters for the torque shown in Figure 9.7.

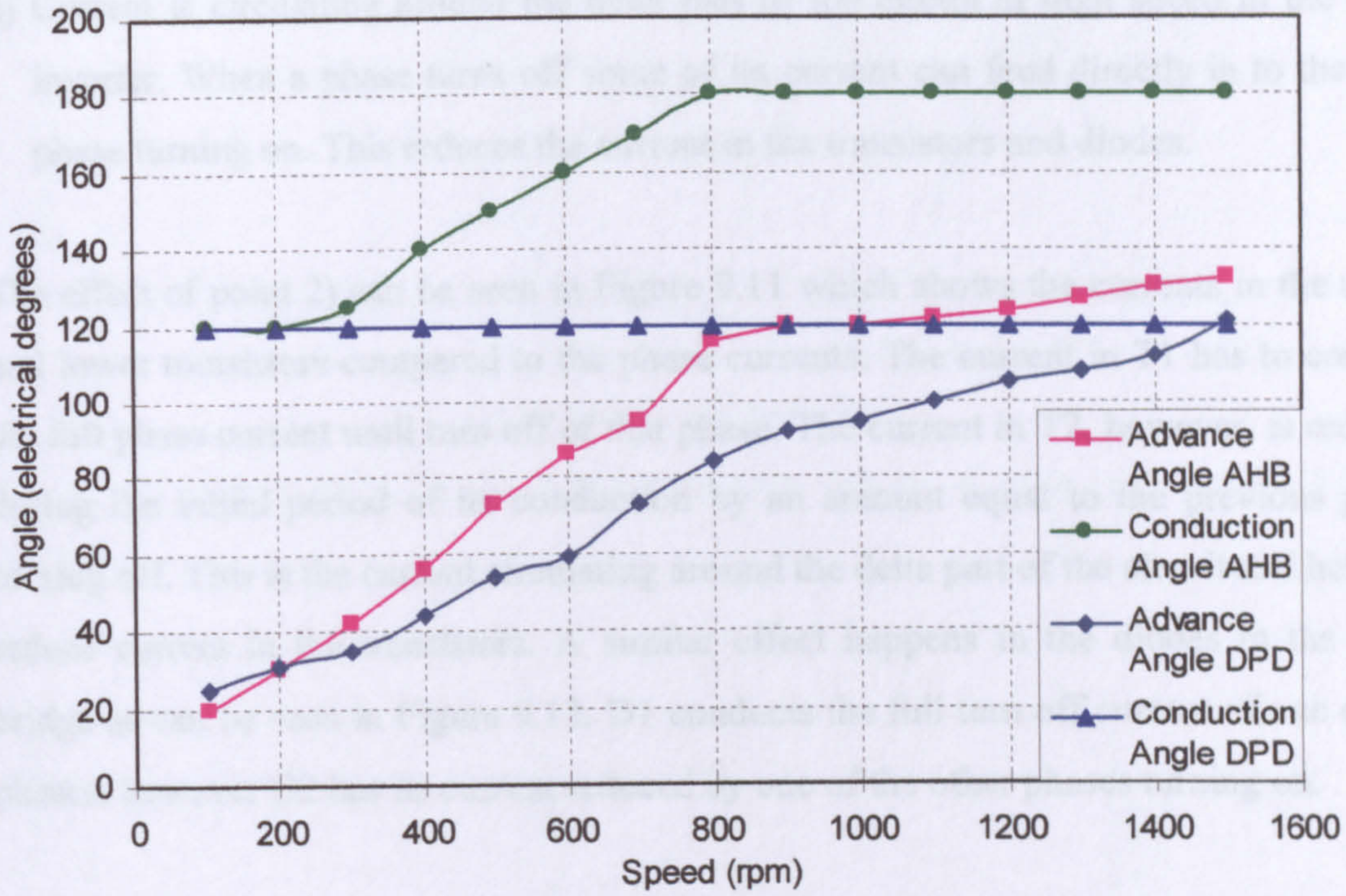

Figure 9.9. Advance and conduction angles used for the DPD and AHB inverters (conduction angle for DPD is inherently fixed at 120°).

9.4.4 Inverter rating

Inverter loss

This is estimated by the DSP in real time as described in Appendix C. Total inverter loss over the whole speed range was collected and is shown in Figure 9.10. These losses correspond to the torque-speed curves of Figure 9.7. Losses in the 'main' inverter i.e. the IGBTs and fast diodes are more important as their cost is much greater than the phase diodes. Therefore two curves are shown, with and without the phase diode loss.

It can be seen that losses in the main part of the inverter are the same at low speed as in the AHB inverter. This is because the phase currents are very similar at this speed and two devices are needed in both inverters to control a phase. At higher speeds though losses in the DPD inverter drop dramatically. This is for two reasons:

1) Conduction angle with the AHB inverter at high speed has been increased to 180° to maximise torque output, thereby increasing inverter losses.

2) Current is circulating around the delta part of the circuit at high speed in the DPD inverter. When a phase turns off some of its current can feed directly in to the next phase turning on. This reduces the current in the transistors and diodes.

The effect of point 2) can be seen in Figure 9.11 which shows the currents in the upper and lower transistors compared to the phase currents. The current in T1 has to conduct the full phase current until turn off of that phase. The current in T2, however, is reduced during the initial period of its conduction by an amount equal to the previous phase turning off. This is the current circulating around the delta part of the circuit and helps to reduce current in the transistors. A similar effect happens in the diodes in the main bridge as can be seen in Figure 9.12. D1 conducts the full turn off current of one of the phases, however D2 has its current reduced by one of the other phases turning on.

If the motor direction is reversed then it is the other pairs of transistors and diodes that have their current reduced. Therefore if bidirectional rotation is needed, silicon sizing cannot be reduced (compared to the use of the AHB inverter if it were controlled with 120° conduction). The only advantage here would be a possible reduction in heatsink size due to the reduction in overall loss.

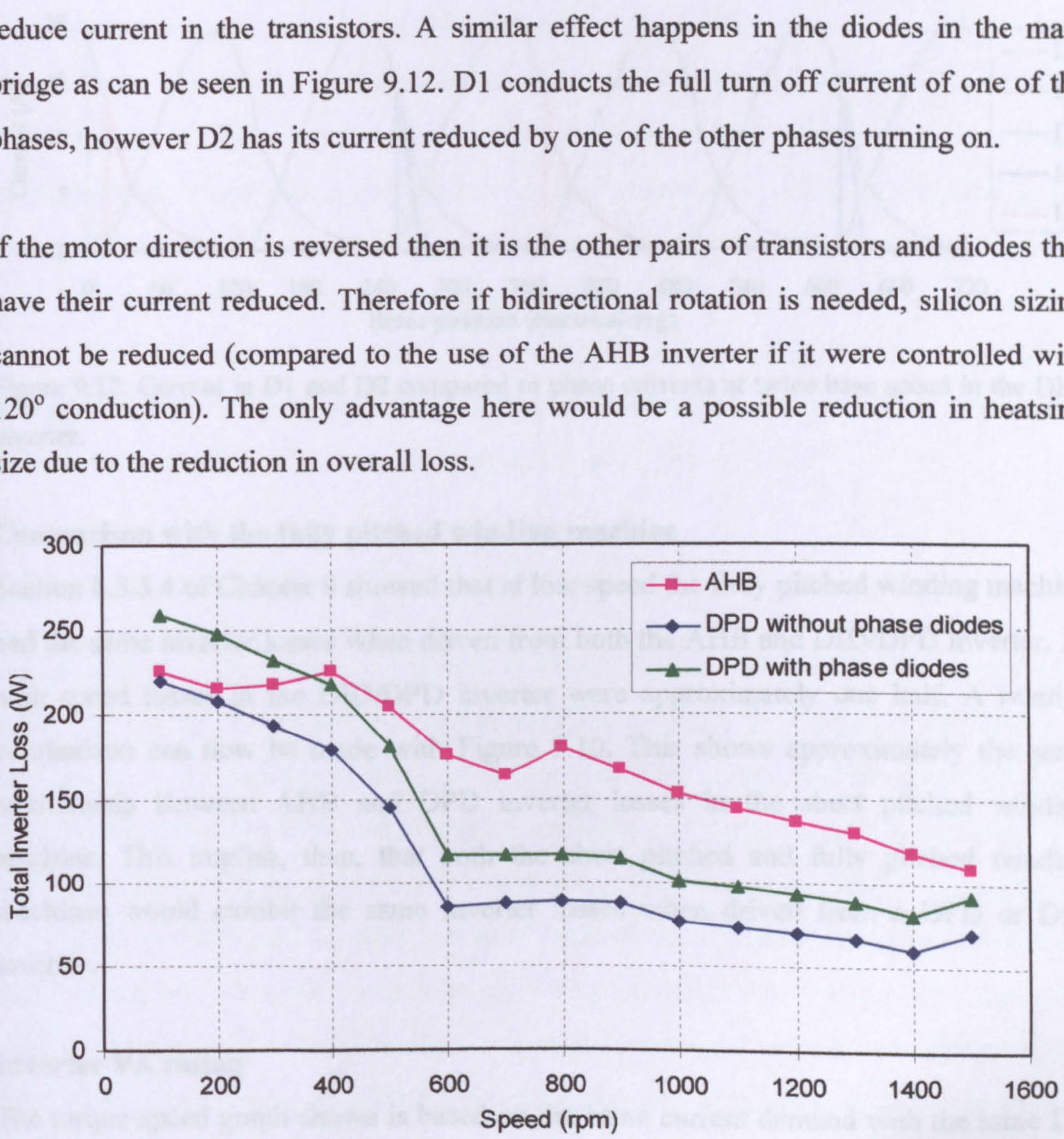

Figure 9.10 Total inverter losses against speed, I_{dem} = 22.4A, V_{dc} = 290V, IRGPH50KD2 IGBT. Switching loss based on 600V. Losses for the delta are shown both with and without phase diode loss.

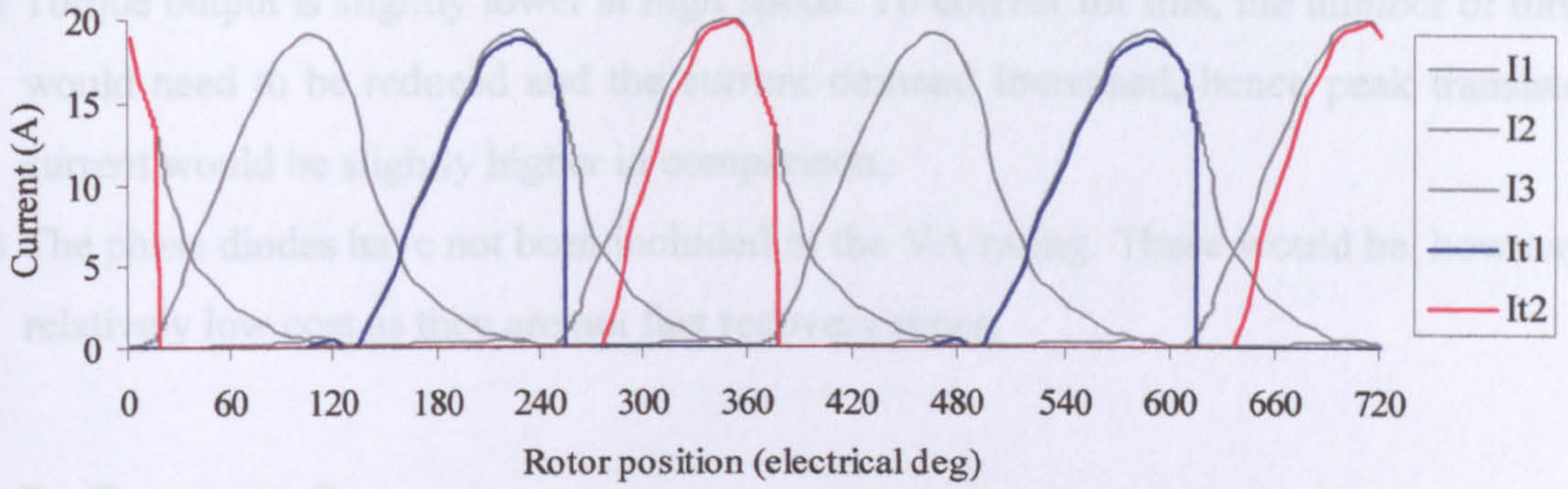

Figure 9.11. Current in T1 and T2 compared to phase currents at twice base speed in the DPD inverter.

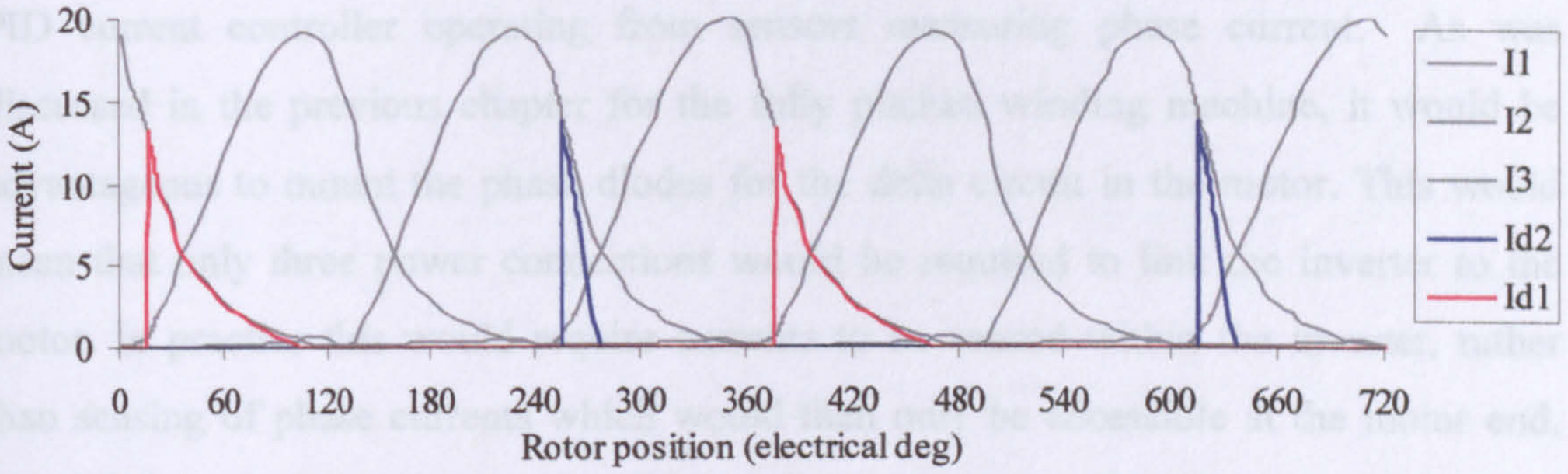

Figure 9.12. Current in D1 and D2 compared to phase currents at twice base speed in the DPD inverter.

Comparison with the fully pitched winding machine

Section 8.3.3.4 of Chapter 8 showed that at low speed the fully pitched winding machine had the same inverter losses when driven from both the AHB and DID/DPD inverter. At high speed losses in the DID/DPD inverter were approximately one half. A relative comparison can now be made with Figure 9.10. This shows approximately the same relationship between AHB and DPD inverter losses in the short pitched winding machine. This implies, then, that both the short pitched and fully pitched winding machines would exhibit the same inverter losses when driven from a DPD or DID inverter.

Inverter VA rating

The torque-speed graph shown is based on the same current demand with the same DC link voltage. Therefore peak transistor current and voltage is the same in both inverters. There are, however, two points to note with the DPD inverter:

1) Torque output is slightly lower at high speed. To correct for this, the number of turns would need to be reduced and the current demand increased, hence peak transistor current would be slightly higher in comparison.
2) The phase diodes have not been included in the VA rating. These would be, however, relatively low cost as they are not fast recovery types.

9.5 Current Sensors

The waveforms shown in the previous sections of this chapter were achieved using a PID current controller operating from sensors measuring phase current. As was discussed in the previous chapter for the fully pitched winding machine, it would be advantageous to mount the phase diodes for the delta circuit in the motor. This would mean that only three power connections would be required to link the inverter to the motor. In practice this would require currents to be sensed within the inverter, rather than sensing of phase currents which would then only be accessible at the motor end. The schemes developed to achieve this are line currents sensing, inverter leg sensing, and DC link current sensing. Over the next few sections the impact of the schemes on current controllability, and hence performance, will be discussed.

9.5.1 Control with Line Current Sensors

An inspection of the current waveforms in Figure 9.4 reveals that the line current I_{L1} is equal to I_1 during the desired conduction period of phase 1. I_{L1} is equal to the difference between I_1 and I_3, and during this period I_3 is zero. This means that control of the phase currents can indeed be achieved simply by sampling of the appropriate line current. This has been demonstrated on the test rig and results are shown in Figure 9.13. Current waveforms are identical to those achieved with phase current sensing throughout the speed range, and therefore overall motor drive performance is unaffected by using this method. The additional benefit is that only two line current sensors are required as the third line current can be calculated. As with phase current sensing, isolation is required between the sensors and the controller.

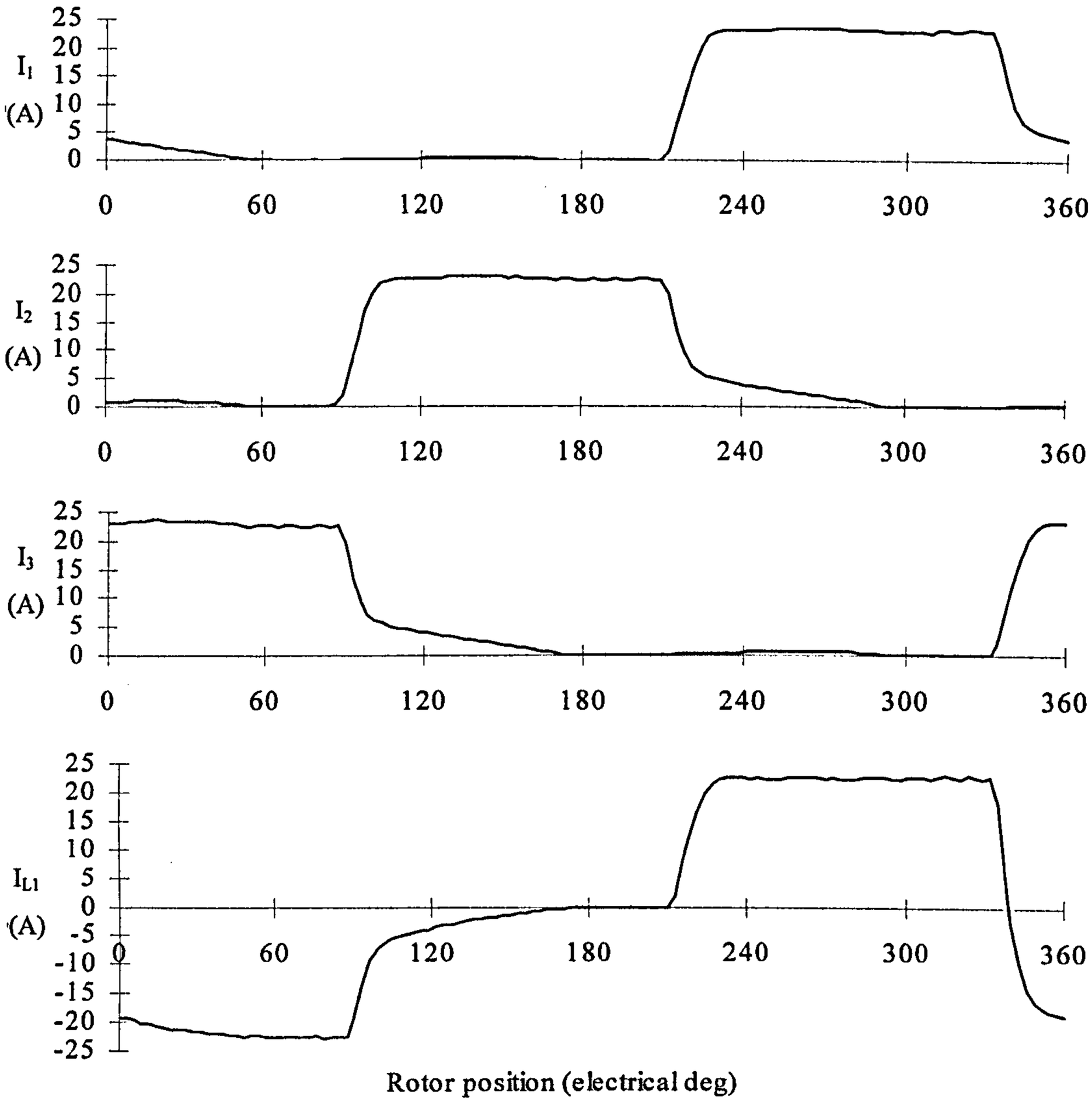

Figure 9.13 Measured current waveforms with current control using line current sensors.

9.5.2 Control with Shunt Resistors in Each Inverter Leg

As with the fully pitched winding machine, the timing of current sampling with inverter leg shunts depends on the position of the shunts, as well as the direction of rotation of the machine.

Example A. Machine turning with phase sequence 1-2-3

Consider an example with phase 1 conducting, phase 3 turning off and phase 2 already off. Here transistors T1 and T4 are on, and line current I_{L2} needs to be sampled to control the phase currents as $I_{L2}=I_2-I_1=I_1$. The current flow in the inverter is shown in Figure 9.14 for this situation. I_{L2} can be measured with a shunt resistor in series with T4.

This means that in this direction of rotation control of the machine can be achieved with shunts resistors referenced to the negative of the DC link. Current sampling can take place in this 'on' state as well as one of the two freewheel states i.e. with T2, T4, T6 on.

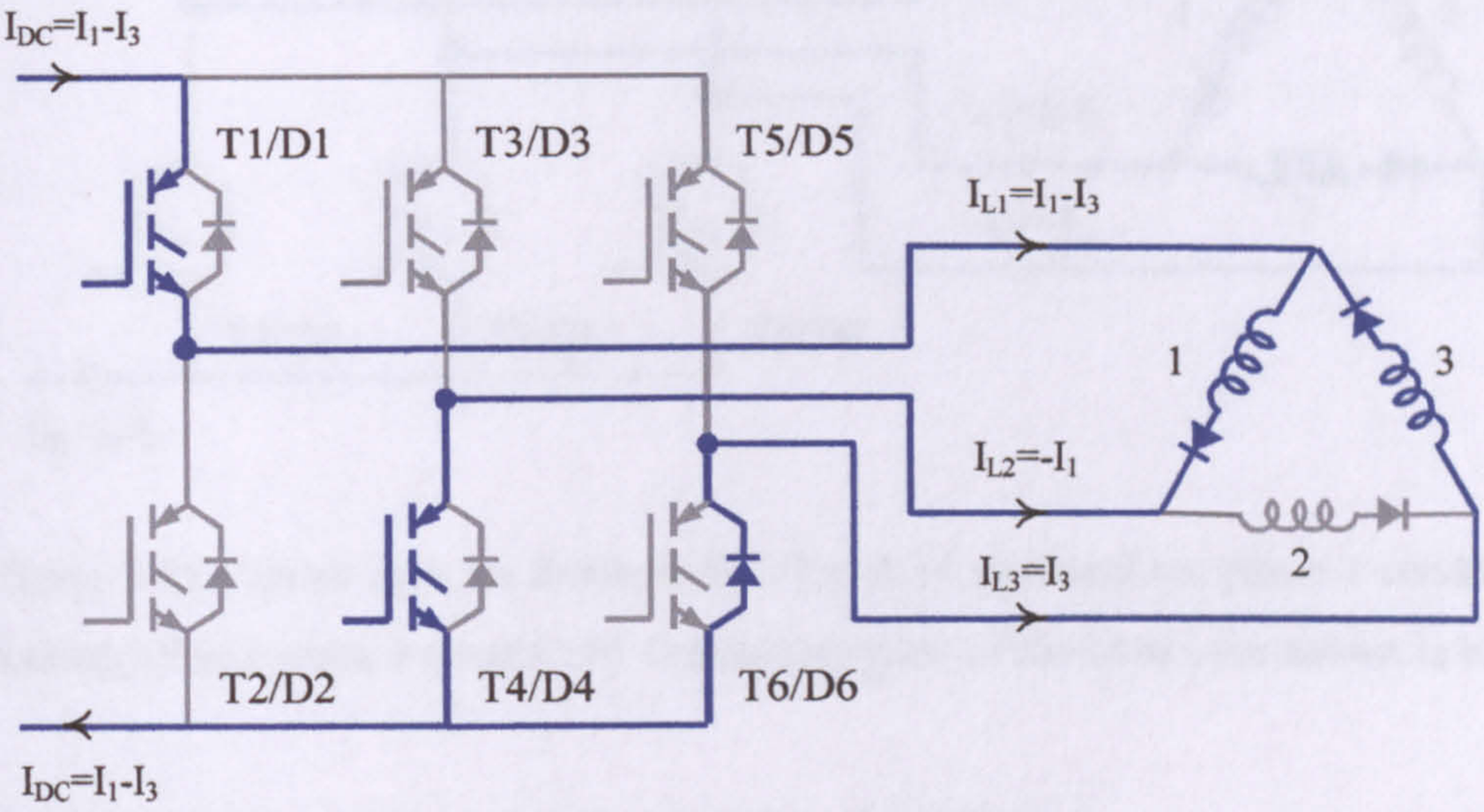

Figure 9.14 Current flow for Example A. T1 and T4 switched on, phase 1 conducting, phase 3 turning off and phase 2 already off. Conducting parts of the circuit are shown in blue.

Example B. Machine turning with phase sequence 1-3-2

With the machine rotating in this direction, phase 1 is conducting, phase 2 turning off and phase 3 is already off. This is shown on Figure 9.15. This time line current I_{L1} needs to be sampled as $I_{L1}=I_1-I_3=I_1$. Unfortunately sampling of this current requires shunt resistors to be placed in the top half of the inverter legs. If shunt resistors were to be placed in the lower half of the inverter legs then sampling of the required current could only take place during of the freewheel states i.e. with T2, T4, T6 on.

The result is that if bidirectional rotation is required then either shunts would be required in both the top and bottom half of the inverter legs, or alternatively current sampling would have to be restricted to just one of the freewheeling states. The latter would mean that it would be impossible to apply full voltage to a winding continuously at the commutation points and sample currents at the same time. This may therefore affect current controllability and consequently machine performance.

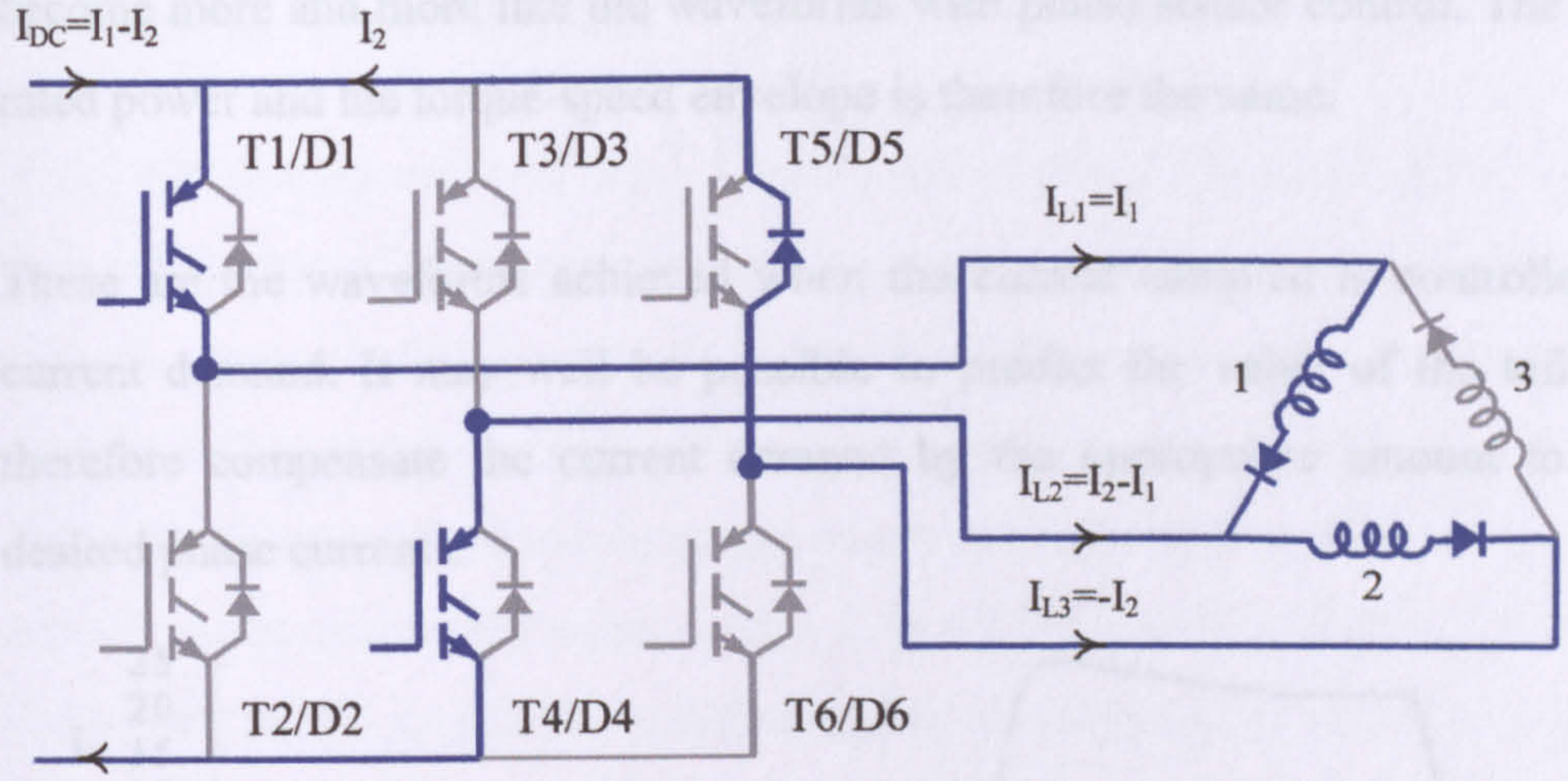

$I_{DC}=I_1-I_2$

Figure 9.15 Current flow for Example B. T1 and T4 switched on, phase 1 conducting, phase 2 turning off and phase 3 already off. Conducting parts of the circuit are shown in blue.

9.5.3 Control with a DC Link Shunt Resistor

Consider again the examples shown in Figure 9.14 and 9.15. The current flow in the DC link is shown with transistors T1 and T4 on i.e. the state that applies a positive voltage to phase 1. The current flowing in the DC link in both cases is the difference between the conducting phase (phase 1) and the phase turning off. The phase current I_1 cannot therefore be directly measured. Additionally, no current sample at all can be made in either of the freewheel states as no DC link current flows.

The current waveforms shown in Figure 9.15 show what happens when this DC link current is used as the controlled parameter and controlled to a constant value. The effect is that the current in the phase turning off is added to the current in phase 1. Notice that the current I_1-I_2 (=-I_{L2}) is now flat topped during the period that phase 1 is on, as that is the parameter now being controlled.

The overall effect on the power electronic rating and the motor efficiency are, in fact, quite small and it is quite realistic to control this inverter drive with this single current sensor. Current demand for the same torque is reduced from 22.4A to 20.9A, however peak device current is in fact 24.7A due to the overshoot of the phase current as it turns on. As the machine approaches base speed and beyond the phase current waveforms

become more and more like the waveforms with phase sensor control. The efficiency at rated power and the torque-speed envelope is therefore the same.

These are the waveforms achieved when the current sampled is controlled to a fixed current demand. It may well be possible to predict the value of the tail current and therefore compensate the current demand by the appropriate amount to achieve the desired phase currents.

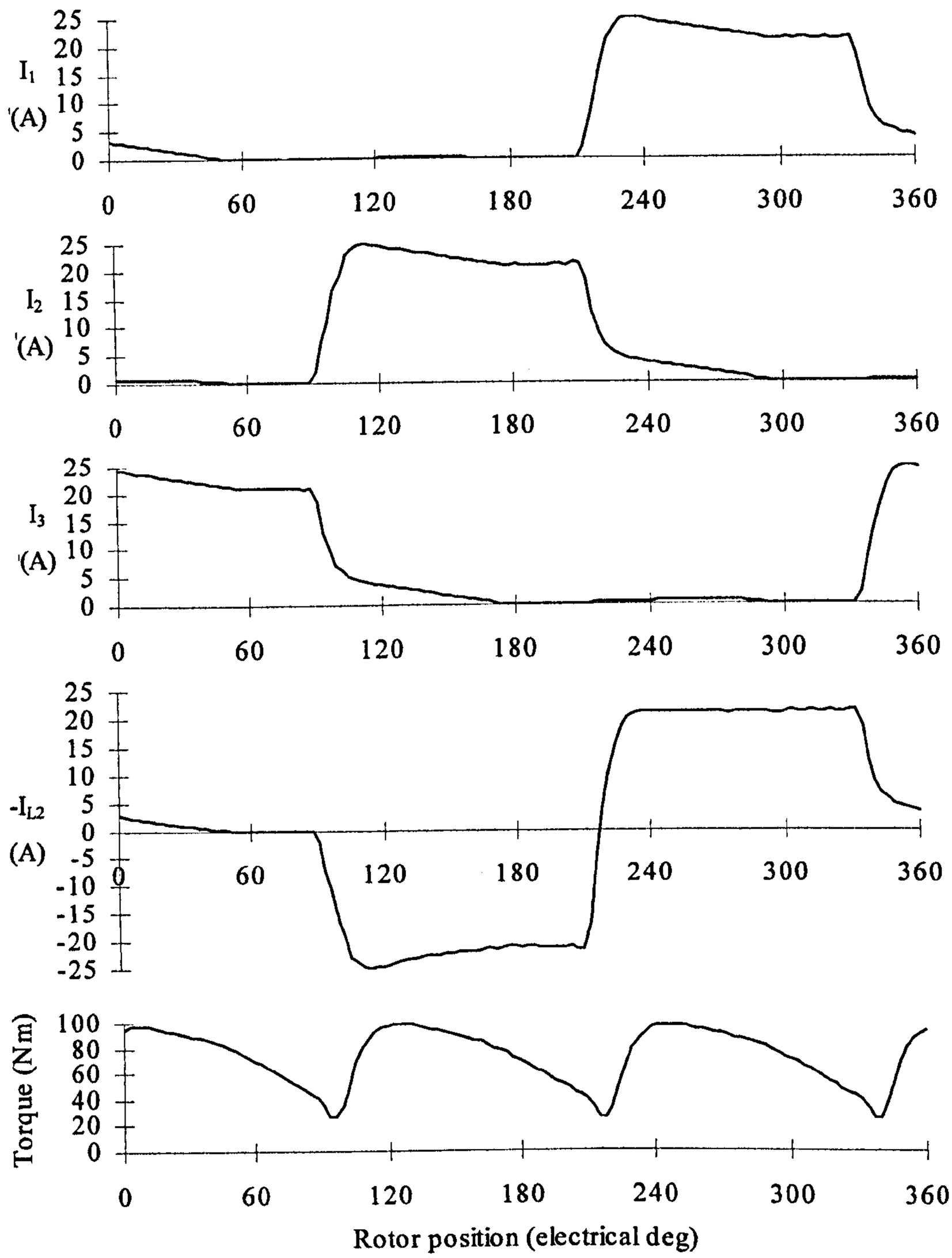

Figure 9.16. Short pitched winding waveforms at 200rpm with one DC link sensor with I_{dem}=20.9A, V_{dc}=290V. Phase currents I_{123} (measured), line current I_{L2}, total machine torque (calculated).

9.6 Dead Time Effects

The DPD inverter requires dead time control to avoid "shoot-through" in the inverter legs. The effect of this dead time on the current waveforms is shown in Figure 9.17. Here the current is being controlled with phase current sensors and a dead time of 2μs, and the effect occurs because of an unwanted switching state during this dead time. Consider an example shown between points A and B below. Phase 1 is under current control at the demanded value, phase 2 is switching off and phase 3 should not be conducting at all. As PWM current chopping is taking place, the switching state cycles between the 1st, 3rd and 4th states shown in Table 9.1 i.e. between the "on" state and the two freewheel states. The problem occurs when moving from the 1st state to the 4th state. Because of the dead time there will be a period when only T4 is on. With current flowing in phases 1 and 2 diodes D2 and D5 conduct, applying positive volts to phase 3.

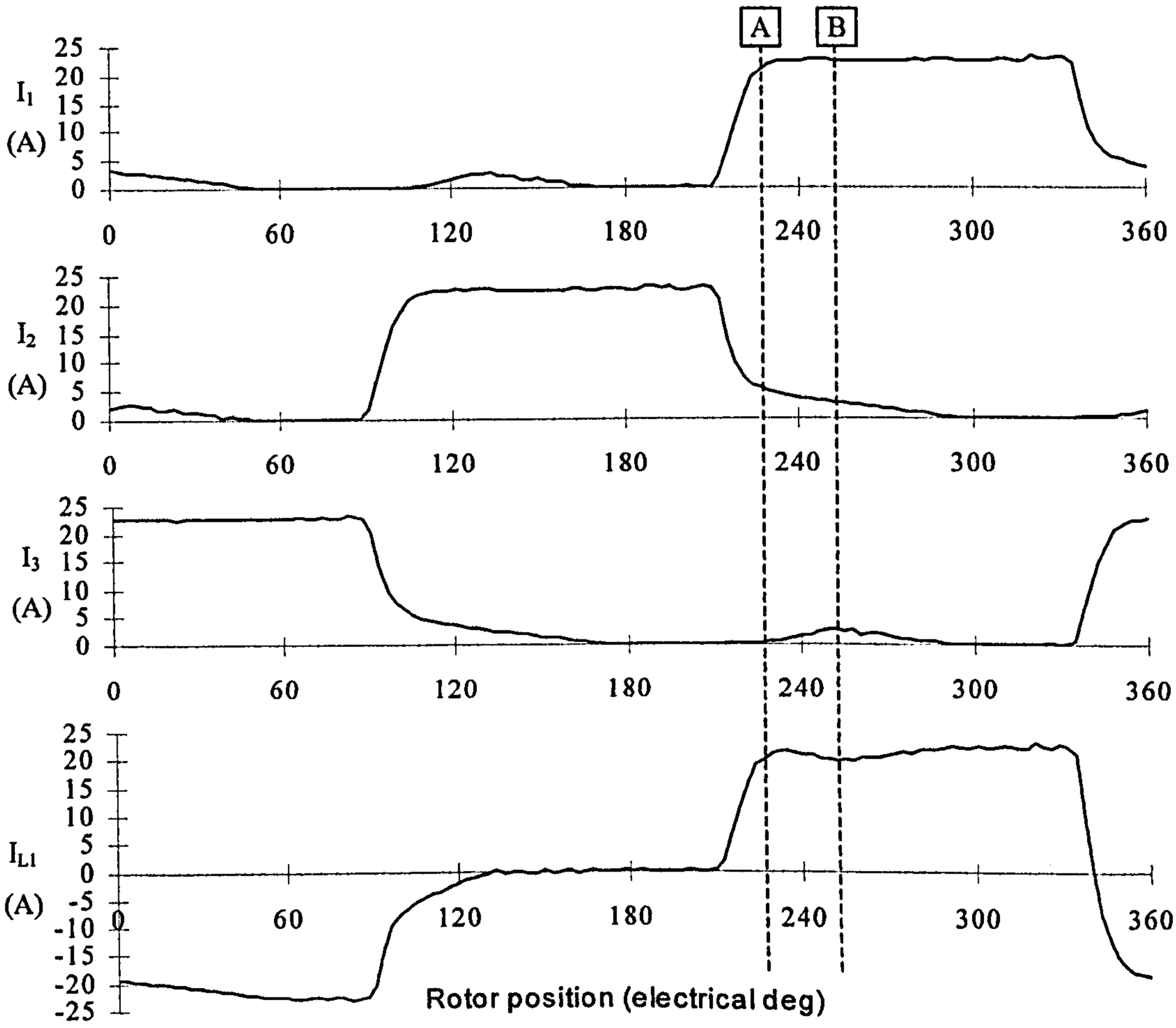

Figure 9.17 The effect of 2μs of dead time. I_{dem}=22.4A, V_{dc}=290V, control with phase current sensing.

This is the undesired state that results in phase 3 conducting with a small amount of current during its "off" period. The current rises until it becomes equal to that in phase 2 (point B in Figure 9.17). The problem becomes self-limiting from this point onwards as, with the currents equal, D5 no longer conducts and a voltage is no longer applied to phase 3. Consequently phase 2 and phase 3 currents fall to zero as one. Inevitably negative torque is generated from this current but the amount is small, as torque is proportional to the square of the current in this unsaturated region of the machine. A scheme, however, very similar to that of the fully pitched winding machine (Appendix D) was developed that overcame the problem. The current waveforms presented throughout this chapter include this scheme and demonstrate that the effect can be eliminated with relatively simple compensating terms in the PWM generator.

9.7 Other "Delta" Type Inverter Topologies

Both the "Delta with Interphase Diodes" (DID) and the "Asymmetric Half Bridge with Interphase Diodes" inverter topologies that were described for the fully pitched winding machine can be used for the short pitched winding machine. A detailed investigation on the test rig however was not carried out, and therefore no results are presented in this chapter.

9.8 Sinusoidal Control of Line Currents

Control of line currents with sinusoidal demands was investigated with the aim of making the control method, as well as the inverter topology, as similar as possible to AC machines. Sinusoidal line currents would normally lead to sinusoidal phase currents, but the presence of the phase diodes means this waveform is offset with a net DC current, hence leading to positive torque production in the short pitched winding SR machine.

Control Strategy

Each line current is sampled and controlled independently to a sinusoidal shape with a PID controller. This differs from the strategy used so far in this chapter where the switch state of the whole bridge is controlled on the basis of one sampled current. Measured phase and line currents are shown in Figure 9.18 with a peak line current demand of 22.4A. This is the same current demand used before with square shaped control. Line

current I_{L1} is equal to I_1-I_3 and, as expected, the phase currents are essentially offset sinusoidal currents. An exact offset sinusoid cannot be produced because the line controller is only able to control the difference between two phase currents, rather than each phase current itself. Unlike induction machines, the variation in phase inductance with position ensures the phase current is not exactly sinusoidal.

The torque produced from phase 1 is also shown in Figure 9.18, together with the total machine torque. This shows that very little negative torque is produced, even though the conduction period has become very large (approximately 300° at this speed). The shape of the current also ensures acoustically quiet operation, as the rate of change of flux in the stator poles rise and fall in a smooth fashion. Sudden changes in flux linkage experienced with square current demands, particularly at turn off, are known to contribute significantly to acoustic noise.

At higher speeds both the line and phase currents become very non-sinusoidal, and these are shown in Figure 9.19 at base speed. This is also reflected in the torque-speed characteristic, which is shown in Figure 9.20 compared to the DPD inverter with square phase current control using the same peak current demand.

Torque per unit copper loss against speed is shown in Figure 9.21 compared to square current control. Copper loss is generally worse for the same torque because the conduction angle is so large. Either small or negative amounts of torque are produced at the start and end of this conduction period, while reasonable amounts of copper loss are being generated. This could potentially be improved slightly by designing the machine to have a more sinusoidal variation of flux linkage with position, as with the prototype design of the fully pitched winding machine described in Chapter 4.

Inverter losses are shown in Figure 9.22. While generally quite similar to square shaped control for the same peak current demand, losses are slightly lower at low speed with sinusoidal control. Figure 9.23 compares torque ripple over the speed range. The benefit of the large conduction angle with sinusoidal control can be seen at low speed, where torque ripple is now much lower.

Inverter rating, then, in terms of both inverter losses and peak VA is very similar to square shaped control, although some increase in both would be necessary to match the torque-speed curves.

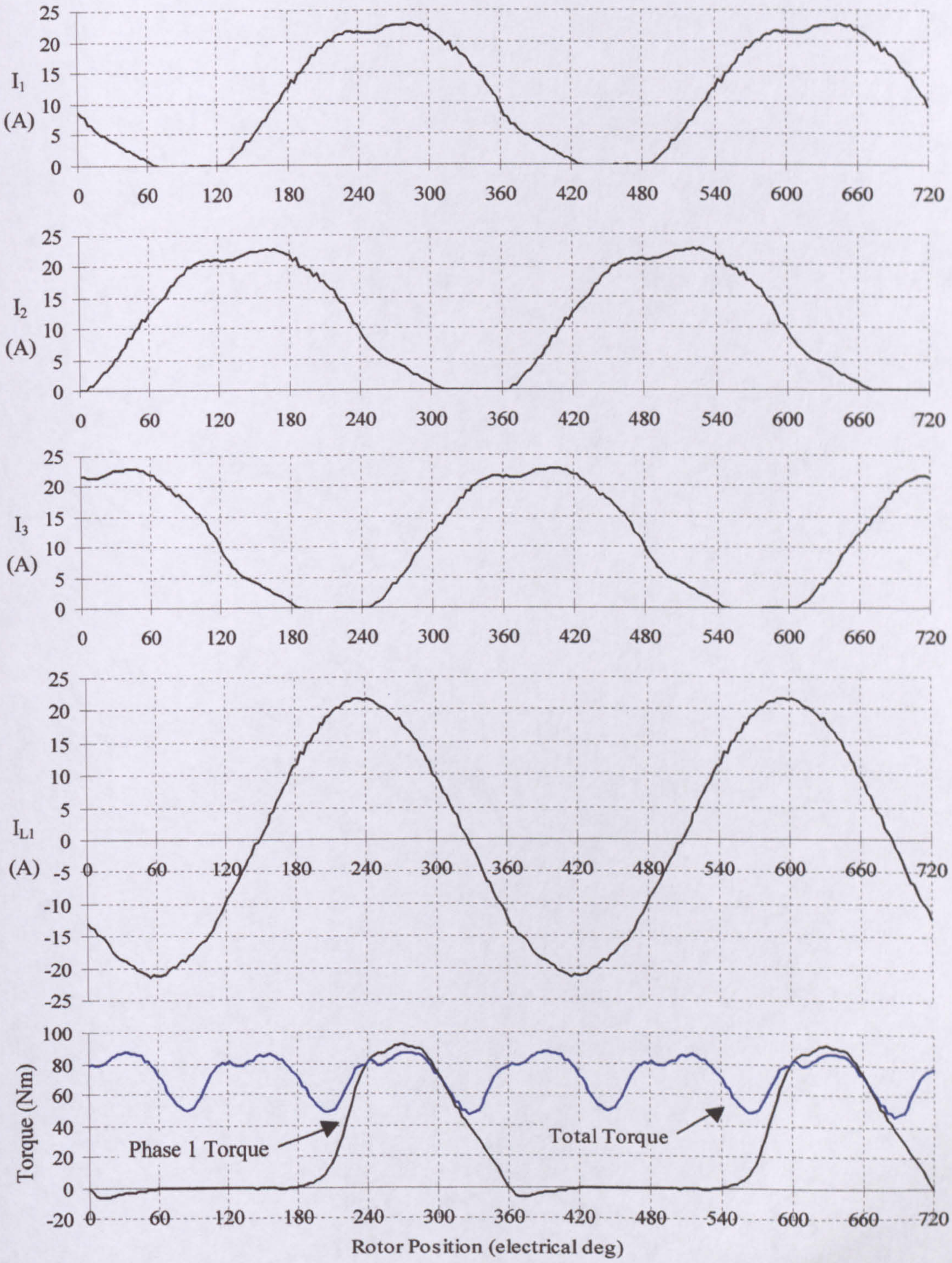

Figure 9.18 Measured phase currents I_{123}, line current I_{L1}, torque due to phase 1 and total torque for the DPD inverter with $I_{dem} = 22.4A$, $V_{dc} = 290V$, speed = 200rpm.

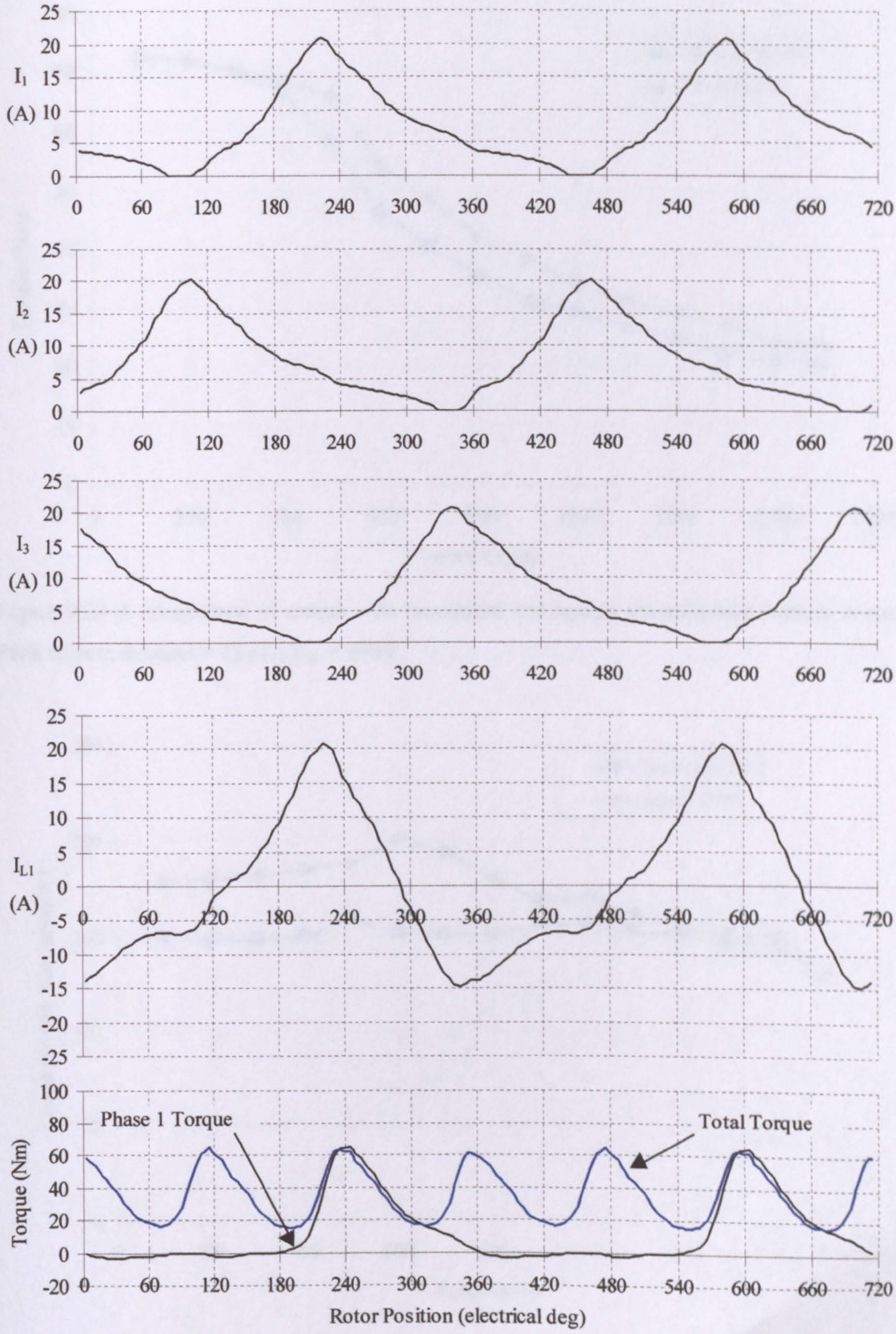

Figure 9.19 Measured phase currents I_{123}, line current I_{L1}, torque due to phase 1 and total torque for the DPD inverter with I_{dem} = 22.4A, V_{dc} = 290V, speed = 750rpm (base speed).

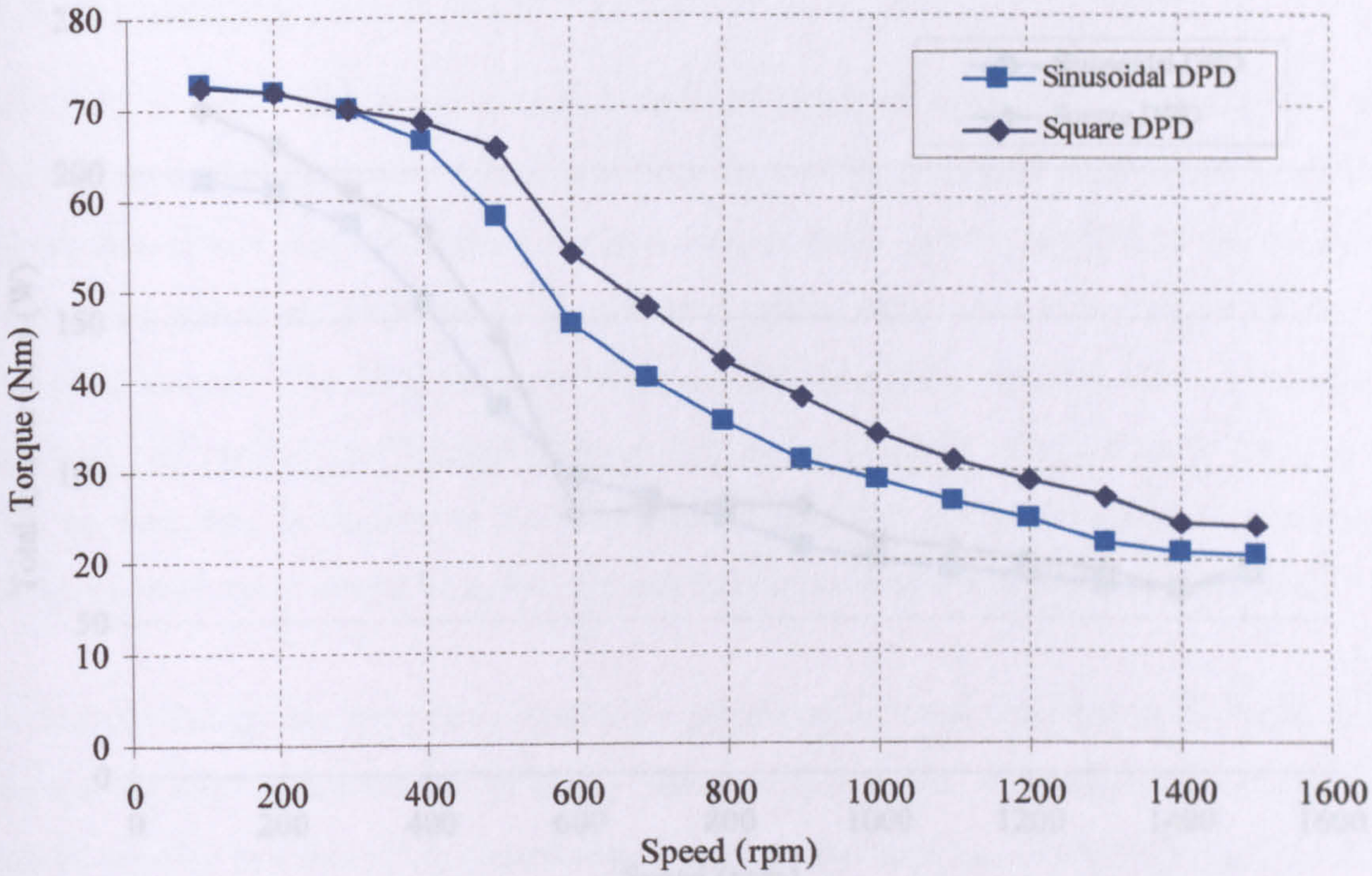

Figure 9.20 A comparison of torque with sinusoidal and square shaped phase current control. Peak current demand = 22.4A, V_{dc} = 290V.

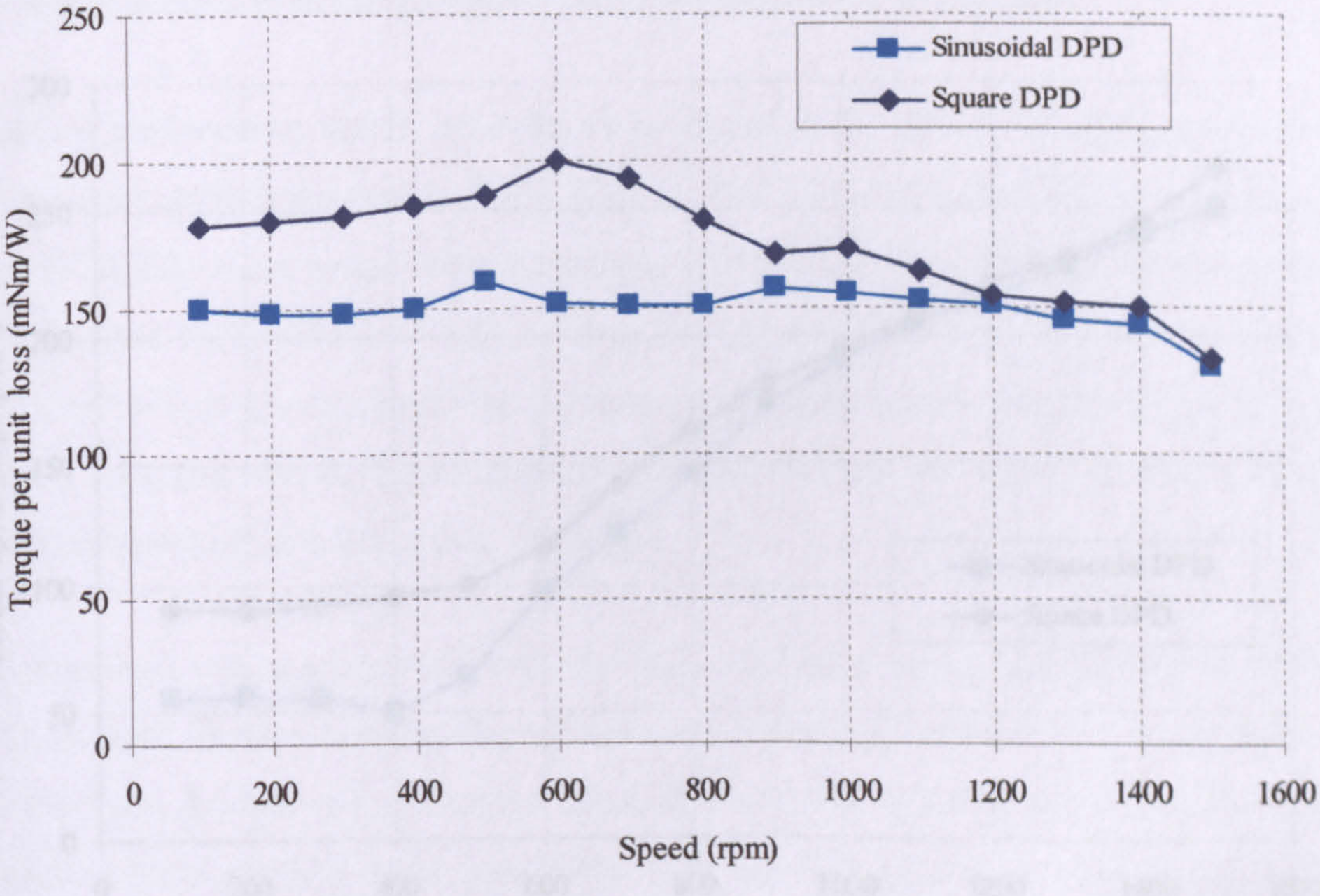

Figure 9.21 Torque per unit copper loss for the torque produced in Figure 9.20.

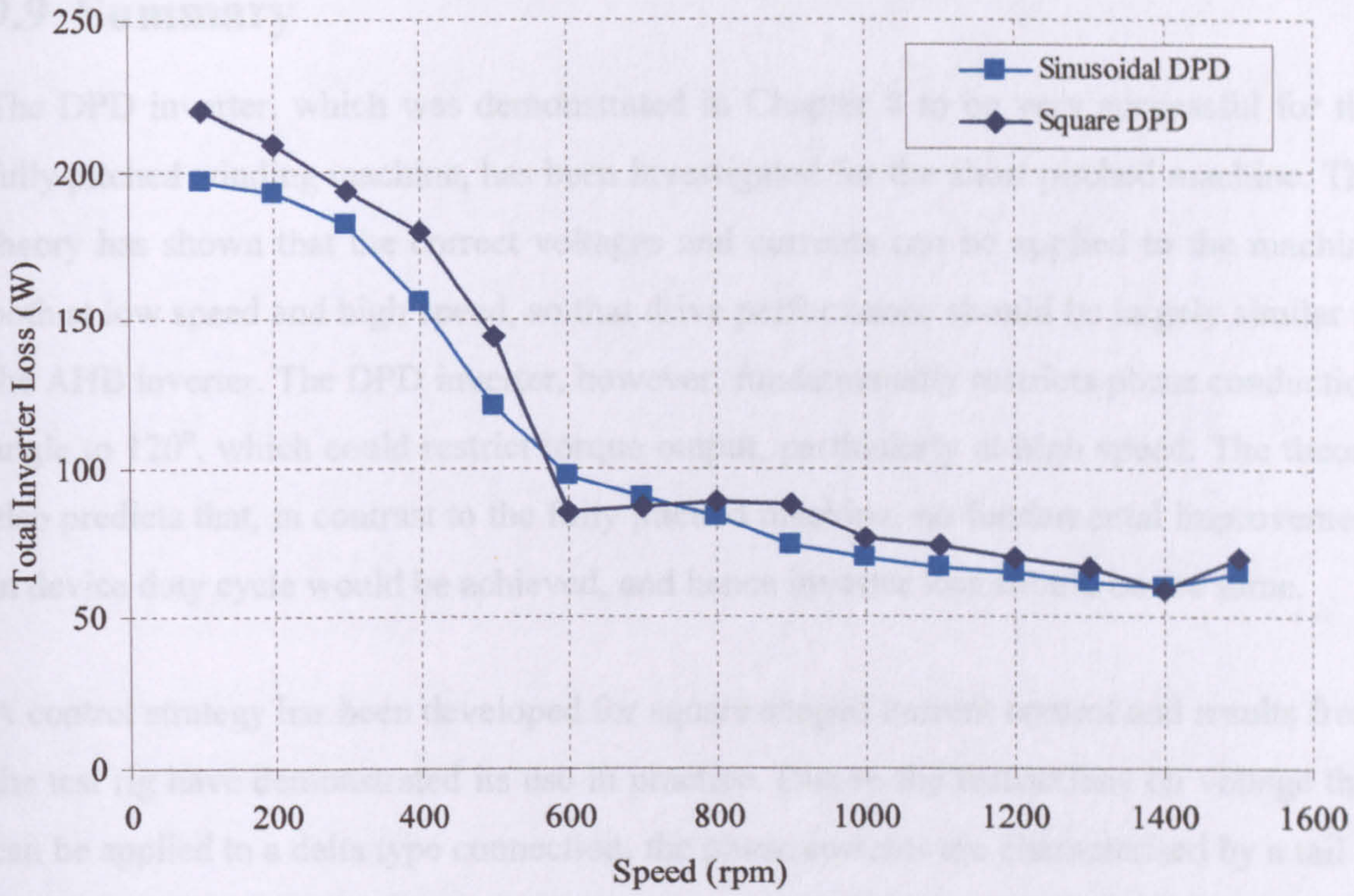

Figure 9.22 Total inverter loss (not including phase diodes) for the torque produced in Fig. 9.20.

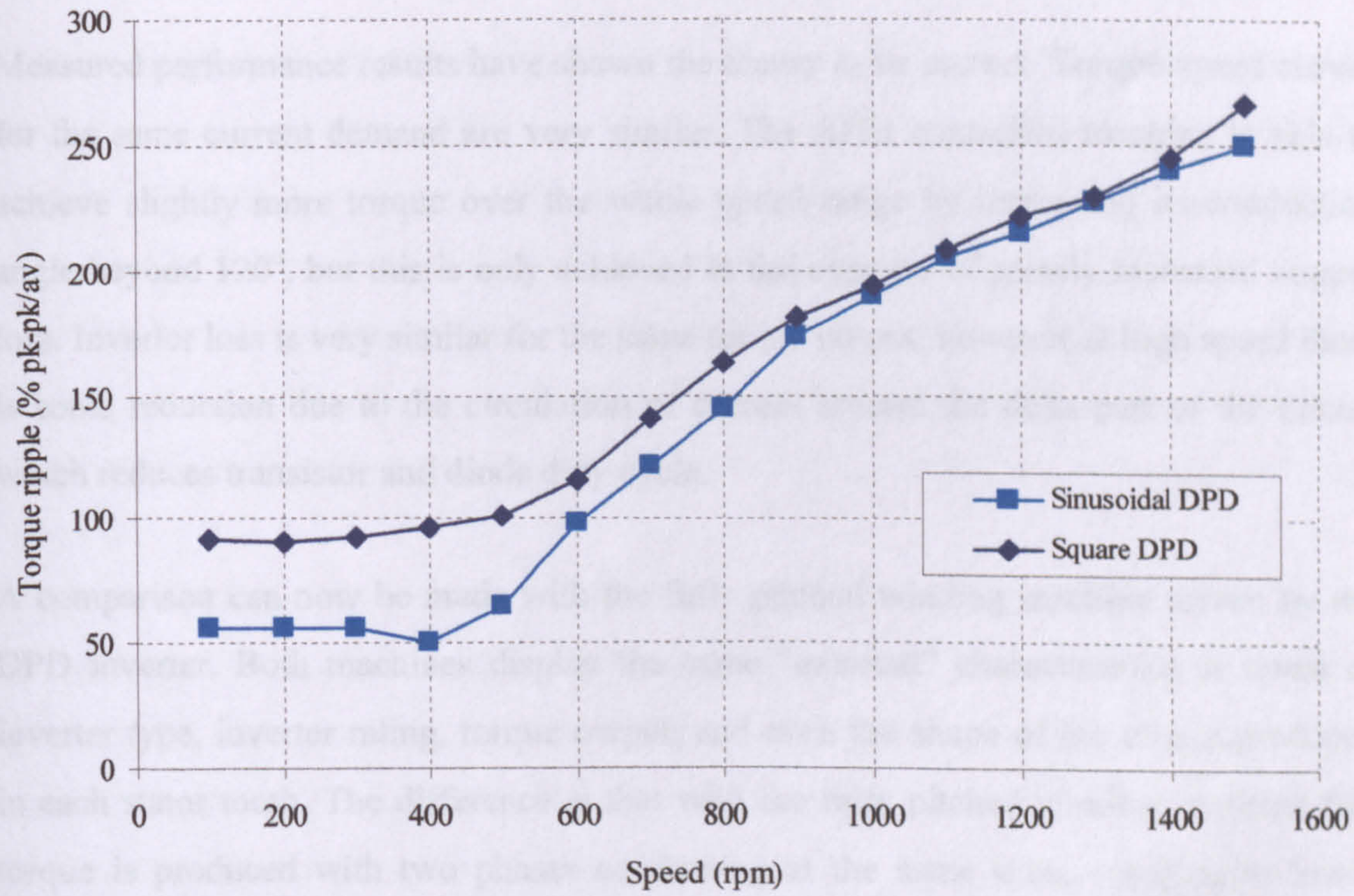

Figure 9.23 Comparison of torque ripple for the torque produced in Fig. 9.20.

9.9 Summary

The DPD inverter, which was demonstrated in Chapter 8 to be very successful for the fully pitched winding machine, has been investigated for the short pitched machine. The theory has shown that the correct voltages and currents can be applied to the machine both at low speed and high speed, so that drive performance should be largely similar to the AHB inverter. The DPD inverter, however, fundamentally restricts phase conduction angle to 120°, which could restrict torque output, particularly at high speed. The theory also predicts that, in contrast to the fully pitched machine, no fundamental improvement in device duty cycle would be achieved, and hence inverter loss should be the same.

A control strategy has been developed for square shaped current control and results from the test rig have demonstrated its use in practice. Due to the restrictions on voltage that can be applied to a delta type connection, the phase currents are characterised by a tail at turn off of a phase. The same effect was seen with the fully pitched winding machine. Interestingly, the shape of this phase current is the same as that of the equivalent single tooth current in the fully pitched winding machine with the DPD inverter. This means that both machines produce the same shaped torque in each stator tooth.

Measured performance results have shown the theory to be correct. Torque-speed curves for the same current demand are very similar. The AHB controlled machine is able to achieve slightly more torque over the whole speed range by increasing its conduction angle beyond 120°, but this is only achieved at the expense of greatly increased copper loss. Inverter loss is very similar for the same torque output, however at high speed there is some reduction due to the circulation of current around the delta part of the circuit which reduces transistor and diode duty cycle.

A comparison can now be made with the fully pitched winding machine driven by the DPD inverter. Both machines display the same "external" characteristics in terms of inverter type, inverter rating, torque output, and even the shape of the torque produced in each stator tooth. The difference is that with the fully pitched winding machine this torque is produced with two phases conducting at the same time, resulting in lower copper losses and hence higher torque output for a given frame size.

Current sensing schemes have been investigated, including control with three phase sensors, two line sensors, three inverter leg shunts, and one DC link shunt. One of the benefits of the DPD inverter is that only three power connections are required between the inverter and the motor. If the motor is remote from the inverter then current sensing must be achieved within the inverter. As with the fully pitched winding machine, line current sensing with two sensors is able to control the machine exactly as with three phase sensors. Sensing with shunts placed in the lower half of the inverter legs (i.e. referenced to the negative DC link) is possible. Current samples, however, can only be made in the "on" state as well as a freewheel state if the machine rotates in one direction only. If bidirectional rotation is required, then shunts must also be placed in the upper half of the inverter legs to be able to continue sampling the current in the "on" state. Control with a single DC link shunt is also possible, but with two limitations. Current sampling can only take place in the "on" state, as no current flows in the DC link during the freewheel states. In addition the current that does flow in the DC link during the "on" state is not the ideal one needed to control the phase currents to a fixed current demand. Some distortion of the current shape occurs, which has a marginal effect on machine performance and inverter rating at low speed only.

Instead of trying to control the phase currents to a fixed current demand, it is possible instead to control the line currents to a sinusoidal shape. This was implemented with a separate PID control loop on each line current and brings the SR drive another step closer to the inverter fed induction motor in terms of the hardware and software required to drive the motor. Results from the test rig have shown that torque-speed curve is slightly lower at high speed, and torque per unit copper loss is affected at low speed due to the long conduction angle. On the other hand torque ripple and acoustic noise are reduced.

In summary, it has been shown that the short pitched SR motor can be driven successfully with a modified three phase bridge. This brings about the opportunity to use standard three phase bridge power electronic modules and benefit from only needing three power connections to the motor, assuming the phase diodes can be mounted in the motor terminal box. Low cost current sensing schemes can be used, and the overall effect on power electronic rating and machine performance is small.

Chapter 10 - CONCLUSIONS

10.1 General

The switched reluctance motor has been extensively developed over the last 30 years with many advances in machine design and control. At the same time the decreasing cost of power electronic components and control electronics has resulted in its commercial viability in an ever increasing number of applications.

SR motors with fully pitched windings have been shown to offer higher torque per unit copper loss due to the increased utilisation of the electric circuit. This leads to higher rated torque for a given frame size and a given temperature rise due to this increase in efficiency. At least two phases must be excited at any one time, as torque is produced from the change of mutual inductance between phases with position. With short pitched windings only one phase is generally excited as torque is produced from the variation of self inductance with position.

10.2 Topologies

A review of the fundamental operation of the machine shows that there are many geometries, number of phases and current waveshapes that are suitable, all of which differ in terms of key criterion, such as torque per unit copper loss and inverter rating. A two phase machine, for example, offers a significant reduction in copper loss as both phases conduct continuously. Operation requires a DC current in one phase and a bipolar current in the other phase. Various excitation patterns are possible with a four phase machine, the most efficient of which is bipolar operation with conduction for ¾ of the time. A simple comparison, ignoring endwinding length, shows that copper loss can be reduced to 16.6% that of a 4 phase short pitched winding machine with two phases excited. The drawback is that 16 power electronic switches are required, although each would conduct a much lower current.

A five phase machine is similar in that a bipolar waveform, conducting for 4/5 of the time, is the most promising. The simplistic analysis shows that copper losses are reduced to 25% the short pitched winding machine, however twenty switches are required if H bridges are used. This could be reduced to 10 switches in a half bridge arrangement with the phases connected in a star.

A three phase machine, utilising six power devices, offers a reduction of 50% in copper loss (ignoring endwindings) and operation with both unipolar and bipolar currents. This was, therefore, selected for detailed assessment and further development of machine design, control, and power electronic topologies.

10.3 Simulation

An accurate dynamic simulation tool is a key element in the comparisons. Based around the use of flux linkage/current/position data, effects such as magnetic saturation are modelled correctly. The use of transformation matrices considerably simplifies the simulation of the fully pitched winding machine with its strong mutual coupling between phases. Direct comparison with test rig results shows very good agreement even at high speed when heavy distortion of the current waveforms occur due to the mutual coupling. Accuracy is further improved at lower speeds due to detailed modelling of digital and analogue PWM current controllers. Deviations from the demanded current occur due to mutual coupling between phases if current controller bandwidth is not sufficient. Direct simulated comparisons with the short pitched winding machine show that because of these effects bandwidth needs to be increased to maintain a stable control system.

10.4 Machine Design

The design of the three phase prototype machine concentrates on maximising efficiency at the same time as reducing copper volume. If the stack design from a short pitched winding machine is taken and wound with fully pitched windings instead, then more copper will be used due to the length of the endwindings. This can be perceived as a disadvantage and therefore detailed design was carried out to minimise this extra copper

while maintaining the advantage the fully pitched winding machine has in terms of torque per unit copper loss. It is also beneficial, in a machine that exhibits greater winding efficiency, to shift the balance between the electric design and the magnetic design in favour of the latter. The design achieves this by decreasing the slot area mainly with an increase in split ratio, and tapering of the stator teeth. The latter increases the average tooth width while maintaining the same tooth width to tooth pitch ratio. FE analysis was used together with the simulation during the design process to ensure that copper volume is reduced while maintaining torque per unit copper loss. With these modifications the extra copper required with fully pitched windings is reduced from 46% to 5.5%.

10.5 Machine Performance

Initial results from a test rig show that the torque-speed curves differ with each mode of operation i.e. unipolar, bipolar squarewave, sinusoidal and sinusoidal star connected. Examination of the flux linkage waveforms explains why this occurs.

At low speed, with 27Nm of torque, the fully pitched machine has between 1.31 and 1.56 times the torque per unit copper loss of a short pitched winding machine, depending on the excitation method used (bipolar squarewave being best). At base speed with 18Nm of torque, the figures are between 1.46 and 1.93 times the torque per unit copper loss. These comparisons are made on the basis of a measured value of phase resistance in the fully pitched winding machine and a theoretical value in the short pitched winding machine.

Torque per unit copper loss varies as a function of torque due to saturation in the magnetic circuit. Comparisons were made at low speed under good current control. It is shown that the bipolar waveforms (i.e. bipolar squarewave and sinusoidal) exhibit relatively greater torque per unit copper loss at lower torques than unipolar operation or the short pitched winding machine. The reason for this is postulated, and this may be of further benefit to low speed operation of fan cooled machines where rated torque is low due to lack of cooling.

Rated torque over the whole speed range is determined from temperature rise tests on the prototype machine. This shows that bipolar squarewave operation is superior to unipolar operation over the whole speed range. Rated torque for unipolar operation at base speed is 23.3Nm compared to 25.7Nm for bipolar squarewave. These results would be further improved if the following are rectified – winding resistance is higher than expected due to unnecessary endwinding length, fill factor is low at 40%, and thermal conductivity between the winding and the stator core appears to be poor. Results are compared to a simulation of the short pitched winding machine for the same loss at each speed. These indicate that at base speed rated torque with unipolar operation would be 21% higher than the short pitched winding machine, and 33.9% higher with bipolar squarewave. Due to its higher torque per unit copper loss at lower torque outputs, bipolar squarewave operation exhibits 40% more torque at low speed.

10.6 Inverter Rating

Inverter ratings are compared in terms of both peak VA and inverter losses, with junction temperature the critical parameter in determining device rating. During very slow speed operation peak current determines the highest junction temperature, however at high speed average device losses are more appropriate. Comparisons show that inverter size in the fully pitched winding machine is generally higher, and it therefore becomes apparent that there is a trade-off of inverter rating and torque per unit copper loss. Sinusoidal operation yields a relatively small increase in torque per unit copper loss, while requiring a relatively large increase in inverter rating. Broadly speaking unipolar, sinusoidal star connected and bipolar squarewave lie on the same gradient of relative increase in torque per unit copper loss versus relative increase in inverter rating.

The number of switches is taken into account in both inverter VA rating and inverter loss comparisons, however it is usually the case that a lower number of switches is beneficial due to space considerations as well as the cost of drive circuits. This may result in bipolar squarewave and sinusoidal operation fairing worse in a practical situation than these figures suggest, as twelve switches are required. Sinusoidal operation may fair relatively better as the topology required is a three phase bridge

where the freewheel diodes can be contained in the same package as the switches. It is also the same topology used with induction motor and brushless DC machines.

10.7 Waveshape Optimisation

A new technique to optimise the demanded current waveshape in the fully pitched winding machine is shown to be very successful. It requires no starting values and is able to quickly scan through many combinations of current waveshape, gradually becoming more and more accurate. The method is able to optimise currents either for maximum torque per unit copper loss or for smooth torque with lowest copper loss. It is able to work at both low and high speed due to the fact that the required change in flux linkage between points can also be taken into account. For a reasonable search time 12 points on the waveform can be considered i.e. 30° (electrical) on a bipolar waveform.

The results show a significant improvement. Compared to squarewave current copper loss is reduced at low speed by 13%. At high speed the squarewave's copper loss increases very rapidly as current demand is increased to maintain a constant power. In contrast the optimised waveshape is able to maintain constant power while maintaining virtually a constant copper loss. Examination of the flux linkage waveforms shows that full voltage control does not yield the highest power output, and that the optimised waveshape is essentially the bipolar equivalent of unipolar operation. This explains why constant power operation can now be achieved. Smooth torque can be achieved up to base speed at the same time as reducing copper loss over bipolar squarewave. The optimisation schemes were implemented with a flux controller to ensure the demanded profiled currents were achieved. As the same method is used to calculate optimised waveforms at any speed, a smooth transition in waveshape can be achieved as the machine moves throughout the speed range.

A delta connected system can also be considered as the optimisation method can take into account the restrictions on the available phase voltages in this topology. Performance is normally very poor with this topology, as the current controller cannot control the phase currents independently. The optimisation technique yields significant

improvements to inverter rating and machine performance, making a delta connected scheme a realistic and attractive topology due to its use of a three phase bridge inverter.

10.8 Novel Inverter Topologies

Three new inverter topologies are proposed for unipolar operation, two of which have been fully developed, namely the DID (Delta with Interphase Diodes) and DPD (Delta with Phase Diodes). Both the DID and DPD topologies achieve similar torque-speed results to the AHB inverter throughout the speed range when operated with a fixed current demand. Inverter losses, however, are reduced at low speed to one half of the AHB inverter, as at any one time only two devices need to conduct to supply two phases. At high speed there is an additional advantage as current is able to feed directly into the next phase turning on via one of the additional diodes, thereby reducing losses further. Machine efficiency is only marginally affected, and therefore it is shown that the fully pitched winding machine can achieve greater efficiency without an increase in inverter rating (both in terms of peak VA as well as inverter losses).

There are further benefits, especially for the DPD inverter, in terms of current sensing arrangements and the packaging of power electronic components. Control with only two line sensors is shown to produce the same current waveforms as three phase sensors. Control with one DC link sensor is possible with some deviation from the demanded level of current. The DPD inverter is simply a standard three phase bridge with the addition of three low cost standard recovery diodes which, if they were mounted in the motor terminal box, would allow only three wires to be required between the motor and inverter.

The DPD inverter is shown to work with the short pitched winding machine. As the sum of the phase voltages must be zero with this topology, conduction periods must be restricted to 120°. Torque-speed performance is only slightly affected. Inverter losses in the main part of the bridge are the same at low speed, but improved at high speed due to the current circulating between phases in the delta configuration. As with the fully pitched winding machine operation is demonstrated with 2 line sensors as well as one DC link sensor.

10.9 Summary of Operating Modes

The following offers a qualitative summary of the performance of each motor drive with each operating mode and the further improvements that have been made to them.

Unipolar – a significant increase in torque per unit copper loss is achievable compared to the short pitched winding machine with many geometries (note that generally the fully pitched winding machine offers the best improvements with longer rather than short aspects ratios and higher pole numbers). Unipolar excitation, however, shows among the least increase in torque per unit copper loss in comparison to other operating modes. Inverter rating is worse than the short pitched winding machine in terms of inverter losses. The DPD and DID inverter topologies, however, rectify this situation, and in fact improve inverter losses during high speed operation. In general, good motor drive performance is achieved at both high and low speeds with square shaped control, making it suitable for a wide range of applications, for example, a general purpose industrial drive.

Bipolar Squarewave – This is the highest performing drive in terms of torque output. It clearly has the highest torque per unit copper loss at the same time as exhibiting relatively low torque ripple. Inverter rating is high and it suffers from the complexity of requiring 12 controlled switches, albeit at a lower rating. Profiling the bipolar currents improves torque per unit copper loss even further, becoming twice that of the short pitched winding machine with square shaped currents. Inverter rating is also improved due to better high speed performance. Smooth torque is achievable up to base speed with profiled currents. This makes this drive more suitable for, perhaps, servo type applications where torque per unit volume and/or smooth torque is paramount.

Sinusoidal (with H bridge) – Torque per unit copper loss is good, however, inverter rating is very high even when compared to bipolar squarewave. Perhaps the only perceivable advantage is that sinusoidal shaped currents offer lower acoustic noise due to lower rates of change of current and flux linkage. Generally speaking a better trade-off of performance versus inverter rating is achieved with bipolar squarewave or sinusoidal star connected.

Sinusoidal Star – Both inverter rating and torque per unit copper loss are average for a fully pitched winding motor drive. A significant advantage, however, is apparent in that a standard three phase bridge topology can be used, allowing either the freewheel diodes to be contained within the same package as the switching devices or alternatively a standard module could be used. Therefore both the inverter topology and the shape of the currents become the same as the induction motor drive. As with unipolar operation, sinusoidal star could be suitable for many applications, although high speed performance is not as good. Some further improvements may be possible if the current profiling optimisation technique was adapted for this topology.

Delta (with bipolar operation) – Low speed performance is very poor as the phase currents cannot be independently controlled, making it an unrealistic drive in the majority of applications. Profiling the line currents, however, significantly improves performance and further analysis of inverter rating may show it to be an alternative to sinusoidal star connected.

10.10 Further Work

The work presented here is a detailed analysis of motor drive performance in three phase machines. Two, four and five phase machines have not been investigated in detail. The simplistic analysis of the potential reduction of copper loss indicates that several suitable excitation patterns and inverter topologies are possible. The two phase machine, for example, potentially offers the same reduction in copper loss as the three phase machine, but further work is required on inverter topologies and control methods to minimise inverter rating. Bipolar operation of the four phase machine appears to offer the largest reduction in copper loss of any fully pitched machine design, although the inverter component count is high. Simulation work would be required to develop control further and assess its true inverter rating and machine performance.

Profiling currents produces significant improvements in performance. Work on the delta topology with bipolar currents is required to check the theoretical analysis and make further improvements. Applying the optimisation technique to the star connected

machine may well also improve its performance. Both of these topologies are interesting as they use standard power electronic topologies.

The DPD and DID topologies are very effective at controlling the fully pitched machine with unipolar currents. Work should be carried out on both the fully pitched and short pitched winding machines to develop this further.

Appendix A - FLUX LINKAGE MEASUREMENT METHOD

Knowledge of the relationship between phase flux linkage, phase current and rotor position is essential in understanding and predicting the performance of the machine. For example it is used in the simulation to predict phase current from knowledge of the applied voltage and the position of the rotor. As explained in Chapter 3 this data can also be used as the basis to calculate the relationship between instantaneous phase torque, current and rotor position.

Flux linkage can either be calculated from finite element analysis (see Chapter 4), or measured on an actual machine. The method for doing the latter is now explained. Equation A.1 shows that the flux linkage is simply the integration over time of the voltage applied to a phase, minus the resistive voltage drop due to the current that is flowing.

$$\Psi = \int_0^t (V - iR)dt \tag{A.1}$$

The DSP was used to control these measurements. It was arranged so that it read the encoder position and outputted it to a display. The rotor could then be manually turned to a desired angle and then locked in that position to perform a set of flux linkage measurements. With the rotor locked the DSP applied voltage to the machine using the inverter. Note that, as explained previously, it was the equivalent per tooth flux linkage that needed to be measured, and so to achieve this two fully pitched winding phases needed to be excited in the fully pitched winding machine. Two windings were therefore connected in series for the purposes of this measurement to ensure that both conducted the same current.

Phase current and applied voltage were then continuously sampled every 25μs so that the integration in Equation A.1 could be performed. The flux linkage needed to be known in steps of 0.5A up to a maximum value of 20A. With a voltage being applied

the current builds up, and every time it reaches one of these current steps the calculated flux linkage is noted by the DSP. A curve of flux linkage against current for one particular position is therefore built up. This process is then repeated for all the other desired rotor positions to build up the family of curves shown in Figure A.1. Table A.1 shows the same data but in a tabulated format.

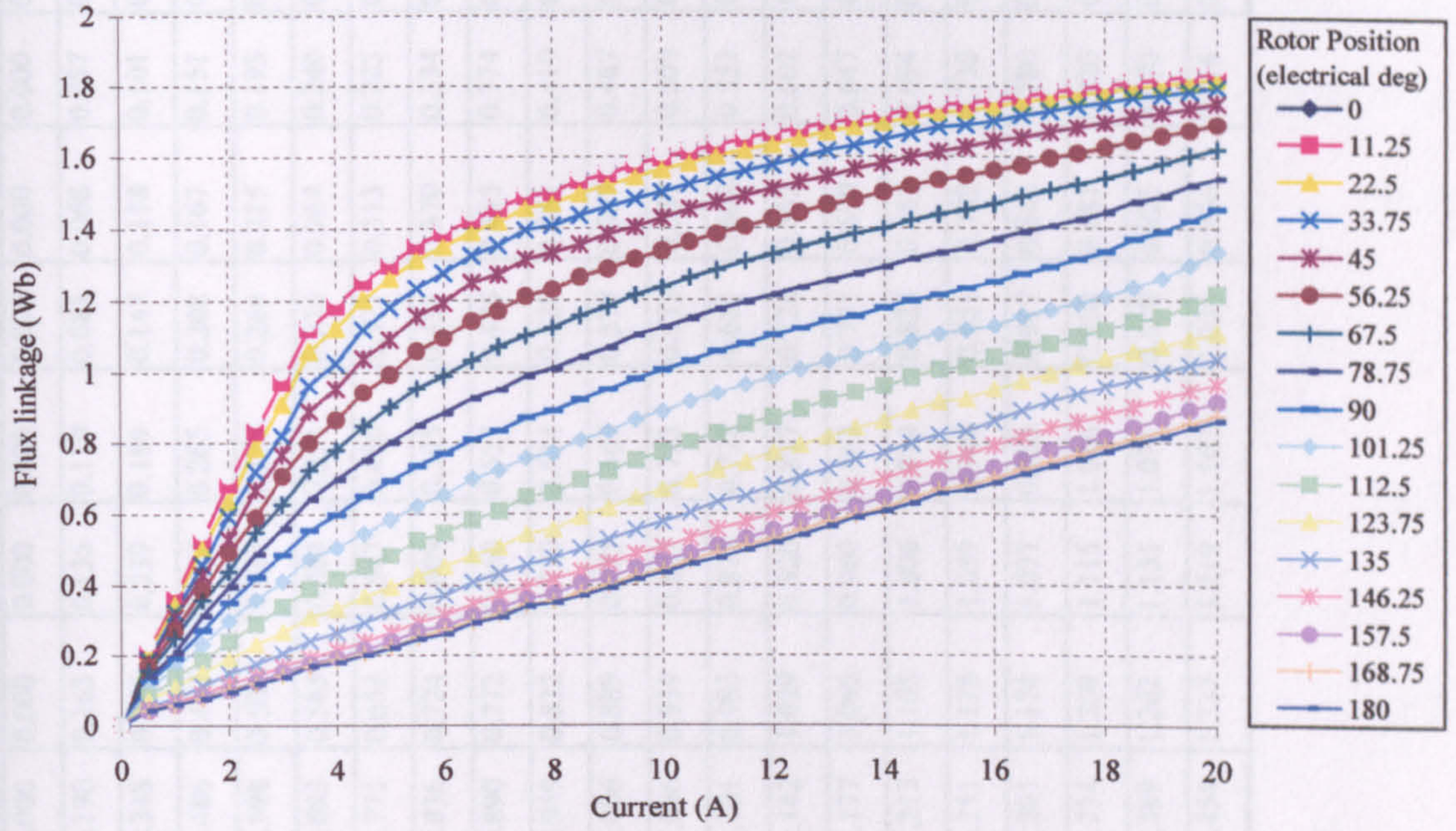

Figure A.1 Measured flux linkage/current/rotor position curves for the prototype machine.

	Rotor Position (electrical degrees)																
I(A)	0	11.25	22.5	33.75	45	56.25	67.5	78.75	90	101.25	112.5	123.75	135	146.25	157.5	168.75	180
0	0.000	0.000	0.000	0.000	0.000	0.000	0.000	0.000	0.000	0.000	0.000	0.000	0.000	0.000	0.000	0.000	0.000
1	0.398	0.358	0.348	0.321	0.307	0.270	0.250	0.209	0.190	0.163	0.135	0.110	0.081	0.068	0.057	0.056	0.060
2	0.708	0.686	0.634	0.593	0.531	0.491	0.438	0.396	0.348	0.296	0.239	0.189	0.147	0.118	0.101	0.103	0.095
3	1.002	0.972	0.909	0.821	0.768	0.709	0.627	0.559	0.486	0.412	0.337	0.265	0.208	0.167	0.151	0.142	0.137
4	1.212	1.186	1.122	1.026	0.954	0.866	0.779	0.699	0.598	0.506	0.417	0.329	0.264	0.215	0.193	0.186	0.178
5	1.324	1.299	1.260	1.181	1.091	0.994	0.902	0.800	0.693	0.585	0.484	0.394	0.324	0.264	0.240	0.223	0.222
6	1.407	1.387	1.348	1.278	1.194	1.094	0.989	0.884	0.771	0.653	0.547	0.450	0.371	0.313	0.283	0.272	0.260
7	1.471	1.457	1.419	1.353	1.274	1.171	1.070	0.950	0.836	0.724	0.609	0.505	0.431	0.370	0.334	0.316	0.308
8	1.521	1.501	1.469	1.409	1.334	1.231	1.124	1.010	0.890	0.772	0.660	0.557	0.475	0.415	0.374	0.352	0.347
9	1.571	1.551	1.519	1.459	1.383	1.288	1.182	1.067	0.949	0.832	0.720	0.614	0.528	0.461	0.419	0.400	0.391
10	1.610	1.597	1.563	1.501	1.428	1.337	1.236	1.123	1.006	0.889	0.775	0.667	0.577	0.507	0.467	0.440	0.434
11	1.648	1.632	1.602	1.544	1.471	1.384	1.283	1.172	1.056	0.939	0.827	0.723	0.632	0.557	0.509	0.491	0.475
12	1.679	1.667	1.633	1.576	1.510	1.427	1.327	1.213	1.101	0.985	0.872	0.772	0.681	0.602	0.553	0.530	0.520
13	1.708	1.696	1.669	1.616	1.546	1.465	1.365	1.255	1.142	1.029	0.920	0.817	0.728	0.652	0.602	0.578	0.564
14	1.734	1.719	1.695	1.648	1.582	1.501	1.399	1.291	1.177	1.065	0.960	0.863	0.771	0.699	0.647	0.615	0.608
15	1.757	1.746	1.723	1.682	1.615	1.535	1.439	1.331	1.213	1.105	1.006	0.914	0.823	0.753	0.694	0.670	0.657
16	1.774	1.763	1.742	1.701	1.643	1.562	1.467	1.367	1.251	1.128	1.039	0.949	0.861	0.792	0.730	0.700	0.688
17	1.795	1.783	1.764	1.729	1.671	1.596	1.507	1.406	1.291	1.174	1.077	0.993	0.917	0.843	0.780	0.747	0.735
18	1.816	1.802	1.785	1.754	1.697	1.627	1.541	1.446	1.334	1.209	1.115	1.036	0.958	0.881	0.820	0.789	0.775
19	1.834	1.822	1.806	1.776	1.726	1.660	1.582	1.490	1.389	1.262	1.155	1.071	0.998	0.925	0.870	0.834	0.816
20	1.854	1.838	1.822	1.800	1.755	1.694	1.622	1.542	1.454	1.337	1.219	1.107	1.036	0.966	0.916	0.877	0.864

Table A.1 Tabulated data for the flux linkage graph of Figure A.1

APPENDIX B -CALCULATION OF COPPER WEIGHT FOR EQUAL COPPER LOSSES

Assume initially that the short pitched and fully pitched winding machines use the same diameter wire and the same number of turns per phase. Due to the extra endwinding length the phase resistance of the fully pitched winding machine is greater by a factor α.

$$R_{FP} = \alpha R_{SP} \tag{B.1}$$

Copper loss is calculated in both machines using the following:

$$Loss_{FP} = 3\left(\frac{2I_{FP}^2 R_{FP}}{3}\right) = 2I_{FP}^2 R_{FP} \tag{B.2}$$

$$Loss_{SP} = 3\left(\frac{I_{SP}^2 R_{SP}}{3}\right) = I_{SP}^2 R_{SP} \tag{B.3}$$

where, for the same the same tooth MMF, and hence torque (assuming unipolar excitation):

$$I_{SP} = 2I_{FP} \tag{B.4}$$

Substituting Equation B.4 and B.1 into B.2 and B.3:

$$Loss_{FP} = 2I^2 \alpha R_{SP} \tag{B.5}$$

$$Loss_{SP} = 4I^2 R_{SP} \tag{B.6}$$

As the wire diameters are the same copper volume is proportional to the ratio of the phase resistances:

$$\frac{CopperVol_{FP}}{CopperVol_{SP}} = \alpha \tag{B.7}$$

If the losses in both machines are then forced to be equal then the resistance of the fully pitched winding must be increased by a further factor of β. Therefore, using Equations B.5 and B.6:

$$\beta = \frac{2}{\alpha} \tag{B.8}$$

To achieve the increase in phase resistance the cross sectional area (CSA) of the wire should be reduced by the factor of β. Copper volume is proportional to the wire CSA, therefore:

$$\frac{CopperVol_{FP}}{CopperVol_{SP}} = \frac{\alpha}{\beta} = \frac{\alpha^2}{2} \tag{B.9}$$

Table 4.1 in Chapter 4 can be used to calculate the value of α for different stack lengths and pole numbers. Therefore, for example, α=1.46 for the 12-8 machine with a stack length of 150mm (and stator OD of 150mm). In this instance, then, the ratio of copper volumes in the two machines would be 1.066 for the same loss and torque output i.e. approximately the same.

Note, however, that to equalise the losses the total cross sectional area of the fully pitched winding has been reduced by the factor β (=1.37, using equation B.8). This means that the slot area could be reduced by the same factor, which would allow, for example, the stator tooth width or the split ratio to be increased. These have the effect of increasing torque for a given MMF.

In this situation described, the MMF is equal in both machines, so the conclusion is that even with the same copper weight and the same copper loss, the fully pitched winding machine would still produce more torque for the same stack size.

Appendix C - TEST RIG DESCRIPTION

C.1 Overview

The test rig used for the newly designed fully pitched winding machine consists of the following main parts – the prototype fully pitched winding SRM, power converter, DSP based controller, DC load machine, and host PC with DSP emulator. A schematic representation of the physical arrangement is shown in Figure C.1.

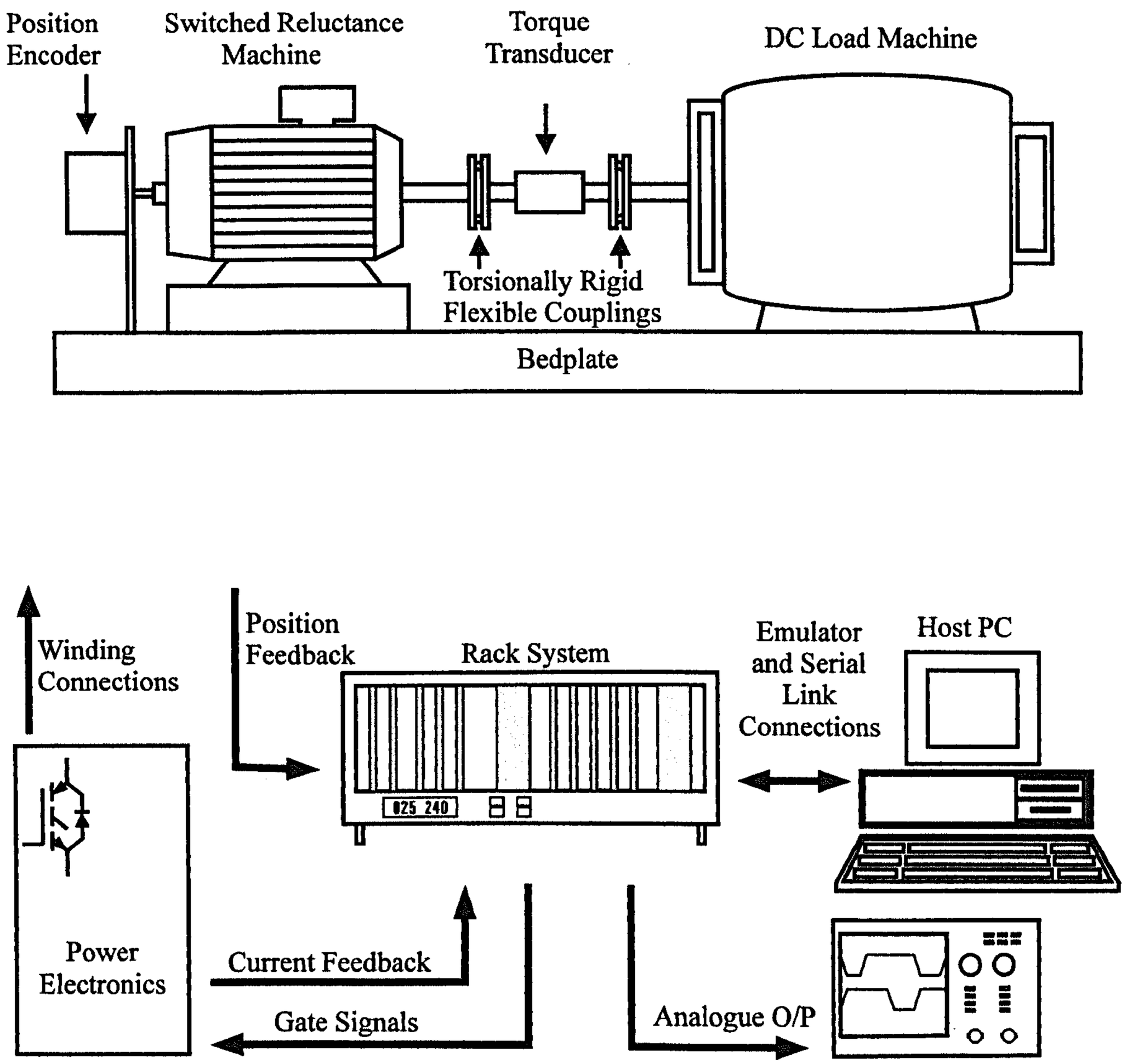

Figure C.1 Physical layout of the test rig.

C.2 Power Converter

A purpose designed voltage source power converter was constructed to enable the different inverter topologies to be easily arranged. The basic connection was three 'H' bridges, which enabled fully independent bipolar control of currents on each phase (see Figure C.2). The same bridge could also be used for unipolar currents in exactly the same way as the standard asymmetric half bridge commonly used with SRMs. In other words devices T2, T3, D1, and D4 were still connected in the circuit but never conduct as the current is unipolar. This arrangement could also be reconfigured to a star or delta connection by only using three of the limbs. Semikron SKM100GB101D IGBTs were used with a nominal maximum rating of 100A, 1200V. The rest of the power circuit was quite standard and consisted of a three phase rectifier, a 5mH DC link inductor and a 2200μF DC link capacitor. The IGBT drivers that were used were supplied by Concept, and these handled the necessary isolation. $V_{ce(sat)}$ overcurrent protection was provided and this was combined with other hardware protection signals such as overvoltage, phase overcurrent and heatsink over temperature, to initiate the tripping of the drive under fault conditions.

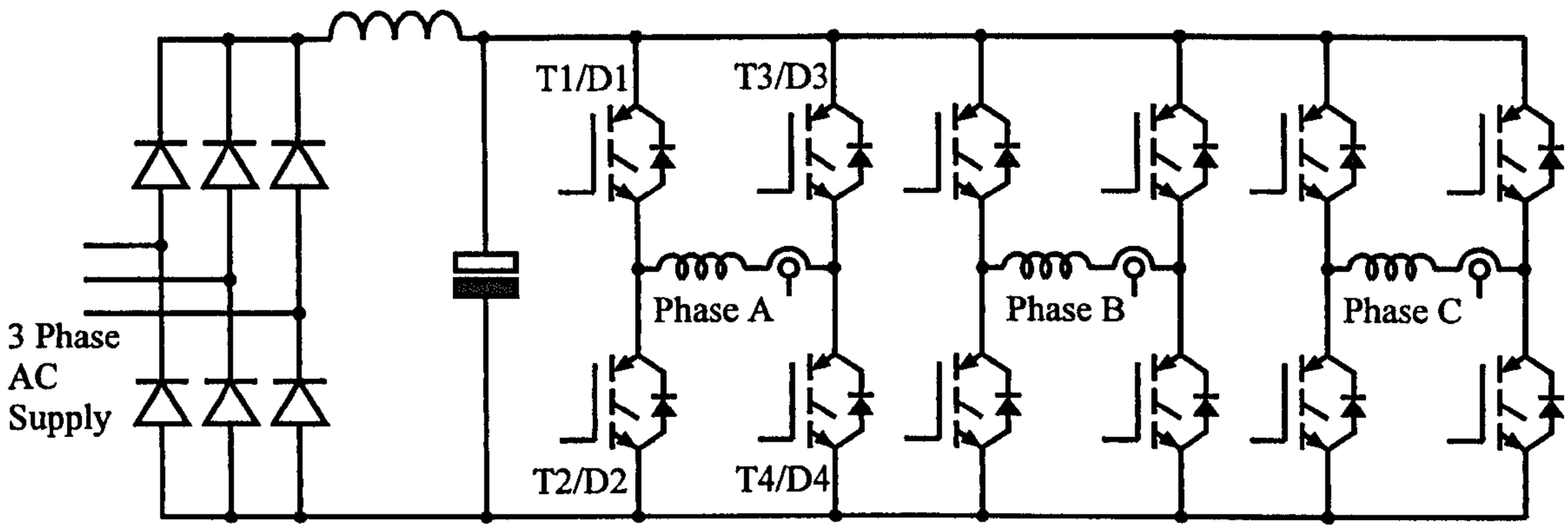

Figure C.2 Power converter in the 'H' bridge configuration, showing rectifier, DC link inductor and capacitor, phase windings and current transducers.

C.3 Controller

Control was centred around the Texas Instruments TMS320C31 DSP (digital signal processor). This is a 32 BIT floating point processor operating at 40MHZ. A rack based

processing system had already been developed as part of the CAPEC (Concerted Action on Power Electronics and Control) funded research in Newcastle University. Further work was carried out to extend the system for the purposes of testing the fully pitched winding SRM. This included a PWM controller based on FPGA programmable logic, a digital to analogue card to output sampled and calculated waveforms to an oscilloscope, and input cards to sample current and rotor position. The separate PWM controller was included to allow the DSP plenty of time for more analytical work such as estimation of torque and calculation of waveforms using the transformation matrices. The DSP itself was linked to a PC based emulator system for software development using a C compiler.

PWM Controller

The purpose of this controller was to convert the voltage reference signals (V_{ref}), supplied from the software based current control loop, into gate signals. As with most PWM schemes this was achieved by comparing the V_{ref} signal to a triangular wave and switching either the lower or upper device accordingly. Each leg of the inverter was operated independently from its own V_{ref} signal. The DSP supplied $+V_{ref}$ to control one leg of a phase and $-V_{ref}$ to the other leg. This enabled the switching frequency seen by the phase winding to be twice that of the switching frequency of the device, keeping switching losses down and taking noise into the inaudible range. The triangle wave and V_{ref} had a resolution of 8 bits.

Features such as the PWM frequency and dead time were programmed by the DSP with an initiating routine. Switching frequency was set to 10kHz, which meant that the current control loop operated every 100μs. Dead time was set to 2μs.

Control Scheme

A schematic of the control scheme is depicted in Figure C.3 with the current loop timing shown in Figure C.4. The whole control system was synchronised to the triangle wave on the PWM card. Synchronisation pulses were sent out at the peak of every triangle wave to initiate the first current control loop in the DSP. The function of this loop was to sample the encoder position and determine the phase current demands. On and off angles for current commutation were input manually with a paddle switch and indicated via an LED display. The rest of the time in this first control loop is taken up calculating

machine performance. Values such as torque, torque ripple, copper loss, inverter loss were estimated during this time and were averaged over several electrical cycles. Waveforms such as phase current, torque, and flux are also sent to the 8 channel DAC card that was developed, for outputting to an oscilloscope.

The DSP spent the time between this first control loop and the second one doing background tasks that did not need to be synchronised to the PWM. The estimated values such as torque, loss etc that had already been calculated were sent via a serial link to the host PC during this time, and displayed on a continuous basis. The DSP periodically stored the sampled waveforms and sent them down the serial link to be captured and stored in ASCII files in the PC. It is these values and waveforms that are the basis for most of the measured results shown in Chapters 5, 6, 7, 8,and 9. Because of the way the waveforms are captured, the results shown are therefore subject to 100μs sampling.

The second control loop was the one that actually contained the PID current control. This was initiated internally in the DSP by a software timer, which in turn was set by the hardware interrupt supplied by the synchronisation pulse. This software timer also outputted a hardware pulse to the ADC cards that initiated the sampling of currents at this point. The current error was then calculated, and voltage references generated via the PID gains. Finally these references were sent to the PWM controller and implemented there at the next synchronisation pulse (t=100μs).

It might be considered more normal to sample the current at the start of the PWM period i.e. t=0, with one control loop handling the voltage reference generation. However this results in a 100μs delay between the sampling of current and the new voltage demand being applied to the machine. This controller lag was found to very significant in affecting the stability of the system. With the speed of the DSP fixed, it was therefore essential to leave the sampling of the current until the last possible moment in the control cycle. To achieve this, any calculations that did not require the newly updated current sample were processed in the first loop, leaving only the minimum amount of work in the second loop. Chapter 6 discusses the impact this has on stability.

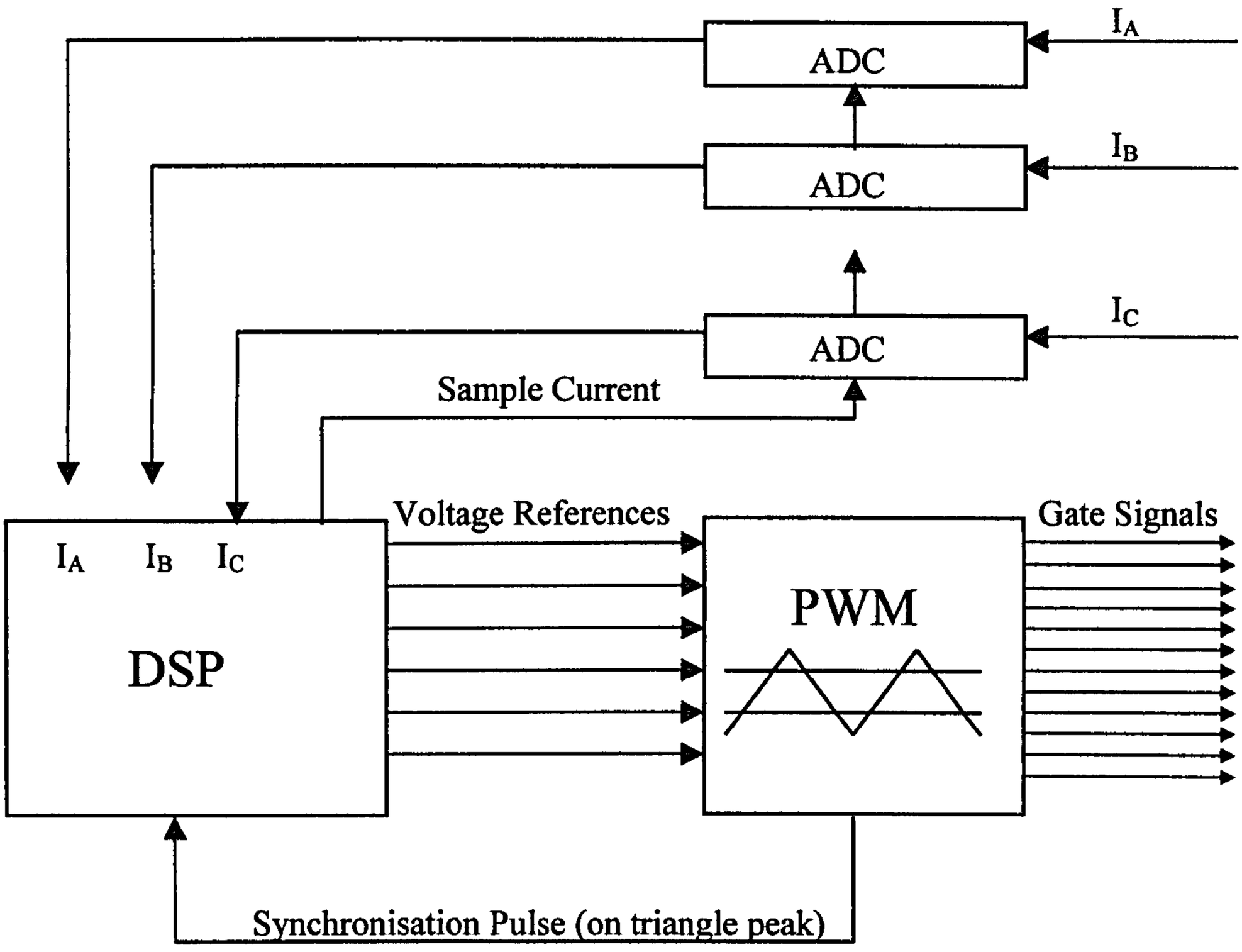

Figure C.3 Current control schematic.

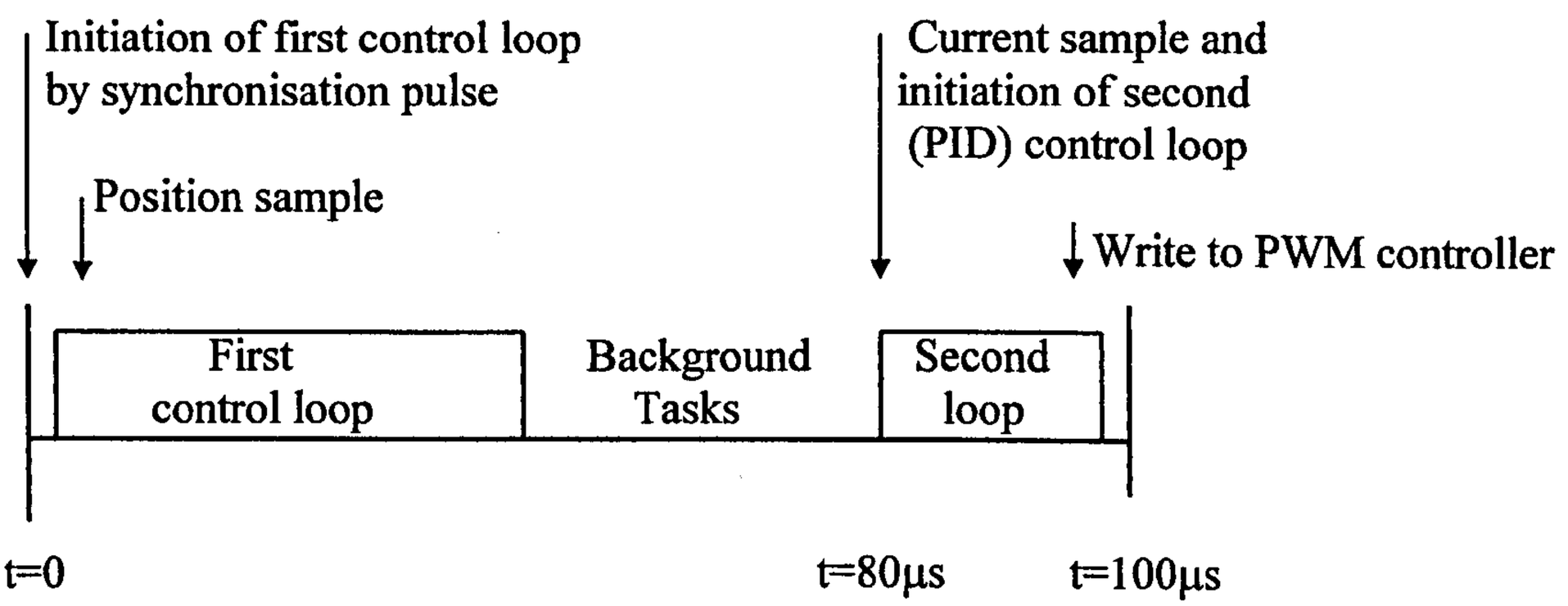

Figure C.4 Current control timing during one PWM cycle.

C.4 Performance Estimation Techniques

This section describes the methods used by the DSP to estimate instantaneous electrical torque and inverter loss in real time.

Torque Estimation

The same method of torque estimation was used as in the simulation i.e. phase current and rotor position were sampled and torque calculated from predetermined characteristics. The DSP measured these values every 100μs and the following calculations were then performed during the first control loop to calculate torque:

- Sampled phase currents were converted into the equivalent single tooth currents using the transformation matrices (Equation 2.8 of Chapter 2).
- Instantaneous electrical torque can then be calculated from the torque/current/rotor position data, which was stored in the DSP as a look-up table. This data that had previously been calculated from the measured flux linkage data using the principle of co-energy (see section 4.3.4 of Chapter 4). The data used is shown again in Figure C.5 and is tabulated at the end of this appendix.

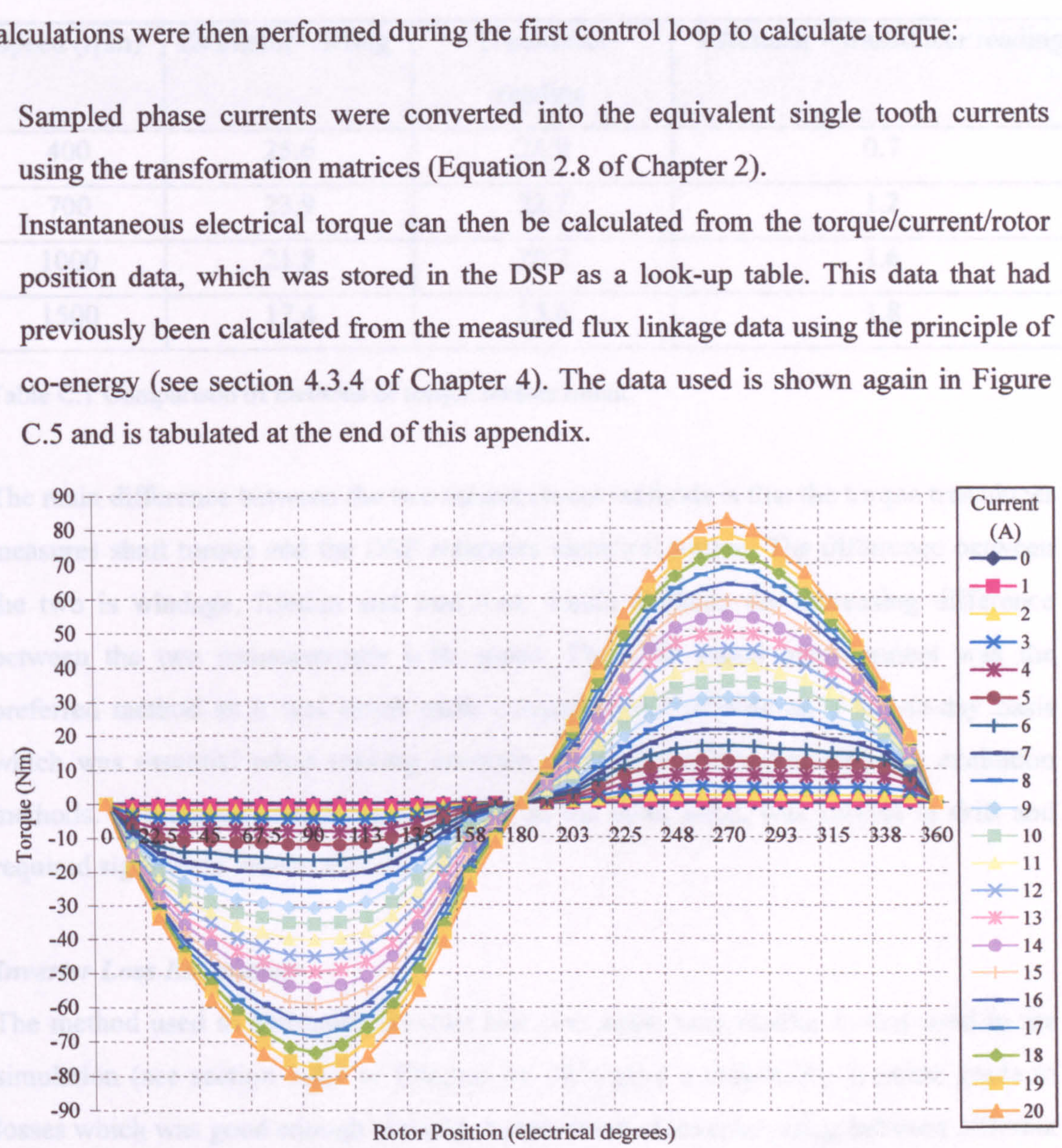

Figure C.5 Electrical torque against current and rotor position for the prototype machine calculated from the measured flux linkage data (curves are shown in steps of 1A for clarity).

The torque values were stored in the look-up table in rotor angle steps of 11.25° (electrical) and current steps of 0.5A. Linear interpolation was used to calculate values between any two points.

The test rig also contained a torque transducer that was located between the SR machine and the DC load machine (see Figure C.1). This was connected to its amplifier box which indicated a measurement of shaft torque. The DSP based torque estimator was compared to the torque transducer with the following results:

Speed (rpm)	Estimator reading	Transducer reading	Estimator – transducer reading
400	25.6	24.9	0.7
700	23.9	22.7	1.2
1000	21.8	20.2	1.6
1500	17.4	15.6	1.8

Table C.1 Comparison of methods of torque measurement.

The main difference between the two measurement methods is that the torque transducer measures shaft torque and the DSP estimates electrical torque. The difference between the two is windage, friction and iron loss, which explains the increasing difference between the two measurements with speed. The DSP based measurement was the preferred method as it was much more consistent and reliable on a day-to-day basis which was essential when making accurate comparisons between different excitation methods. The torque transducer amplifier, on the other hand, was subject to drift and required significant time to warm up.

Inverter Loss Estimation

The method used to determine inverter loss was again very similar to that used in the simulation (see section 3.4.2 of Chapter 3). This gave a reasonably accurate guide to losses which was good enough to make comparisons of inverter rating between different methods of excitation.

Device conduction losses were approximated using a y = mx + c type of characteristic for IGBT V_{ce} drop and diode V_f drop. Switching losses were based on knowing the energy dissipated for each switch on and off of the device at a given voltage and current which could easily be determined from the device datasheet. This value was then used in proportion to the actual values being switched. This method therefore takes in account the effect of IGBT tail currents and reverse recovery losses in the IGBTs due to the diodes. The PWM V_{ref} value was used to decide whether a device is going to switch or not within a given PWM period. It was also used to determine the conduction period of the IGBTs and diodes for the conduction loss calculation.

I	Rotor Position (electrical degrees)															
	0	11.25	22.5	33.75	45	56.25	67.5	78.75	90	101.25	112.5	123.75	135	146.25	157.5	168.75
0	0.0	0.0	0.0	0.0	0.0	0.0	0.0	0.0	0.0	0.0	0.0	0.0	0.0	0.0	0.0	0.0
1	0.0	-0.5	-0.4	-0.5	-0.4	-0.5	-0.7	-0.6	-0.5	-0.7	-0.6	-0.6	-0.5	-0.2	-0.1	0.0
2	0.0	-1.6	-1.8	-2.1	-1.9	-2.0	-2.3	-2.2	-2.1	-2.4	-2.3	-2.1	-1.6	-0.9	-0.4	-0.1
3	0.0	-3.3	-4.2	-4.5	-4.3	-4.4	-4.5	-4.7	-4.7	-5.0	-4.8	-4.4	-3.4	-1.9	-0.9	-0.3
4	0.0	-5.0	-7.4	-7.8	-7.4	-7.7	-7.8	-8.1	-8.1	-8.4	-8.2	-7.3	-5.7	-3.2	-1.4	-0.5
5	0.0	-6.6	-10.2	-11.2	-10.9	-11.5	-11.6	-12.1	-12.3	-12.4	-11.9	-10.5	-8.2	-4.8	-2.1	-0.9
6	0.0	-7.8	-12.6	-14.4	-14.6	-15.6	-15.8	-16.5	-16.8	-16.7	-15.9	-14.0	-10.9	-6.5	-3.0	-1.3
7	0.0	-9.0	-14.7	-17.3	-18.4	-19.9	-20.2	-21.1	-21.5	-21.3	-20.3	-17.6	-13.7	-8.5	-3.9	-1.7
8	0.0	-10.0	-16.7	-20.2	-22.1	-24.2	-24.7	-25.8	-26.2	-25.9	-24.7	-21.4	-16.6	-10.5	-5.1	-2.3
9	0.0	-11.1	-18.6	-23.0	-25.6	-28.3	-29.2	-30.6	-30.9	-30.5	-29.1	-25.3	-19.7	-12.6	-6.3	-2.9
10	0.0	-12.1	-20.5	-25.8	-29.0	-32.2	-33.6	-35.3	-35.7	-35.2	-33.6	-29.3	-22.9	-14.8	-7.6	-3.5
11	0.0	-13.1	-22.4	-28.5	-32.3	-36.1	-38.0	-40.0	-40.5	-39.9	-38.1	-33.3	-26.2	-17.1	-8.9	-4.1
12	0.0	-14.1	-24.2	-31.1	-35.5	-39.8	-42.3	-44.7	-45.2	-44.5	-42.5	-37.3	-29.6	-19.6	-10.3	-4.8
13	0.0	-14.9	-25.9	-33.6	-38.6	-43.5	-46.6	-49.3	-49.8	-49.1	-46.8	-41.2	-33.0	-22.2	-11.8	-5.6
14	0.0	-15.8	-27.4	-35.9	-41.6	-47.3	-50.8	-53.9	-54.4	-53.5	-51.0	-45.1	-36.4	-24.8	-13.4	-6.3
15	0.0	-16.5	-28.8	-38.2	-44.6	-50.9	-55.0	-58.5	-59.0	-57.8	-55.0	-48.9	-39.7	-27.4	-15.1	-7.1
16	0.0	-17.2	-30.1	-40.3	-47.5	-54.5	-59.1	-62.9	-63.7	-62.2	-58.8	-52.6	-42.9	-30.0	-16.9	-7.9
17	0.0	-17.9	-31.2	-42.3	-50.3	-57.9	-63.0	-67.3	-68.5	-66.5	-62.5	-56.0	-46.0	-32.8	-18.8	-8.7
18	0.0	-18.5	-32.2	-44.1	-53.0	-61.1	-66.8	-71.6	-73.3	-70.9	-66.1	-59.3	-49.2	-35.6	-20.7	-9.6
19	0.0	-19.1	-33.2	-45.8	-55.5	-64.2	-70.4	-75.6	-78.1	-75.6	-69.8	-62.5	-52.3	-38.4	-22.6	-10.6
20	0.0	-19.7	-34.0	-47.3	-57.8	-67.0	-73.6	-79.3	-82.5	-80.4	-74.1	-65.9	-55.2	-40.9	-24.4	-11.7

I	Rotor Position (electrical degrees)																
	180	191.25	202.5	213.75	225	236.25	247.5	258.75	270	281.25	292.5	303.75	315	326.25	337.5	348.75	360
0	0.0	0.0	0.0	0.0	0.0	0.0	0.0	0.0	0.0	0.0	0.0	0.0	0.0	0.0	0.0	0.0	0.0
1	0.0	0.0	0.1	0.2	0.5	0.6	0.6	0.7	0.5	0.6	0.7	0.5	0.4	0.5	0.4	0.5	0.0
2	0.0	0.1	0.4	0.9	1.6	2.1	2.3	2.4	2.1	2.2	2.3	2.0	1.9	2.1	1.8	1.6	0.0
3	0.0	0.3	0.9	1.9	3.4	4.4	4.8	5.0	4.7	4.7	4.5	4.4	4.3	4.5	4.2	3.3	0.0
4	0.0	0.5	1.4	3.2	5.7	7.3	8.2	8.4	8.1	8.1	7.8	7.7	7.4	7.8	7.4	5.0	0.0
5	0.0	0.9	2.1	4.8	8.2	10.5	11.9	12.4	12.3	12.1	11.6	11.5	10.9	11.2	10.2	6.6	0.0
6	0.0	1.3	3.0	6.5	10.9	14.0	15.9	16.7	16.8	16.5	15.8	15.6	14.6	14.4	12.6	7.8	0.0
7	0.0	1.7	3.9	8.5	13.7	17.6	20.3	21.3	21.5	21.1	20.2	19.9	18.4	17.3	14.7	9.0	0.0
8	0.0	2.3	5.1	10.5	16.6	21.4	24.7	25.9	26.2	25.8	24.7	24.2	22.1	20.2	16.7	10.0	0.0
9	0.0	2.9	6.3	12.6	19.7	25.3	29.1	30.5	30.9	30.6	29.2	28.3	25.6	23.0	18.6	11.1	0.0
10	0.0	3.5	7.6	14.8	22.9	29.3	33.6	35.2	35.7	35.3	33.6	32.2	29.0	25.8	20.5	12.1	0.0
11	0.0	4.1	8.9	17.1	26.2	33.3	38.1	39.9	40.5	40.0	38.0	36.1	32.3	28.5	22.4	13.1	0.0
12	0.0	4.8	10.3	19.6	29.6	37.3	42.5	44.5	45.2	44.7	42.3	39.8	35.5	31.1	24.2	14.1	0.0
13	0.0	5.6	11.8	22.2	33.0	41.2	46.8	49.1	49.8	49.3	46.6	43.5	38.6	33.6	25.9	14.9	0.0
14	0.0	6.3	13.4	24.8	36.4	45.1	51.0	53.5	54.4	53.9	50.8	47.3	41.6	35.9	27.4	15.8	0.0
15	0.0	7.1	15.1	27.4	39.7	48.9	55.0	57.8	59.0	58.5	55.0	50.9	44.6	38.2	28.8	16.5	0.0
16	0.0	7.9	16.9	30.0	42.9	52.6	58.8	62.2	63.7	62.9	59.1	54.5	47.5	40.3	30.1	17.2	0.0
17	0.0	8.7	18.8	32.8	46.0	56.0	62.5	66.5	68.5	67.3	63.0	57.9	50.3	42.3	31.2	17.9	0.0
18	0.0	9.6	20.7	35.6	49.2	59.3	66.1	70.9	73.3	71.6	66.8	61.1	53.0	44.1	32.2	18.5	0.0
19	0.0	10.6	22.6	38.4	52.3	62.5	69.8	75.6	78.1	75.6	70.4	64.2	55.5	45.8	33.2	19.1	0.0
20	0.0	11.7	24.4	40.9	55.2	65.9	74.1	80.4	82.5	79.3	73.6	67.0	57.8	47.3	34.0	19.7	0.0

Table C.2 Tabulated data for the torque/current/angle graph shown in Figure C.5.

Appendix D - PWM TECHNIQUES FOR DID AND DPD INVERTERS

D.1 PWM Generation

The switching states for control of a fully pitched winding machine with a DPD inverter are shown in Table D.1. These are used as the basis for the PWM methodology. The table details three basic switching states for each one third period of the electrical period – one 'on' state and two freewheeling states. Notice that the 'on' state only requires two switches to be turned on. In a standard three phase bridge drive circuit the two devices in a each half bridge are often controlled as a pair so that one of the devices is always on and the other is off (apart from in the dead time period when both are off). This can make control easier as one PWM generator is used to control a pair of devices, as one is the compliment of the other.

Phases desired on	Switches On	Condition	Phase A Voltage	Phase B Voltage	Phase C Voltage
A & B	T1, T6	$I_A > I_B$	0	$+V_{dc}$	$-V_{dc}$
	T1, T6	$I_A < I_B$	$+V_{dc}$	0	$-V_{dc}$
	T1, T3, T5	-	0	0	0
	T2, T4, T6	-	0	0	0
B & C	T3, T2	$I_B > I_C$	$-V_{dc}$	0	$+V_{dc}$
	T3, T2	$I_B < I_C$	$-V_{dc}$	$+V_{dc}$	0
	T1, T3, T5	-	0	0	0
	T2, T4, T6	-	0	0	0
C & A	T5, T4	$I_C > I_A$	$+V_{dc}$	$-V_{dc}$	0
	T5, T4	$I_C < I_A$	0	$-V_{dc}$	$+V_{dc}$
	T1, T3, T5	-	0	0	0
	T2, T4, T6	-	0	0	0

Table D.1 Summary of the useful switching states for current control and the resulting winding voltages.

If this is the case with this inverter then a slight complication is added because in the 'on' state only two devices are actually required on rather than three. If the complimentary switching is to be used then the controller has to decide to turn on another switch. This of course must not affect the voltages that are applied to the winding.

The PWM is generated as follows. The PID control loop decides the duty cycle to apply to the whole bridge made on the basis of the current sampled in the phase that is in the first half of its conduction period. The duty cycle, or voltage reference (V_{ref}), is then sent to the PWM generator. In the case of the test rig the PID control loop was implemented in the DSP and the PWM generator in an FPGA. That voltage reference is then compared to a triangle wave, which is generated at the desired switching frequency of the transistors. The negative of V_{ref} is also generated (with V_{ref}=0 being at the centre of the triangle wave). It then depends on which phases are desired on as to which pairs of transistors receive $+V_{ref}$ and which ones receive $-V_{ref}$. An example is given in Figure D.1 with phases A and B desired on, and phase C desired off. The resulting voltages that would be applied to the winding by the inverter are also shown. It can also be seen that with this method the frequency of the applied voltage to the motor is twice that of the switching frequency of the transistors. This enables inaudible operation to be more easily achieved and spreads losses more evenly between devices.

Notice that with phases A and B on, only devices T1 and T6 actually need to be turned on. In the example in Figure D.1 the controller has decided to turn T3 on as well at this time because of the situation described above with complimentary switching. The alternative would have been to turn T4 on as this is the other half of the pair. However the controller made this decision because it knew that I_A was greater than I_B, which means that diode D3 would already be conducting with the difference of the two phase currents. Turning T3 on therefore does not affect the voltages applied to the winding and achieves the desired goal of complimentary switching all the devices. This therefore requires knowledge of whether certain phase currents are greater or smaller than the others for the scheme to work. If this is not known then individual PWM generators would be needed for each device. This situation would occur when sensing only DC link current or inverter leg currents.

Note that negative volts should not be allowed to be applied to the phase that is in the first half of its conduction period i.e. the phase that the current sample is being taken from to determine the PWM duty cycle. Negative volts should never be needed on the phase that is in the first half of its conduction period, but if it were applied then this would mean that negative volts could not be applied to the phase turning off. To prevent this from happening $+V_{ref}$ should not be allowed to fall below zero.

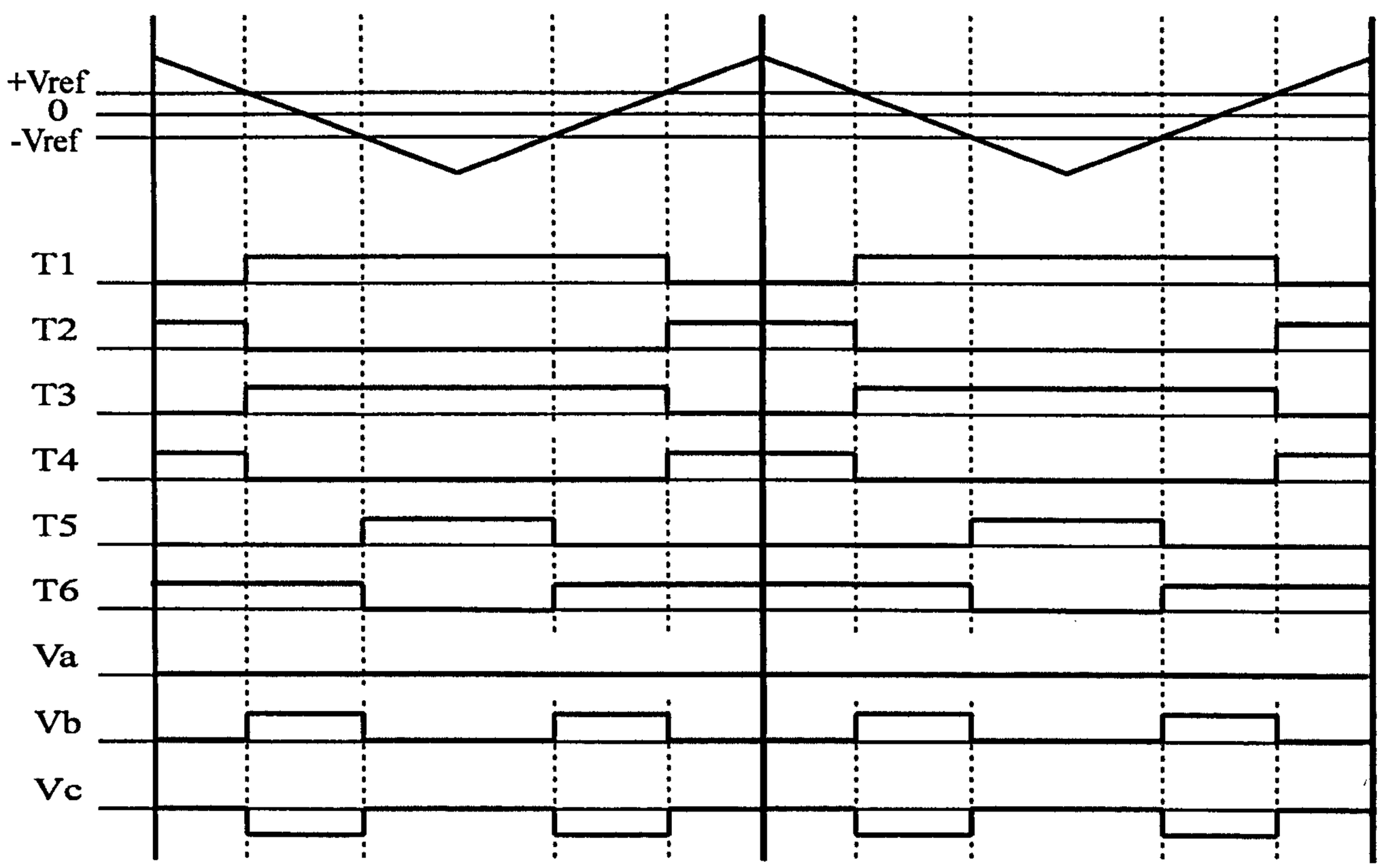

Figure D.1 PWM strategy for the example with phases A and B on, phase C off, and $I_A > I_B$. Two PWM periods shown. DPD inverter.

D.2 Dead Time Effects and Compensation

Chapters 8 and 9 described the effects of dead time on the current waveform with the DPD inverter. This section describes in more detail the dead time compensation scheme that is used to bring the waveforms back to the desired shape.

Figure D.2 shows the PWM generation including the dead time control between the upper and lower devices. The resulting voltages applied to the winding are also shown. This waveform assumes perfect switching which is clearly not possible as dead time control would not be needed in the first place, but it does give a qualitative view as to what the effect is. It can be seen that, during the dead time period, phase A receives negative volts rather than the zero volts that are required, and phase C receives zero volts rather than negative volts. This explains, for example, why in Figure 8.26 of Chapter 8 the waveforms become distorted - the commutation spike comes down faster than it would normally do because it is receiving negative volts when it should be receiving none. These negative volts should be being applied to the phase turning off and that is why the tail lasts longer than it should. The result is that the tail current and the commutation spike do not cancel each other out resulting in the line current and the equivalent single tooth currents becoming distorted from the ideal.

A method was therefore developed to counteract this effect. A compensating value can be added to the voltage reference, V_{ref}, of appropriate pairs of switches. The result is that those waveforms shift in time slightly as shown in Figure D.3. The voltage outputs from the inverter are then restored to the correct shapes. This method has been shown to work well on the test rig and, as Figure 8.27 shows in Chapter 8, the current waveforms are indeed restored to the correct shape. This has been tried with various values of dead time up to 8μs with complete success. The only complication is that the V_{ref} compensation value depends not only on the dead time that is being used, but also on the current switched and the DC link voltage. This is thought to be due to the variation in switching time with current, which affects the effective dead time period. In a real application the DC link voltage may not vary enough to affect the value, but the current switched will vary.

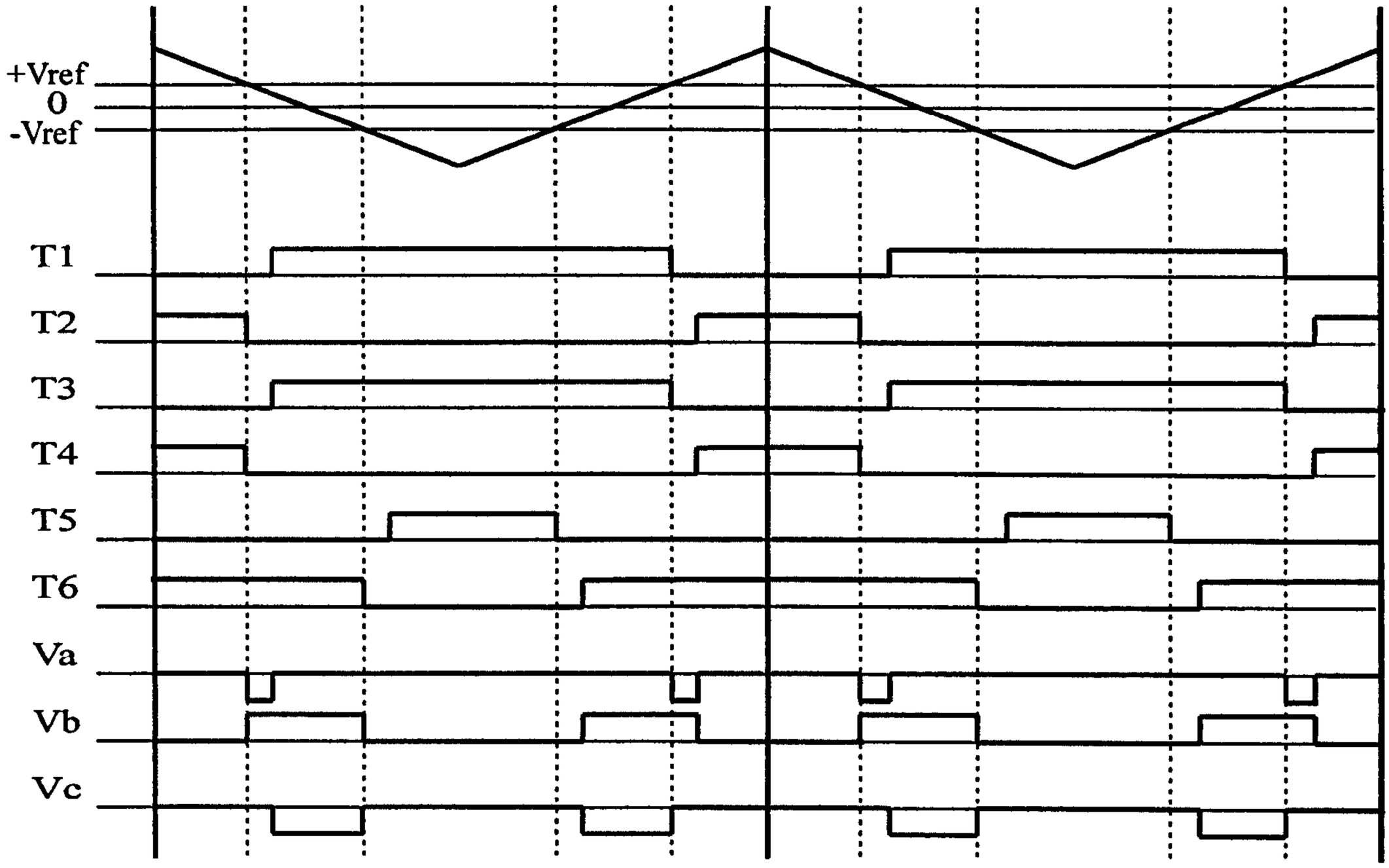

Figure D.2. PWM generation in the DPD inverter including dead time control. The resulting idealised voltage output from the inverter on each phase also shown (assuming $I_A > I_B > I_C$).

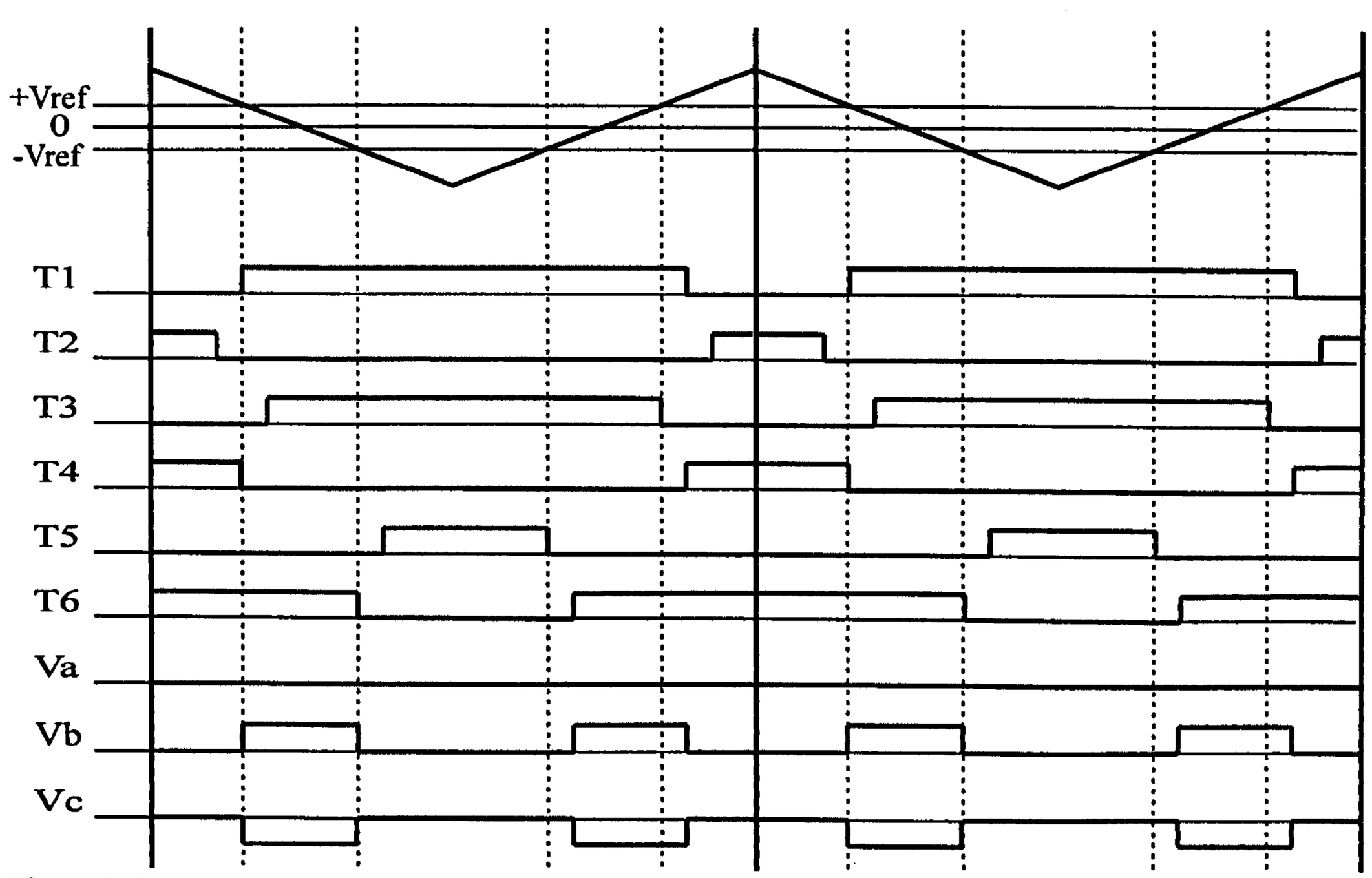

Figure D.3. As Figure D.2, but with dead time compensation on T1/T2.

However it should be quite possible to use a simple linear equation to determine the V_{ref} compensating value based on the current being switched, and it is not critical to compensate for this effect entirely.

Finally, with the DPD inverter, the following transistors should be paired together if complimentary switching is required –

Pair 1 - T1 and T6

Pair 2 - T2 and T3

Pair 3 - T4 and T5

DID inverter

Figure D.4 shows an example of PWM in the DID inverter together with the resulting phase voltages, assuming idealised transistors.

In this type of inverter dead time control is not required, as the shoot through situation cannot occur. On the test rig, however, the same PWM controller was used on both types of inverter and it was found that using a small amount of dead time together with the compensation technique improved the shape of the current waveforms. Without any dead time at all the waveforms were slightly distorted, but not as much as with the DPD inverter. This effect occurs with the DID inverter as well because the transistors do not switch instantaneously, meaning that there is some overlap between the switching of complimentary pairs. This does not cause a shoot through in this inverter, but does distort the current. The amount of overlap depends on the current switched, and therefore to correct the effect under all conditions some dead time should be included, and then voltage reference compensation terms added that are a function of current (as with the DPD inverter).

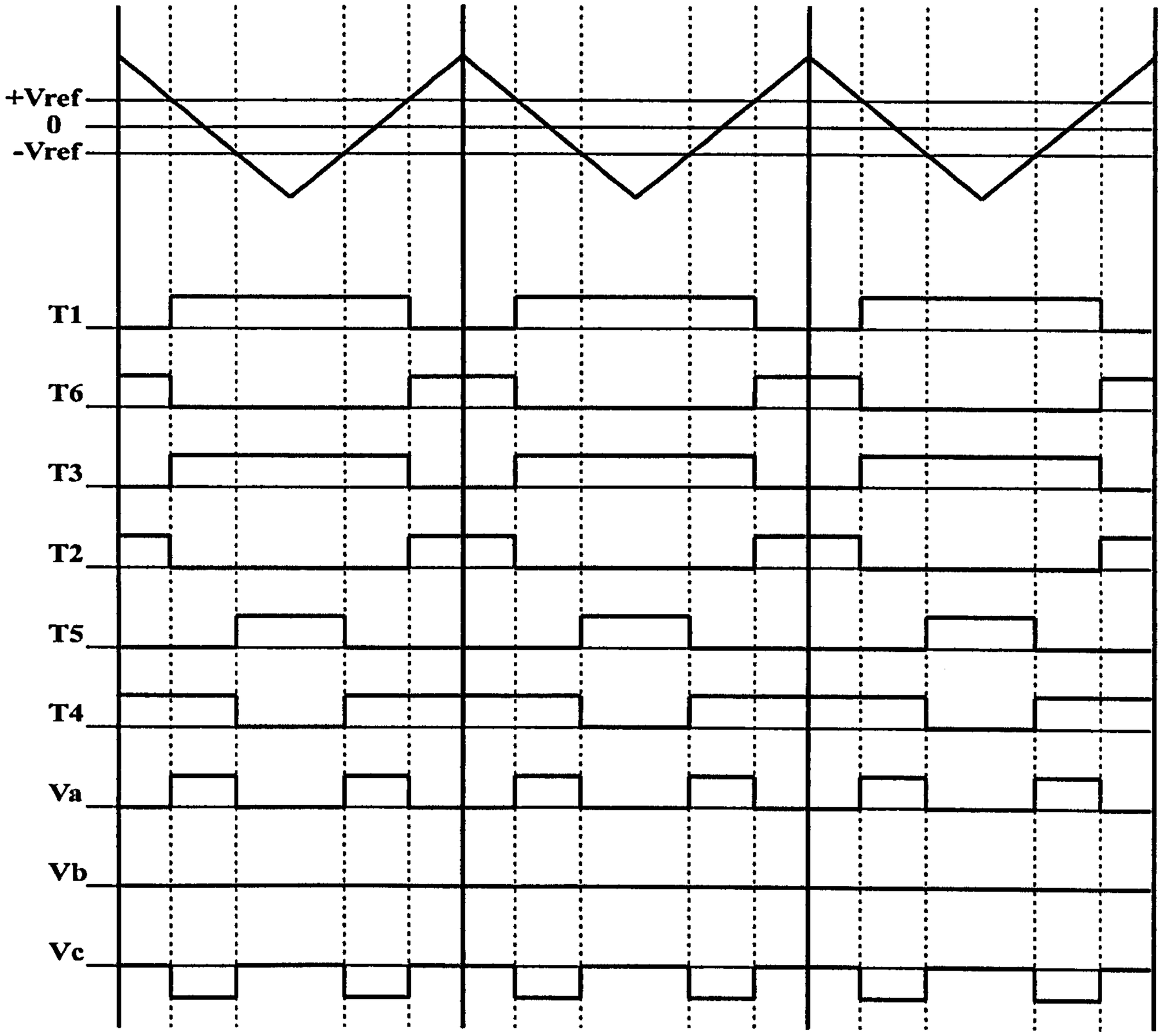

Figure D.4. PWM generation in the DID inverter. The resulting idealised voltage output from the inverter on each phase also shown with $I_A > I_B > I_C$.